INDIAN AGRICULTURAL
RESEARCH INSTITUTE, NEW DELHI

I. A. R. I. 6.
MGIPC—S4—10 AR—21-6-49—1,000.

PROCEEDINGS

OF THE

ROYAL SOCIETY OF LONDON

SERIES A. MATHEMATICAL AND PHYSICAL SCIENCES

VOL 178

LONDON
Printed and published for the Royal Society
By the Cambridge University Press
Bentley House, N.W.1

15 August 1941

PRINTED IN GREAT BRITAIN BY
WALTER LEWIS, M.A.
AT THE CAMBRIDGE UNIVERSITY PRESS

CONTENTS

SERIES A VOL 178

No. A 972. 9 May 1941

PAGE

Relaxation methods applied to engineering problems. VII. Problems relating to the percolation of fluids through porous materials. By F. S. Shaw and R. V. Southwell, F.R.S. 1

On the specific heat of the sodium chloride crystal. By E. W. Kellermann 17

The kinetics of the polymerization of isoprene on sodium surfaces. By J. L. Bolland 24

Structure and molecular anisotropy of sorbic acid, $CH_3.CH:CH.CH:CH.COOH$. By K. Lonsdale, J. M. Robinson and I. Woodward. (Plates 1–4) 43

The sun's magnetic field and the diurnal and seasonal variations in cosmic ray intensity. By L. Jánossy and P. Lockett 52

The flame spectrum of carbon monoxide. II. Application to 'after-burning'. By A. G. Gaydon 61

The determination of the vapour-pressure curve of liquid helium below 1·6° K using a magnetic thermometer. By B. Bleaney and R. A. Hull 74

The effective susceptibility of a paramagnetic powder. By B. Bleaney and R. A. Hull 86

A stress-strain curve for the atomic lattice of iron. By S. L. Smith and W. A. Wood 93

The catalytic isomerization of butene-1. By G. H. Twigg 106

No. A 973. 12 June 1941

A self-consistent field for methane and its applications. By R. A. Buckingham, H. S. W. Massey, F.R.S. and S. R. Tibbs 119

Bose-Einstein statistics and degeneracy. By D. S. Kothari and B. N. Singh 135

The production of waves by the sudden release of a spherical distribution of compressed air in the atmosphere. By J. J. Unwin 153

PAGE

Precise measurements of the energies of β-rays from radium (B + C). By A. F. A. Harper and N. F. Roberts 170

The γ-ray transition of radio-bromine. By R. E. Siday 189

On transition from laminar to turbulent flow in the boundary layer. By A. Fage and J. H. Preston. (Plate 5) 201

Further investigations of solid *n*-paraffins. (Repulsion potential and compressibility.) By A. Müller 227

No. A 974. 31 July 1941

The electronic charge. By V. D. Hopper and T. H. Laby. (Plate 6) . 243

General classical theory of spinning particles in a Maxwell field. By H. J. Bhabha and H. C. Corben 273

General classical theory of spinning particles in a meson field. By H. J. Bhabha 314

Spectroscopic observations on hydrocarbon flames in atomic oxygen. By K. H. Geib and W. M. Vaidya. (Plate 7) 351

A spectroscopic investigation of hydrocarbon flames. By W. M. Vaidya. (Plates 8–10) 356

Chemical equilibria of thermal associations. By A. Wassermann . . 370

The diffusion and thermal diffusion of hydrogen-deuterium, with a note on the thermal diffusion of hydrogen-helium. By H. R. Heath, T. L. Ibbs and N. E. Wild 380

Thermal diffusion in hydrogen-deuterium mixtures. By K. E. Grew . 390

No. A 975. 15 August 1941

Critical and co-operative phenomena. VI. The neighbour distribution function in monatomic liquids and dense gases. By J. Corner and J. E. Lennard-Jones, F.R.S. 401

On the electron diffraction of multilayers of esters of fatty acids. I. By A. Cameron and G. D. Coumoulos 415

On the electron diffraction of multilayers of esters of fatty acids. II. The structure of multilayers of the esters. By G. D. Coumoulos and E. K. Rideal, F.R.S. (Plates 11, 12) 421

PAGE

The catalysis of the parahydrogen conversion by tungsten. By D. D. Eley and E. K. Rideal, F.R.S. 429

The interchange of hydrogen in the adsorbed film on tungsten. By D. D. Eley 452

On the α/β brass type of equilibrium. By K. W. Andrews and W. Hume-Rothery, F.R.S. 464

Deuteron-induced fission in uranium and thorium. By D. H. T. Gant and R. S. Krishnan 474

On the dielectric strength of mixed crystals. By H. Fröhlich. . . . 493

Perturbation theory for the self-consistent field. By H. W. Peng . . 499

Two-phase equilibrium in binary and ternary systems. IV. The system ethane-propylene. By H. Lu, D. M. Newitt and M. Ruhemann . . 506

Systematic constructional tables for thin cemented aplanatic lenses. By Edna D. Brown and T. Smith, F.R.S. 525

Index 526

Relaxation methods applied to engineering problems

VII. Problems relating to the percolation of fluids through porous materials

By F. S. Shaw, B.E. (*Western Australia*) and
R. V. Southwell, F.R.S.

(*Received* 3 *January* 1941)

The accepted theory of percolation of fluids through porous materials (which is based on Darcy's law of resistance) indicates that the velocities can be calculated from a velocity-potential which, in two-dimensional motion, is plane-harmonic within the fluid field. The associated stream function, and the fluid pressure, are also plane-harmonic, so in cases where all boundaries are known their determination is an ordinary problem in plane-potential theory. But in cases where a free surface exists (as in the percolation of water through earth dams), its shape is not known a priori, consequently orthodox methods cannot be applied.

Here the relaxation method developed in earlier papers is shown to be applicable without special assumptions, and to yield results of more than sufficient accuracy. Three typical examples are treated, the third involving 'refraction' of the lines of flow and pressure at the junction of two materials of different porosity.

Introduction and summary

1. Among the problems treated in Part III of this series (Christopherson and Southwell 1938) was one which by orthodox analysis is quite intractable, —the problem of torsion for a homogeneous prism stressed beyond its elastic limit. Here, while some parts of the material still obey Hooke's law, in other parts (on account of 'yielding' due to overstrain) the shear stress has a constant limiting intensity. What makes the problem intractable by orthodox methods is the fact that the overstrained region cannot be defined a priori, being dependent on the distribution of stress in the parts which remain elastic. By relaxation methods, with their more tentative approach, this difficulty was surmounted easily.

In view of this success with one 'unknown boundary problem' it was natural to look for others in different fields, and a case of some practical importance was found in the theory of fluids percolating through porous material such as sand or peat. This theory, of which the foundations appear to have been laid by Forchheimer (1886) and Boussinesq (1904),* is now generally accepted: it involves a potential function ϕ which (in two-dimensional problems) is plane-harmonic like the velocity-potential of inviscid fluid theory, notwithstanding that resistance of the viscous-fluid type is implied in 'Darcy's law' which is the basis of its governing equations. In many cases (e.g. the peat-drainage problems discussed by Richardson (1908)) the boundaries of the percolating fluid are known initially and the boundary conditions are of normal kind; but in cases where the percolating fluid has a free surface, e.g. when water leaks through the material of a retaining wall, the form of this surface is determined by the joint actions of gravity and of resistance to percolation, therefore cannot be predicted. Retaining walls have been discussed in recent papers by Davison and Rosenhead (1940) and by Casagrande (1937): the latter contains an extensive bibliography.

2. Casagrande's paper explains very clearly the essentials of the problem and the nature of the free surface in a retaining wall. His method† for determining ϕ entails free-hand sketching of stream-lines and of their orthogonals, therefore requires that the free surface—which is one of the family of stream-lines—be either known a priori, or guessed, or obtained by trial and error. Davison and Rosenhead, by a skilful use of Schwarz-Christoffel transformations, escape the necessity of defining free surfaces a priori; but they have not, on the other hand, completely solved the problem indicated in figure 1 (which is based on figures 1 and 4 of their paper), except on the assumption of evaporation from the free surface in excess of a specified limit. This problem concerns the leakage of water through a retaining wall having vertical sides BL, CM: the head of water on each side is specified, and leakage *under* the wall is prevented by an impermeable stratum. If the evaporation is sufficient, the free surface inside the wall tends smoothly to the level on the downstream side; but otherwise it reaches this (vertical) side at a point (E) above that level, and fluid seeping through to air drains freely down the wall. Davison and Rosenhead formulate two boundary conditions to be satisfied on a free surface extending from A to D (figure 1), then proceed to conformal transformation; but what results in the second case is a curve of the type sketched in broken lines, implying not only seepage through the downstream face but also return flow back into the wall. As they remark, only the first of these implications can be accepted: the second is unrealizable, so the total percolation is not given correctly.

---

* Cf. Davison (1936 *a*, p. 881).

† Casagrande (1937, § D) attributes the graphical method to Forchheimer.

3. Our 'relaxation' treatment of this problem, described in §§7–11, focuses attention not on ϕ but on the 'average pressure p' (which also is plane-harmonic). No serious difficulty was encountered, since the free surface was found to be stable in the sense that an incorrect assumption regarding its shape led to 'out-of-balance forces' which could be liquidated only by amending that assumption. As found by computation it joins the upstream face horizontally and the downstream face tangentially (i.e., in this problem, vertically: cf. figure 5). These features accord with Casagrande's description (1937, §§E, F).

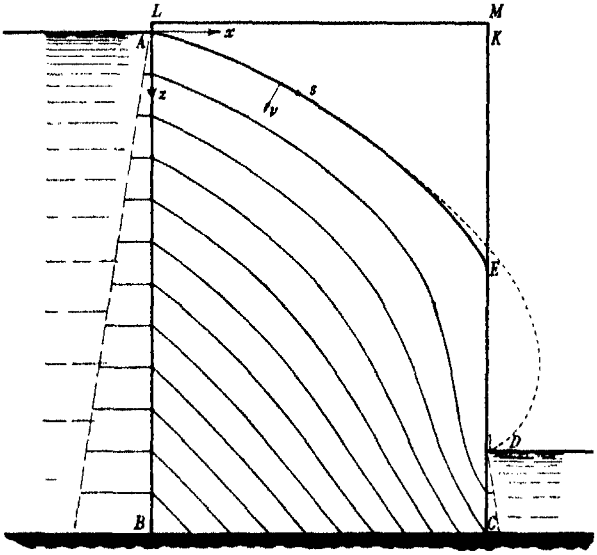

FIGURE 1

4. Having found the method successful in this instance, we next applied it to a harder example suggested by figure 13 of Casagrande's paper. Here (figure 2) the upstream and downstream faces of the wall are 'battered', the subsoil (in figure 1 taken as quite impermeable) is assumed to offer the same resistance to percolation as the wall, and a 'blanket' of permeable material (e.g. graded rubble) is provided, in accordance with modern practice, with the aim of preventing erosion due to drainage down the exposed (i.e. downstream) face.

5. In view of the need for brevity it was not considered necessary to include examples which, being straightforward applications of potential theory, present no problem not already considered in Part III (Christopherson and Southwell 1938). We have, however, treated a case (figure 3) in which

two distinct strata are involved, having resistances to percolation in the ratio 1 : 4. Such cases are confronted in practice, and they entail boundary conditions of somewhat special kind, in that the stream-lines are 'refracted' where they cross the common surface of two different strata. In figure 3 this common surface is horizontal: the general case presents no greater difficulty, but would of course entail rather more labour.

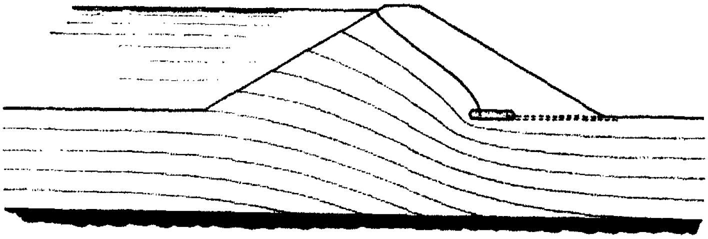

FIGURE 2

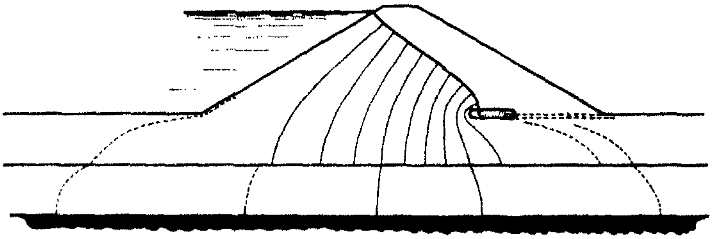

FIGURE 3

Evaporation occurring within the retaining wall will modify the boundary condition to be satisfied at the free surface (cf. § 2); but its effect is not likely to be important, and we have not considered it in this paper. What matters is that we should be able to predict, with reasonable accuracy, the nature of the flow and of the pressures which it induces: our treatment focuses attention on these pressures from the first. Terzaghi (1933, 1934*a*, *b*) first called attention to their importance, and Casagrande stresses the value of a method which will determine them approximately, even at the cost of several days of labour (1937, § F, *d*). Our method, as we believe, can be applied with complete confidence in its accuracy, and even in inexperienced hands will lead without difficulty to positive results. Slightly modified, it should be capable of dealing with stratified and therefore anisotropic soils (Casagrande 1937, § G).

For brevity, knowledge of Parts III and V of this series (Christopherson and Southwell 1938; Gandy and Southwell 1940) is presumed in the account which follows.

THE MATHEMATICAL PROBLEM

6. Adopting the notation of Davison and Rosenhead (1940, § 1), we take

Ox as the horizontal axis and Oy, directed upwards, as the vertical axis; and we write

p for the average pressure at a point x, y,
u and v for the components of percolation velocity along Ox and Oy.

The components of frictional force are defined, in agreement with Darcy's law,* as $\rho g u/k$ and $\rho g v/k$, ρ denoting the density of the fluid and g the acceleration due to gravity. k is the 'percolation coefficient' or 'coefficient of permeability' (Casagrande): it measures the flow per unit time (of the fluid considered) through a unit cube (figure 4) of the permeable material, when a unit difference of head is maintained between two opposite vertical faces and when flow through the other faces is prevented.

The equation of continuity is

$$\frac{\partial u}{\partial x}+\frac{\partial v}{\partial y}=0, \qquad \text{(i)}$$

and the equations of motion are

$$\left.\begin{aligned} -\frac{\partial p}{\partial x}-\frac{\rho g}{k}u &= 0,\\ -\frac{\partial p}{\partial y}-\frac{\rho g}{k}v-\rho g &= 0,\end{aligned}\right\} \qquad \text{(ii)}$$

showing that u, v have the expressions

$$u=\frac{\partial \phi}{\partial x},\quad v=\frac{\partial \phi}{\partial y}, \qquad \text{(iii)}$$

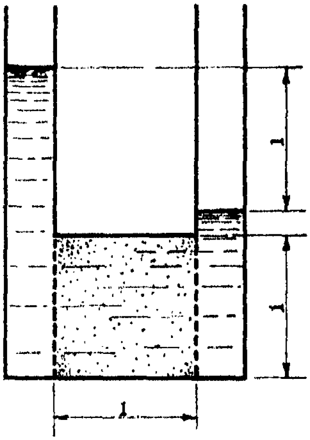

FIGURE 4

in terms of a velocity-potential ϕ defined by

$$\phi=-k\left(\frac{p}{\rho g}+y\right). \qquad (1)$$

On substitution from (iii) in (i) we find that

$$\left.\begin{aligned} &\nabla^2\phi=0,\\ \text{also}\qquad &\nabla^2 p=0 \text{ in virtue of (ii).}\end{aligned}\right\} \qquad (2)$$

---

* Casagrande states (1937, p. 134): 'The reader may be assured that this law is valid for the study of seepage through dams.'

We shall find it convenient to introduce the symbol z for the vertical co-ordinate measured *downwards* from an origin (A) in the upstream face of the retaining wall at the level of the water surface, as shown in figure 1. Then along AB (since the fluid is sensibly at rest) we have

$$p/\rho g = z. \tag{3}$$

Along AE (the free surface*) and ED (the 'seepage surface')

$$p/\rho g = 0. \tag{4}$$

Along DC (since the fluid is sensibly at rest)

$$p/\rho g = z - z_D. \tag{5}$$

Along the impermeable base BC, $v = \partial\phi/\partial y = 0$, therefore by (1)

$$\frac{\partial}{\partial z}(p/\rho g) = -\frac{\partial y}{\partial z} = 1. \tag{6}$$

(We have assumed in (4) that p is measured from atmospheric pressure as datum. In the nature of the case, if another datum were chosen we could make a constant addition to $p/\rho g$.)

PROBLEM I. SEEPAGE THROUGH A RETAINING WALL HAVING VERTICAL SIDES

7. We have still to discuss, for this problem, a further condition which must be satisfied at the free surface AE.

By definition, $\partial\phi/\partial\nu = 0$ for all points on AE, ν denoting the direction of the normal to the curve. Hence, according to (1), we have

$$\frac{\partial}{\partial \nu}(p/\rho g) = -\frac{\partial y}{\partial \nu} = \frac{\partial z}{\partial \nu} = \frac{\partial x}{\partial s} \quad \text{(cf. figure 1)},$$

s denoting distance from A along the curve AE. Combined with (4) which must also be satisfied on AE, this yields two equivalent conditions as under:

$$\left.\begin{aligned} &\frac{\partial}{\partial z}(p/\rho g) = l\frac{\partial}{\partial \nu}(p/\rho g) = l^2, \\ &\frac{\partial}{\partial x}(p/\rho g) = -m\frac{\partial}{\partial \nu}(p/\rho g) = -lm, \\ &l,\ m \text{ denoting the direction-cosines } \frac{\partial x}{\partial s},\ \frac{\partial z}{\partial s}. \end{aligned}\right\} \tag{7}$$

Therefore at A, where $p/\rho g$ must also satisfy (3),

$l^2 = 1$, i.e. the curve AE is horizontal, and at E, where (unless this point coincides with D) $p/\rho g$ must also satisfy (4),

---

* Casagrande (1937, § E) terms this the 'line of seepage'.

$$l^2 = 0, \text{ i.e. the curve } AE \text{ is tangential to } ED.$$

At both points (since $l^2+m^2 = 1$) lm will vanish and so (on the curve AE)

$$\frac{\partial}{\partial x}(p/\rho g) = 0 \text{ according to the second of (7).}$$

We can (initially) make no other assertion about the form of AE, which obviously depends upon the pressure-distribution inside the retaining wall, and would be altered, for example, if the wall included an impermeable obstruction.

8. We can, on the other hand, see the nature of the double boundary condition by analogy. Let w stand for the plane-harmonic function $p/\rho g$, and let it be interpreted as the transverse displacement of a uniformly tensioned membrane (e.g. soap film). Then along AB, DC the value of w is determined by (3) and (5), and it is zero, by (4), at every point in AE and ED. The form of AE (including the position of E) must satisfy the condition

$$\int_0 \frac{\partial w}{\partial \nu}\, ds = x, \tag{8}$$

which is derived by integration of the first equation in § 7.

Now when w is interpreted as above, $\partial w/\partial \nu$ measures the line-intensity of the pull exerted, in the direction of w, by the membrane on the boundary. We see from (8) that this line-intensity must be such that the pull on any element δs is proportional to the corresponding element δx: in other words, the edge AE of the membrane must be held down (so that $w = 0$) by forces having *uniform line-intensity with respect to x*. The circumstances are like those of a gas-balloon held down during inflation by 'shot-bags'; but with this difference, that here the tendency of the membrane to lift comes not directly (from applied pressure) but indirectly by transmission, due to its tension, of the displacements imposed at its edges AB, DC.

The relaxation method of Part III was, in point of fact, based on a 'membrane analogue' of this kind. In effect it replaced the tensioned membrane by a tensioned net of uniform mesh, and its results hold strictly in respect of this net, therefore are assumed (by an appeal to intuition) to be approximate results for the membrane. Making the assumption, we now deduce a process whereby the form of AE can be determined within the accuracy permitted by the particular size of mesh. Intuitively it is evident that the results obtained with any one mesh size will constitute a good starting assumption for 'advance to a finer net' (Part III, § 13).

9. Suppose in the first place, that p is zero along AK, KE (figure 1), and that we solve the potential problem thus presented. It can be predicted that w, since it vanishes along both arms of the angle AKE, will be very small in the region immediately adjacent to this angle; so towards the end K, at any rate, of AK we may expect that $\partial w/\partial \nu$ (in this instance $\partial w/\partial z$) will have values less than is required by (7) with $l = 1$. It is certain that the boundary must be moved downwards except at its end A (where the relations (7) are already satisfied).

It is also evident on physical grounds (and can in fact be proved mathematically) that depression of any internal point of the membrane will entail depressions everywhere: therefore we can certainly move the boundary downwards so long as the resulting changes in the boundary slopes, *assuming w to remain unchanged at all internal nodes*, are not so great that at any point the analogue of $(\partial w/\partial \nu)\,ds > dx$. Now the 'net analogue' of $(\partial w/\partial \nu)\,\delta s$ is *the pull exerted on an element δs of the boundary by those strings which come to it.* If then we accept all consequences of the 'net approximation' (and this is the only logical course), then we can with certainty depress the boundary through *some* distance, after which we must trace the consequences on w at interior points. These points will also be depressed, reducing the boundary slopes; so now we can depress the boundary further, then recalculate internal values of w, and so on.*

10. Having determined $p/\rho g$ at all internal points of the chosen net, we can estimate the total 'leakage' (i.e. the quantity flowing in unit time through unit thickness of the retaining wall).

By definition, this quantity

$Q = \int u\,dz$, when the integral extends over any vertical line drawn from AE to the impermeable base BC,

$$= \int \frac{\partial \phi}{\partial x}\,dz = -k\int \frac{\partial}{\partial x}\left(\frac{p}{\rho g}\right)dz, \text{ by (1).}$$

On the upstream face $(p/\rho g)$ ranges from 0 at the free surface A to $p_0/\rho g = D$, by (3), at B, D denoting the depth of the impermeable base. Consequently if $p/\rho g$ at any point be measured as a fraction of D, then

$$\left.\begin{array}{c} Q = -kD\displaystyle\int \frac{\partial P}{\partial x}\,dz, \\ \text{where } P \text{ stands for } p/\rho g D. \end{array}\right\} \qquad (9)$$

---

* Actually we depress the boundary further than is immediately justified, *anticipating* the consequent depression of interior points.

The integral in (9) is non-dimensional like P (x and z being measured in the same units); so Q is given by (9) as a fraction of kD, i.e. (cf. § 6) as a fraction of the flow per unit time through the unit cube of figure 4, when an excess head D of the fluid is maintained on its left-hand side.

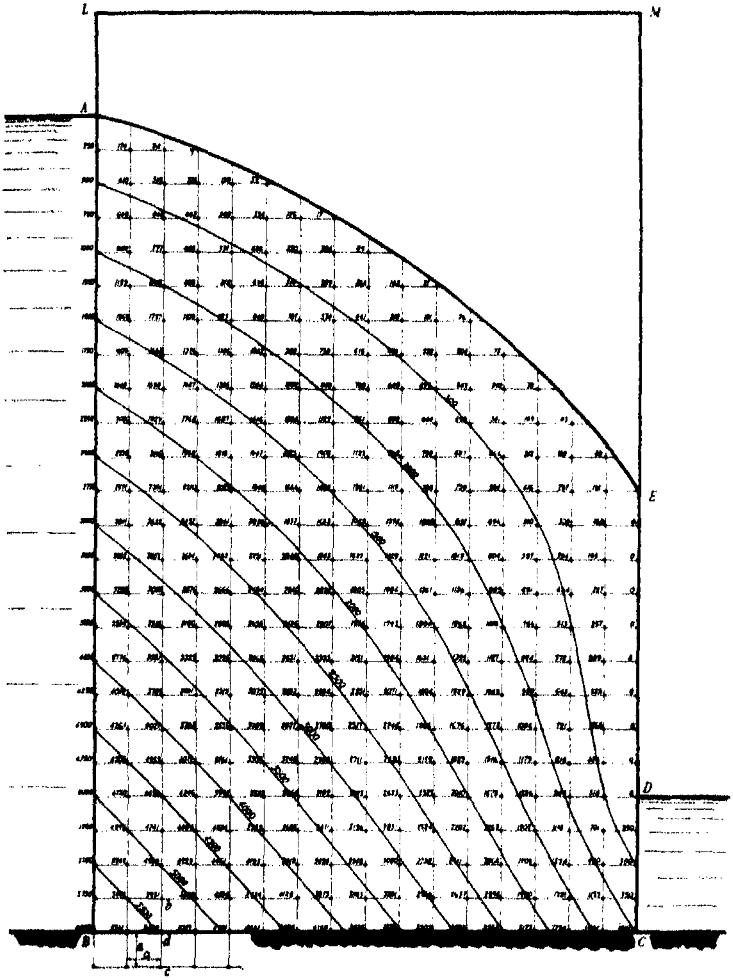

FIGURE 5

11. Figure 5 exemplifies these methods as applied with the use of a rectangular net. The depths of water on the two sides of the wall were taken in the ratio 6 : 1, and (with the object of eliminating decimals) a large and arbitrary value 6000 was given to D (§ 10). Values of $(p/\rho g)$ could then be attached to nodal points on the two sides of the wall, and relaxation begun.

The condition (6) was satisfied (approximately) along BC by including one horizontal row of fictitious nodal points immediately below that line, as indicated by the point c in figure 5, and by identifying, for example, the gradient of $(p/\rho g)$ at d with the gradient of its chord bc; i.e. by identifying

$$\left[\frac{\partial}{\partial z}(p/\rho g)\right]_d \text{ with } \frac{(p/\rho g)_c-(p/\rho g)_b}{2a}, \tag{10}$$

where a ($=250$ in figure 5) denotes the side of any square mesh.

Figure 5 is in fact the last of three successive nets (Part III, § 13) on which Problem I was attacked. Except for the determination of the free surface AE, computation might have been ended earlier: even the coarsest net (with mesh-side four times as great) gave a satisfactory picture of the general flow, and on all three the free surface (as expected) proved to be 'stable' in the sense of § 3. Actually, in the neighbourhood of the boundary, advance was made to *two still finer nets*: thereby we satisfied ourselves regarding the rapid curvature of AE both at A and E, whereby the conditions (7) are in fact satisfied, yet the general shape of the free surface approximates to a line of constant slope.*

Contours of constant pressure are shown, but it should be emphasized that no graphical representation can attain to the accuracy of the recorded numbers (which are believed to be correct to 1 in the last digit). *The contours are not lines of flow,* since the stream-lines cut the ϕ-lines orthogonally, ϕ being related with $(p/\rho g)$ by (1). It would of course be a simple matter to deduce values of ϕ, and the stream-function ψ could then be determined by the methods of Part V (Gandy and Southwell 1940); but from a practical standpoint what concerns us is the fluid pressures induced in the retaining wall, so it would seem preferable to concentrate attention on these (as we have done) from the first. The computed 'leakage' Q (§ 10) is $0{\cdot}729kD$.

PROBLEM II. EARTH WALL CONTAINING A PERMEABLE 'BLANKET' ON SUBSOIL OF THE SAME MATERIAL

12. Figure 6 shows, similarly, our accepted solution of this problem. The wall or levee is battered on both sides, and is assumed (§ 4) to be of the same material as the subsoil, which extends down to an impermeable stratum at a depth below ground level equal to the depth of the fluid on the 'upstream' side. A 'blanket' of coarse rubble (cf. figure 2) is assumed to maintain atmospheric pressure along the line AB, and figure 6 shows that it is

---

* Figure 5 may be compared with figure 9 (b) of Casagrande's paper.

effective in preventing seepage through the wall. The free surface (OA) is such as it would have been impossible to predict, but is determined with certainty by our method. The inflexion accords with Casagrande's description (1937, § F, *e*).

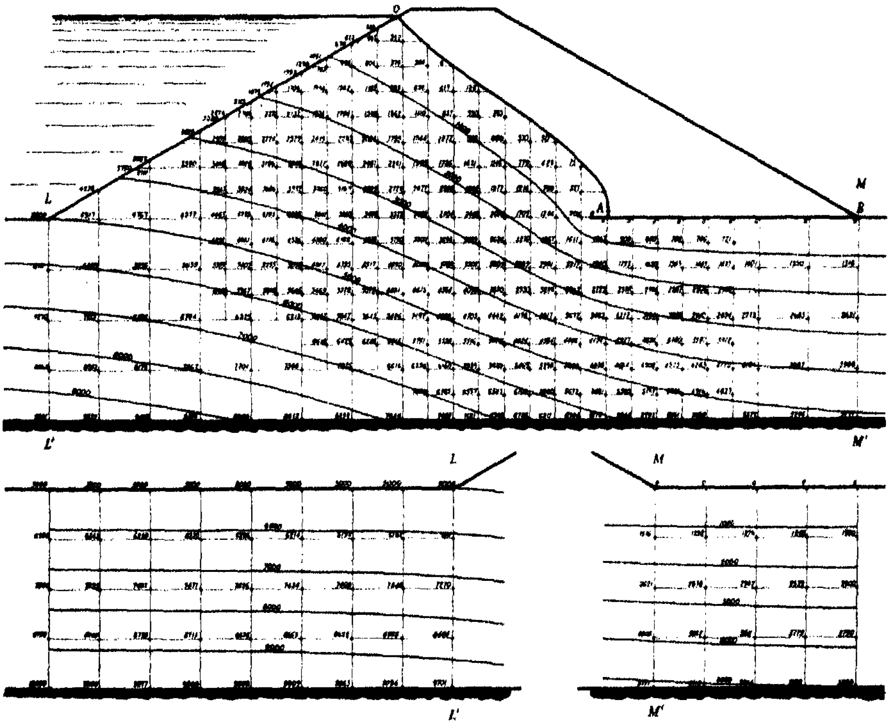

FIGURE 6

PROBLEM III. THE SAME WALL RESTING ON A SUBSOIL CONTAINING TWO DIFFERENT STRATA

13. Here (figure 7) the same depth of subsoil (down to the impermeable stratum) is assumed to contain two distinct strata, separated by a horizontal surface, of which the lower offers four times as much resistance as the upper to percolation. The shape of the retaining wall, and the level of the water on its upstream side, are unaltered: consequently the difference between this problem and the last comes solely from increased resistance to flow in the lower stratum. Mathematically, Problem III is of interest as exemplifying the 'refraction' which occurs at the common surface of two different materials.

The pressure will be plane-harmonic in each of the two strata, and it will be continuous (i.e. single-valued) at their common surface; also the velocity across this surface must have the same value on either side. Since the normal velocity is given (§ 6) by

$$\frac{\partial \phi}{\partial \nu} = -\frac{\rho g}{k}\frac{\partial p}{\partial \nu} - k\cos(y, \nu),$$

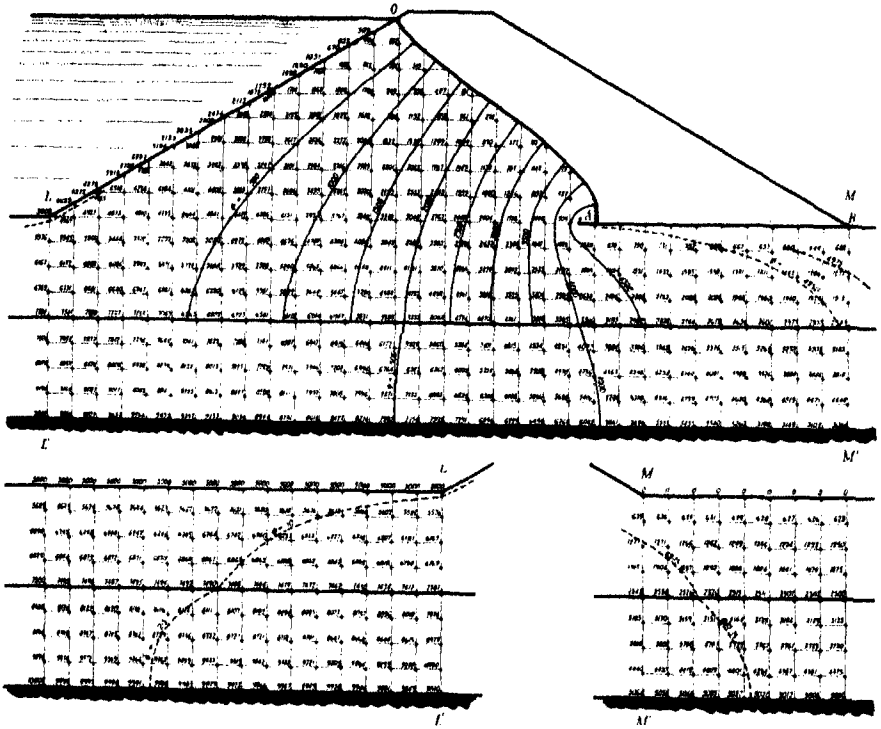

FIGURE 7

we have at a *horizontal* common surface the condition

$$k_{\mathrm{I}}\left\{\left(\frac{\partial w}{\partial y}\right)_{\mathrm{I}} + 1\right\} = k_{\mathrm{II}}\left\{\left(\frac{\partial w}{\partial y}\right)_{\mathrm{II}} + 1\right\},$$

w standing as in § 8 for $p/\rho g$, and suffixes I and II distinguishing values in the two strata. This equation reduces to

$$\left.\begin{aligned} 4\left(\frac{\partial w}{\partial y}\right)_{\mathrm{I}} + 3 &= \left(\frac{\partial w}{\partial y}\right)_{\mathrm{II}}, \\ k_{\mathrm{II}} &= \tfrac{1}{4}k_{\mathrm{I}}. \end{aligned}\right\} \qquad (11)$$

when, as assumed in § 5,

14. Let the net be so chosen that one row of nodal points lies on the common boundary of the two strata. Then at all points which lie inside either stratum we have the usual relation (Part III, § 8)

$$\Sigma_{a,4}(w) - 4w_0 = 0 \tag{12}$$

as the finite-difference approximation to $\nabla^2 w = 0$; but now we require a corresponding relation to be satisfied at points on the common boundary.

Suppose first that a row of points lies just within the stratum (I), as indicated by row C of figure 8*a*, and consider the representative point *O*. Inside the shaded region w (being plane-harmonic) may be interpreted as transverse displacement of a tensioned membrane, and if this membrane extended beyond the common boundary to row D, w would have at the point numbered 2 a value w_2' such that

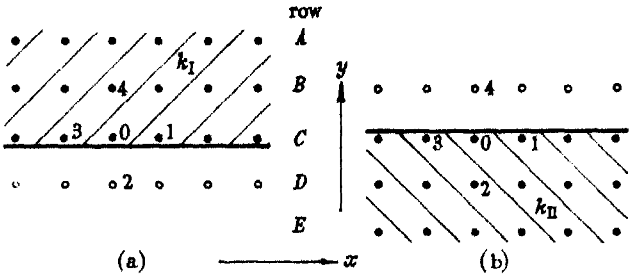

FIGURE 8

$$w_1 + w_2' + w_3 + w_4 = 4w_0, \tag{i}$$

in accordance with (12). Similarly in figure 8*b*, where row C falls just within the stratum (II), inside the shaded region w is plane-harmonic and may be interpreted as transverse displacement of a tensioned membrane, and if this second membrane extended beyond the common boundary to row B, w would have at the point numbered 4 a value w_4' such that

$$w_1 + w_2 + w_3 + w_4' = 4w_0, \tag{ii}$$

in accordance with (12).

Now let row C, *in both diagrams*, coincide exactly with the common boundary. Then, in the mechanical analogue, this boundary becomes the junction of two membranes stretched with different tensions, and so w_0, w_1, w_3 have the same significance both in (i) and in (ii); but while w_2 in (ii) and w_4 in (i) have real significance, the quantities w_2' and w_4' (interpreted as above) can have other values. By subtraction we obtain from (i) and (ii)

$$w_2 - w_2' = w_4 - w_4'. \tag{iii}$$

15. We now consider the boundary condition (11) of § 13. It must hold at all points of the common boundary, e.g. at point O when this boundary contains row C; and with neglect of terms of order a^3 we can replace

$$\left.\begin{aligned} &2a\left(\frac{\partial w}{\partial y}\right)_{\text{I}} \text{ at point } O \text{ by } w_4 - w_2', \\ &2a\left(\frac{\partial w}{\partial y}\right)_{\text{II}} \text{ at point } O \text{ by } w_4' - w_2, \end{aligned}\right\} \tag{iv}$$

when w_2', w_4' have the same significance as in § 14. So the finite-difference approximation to (ii) is

$$4(w_4 - w_2') + 6a = w_4' - w_2. \tag{v}$$

Eliminating w_4' between (iii) and (v), we obtain

$$5w_2' = 6a + 2w_2 + 3w_4, \tag{vi}$$

whence, and from (iii), it follows that

$$5w_4' = 6a - 3w_2 + 8w_4.$$

Finally, on substituting from (vi) in (i) we have

$$5(w_1 + w_3) + 2(w_2 + 4w_4) + 6a = 20w_0 \tag{13}$$

as the finite-difference relation which replaces (12), § 14, at nodal points on the common boundary.

16. Introducing the concepts of the relaxation method (Part III, § 10), we may write this result in the form

$$\mathbf{F}_0 = 6a + 5(w_1 + w_3) + 2(w_2 + 4w_4) - 20w_0, \tag{14}$$

$\mathbf{F}_0$ denoting the 'residual force' at O. (In this instance no 'external forces' are operative.) We can use (14) to calculate the 'initial forces' implied in any trial solution, and we can deduce from it the effect on the $\mathbf{F}$'s of imposing an isolated displacement on any nodal point. Our solution must bring all residual forces (sensibly) to zero.

In particular, if in the trial solution w_0, w_1, w_2, w_3, w_4 have values satisfying (12), i.e. if

$$w_1 + w_2 + w_3 + w_4 = 4w_0, \tag{15}$$

then the initial force at O is given by

$$(\mathbf{F}_0)_{\text{init.}} = 3(2a - w_2 + w_4). \tag{16}$$

We started our investigation of Problem III by adopting as a trial solution our final results for Problem II, then using (16) to calculate the forces requiring liquidation. Consequently at the start (i.e. before further relaxation was attempted) it was only on the common boundary of the two strata that the initial forces had sensible magnitudes.

17. Figure 7 records the results of the liquidation process, which presented no new feature or difficulty. Comparing its figures with those of figure 6, we see that the relatively impermeable lower stratum has a sensible effect on the pressure even up to the level of the 'blanket', but that the 'hydrostatic' part due to gravity (which of course is unaffected) predominates in both cases. On this account, while recording values of pressure, we have plotted contours of the velocity-potential ϕ, as related with p by (1) with $k_{\mathrm{I}} = 1$, $k_{\mathrm{II}} = 0{\cdot}25$. These clearly indicate continuity of $v = \partial\phi/\partial y$ associated with discontinuity of $u = \partial\phi/\partial x$, in accordance with the predictions of § 13. The stream-lines, which cut them orthogonally, will evidently pass from one stratum to the other with sudden changes of direction at the common surface.

The computed 'leakage' Q (§ 10) has the value $0{\cdot}317k_1D$ in Problem III, as compared with $0{\cdot}371k_1D$ in Problem II.

APPENDIX

Junction of free surface with downstream face of retaining wall. General case

We showed in § 7 that the free surface AE of figure 1 meets the vertical face DM of the retaining wall (where the pressure is atmospheric) tangentially. It is of interest to consider similarly the general case of seepage through a face having any given inclination to the horizontal.

In figure 9, AE represents the free surface, along which the fluid is assumed to move from A to E, i.e. in the direction of s increasing. Consequently $\partial\phi/\partial s$ is everywhere positive, and so according to (1), since $(p/\rho g)$ is constant (and k necessarily positive) on AE,

$$\frac{\partial y}{\partial s} < 0, \quad \text{i.e.}\ \frac{\partial z}{\partial s} > 0.$$

This means that AE must everywhere be inclined *downwards* from the horizontal: i.e. θ, in figure 9, is everywhere positive.

Again, in that part of the wall which is penetrated by the fluid $(p/\rho g)$, being plane-harmonic, can have no minimum value; and on the boundaries of this region it is either zero or positive or is required (at the impermeable stratum) to have zero normal gradient. It can be shown that in consequence $\partial/\partial\nu\,(p/\rho g)$ must be positive or zero at every point in AE; and since (§ 7) this normal gradient $= \partial x/\partial s$, it follows that θ cannot exceed $\frac{1}{2}\pi$.

Now on AE, since this is both a stream-line and a line of constant pressure, the conditions (7) must be satisfied at every point. Along ED (which is *not* required to be a stream-line) we have merely

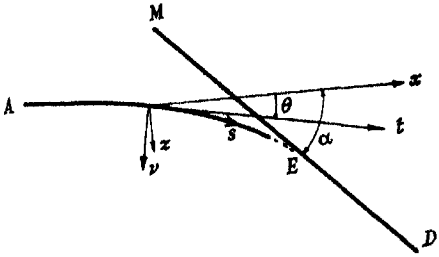

FIGURE 9

$$\cos\alpha\frac{\partial p}{\partial x}+\sin\alpha\frac{\partial p}{\partial z} = 0.$$

Therefore at E, *since the velocities and therefore the pressure-gradients must be single-valued*, we have

$$l(l\sin\alpha - m\cos\alpha) = 0,$$

or

$$\cos\theta\sin(\alpha-\theta) = 0,$$

indicating as alternative possibilities *either* $\theta = \pm\frac{1}{2}\pi$ *or* $\theta = \alpha + n\pi$ (n integral or zero).

Since, as we have just seen, $0 \leqslant \theta \leqslant \frac{1}{2}\pi$, the second alternative is acceptable only when α lies between 0 and $\frac{1}{2}\pi$—i.e. when the downstream face has positive batter: in that event AE will meet MD tangentially, as in § 7. When α lies between $\frac{1}{2}\pi$ and π, i.e. when the downstream face is overhung, only the first alternative is acceptable: then AE is vertical at its point of intersection with MD. (In the nature of the case $0 \leqslant \alpha \leqslant \pi$.)

Casagrande (1937, Appendix I, § C) and Davison (1936*b*) reach the same conclusions by somewhat different reasoning.

References

Boussinesq, J. 1904 *J. Math. pures appl.* (5), **10**, 11–16, 363–394.
Casagrande, A. 1937 *J. New Engl. Wat. Wks Ass.*, **51**, 131–172.
Christopherson, D. G. and Southwell, R. V. 1938 *Proc. Roy. Soc.* A, **168**, 317–350.
Davison, B. 1936*a* *Phil. Mag.* (7), **21**, 881–903.
Davison, B. 1936*b* *Phil. Mag.* (7), **21**, 904–922.
Davison, B. and Rosenhead, L. 1940 *Proc. Roy. Soc.* A, **175**, 346–365.
Forchheimer, P. 1886 *Z. Arch. Ing. Ver. Hannover*, **32**, 539–564.
Gandy, R. W. G. and Southwell, R. V. 1940 *Phil. Trans.* A, **238**, 453–475.
Richardson, L. F. 1908 *Proc. Roy. Dublin Soc.* **11** (N.S.), 295–316.
Terzaghi, K. 1933 1er *Congr. Grands Barrages* (Stockholm).
Terzaghi, K. 1934*a* *Die Bautechnik*, no. 29.
Terzaghi, K. 1934*b* *Der Bauingenieur*, no. 29/30.

On the specific heat of the sodium chloride crystal

By E. W. Kellermann
University of Edinburgh

(*Communicated by M. Born, F.R.S.—Received* 21 *June* 1940)

Based upon previous calculations of about 280 proper frequencies of the sodium chloride lattice, these frequencies have been used to determine the specific heat of NaCl according to Born's theory. It is shown that this number of frequencies is sufficiently large to make the determination of the frequency distribution and, therefore, of the specific heat possible. Agreement with experiment is obtained. It is shown in agreement with Blackman's investigations that the deviations from Debye's theory as found experimentally are due to Debye's assumption of a ν^2 law for the frequency distribution instead of the distribution following from the atomic theory.

Introduction

The desirability of comparing Born's theory of the specific heat of crystals (1923) with experimental data and with the results of Debye's theory (1912) has often been emphasized. Blackman's investigations (1935*a*, *b*, 1937) have already clearly illustrated that Born's theory is fitted to explain the behaviour of the specific heat at low temperatures; however, the difficulties in calculating the frequency spectrum of a crystal, under assumptions on the forces which approximate the forces in a real crystal more closely than Blackman's models, have so far been the main obstacle in carrying out an actual comparison. [Other calculations for a crystal model have been made by P. Ch. Fine (1939).]

In a recent paper (1940) (in the following quoted as (K. 1940)), I have calculated about 280 proper frequencies of the sodium chloride crystal according to Born's theory and obtained the frequency distribution curve for this lattice.

It will be shown here that already with this comparatively small number of frequencies and in spite of other minor approximations, a calculation of the specific heat from this distribution curve gives results in satisfactory agreement with experiment and can account for the variation of Debye's critical temperature θ which according to Debye's theory should be constant.

1. DETERMINATION OF THE FREQUENCY SPECTRUM AND SPECIFIC HEAT

I shall calculate the specific heat of sodium chloride using the results of my previous paper.

Let $N(\nu)$ be a function describing the distribution (density) of proper frequencies ν in a crystal, then the specific heat of 1 mole of the crystal is given by

$$C_v = k\int_0^\infty N(\nu)\,E\left(\frac{h\nu}{kT}\right)d\nu. \tag{1.0}$$

Here $E(x)$ is the Einstein function

$$E(x) = \frac{x^2e^x}{(e^x-1)^2}, \tag{1.1}$$

h and k are Planck's and Boltzmann's constants respectively, and T is the absolute temperature.

The function $N(\nu)$ is normalized so that its integral taken over the whole of the spectrum gives the total number of frequencies in one mole of the crystal. If the cell of the lattice contains as many atoms (or ions) as the chemical molecule, say s, and there are N cells per mole (N is Avogadro's number), then there are $3sN$ proper vibrations per gramme molecule, and the normalizing integral for the function $N(\nu)$ is

$$\int_0^\infty N(\nu)\,d\nu = 3sN \quad (s=2,\text{ for NaCl}). \tag{1.2}$$

In general, the frequencies of a crystal can only be obtained by numerical methods, since the derivation of an analytical expression for the function $N(\nu)$ is very involved. Even to obtain a good numerical approximation is difficult since the calculation of the frequencies is already tedious, and the determination of an unlimited number of frequencies is not feasible. At first sight, this seems to be a disadvantage of a calculation of the specific heat, based upon a relatively meagre number of frequencies. Considering the practically infinite number of waves $\exp\{2\pi i(\mathbf{k},\mathbf{r})\}$ (cf. K. 1940) with wave vector **k** which represents the normal modes of vibration of a crystal, one ought to calculate a very high number of frequencies and count the number of frequencies in equal volume elements of the phase ($\mathbf{k}-$) space, in order to get a really good approximation to the distribution function $N(\nu)$.

It will, however, be seen in the following that the present calculation is sufficient to give a relatively close approximation.

In the previous paper (K. 1940) I have calculated about 280 frequencies corresponding to 48 points of the phase space, defined in suitable units by

$$0 \leqslant k_z \leqslant k_y \leqslant k_x \leqslant 10, \quad [\mathbf{k} = (k_x, k_y, k_z)]$$

$$k_x + k_y + k_z \leqslant 15,$$

$$k_x, k_y, k_z, \quad \text{all odd or all even.}$$

Since from reasons of symmetry, each vector **k** in this interval determines a further number of frequencies in the whole of the phase space (the average weight factor is about 24), the number of frequencies calculated determines about 6700 frequencies in the whole of the phase space. As already mentioned there, the distribution curve plotted previously (K. 1940, p. 547) contained a slight error in the counting of the frequencies (more precisely, in the weight factor of several frequencies). I have, therefore, plotted the corrected distribution curve here (figure 1) in otherwise the same way as in the former paper.

The features of the curve are essentially the same as those of the older graphs. The main deviations are a slight shift of some of the maxima, as given below in detail, and a change of the normalization constant $6N \times 0{\cdot}32 \times 10^{-13}$ sec., instead of $6N \times 0{\cdot}33 \times 10^{-13}$ sec. For small frequencies the distribution function is proportional to ν^2 ($N(\nu) = K\nu^2$), and the constant K is here found to be

$$K = 1{\cdot}1 \times 10^{-38}\,\text{sec.}^3$$

There might be another small maximum at the end of the spectrum. But the number of frequencies calculated is not large enough to enable us to draw definite conclusions.

In the main one finds again (cf. K. 1940) three definite maxima (figure 1). The frequencies belonging to longitudinal optical waves (*l.o.*), to longitudinal acoustic (*l.a.*), transverse optical (*t.o.*), and transverse acoustic waves (*t.a.*) have been collected separately (figure 2) as before (K. 1940, p. 547). It is seen that the main maximum at the frequency of the residual rays in

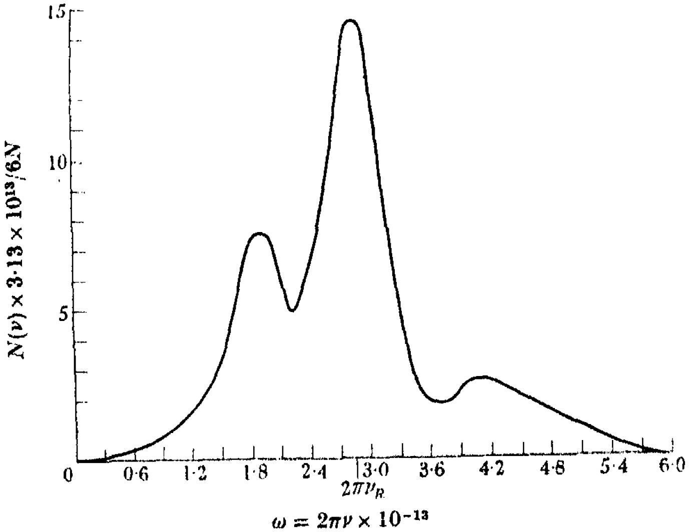

FIGURE 1. Frequency distribution of the sodium chloride crystal. ν_R, frequency of residual rays.

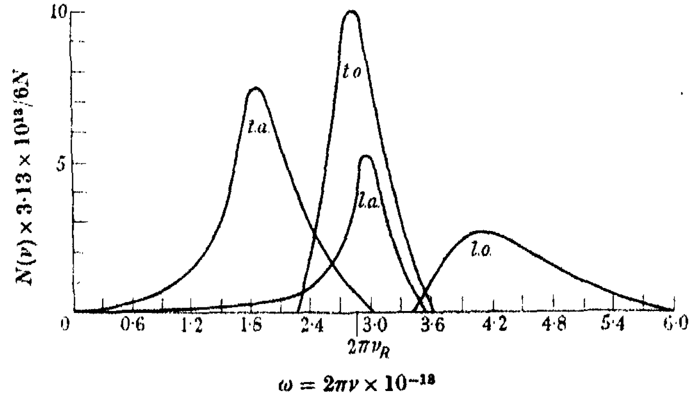

FIGURE 2. Frequency distribution, analysed. ν_R, frequency of residual rays.

figure 1 is due to the two maxima (*t.o.*) at $\omega = 2{\cdot}85 \times 10^{13}$ sec.$^{-1}$ and (*l.a.*) at $\omega = 3{\cdot}0 \times 10^{13}$ sec.$^{-1}$ respectively, as compared with $2{\cdot}85 \times 10^{13}$ and $2{\cdot}9 \times 10^{13}$ sec.$^{-1}$ in the older paper. Two more maxima, (*t.a.*) and (*l.o.*), are found, one at $\omega = 1\cdot9\times10^{13}$ sec.$^{-1}$ and the other at $\omega = 4\cdot1\times10^{13}$ sec.$^{-1}$ (previously: $1\cdot8\times10^{13}$ and $4\cdot2\times10^{13}$). For our purposes the maximum at $\omega = 1\cdot9\times10^{13}$ sec.$^{-1}$ is the most interesting, since it shows clearly the deviation of the spectrum of a real crystal from a Debye distribution which is a ν^2 curve going up to a maximum near the residual rays frequency where it is cut off.

It is encouraging to find good agreement with Blackman's calculation (1937). Blackman has calculated the frequencies corresponding to 30,000 points of the phase space for a simplified model of a crystal. I have not calculated so many frequencies, but Blackman's arguments, which indicate that it is not necessary to calculate too large a number of frequencies, also hold in my case, quite apart from the agreement of this calculation with experiment.

In addition to Blackman's arguments (1937, p. 423), one has only to consider the graphs of the frequencies as functions of the phase vector **k** (K. 1940, p. 543). It is seen that all these curves are smooth. Now the density $N(\nu)$ is proportional to the volume in phase space between two surfaces of constant frequency and, therefore, will also be a smooth curve.

The density curve as calculated by Blackman is very similar to the curve plotted in this paper. Both graphs show the same characteristic property, namely, the four maxima. In neither case can the possibility of the presence of further maxima be ruled out, but again in neither case is the accuracy of the calculation high enough to make a definite statement possible. However, the contribution of such maxima to the specific heat can safely be neglected.

I have calculated the specific heat partly numerically and partly graphically. The Einstein function has been tabulated (Nernst 1918; Landolt-Börnstein 1927), and the values of the distribution function $N(\nu)$ have been taken from figure 1. In this way the function $N(\nu)\,E(h\nu/kT)$ has been plotted and integrated by means of a planimeter for various values of T. I have calculated C_v for six temperature values with 10° interval in that region where a deviation from Debye's theory is observed. The results are given in table 1, the units being cal./° K.

TABLE 1

T	C_v
20	0·157
30	0·577
40	1·19
50	1·84
60	2·45
100	4·12

2. Comparison with experiment

In order to compare the calculated values of the specific heat with experimental results, and, at the same time, to illustrate the deviations from Debye's theory, I have plotted a Θ curve (figure 3), i.e. instead of plotting the C_v values directly against the temperature, I have determined at various temperatures the characteristic temperature Θ, belonging to the C_v values according to Debye's theory. The Θ value at zero temperature can be calculated without the knowledge of the frequency spectrum (Born and Kármán 1912).

One finds
$$\Theta = \frac{h}{k}\left(\frac{3}{4\pi\Omega}\right)^{\frac{1}{3}}\bar{v}, \tag{2.0}$$

where Ω is the atomic volume and $\bar{v}$ is the mean velocity of propagation of the waves in the crystal. At low temperatures only long waves need be considered, which means that one can use the elastic data for the calculation of the mean velocity $\bar{v}$. An approximation method for the calculation of $\bar{v}$ has been given by Hopf and Lechner (1914; cf. also K. Fuchs 1936). Using the elastic constants as calculated in the preceding paper (K. 1940) one finds for NaCl
$$\Theta = 313^\circ\,\mathrm{K}$$
at zero temperature.

Results of experiments on the temperature dependence of Θ for NaCl have been published by Clusius, Goldman, and Perlick (cf. Keesom 1934). While at high temperature Θ has a constant value ($\Theta = 281^\circ$ K), these authors have found a minimum of Θ($\Theta = 275^\circ$ K at $T = 40^\circ$) and a rise again for still lower temperatures ($\Theta = 310^\circ$ K at $T = 10^\circ$ K). Various suggestions have been put forward to explain this deviation from Debye's theory. The results of this calculation, however, furnish a conclusive proof that Blackman's explanation has been correct. The failure of Debye's theory to account for the temperature dependence of Θ is due to the assumption of a ν^2 law for the frequency distribution instead of a spectrum of the kind as plotted in figure 1, which conforms to the actual properties of a crystal.

The curve of the calculated Θ values (figure 3) coincides with the curve obtained from the measurements by Clusius and collaborators between $T = 10^\circ$ and $T = 40^\circ$ K. I have been unable to find experimental data, measured between $T = 40^\circ$ and $T = 100^\circ$ K, i.e. for the right-hand side of the minimum, but it is seen that Θ approaches the constant value 281° K which is found at higher (room) temperatures.

This agreement with experiment is rather remarkable. It not only suggests that the number of frequencies calculated is large enough for the determination of the spectrum, but it also justifies some other approximations in the preceding calculations (K. 1940), for instance the neglecting of polarizability and forces, other than Coulomb forces, between next nearest neighbours. The only constant entering the calculations is the compressibility κ in the constant A of the repulsive potential (K. 1940, p. 531). Actually the experimental value of κ, as measured at room temperature, has been used. But even if this value is corrected, assuming a temperature coefficient of κ of about 10^{-15} cm.^{2}/dyne × degree for $\partial\kappa/\partial T$, the final results do not change appreciably, as can be seen by recalculating Θ (2.0) for $T = 0$ with the corrected value of κ. The effect of this, as of the other approximations, is within the limits of error of the calculation.

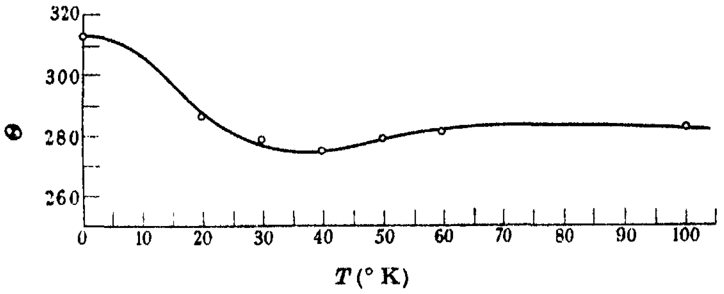

FIGURE 3. Temperature dependence of Θ. The smooth line is drawn from experiments. ○, calculated values.

The result of this calculation makes it desirable to calculate the frequency spectrum of KCl or other crystals for which more experimental data are available. If the coefficients due to the electric forces, as tabulated (K. 1940), are used in the equation of motion and the same method for the actual calculation of the frequencies is applied as used there, this would not be too arduous.

I wish to thank Professor M. Born for the interest he has taken in this paper. I am also grateful to Dr K. Fuchs for many helpful discussions.

REFERENCES

Blackman, M. 1935*a* *Proc. Roy. Soc.* A, **148**, 365.
Blackman, M. 1935*b* *Proc. Roy. Soc.* A, **149**, 117.
Blackman, M. 1937 *Proc. Roy. Soc.* A, **159**, 416.
Born, M. 1923 *Atomtheorie des festen Zustandes.* Leipzig.
Born, M. and Kármán, Th. 1912 *Phys. Z.* **13**, 297.

Debye, P. 1912 *Ann. Phys., Lpz.*, **39**, 789
Fine, P. Ch. 1939 *Phys. Rev.* **56**, 355.
Fuchs, K. 1936 *Proc. Roy. Soc.* A, **153**, 622.
Hopf, L. and Lechner, G. 1914 *Verh. dtsch. Phys. Ges.* **16**, 643.
Keesom, W. H. 1934 *Phys. Z.* **35**, 939.
Kellermann, E. W. 1940 *Phil. Trans.* A, **238**, 513.
Landolt-Börnstein 1927 *Physikalisch-Chemische Tabellen*, **1**. Erg. Bd. Berlin.
Nernst, W. 1918 *Die theoretischen und experimentellen Grundlagen des neuen Wärmesatzes*. Halle.

The kinetics of the polymerization of isoprene on sodium surfaces

By J. L. Bolland
British Rubber Producers' Research Association,

(*Communicated by Eric K. Rideal, F.R.S.—Received 4 November* 1940—*Revised* 19 *December* 1940)

The kinetics of the polymerization of isoprene liquid and vapour occurring on sodium surfaces have been investigated at 60 and 25° C. In the case of the liquid phase polymerization diffusion of monomer to the catalytic surface is shown to be the rate-controlling factor, except when the sodium surface is in the form of a sphere of sufficiently small dimensions.

The kinetics of the polymerization in presence of toluene are consistent with the view that polymeric chains are initiated by formation of free radicles on the sodium surface, the subsequent propagation occurring while the polymer is still attached to the sodium: termination occurs exclusively by interaction with toluene. In absence of toluene an alternative termination reaction, leading to cross linking and requiring 4·6 kcal. more activation energy than the process involving toluene, comes into play.

INTRODUCTION

In recent years an increasing amount of study has been devoted toward gaining a better understanding of the fundamental nature of polymerization reactions. Perhaps the most successful method of approach so far employed has been the systematic study of the kinetics of a wide variety of polymerizations, thermal, catalytic and photochemical. As yet, however, little attention has been directed toward one very important type of polymerization, namely, the polymerization of conjugated compounds in presence of alkali metals. The kinetic method has therefore been applied to the polymerization of isoprene on sodium as a representative example of this class of reactions.

EXPERIMENTAL

The convenient and accurate dilatometric method of following the course of the polymerization was used. From measurements of the limiting value to which the diminution in volume tends on prolonged polymerization, checked by measurements of the density of thoroughly dried polyisoprene, it has been shown that the maximum fractional decrease in volume amounts to 0·25 and is independent of molecular weight, certainly within the limits 3000–80,000.

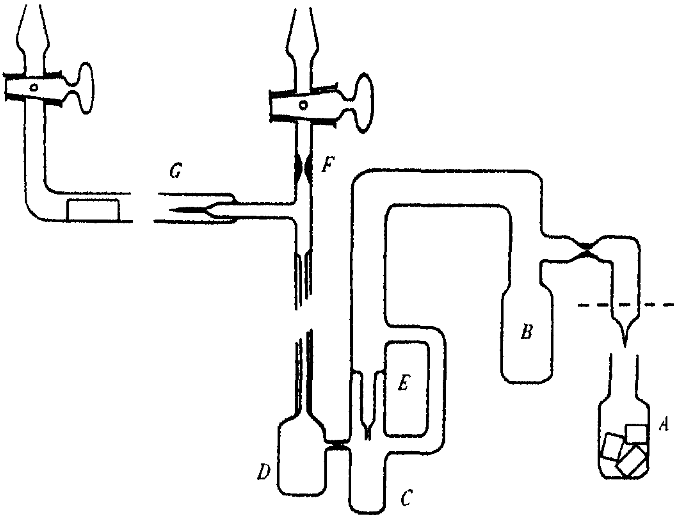

FIGURE 1. Preparation of sodium surfaces.

The simplest method of preparing a sodium surface on which polymerization might be conducted is undoubtedly by distillation of sodium under high vacuum conditions onto the cool walls of the reaction vessel, which may then be sealed off from the sodium supply. Such films are, however, quite unsuited for kinetic measurements, since their non-uniformity prevents the effective area of the sodium catalyst being estimated with any degree of accuracy. It has accordingly been found necessary to conduct experiments on the readily measurable surface area of an appreciable quantity of solid sodium introduced into the reaction vessel by the following method. After thorough evacuation and flaming of the pyrex apparatus sketched (figure 1), fragments cut from the centre of a large piece of sodium were sealed in. After distillation of the requisite amount of sodium from *A* to *B* and then from *B* to *C* at 10^{-5} mm. pressure, the apparatus was detached from the main vacuum line and immersed in an oil bath at *ca.* 140° C. The desired amount of purified molten sodium could be poured into the reaction vessel (D) which was then sealed off from the remainder. Normally, sufficient sodium was introduced into the reaction vessel to cover the bottom completely, giving a plane surface of area equal to that of the cross section of the reaction vessel; it was then permissible to eliminate the internal dropper E. On certain occasions, however, it was found necessary to introduce only very small globules of sodium. In such cases the internal dropper, E, was of value in regulating the amount of sodium transferred to C. The by-pass tube facilitated evacuation of the sodium during the distillations, and also allowed for the return of the sodium in C if too much had been shaken through the dropper. Using such a technique it was possible with reasonable certainty to introduce globules of 3 mm. diameter into the reaction vessel. Following the introduction of sodium the reaction vessel was reattached to the vacuum line, and sealed off at F after filling with the required volumes of isoprene and diluent (as measured in calibrated side tubes) by liquid air distillation. In certain instances when it was desired to recover unpolymerized isoprene from such reaction vessels 'breakable seals' of the type indicated in figure 1 (G) were attached.

The polymerizations were carried out in 60 and 25° C thermostats, controlled by toluene-mercury regulators to 0·01° C.

The molecular weights of the polymers obtained were calculated from measurements of the viscosity of dilute solutions in benzene, using a small volume Ostwald viscometer (flow time for benzene *ca.* 80 sec.) using the well-known relation

$$\text{mol. wt} = K \lim_{c\to 0} \frac{\log \eta_r}{c},$$

where η_r represents the relative viscosity of a benzene solution of concentration c (g./100 c.c. solution). The value adopted for the constant K was 60,000 (Gee 1940).

Crude isoprene was obtained by the cracking of dipentene, using a modification of Whitby and Crozier's (1932) form of isoprene lamp. The isoprene fraction of the volatile product was converted into the corresponding sulphone which was twice recrystallized from water, dried and decomposed by heating with caustic alkali. The regenerated isoprene, after washing well with alkali and with water and then drying, was distilled at once over sodium within 1° C range (b.p. 34° C). The yield from the sulphone was 86 %. For details of the method of cracking and practical assistance we are indebted to Dr E. H. Farmer.

Of the hydrocarbon diluents employed, the toluene was a B.D.H. sulphur-free product, the benzene was of Analar grade, and the cyclohexane was supplied by B.D.H. as spectroscopically pure. All three solvents were stored in sodium-coated tubes separated from the main vacuum line by taps and mercury cut-offs.

Polymerization of pure isoprene on a clean sodium surface at 60° C is preceded by a short inhibition period, during which no polymerization can be detected, and normally extending to about 30 min., though experience has shown that this period is particularly sensitive to any slight oxidation of the sodium surface. The first visual sign of the commencement of polymerization is the gradual formation of a crimson zone surrounding the contours of the sodium to a depth of *ca.* 2–3 mm. As polymerization proceeds it may be shown, by inverting the reaction vessel, that a distinct solid layer consisting of swollen polymer forms round the sodium surface, and this gradually increases in depth till the reaction vessel is completely filled.

A typical curve representing the progress of polymerization of 100 % isoprene on 'plane' sodium surfaces at 60° C is given in figure 2. It is important to note that the curve shows a relatively sharp maximum. From visual estimates of the thickness of the polymer layer at somewhat later stages in the polymerization, it is estimated that the maximum rate of polymerization occurred when a layer of *ca* 6 mm. had been formed on the surface.

Kinetics of polymerization in presence of toluene

The kinetic data obtained when polymerization runs are carried out in presence of added amounts of toluene on plane sodium surfaces give, in the main, curves of the type indicated in figure 2. The variation of the maximum

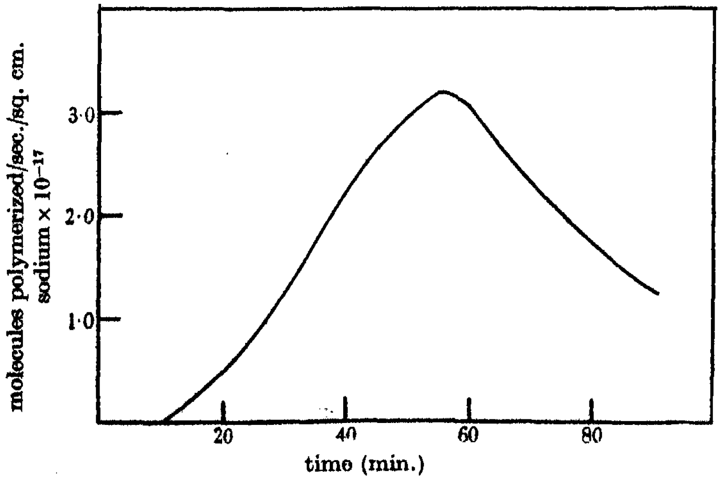

FIGURE 2. Polymerization of isoprene on plane sodium surface at 25° C.

rate of polymerization at 60° C with the amount of toluene added is as indicated by the data given in table 1.

Table 1

molar % toluene	max. rate of polymerization mol. polymerized/sec./sq. cm. sodium $\times 10^{-17}$	mol. wt
4·65	3·24	80,000
5·7	3·18	84,000
8·61	3·23	70,000
10·7	2·65	59,500
17·7	2·02	31,200
35·0	2·0	20,600
48·5	1·08	10,800
65·9	0·32	3,800

It is noteworthy that while the addition of 35 molar % toluene reduces the molecular weight of the polyisoprene by a factor of *ca.* 4 the maximum rate of polymerization is diminished by only 36% under such a change of conditions. Polymerization runs, in which sodium surfaces of various configurations were used, have shown that this lack of correlation between the rate of polymerization and the chain length of the polymer produced resulted from the fact that the diffusion of the monomer through the intervening polymer layer to the site of reaction was the factor determining the observed rate of polymerization. The details of these experiments, and the maximum rates of polymerization measured, are given in table 2, while the course of the runs is indicated graphically in figure 3.

Table 2. Polymerization of isoprene + 8·61 molar % toluene at 60° C

description of surface	max. rate of polymerization mol./sec./sq. cm. sodium $\times 10^{-17}$
(*a*) plane	$3{\cdot}2_3$
(*b*) hemispherical, $r_1 = 0{\cdot}20$ cm.	9·7
(*c*) hemispherical, $r_1 = 0{\cdot}14_7$ cm.	11·0

Provided the extent of the induction period depends on characteristics of the surface and not on those of the liquid, it may be shown that the probability of observing the complete course of the induction period, before diffusion becomes the rate-controlling factor, is much increased by the use of curved surfaces. Thus in figure 4 curves have been constructed relating

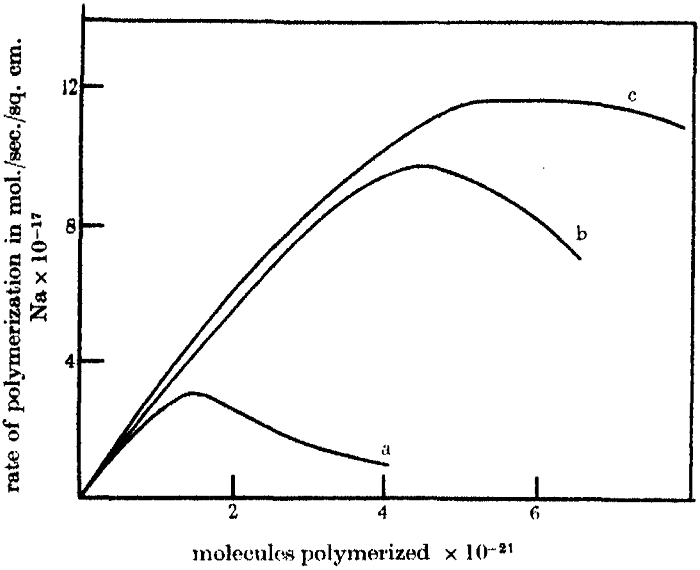

Figure 3. Polymerization of isoprene at 25° C on (*a*) a plane sodium surface, and hemispherical surfaces of radii, (*b*) 0·20 cm., and (*c*) 0·14, cm.

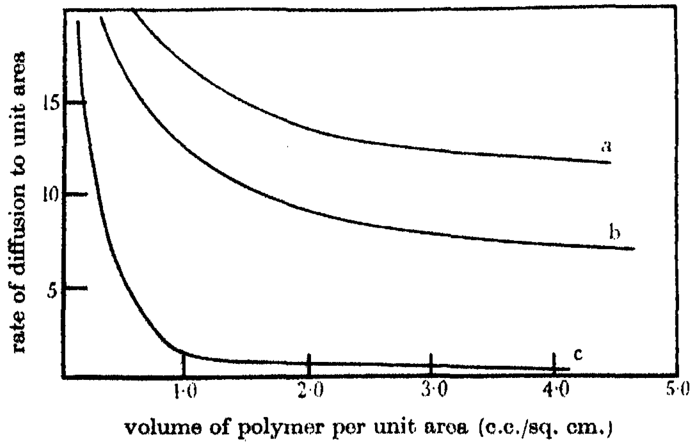

Figure 4. Diffusion of isoprene to sodium surfaces of various shapes: (*a*) hemisphere of radius 0·10 cm., (*b*) hemisphere of radius 0·15 cm., and (*c*) plane surface.

the rate of diffusion (to unit surface area) with extent of reaction (per unit area) based on the following equations, which are derived on the assumption that Fick's law holds:

$$\text{for a plane surface,}\qquad \frac{\text{rate of diffusion}}{\text{unit area}} = \frac{D\Delta C}{t},$$

where t is the thickness of polymer layer, D the diffusion coefficient and ΔC the difference in monomer concentrations at the polymer-liquid and polymer sodium interfaces;

$$\text{for spherical surfaces,}\qquad \frac{\text{rate of diffusion}}{\text{unit area}} = \frac{D\Delta C}{r_1(1-r_1/r_2)}, \tag{1}$$

where r_1 and r_2 are respectively the radii of curvature of the surface and the polymer-liquid interface.

The fact that the observed maximum rate of polymerization is in fact increased by the use of spherical sodium surfaces demonstrates the existence of the diffusion effect, while the stationary nature of the maximum rate in the case of the smaller hemispherical surface indicates that the true maximum rate of polymerization was attained before the rate of diffusion became the rate-controlling factor.

That the maximum rate of polymerization observed on surface (*c*) should be uninfluenced by diffusion seems reasonable may be shown as follows. The maximum rate is attained when 1·16 c.c. (dry) polymer have been formed. Swelling measurements show that polyisoprene swells to twice its volume in presence of isoprene at 60° C. Allowing for this factor, it may be shown that the radius of curvature (r_2) of the polymer liquid phase interface (assumed hemispherical, since the radius of curvature of the sodium surface was much smaller than the cross-sectional diameter of the reaction vessel) is 10·5 mm. when the maximum rate of polymerization is attained. Inserting the relevant values in equation (1) $D\Delta C$ is found to be $2{\cdot}1 \times 10^{17}$ mol./sec./cm. Unfortunately, the value of D for this actual system has not been measured; Abkin and Medvedev (1939) have, however, determined the same quantity for the very similar system butadiene-polybutadiene, and extrapolation of their results would indicate a value of *ca.* $1{\cdot}5 \times 10^{-3}$ cm.^{2} sec.$^{-1}$ at 60° C. If this value is applied to the present case, $\Delta C = 1{\cdot}4 \times 10^{20}$ mol./c.c. The saturation concentration—that at the polymer-liquid boundary—is estimated at $3{\cdot}0 \times 10^{21}$ mol./c.c., on the grounds that isoprene swells the polymer to twice its normal size with little total volume change. In this case then it seems reasonable to assume that the monomer concentration in the neighbourhood of the sodium is but little removed from the saturation concentration.

By conducting polymerizations on hemispherical sodium surfaces of sufficiently small dimensions it has been found possible to determine the true maximum rate of polymerization over substantially the whole range of toluene concentrations. These results are incorporated in table 3.

TABLE 3

toluene conc. (molar %)	isoprene conc. / toluene conc.	max. rate of polymerization mol./sec./sq. cm. sodium × 10^{-17}	chain length	$K \times 10^{-17}$	K_1
2·90	29·9	32·5	—	1·06	—
8·61	9·40	11·0	1780	1·17	189
22·9	3·37	4·0	580	1·19	172
35·0	1·86	2·0	330	1·07	177
48·5	1·06	1·08	156	1·02	148
65·9	0·36	0·32	56	0·89	175
			Mean	1·07	172

K and K_1 are constants defined by equations (2) and (3) below.

It is evident from table 3 that the maximum rate of polymerization is related to the concentrations of isoprene and toluene by the following simple relationship:

$$R_{\max} = K\frac{[\text{isoprene}]}{[\text{toluene}]}. \tag{2}$$

The mean chain lengths of the polymers obtained in these experiments are also included in table 3, and it is evident that a parallel relationship exists between the chain length and the isoprene concentration, viz.

$$\text{chain length} = K_1\frac{[\text{isoprene}]}{[\text{toluene}]}. \tag{3}$$

A similar series of experiments performed at 25° C, using hemispherical beads where necessary, yielded quite analogous results, though here it was unfortunately not found possible to extend the measurement of true maximum rates of polymerization to quite such high isoprene concentrations. The data are given in table 4.

Polymerization of undiluted isoprene

Examination of the polymer obtained by polymerizing undiluted isoprene shows that the larger portion of it is quite insoluble in benzene. Thus in one typical instance a sample mechanically shaken with benzene for about 30 days in a tube which had previously been carefully evacuated gave an insoluble residue amounting to 65 % by weight; the mean molecular weight

TABLE 4

toluene conc. (molar %)	$\frac{\text{isoprene}}{\text{toluene}}$	max. rate of polymerization mol./sec./sq. cm. sodium × 10^{-17}	chain length	$K \times 10^{-16}$	K_1
8·6	9·4	1·48	2720	1·58	290
25·6	2·92	0·49	880	1·68	320
45·7	1·19	$0{\cdot}17_5$	412	1·47	346
63·7	0·57	$0{\cdot}10_8$	188	1·89	303
			Mean	1·65	315

of the soluble portion was found to be 210,000. Further shaking of the portion insoluble in benzene with 10 % ethyl alcohol in benzene resulted in no further solution being effected. As in the case of reaction mixtures containing toluene, the observed maximum rate of polymerization was very markedly increased by substitution of hemispherical for plane sodium surfaces. It was, however, never found practicable to prepare a surface of sufficiently small dimensions to allow for observation of a rate of polymerization greater than $1{\cdot}66 \times 10^{18}$ mol./sec./sq. cm.; in this particular run there was no appreciable interval following attainment of the maximum rate of polymerization during which the rate of polymerization remained constant. The conclusion is therefore that the true rate of polymerization of 100 % isoprene exceeds $1{\cdot}66 \times 10^{18}$ mol./sec./sq. cm. (It will be noted that in one case (see table 3) a higher rate of polymerization has been measured: conditions were specially favourable in that particular run, since the diameter of the bead was only $2{\cdot}0_4$ mm. as compared with the 3·0 mm. for the second smallest bead prepared during these experiments, and, moreover, the isoprene used was derived from a sample which had previously been partly polymerized; there is good reason to believe that this latter factor should have diminished the extent of the induction period.)

Nature of induction period

It seems almost certain that the induction period observed in the polymerization reaction under consideration must arise from one of two possible causes. The induction period may represent the time taken for the establishment of the maximum (stationary) number of centres from which polymerization may proceed, or alternatively the period during which are destroyed adventitious impurities in the isoprene (or solvents), which may inhibit the initiation of polymerization chains, or by their interaction bring polymerization chains to a premature termination.

A series of experiments, in which the polymerization of 100 % isoprene on plane sodium surfaces was interrupted at some point during the induction period, showed that the molecular weight of the polymer formed during the induction period is quite significantly lower than that of the soluble portion of the polymer obtained from completed reactions:

molecules isoprene polymerized at interruption/sq. cm. sodium $\times 10^{-19}$	mol. wt
7·5	5,800
17·5	14,600
23·5	24,000
27·1	13,400
164	48,000

(The maximum rate of polymerization on a plane surface occurs after polymerization of *ca.* 180×10^{19} mol./sq. cm.)

While these figures are not very concordant among themselves they indicate that the molecular weight gradually increases throughout the induction period to a value which is still significantly smaller than the final mean molecular weight of the soluble portion of the polymer. In order to decide whether the induction period and/or this initial depression of the molecular weight were due to the presence of a trace of some efficient chain terminator, a 6 c.c. sample of isoprene was subjected to a series of successive partial polymerizations. The reaction vessels used for this purpose were provided with breakable seals (figure 1 (*G*)). On attainment of the maximum rate of polymerization the remaining unpolymerized isoprene was transferred to a similar reaction vessel via the breakable seal. Benzene was then distilled into the first reaction vessel in sufficient quantity to effect the solution of the polymer (carried out *in vacuo*). This cycle was carried out four times with the results shown in table 5.

As is evident from table 5, with each partial polymerization the mean chain length during the induction period shows an undoubted upward trend, while the induction period becomes shorter and shorter. We conclude that a contributory factor to the induction period is the presence of adventitious traces of impurity in the isoprene, even when purified with extreme care. It was observed that while the initial stages of the first polymerization of the above series were accompanied by the development of the (normal) crimson coloration near to the surface, in the subsequent runs such coloration was quite absent. In view of the observations made by V. N. L'vov (1937) that the products resulting from the copolymerization of butadiene and isobutylene in presence of sodium were of an intense cherry red colour (and extremely sensitive to the influence of moisture and air), and also that the presence of isobutylene has a marked effect in reducing the chain length of sodium-catalysed polyisobutadienes, it seems quite likely that the impurity concerned is in fact a mono-olefine.

TABLE 5

Temperature = 60° C.

	vol. isoprene used (c.c.)	vol. isoprene recovered (c.c.)	chain length	max. rate of polymerization mol./sec./sq. cm. sodium $\times 10^{-17}$	$P \times 10^{-21}$
I	5·10	4·37	705	3·55	1·69
II	3·94	2·16	1160	3·87	1·25
III	2·16	1·70	1330	4·28	0·93
IV	1·56	1·23	1690	4·44	0·57
V	1·08	0·93	425	—	—
VI	0·93	—	398	—	—

P represents the number of molecules of isoprene polymerized at the point when the maximum rate of polymerization is attained.

The last two experiments included in table 5 represent an attempt to detect whether the addition of monomer molecules to polymer chains is a relatively slow process (of the type suggested for the photochemically initiated polymerization of methyl methacrylate (Melville 1937), so that the completion of a polymer chain might occupy several minutes. Run V, using isoprene from run IV, served as a control, conducted similarly to the previous four experiments. In the case of run VI, using the isoprene recovered from V, the reaction was interrupted at the same stage (as measured by the contraction), and by inverting the reaction vessel it was arranged that the polymer already formed should have an opportunity of continuing growth in absence of sodium. The extent of reaction permitted on the catalytic surface was regulated so that it was still possible to disperse the polymer quite rapidly in the remaining isoprene by manual shaking. On leaving the inverted reaction vessel at the previous polymerization temperature (60° C) for 24 hr., the remaining isoprene was found to have polymerized on the sodium surface, while, as will be seen from table 5, the polymer removed from the catalytic surface did not undergo any further growth. It is unfortunate that the insoluble nature of the polymer formed subsequent to the completion of the induction period (when it could be assumed that all adventitious chain terminators would have been eliminated) prevents repetition of such experiments during the later stages of the polymerization.

It is to be noted that the results presented in table 5 cannot well be explained completely in terms of the presence of adventitious inhibitors. Thus it was found that only 35 % of samples of polyisoprene obtained by complete polymerization of undiluted isoprene was soluble in benzene. It is to be supposed that the soluble portion resulted from the early stages of the polymerization, owing to the interaction of inhibitors, and any possible premature chain terminating effect due to the state of the surface. Assuming for the moment that the predominating factor is the presence of inhibitors, each molecule of which terminates one chain only, it follows from the molecular weight of the soluble portion (210,000) that the concentration of inhibitor is $1{\cdot}13 \times 10^{-2}$ molar %. On the other hand, by polymerizing a sample of isoprene in successive stages (as in table 5), it is possible to obtain from it at least 70 % soluble polymer of mean molecular weight 73,000, corresponding to an inhibitor concentration of $6{\cdot}5 \times 10^{-2}$ molar %. It must therefore be supposed that an additional contributory factor is in operation in determining the molecular weight during the early stages of polymerization. Since the care taken in preparing the catalytic surfaces should rule out the presence of possible inhibitors on the sodium surface, it would seem that the effect must be due to some more fundamental characteristic of the sodium surface during the induction period.

Polymerization of isoprene vapour on sodium

It is well known that conjugated substances readily polymerize on sodium even when their vapour pressure is much less than the saturation value. A system of this type is more suitable for kinetical study than the corresponding liquid system, since the effective monomer concentration may be readily altered without introducing diluents which may well have a complicating effect on the kinetics. Moreover, an additional advantage accrued in the case of isoprene, since, in distinction to the liquid phase reaction, a stationary maximum rate of polymerization was observed in absence of toluene.

The apparatus employed consisted of a suitable reaction vessel, round which water at 25 or 60° C could be circulated, attached to a constant pressure gas burette of the normal type. The burette was controlled manually, variations from the initial pressure being observed through a telescope focussed on the meniscus of a wide-limbed mercury differential manometer. Sodium films were deposited on the walls of the reaction vessels in two ways: thicker sodium films were introduced by distillation from a side tube which was then sealed off, while small yet measured amounts of sodium were in some instances introduced, using the method described by Burt (1925), whereby sodium could be electrolysed through the soda glass walls of the reaction vessel; the strength and duration of the electrolytic current gave an accurate estimate of the amount of sodium introduced in this way.

Figure 5 represents the course of a polymerization carried out on a thin film of sodium, consisting of 1·12 mg. introduced electrolytically. The temperature was 25° C and the vapour pressure of isoprene *ca.* 370 mm. It will be noted that the rate of polymerization gradually reaches a maximum value which is maintained for some time before finally diminishing again.

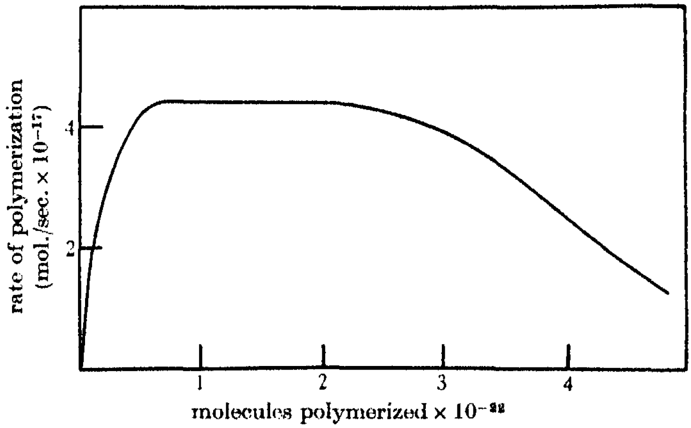

FIGURE 5. Polymerization of isoprene vapour ($p = 380$ mm. Hg) on a thin sodium surface at 25° C.

A few experiments carried out on thicker sodium films yielded results the general nature of which agree well with those obtained by Abkin and Medvedev (1936, 1939) from a careful study of the analogous butadiene reaction. They may be summarized as follows. The rates of reaction in the pressure range 100–350 mm., measured on one particular sodium surface following the completion of the induction period, were found to conform to the following expressions:

$$\text{at } 25^\circ\text{ C}, \; R = 5{\cdot}80 \times 10^{10} p^{2.7} \text{ mol./sec.,}$$

and

$$\text{at } 60^\circ\text{ C}, \; R = 3{\cdot}85 \times 10^{13} p^{1.4} \text{ mol./sec.,}$$

where p is the gas phase pressure of isoprene in mm. Hg. The absorption isotherms of isoprene on the polymer which had previously been allowed prolonged exposure to oxygen were determined over the same pressure range and found to approximate to the forms

$$\text{at } 25^\circ\text{ C}, \; C = 1{\cdot}52 \times 10^{14} p^{2.5},$$

and $$\text{at } 60^\circ\text{ C, } C = 3{\cdot}00\times 10^{16} p^{1.25},$$

where C represents the concentration of isoprene in the polymer in mol./c.c.

These empirical relations yield the following expressions for the rate of polymerization in terms of the isoprene concentration:

$$\text{at } 25^\circ\text{ C, } R = 2{\cdot}50\times 10^{-5} C^{1.08}\text{ mol./sec.,}$$

and $$\text{at } 60^\circ\text{ C, } R = 1{\cdot}35\times 10^{-5} C^{1.12}\text{ mol./sec.,}$$

in agreement with the first order nature of the analogous butadiene reaction, as found by Abkin and Medvedev.

In the concentration range common to the measurements at 60 and 25° C (viz. $1{\cdot}5\times 10^{19}$ to $6{\cdot}0\times 10^{19}$ mol./c.c. polymer), the ratio of the rates of polymerization (at equal monomer concentrations) has a mean value of 3·08, corresponding to an activation energy of 6·4 kcal.; the figure is similar to the activation energy of the butadiene polymerization obtained by Abkin and Medvedev, viz. 7·3 kcal.

Interpretation of kinetic data

There is no reason to suppose that the polymerization of isoprene on sodium departs from the generally recognized view that such reactions are of a chain character, involving three distinct phases, namely, initiation, propagation and termination of the chains. It will be convenient to consider in that order the nature of these three processes in the light of the information outlined above.

It has been shown that the kinetic data relating to the polymerization of liquid isoprene suggest the validity of the equations

$$R = K\frac{[I]}{[T]}, \tag{2'}$$

and

$$\nu = K_1\frac{[I]}{[T]}, \tag{3'}$$

where R and ν represent the rate of polymerization and the chain length of the polymer formed: $[I]$ and $[T]$ refer to the concentrations of isoprene and toluene. It is evident from these equations that the rate of initiation of chains ($= R/\nu$) is independent of isoprene or toluene concentrations. Assuming the zero order nature of the initiation process, it may readily be shown by the normal stationary state procedure that the only type of terminating reaction consistent with equation (2′) involves the interaction of the active propagating centre with toluene.

Nature of initiation reaction

The various possible alternatives may in the first place be classified according as to whether or not the initiation process involves the irreversible incorporation of sodium into the chain centre. Incineration of samples of polyisoprene, obtained from the polymerization of 100 % isoprene and of isoprene mixed with an equal proportion of toluene, failed to reveal the presence of even traces of sodium in the polymer. In the latter case the detection of sodium should have been extremely easy, since the incineration of the 1 g. sample would have yielded 0·01 g. sodium sulphate for each sodium atom incorporated per polyisoprene molecule. It must accordingly be assumed that the reaction mechanism must be such that at no stage is sodium incorporated in the polymer chain. Some confirmation of the absence of sodium in the finished polymer arises from the experiment mentioned above in which polymerization was carried out on 1·12 mg. sodium at 25° C. During this reaction 12 g. isoprene were polymerized, without the sodium deposit showing any marked decrease in size or density. It is to be noted that even if all the sodium were incorporated in the polymer so that each polymer chain contained one sodium atom the molecular weight would be 250,000.

This evidence conflicts with the views of Abkin and Medvedev (1936, 1939) regarding the mechanism of the polymerization of butadiene vapour on sodium. They conclude that the initiation reaction consists of the formation of definite disodium complexes of the type

$$\mathrm{Na{-}CH_2{-}CH{=}CH{-}CH_2{-}Na},$$

the chain growth thereafter occurring by successive insertions of manomeric molecules between one of the sodium atoms and the hydrocarbon portion of the complex. As no termination reaction is specifically mentioned, this mechanism would lead to the expectation that the finished polymer would contain two sodium atoms per molecule.

From the experimental data available it is possible to estimate the activation energy required in the initiation process. The overall activation energy of the polymerization (ΔE) may be resolved into three components, representing the activation energies associated respectively with the initiation (ΔE_i), the propagation (ΔE_p) and the termination processes (ΔE_t), thus

$$\Delta E = \Delta E_i + \Delta E_p - \Delta E_t.$$

ΔE may readily be calculated as 11·0 kcal. from the variation of the quantity K with temperature (tables 3 and 4), while the temperature variation of K_1 (tables 3 and 4) yields a value for ($\Delta E_p - \Delta E_t$) of $-3{\cdot}4$ kcal. The activation energy of the initiation reaction is accordingly 14·4 kcal.

The initiation reaction is almost certainly in itself a composite reaction, consisting of three possible consecutive phases: the adsorption of an isoprene molecule to the neighbourhood of the sodium surface, any activation on the surface, and possibly desorption of the activated complex so formed. The activation energy measured will correspond to the slowest process. It is unfortunate that no detailed study of the adsorption of conjugated hydrocarbons on alkali metals has been made, with the result that no decision has been reached as to the mode of adsorption involved. There seem good grounds for supposing that the chemisorption of isoprene concerns the attachment of the isoprene in the form

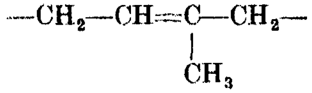

$$-CH_2-CH{=}\underset{\displaystyle CH_3}{\underset{|}{C}}-CH_2-$$

to the positive ions forming the sodium crystalline lattice. From a consideration of the mutual forces between the isoprene molecule and sodium ion, it must be supposed that the maximum value of the activation energy required for the formation of such an adsorption complex would be the resonance energy of the isoprene molecule. While this quantity has not been determined, it should not vary greatly from the figure of 5 kcal. obtained by theoretical and experimental methods for the butadiene molecule (Lennard-Jones and Coulson 1939). It may be concluded therefore that the activation of the isoprene at the catalytic surface is not the rate-determining factor.

It is therefore necessary to identify the 14·4 kcal. energy with a desorption process, involving the cleavage of a carbon-sodium linkage. Two alternative mechanisms which include such a step must be considered: in the first, the adsorbed isoprene molecule leaves the catalytic surface in active form, the chain propagation occurring thereafter away from the sodium surface; the second alternative is that the chain growth of each polymer molecule occurs while the molecule is still attached to the catalytic surface by the original carbon-sodium linkage, desorption of the finished polymer molecule occurring at some time subsequent to the termination of the chain growth. In both cases the factor controlling the rate of initiation is thus in effect the rate at which sites on the catalytic surface are vacated. In view of the experimental fact that the rate of initiation is independent of isoprene (and toluene) concentration, it is necessary to suppose that in the first case in the concentration range examined the catalytic surface is always saturated with isoprene molecules, while in the second case the additional assumption must be made that the termination of the chain growth in no way affects the lifetime of the polymer molecule adsorbed on the surface. While there is no readily apparent method of deciding experimentally between these alternatives it is felt that the adsorption complex $\mathrm{Na{-}CH_2{-}CH{=}CH{-}CH_2{-}}$ represents a more likely initiation centre than a desorbed isoprene molecule, which would so readily revert to its stable configuration.

Nature of propagation reaction

In view of the conclusions drawn as to the nature of the initiation reaction it follows that the propagation reaction must be of the free radical type. Evidence has been provided (Midgley 1937; Ziegler, Grimm and Willer 1939) that conjugated molecules may become incorporated in polymer chains in the 1–2 sense, e.g.

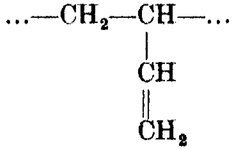

$$\ldots\mathrm{{-}CH_2{-}}\underset{\substack{|\\ \mathrm{CH}\\ \|\\ \mathrm{CH_2}}}{\mathrm{CH}}\mathrm{{-}}\ldots$$

as well as in the 1–4 sense, e.g. $\ldots\mathrm{{-}CH_2{-}CH{=}CH{-}CH_2{-}}\ldots$. That both modes of addition are in operation in the present case also has been suggested by X-ray observations carried out by Dr G. A. Jeffrey. Polyisoprene samples, both in the unstretched and stretched condition, failed to give any indication of the X-ray phenomena associated in the case of rubber with regularity of structure. The possibility that the lack of structure was attributable to the irregular distribution of isoprene units orientated in the two possible ways

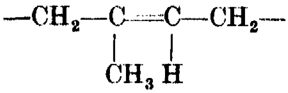

$$\mathrm{{-}CH_2{-}}\underset{\substack{|\\ \mathrm{CH_3}}}{\mathrm{C}}{=}\underset{\substack{|\\ \mathrm{H}}}{\mathrm{C}}\mathrm{{-}CH_2{-}}$$

and

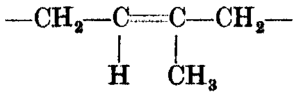

$$\mathrm{{-}CH_2{-}}\underset{\substack{|\\ \mathrm{H}}}{\mathrm{C}}{=}\underset{\substack{|\\ \mathrm{CH_3}}}{\mathrm{C}}\mathrm{{-}CH_2{-}}$$

was eliminated by submitting a sample of polybutadiene—prepared under the same conditions as the polyisoprene—to X-ray examination. Since, in this case also, no evidence of regularity of structure could be obtained, it must be assumed that both modes of polymerization, 1–2 and 1–4, do actually occur.

Nature of termination reaction

There is good reason to suppose that toluene acts as an effective terminating agent through chemical interaction with the centre of growth, as distinct from the physical interaction normally associated with 'solvent action', since it was found that addition of cyclohexane produced no appreciable effect on the polyisoprene formed. Thus in one instance, in which 38 molar % cyclohexane was added to the isoprene, the polymer obtained at 60° C was only 30 % soluble; the molecular weight of the soluble portion being

217,000 in excellent agreement with the data obtained for polymers obtained from undiluted isoprene. Benzene, on the other hand, produces an effect comparable with that of toluene: in one experiment at 60° C, using 46·7 molar % benzene, the maximum rate of polymerization (and judging from the fact that the maximum rate of polymerization was maintained for a considerable portion of the reaction it represented the true maximum rate of polymerization) was $2{\cdot}1 \times 10^{17}$ mol./sec./sq. cm. and the mean chain length was 530. This would indicate that the rate of production of initiation centres was $4{\cdot}0 \times 10^{14}$ per sec.—a figure in reasonable agreement with that obtained in presence of toluene, viz. $6{\cdot}5 \times 10^{14}$. From the ratio of molecular weights obtained under equal molar concentrations of toluene and benzene it may be deduced that the termination reaction involving toluene is some 3·6 times more efficient than that involving benzene.

The kinetic evidence shows that even where only 2·9 molar % toluene is present the termination of polymer chains is wholly effected by toluene: this is also in agreement with the complete solubility of the polymer obtained at such low toluene concentrations—as contrasted with the partial insolubility of the polymer obtained when no toluene is present. In absence of toluene therefore an alternative termination mechanism, the efficiency of which is considerably less than that involving toluene, must come into play. The onset of insolubility may be due to one of two characteristics of the additional termination mechanism; the deactivation of each growing chain may be accomplished by interaction with points in other polymer molecules which are of abnormal chemical activity (e.g. pendant vinyl groups formed, when propagation of the polymer chain occurred by 1–2 addition) thus producing a net or cross linked structure; alternatively, the efficiency of the terminating reaction may be so small that the polymer becomes of such dimensions as to become inextricably entangled with other polymer molecules, even in the presence of solvent. This latter condition would give rise to an almost infinitely great rate of polymerization, but since even the highest rate of polymerization observed experimentally appeared to be controlled by the rate of diffusion, there are no experimental grounds for dismissing this possibility. It is, however, rendered less likely by the observation of Bronsted and Volqvartz (1939) that polystyrenes of molecular weight of the order of 1,000,000 could be dissolved in benzene.

Polymers of similar insolubility are obtained when isoprene at pressures below the saturation vapour pressure is allowed to polymerize on sodium surfaces. It is reasonable to suppose that the nature and energetics of the initiation, propagation and termination reactions concerned in this 'gas phase' polymerization are identical with those of the corresponding reactions involved in the later stages of the polymerization of undiluted liquid isoprene. From the fact that a stationary maximum rate of polymerization is established in the case of the 'gas-phase' reaction, it must be assumed that a termination reaction is in operation. In order to explain the overall energy of activation of the liquid phase reaction being some 4·6 kcal. greater than that of the gas phase reaction, it is necessary to suppose that the termination reaction, which produces insolubility, requires 4·6 kcal. greater activation energy than the termination reaction involving toluene.

Thanks are due to Professor E. K. Rideal, F.R.S., for the facilities allowed at the Laboratory of Colloid Science, Cambridge, where part of the work was performed, and also to Dr G. Gee for much helpful advice and criticism. The above work has been carried out as part of the programme of fundamental research on rubber undertaken by the Board of the British Rubber Producers' Research Association.

REFERENCES

Abkin, A. and Medvedev, S. 1936 *Trans. Faraday Soc.* **32**, 286–295.
Abkin, A. and Medvedev, S. 1939 *J. Phys. Chem. Russ.* **13**, 705–718.
Bronsted, J. N. and Volqvartz, K. 1939 *Trans. Faraday Soc.* **35**, 576–579.
Burt, R. C. 1925 *J. Opt. Soc. Amer.* **11**, 88–92.
Gee, G. 1940 *Trans. Faraday Soc.* **36**, 1171–1178.
Lennard-Jones, J. E. and Coulson, C. A. 1939 *Trans. Faraday Soc.* **35**, 811–823.
L'vov, V. N. 1937 *J. Gen. Chem.* (*U.S.S.R.*), **7**, 928–946.
Melville, H. W. 1937 *Proc. Roy. Soc.* **A**, **163**, 511–542.
Midgley, T. 1937 *Chemistry and technology of rubber*, p. 684, 1st ed. New York: Reinhold Publishing Corporation.
Whitby, G. S. and Crozier, R. N. 1932 *Canad. J. Res.* **6**, 203–225.
Ziegler, K., Grimm, H. and Willer, R. 1939 *Ann. Phys. Chem.* **542**, 90–122.

Structure and molecular anisotropy of sorbic acid, $CH_3.CH:CH.CH:CH.COOH$

By Kathleen Lonsdale, J. Monteath Robertson
and Ida Woodward

Royal Institution, London, and The University, Sheffield

(*Communicated by Sir William Bragg, P.R.S.—Received* 18 *November* 1940)

[Plates 1–4]

A preliminary study of sorbic acid has shown that the monoclinic unit cell contains eight molecules, these being linked in pairs by hydrogen bonds about the symmetry centres of the crystal, with the long chain axis of the molecule in or near to the (010) plane and inclined at between 10° and 15° to the *a* axis in the obtuse angle β. The molecular chains must be rotated so as to bring some of the atoms out of the (010) plane, and an approximate measure of this rotation is provided by measurements of optical and magnetic anisotropy, which give ± 35° as the angle between the *b* axis and the normal to the molecular plane. The magnetic anisotropy due to resonance in the conjugated carbon chain is about half as large as that in the benzene ring and falls into line with previous observations on non-cyclic conjugated compounds. The orientation of the molecules has been confirmed by observation of the size and shape of the diffuse spots occurring on well-exposed Laue photographs taken with radiation from a copper target, and the usefulness of these photographs as a secondary method of structure determination has been emphasized.

Introduction

Sorbic acid, $CH_3.CH:CH.CH:CH.COOH$, is of particular interest because it is probably the simplest case of a compound containing an open conjugated chain which is readily obtained in single crystals at ordinary temperatures. Moreover, the related hydrocarbon $CH_2:CH.CH:CH_2$, 1·3-butadiene, is one basis of an artificial rubber, and any information as to the configuration and physical properties of the chain is bound to be useful in that connexion. Theoretical considerations (Pauling and Sherman 1933) and some experimental evidence (Mulliken 1939*a*) indicate that butadiene molecules have a plane, *trans*-configuration. The electron diffraction data (Schomaker and Pauling 1939) are said to be 'not incompatible with a mixture of *cis* and (predominantly) *trans* molecules', the following parameters being given: $C—H = 1·06\,A$ (assumed), $C=C = 1·35 \pm 0·02\,A$, $C—C = 1·46 \pm 0·03\,A$, angle $C=C—C = 124° \pm 2°$; while later absorption data indicate the possible presence of 20 % *cis* molecules (Mulliken 1939*b*). The theoretical values given for the double and single carbon to carbon bonds in this substance are:

(Lennard-Jones 1937): C—C = 1·41 A, C═C = 1·34 A;
(Penney 1937): C—C = 1·43 A, C═C = 1·34 A.

The X-ray method, used to its full power, is capable of giving very exact information as to the atomic distances and angles in molecules, when suitable single crystals are available. In the following paper, a preliminary structure is outlined for sorbic acid. It is hoped to refine the structure at a later date by Fourier series methods, and to obtain precise measurements of the bond lengths in the conjugated chain.

The existence of conjugation, or resonance, implies the presence of electrons whose density is spread over molecular orbitals, embracing several nuclei. These large plane electronic orbits give rise to an additional diamagnetic susceptibility normal to the plane of the molecule. Only in the case of *cyclic* conjugated compounds is there a satisfactory theoretical discussion of this effect (London 1937), but the effect has been observed in a number of open chain compounds also (Lonsdale 1939). Since 1·3-butadiene is a gas, the magnetic anisotropy of its molecules cannot be directly observed, but measurements are given here of the anisotropy of crystalline sorbic acid, and the anisotropy of the molecule itself is deduced.

It has been found that Laue photographs of sorbic acid, if taken with X-rays containing a large proportion of Cu $K\alpha$ and well exposed, show, in addition to the normal Laue spots, a great many diffuse spots of a totally different character (plate 1). The cause of these diffuse spots is at present the subject of discussion (Preston 1939; Zachariasen 1940; Raman and Nilakantan 1940; Raman and Nath 1940; Bragg 1940), but it is clear from the photographs that the shape and size of the diffuse spots are intimately related to the structure of the crystal and that a study of such spots may prove a useful secondary method of structure determination.

CRYSTAL DATA

Sorbic acid: $C_6H_8O_2$; $M = 112$; melting-point 134°·5 C; density calculated, 1·187; measured, 1·204 at 19°/4°. Monoclinic, $a = 20{\cdot}00 \pm 0{\cdot}05$, $b = 4{\cdot}03 \pm 0{\cdot}02$, $c = 15{\cdot}83 \pm 0{\cdot}03$ A, $\beta = 102°{\cdot}5$. (hkl) reflexions absent when $(h+k)$ is odd, ($h0l$) absent when h or l is odd; space group, C_s^4 *b* ii (Cc) (monoclinic hemihedry) *or* C_{2h}^6 *b* ii (C 2/*c*) (monoclinic prismatic). Eight molecules per unit cell; no molecular symmetry. Volume of the unit cell, 1246 A^3. Absorption coefficient for X-rays, $\lambda = 1{\cdot}54$, $\mu = 8{\cdot}51$ per cm. Total number of electrons per unit cell = $F(000) = 480$. Optically positive; $\alpha \doteqdot \beta < \gamma$; α along b, β nearly along c, and γ nearly perpendicular to (100).

EXPERIMENTAL X-RAY WORK

The crystals used in this work were obtained from acetone solution in the form of small laths, with the b axis along the length of the lath. Rotation and moving film photographs were taken, with Cu $K\alpha$ radiation, about the three crystallographic axes and various cell diagonals. These showed that the body diagonal was normal, but the presence of an identical molecule was disclosed at the centre of the (001) face, a periodicity of 10·17 A being found along this diagonal instead of the calculated value of 20·40 A. This confirmed the general halvings observed on the moving film photographs reported above.

Of the two possible space groups, C_{2h}^6 ($C\,2/c$) in the prismatic class seems the most probable, as the crystals show no sign of hemihedry and the unit cell is found to contain the eight (asymmetric) molecules which are necessary to complete the symmetry of the group $C\,2/c$. This space group is confirmed by the results of the structure analysis given below.

For the intensity measurements, small specimens of between 0·05 and 0·1 mg. weight were selected, and moving-film photographs were taken with long exposures on series of superimposed films (de Lange, Robertson and Woodward 1939). This arrangement enabled the intensities to be recorded and measured on the integrating photometer over a range of about 2000 to 1. The shape of the crystal specimen was taken into account, and approximate absorption coefficients were calculated for each reflexion.

The absolute values of the structure factors were obtained by comparison with a diamond standard on the two-crystal moving-film spectrometer. Sorbic acid crystals are slightly volatile, and so the specimen employed for the absolute measurements (a small specimen completely bathed in the radiation) was weighed immediately after making the exposure. Its mass was 0·046 mg.

STRUCTURE ANALYSIS

It seemed likely on general grounds that the sorbic acid molecules would be associated in groups of two by hydrogen bonding between opposite carboxylic oxygen atoms, as in the stable formic and acetic acid dimers. The conjugated chains may intensify this effect and will in any case maintain the molecules in fairly rigid planar configurations. It also seemed probable that the dimers might form a series of centro-symmetrical units in the crystal.

These expectations are confirmed by a study of the cell dimensions and structure factors. The short *b* axis and the long *a* and *c* axes indicate that the molecular chains must lie mainly in the (010) plane. It is at once apparent, however, that the atoms cannot all lie strictly in this plane, because such an arrangement would give the (020) structure factor a maximum value, whereas it is actually quite small ($F(020) = 34$; possible maximum about 166). It is thus almost certain that the molecular chains are rotated somewhat about their long axes, bringing some of the atoms out of the (010) plane. As a first approximation, however, we may regard the atoms as lying in the (010) plane, without much error as far as the view of the structure along the *b* axis is concerned. In this preliminary account of the structure we shall not consider rotations of the chain axis.

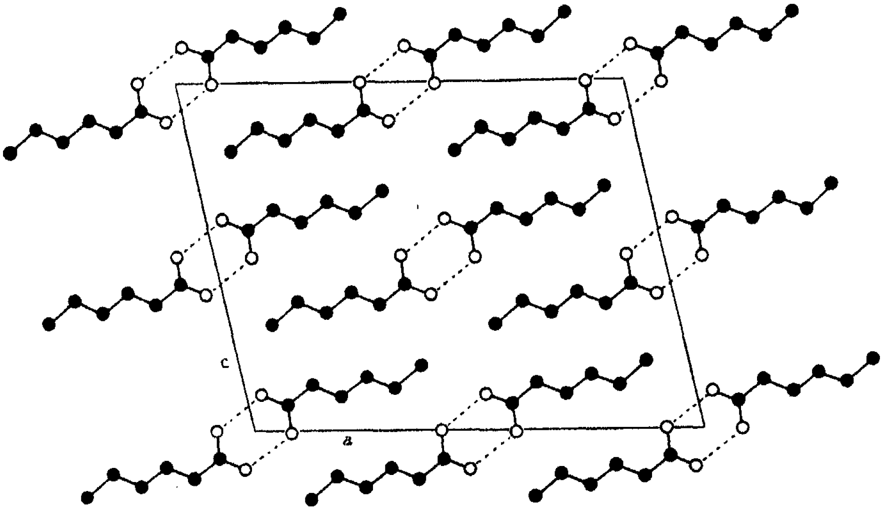

FIGURE 1. Sorbic acid. Projection on (010).

● carbon ----- hydrogen bonds
○ oxygen —— unit cell boundary

Further information regarding the orientation of the molecules in the (010) projection is provided by some outstanding features among the intensities of the (*h*0*l*) planes. All the atoms must be nearly in phase for the (16,00) reflexion ($F(16,00) = 75$; possible maximum about 80), and the $(18,0\bar{4})$ is nearly as strong. Among planes of larger spacing the reflexions from $(20\bar{4})$ and (004) are the most outstanding.

These and other similar considerations enable us to fix the structure with some certainty, and the result is shown in figure 1.

The molecules are linked in pairs by hydrogen bonds about the symmetry centres of the crystal, with the long chain axis of the molecule inclined at between 10° and 15° to the *a* crystal axis. In the structure shown, the hydrogen bonds linking the adjacent carboxyl groups have a length of 2·6 A, but this figure cannot be determined with much certainty at present. The values assumed for other bond lengths and valency angles are: C=C = 1·34, C—C conjugated = 1·44, C—C terminal = 1·54 A; angles 120°.

TABLE 1. MEASURED AND CALCULATED VALUES OF SOME $(h0l)$ STRUCTURE FACTORS

hkl	$2\sin\theta(\lambda = 1{\cdot}54)$	F measured	F calculated
200	0·158	6	+ 9
400	0·315	39	− 40
600	0·473	59	− 52
800	0·630	60	− 40
10,00	0·788	11	+ 15
12,00	0·946	31	+ 24
14,00	1·103	26	+ 9
16,00	1·261	75	− 67
18,00	1·418	8	− 4
20,00	1·576	9	+ 1
22,00	1·734	20	+ 9
002	0·199	53	+ 55
004	0·398	96	− 115
006	0·597	8	+ 21
008	0·796	38	+ 50
00,10	0·996	40	+ 48
00,12	1·195	21	+ 13
00,14	1·394	12	+ 2
00,16	1·593	13	+ 10
204	0·459	43	− 22
202	0·278	26	+ 11
$20\bar{2}$	0·223	63	+ 82
$20\bar{4}$	0·395	146	+ 125
404	0·560	72	− 54
$40\bar{4}$	0·450	11	+ 2
604	0·680	125	− 86
$18,0\bar{4}$	1·384	50	− 40

On this basis the values shown in table 1 are calculated for some of the $(h0l)$ structure factors. The agreements obtained with the measured values show that the proposed structure is on the right lines. As expected, there are certain discrepancies owing to the fact that no account has yet been taken of movements bringing the atoms out of the (010) plane.

MAGNETIC ANISOTROPY: EXPERIMENTAL

The diamagnetic anisotropy of sorbic acid crystals is relatively small, and therefore large crystals of mass about 3 mg. were used for measurement. It was found that well-developed thick needles could be grown from an 80–100° B.P. petroleum ether solution, by very slow evaporation. The *b* axis lies along the length of the needles and the side faces are $\{100\}$ (largest face), $\{001\}$ $\{103\}$ $\{70\bar{6}\}$ and sometimes $\{10\bar{1}\}$ $\{10\bar{5}\}$. Laue and rotation photographs were taken of smaller crystals optically identical with the larger ones used for the magnetic work.

Magnetic measurements were difficult to obtain accurately, as successive crystals gave different results, and data for the same crystal varied even during the time of observation although no apparent change took place in the crystals themselves (the loss of weight in a large crystal over the time of a single experiment was negligible). In particular the orientation of the crystals was apt to change gradually from an initial stage in which the (100) plane was normal to the field H to a final stage in which the field direction made an angle of 10–20° with the (100) normal, almost as if the molecules were being rearranged by the magnetic field, this change in orientation always being accompanied by a *decrease* in the anisotropy $(\chi_1 - \chi_2)$. The final readings, however, agreed moderately well for different crystals and are as follows:

$$\chi_3 \text{ (along } b) > \chi_2 > \chi_1, \quad \chi_1 - \chi_3 = 6{\cdot}8 \pm 0{\cdot}2,$$

$$\chi_2 - \chi_3 = 5{\cdot}7 \pm 0{\cdot}2, \quad \chi_1 - \chi_2 = 1{\cdot}1 \ (\times 10^{-6}).$$

$$\text{Angle } \chi_1 : c, \text{ measured positive in obtuse } \beta, \ \psi = 80^\circ (\pm 10^\circ).$$

The absolute susceptibility was measured in a mixture of SrBr and $NiCl_2$, the solutions being previously saturated with sorbic acid, which is soluble in H_2O. The crystals used were all first examined optically. The measured density was 1·204 at 19°/4°, and $\kappa_{\text{min.}} = -0{\cdot}598 \pm 0{\cdot}006 \ (\times 10^{-6})$. Hence $\chi_1 = -55{\cdot}8$, $\chi_2 = -56{\cdot}9$, $\chi_3 = -62{\cdot}6 \ (\times 10^{-6})$. The mean susceptibility is $-58{\cdot}4$, as compared with $-56{\cdot}9$, the value calculated from Pascal's additive data.

DISCUSSION OF MOLECULAR ANISOTROPY

The minimum optical polarizability and maximum diamagnetic susceptibility coincide in direction in the crystal, both being along the *b* axis. This coincidence is typical of aromatic compounds, and of aliphatic compounds such as maleic and succinic acids which contain a high proportion of double

Lonsdale, Robertson & Woodward   *Proc. Roy. Soc., A, vol.* 178, *plate* 1

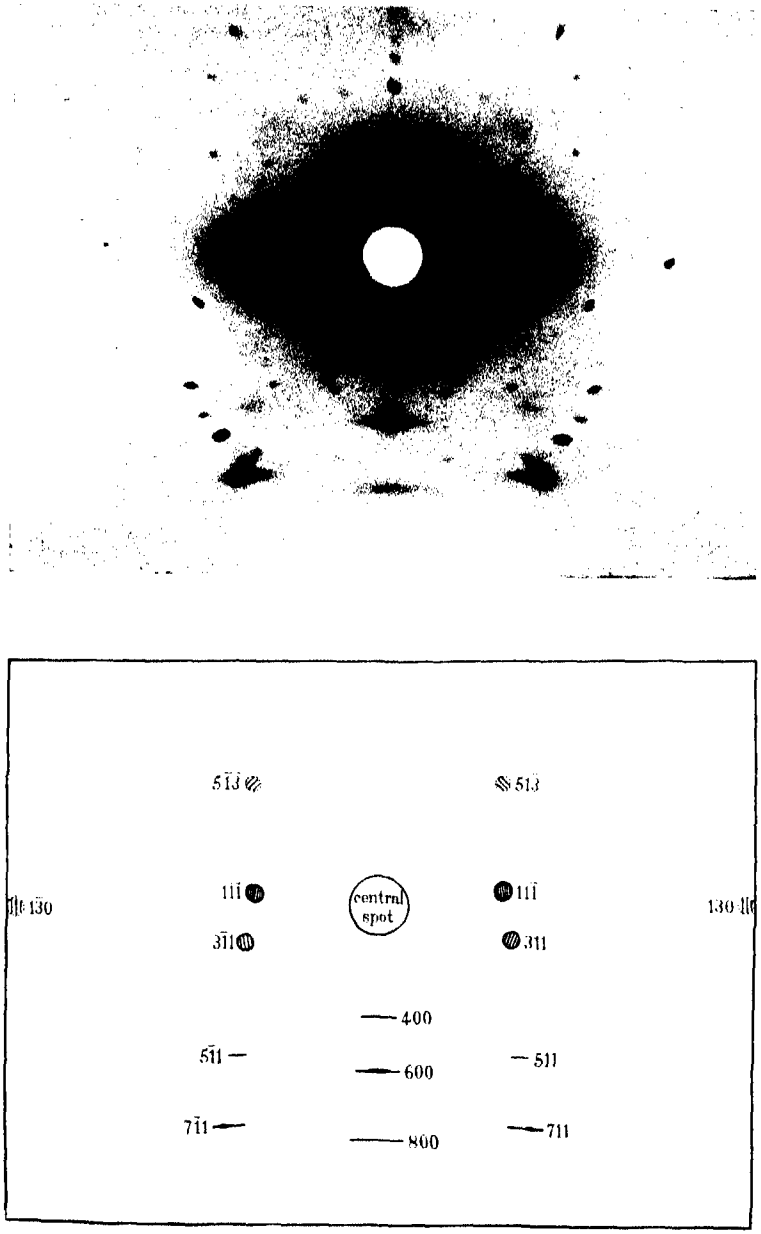

(*a*) Sorbic acid: Filtered Cu radiation, 4 cm. *b* axis horizontal; X-ray beam at 88°·3 to *a* axis, 14°·2 to c axis. Showing fine diffuse spots: (400) (600) (800) (511) (711) and broad diffuse spots: ($11\bar{1}$) (311) ($51\bar{3}$) (130).

(*Facing p.* 48)

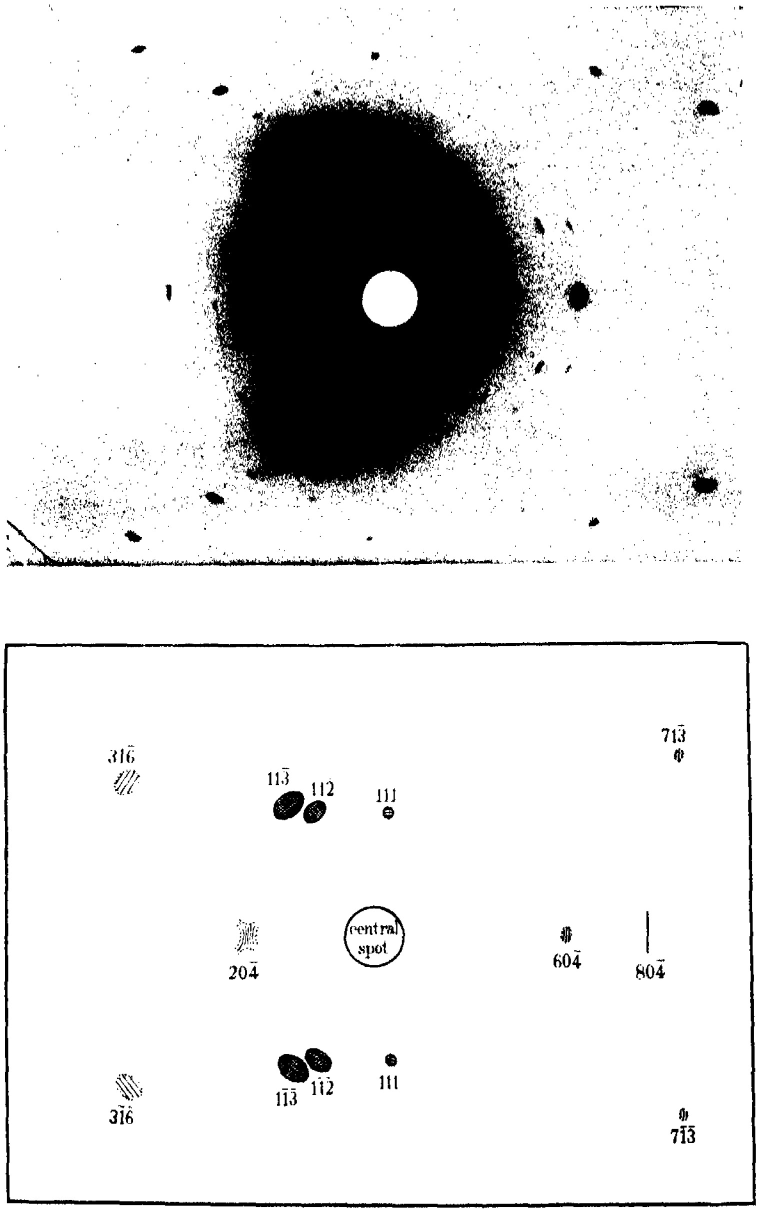

(*b*) Sorbic acid: Filtered Cu radiation, 4 cm. *b* axis vertical; X-ray beam at 41°·9 to *a* axis, 60°·6 to *c* axis. Showing strong $(11\bar{2})$ $(11\bar{3})$ diffuse spots.

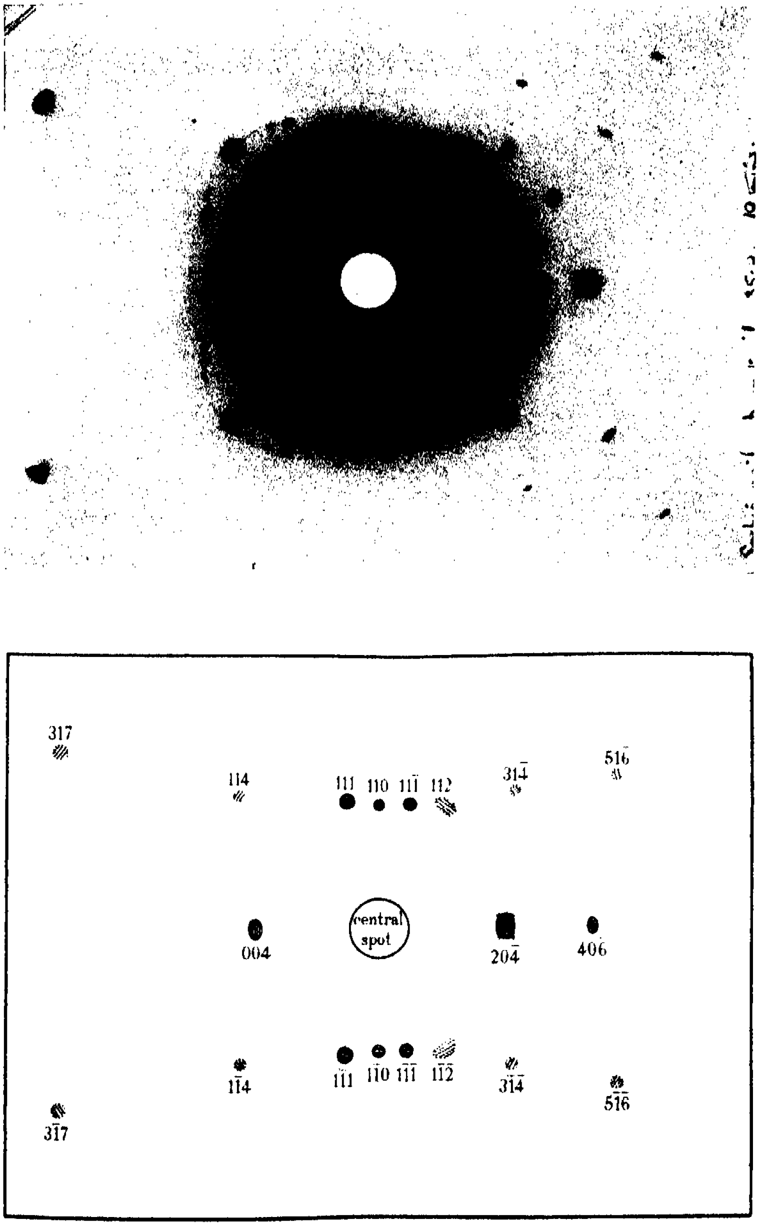

(c) Sorbic acid: Filtered Cu radiation, 4 cm. *b* axis vertical, X-ray beam at 11°·9 to *a* axis, 90°·6 to *c* axis. Showing (004) and (stronger) (20$\bar{4}$) diffuse spots on central layer line.

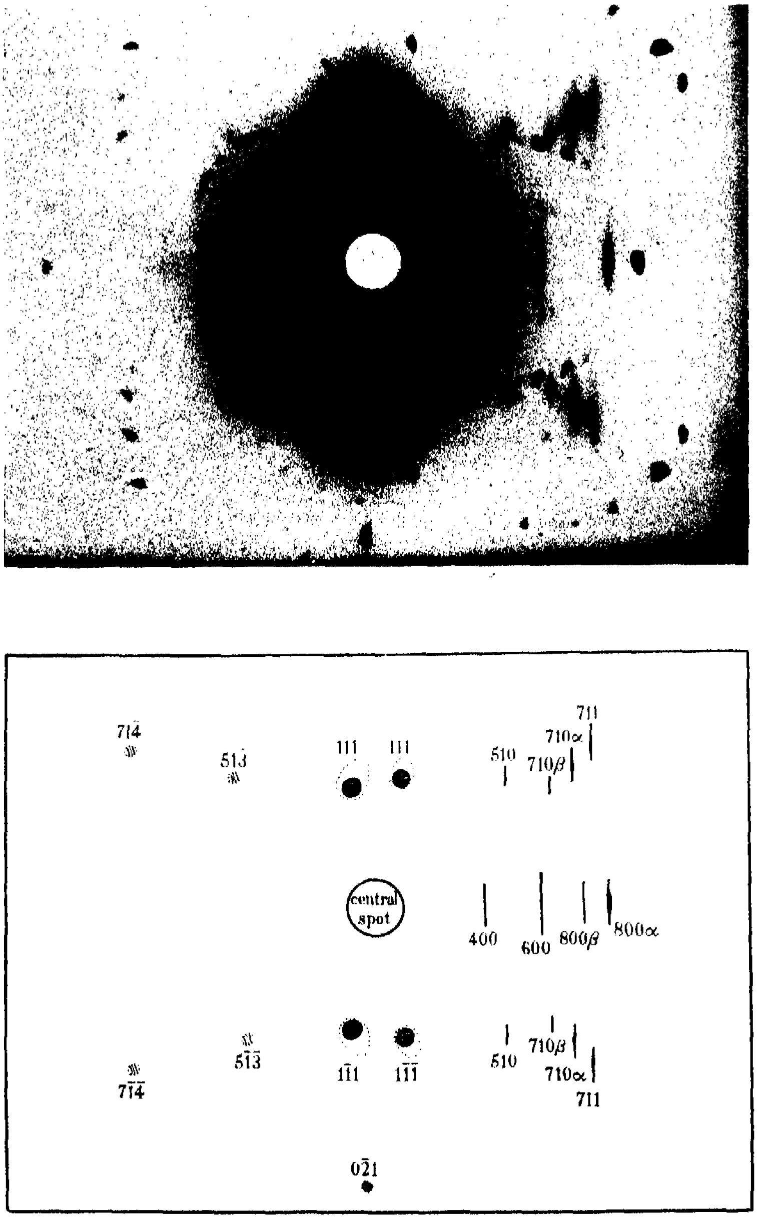

(*d*) Sorbic acid: Unfiltered Cu radiation, 4 cm. *b* axis vertical, X-ray beam at 81°·9 to *a* axis, 20°·6 to *c* axis. Showing contrast between fine and broad types of diffuse spot.

bonds. In aliphatic compounds containing only single bonds the maximum diamagnetic susceptibility is *along* the chain length. Thus in *d*-mannitol, $CH_2OH.CHOH.CHOH.CHOH.CHOH.CH_2OH$, the susceptibility along the carbon backbone exceeds those in the cross-section by 13·3 and 7·7 units (Lonsdale 1939). In respect of dimensions only, one might expect a similar anisotropy in sorbic acid, which contains an equal number of carbon atoms. The direction of the acute bisectrix in an optically positive crystal generally indicates the length of the molecule, which probably, therefore, lies nearly normal to the (100) plane. That this is so has already been proved by the preliminary X-ray study.

As far as the molecular dimensions alone are concerned, therefore, one would expect the magnetic susceptibility normal, or nearly normal, to (100) to exceed that in other directions by 13·3→7·7 units, whereas in fact the susceptibility χ_3 along the b axis is 5·7 greater and χ_1 is only 1·1 less than χ_2, which is almost coincident with the molecule length in the crystal.

Let us suppose that the diamagnetic susceptibilities of the sorbic acid molecule in respect of dimensions alone are K_1 (along length), K_2 (along width) and K_3 (normal to plane of atoms), and that the presence of the conjugated carbon chain terminated by an acid group introduces an added diamagnetism k normal to the plane of the molecule. Then we may expect $K_1 - K_2 \fallingdotseq -7{\cdot}7$, $K_1 - K_3 \fallingdotseq -13{\cdot}3$ $(\times 10^{-6})$. If, as seems most probable, χ_2 and K_1 coincide, then $K_1 = -56{\cdot}9$, $K_2 \fallingdotseq -49{\cdot}2$, $K_3 \fallingdotseq -43{\cdot}6$ $(\times 10^{-6})$. The tilt of the molecular normal away from the b axis will be given by θ, where

$$\chi_1 = K_2 \cos^2\theta + (K_3 + k)\sin^2\theta = -55{\cdot}8\ (\times 10^{-6}),$$

$$\chi_3 = K_2 \sin^2\theta + (K_3 + k)\cos^2\theta = -62{\cdot}6\ (\times 10^{-6}).$$

Hence

$$K_2 + K_3 + k = -119{\cdot}4\ (\times 10^{-6}),$$

$$k \fallingdotseq (-119{\cdot}4 + 49{\cdot}2 + 43{\cdot}6) = -25{\cdot}6\ (\times 10^{-6}),$$

$$\sin^2\theta \fallingdotseq 0{\cdot}33, \quad \theta \fallingdotseq \pm 35^\circ.$$

This calculation is admittedly only approximate, but the results agree well with expectation. The added anisotropy due to the double bond character, −25·6, is about −5·1 for each carbon atom with a double-bond linkage; the same value has been found in all open chain substances so far investigated. It is worth noting that this anisotropy is nearly half as much as that of the benzene ring, although the chain is open. The additional anisotropy found in all these compounds, therefore, is a consequence of the resonance and not exclusively of the cyclic character of the compounds.

A tilt of the molecular normal away from the b axis of the order of ± 35° could easily explain the small value of the (020) structure factor; but it does not necessarily follow that the rotation takes place exactly about the chain axis.

DIFFUSE SPOT PHOTOGRAPHS

When Laue photographs of small crystals were being taken for identification purposes, using X-radiation from a copper target, it was observed that many of these photographs showed particularly well-developed diffuse spots of different shapes, these being due to the characteristic radiation in the X-ray beam. Examples of these are shown in plates 1–4.

Previous observation had shown that in layer structures, such as hexamethylbenzene, urea nitrate, etc., the diffuse spot corresponding to the layer plane was large (in all directions, but especially at right angles to the radial 'white radiation' streak), intense, and persistent over a wide variation of crystal orientation (Lonsdale 1940), while in chain structures, such as those of the paraffins and long-chain fatty acids, the diffuse spots corresponding to planes normal, or nearly normal, to the chain length are very fine streaks. In the sorbic acid photographs *both* types of spots appear. By comparison of the accompanying diagram (figure 2), which shows planes giving these two types of diffuse spots in the $(h0l)$ zone, with the structure shown in figure 1, it will be seen that the large intense spots correspond to planes which are nearly *parallel* to the chain length, while the fine, streaky spots correspond to planes more nearly *perpendicular* to the chain length. Other diffuse spots, corresponding to planes not in the $(h0l)$ zone, are:

Large: (110) (130) (111) (114) (118) $(11\bar{1})$ $(11\bar{2})$ $(11\bar{3})$ $(11\bar{4})$ $(11\bar{5})$
$(11\bar{6})$ $(11\bar{7})$ (315) (317) $(31\bar{3})$ $(31\bar{4})$ $(31\bar{5})$ $(31\bar{6})$ $(31\bar{7})$ $(51\bar{2})$
$(51\bar{3})$ $(51\bar{4})$ $(51\bar{6})$ $(71\bar{2})$ $(71\bar{3})$ $(71\bar{4})$ $(71\bar{6})$ $(91\bar{3})$ (021)

Fine: (510) (511) (512) $(51\bar{1})$ (710) (711) (712) (713) (910) $(91\bar{1})$

This list is not intended to be exhaustive, but at least one important conclusion may be drawn from a comparison of the relative intensities of the observed diffuse spots. The most intense 'layer' spots are those due to the $\{11\bar{3}\}$ planes, with $\{11\bar{2}\}$ next in intensity. This indicates that the molecules are tilted, possibly about the mean axis of each dimer, so that the atoms lie in planes which are nearly parallel to $\{11\bar{3}\}$, or which lie between $\{11\bar{3}\}$ and $\{11\bar{2}\}$. In fact, we find that $\{11\bar{3}\}$ planes make an angle of about 37°·5 and $\{11\bar{2}\}$ planes an angle of about 27°·5 with (010). The angle of tilt of about ± 35° given by the magnetic results is thus confirmed by the indications of the diffuse spots.

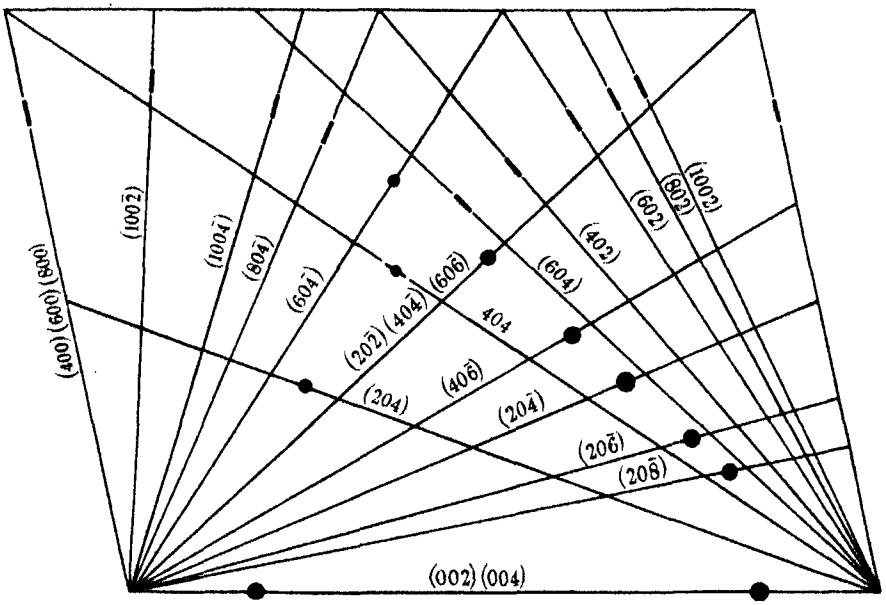

FIGURE 2. Sorbic acid: ($h0l$) zone.

—●— planes giving broad diffuse spots.

—▬— planes giving fine diffuse spots.

Such a method of deducing approximate molecular orientations may prove to be very useful in the case of molecules which, though complicated in formula, possess a reasonably well-defined layer or chain character.

Our thanks are due to Professor Linstead, Professor Lowenbein and Dr Oldham for various specimens of sorbic acid. Mr H. Smith gave valuable assistance in the taking of the diffuse spot photographs. All the experimental work was carried out in the laboratories of the Royal Institution. One of us (J. M. R.) is indebted to the Royal Society for a grant which has made it possible for the structure analysis to be continued at Sheffield University.

REFERENCES

Bragg, W. H. 1940 *Nature, Lond.*, **146**, 509.
de Lange, Robertson and Woodward 1939 *Proc. Roy. Soc.* A, **171**, 398, 404.
Lennard-Jones 1937 *Proc. Roy. Soc.* A, **158**, 280.
London 1937 *J. Phys. Radium*, **8**, 397.
Lonsdale 1939 *Proc. Roy. Soc.* A, **171**, 541.
Lonsdale 1940 *Molecular anisotropy of urea and of related compounds* (in the Press).
Mulliken 1939*a* *J. Chem. Phys.* **7**, 121.
Mulliken 1939*b* *J. Chem. Phys.* **7**, 373.
Pauling and Sherman 1933 *J. Chem. Phys.* **1**, 679.
Penney 1937 *Proc. Roy. Soc.* A, **158**, 306.
Preston 1939 *Proc. Roy. Soc.* A, **172**, 116.
Raman and Nath 1940 *Proc. Indian Acad. Sci.* **12**, 83.
Raman and Nilakantan 1940 *Proc. Indian Acad. Sci.* **11**, 389, 398; **12**, 141.
Schomaker and Pauling 1939 *J. Amer. Chem. Soc.* **61**, 1773.
Zachariasen 1940 *Phys. Rev.* **57**, 597.

The sun's magnetic field and the diurnal and seasonal variations in cosmic ray intensity

BY L. JÁNOSSY AND P. LOCKETT
Physical Laboratories, University of Manchester

(*Communicated by P. M. S. Blackett, F.R.S.—Received* 19 *November* 1940)

The diurnal and seasonal variations in the vertical cosmic ray intensity, produced by a solar magnetic dipole field, are calculated at latitudes 0 and 45°, and compared with 'observed' data.

It appears that the diurnal variation at latitude 45° can be largely accounted for by assuming the existence of a solar dipole of moment $1 \cdot 1 \times 10^{34}$ gauss cm.^{3}, a value which is consistent with observational evidence. The diurnal variation at the equator, however, cannot be explained by the hypothesis of a solar magnetic dipole field.

The seasonal variation in intensity inferred by the above value for the solar dipole moment is of the same order of magnitude as the observational variation, but shows a phase discrepancy of two months.

I. INTRODUCTION

As a result of measurements of the Zeeman effect in solar spectra, Hale, Seares, Van Maanen and Ellerman (1918) were led to conclude that there exists a permanent magnetic field at the surface of the sun, with distribution such as might be attributed to a uniformly magnetized sphere, and of strength at the equator about 30 gauss. The more recent spectroscopic measurements of Evershed (1939), however, fail to indicate the presence of a magnetic field at the surface of the sun.

If we assume that a magnetic field exists at the surface of the sun, of the form indicated by Hale's observations, it is still doubtful whether this field will extend far beyond the sun. Chapman (1928) shows that a magnetic dipole field proceeding from within the sun will generate electric currents in the sun's ionized atmosphere, which may limit the outward extension of the field.

Thus the existence of a magnetic field, originating within the sun and extending into free space, is uncertain. The presence of such a field would affect cosmic ray phenomena in three main ways. It would produce:

(1) A lower limit in the cosmic ray energy spectrum incident on the earth. This fact was pointed out by Jánossy (1937) and later by Vallarta (1937) as a possible explanation of the latitude 'cut-off' effect.

(2) A diurnal variation in cosmic ray intensity.

(3) A seasonal variation both in the amplitudes and phase of the diurnal variation and in the intensity itself.

The effects (2) and (3) are suitable for comparison with experimental data, and may be used to give evidence about the existence of an extended solar dipole field.

In the following paper we have calculated the amplitude and phase of these two effects and compared the results with experimental data for the diurnal and seasonal variations.

II. THE DIURNAL VARIATION CAUSED BY A SOLAR MAGNETIC FIELD

A. *Brief outline of the theory*

We assume that:

(1) The solar magnetic field can be represented as a dipole field. We take the sun's dipole to be perpendicular to the ecliptic and in the same direction as the earth's dipole.

(2) The incoming cosmic radiation consists of positive and negative particles in approximately equal numbers.

The calculation of the diurnal variation in cosmic ray intensity is based upon the theory of the forbidden cone. This arises out of the general theory of the motion of charged particles in the field of a magnetic dipole, and was first developed by Störmer (1930, 1931, 1934) and later extended by Lemaitre and Vallarta (1933).

Suppose P is a point in the equatorial plane of a dipole (moment M), distant R cm. from the centre of the dipole. Störmer shows that charged particles coming from infinity may approach P only from certain directions, determined by the energy of the particle in the following ways:

If V is greater than a certain energy $V_{\text{max.}}$ given by

$$V_{\text{max.}} = \frac{300M}{R^2},$$

the particles may approach P from any direction.

If V is less than another energy $V_{\text{min.}}$ given by

$$V_{\text{min.}} = \frac{300M}{R^2}(\sqrt{2}-1)^2,$$

the particles are unable to approach P from any direction.

If $V_{\text{min.}} < V < V_{\text{max.}}$ the particles can approach P only from certain directions, all other directions being forbidden. These forbidden directions form a circular cone, with axis perpendicular to the line joining P to the dipole, and angle 2θ given by

$$R^2 \cos\theta = 2R\sqrt{(300M/V)} - 300M/V. \tag{1}$$

Take the point P to be a point on the earth, and consider charged particles approaching the earth. As a result of the sun's magnetic field, for all energies $V_{\text{min.}} < V < V_{\text{max.}}$ there is at the earth a forbidden cone, with axis perpendicular to the direction sun-earth. As a result of the rotation of the earth, to an observer on the earth the forbidden directions appear to move round the earth. This movement leads to the cut out of certain energies at certain times of the day (called by us the forbidden hours), and this produces a daily variation in cosmic ray intensity.

Both the duration and position of the forbidden hours are affected by the presence of the earth's magnetic field, which is superposed on the sun's field. Before the forbidden hours can be calculated, the asymptote to the orbit of the particle in the earth's field must be found. This asymptote is determined by two angles—ϕ_∞, the angle through which the meridian plane containing the particle rotates as the particle passes from remote space to the earth, and n_∞, the inclination of the asymptote to the ecliptic. At the equator these two angles are easily found, but at higher latitudes they can be found only by numerical integration.

In our calculation we have considered only particles which approach the earth vertically, so that the forbidden hours are uniquely determined by the energy and latitude.

The duration of the forbidden hours for any energy depends upon 2θ, the angle of the forbidden cone due to the sun's magnetic field, and also upon n_∞. For particles approaching the earth at the equator, n_∞ is zero and the duration of the forbidden hours is $2\theta/15$ hours, if θ is expressed in degrees. At higher latitudes n_∞ is not zero, and it can be shown that the duration is reduced to a value $2w/15$ hours, where $2w$ is the effective angle of the forbidden cone and is given by

$$\cos w = \cos\theta/\sin n_\infty. \tag{2}$$

The position of the forbidden hours is determined by the angle ϕ_∞ and also by w. We find that for positive particles the forbidden hours extend from $(90-\phi_\infty-w)/15$ to $(90-\phi_\infty+w)/15$ a.m. For negative particles they extend from $(90+\phi_\infty-w)/15$ to $(90+\phi_\infty+w)/15$ p.m.

Using the forbidden hours for different energies the diurnal variation curve can be calculated if we know the primary cosmic ray energy spectrum. We assume the number of particles of energy between E and $E+dE$ to be proportional to $dE/E^{2\cdot8}$. This is the energy spectrum derived by Johnson (1938), using the ionization-depth curves of Bowen, Millikan, Neher and Haynes (1936, 1937). Heitler (1937), gives a similar spectrum.

B. *Calculation of the diurnal variation curve*

We have worked out the daily variation curve for the vertical intensity at latitudes 0 and 45° for two values of M_s, the solar magnetic moment.

(*a*) $M_s = 1\cdot7\times10^{34}$ gauss cm.^{3}. This was the value suggested by Jánossy in his previous work, and corresponds to a latitude 'cut-off' at 50°. The theoretical curves obtained at latitudes 0 and 45° are given in curves (1) and (2).

(*b*) $M_s = 1\cdot1\times10^{34}$ gauss cm.^{3}. This value was chosen so that the daily variation at the equator was zero. That found at latitude 45° is given in curve (3).

In these calculations we have not considered atmospheric absorption. Most of the particles observed at sea level are of secondary origin, largely mesons, and probably the whole diurnal variation at sea level is due to mesons. Since the mode of production of these mesons is still uncertain, it is not possible at present to take atmospheric absorption into quantitative account. We can easily see, however, that the effect of this factor will be to reduce considerably the amplitude of the theoretical daily variation. As similar energies are involved in producing the daily variation and in the latitude effect, the reduction in amplitude which occurs in passing from the top of the atmosphere to sea level will probably be similar in the two cases.

The reduction in the case of the latitude effect is certainly great, for experimental data show that the amplitude of this effect is reduced from 33 to 10 % in passing from 4360 metres to sea level (Compton 1933).

C. *Comparison of the theoretical curves with 'observed' data*

Measurements of the diurnal variation have been made by several observers at different latitudes. Some of the most extensive measurements were made on the Pacific Ocean between 1936 and 1937, by Compton and Turner, who obtained the diurnal variation curves for latitudes from 50° N to 40° S. The results of these measurements and also those of earlier observers have been collected by J. L. Thompson (1938). All observers show a small but definite diurnal variation with a maximum intensity in the neighbourhood of midday.

The phase and general shape of the 'observed' and theoretical curves at the same latitude, should be comparable. We compare them in Table 1.

TABLE 1

M_s	latitude	theoretical curves in	comparison of phase with that of corresponding 'observed' curve
$1\cdot7 \times 10^{34}$ gauss cm.^{3}	0	curve (1)	Phase in contradiction
	45°	curve (2)	Phase in agreement
$1\cdot1 \times 10^{34}$ gauss cm.^{3}	0	—	No theoretical effect
	45°	curve (3)	Phase in agreement

We found that with $M_s = 1\cdot7 \times 10^{34}$ gauss cm.^{3} the phase of the theoretical curve at the equator is in direct contradiction with that of the experimental curve. As a result we decided that this value of magnetic moment is unlikely and that $M_s = 1\cdot1 \times 10^{34}$ gauss cm.^{3}; which is such that the effect at the equator is zero, is a more probable value for the solar dipole moment. This value of M_s leads to a field of about 30 gauss at the surface of the sun, which is consistent with Hale's measurements. In addition the latitude 'cut-off' which it produces (at about latitude 54°) is quite compatible with experimental data (Compton and Turner 1937).

With this value of M_s, the phase of the theoretical curve agrees with that of the 'observed' curve. No exact agreement in the shape of the 'observed' and theoretical curves could be expected because:

(1) We have not considered atmospheric absorption.

(2) The shape of the 'observed' curve is probably due in part to the cosmic ray temperature effect (Blackett 1938). This effect will probably produce a diurnal variation opposite to that observed; it is likely to give rise to a midday minimum.

(3) The 'observed' curves all refer to the total intensity from all directions, whereas the theoretical curves refer to the vertical intensity only. We can easily see that if the resultant intensity from all directions is considered, the theoretical curve will be modified, the minimum will be less abrupt, and the maximum more localized, which will give better agreement with the 'observed' curve.

For the same three reasons the amplitude of the theoretical curve will be very much greater than that of the 'observed' curve.

D. *Conclusion*

As far as our theoretical curve and the 'observed' curve are comparable, it seems that the daily variation at latitude 45° can qualitatively be largely accounted for by the hypothesis of a solar magnetic field. This is in agreement with the calculations which have recently been made by Vallarta and Godart (1939).

The daily variation at the equator, however, cannot be accounted for by this hypothesis. Vallarta and Godart (1939) show that a possible explanation of the effect at low latitudes is the change of ionization of the ionosphere.

III. THE SEASONAL VARIATION

A. *In the diurnal variation in intensity*

In the above calculations we have neglected the inclination of the earth's axis to the normal to the ecliptic. This inclination produces a seasonal variation of six-month period in the diurnal variation in intensity, for the effective angle of the forbidden cone of the sun depends upon the relative orientations of the earth's axis, and that of the forbidden cone.

We find that in summer and winter the effective angle is exactly as in section II. A (i.e. it is given by formula (2)), but in autumn and spring, it is given by (3) and (4) below.

Autumn:

$$\sin n_\infty \cos w = \cos\theta \cos i - \tan i(\cos n_\infty - \cos\theta \sin i). \tag{3}$$

Spring:

$$\sin n_\infty \cos w = \cos\theta \cos i + \tan i(\cos n_\infty + \cos\theta \sin i). \tag{4}$$

[i = inclination of the earth's axis to the normal to the ecliptic.]

Using the above values of w we have calculated the diurnal variation curves in autumn and spring (see curve (4)). We find that the amplitude of the diurnal variation is least in autumn and spring and greatest in summer and winter (curve (3)), the variation in amplitude being about 8 %. Also the position of the minimum varies slightly with season from one hour before midnight in spring to one hour after midnight in autumn.

Observational evidence for such a seasonal effect is as yet lacking, possibly because the smallness of the actual diurnal variation makes any small seasonal fluctuation in it very difficult to detect.

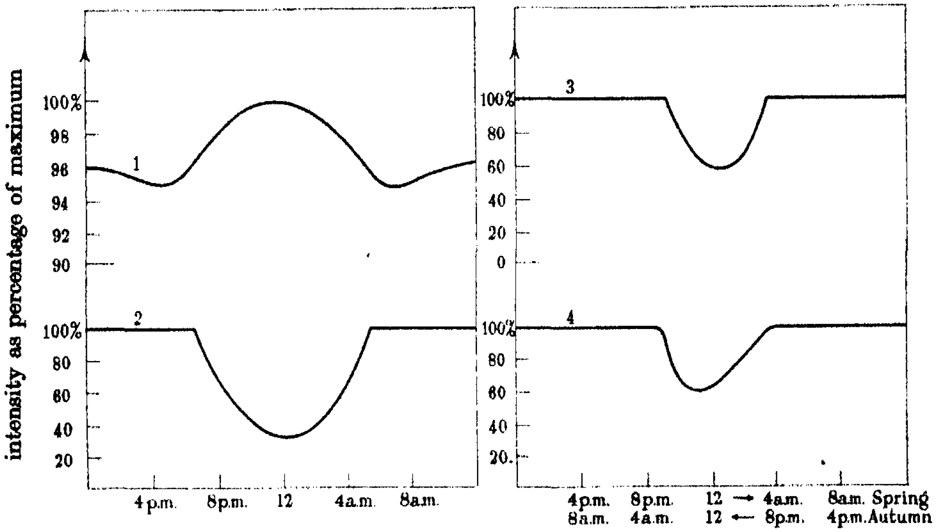

FIGURE 1. Diurnal variation. Curve 1, at equator; curve 2, at latitude 45°; curve 3, at latitude 45°, summer and winter; curve 4, at latitude 45°, autumn and spring. In curves 1 and 2. M_s is assumed equal to $1\cdot7 \times 10^{34}$ gauss cm.^{3}, in curves 3 and 4 to $1\cdot1 \times 10^{34}$ gauss cm.^{3}.

B. *In the intensity itself*

The unaffected daytime intensity has the same value in the curves (3) and (4). This means that the daily mean cosmic ray intensity must vary with season. At latitude 45°, it will be greatest in March and September and least in June and December. Also the amplitude of this theoretical variation will be about 1 %.

The observational data given by different observers for this effect are not very consistent. Some of the most complete observations have recently been made by Gill (1939). From his data we should expect, at 45°, a seasonal variation of amplitude 0·5 % with maximum intensity in May and November.

Thus the amplitude of the variation predicted by our theory is compatible with experimental data, but the phase differs by two months.

This phase discrepancy may possibly be accounted for by the cosmic ray temperature effect (Blackett, 1938).

It is interesting to note that other possible explanations of the seasonal effect, considered by Vallarta (1939), give a three-month phase discrepancy with the 'observed' curves.

APPENDIX*

The solar daily variation of cosmic ray intensity at sea level, though now well established, is very small, only ± 0·2 %; it appears to consist of a simple diurnal sine-wave. Between 25° S and 55° N latitude both the amplitude and phase are found to be approximately independent of the latitude (Wollan, 1939); the local time of maximum according to Forbush (1937) is 11 a.m. Vallarta and Godart (1939), like the authors of the present paper, have considered whether the heliomagnetic field can account for the observed daily variation; an important element in their theory (not referred to in the present paper) is the ratio of the numbers of the positively and negatively charged primary cosmic rays. By a suitable choice of this ratio they obtain calculated values of the amplitude and phase of the daily variation, which are in good agreement with the measurements for latitudes greater than 40°; for lower latitudes they find that the influence of the sun's field becomes negligible, and they seek the cause of the daily variation in those latitudes in the changes of ionization in the ionosphere. On general grounds, however, it does not seem likely that a phenomenon whose geographical distribution is very simple is caused by two totally different agencies, one heliomagnetic and the other geomagnetic, whose effects combine so smoothly to give no variation with latitude over the critical region (40°). This general argument bears also on the discussion in the present paper. It seems more likely that the average daily variation is due to one main cause. According to Wollan, Gunn has suggested that this is probably the daily variation of the geomagnetic field.

The calculation of the heliomagnetic effects for two different values of the heliomagnetic moment is of much interest; but the existing state of our knowledge of the general heliomagnetic field is compatible with much lower values of the effective dipole moment M_s (for phenomena well outside the sun), owing to the possible radial limitation of the sun's field, and its non-dipolar character at the surface of the sun. But if the value of M_s is taken to be appreciably smaller than that assumed in the present paper, no diurnal variation would result at sea level, as for such values of M_s the particles affected cannot penetrate the earth's atmosphere.

---

* Added by a referee, with the consent of the authors.

According to the theory in the present paper, the daily variation of cosmic ray intensity due to the heliomagnetic field is of a definite type, consisting of a night-time depression in a curve which for the greater part of the day is horizontal (cf. curves 2–4). When harmonically analysed, such a curve would have higher harmonic components not all negligible compared with the first and having definite amplitude and phase relations to the first (diurnal) component. The data, as discussed by Thompson (1938), do not agree with this expectation, but an agreement can hardly be expected since the present paper deals with the vertical intensity only and the variation of the intensities in inclined directions will certainly alter the shape of the total variation.

REFERENCES

Bartels 1935 *Terr. Mag.* **40**, 1.
Blackett 1938 *Phys. Rev.* **54**, 973.
Bowen, Millikan and Neher 1937 *Phys. Rev.* **52**, 80.
Chapman 1928 *Mon. Not. R. Astr. Soc.* **139**, 57.
Compton 1933 *Phys. Rev.* **43**, 387.
Compton and Turner 1937 *Phys. Rev.* **52**, 802.
Evershed 1939 *Mon. Not. R. Astr. Soc.* **99**, 438.
Forbush 1937 *Terr. Mag.* **42**, 1.
Gill 1939 *Phys. Rev.* **55**, 429.
Hale, Seares, Van Maanen, and Ellerman 1918 *Astrophys. J.* **47**, 206.
Heitler 1937 *Proc. Roy. Soc.* A, **161**, 261.
Lemaitre and Vallarta 1933 *Phys. Rev.* **43**, 87.
Jánossy 1937 *Z. Phys.* **104**, 430.
Johnson 1938 *Phys. Rev.* **53**, 499.
Millikan, Neher and Haynes 1936 *Phys. Rev.* **50**, 992.
Störmer 1930 *Z. Astrophys.* **1**, 237.
Störmer 1931 *Terr. Magn. Atmos. Elect.* **3**, 31.
Störmer 1934 *Publ. Univ. Obs. Oslo*, No. 10.
Thompson 1938 *Phys. Rev.* **54**, 93.
Vallarta 1937 *Nature, Lond.*, **139**, 839.
Vallarta 1938 *An outline of the theory of the allowed cone.* Univ. Toronto Press.
Vallarta and Godart 1939 *Rev. Mod. Phys.* **11**, 180.
Wollan 1939 *Rev. Mod. Phys.* **11**, 160.

The flame spectrum of carbon monoxide

II. Application to 'afterburning'

By A. G. Gaydon, Ph.D., A.Inst.P., *Leverhulme Research Fellow*
Chemical Technology Department, Imperial College, London, S.W. 7

(*Communicated by A. C. G. Egerton, Sec.R.S.—Received* 29 *November* 1940)

In a previous paper it has been shown, from a study of the spectrum of the carbon monoxide flame, that the molecules of CO_2 formed by the combustion are initially in a highly excited state of internal vibration. An attempt is made here to derive approximate values for the lifetimes of these vibrationally activated molecules.

The orders of magnitude of the radiative lifetime for the three types of vibration are derived. From data obtained from supersonic dispersion in CO_2 the relaxation times, or collision lifetimes, are discussed with especial emphasis on the effect of moisture on the collision-life of the activated molecules. A section is also devoted to the possibility of the close resonance between the vibrations ν_1 and ν_2 of CO_2 resulting in a high percentage of dissociation after the combustion of the dry gas.

The results give a good interpretation of the experiments of Garner and colleagues on the marked effect of moisture and other catalysts on the infra-red emission of the flame, and the general failure to observe a strong emission band at $14{\cdot}9\,\mu$. The results of the theory go far towards explaining the latent energy of the combustion observed by David and colleagues.

The lifetime of the activated molecules is calculated to be not more than a few tenths of a second, but dissociation and recombination processes might lengthen this time. For moist gases the lifetime will be very much less, and the infra-red radiation from the flame and the latent energy of the products should similarly be much reduced, in agreement with experiment. The vibrationally activated molecules are to be regarded as essentially normal molecules of CO_2 in which the vibrational energy has not had time to reach equipartition with the energy in other degrees of freedom; spectroscopically there is no evidence to show that they are electronically excited or peculiar in any other way.

Experiments on the absorption spectrum of a long length of burning gas show strong absorption due to hot oxygen, this being particularly marked when the gases are dry. This is interpreted as being due to transfer of the vibrational energy from the CO_2 to the O_2 molecules, the absorption spectrum of which is thereby shifted to longer wave-lengths.

INTRODUCTION

In a recent paper (Gaydon 1940) the spectrum of the flame of carbon monoxide burning in air or oxygen has been described, and new measurements and an attempt at a partial analysis of the spectrum were presented. It was concluded that the visible and ultra-violet emission spectrum of the flame was probably due to molecules of carbon dioxide undergoing an electronic transition to the ground electronic state, and that after this transition the CO_2 molecules would be left with a considerable amount of vibrational energy, due to the change of shape or size of the molecule during the transition, and that this vibrational energy might persist for some time before thermal equilibrium with the other degrees of freedom was attained.

It is the purpose of the present paper to describe some additional experimental work in which the absorption spectrum of a long length of the flame has been examined, and then to discuss the bearing of the conclusions reached in the first paper on the phenomenon of 'afterburning' which is often so marked in the combustion of carbon monoxide. This also involves a discussion of the infra-red radiation from the carbon monoxide flame, and reference to relaxation times obtained from supersonic measurements in carbon dioxide.

A detailed understanding of the cause of the apparent 'afterburning' of carbon monoxide is of interest because of the effect of this afterburning on the efficiency of the combustion and its relation to the completeness of combustion and amount of unburnt carbon monoxide discharged into the atmosphere from the internal combustion engine and from gas flames. If the afterburning is not a real phenomenon, as thought probable by Lewis and von Elbe (1934), but is only due to pockets of unburnt gas and necessary pressure and temperature changes in the combustion vessel, then technical improvements in the design of burners and combustion chambers might eliminate the trouble. If, however, as believed by David and colleagues, there is a real activation of the molecules formed in the combustion, then such methods cannot be expected to give complete success, and chemical or physical expedients must be sought.

ABSORPTION SPECTRUM OF THE FLAME

It was postulated in the previous paper that, after the combustion, the CO_2 molecules formed would be in the ground electronic state but in high vibrational levels of this state. If this postulate were correct and the CO_2 molecules persisted for some while in these high vibrational levels, then it might be possible to observe absorption therefrom, and this absorption might be expected to lie to longer wave-lengths than the normal absorption by cold CO_2. The main absorption bands of CO_2 are in the extreme ultra-violet below 1150 A, but there is a weaker system which can be extended to 1700 A at high pressure (Price and Simpson 1938). Any considerable extension of this system should bring it within the range of quartz instruments.

It is known that a simple carbon monoxide-air flame at an ordinary jet does not absorb in the quartz region, and hence it was decided to investigate the absorption spectrum of a longer length of burning gas and its freshly formed combustion products.

The combustion occurred in a silica tube 60 cm. long and 1·5 cm. internal diameter as shown in figure 1. Carbon monoxide and oxygen from cylinders were fed in at three and two side tubes respectively. The relative flows of the gases were recorded with two flowmeters. No special precautions were taken to purify the gases apart from drying (see later). Patches of flame were localized at four places indicated by shading in the figure, and the tube was heated to a bright red at these places. During some of the experiments the tube was lagged by wrapping with asbestos cord. A powerful hydrogen discharge tube of the type described by Hunter and Pearse (1936) was used as a source of continuum and spectrograms were taken on a small quartz instrument and on a medium size (Hilger E. 2) quartz spectrograph using special ultra-violet sensitive plates. The small instrument allowed the spectrum to be studied as far as the limit of transparency of air (around 1950 A), but the E. 2 was limited to wave-lengths greater than 2100 A by the geometrical design. The absorption spectrum was studied by viewing the tube end-on, an approximately parallel beam of light between two quartz lenses being used.

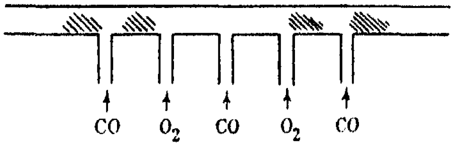

FIGURE 1

The absorption was found to consist of an apparently complex band system, with partially resolved rotational structure, at the short wave-length end of the region studied. Using a very fast flow of dried gases the absorption extended to nearly 2600 A. It was at first thought that the system was of the same type as the CO flame emission bands, but closer inspection revealed that the band system was part of the Schumann-Runge system of oxygen, which extends into the quartz region when absorption is observed through heated oxygen. The apparent complexity is due to the long rotational branches caused by the high temperature and to the bands being so strongly degraded to the red.

This absorption seemed qualitatively rather stronger than might have been expected from a consideration of the temperature and length of absorbing column of hot oxygen, and its interest is increased by the marked effect of moisture on the intensity of the absorption. When the gases were dried by passing through long tubes filled with phosphorus pentoxide, the absorption was markedly stronger than when using the same flows of undried or deliberately moistened gases. It may be noted here that David (see later references and discussion) has recorded that there is a definite rise of temperature when a trace of moisture is present, and therefore the oxygen might have been expected to be hotter and to absorb more, not less, strongly when moist. It seems that this absorption by oxygen, which of course occurs from high vibrational levels of the ground electronic state of O_2, is stimulated in some special way by the combustion and is not entirely due to temperature effects. The vibrationally excited CO_2 molecules, whose absorption spectrum lies farther to the ultra-violet than that of oxygen and is therefore masked, presumably are able to pass some of their vibrational energy on to the oxygen molecules by collision, and thus these acquire a high vibrational temperature resulting in the observation of strong absorption by these molecules.

THE AFTERBURNING AND LATENT ENERGY OF COMBUSTION OF CARBON MONOXIDE

It is well known that the combustion of carbon monoxide is usually incomplete immediately after the explosion wave has travelled through the gases. David, Brown and El Din (1932) have shown, from studies of the maximum pressure reached during explosions in closed vessels of various sizes, that combustion is not complete at the moment that maximum pressure is reached. Ellis and Wheeler (1927) and Ellis and Morgan (1934) note the afterburning, and record that the temperature continues to rise after the flame front has passed through the gases, indicating that the combustion processes are not complete. Lewis and von Elbe (1934) have criticized these papers and conclude that afterburning is not a real phenomenon, and is only a manifestation of the pressure and temperature changes which are bound to occur following an explosion in a closed vessel, and that David, Brown and El Din's results may be due partly to pockets of unburnt gas. Lewis and von Elbe support their criticism by experiments on explosions of oxygen and hydrogen. For oxygen-hydrogen mixtures evidence for afterburning is certainly not conclusive, but for carbon monoxide, which when pure and dry shows a remarkable reluctance to burn quickly or to completion, the existence of some form of afterburning seems to be fairly well established. Photographs of CO-O_2 explosions by Bone, Fraser and

Winter (1927) and others show a very marked increase in luminosity in the centre of the vessel as the pressure wave travels back after the explosion, and Prof. Egerton has suggested that this is probably connected with the internal energy of the CO_2 molecules. Withrow and Rassweiler (1931) and Rassweiler and Withrow (1932) have studied the afterburning in the internal combustion engine and have obtained good spectrograms showing that the emission spectrum is identical with that of the carbon monoxide flame, and therefore presumably due to molecules of CO_2. David (1936, 1937*a*, 1937*b*) and David and Pugh (1937, 1940) from comparison of measured and calculated flame temperatures have concluded that there is a considerable amount of latent energy which is not immediately released by the combustion and which is attributed to long-lived metastable molecules formed in the flame front. This latent energy varies from 1 % to 28 % and is most marked in flames of dry carbon monoxide, but is greatly reduced by the presence of a trace of water vapour which, while lowering the theoretical flame temperature, is found in practice to result in a marked rise of temperature. For the internal combustion engine the latent energy is less, being variously given as from 1 % to 4 %. It will also be noted later, in discussing the infra-red radiation, that Garner and colleagues also obtain independent evidence for this activation of the newly formed CO_2 molecules.

INFRA-RED RADIATION

The infra-red radiation from a carbon monoxide flame consists principally of a very intense band at $4{\cdot}4\mu$ and another rather less intense at $2{\cdot}8\mu$. These bands have been identified with the infra-red absorption bands of CO_2 at $4{\cdot}25\mu$ (corresponding to the fundamental asymmetrical valence vibration $\nu_3 = 2350\,\text{cm.}^{-1}$) and $2{\cdot}7\mu$ (corresponding to the sum of the combination bands $\nu_3+\nu_1$ and $\nu_3+2\nu_2$). The other active fundamental of CO_2, the transverse vibration $\nu_2 = 667\,\text{cm.}^{-1}$, shows strong absorption at $14{\cdot}9\mu$, but there is no satisfactory record of this having been obtained in emission, which at first sight is very surprising. Rubens and Aschkinass (1898) studied CO_2 to 20μ and observed the absorption band (at $14{\cdot}7\mu$) and record emission at $14{\cdot}1\mu$, but the identity of this with the absorption is uncertain. Bailey and Lih (1929) failed to observe a band in emission in this region but state that this failure may be due to a thin film of collodion on their prism; Garner and Johnson (1927) also studied this region without observing any emission band and say that the sensitivity of their instrument was such that an intensity of one fiftieth of that of the band at $4{\cdot}4\mu$ would have been sufficient for detection.

The infra-red emission from flames and explosions of carbon monoxide has been the subject of exhaustive study by Garner and colleagues (Garner, Johnson and Saunders 1926; Garner and Johnson 1928) who record that the emission is greatly reduced by the addition of certain catalysts, such as water or ethyl nitrate, although the flame temperature is increased by this addition. For the pure gas (Garner, Hall and Harvey 1931) the CO_2 molecules produced by the combustion are believed to contain a large fraction of the total energy of the combustion. This forms at least 24 % of the total energy set free. These molecules are, they say, very stable towards collisions, but can lose their energy either by the emission of radiation or by resonance to other molecules of CO_2. As a result of resonance the activated molecules possess an appreciably longer duration of life.

LIFETIME OF VIBRATIONALLY ACTIVATED MOLECULES

It has been pointed out in the first paper that there is reason to believe that immediately after the initial combustion process and accompanying electronic rearrangement, the CO_2 molecules so formed will be in a vibrationally activated state. It would be of great interest if some estimate of the average lifetime of such activated molecules could be obtained. Loss of vibrational energy can occur either by radiation, with emission of the characteristic infra-red bands of CO_2, or by transfer of the energy to other degrees of freedom by collision with other molecules. For CO_2 there are three fundamental vibrational frequencies and these three types of vibration will probably have different lifetimes. It is probable that all three will be excited fairly highly during the electronic transition, but, if the tentative hypothesis put forward in the earlier paper that the excited electronic state is triangular is correct, then the transverse vibration ν_2 may be the most strongly activated.

It is possible, in theory, to calculate the radiative lifetime for any vibration from a quantitative knowledge of the absorption coefficient of the gas for the particular infra-red vibration band. This calculation is based on the Einstein derivation of the Planck radiation law and the method has been given in detail by Tolman (1924). The calculation involves a knowledge, from experimental data, of $\int_0^\infty \alpha . d\nu$, α being the absorption coefficient and ν the frequency. Unfortunately the resolving power and purity of spectrographs used for the infra-red is insufficient to resolve the structure of the bands fully, the natural line width of the rotational structure being less than the instrumental width; thus the lines are observed as broader and less intense than is really the case, and the value determined for $\int \alpha . d\nu$ will almost invariably be too low; this is shown by the fact that the observed absorption does not vary linearly with the thickness and density of the absorbing gas. Approximate calculations have, however, been made using the experimental data of Martin and Barker* (1932). These calculations are based on a number of assumptions and approximations and should only be regarded as giving a rough value for the radiative lifetime; any increase in the value for $\int \alpha . d\nu$ such as might be observed by the use of a spectrograph of still higher resolving power would decrease the calculated lifetime.

For the asymmetric vibration ν_3, which corresponds to the $4{\cdot}4\mu$ band, a figure of the order 0·01 sec. has been obtained for the upper limit for the

---

* Martin and Barker show curves of deflexion (proportional to light intensity) against wave-length. These curves were measured up, and, assuming a base line passing through the points of maximum deflexion to give the deflexion corresponding to light from the source without absorption, a new curve between wave-number (reciprocal of the wave-length) and absorption coefficient ($-\log_e$ of the transmission) was plotted. This was done for all the curves given, those corresponding to various stated equivalent thicknesses of absorbing gas. From the area under each of these curves for the whole band the value of $\int_0^\infty \alpha . d\nu$ was obtained directly as the product of this area and the velocity of light (to reduce the wave-numbers to frequencies). The values of $\int_0^\infty \alpha . d\nu$ were then inserted in Tolman's formula

$$A_{21} = \frac{8\pi\nu^2}{c^2 N_1} \frac{\rho_1}{\rho_2} \int_0^\infty \alpha . d\nu,$$

where

A_{21} = chance per sec. of molecules radiating = 1/radiative life,
ν = frequency,
ρ_1 and ρ_2 a priori probabilities of initial and final states,
N_1 = no. mol. per unit vol. in initial state (i.e. for absorption for the cold gas, the lowest state).

The following assumptions were made:

$N_1 = 2{\cdot}7 \times 10^{19} \times$ equivalent thickness of absorbing gas in cm., i.e. practically all the molecules are in the lowest state at the temperature of the measurements.

$\rho_1/\rho_2 = 1$. This is probably not strictly correct, but is unlikely to be in error by more than a factor of 2.

The several curves gave values of A_{21} which were not, as they should be, the same, but which in practice decreased somewhat with increasing equivalent thickness of gas, owing to inadequate resolving power of the instrument. A rough extrapolation to zero equivalent thickness of absorbing gas was made, and this was taken as the value of A_{21} from which the value of the radiative lifetime ($1/A_{21}$) used in the following discussion was calculated.

average time for the transition from $v_3 = 1$ to $v_3 = 0$. The lifetime for transitions involving unit decrease in vibrational quantum number for more highly excited molecules (e.g. $v_3 = 10$ to $v_3 = 9$) may be a little longer, and the total time for radiation of the energy stored in the asymmetric vibration, which would mostly be radiated in successive steps in which the vibrational quantum number decreased a unit at a time, might amount to a few tenths of a second at the most.

For the transverse vibration ν_2 corresponding to the absorption band at $14 \cdot 9\mu$, a similar calculation gives a lifetime not exceeding 0·2 sec. for the transition $v_2 = 1$ to $v_2 = 0$.

The symmetrical valence vibration ν_1 is of course inactive in the infra-red and does not emit any radiation corresponding to the fundamental frequency itself. Some energy may be lost by radiation of the combination band $\nu_3 + \nu_1$ at $2 \cdot 8\mu$. No exact calculation of the lifetime has been made, but it may be assumed that the radiative lifetime for this vibration is relatively long.

The order of the lifetime of vibrationally excited CO_2 molecules can also be obtained from supersonic dispersion and absorption.* The relaxation time calculated from these supersonic measurements corresponds to the time for the vibrational energy to be transferred to translational and rotational energy by collision. The results obtained by this method are mostly for atmospheric temperature and pressure, although Eucken and Nümann (1937) have studied CO_2 at 673° K at which temperature the relaxation time is given as $2 \cdot 0 \times 10^{-6}$ compared with $7 \cdot 0 \times 10^{-6}$ sec. at 293° K. The relaxation time corresponds to transitions between $v = 1$ and $v = 0$, and the time lag for vibrational energy transfer at high temperatures and for highly excited molecules may be rather different; the vibrational energy will not be transferred at a single collision but in successive small steps, the highly excited molecules quickly losing some of their energy but with the final steps taking a time similar to that derived from the supersonic determinations. The absorption of sound and the supersonic dispersion of carbon dioxide are greatly affected by trace impurities, especially water vapour, and several authors have studied the effect of moisture quantitatively.

* Other methods, such as resonance fluorescence and molecular recombination rates, give information about the transfer of vibrational energy on collision, and the results from these methods are often at variance with the value of the relaxation time from supersonic measurements. For CO_2 the only numerical data are for the relaxation time. The resonance fluorescence method, as pointed out by Dwyer (1939) who has obtained direct evidence for the persistence of vibrational energy in I_2, only gives values for the electronically excited gas. The recombination method also appears to involve three-body collisions, which will have a different probability of producing energy transfer from the two-body collisions necessary for supersonic dispersion and combustion phenomena.

The main sound-absorption peak corresponds to the time lag in transfer of energy to and from the transverse vibration ν_2. For pure CO_2 the relaxation time has been determined by several investigators, who concur in giving a value of around 5×10^{-6} sec. at room temperature. According to Eucken and Becker (1934) the vibrational energy will only be converted into other forms for one collision in 51,000 for pure CO_2, but one collision in 34 with a water molecule is effective in producing transfer; a concentration of 3 % of water vapour reduces the relaxation time from $5{\cdot}7 \times 10^{-6}$ sec. to $0{\cdot}09 \times 10^{-6}$ sec.

The symmetrical valence vibration ν_1, having a higher frequency than ν_2, contributes less to the specific heat of the gas and has a less marked effect on the sound absorption and dispersion. On classical grounds the symmetrical vibration would be expected to transfer its energy by collision much less easily than does the transverse vibration, but Eucken and Nümann (1937) have expressed the opinion that the symmetrical vibration is excited as easily as the transverse vibration, not because of the equality of sensitiveness to impact but because of the very rapid adjustment of equilibrium of the energy in the two forms of vibration (see later section on dissociation). Recently Pielemeier, Saxton and Telfair (1940) have observed a shelf on the sound absorption-frequency curve which they interpret as corresponding to ν_1, the relaxation time for which may therefore be a little longer than for ν_2; also it appears that the transfer of energy from this form of vibration is rather less dependent on the presence of moisture.

The asymmetric valence vibration ν_3 has such a high frequency that it contributes very little to the specific heat at room temperature and does not therefore produce dispersion or absorption of sound. The collision lifetime of this vibration should be longer than for the transverse vibration.

We may now compare the radiative and collision lives of CO_2 molecules for the three types of vibration.

The transverse vibration ν_2 has a collision life of 5×10^{-6} sec. against a radiative lifetime of rather less than 0·2 sec. Thus energy initially stored in this form of vibration will be transferred to other degrees of freedom by collision before there is time for any appreciable radiation of the characteristic infra-red band at $14{\cdot}9\mu$. This explains the failure of Garner and Johnson and others to observe this radiation from the flame, a result which at first sight seemed rather surprising.

For the asymmetric vibration ν_3 the radiative lifetime has been calculated to be rather less than 0·01 sec.; we have no definite knowledge of the relaxation time for this mode of vibration. It is known from the work of Garner and colleagues that a flame of carefully dried carbon monoxide does radiate the infra-red band at 4·4μ very strongly (up to 24 % of the total energy of the combustion). Thus experimentally the collision life, in pure CO_2, must be longer than the radiative lifetime. Also from Garner's work we know that the radiation at 4·4μ is very much less if the gas is slightly moist or if other catalyst is added. Thus it may be assumed that for this vibration also the relaxation time (or collision life) is greatly reduced by the presence of moisture and so the vibrational energy is lost by collision with water molecules rather than by radiation.

The symmetrical vibration ν_1 has a relaxation time of around 10^{-5} sec., and since this vibration is inactive in the infra-red the energy is of course lost principally by collision (perhaps after transfer to the transverse form of vibration). The combination band $\nu_3+\nu_1$ and $\nu_3+2\nu_2$ at 2·8μ does emit some radiation and it is interesting to note that Garner and Johnson found that this band was less sensitive to the presence of water than the other band; this may be linked with the less marked effect of moisture on the relaxation time for ν_1 recorded by Pielemeier, Saxton and Telfair.

The above deductions may be summarized as follows. For the combustion of pure dry carbon monoxide the energy stored in the asymmetric valence vibration is lost mostly by radiation in a time of not more than a few tenths of a second, while the energy in the other two vibrations will be transferred to other degrees of freedom (heat energy) in a time of the order 10^{-4} sec. In the presence of moisture or other catalyst the vibrational energy of all forms will mostly be transferred by collision in a very much shorter time. These conclusions may require some revision if, as suggested in the next section, there is much dissociation and recombination, which would lengthen the apparent life of the activated molecules.

DISSOCIATION

It has been suggested by Rosen (1933) that for molecules with more than one vibrational degree of freedom there is a possibility of resonance between the vibrations resulting in a transfer of energy from one form of vibration to another, and if the total energy of the vibrations exceeds the dissociation energy of any one form there will be a chance that the molecule will dissociate spontaneously. Rosen makes an attempt to evaluate this chance quantitatively in a specific case by making a number of simplifying assumptions. Rice (1933) has commented on details of this treatment, but accepts the main conclusion that in certain cases there will be a finite chance of dissociation before the molecule can lose its vibrational energy by collision.

Rosen points out that any degeneracy, such as does in fact occur for CO_2 where $\nu_1 = 2\nu_2$ very exactly (Dennison 1932), will greatly increase this effect.

Thus if the vibrationally activated molecules of CO_2 formed by the combustion are not quickly de-activated by collision with molecules of water or other catalyst, then many of the molecules will dissociate again. This agrees with the observation that the combustion of pure carbon monoxide is always far from complete, only 80 % to 90 % being burnt if the gas is dried carefully. As an alternative viewpoint of the same effect it may be seen that if the molecules are vibrationally activated so that they are not in thermal equilibrium then a greater amount of dissociation may be expected than would occur for thermal equilibrium at that temperature, i.e. the vibrational temperature which determines the amount of dissociation will be much higher than the recorded temperature of the flame.

CONCLUSIONS

It is now possible to weld together the various deductions and observations given in the previous rather disconnected sections and in the previous paper, to form a general picture of the later stages of the combustion processes as a whole.

It seems that in the formation of a molecule of CO_2 from carbon monoxide and oxygen, since the carbon atom in the CO_2 molecule is not in its lowest electronic state, there must be an electronic rearrangement in the newly formed molecule. This rearrangement may occur either by the emission of radiation, giving the well-known flame spectrum, or more frequently on collision. In either case, since there is reason to believe, from a study of the spectrum, that the equilibrium size or shape of the molecule is very different in the two electronic states, a large part of the energy will be left as internal vibrational energy of the molecule when it reaches the ground electronic state. This vibrational energy will, in the pure gas, persist for an appreciable fraction of a second, during which the hot gases will not be in thermal equilibrium and will therefore be below the theoretical maximum temperature of the combustion (in agreement with David's observations). They will lose some of their energy by infra-red radiation of wave-length $4{\cdot}4\mu$, will suffer a considerable amount of dissociation (resulting in apparent incompleteness of the combustion) and may pass some of their vibrational energy on to other molecules such as nitrogen or oxygen (as observed in the absorption spectrum of the flame of the dry gas). When combustion occurs in the presence of a catalyst the excess vibrational energy of the newly formed CO_2 molecules will be quickly passed on to molecules of the catalyst and the infra-red radiation, the amount of dissociation and the vibrational energy transferred to oxygen molecules will all be reduced.

Thus the above discussion seems to account fairly well, at least qualitatively, for the peculiarities of the combustion of carbon monoxide. The long-lived metastable molecules postulated by David to account for the latent energy of the combustion are not of an essentially peculiar structure or type; the absence of absorption in the visible or near ultra-violet by liquid carbon dioxide shows that there are no low-lying electronic levels for this molecule and hence the metastable molecules cannot be electronically excited. The latent energy is merely due to delay in the vibrational energy reaching equipartition with that in other degrees of freedom. To some extent this is probably partly so for the combustion of all substances, but when carbon dioxide is the final product the effect is present to an unusual extent because firstly of the difference in shape or size of the CO_2 molecule in its two electronic states and secondly because of the degeneracy resulting from the almost perfect equality $\nu_1 = 2\nu_2$ for CO_2 which increases the dissociation.

The possibility of the afterburning being due to internal vibrational energy has been mentioned by previous authors. David and Davies (1930) dismiss the possibility because they say that this would not account for the afterburning being of such long duration. Lewis and von Elbe (1935) also refer to the lag in the equipartition of the vibrational energy. No quantitative estimate in the delay in equipartition seems to have been attempted, however, and especially the significance of moisture on the lifetime of vibrationally activated molecules seems to have been overlooked. The dissociation resulting from the degeneracy is also probably important in lengthening the afterburning. The quantitative objections raised by Egerton and Ubbelhode (1934) to David's view that the afterburning is due to metastable molecules will not apply to the above reasoning, as the latent energy, which is about a quarter of the total combustion energy, will, for the dry gas, be radiated in the infra-red in agreement with Garner's observations.

The luminescence of the afterburning is probably due to recombination of molecules which have dissociated after the initial combustion. The strong excitation of the OH radiation in the flame and the afterburning gas is probably associated with the energy acquired by the water molecules on collision which may result in their dissociation and excitation. The afterglow of carbon dioxide in an electric discharge (Fowler and Gaydon 1934) persists longer than does the afterburning due to combustion at atmospheric pressure, which is in agreement with expectations if the phenomenon depends on the collision-life of the activated molecules, which will be longer at reduced pressure.

I wish to express my thanks to Professor A. C. Egerton and Dr D. M. Newitt for their continued interest and helpful suggestions.

REFERENCES

Bailey, C. R. and Lih, K. H. 1929 *Trans. Faraday Soc.* **25**, 29.
Bone, W. A., Fraser, R. P. and Winter, D. A. 1927 *Proc. Roy. Soc.* A, **114**, 402.
David, W. T. 1936 *Phil. Mag.* **21**, 280.
David, W. T. 1937*a*. *Phil. Mag.* **23**, 345.
David, W. T. 1937*b* *Engineering*, **144**, 531.
David, W. T., Brown, J. R. and El Din, A. H. 1932 *Phil. Mag.* **14**, 764.
David, W. T. and Davies, W. 1930 *Phil. Mag.* **9**, 390.
David, W. T. and Pugh, B. 1937 *Nature, Lond.*, **140**, 1098.
David, W. T. and Pugh, B. 1940 *Nature, Lond.*, **145**, 896.
Dennison, D. M. 1932 *Phys. Rev.* **41**, 304.
Dwyer, R. J. 1939 *J. Chem. Phys.* **7**, 40.
Egerton, A. C. and Ubbelhode, A. R. 1934 *Nature, Lond.*, **134**, 848.
Ellis, O. C. and Morgan, E. 1934 *Trans. Faraday Soc.* **30**, 287.
Ellis, O. C. and Wheeler, R. V. 1927 *J. Chem. Soc.* p. 310.
Eucken, A. and Becker, R. 1934 *Z. phys. Chem.* B, **27**, 219.
Eucken, A. and Nümann, E. 1937 *Z. phys. Chem.* B, **36**, 163.
Fowler, A. and Gaydon, A. G. 1934 *Proc. Roy. Soc.* A, **142**, 362.
Garner, W. E., Hall, D. A. and Harvey, F. E. 1931 *J. Chem. Soc.* p. 641.
Garner, W. E. and Johnson, C. H. 1927 *Phil. Mag.* **3**, 97.
Garner, W. E. and Johnson, C. H. 1928 *J. Chem. Soc.* p. 280.
Garner, W. E., Johnson, C. H. and Saunders, S. W. 1926 *Nature, Lond.*, **117**, 790.
Gaydon, A. G. 1940 *Proc. Roy. Soc.* A, **176**, 505.
Hunter, A. and Pearse, R. W. B. 1936 *J. Sci. Instrum.* **13**, 403.
Lewis, B. and von Elbe, G. 1934 *J. Chem. Phys.* **2**, 659.
Lewis, B. and von Elbe, G. 1935 *Phil. Mag.* **20**, 44.
Martin, P. E. and Barker, E. F. 1932 *Phys. Rev.* **41**, 291.
Pielemeier, W. H., Saxton, H. L. and Telfair, D. 1940 *J. Chem. Phys.* **8**, 106.
Price, W. C. and Simpson, D. M. 1938 *Proc. Roy. Soc.* A, **169**, 501.
Rassweiler, G. M. and Withrow, L. 1932 *Industr. Engng Chem.* **24**, 528.
Rice, O. K. 1933 *J. Chem. Phys.* **1**, 625.
Rosen, N. 1933 *J. Chem. Phys.* **1**, 319.
Rubens and Aschkinass 1898 *Astrophys. J.* **8**, 191.
Tolman, R. C. 1924 *Phys. Rev.* **23**, 693.
Withrow, L. and Rassweiler, G. M. 1931 *Industr. Engng Chem.* **23**, 769.

The determination of the vapour-pressure curve of liquid helium below 1·6° K using a magnetic thermometer

By B. Bleaney and R. A. Hull
Clarendon Laboratory, Oxford

(*Communicated by F. A. Lindemann, F.R.S.—Received* 17 *December* 1940)

The vapour-pressure curve of liquid helium below 1·6° K has been determined using the susceptibility of various paramagnetic salts as the thermometer. It is found that the results agree with the theoretical curve recently calculated by Bleaney and Simon to within the experimental error of 0·004° down to 1° K, and differ from the 'scale 1937' of Schmidt and Keesom, e.g. by 0·03° at 1° K.

1. Introduction

The history of the experimental determination of the vapour pressure of helium has been outlined in a recent paper by Bleaney and Simon (1939), where the thermodynamic relations between the vapour pressure and the other physical properties of liquid and gaseous helium are developed explicitly, and it is shown that the most recent measurements of vapour pressure (Schmidt and Keesom 1937, afterwards referred to as 'scale 1937') do not obey these relations below 1·6° K. Then, starting from these relations, a new scale was calculated, scale 1939, and the present paper records some experimental tests of this scale.

The Leiden measurements have been carried out with a constant-volume gas thermometer, for which the only available gas is helium itself, and the pressure in the gas thermometer must therefore be less than the vapour pressure. At the lowest temperatures this means the use of a pressure so small that its measurement is inherently difficult and involves several appreciable corrections. It is desirable to find some other type of thermometer that preserves its accuracy as the temperature is lowered.

At temperatures in the region below 1° K, attained by the method of adiabatic demagnetization of a paramagnetic salt, the simplest thermometric property to measure is the susceptibility of the salt, and hence the 'magnetic thermometer' has been developed. A temperature scale T^* has been defined by assuming that the susceptibility of a spherical sample (following Kurti and Simon 1938) is inversely proportional to the temperature, according to Curie's law. As the thermometric sensitivity of a salt which obeys Curie's law is proportional to the inverse square of the temperature, the magnetic thermometer is particularly suitable for use at low temperatures. It is true that at the lowest temperatures this Curie scale can no longer hold good: but with salts whose 'characteristic temperature' is of the order of a few hundredths of a degree, the deviation is very small at 1° K and can be calculated as will be shown later.

The salts we used were manganese ammonium sulphate and potassium chrome alum. The latter has a volume susceptibility only one-third of the former, and its sensitivity as a thermometer is proportionately smaller; on the other hand, the deviations from Curie's law are much smaller and can be accurately calculated from the measurements of Casimir, de Haas and de Klerk (1939) and of one of us (Bleaney, unpublished).

At 1° K a 1 % change in vapour pressure corresponds to a 0·1 % change in temperature; these were the accuracies aimed at in the measurement of pressure and temperature.

2. The apparatus

The apparatus resembled closely that commonly used in this laboratory for experiments with the magnetic method. A supply of liquid helium was obtained in a Simon expansion liquefier, and below this was the experimental vessel consisting of a helium bath in which the paramagnetic sample was immersed. This vessel was made of glass to avoid supraconductive disturbances, and is shown in figure 1. Its temperature was controlled by pumping continuously through tube A, and the vapour pressure was measured through tube B, which dipped below the surface of the bath. These tubes were connected to the metal liquefier by platinum-glass seals. Tube A had an internal diameter of 6 mm. with a 1 mm. constriction at the bottom. The latter followed the procedure devised by Cooke and Hull (1939) for reducing the abnormal evaporation caused by the creeping film of He II, and thus attaining the lowest possible temperature. There is also, of course, a similar film in tube B, which means that the temperature can never be as low as in experiments where there is only one tube in connexion with the bath. In fact 0·94° was reached when tube B had diameter 0·76 mm. and 1·0° when B had diameter 2·2 mm.

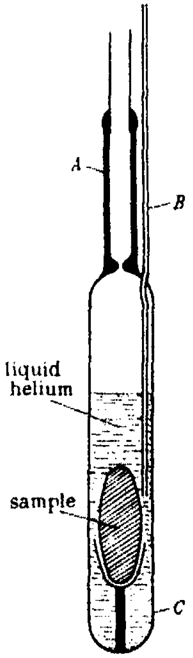

FIGURE 1

The sample of paramagnetic salt was of fine powder compressed to the shape of a 4 : 1 ellipsoid. It rested in an egg-shaped cup of glass sealed into the glass vessel. To insert the sample, the vessel shown in figure 1, at present in two halves, was turned upside down, the sample put in and then the glass seal made at the point C. The vessel was righted when cold and the sample slid into position. It could then be attached by the platinum tubes to the liquefier. This procedure, together with the length of the vessel, avoided any danger of decomposing the salt by heat.

The measurement of temperature

The susceptibility of the sample was determined by measuring the mutual induction of two coils surrounding it. The primary coil was wound with extra turns at the ends so as to keep the magnetic field constant to 0·1 % over the volume of the sample. The mutual induction was measured by reversing a known current in the primary coil and observing the deflexion of a ballistic galvanometer in the circuit of the secondary coil. The deflexions were reduced to the equivalent deflexion corresponding to the reversal of a standard current in the primary coil. A correction, which was always less than 0·2 %, was applied for the difference between the tangent of the angle of deflexion (which was the measured quantity) and the angle itself.

The current in the primary coil is a measure of the magnetic field in the absence of the sample, which is not the same as the magnetic field experienced by the elementary dipoles, owing to the Lorentz and demagnetizing fields. It has been shown (see e.g. Kurti and Simon 1938) that when allowance is made for this difference, Curie's law takes the form $1/\kappa \propto (T^* - \Delta)$, κ being the measured apparent volume susceptibility, where Δ is given by

$$\Delta = c\left(\tfrac{4}{3}\pi - N\right),$$

c = Curie constant per c.c. of compact crystal, and N = demagnetizing factor. Although this expression gives the value of Δ for a compact crystal, it is also valid for the powder, as the degree of compression was so great that the sample density was within 1 % of the crystalline density.

A more accurate expression for the Lorentz field has been obtained by Van Vleck (1937), which differs from Lorentz's expression by an amount only appreciable at the lowest temperatures. It will be considered later, together with the effect of the crystalline splitting of the energy levels.

The measurement of pressure

Pressures down to 3 mm. were measured on a precision mercury manometer kindly lent by Dr Lambert of the Inorganic Chemistry Department, Oxford; the readings were consistent and accurate to within 0·04 mm. For pressures below 3 mm. a McLeod gauge was constructed in which the lowest pressures obtained (0·1 mm. Hg) could be read with an accuracy of 1 %. At 3 mm. its readings were compared with those of the mercury manometer and agreement was obtained to within 1 %.

Corrections had to be made for two effects. First, the tubes between the helium bath and the manometers passed through several severe temperature gradients from liquid-helium temperature to room temperature. At the lowest pressures, therefore, a correction had to be applied for the thermo-molecular pressure difference. This correction was negligible for temperature gradients other than that between room temperature and liquid-oxygen temperature, and was calculated for this gradient from the formula (VII*a*) of Weber and Schmidt (1936). The correction amounted to 7 % at 0·1 mm. Hg, and 1 % at 0·3 mm. Hg; it was thus appreciable only below 1·1° K.

The second correction arises from the presence of the creeping film of liquid He II in tube B. The film evaporates at a warmer part of the tube and, as the gas is not being pumped away, it must return to the bath (where it recondenses). This downward flow produces a small pressure difference which can be calculated from Poiseuille's law if one assumes the position where the evaporation is taking place in tube B. If the appropriate length of tube is l cm. of diameter a mm., the difference of the squares of the pressures (in mm. Hg) at the point of evaporation (i.e. also at the manometers) and at the bath is given by*

$$\Delta(p^2) = 1{\cdot}3 \times 10^{-4} \quad lT^2/a^3.$$

Making the plausible assumption that the film evaporates somewhere near the platinum glass seal, this formula gives for the tube first used ($a = 0{\cdot}76$ mm.), $\Delta(p^2) = 4 \times 10^{-3}$ at 1° K, equivalent to a 20 % correction to the measurement of p. For the later experiments a 2·2 mm. tube was used, diminishing $\Delta(p^2)$ by a factor 30 and making the correction negligible.

3. THE EXPERIMENTS

The 'magnetic thermometer' was calibrated at the boiling-points of oxygen, hydrogen and helium. The first of the calibration points was observed after the apparatus had been cooled by immersion in liquid oxygen for some hours, helium exchange gas being present in the vacuum case and experimental chamber. In order that the coils of the mutual inductance might have the same resistance as during the rest of the experiment, it was necessary for them to be immersed in liquid hydrogen. The vacuum case and experimental chamber were therefore evacuated and the liquid oxygen surrounding the apparatus replaced by liquid hydrogen. This had the further advantage of avoiding any disturbance due to the paramagnetism of liquid oxygen. The heat flow to the sample was small, and its temperature remained unchanged while the galvanometer deflexion was read. It was only after this calibration point had been observed that the sample and the rest of the apparatus inside the vacuum case were cooled to the boiling-point of liquid hydrogen.

---

* When $\Delta p \ll p$, this formula is identical with the formula given by Bleaney and Simon (1939).

The liquid hydrogen in the Dewar vessel was at atmospheric pressure, which was measured on a Fortin's barometer, and ample exchange gas was maintained in the vacuum case and experimental chamber to ensure that the sample was at the actual temperature of the liquid hydrogen. This temperature was obtained from the vapour-pressure curve of hydrogen, and the galvanometer deflexion read. The liquefaction of helium then proceeded as usual.

Liquid helium was transferred into the experimental chamber by condensation, and when sufficient had been obtained to ensure that the sample would remain covered throughout the measurements, the third calibration point was taken. To maintain a constant pressure in the helium bath it was connected to the atmosphere via a tube open under water. The water prevented the ingress of air which might solidify and block the tube in the cryostat. The pressure was read on the mercury manometer, and hence the temperature was obtained from Schmidt and Keesom's scale 1937.

The temperature of the helium bath was adjusted by varying the pumping speed; the time taken to reach equilibrium in the bath after adjustment of the speed was several minutes at the higher temperatures, but quite rapid in the He II region. This is due to the enormously greater heat conductivity of He II. Temperature gradients in the bath in the He I region were avoided by never allowing the temperature to rise, so that the bath was always well stirred up by the action of pumping.

4. RESULTS

Since the compensation of the magnetic thermometer was not accurately adjusted to zero, an additive constant was introduced into the equation connecting the galvanometer deflexion with the temperature. The deflexion observed on reversing the current in the primary was reduced to that deflexion δ_1, which would be produced by reversing a current of 1 amp. We have then

$$\delta_1 - a = \frac{k}{T^* - \Delta}.$$

The values of the constants k and a were obtained from the calibration points.

To compare the experimental results with the vapour-pressure scale of Bleaney and Simon, it is most convenient to compare the temperature given by the magnetic thermometer (T^*) with that deduced from the vapour pressure using the scale 1939. The equation of the latter is

$$\log_{10} p_{\text{cm.}} = -\frac{3{\cdot}117}{T} + 2{\cdot}5 \log_{10} T - 0{\cdot}00227\,T^3 + 1{\cdot}196 + D,$$

where D is a small term* which cannot be conveniently expressed explicitly; its values are given in the original paper (Bleaney and Simon 1939, there called Δ). In the calculation of the scale 1939 the theoretical values of de Boer and Michels (1939) were assumed for the second virial coefficient B of helium gas in the absence of experimental determinations below 2° K. Such experiments have now been reported by Keesom and Walstra (1939), whose values are in good agreement with the values assumed by Bleaney and Simon. Since even relatively large errors in their assumed B-T relation cannot seriously affect the calculated vapour pressure below 1·6° K, no adjustment of the scale 1939 is necessary.

Experiment 1

In the first experiment manganese ammonium sulphate was used for the sample, weight 4·46 g., in the form of a 4:1 ellipsoid, for which the value of Δ is 0·066°. Calibration points were taken at the boiling-points of hydrogen and helium, the readings being:

$$T = 20{\cdot}39, \quad \delta_1 = 1{\cdot}63, \quad \frac{1}{T - 0{\cdot}066} = 0{\cdot}0492,$$

$$T = 4{\cdot}217, \quad \delta_1 = 10{\cdot}72, \quad \frac{1}{T - 0{\cdot}066} = 0{\cdot}2409.$$

---

* **Below 1·4° K the T^3 term and D are together so small that they can be neglected without introducing an error of more than 1 % in p, or 0·1 % in T.**

These values give $k = 47{\cdot}42$, $a = -0{\cdot}70$; the calibration formula is therefore

$$T^{*} - 0{\cdot}066 = \frac{47{\cdot}42}{\delta_1 + 0{\cdot}70}.$$

The results are shown in table 1.

TABLE 1

δ_1 cm.	p mm. Hg	thermo-molecular correction %	p_1 mm. Hg	$\Delta(p^3)$ mm. Hg $\times 10^{-3}$	p_2 mm. Hg	T_{1939}	T^{*}	$T^{*} - T_{1939}$
12·59	417·1	—	—	—	—	3·641	3·634	−0·007
13·21	347·4	—	—	—	—	3·491	3·475	−0·016
14·01	270·9	—	—	—	—	3·287	3·290	+0·003
16·61	133·2	—	—	—	—	2·804	2·803	−0·001
19·88	57·8	—	—	—	—	2·361	2·370	+0·009
22·09	34·58	—	—	—	—	2·143	2·147	+0·004
23·18	26·50	—	—	—	—	2·044	2·052	+0·008
25·39	15·96	—	—	—	—	1·875	1·884	+0·009
28·63	7·87	—	—	—	—	1·680	1·683	+0·003
31·24	4·60	—	—	—	—	1·553	1·552	−0·001
32·31	3·63	—	—	—	—	1·503	1·503	0·000
33·72	2·67	—	—	—	—	1·443	1·443	0·000
36·43	1·565	—	—	—	—	1·344	1·343	−0·001
38·60	1·02	—	—	—	—	1·274	1·273	−0·001
41·04	0·642	—	—	5·8	0·637	1·203	1·202	−0·001
41·79	0·559	—	—	5·6	0·554	1·183	1·182	−0·001
44·52	0·351	0·8	0·348	5·5	0·342	1·117	1·115	−0·002
46·63	0·237	2·2	0·232	4·8	0·222	1·067	1·068	+0·001
48·53	0·176	3·4	0·170	4·4	0·156	1·027	1·029	+0·002
50·44	0·135	4·5	0·129	4·1	0·112	0·993	0·993	0·000
53·23	0·097	7·1	0·090	3·6	0·067	0·943	0·945	+0·002

In the first column of the table is shown the measured value of δ_1 already corrected for the tangent of the angle of deflexion of the light reflected from the galvanometer mirror. A further correction has also been applied, the necessity for which was discovered at the end of the experiment. As a check after readings had been taken for 11 hr., the calibration points were observed again, and it was found that the values of δ_1 were lower by 0·10 cm. This change was traced to the slight heating of the mutual inductance used as compensator, which resulted in an increase of its value, that is, effectively to a numerical increase in the constant a. The effect of this increase was small at the lowest temperatures, amounting only to an error in T^{*} of 0·002° at 1° K. An accurate correction could therefore be made by interpolation.

The observed values of the vapour pressure are given in column 2, (p), and the thermomolecular pressure correction (where not negligible) in the following column as a percentage of p. The fourth column gives the pressure (p_1) after the correction of column 3 has been applied. The fifth column shows the correction due to the creeping film $\Delta(p^2)$, and the following column gives the pressure (p_2) after applying this second correction; p_2 is the vapour pressure of the helium bath, and from it the temperature of the bath has been obtained using the scale 1939. This is given in column 7 (T_{1939}). The temperature obtained from the calibration of the paramagnetic salt (T^*) is shown in column 8, and in the last column the values of the differences $T^* - T_{1939}$ are given.

It will be seen from the figures in columns 4, 5 and 6 that near 1° K the pressure difference caused by the evaporation of the creeping film is by no means small compared with the vapour pressure. At the lowest temperature reached, the measured pressure was nearly 50 % higher than the vapour pressure owing to this effect; it was obvious that such a correction could not be accurately estimated, and in the following experiments it was directly eliminated by an alteration in the experimental vessel.

Experiment 2

The sample of manganese ammonium sulphate was the same as that used in the first experiment, but in a different experimental vessel. The new vessel had a larger tube (2·2 mm. bore) in order to eliminate the correction to the measured pressure for the creeping effect. The correction was now

$$\Delta(p^2) = 2 \times 10^{-4}\,(\text{mm.}^2)$$

at 1°, and this affects the vapour pressure (0·1 mm.) by less than 1 %. The correction was therefore neglected.

The calibration points were as follows:

$$T = 90{\cdot}1^\circ, \quad \delta_1 = 0{\cdot}16, \quad \frac{1}{T - 0{\cdot}066} = 0{\cdot}0111,$$

$$T = 20{\cdot}34^\circ, \quad \delta_1 = 1{\cdot}96, \quad \frac{1}{T - 0{\cdot}066} = 0{\cdot}0493,$$

$$T = 4{\cdot}212^\circ, \quad \delta_1 = 10{\cdot}82, \quad \frac{1}{T - 0{\cdot}066} = 0{\cdot}2412.$$

The best straight line through these points was

$$T^* - 0{\cdot}066 = \frac{46{\cdot}25}{\delta_1 + 0{\cdot}34},$$

and this has been used to calculate the temperatures.

The results are given in table 2. The columns are as before, except that there is no correction to be applied for the creeping film effect.

The good agreement between these values and those of experiment 1 shows that the correction applied there for the effect of the creeping film was substantially correct. The difference between the values of experiments 1 and 2 at 1° K is only about 0·003°, or 3 % in p, whereas at the lowest temperature attained in experiment 1 the correction for the creeping film effect amounted to 50 % of the vapour pressure.

TABLE 2

δ_1 cm.	p mm. Hg	thermo-molecular correction %	p_1 mm. Hg	T_{1939}	T^*	$T^* - T_{1939}$
14·30	251·2	—	—	3·237	3·225	−0·012
16·88	123·8	—	—	2·760	2·752	−0·008
21·12	41·97	—	—	2·226	2·221	−0·005
21·71	36·4	—	—	2·164	2·163	−0·001
22·75	28·23	—	—	2·065	2·069	+0·004
25·15	16·0	—	—	1·875	1·880	+0·005
27·70	9·00	—	—	1·714	1·715	+0·001
30·19	5·17	—	—	1·580	1·581	+0·001
30·21	5·15	—	—	1·579	1·579	0·000
31·48	3·94	—	—	1·519	1·519	0·000
32·94	2·83	—	—	1·454	1·456	+0·002
33·24	2·61	—	—	1·438	1·443	+0·005
34·76	1·92	—	—	1·380	1·383	+0·003
36·50	1·35	—	—	1·318	1·322	+0·004
38·25	0·943	—	—	1·261	1·264	+0·003
40·35	0·61	—	—	1·198	1·203	+0·005
40·54	0·60	—	—	1·195	1·197	+0·002
44·28	0·294	1·2	0·290	1·098	1·102	+0·004
46·98	0·179	3·2	0·173	1·039	1·043	+0·004
49·07	0·126	4·9	0·120	1·000	1·002	+0·002
49·30	0·118	5·6	0·111	0·992	0·998	+0·006

Experiment 3

In the third experiment an ellipsoid of 'Analar' potassium chrome alum of the same dimensions as before was used. The experimental vessel was that with the wide bore tube.

Since the susceptibility of this substance is only one-third that of manganese ammonium sulphate, correspondingly smaller deflexions were obtained. For this reason a current of about one ampere was used continuously in the primary coil of the magnetic thermometer, which eventually heated the mutual inductance compensator and changed its value. This limited the number of observations that could be taken in this experiment.

The calibration points were:

$$T = 20{\cdot}40^\circ,\quad \delta_1 = 1{\cdot}23,\quad \frac{1}{T - 0{\cdot}022} = 0{\cdot}0492,$$

$$T = 4{\cdot}222^\circ,\quad \delta_1 = 4{\cdot}21,\quad \frac{1}{T - 0{\cdot}022} = 0{\cdot}2370,$$

whence

$$T^{*} - 0{\cdot}022 = \frac{15{\cdot}80}{\delta_1 - 0{\cdot}45}.$$

The results are given in table 3.

TABLE 3

δ_1 cm.	p mm. Hg	thermo-molecular correction %	p_1 mm. Hg	T_{1939}	T^{*}	$T^{*} - T_{1939}$
6·86	74·6	—	—	2·488	2·487	−0·001
7·86	35·44	—	—	2·153	2·149	−0·004
9·60	10·28	—	—	1·750	1·749	−0·001
10·80	4·64	—	—	1·555	1·549	−0·006
11·30	3·16	—	—	1·476	1·478	+0·002
12·40	1·52	—	—	1·339	1·343	+0·004
15·47	0·232	2·1	0·228	1·070	1·073	+0·003

5. DISCUSSION

The values of the difference T (magnetic) − T (scale 1939) given in the last columns of tables 1, 2 and 3 are shown graphically in figure 2. The difference between the scale 1937 and the scale 1939 below 1·6° is shown as a broken line; above this temperature the two scales coincide. The experimental accuracy can be estimated as follows: the temperature was measured to 0·1 %; the pressure to 1 %, corresponding to 0·1 % in the temperature; the calibration of the magnetic thermometer for manganese ammonium sulphate should be accurate to 0·2 % (0·5 % for chrome alum). It will be seen that these figures are consistent with the scatter of the experimental points, which all lie between −0·002 and +0·005°.

The mean of the scattered points lies somewhat on the positive side, as would be expected if the susceptibility of the paramagnetic salts deviates at all from Curie's law at 1°. The magnitude of these deviations, which are due to interactions of the magnetic dipoles with each other and with the crystalline electric field, can be estimated from the calculations of Hebb and Purcell (1937). One correction has already been made here for the mutual interaction of the dipoles, viz. the Lorentz correction. The mutual interaction has been more rigorously calculated by Van Vleck (1937), whose formula differs from the Lorentz formula by a second order term which is less than +0·001° for chrome alum, and equals +0·006° for manganese ammonium sulphate. The deviation due to the interaction with the crystalline field is +0·002° for chrome alum; the exact formulae have not been evaluated for the manganese salt, but since the anomalous specific heat due to this interaction is about twice as large as for chrome alum, the deviation is probably about +0·004°.* The estimated deviations are together +0·003° for chrome alum, and about +0·01° for manganese ammonium sulphate. It should be noted that these deviations refer to 1° K; the deviations fall off with the inverse of the temperature.

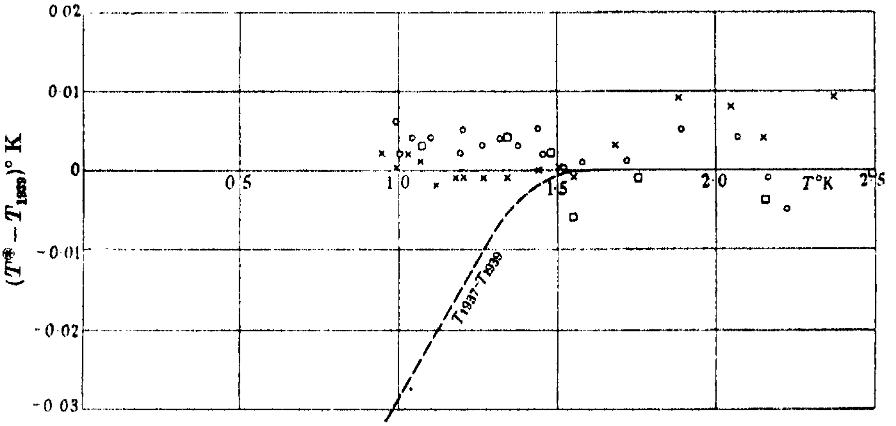

FIGURE 2. ×, experiment 1, manganese ammonium sulphate. ○, experiment 2, manganese ammonium sulphate. □, experiment 3, potassium chrome alum.

The mean of the differences between the temperatures deduced from the susceptibility and from the scale 1939 vapour pressure is +0·003° for both salts. This is the same as the estimated deviation for chrome alum, but less than that estimated for the manganese salt. As there is some uncertainty in the latter estimation, we may say that the experimental determination of the vapour pressure agrees with the thermodynamically calculated scale 1939 within the experimental error.† It should be pointed out that the discrepancy between these temperatures and scale 1937 is 0·029° at 1° K, which is considerably greater than the corrections that have just been discussed.

---

* The deviation due to the crystalline splitting can also be estimated by using the formulae derived by Hebb and Purcell (1937) for a similar substance, iron ammonium alum, together with the splitting parameter value found experimentally for manganese ammonium sulphate by Cooke and Hull (unpublished). This method also gives +0·004°.

† Some measurements of vapour pressure made during experiments not specifically designed for this purpose, but using the susceptibility of a paramagnetic salt for the measurement of temperature, have been kindly communicated to us by

In view of the fundamental importance of a correct knowledge of the vapour pressure-temperature scale of helium, we regret very much that circumstances did not allow us to carry out more measurements as we had planned. Since the deviation from Curie's law for chrome alum is both small and accurately known, this is the most suitable salt, and the disadvantage of its small susceptibility could be overcome by increasing the number of turns on the mutual inductance coils by a factor three say, when the calibration could be made as accurately as for manganese ammonium sulphate in the present apparatus. Iron alum could also be used, for its susceptibility is not much smaller than that of manganese ammonium sulphate, and the deviations from Curie's law are known from the experiments of Kurti, Lainé, Simon and Squire (unpublished).

We are indebted to Professor F. Simon, at whose suggestion this experiment was made, for many helpful discussions.

We also wish to thank the Government Grant Committee of the Royal Society for aid in the purchase of apparatus.

REFERENCES

Bleaney, B. and Simon, F. 1939 *Trans. Faraday Soc.* **35**, 1205.
Boer, J. de and Michels, A. 1939 *Physica*, **6**, 409.
Casimir, H. B. G., Haas, W. J. de and Klerk, D. de 1939 *Physica*, **6**, 365.
Cooke, A. H. and Hull, R. A. 1939 *Nature, Lond.*, **143**, 799.
Hebb, M. H. and Purcell, E. M. 1937 *J. Chem. Phys.* **5**, 338.
Keesom, W. H. and Walstra, W. K. 1939 *Physica*, **6**, 1146.
Kurti, N. and Simon, F. 1938 *Phil. Mag.* **26**, 849.
Van Vleck, J. H. 1937 *J. Chem. Phys.* **5**, 320.
Weber, S. and Schmidt, G. 1936 *Commun. Phys. Lab. Univ. Leiden*, no. 246*c*.

Dr H. G. B. Casimir of Leiden. These are shown in the following table, together with the values of scale 1939. On the whole the magnetic temperatures are a little higher than the scale 1939, as is expected. These figures afford satisfactory confirmation of those obtained by us, while differing from the scale 1937 by about 0·03°.

substance	vapour pressure mm. Hg	magnetic temp.	temperature scale 1939
potassium chrome alum	0·51	1·178	1·171
	0·48	1·170	1·162
iron ammonium alum	0·42	1·134	1·144
	0·48	1·166	1·162
	0·50	1·173	1·168

The effective susceptibility of a paramagnetic powder

By B. Bleaney and R. A. Hull

Clarendon Laboratory, Oxford

(*Communicated by F. A. Lindemann, F.R.S.—Received* 17 *December* 1940)

The effective susceptibility (that is, the magnetic moment divided by the external magnetic field) of a paramagnetic powder loosely packed into an ellipsoidal container has been measured against the vapour pressure of liquid helium, and hence, using the results of the preceding paper, against the susceptibility of the compact salt. The definition of the 'Curie' temperature scale is based on the latter, and it is found that the correction to be applied in calculating the Curie temperature from the effective susceptibility of the powder agrees with that given by a theoretical expression derived from Breit's calculation of the demagnetizing field of a powder. This is of importance both in experiments using a loosely packed powder and in experiments using a paramagnetic powder mixed with a non-magnetic material.

The determination of the susceptibility of paramagnetic salts has become of exceptional importance in the temperature region below 1° K, and also in the liquid helium range itself, especially as the temperature scale is intimately connected with it. The correct procedure to be adopted for evaluating the susceptibility from measurements at these temperatures requires some consideration since, owing to the very high intensity of magnetization, the true field inside the sample (which enters into the definition of susceptibility) can differ considerably from the external field, i.e. the field present before the introduction of the sample. For an ellipsoidal sample of compact material this true field can be obtained simply by subtracting from the external field the demagnetizing field $N(M/V)$, N being the demagnetizing factor which can be calculated from the shape of the sample using Maxwell's formulae, and M/V the magnetic moment per unit volume. If, however, the sample is not homogeneous, e.g. a powdered material or mixture, the expression for the demagnetizing field will be more complicated and the theory has not yet been worked out for the general case.

The demagnetizing field has been calculated by Breit (1922) for a number of special cases, such as a space lattice of spheres or of spherical holes. The calculation showed that the average value of the field within the powder particles (H_2) is less than the average field (H_1) within the sample as a whole by an amount $\frac{4\pi}{3}\frac{1-f}{f}\frac{M}{V}$‡, i.e.

$$H_2 = H_1 - \frac{4\pi}{3}\frac{1-f}{f}\frac{M}{V},$$

where f = filling factor = sample density/crystal density. Owing to the demagnetizing effect of the external shape we have

$$H_1 = H - N(M/V),$$

where H is the external field in the absence of the sample. Combining these equations we have

$$H_2 - H = -N(M/V) - \frac{4\pi}{3}\frac{1-f}{f}\frac{M}{V}. \tag{1}$$

The quantity on the right of this equation may be called the demagnetizing field of the powder.

The quantities in which we are interested are (*a*) the ratio of the intensity of magnetization M/V to the external field H; this ratio will be called the 'effective susceptibility' κ, since it is the quantity usually measured; (*b*) the ratio of the intensity of magnetization to the field H_0 acting on the magnetic dipoles; this ratio, denoted by κ_0, enters into the definition of the 'Curie scale' of temperature (see, for instance, Kurti and Simon 1938*a*). For it is generally assumed that Curie's law will hold if it is the quantity κ_0 that is taken to be inversely proportional to the absolute temperature rather than the susceptibility as defined in electromagnetic theory; and at temperatures where Curie's law is no longer true it is usual to define a new scale (the Curie or T^* scale) by extrapolation of Curie's law, i.e.

$$T^* = c/\kappa_0,$$

c being the Curie constant per c.c.

Now the fields H_2 and H_0 are connected by the well-known relation of Lorentz

$$H_0 = H_2 + \frac{4\pi}{3}\frac{1}{f}\frac{M}{V}.$$

---

‡ This follows from equation (1′) of Breit, which, written with the above notation, becomes

$$\frac{4\pi\left(\frac{M}{V}\middle/H_1\right)}{f\,4\pi\left(\frac{M}{fV}\middle/H_2\right)} = \frac{1}{1+\frac{1-f}{3}\,4\pi\left(\frac{M}{fV}\middle/H_2\right)}.$$

This reduces to the above expression.

Here the factor $1/f$ enters because (M/V) is the average intensity of magnetization of the powder, and the Lorentz field naturally depends on the intensity of magnetization inside the crystalline particles. Hence from equation (1) we have

$$H = H_0 + N\frac{M}{V} + \frac{4\pi}{3}\frac{1-f}{f}\frac{M}{V} - \frac{4\pi}{3}\frac{1}{f}\frac{M}{V}$$

$$= H_0 - (4\pi/3 - N)(M/V),$$

i.e.

$$\frac{1}{\kappa} = \frac{H}{\frac{1}{f}\frac{M}{V}} = \frac{1}{\kappa_0} - f\left(\frac{4\pi}{3} - N\right) = \frac{1}{c}(T^* - \Delta), \tag{2}$$

where

$$\Delta = cf(4\pi/3 - N).$$

Hence the 'effective susceptibility' κ is inversely proportional to $(T^* - \Delta)$.

In his monograph on *Magnetism and very low temperatures** Casimir has pointed out that the above calculation cannot be considered absolutely reliable in the general case, as for example with 'salt crystals crushed in a mortar and compressed to a density corresponding to $f = 0{\cdot}6$ or $f = 0{\cdot}7$'. He considers it more advisable to use only very dense powders or solid material (since no doubt arises about the expression for Δ when $f = 1$) rather than to perform special experiments to test the above result. The difficulty cannot be avoided in this way, however, when a mixture of a paramagnetic salt with a non-paramagnetic salt is used; such mixtures are often necessary when it is desired to investigate the properties of substances not in themselves suitable for cooling by adiabatic demagnetization, at temperatures only obtainable by this method (Kurti and Simon 1935). Also, loose powders of paramagnetic salt have to be used in the capsule technique employed by various workers (Kurti, Rollin and Simon 1936; Kurti and Simon 1938*b*; Shire and Allen 1938).

The purpose of the experiment described in this paper is therefore to determine the value of Δ for a loosely packed salt, actually with a filling factor of about one-half. From equation (2) it will be seen that this involves the measurement of the effective susceptibility κ and of T^*, i.e. the true susceptibility. The former is measured by a mutual inductance method; the latter is determined from the vapour pressure of helium, using the results of the preceding paper.

---

* We are considerably indebted to this monograph for parts of the theoretical exposition above.

EXPERIMENTAL PROCEDURE

Since the value of Δ is a few hundredths of a degree, it is obvious that its determination involves the measurement of temperatures in the liquid helium range, and particularly near 1° K, to an accuracy of 0·1 %. Such accuracy requires special apparatus such as that used for the measurement of the vapour pressure of liquid helium using the susceptibility of a compact paramagnetic salt as thermometer (see preceding paper). It is clear that once the vapour-pressure curve was established, the same apparatus could be used for the measurement of the effective susceptibility of a loosely packed powder.

The experimental procedure will only be briefly outlined, since full details are given in the preceding paper. Manganese ammonium sulphate was chosen as the paramagnetic salt since it has a high Curie constant, and the value of Δ is therefore comparatively high. It was roughly powdered in a mortar and loosely packed into a container whose shape was that of a 4 : 1 ellipsoid. This container was made of 'Perspex', turned as thin as possible and pierced by a number of small holes to ensure good thermal contact between the salt and the liquid helium bath in which it was immersed. The filling factor f was 0·55.

The temperature of the bath was determined from its vapour pressure using the 'scale 1937' down to 1·6° K and the more accurate 'scale 1939' below that point. The pressure was measured by a precision mercury manometer above 3 mm. Hg; lower pressures were measured by a special McLeod gauge, accurate to 1 %, corresponding to 0·1 % in temperature. The effective susceptibility was measured by a mutual inductance method, observations being made at the boiling-points of oxygen and hydrogen, and from the boiling-point of helium down to 1° K.

RESULTS

The effective susceptibility κ was measured by surrounding the sample by two coils, and measuring the deflexion δ of a ballistic galvanometer in the circuit of the secondary coil when a known current was reversed in the primary coil. The deflexion δ was reduced to the value δ_1, corresponding to the reversal of unit current. The deflexion in the absence of the sample was not quite balanced out by an external mutual inductance, so that κ was not proportional to δ_1 but to $\delta_1 - a$, where a is a small constant. We have then

$$T^* - \Delta = k/(\delta_1 - a). \qquad (3)$$

In the general case when this formula is used for the determination of T^* the value of Δ is known, and the constants k and a are obtained from two or more calibration points. In this experiment Δ is the unknown, and the simplest procedure is to write (3) in the form

$$T^*(\delta_1 - a) = \Delta(\delta_1 - a) + k. \tag{4}$$

This is of the form $y = \Delta x + k$, and hence on plotting $y = T^*(\delta_1 - a)$ against $x = (\delta_1 - a)$, a straight line should be obtained whose slope gives the correct value of Δ. As it is not possible to determine the value of a directly by removing the sample, equation (4) can only be used to determine Δ if the value of a obtained by calculation from two observed points is independent of Δ. To the accuracy required, which is the same (0·01 cm.) as the accuracy of measurement of δ_1, this is so, for the value of a can be obtained from the values of δ_1 observed at the boiling temperatures of oxygen and hydrogen. Compared with these temperatures Δ is very small and can be neglected.

The values of δ_1 and T at the boiling-points of oxygen and hydrogen are

$$\delta_1 = 0{\cdot}09 \quad T = 90{\cdot}1^\circ,$$
$$\delta_1 = 1{\cdot}40 \quad T = 20{\cdot}3^\circ.$$

Substituting these values in equation (3) the value of a is obtained as $-0{\cdot}29$.

The results obtained in the liquid helium range are given in table 1. In the first two columns the values of δ_1 and the vapour pressure are given, the latter being the measured pressure corrected for the thermolecular pressure difference and the creeping film effect as described in the preceding paper. These corrections are negligible except at the last two points.

The value of T^* is not appreciably different from T except at the lowest temperatures, and the value of $T^* - T$ is obtained from the preceding paper.

TABLE 1

δ_1 cm.	vapour pressure mm.	T °K	T^*	$x = (\delta_1 - a)$	$y = T\circledast(\delta_1 - a)$
7·99	754	4·209	4·209	8·28	34·85
10·62	245·3	3·216	3·216	10·91	35·08
13·72	78·3	2·510	2·510	14·01	35·17
16·33	33·1	2·125	2·125	16·62	35·32
19·83	10·36	1·753	1·755	20·12	35·31
23·78	3·07	1·470	1·473	24·07	35·46
27·95	0·92	1·258	1·261	28·24	35·61
30·37	$0{\cdot}47_8$	1·160	1·164	30·66	35·69
35·24	0·130	1·008	1·012	35·53	35·96
35·33	0·129	1·007	1·011	35·62	36·01

There the vapour pressure of helium was compared with the true susceptibility of a compact sample of manganese ammonium sulphate, so that by using those results the true susceptibility of our loosely packed sample is obtained, indirectly, from that of the compact sample. Thus the effect of the small deviation of the salt from Curie's law is eliminated.

Using for a the value $-0{\cdot}29$ obtained above, the values of $x = \delta_1 - a$, and of $y = T^*(\delta_1 - a)$ are calculated and shown in figure 1, and from the slope of the straight line drawn through the points the value of Δ is obtained as $0{\cdot}038°$. The values of T^* and of δ_1 should each be accurate to 0·1 %, and the error in the value of y should not therefore be more than 0·2 %. It will be seen that the maximum deviations of the experimental points from the straight line are of this order. As the range of values of x is about 30, it follows that the accuracy of the determination of Δ, the slope of the straight line, is about $\pm 0{\cdot}002 \times 35/30 = \pm 0{\cdot}002°$.

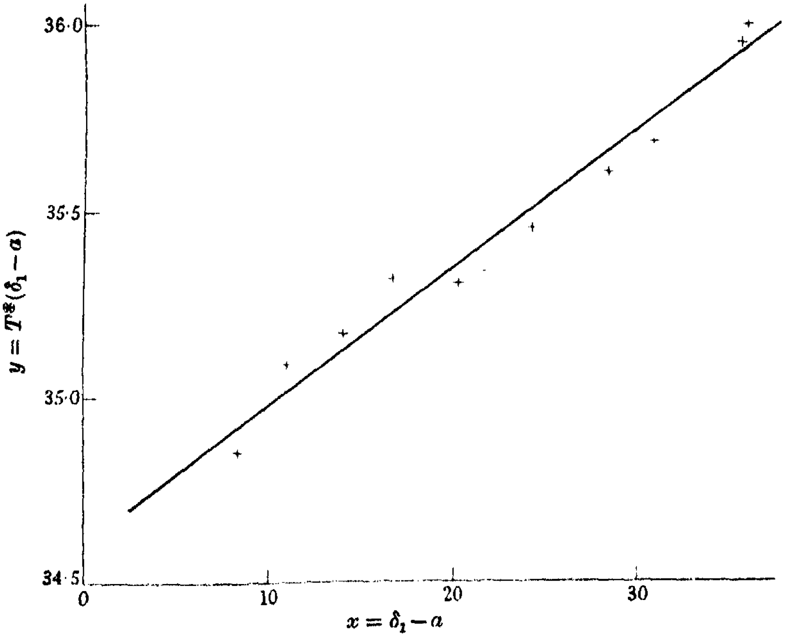

FIGURE 1

This experimental value of Δ has now to be compared with that given by the theoretical expression

$$\Delta = fc(4\pi/3 - N)$$

where $f = 0{\cdot}55$, $c = 2{\cdot}00 \times 10^{-2}$, $N = 0{\cdot}95$ for a 4 : 1 ellipsoid with major axis parallel to the field.

Inserting these figures, we have $\Delta = 0{\cdot}037°$. This value is in agreement with the experimental value of $0{\cdot}038 \pm 0{\cdot}002°$ and differs considerably from the value 0·066° for a compact sample. It should be noted that at the lowest temperatures which can be attained by adiabatic demagnetization of manganese ammonium sulphate (about 0·1°), the use of the incorrect value of Δ would introduce an error of about 30 % in the temperature.

CONCLUSION

The good agreement between the theoretical value 0·037° of Δ and the experimental value of $0{\cdot}038° \pm 0{\cdot}002$ indicates that the expression for the demagnetizing field derived by Breit for certain special forms of space lattice can be used in the general case of a powder formed by crushing salt crystals.

For the calculation of the 'Curie' temperature the experiment shows that the expression $\Delta = fc(4\pi/3 - N)$ is certainly still valid for loosely packed salts with an f-value of one-half.

REFERENCES

Breit, G. 1922 *Commun. Phys. Lab. Univ. Leiden*, Suppl. no. 46.
Kurti, N., Rollin, B. V. and Simon, F. 1936 *Physica*, **3**, 266.
Kurti, N. and Simon, F. 1935 *Proc. Roy. Soc.* A, **151**, 610.
Kurti, N. and Simon, F. 1938*a* *Phil. Mag.* **26**, 849.
Kurti, N. and Simon, F. 1938*b* *Nature, Lond.*, **142**, 207.
Shire, E. S. and Allen, J. F. 1938 *Proc. Camb. Phil. Soc.* **34**, 301.

A stress-strain curve for the atomic lattice of iron

By S. L. Smith, D.Sc., F.C.G.I., *Engineering Department*,
and W. A. Wood, D.Sc., *Physics Department*,
National Physical Laboratory, Teddington, Middlesex

(*Communicated by G. W. C. Kaye, F.R.S.—Received* 24 *December* 1940)

Measurements have been made on the stress-strain relationship for the atomic lattice of iron (purity 99·95 %). The changes in dimensions of the atomic lattice of tensile specimens have been determined in the direction perpendicular to the applied stress and compared with the contraction in external dimensions which occurs in the same direction. It has been shown that the lattice stress-strain curve, obtained by plotting the lateral change in lattice spacing against the tensile stress, exhibits three main characteristics. Up to the external yield point, the lattice contraction is directly proportional to the applied stress. Beyond the yield point, the lattice contraction slows down as the stress increases. Finally, at still higher stresses, the lattice tends to expand. A further set of experiments, in which cycles of stress are employed, show that when a stress greater than the yield stress is applied and then removed from a specimen, the lattice is left with a permanent expansion which depends in a regular manner upon the value of the stress applied. It is concluded that beyond the external yield point, the iron lattice undergoes two distinct modifications. First, the lattice spacing tends to contract elastically, in conformity with the external elastic contraction exhibited by the specimen in the same direction (perpendicular to the applied stress). Second, the lattice tends to deform in a manner which leads to a superposed expansion of lattice spacing. The actual change of spacing at a particular stress is then the resultant of the two effects; a process which explains the unexpected shape of the lattice stress-strain curve, and affords systematic information on the problem of internal strains in metals. Further experiments indicate that the permanent expansion of the lattice after loading occurs not only in the direction perpendicular to the applied stress, but also in the direction of the stress; the permanent lattice deformation thus represents a decrease in density of the test specimen. Finally, the results of some experiments are recorded on the effect of temperature on the lattice expansion effect, and it is shown that recovery of the lattice can be produced by mild heat treatment at a temperature much lower than that required to renew the properties of the metal by recrystallization.

Subjected to external stress, a metal deforms by two distinct processes. First, the atoms move from their normal positions in the lattice until equilibrium is restored. Second, if the yield point is exceeded, groups of atoms undergo relative translations within the grains by internal gliding and by breakdown into smaller units which have a lower limiting size. The latter process in the main is irreversible; in consequence, after removal of the applied stress, the grains are left with a permanent change in internal structure and external shape. This constitutes the plastic deformation which in recent years has been intensively studied by metallographic and X-ray methods, and of which at least the principal features have been elucidated (e.g. Andrade 1940; Gough 1933; Gough and Wood 1936, 1938; Orowan 1940; Taylor 1934; Wood 1939, 1940).

Less is known of the first process. This is largely because no direct method has been available for measuring the atomic displacements prior to the development of precise X-ray diffraction methods, and until the changes in X-ray structure associated with plastic deformation could be classified and allowed for. Previously, the atomic displacements have been deduced indirectly from the nature of the external deformation. Thus when the applied stress is within the limit of proportionality, so that Hooke's Law is obeyed and plastic deformation excluded, the external deformation disappears as the stress is removed; it is then reasonable to assume that the atoms have reverted to their original arrangement and spacing, and that the average amplitude of the atomic displacements is expressed by the external elastic moduli. If, however, the applied stress exceeds the yield point, producing plastic deformation, the metal is left permanently deformed. It is then impossible to tell from the external changes how much of this deformation is of the plastic type and how much is due to a permanent deformation of the lattice, arising because the atoms have not returned to their initial arrangement. It is, therefore, necessary to supplement the external measurements in this respect. This can be done by the X-ray measurements.

The present paper describes a 'lattice stress-strain curve' for pure iron (purity 99·95 %) subjected to tensile stress. This curve relates the observed atomic displacements to the applied tensile stress. It is thus complementary to the external stress-strain curve, obtained in mechanical testing, which relates the stress to the observed external strain. The authors have developed a combined tensile-testing machine and X-ray spectrometer by which the two curves can be obtained at the same time on the same specimen, and thus under strictly comparable conditions. This apparatus has been used in the present research and as its main features have been indicated in a previous paper (Smith and Wood 1940), it is proposed to proceed at once to a description of the results. These bring out some systematic properties of the metallic lattice not hitherto observed.

1. EXTERNAL TENSILE STRESS-STRAIN CURVE

The specimens were flat tensile specimens machined to the standard shape and dimensions shown in figure 1. They were annealed in vacuo under the same conditions until, as shown by preliminary X-ray tests, the grains were free from the effect of residual strains. The external stress-strain curve was then much the same for each specimen tested and it will suffice to reproduce the typical curve shown in figure 2. In this curve the stress was calculated from the applied load divided by the initial area of cross-section of the test specimen, and the measurements were discontinued when the specimen necked prior to fracture. In the range thus investigated, the change in section during the loading of the specimen was not so large as to cause the plotted stress to differ materially from the actual stress. The ultimate stress given below is the maximum load

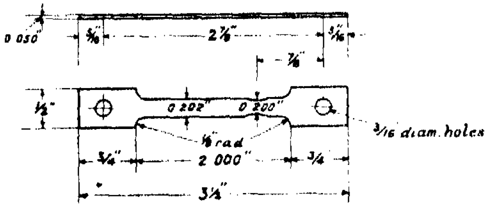

FIGURE 1. Shape of X-ray tensile specimen.

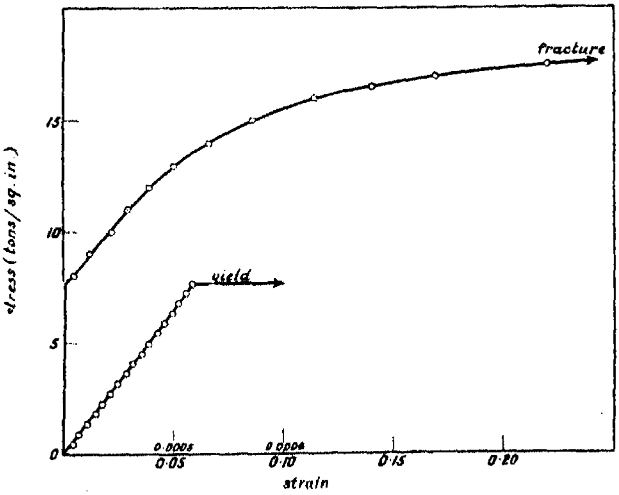

FIGURE 2. External tensile stress-strain curve.

reached before the specimen necked and fractured divided by the original area of cross-section. It will be seen that the curve follows the usual course for a ductile metal, showing an initial elastic range followed by a definite yield and then a much larger range of plastic deformation until fracture. The principal mechanical data were:

Young's modulus	13×10^3 tons/sq. in.
Poisson's ratio	0·27
Yield point	7·5 tons/sq. in.
Ultimate stress	18 tons/sq. in.

1 ton per sq. in. = $1{\cdot}545 \times 10^8$ dynes per sq. cm.

2. LATTICE STRESS-STRAIN CURVE

As a specimen is stretched it contracts by a related amount in the perpendicular direction. It is immaterial, as far as the characteristics of external deformation are concerned, whether one considers the elongation or the contraction. But when the measurements involve the lattice strains, it is necessary to define the dimension investigated, since the grains are not isotropic. The lattice strain will depend on the crystallographic direction chosen for investigation, and the orientation of that direction relative to the direction of stress.

This dimension is set largely by exigencies of technique. First, the diameter of an X-ray diffraction ring is most sensitive to changes of lattice spacing when the ring is formed by reflexion backwards, as nearly as possible along the line of the incident beam. The atomic planes reflecting backwards in this way will be those practically perpendicular to the incident beam. Second, of possible directions for the incident beam, it is simplest to choose the one perpendicular to the length of the tensile specimen, in order to avoid clamps and ancillary apparatus connected to the ends of the specimen. Consequently, the planes most conveniently investigated are planes almost parallel to the length of the specimen. The exact inclination depends on the Bragg reflexion angle for each set of planes. For the (310) planes, and with the characteristic Co K-radiation as incident wave-length, this angle is 80·7°. When the incident beam is perpendicular to the length of the specimen, X-ray observations on the (310) planes then refer to those (310) planes inclined at $90\text{–}80{\cdot}7^\circ = 9{\cdot}3^\circ$ to the length of the specimen. To a first approximation, these may be regarded as parallel to the length of the specimen. As the specimen extends, its cross-section diminishes and these planes will therefore be brought closer together. It is the variation in spacing of these planes which forms the subject of the present measurements.

It will be noted that the X-ray method is selective. A proportion only of the total number of grains in the cross-section of a polycrystalline specimen will be so oriented that the (310) planes in each grain are inclined in the manner required. Measurements on the (310) diffraction ring will refer only to this group of grains. Another diffraction ring, (*hkl*) say, would respond to the changes in another group of grains in which the (*hkl*) planes were oriented at the appropriate Bragg angle to the incident beam. To obtain this (*hkl*) ring in the sensitive large-angle range would mean using some incident wave-length other than the Co *K*-radiation. At present the choice of wave-lengths is limited. There is no reason why sometime this limitation should not be overcome by the development of higher-powered X-ray tubes in conjunction with a monochromatizing crystal which would select from the white background-radiation a waveband sufficiently narrow and intense for the purpose. The present measurements on the (310) group suffice, however, to bring out the features in the behaviour of the metallic lattice to which it is desired to draw attention. These are likely to differ only in magnitude for the other groups of grains.

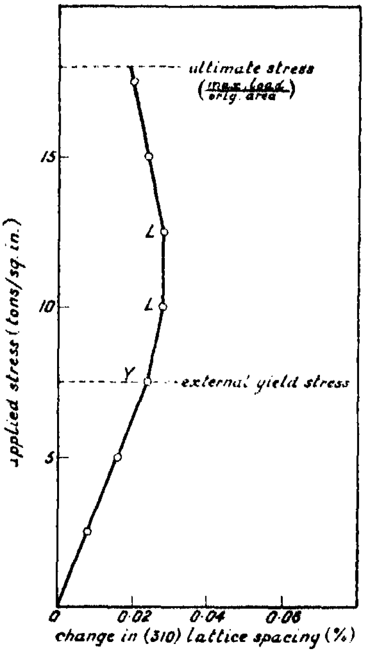

FIGURE 3. Lattice stress-strain curve for (310) planes approximately parallel to direction of applied stress.

The observations on the (310) lattice spacing, made in the manner defined above, then lead to the stress-strain curve shown in figure 3.

The contraction in spacing is expressed as the percentage change from the initial (310) spacing of 0·904 A. The stresses at which external yield and maximum load are reached are also indicated on the graph. It will be seen that the change in spacing shows two novel features which could not have been deduced from the external deformation. These occur after the external yield point, *Y*; below this point, as might have been anticipated, the contraction is proportional to the applied stress, the lattice obeying Hooke's law. At the external yield point, there is no sharp change in lattice dimensions to correspond with the marked increase in rate of external deformation as plastic strain sets in. The lattice behaves actually in the opposite sense. As the stress is increased, the initial rate of lattice contraction falls off and the contraction approaches a limiting value, shown on the curve by *LL*. This is the first feature. The second feature is that, as the stress is still further increased, the lattice spacing tends to recover and expand. Fracture soon follows this stage. These two observations, the limited contraction and the subsequent partial expansion, stand in contrast to the continued contraction in the external cross-section.

It will be shown in the next section that these effects are associated with a permanent deformation of the lattice which sets in after the external yield. It is desired first to remark on the quantitative measurements.

Pure iron lends itself to accurate measurements. It has been proved in previous work that during progressive plastic strain the initially annealed grains are broken down into widely oriented crystallites characterized by a lower limiting size (Wood 1939). In practice, if this size is less than about 10^{-5} cm., then the diffraction rings, especially those occurring at large reflexion angles, become abnormally diffuse (Scherrer effect). If therefore an accurate determination is required of changes in diameter of the rings over a wide range of deformation, it is advantageous to have a metal with a relatively high limiting crystallite size. The rings will then remain sufficiently sharp throughout the range of measurement to permit of accurate comparison. Pure iron satisfies this condition. The α_1 and α_2 components of the (310) diffraction ring are always resolved.

Measurements of the ring diameters were made by a travelling microscope or, when further detail was required, by a Moll microphotometer. The variation in diameter of the ring was directly proportional, over the ranges involved, to the changes in (310) spacing; a change in diameter of 1 mm. corresponded to a change in spacing of 0·037 %. This calibration figure was obtained by calculation; the distance of specimen to photographic film was known from direct measurement so that the lattice spacing corresponding to a number of assumed ring diameters in the observed range of variation could be calculated and from the results the rate of change of spacing with change in diameter then obtained to give the calibration constant mentioned.

The slope of the line in the initial linear range of the lattice stress-strain curve then gives the percentage contraction of the (310) lattice spacing per unit increase in stress (ton/sq. in.). This change is in the direction inclined to the incident beam at the angle of 9·3°. The change actually in the direction of the beam, or perpendicularly to the length of the specimen, since the angle is small, will be given with reasonable accuracy on dividing the previous result by cos 9·3°. This result may then be compared with the external elastic contraction in the same direction; this is given by the extensometer measurements of the change in length of the specimen per unit increase in stress and the observed value of Poisson's Ratio for the material. These quantitative results are summarized as follows:

Change in (310) spacing per unit stress (tons/sq. in.) as directly observed	$0{\cdot}0029_6$ %
Change in (310) spacing per unit stress (tons/sq. in.) in direction perpendicular to length of specimen	0·0030 %
External contraction per unit stress (tons/sq. in.) in direction perpendicular to length of specimen	0·0021 %

3. LATTICE STRESS-STRAIN CURVE FOR CYCLES OF STRESS

In the above experiments, the lattice measurements were made while a specimen was progressively loaded until maximum load. In the experiments described in the present section, the changes were determined as a specimen was loaded to a particular stress and the stress then removed. The results thus indicate the extent to which the lattice changes are reversible.

In the first instance, one specimen was treated as follows. Loads of 5, 7½ (yield point), 10, 12½, 15 and 17½ tons/sq. in. were selected. The specimen was loaded to 5 tons/sq. in. and the load then removed. X-ray photographs were obtained from the specimen in the initial state, at the load of 5 tons/sq. in., and upon removal of this load. The process was repeated with the same specimen for the further loads selected. X-ray photographs were thus obtained at 7½, 10, 12½, 15 and 17½ tons/sq. in. and at zero load between each of these points. The percentage variation in the lattice spacing under these loads and the extent of recovery after each load was removed are plotted against the respective stresses in figure 4. The graph brings out the following characteristics in the behaviour of the lattice.

(i) Regarding the behaviour below the external yield point, indicated on the graph at Y. In this range the lattice spacing, which is contracted under load, returns on unloading to its initial value. Therefore in the external primitive elastic range the lattice changes are reversible.

(ii) Regarding the behaviour when the external yield stress has been exceeded. Then the contracted lattice spacing does not return to its original normal value upon removal of the load, but to a value in excess of the original. The lattice spacing is left with a permanent expansion. The extent of the changes is shown in figure 4. On unloading from L_1, the point corresponding to 10 tons/sq. in., the lattice spacing does not return to the origin O, but to the value at M_1. The lattice thus exhibits the residual expansion OM_1. Similarly, on unloading from 12½, 15 and 17½ tons/sq. in., the points L_2, L_3 and L_4, the lattice spacing returns to M_2, M_3 and M_4, and

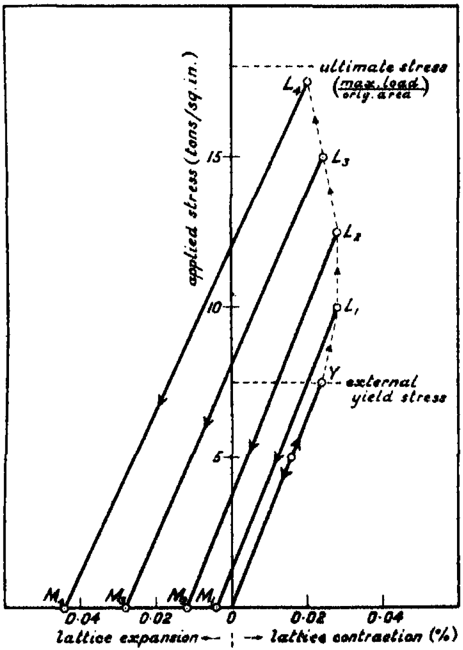

FIGURE 4. Changes in (310) lattice spacing under cycles of applied stress.

the lattice is left with the further increased expansions of OM_2, OM_3 and OM_4 respectively. Had these residual deformations been of the nature of a contraction, then it might have been concluded that the lattice had exhibited incomplete or retarded recovery from the contraction produced by the external stresses. The observation of a residual expansion is a different matter, proving that the lattice has undergone modifications of a radical character during the external plastic deformation.

(iii) The lines L_1M_1, L_2M_2, ... are, within experimental limits, parallel to the line OY which represents the lattice stress-strain relation in the range of primitive elasticity. This point was confirmed by experiments on other specimens which were examined in further detail than the single specimen to which figure 4 specifically applies. Thus a specimen was loaded to L_1 and the lattice changes measured as the load was removed in steps of 2 tons/sq. in. It was found that the curve on unloading was linear and followed the line L_1M_1. On reloading from M_1 in steps the curve again followed the path M_1L_1 until the point L_1 was reached, when it began to follow the main curve L_1L_2, ... Similar changes were exhibited by specimens loaded to L_2, L_3 and L_4 and examined in the same way. Figure 4 may thus be regarded as a composite graph giving the general behaviour of the lattice on loading and unloading. The parallelism of the lines L_1M_1, L_2M_2, ... means that the stress-strain modulus of the deformed lattice is appreciably the same as that of the initial perfect lattice, and probably explains why ordinary mechanical tests of stress-strain relations have not previously indicated directly the building up of the extensive internal strains revealed by the present X-ray tests.

(iv) The final point is concerned with the total range of reversible lattice strain associated with any particular load. When the specimen has been loaded to L_1, the previous tests showed that on unloading and re-loading the lattice changes were in linear relation to the stress over the range M_1L_1. The total range of reversible lattice strain associated with L_1 is the projection of M_1L_1 upon the x-axis. It was found that this total range at each stress was practically directly proportional to the value of the stress. The total permissible range of elastic lattice strain therefore increases with the applied stress but does so, not because the atoms are being brought closer and closer together, but because they commence their movement from positions which are farther apart.

The preceding observations offer an explanation of the peculiar shape of the basic lattice stress-strain curve given in figure 3. When a specimen is stressed beyond the external yield point, two distinct factors are brought into play. First, the lattice spacing tends to contract, in conformity with the external elastic contraction taking place in the specimen in the related direction. Secondly, the lattice tends to deform in a manner which leads to a superposed expansion of the spacing. At any particular stress, the change in spacing observed is the resultant of the two effects. The limiting lattice contraction and the subsequent tendency of the lattice to expand at the higher stresses means that the rate of expansion through deformation gains on and ultimately surpasses the rate of the more normal elastic contraction. It has been found possible to separate the two effects because the expansion persists after the stress has been removed.

The magnitude of the residual expansion of the lattice is of the same order as the elastic changes, as shown by the following data. The internal strain is thus not a second order effect.

External elastic contraction at yield point (7·5 tons/sq. in.)	0·016 %
Lattice spacing contraction at yield point	0·022 %
Limiting value of lattice contraction (at 12·5 tons/sq. in.)	0·026 %

Permanent expansion of lattice spacing (OM_1, OM_2, ..., figure 4):

After 7½ tons/sq. in.	Nil
After 12½ tons/sq. in.	0·011 %
After 17½ tons/sq. in.	0·041 %

4. Lattice expansion effect

The following further experiments were made on the permanent lattice expansion revealed by the experiments described above:

(i) The lattice strain so far discussed refers to the (310) spacing measured in a direction practically perpendicular to the applied stress. The point arises, whether any permanent strain is exhibited by the lattice in the direction of the applied stress, and whether that strain is also an expansion. It is hoped, when conditions permit, to examine this question directly by adapting the apparatus so that the incident beam may be made to strike the specimen at any of a wide range of angles inclined to the stress direction. The following test, however, gives an indication of the nature of the lattice strain in the stress direction. A tensile specimen of circular section, diameter 0·36 in., was loaded to 15·5 tons/sq. in. in a standard tensile testing machine. This stress was sufficient to produce an easily measured residual expansion of the lattice when photographed, as in the preceding tests, with the beam perpendicular to the direction of the applied stress. After unloading, it was then sawn in two perpendicularly to the direction of stretching. The exposed flat surfaces were carefully turned in the lathe with the object of removing the layers likely to be affected by the sawing. An X-ray photograph, taken with the incident beam at right angles to the turned surface, then recorded any permanent lattice deformation which might have been produced in the direction of the applied stress. Other photographs were taken after the surface had been etched to remove further cold-worked layers. With the back-reflexion spectrometer used, the diameter of the (310) diffraction ring at the various stages of test was:

	cm.
(1) Perpendicular to applied stress:	
Initial state	6·68
After loading	6·75
(2) Parallel to applied stress:	
Initial state	6·68
After loading: surface of section turned	6·75
surface of section also etched	6·75

The measurements therefore indicate that the lattice expands in the direction of the applied stress as well as at right angles, and that the increase is of the same order. The permanent expansion of the lattice is therefore not confined to the (310) spacing measured as described in the preceding sections, but appears to be a three dimensional effect, involving an increase in volume of the unit cell and thus a decrease in density of the test specimen. In passing, it is of interest to note that it is generally accepted, from data based on density measurements, that the density of a cold-worked metal tends to decrease; the present lattice change may be a factor contributing to this decrease.

(ii) A number of specimens were loaded to stresses in excess of the yield point and then heat treated in vacuo. The object was to determine the order of temperature required to remove the internal lattice strain. It was found that temperatures in excess of some 300° C would cause the expanded spacing to revert appreciably to the normal value. The recovery thus could take place at temperatures distinctly lower than the recrystallization temperature of the metal. These experiments were conducted mainly to ascertain that point, whether the lattice strain was susceptible to mild heat treatment, rather than to make a detailed study of the decrease of strain with temperature and time. The point is of interest because it is

Diameter of diffraction ring before heat treatment:	cm.
Initial state	6·68
Under load of 14 tons/sq. in.	6·61
After removal of load	6·73
Diameter after heat treatment:	
After 1 hr. at 100° C	6·73
After 1 hr. at 200° C	6·73
After 1 hr. at 300° C (recovered)	6·69

known that a number of mechanical properties of a cold-worked metal may be greatly affected by heat treatment at temperatures much lower than those required to renew the properties by recrystallization. The observations may be illustrated by the measurements (p. 103) on a specimen loaded to 14 tons/sq. in.

5. DISCUSSION

The results indicate that the metallic lattice is capable of existing at room temperature with lattice dimensions which may vary over an appreciable range. The effect in pure iron is shown to be quite marked. On the other hand, the effect in copper subjected to tensile stress and studied in the previous work (Smith and Wood 1940) was not detected. Copper, however, after plastic deformation, gives extremely diffuse diffraction rings which would tend to mask small lattice changes. The extent of the permanent lattice changes left after stressing therefore in general is likely to vary from metal to metal. With the accumulation of similar X-ray data on available metals, it should thus be possible to classify metals in respect of their susceptibility to internal lattice strains. It should also be possible, with a systematic knowledge of the lattice stress-strain curves, to tell when the degree of internal strain exhibited by a metal after particular mechanical treatment approaches the dangerously high value associated with the breaking stress. It is hoped to apply this point for instance to fracture by fatigue. This variability of lattice spacing may also prove of technical interest in problems involving the creep and recovery of metals. The completely stable lattice dimensions are presumably those obtained when all traces of internal strain have been removed by suitable heat treatment. There would always be a tendency for the abnormal lattice spacing to revert to this stable value, even at room temperature. Such changes may explain the after-recovery in external dimensions often noted in metals which have been subjected to severe cold work.

The relation between stress and lattice strain appears to be linear below the yield point and again when a specimen is unloaded and subsequently reloaded to a given stress. Observations of this type are always subject to the degree of accuracy obtainable with the available technique. It is possible that future developments may demonstrate slight deviations from these linear relationships. Indeed, when technique permits, it might be useful to look for such deviations in connexion with problems of mechanical hysteresis and internal damping. The point remains, however, that these deviations will be of a second order, and that the present measurements map out the main course of the changes which characterize the response of the lattice to external tensile stress.

The permanent lattice strain exhibited after stressing, and its systematic relation to the value of the applied stress, are perhaps the most important of the present observations. This strain appears to be of a regular character. An irregular distortion of the lattice might be expected to produce an abnormal diffusion of the diffraction rings. There is, however, no evidence of any special diffusion from this source; the sharpness of the rings is substantially the same when the amounts of internal strain are very different, and does not vary appreciably between the loaded and unloaded conditions of a specimen. The effect on the diffraction rings resembles rather that of raising the temperature of the specimen since, though there is no abnormal diffusion of the rings, there is the same tendency of their intensity to diminish in relation to the intensity of the background radiation. As a matter of interest, the rise in temperature required to produce the same lattice expansion as that remaining after unloading a specimen from the vicinity of the breaking stress would be of the order of 40° C.

The comparison between the elastic contraction of the (310) lattice spacing and the external elastic contraction of the test specimen is of interest. As shown in section 2, the lattice contraction per unit stress is 0·003 %, while the corresponding value for the external contraction, calculated from the elastic extension and Poisson's Ratio, is 0·002 %, a difference which is beyond error of measurement. Such a difference is, however, to be expected. The external contraction is the integrated effect of lattice contractions from grain to grain across the section. These contractions will vary according to the crystallographic orientation of a grain relative to the stress direction. In the previous work on copper a special point was made of measuring the contraction in two groups of grains, in one of which the (331) planes were parallel to the applied stress and in the other the (400) planes. It was shown that the lattice contraction per unit stress was distinctly different in the two cases, and attention was drawn to the interesting state of affairs which must arise at the boundaries of contiguous grains of different orientation which, according to the experimental evidence, are contracting at different rates. It was suggested for instance that this incompatibility might be responsible for the striking disruption of the grains which is a feature of the yield point of a metal. The present observation of a difference between the (310) contraction and the average contraction, represented by the external measurements, indicates that the same effect characterizes also the behaviour of polycrystalline iron under stress.

In conclusion, the authors express their thanks to Dr G. W. C. Kaye, F.R.S., for his continued interest in the work. Mr R. C. A. Thurston, B.Sc., assisted in the preparation and mechanical testing of a number of specimens.

REFERENCES

Andrade, E. N. da C. 1940 *Proc. Phys. Soc.* **52**, 54.
Gough, H. J. 1933 *Proc. Amer. Soc. Test. Mat.* **33**, 53 (Marburg Lecture).
Gough, H. J. and Wood, W. A. 1936 *Proc. Roy. Soc.* A, **154**, 510.
Gough, H. J. and Wood, W. A. 1938 *Proc. Roy. Soc.* A, **165**, 358.
Orowan, E. 1940 *Proc. Phys. Soc.* **52**, 8.
Smith, S. L. and Wood, W. A. 1940 *Proc. Roy. Soc.* A, **176**, 398.
Taylor, G. I. 1934 *Proc. Roy. Soc.* A, **145**, 362.
Wood, W. A. 1939 *Proc. Roy. Soc.* A, **172**, 231.
Wood, W. A. 1940 *Proc. Phys. Soc.* **52**, 110.

The catalytic isomerization of butene-1

BY G. H. TWIGG

Department of Colloid Science, The University, Cambridge

(*Communicated by Eric K. Rideal, F.R.S.—Received* 24 *December* 1940)

It has been shown that butene-1 undergoes isomerization to butene-2 on a nickel catalyst in the presence of hydrogen. By using deuterium, this double-bond migration has been examined simultaneously with the exchange and hydrogenation reactions. The kinetics of double-bond migration and hydrogenation at 65° C were found to be identical, the rate of reaction in both cases being proportional to the square root of the butene pressure and to the square root of the hydrogen pressure. Energies of activation for the three reactions were measured over the temperature range 76–126° C and the following values found:

Exchange	9·0 kcal.
Hydrogenation	2·5 ,,
Double-bond migration	5·9 ,,

At the lowest temperatures, the rate of double-bond migration was about six times that of exchange. These facts are in agreement with the theory that the catalytic exchange between olefines and deuterium takes place through the formation of an associative complex. The rate-determining step in the double-bond migration is the second, fast step of the exchange reaction, viz.

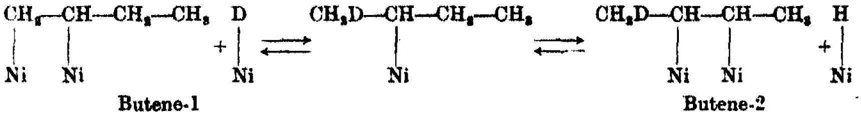

$$\underset{\mathrm{Ni}}{\mathrm{CH_2}}{-}\underset{\mathrm{Ni}}{\mathrm{CH}}{-}\mathrm{CH_2}{-}\mathrm{CH_3} + \underset{\mathrm{Ni}}{\mathrm{D}} \rightleftharpoons \mathrm{CH_2D}{-}\underset{\mathrm{Ni}}{\mathrm{CH}}{-}\mathrm{CH_2}{-}\mathrm{CH_3} \rightleftharpoons \mathrm{CH_2D}{-}\underset{\mathrm{Ni}}{\mathrm{CH}}{-}\underset{\mathrm{Ni}}{\mathrm{CH}}{-}\mathrm{CH_3} + \underset{\mathrm{Ni}}{\mathrm{H}}$$

In an early paper on the chemistry of deuterium, Farkas, Farkas and Rideal (1934) showed that when ethylene and deuterium interact on a nickel catalyst, exchange takes place between the hydrogen of the ethylene and the deuterium. Investigations which have since been carried out on this exchange reaction (Twigg and Rideal 1939; Conn and Twigg 1939) indicated that the reaction proceeded through an associative mechanism, viz.

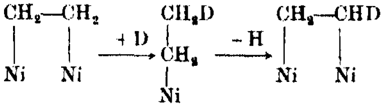

$$\underset{\mathrm{Ni}\quad\;\mathrm{Ni}}{\mathrm{CH_2{-}CH_2}} \xrightarrow{+\mathrm{D}} \begin{matrix}\mathrm{CH_2D}\\ |\\ \mathrm{CH_2}\\ |\\ \mathrm{Ni}\end{matrix} \xrightarrow{-\mathrm{H}} \underset{\mathrm{Ni}\quad\;\mathrm{Ni}}{\mathrm{CH_2{-}CHD}}$$

In these papers, it was predicted that on the basis of this mechanism, migration of the double bond in the higher olefines would take place on a nickel catalyst in the presence of hydrogen, as, for example,

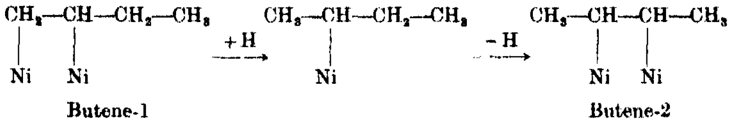

$$\underset{\mathrm{Ni}\quad\mathrm{Ni}\qquad\qquad}{\mathrm{CH_2{-}CH{-}CH_2{-}CH_3}} \xrightarrow{+\mathrm{H}} \underset{\qquad\mathrm{Ni}\qquad\quad}{\mathrm{CH_3{-}CH{-}CH_2{-}CH_3}} \xrightarrow{-\mathrm{H}} \underset{\qquad\mathrm{Ni}\quad\mathrm{Ni}\qquad}{\mathrm{CH_3{-}CH{-}CH{-}CH_3}}$$

The existence of double-bond migration under these circumstances has been verified in a qualitative manner (Twigg 1939) using the transformation of butene-1 to butene-2. The present work deals with the quantitative investigation of this reaction and its relation to the exchange and hydrogenation reactions. The evidence derived from this work gives further support to the associative mechanism for exchange postulated above.

APPARATUS AND TECHNIQUE

The apparatus used in these experiments is, with slight modifications, the same as that used previously for the exchange reaction between ethylene and deuterium (Twigg and Rideal 1939). For ease and speed of working, the deuterium content only of the hydrogen during exchange was measured, and the original fine-wire deuterium analyser was replaced by one having a close-coiled tungsten spiral. The effect of this was to make the resistance-composition calibration curve almost linear and to render the curves for equilibrium and non-equilibrium hydrogen coincident (Melville and Bolland 1937). This enabled the deuterium content to be measured without bringing the hydrogen to equilibrium. The apparatus was further modified so that the small sample of gas taken from the reaction vessel for the analysis of the deuterium could be used also for the analysis of the double-bond migration, and the two reactions thus followed simultaneously. A three-way tap was inserted between the pipette leading from the reaction vessel and the analytical system. Samples of the reacting gases are taken from the reaction vessel, and passed through a trap cooled in liquid air. The butene is condensed and the hydrogen passes on to the original analyser where the deuterium content is measured. The liquid air is then removed, and by turning the three-way tap, the butene is passed into a second analyser.

Analysis of the butene is effected by measuring the vapour pressure at − 80° C; the analyser is shown in figure 1. The butene enters at D, and is compressed into the narrow tube A_2C by raising the mercury. This tube bends over and dips into a bath of solid CO_2 and acetone. The vapour pressure of the butene is read off as the difference in levels of the mercury in BC and the adjacent tube.

In this analyser, it was originally intended to measure the vapour pressure of the butene by means of the thermal conductivity, using the Pirani gauge A_1A_2. However, this was not possible as the butene-2 produced was a mixture of *cis* and *trans* forms which were surprisingly found to have widely different coefficients of thermal conductivity. These results, however, indicate that the Pirani method is very suitable for the analysis of mixtures of *cis* and *trans* butene-2 which are otherwise difficult to distinguish on account of the close identity of their physical properties.

Each of the vapour-pressure values was the mean of five separate measurements and the probable error is ± 0·1 mm. or less. In the case of mixtures, the vapour pressure depends on the size of the sample and the degree of compression, owing to the difference in composition between liquid and vapour phases. This is shown in table 1 and the calibration curve (figure 2) for mixtures of butene-1 and *trans* butene-2; δp_m is the difference between

TABLE 1

% *trans* butene-2		p (mm.)	δp_m (mm.)
0		13·15	4·40
16·8	1 dose	12·35	3·60
	2 doses	12·40	3·65
41·8	1 dose	11·20	2·45
	2 doses	11·45	2·70
57·1	1 dose	10·40	1·65
	2 doses	10·65	1·90
79·0	1 dose	9·65	0·90
	2 doses	9·70	0·95
100		8·75	0·0

the vapour pressure of the mixture and that of *trans* butene-2. The calibration was made with single and double samples. The points lie just below the straight line and, as would be expected, the values for a single dose lie below those for two doses. The size of butene sample taken during an experiment varies between 1 and 1½ doses as the reaction proceeds. The curve used was that drawn for single doses. The standard vapour-pressure values for butene-1, *trans* butene-2 and butane varied slightly with the atmospheric pressure and were redetermined before each experiment.

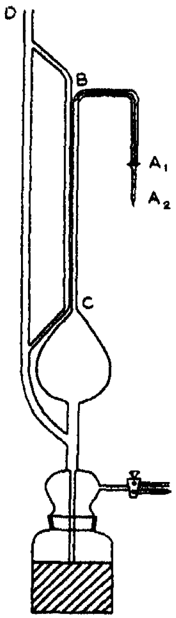

FIGURE 1

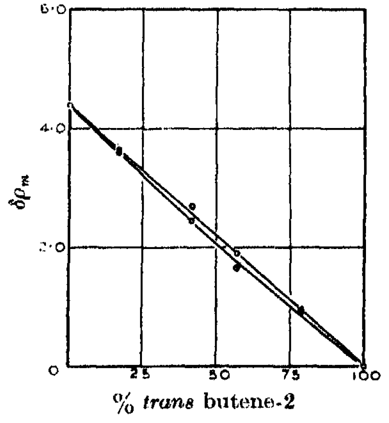

FIGURE 2

The analysis is greatly complicated by the presence of butane produced by hydrogenation of the butene, and the method of correcting for this is somewhat involved. Measurements were made on different mixtures of butene-1 and butene-2 to which were added varying quantities of butane. The values fell into two groups, those where the vapour pressure of the mixture was greater than that of butane, and those where it was less. In the first case it was seen that the curves obtained on plotting the vapour pressure against the butane content for given butene-1-butene-2 mixtures were similar in shape. Accordingly, on the assumption that all the curves with different butene-1-butene-2 ratios had the same form, a single correction curve (figure 3 A) was made by altering, by means of formula (1), the observed values (δp) to values (δp^*) which they would have had if the butene-2 concentration had been zero. The values of δp, δp^*, etc. are reckoned from that of pure *trans* butene-2 as zero. The correction for the presence of butane in the butene is then derived as follows. The dotted curve of figure 3 represents the vapour pressure of a mixture of butane with the unknown mixture of butene-1 and butene-2. Then δp is the observed vapour pressure of the total mixture, and δp_m that of the butene-1-butene-2 mixture without butane. Since the two curves are similar, then

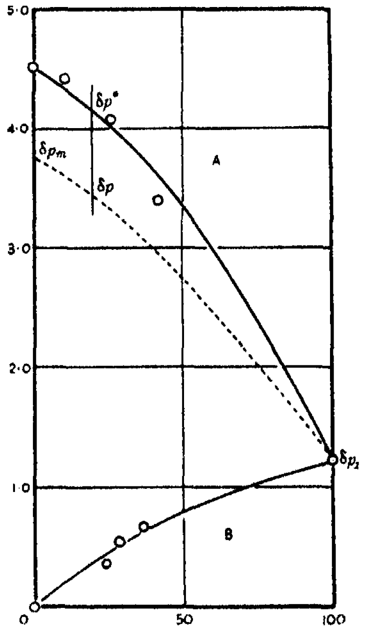

FIGURE 3

$$\delta p_m = \delta p_0 - (\delta p^* - \delta p)\frac{\delta p_0 - \delta p_s}{\delta p^* - \delta p_s}, \qquad (1)$$

where δp_0 is the vapour pressure of butene-1 and δp_s that of butane. The butane content is obtained by following the hydrogenation reaction, and δp^* is then found from the correction curve. The values of δp_m thus obtained from formula (1) are then used in conjunction with the graph of figure 2. A similar procedure was adopted in the case where the vapour pressure was less than that of butane, except that the correction curve (figure 3, B) is drawn for mixtures of butane with *trans* butene-2. Formula (1) is again applied but with δp_0 now equal to zero. Table 2 shows the course of the double-bond migration with these corrections applied. It will be seen that the correction becomes very considerable towards the end of the reaction, but despite this, the error in the butene-2 concentration is estimated to be not more than ± 3 %.

TABLE 2. REACTION 220, 76° C

t min.	Z % butane	vapour pressure mm. Hg	δp mm.	δp_m mm.	% butene-2
16	6	11·38	2·76	2·81	35
33	10	10·16	1·54	1·56	63
62	17	9·52	0·90	0·84	79
143	32	9·32	0·70	0·31	92

The course of the reaction with time is derived as follows:

$$\underset{1-y}{\text{Butene-1}} \quad \underset{k_2}{\overset{k}{\rightleftharpoons}} \quad \underset{y}{\text{Butene-2}}$$

Let y be the fraction of butene-2 in the mixture, $p_{\text{bu.}}$ the total pressure of the butenes, $p_{\text{hyd.}}$ the hydrogen pressure, k_1 and k_2 the velocity constants of forward and back reactions, c_1, c_2 and $c_{\text{hyd.}}$ the surface concentrations of butene-1, butene-2 and hydrogen respectively. Then

$$p_{\text{bu.}}\frac{dy}{dt} = k_1 c_1 c_{\text{hyd.}} - k_2 c_2 c_{\text{hyd.}}, \tag{2}$$

and

$$\frac{k_1}{k_2} = K = \frac{y_{\text{eq.}}}{1-y_{\text{eq.}}}, \tag{3}$$

where $y_{\text{eq.}}$ is the equilibrium value of y. If we make the assumption that butene-1 and butene-2 have the same adsorbabilities on the catalyst, then

$$\frac{c_1}{c_2} = \frac{1-y}{y}. \tag{4}$$

Substituting in equation (2), we get

$$\begin{aligned} p_{\text{bu.}}\frac{dy}{dt} &= k_1(c_1+c_2)\,c_{\text{hyd.}}\left[1-y-\frac{y}{K}\right] \\ &= k_1(c_1+c_2)\,c_{\text{hyd.}}\,\frac{y_{\text{eq.}}-y}{y_{\text{eq.}}} \\ &= k_1\theta(p_{\text{bu.}}, p_{\text{hyd.}})\frac{y_{\text{eq.}}-y}{y_{\text{eq.}}}, \end{aligned}$$

where $\theta(p_{\text{bu.}}, p_{\text{hyd.}})$ is a function of the butene and hydrogen pressures.

Integration gives the final result

$$y_{\text{eq.}} - y = y_{\text{eq.}} e^{-\alpha t}, \tag{5}$$

where
$$\alpha = \frac{k_1 \theta(p_{\text{bu.}}, p_{\text{hyd.}})}{p_{\text{bu.}} . y_{\text{eq.}}}.$$

From the curve of $\log y_{\text{eq.}} - y$ against time, the initial rate of reaction is obtained by the formula

$$\left(\frac{dy}{dt}\right)_0 = -y_{\text{eq.}} \frac{d}{dt} \log (y_{\text{eq.}} - y) = \frac{k_1 \theta(p_{\text{bu.}}, p_{\text{hyd.}})}{p_{\text{bu.}}}. \tag{6}$$

The value of $y_{\text{eq.}}$ used in applying equation (5) was determined experimentally. The equilibrium was approached from both sides, butene-1 being used in one case, and *trans* butene-2 in the other. The two agreed in giving $y_{\text{eq.}}$ equal to about 93 %. This is somewhat lower than is found by extrapolating the thermal data of Todd and Parks (1936), which gives for $y_{\text{eq.}}$ the value of 96–97 % in the temperature range 70–130° C. The value of 93 % was used in working out the present experiments.

The light hydrogen and deuterium were obtained and purified as described previously (Twigg and Rideal 1939). The butene-1 was kindly supplied by the Anglo-Iranian Oil Co., Ltd., and was purified by distillation from liquid air, the middle fraction only being taken. I am greatly indebted to Professor G. B. Kistiakowsky for samples of pure *cis* and *trans* butene-2. The catalyst consisted of a 0·1 mm. diameter nickel wire and it was heated by means of a furnace round the reaction vessel.

RESULTS

It was first verified that no double-bond migration occurred in the absence of hydrogen. Butene-1 was left in the reaction vessel for 20 min. at 133° C; no transformation to butene-2 could be detected.

The kinetics of the double-bond migration were determined at 65° C. Light hydrogen was used for this and the exchange reaction was not observed. The kinetics of the hydrogenation were determined simultaneously. Table 3 shows the results obtained.

Here $(dy/dt)_0$ and $-(dp/dt)_0$ represent the initial rates of double-bond migration (D.B.M.) and hydrogenation respectively. The fifth entry in the table gives, from equation (6), values of $k_1 \theta(p_{\text{bu.}}, p_{\text{hyd.}})$ corrected for varying activity a of the catalyst. The activity was determined by means of a standard hydrogenation reaction using ethylene. Comparison of these values shows that, approximately, $\theta = p_{\text{bu.}}^{\frac{1}{2}}\, p_{\text{hyd.}}^{\frac{1}{2}}$. That is, the rate of double-bond migration is proportional to the square root of the butene pressure and to the square root of the hydrogen pressure. The figures in the second last line show that similarly the rate of hydrogenation is proportional to the square root of the butene pressure and the square root of the hydrogen pressure. Further evidence that the kinetics of the two reactions are identical is given by the constancy of the figures in the last line of the table, which give the ratio of the rates of the two reactions. The significance of this result is to be found in the close connexion which it shows between the two reactions. This is to be compared with the results found previously for ethylene (Twigg and Rideal 1939) which showed that the exchange and hydrogenation reactions of ethylene had identical kinetics. Thus all three reactions—exchange, hydrogenation, and double-bond migration—are controlled by the same adsorption factors. Comparison with the previous results (Twigg and Rideal 1939) shows that, despite the lower temperature used here, the rates of the butene reactions are not independent of the olefine pressure, and consequently the surface of the catalyst is not completely covered with butene, in contrast to the case of ethylene, where it is. This is to be expected on the basis of calculations made on the fitting of olefines on to the nickel surface (Twigg and Rideal 1940). In this paper it was shown that, owing to their size, methyl-substituted ethylenes should be incapable of covering the whole catalyst surface. The fact that the order

TABLE 3. 65° C

	reaction 213	reaction 215	reaction 216
p_{H_2} (mm.)	8·2	32·3	31·9
$p_{\text{bu.}}$ (mm.)	8·4	8·4	31·9
Activity a	2·1	1·3	1·1
$\left(\frac{dy}{dt}\right)_0 \times 10^3$	1·59	2·08	0·92
$\frac{1}{a} p_{\text{bu.}} \left(\frac{dy}{dt}\right)_0 \times 10^3$	6·4	13·2	26·6
$-\left(\frac{dp}{dt}\right)_0 \times 10^2$	5·7	6·4	11·8
$-\frac{1}{a}\left(\frac{dp}{dt}\right)_0 \times 10^2$	2·7	4·9	10·7
$\frac{\text{D.B.M.}}{\text{Hydrogenation}}$	2·4	2·7	2·5

of reaction with respect to the hydrogen pressure is less in the present case than with ethylene is to be expected on account of the lower temperature.

The three reactions—exchange, hydrogenation, and double-bond migration—were examined simultaneously over the temperature range 76–126° C and energies of activation were determined. Equal quantities of deuterium and butene-1, 10·7 mm. of each, were used. Table 4 gives the results obtained; the initial rates of the three reactions are corrected for varying activity of the catalyst. The values for the ratio of the rate of double-bond migration to rate of exchange, D.B.M./E., are derived from the equation

$$\frac{\text{D.B.M.}}{\text{E.}} = p_{\text{bu}}\left(\frac{dy}{dt}\right)_0 \Big/ p_{\text{D}_2}\left(\frac{du}{dt}\right)_0.$$

Graphs of the log of the rate against $1/T$ for exchange and double-bond migration are shown in figure 4. The energies of activation found were:

Exchange	9·0 kcal.
Hydrogenation	2·5 kcal.
Double-bond migration	5·9 kcal.

It is to be noted that the values for the exchange and hydrogenation reactions agree with the corresponding values for butene-2 (Twigg 1939). This agreement is to be expected in the case of the exchange reactions, since both butenes are interconverted during the process of exchange of all the hydrogen atoms in the molecule.

TABLE 4

	Hydrogenation	Exchange	D.B.M.	
T° C	$\frac{1}{a}\left(\frac{dp}{dt}\right)_0$	$\frac{1}{a}\left(\frac{du}{dt}\right)_0$	$\frac{1}{a}\left(\frac{dy}{dt}\right)_0$	$\frac{\text{D.B.M.}}{\text{E.}}$
76·0	$9{\cdot}4 \times 10^{-2}$	$0{\cdot}49 \times 10^{-2}$	$3{\cdot}01 \times 10^{-2}$	6·1
86·5	10·0	0·57	3·57	6·2
101·5	10·9	0·93	5·05	5·6
114·5	12·2	1·39	7·0	5·0
126·0	15·9	1·97	7·5	3·8

The most noteworthy feature of the results is that the double-bond migration is much faster than the exchange reaction. The ratio D.B.M./E. is equal to the ratio of the number of butene molecules isomerized to the number of deuterium molecules transformed to light hydrogen molecules. This means that, at the lowest temperatures, approximately twelve molecules are isomerized per deuterium atom transformed. In a previous paper (Twigg and Rideal 1939) it was shown in the case of ethylene that the slow initial step involving the adsorption of the hydrogen, according to the reaction

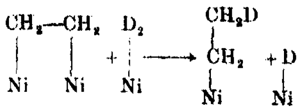

$$\underset{\text{Ni}}{\text{CH}_2}-\underset{\text{Ni}}{\text{CH}_2} + \underset{\text{Ni}}{\text{D}_2} \longrightarrow \underset{\text{Ni}}{\overset{\text{CH}_2\text{D}}{\text{CH}_2}} + \underset{\text{Ni}}{\text{D}} \qquad \text{(i)}$$

is followed by a fast reaction involving atoms and of the type

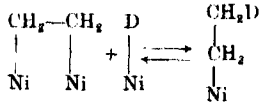

$$\underset{\text{Ni}}{\text{CH}_2}-\underset{\text{Ni}}{\text{CH}_2} + \underset{\text{Ni}}{\text{D}} \rightleftarrows \underset{\text{Ni}}{\overset{\text{CH}_2\text{D}}{\text{CH}_2}} \qquad \text{(ii)}$$

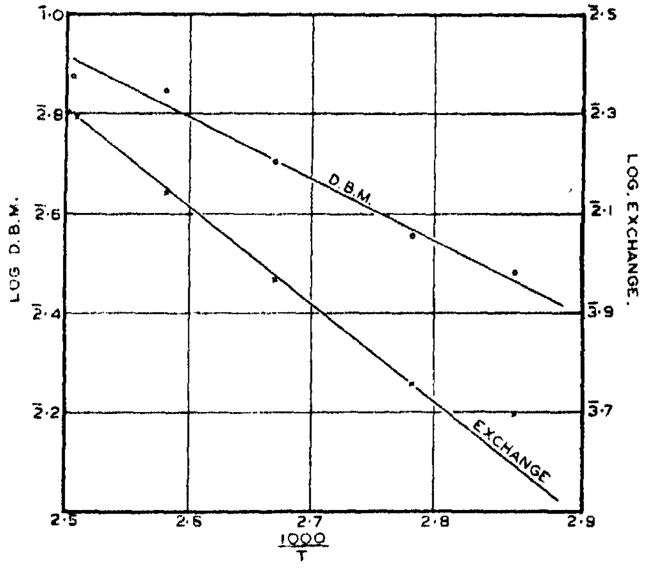

FIGURE 4

By this second reaction, every molecule entering the adsorption layer underwent a number of exchanges before desorption. For ethylene, this number appears to be about four to six per deuterium atom. It thus seems that these processes are again operative in the case of butene, and that the double-bond migration is effected by the fast second reaction, which in the case of butene becomes

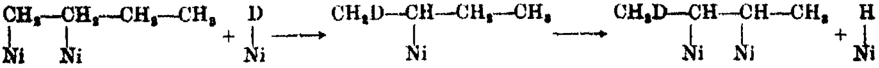

$$\underset{\text{Ni}}{\text{CH}_2}-\underset{\text{Ni}}{\text{CH}_2}-\text{CH}_2-\text{CH}_3 + \underset{\text{Ni}}{\text{D}} \longrightarrow \text{CH}_2\text{D}-\underset{\text{Ni}}{\text{CH}}-\text{CH}_2-\text{CH}_3 \longrightarrow \text{CH}_2\text{D}-\underset{\text{Ni}}{\text{CH}}-\underset{\text{Ni}}{\text{CH}}-\text{CH}_3 + \underset{\text{Ni}}{\text{H}}$$

If this reaction were absent, and reactions of the type (i) only operated, then a maximum of one butene molecule could be isomerized per deuterium atom exchanged.

The rate of exchange has been shown previously to be controlled by the first step (i), since that determines the rate at which the light hydrogen produced by the second step exchanges with the deuterium in the gas phase. The double-bond migration, however, is not dependent on the rate at which the hydrogen enters or leaves the adsorbed layer but is controlled alone by the hydrogen in the layer. Thus the double-bond migration is controlled either by step (ii) or by the evaporation of butene from the surface.

It seems improbable that evaporation is the slow rate-determining step for the following reasons. The fact that the rate of double-bond migration is proportional to the half-power of the butene pressure is evidence that only part of the surface is covered by the butene. It has also been shown previously (Twigg and Rideal 1940) that methyl-substituted ethylenes do not cover the whole surface of the catalyst and that hydrogen is also present on the surface. Unless this hydrogen exists only in small quantity and as isolated immobile atoms, the butene-1-butene-2 equilibrium would be established over the whole surface by means of reaction (ii). Since this equilibrium is not affected by hydrogen, the pressure of hydrogen would not determine the type of molecule desorbed; the rate of double-bond migration would be controlled only by the rate of desorption of butene from a nickel surface and thus would be independent of the hydrogen pressure, contrary to what was found.

The velocity of step (ii) will depend on the surface hydrogen concentration. Since the hydrogen enters the surface by means of reaction (i), the concentration will be determined by the equilibrium point of that reaction and therefore will be proportional to the concentration of hydrogen molecules in the van der Waals layer. This accounts for the identity in kinetics of the three reactions—exchange, hydrogenation, and double-bond migration.

These experiments on double-bond migration thus fit in with the other work on the exchange reaction and give further confirmation to the theory that exchange takes place through the associative mechanism. A. Farkas (1939) has asserted that double-bond migration can occur through the dissociative mechanism, and has suggested the following scheme to account for this:

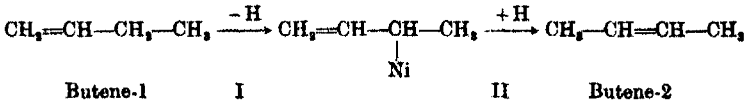

$$CH_2{=}CH{-}CH_2{-}CH_3 \xrightarrow{-H} CH_2{=}CH{-}\underset{\substack{|\\ Ni}}{CH}{-}CH_3 \xrightarrow{+H} CH_3{-}CH{=}CH{-}CH_3$$

Butene-1 I II Butene-2

This mechanism can be criticized on several grounds. The hydrogen atom which is abstracted from the butene-1 molecule on adsorption is restored in the second step in a different way. This step is highly artificial and demands the simultaneous performance of several acts. The hydrogen atom is restored to a carbon atom distant from the point of attachment of the molecule to the surface, and simultaneously, the double bond has to switch from the 1- to the 2-position, and the nickel-carbon bond has to be broken. The artificiality of this scheme can be seen more clearly by considering the reverse of the second step. Here, in order that the molecule may be adsorbed, it has to lose a hydrogen atom from one carbon atom, attach itself to the surface by means of a distant carbon atom, and at the same time switch round the double bond.

The chief criticism of Farkas's mechanism, however, is offered by the results of the experiments described above. If the mechanism which he has advanced were correct, then step I, together with its reverse, or step II and its reverse, would bring about exchange but no double-bond migration; for the latter, both steps I and II are necessary. Consequently, the rate of the double-bond migration will be controlled by the slower of the two steps, whereas the exchange will be controlled by the faster; that is, the double-bond migration can never be faster than exchange, and in the most favourable case, a maximum of one butene molecule could be isomerized for each deuterium atom exchanged. The present experiments show that this is far from being so, and that double-bond migration is much faster than exchange. Similarly, if Farkas's mechanism were correct, the energy of activation for double-bond migration could never be less than that for exchange; the opposite was found to be the case. This explanation of double-bond migration on the dissociative theory for exchange must be regarded as inadequate, whereas the associative theory gives a consistent picture of the whole reaction.

The author has much pleasure in thanking Professor E. K. Rideal for his helpful advice and stimulating discussion. He also desires to record his thanks to the Carnegie Trust for a Research Fellowship.

REFERENCES

Conn and Twigg 1939 *Proc. Roy. Soc.* A, **171**, 70.
Farkas 1939 *Trans. Faraday Soc.* **35**, 906.
Farkas, Farkas and Rideal 1934 *Proc. Roy. Soc.* A, **146**, 630.
Melville and Bolland 1937 *Trans. Faraday Soc.* **33**, 1316.
Todd and Parks 1936 *J. Amer. Chem. Soc.* **58**, 134.
Twigg 1939 *Trans. Faraday Soc.* **35**, 934.
Twigg and Rideal 1939 *Proc. Roy. Soc.* A, **171**, 55.
Twigg and Rideal 1940 *Trans. Faraday Soc.* **36**, 533.

A self-consistent field for methane and its applications

By R. A. Buckingham, Ph.D.,* H. S. W. Massey, F.R.S.
and S. R. Tibbs, Ph.D.
University College, London

(*Received* 6 *November* 1940)

An approximate self-consistent field for methane has been obtained by first averaging the proton distribution over all orientations so as to obtain a spherically symmetrical field due to all the nuclei. The eight-electron problem then presented was solved by the usual self-consistent field method without exchange. Rapid convergence to self-consistency was found by using as initial approximations the charge distributions given by Coulson for the two-quantum orbitals of the tetrahedral system, averaged over all orientations.

The self-consistent wave functions are used to calculate the charge distribution, energy, diamagnetic susceptibility and polarizability of the molecule and also the van der Waals forces between two molecules. The scattering of slow electrons by the self-consistent field obtained is also investigated in detail and compared with observations of total collision areas and angular distributions for methane. The observed similarity of behaviour between argon and methane in scattering slow electrons is reproduced by the theory provided the same approximation of using the self-consistent field without exchange is employed for each. Comparison of observed and calculated values of the quantities investigated indicate that the methane field is little less satisfactory than the corresponding fields for atoms.

The principles underlying the self-consistent field method are frequently employed in discussing molecular and nuclear problems, but the detailed numerical applications have largely been confined to atoms. This is because of the difficulty of solving the wave equation for individual electrons when the effective potential energy concerned is not spherically symmetrical, a difficulty present even for atoms when the occupied orbitals are not all of s type. The energy of a particular electron, due to its coulomb interaction with an electron in a $p, d, f, \ldots$ or other orbital with $l \neq 0$, is not a function only of the distance of the electron from the nucleus, so it is necessary to average the interaction energy over all orientations of the axis of quantization before inclusion in the particular wave equation. This process is not effective for molecules because of the lack of spherical symmetry in the distribution of atomic nuclei, but for those molecules possessing a high degree of symmetry, such as the tetrahedral molecules CH_4, CCl_4, SiH_4, etc., it is possible to extend the averaging method to the nuclear distribution also, without departing too far from reality. If the nuclear distribution is averaged over all orientations about the central nucleus, the system becomes similar to an atom with part of its nucleus removed and distributed uniformly in a spherical shell around the residual nucleus as centre. Once a spherically symmetrical nuclear distribution is obtained, the usual procedure may be employed to find the self-consistent distribution of electrons.

---

* Exhibition of 1851 Senior Research Student.

The averaging of the nuclear distribution before carrying out the calculations is more open to criticism than that of electron distributions in the usual applications to atoms; the motion of the nuclei is so slow that the molecular electrons follow the nuclear distribution in detail rather than move in the time average of the field due to it. Nevertheless, if the symmetry is high the time average of the distribution will not differ greatly from an instantaneous distribution and the results obtained should be of sufficient accuracy to be of value.

In this paper we apply the method in detail to the simplest case, that of methane. The self-consistent electron wave functions are obtained and employed to calculate the charge distribution, energy, diamagnetic susceptibility and polarizability of the molecule and also the van der Waals forces between two molecules. The scattering of slow electrons by the self-consistent field derived is also investigated in detail. Comparison of the calculated and observed results reveals reasonable agreement, shows the method to be capable of yielding valuable information and indicates the directions in which the theory is at fault.

We employ the same notation and units as in the usual applications (Hartree and Black 1933) of the self-consistent field method to atoms.

THE SELF-CONSISTENT WAVE FUNCTIONS

In the methane molecule the four protons are at a distance $2a_0$ from the carbon nucleus. We average this distribution over all orientations; so the potential energy of an electron at distance r from the carbon nucleus, due to all nuclei, is taken as

$$\left.\begin{aligned} V_n &= -2-6/r, \quad r<2, \\ &= -10/r, \qquad r>2. \end{aligned}\right\} \tag{1}$$

The ground state of this system will be a $(1s)^2(2s)^2(2p)^6$ term. The corresponding wave functions $rP(1s\,|\,r), rP(2s\,|\,r), rP(2p, r)$ will satisfy the usual self-consistent equations:

$$\left.\begin{aligned} P''(1s\,|\,r) + 2[\epsilon_{1s} - V_n - \{Z_p(1s) + 2Z_p(2s) + 6Z_p(2p)\}/r]\,P(1s\,|\,r) &= 0,\\ P''(2s\,|\,r) + 2[\epsilon_{2s} - V_n - \{2Z_p(1s) + Z_p(2s) + 6Z_p(2p)\}/r]\,P(2s\,|\,r) &= 0,\\ P''(2p\,|\,r) + 2[\epsilon_{2p} - V_n - 1/r^2 - \{2Z_p(1s) + 2Z_p(2s) + 5Z_p(2p)\}/r]\,P(2p\,|\,r) &= 0. \end{aligned}\right\} \tag{2}$$

$r^{-1}Z_p(\alpha\beta)$ is the averaged potential at r due to an electron in the $\alpha\beta$ orbital and it satisfies

$$Z''_p = -r^{-1}P^2(\alpha\beta\,|\,r), \tag{3}$$

with $$Z_p(0) = 0, \quad Z_p(\infty) = 1.$$

To solve these equations conveniently it is necessary to start with a good first approximation. It is not possible to obtain much help from atomic field calculations, as V_n is a type of nuclear field which does not occur in such cases. Instead, use was made of an investigation of the methane molecule from the standpoint of molecular orbitals, due to Coulson (1937). The two-quantum orbitals of an electron in the field of tetrahedral symmetry existing in the methane molecule are of two types, usually designated $2s_a$, $2t$ respectively (van Vleck and Sherman 1935). If $\psi(\mathrm{C}; 2s)$, $\psi(\mathrm{C}; 2p_x)$ are the wave functions for the $2s, 2p_x$ orbitals respectively of a carbon atom, $\psi(\mathrm{H})$ that for a hydrogen atom, then Coulson writes, for the methane orbitals,

$$\left.\begin{aligned} \psi(2s_a) &= \lambda_s\psi(\mathrm{C}; 2s) + \mu_s\{\psi(\mathrm{H}_1) + \psi(\mathrm{H}_2) + \psi(\mathrm{H}_3) + \psi(\mathrm{H}_4)\},\\ \psi(2t_x) &= \lambda_t\psi(\mathrm{C}; 2p_x) + \mu_t\{\psi(\mathrm{H}_1) + \psi(\mathrm{H}_2) - \psi(\mathrm{H}_3) - \psi(\mathrm{H}_4)\}, \end{aligned}\right\} \tag{4}$$

with $\psi(2t_y)$, $\psi(2t_z)$ following in cyclic order, the suffixes 1, 2, 3, 4 distinguishing the different hydrogen atoms. These satisfy the symmetry requirements given by van Vleck and Sherman and μ_s/λ_s, μ_t/λ_t may be determined by a variation method. This was done by Coulson using simplified forms for $\psi(\mathrm{C}; 2s)$, $\psi(\mathrm{C}; 2p)$ involving an effective nuclear charge Z_c. A value $Z_c = 1{\cdot}72$ was found to give the correct energy and for it $\lambda_s/\mu_s = 8{\cdot}22$, $\lambda_t/\mu_t = 1{\cdot}70$. To estimate the functions Z_p for substitution in (2), we then chose in (3)

$$\left.\begin{aligned} &P^2(2s) = r^2\,\overline{|\,\psi(2s_a)\,|^2}, \quad P^2(2p) = \tfrac{1}{3}r^2\Sigma_x\,\overline{|\,\psi(2t_x)\,|^2},\\ &P^2(1s) = r^2\,|\,\psi(\mathrm{C}; 1s)\,|^2, \end{aligned}\right\} \tag{5}$$

where the averaging is over all orientations of the hydrogen nuclei. $\psi(\mathrm{C}; 1s)$, $\psi(\mathrm{C}; 2s)$, $\psi(\mathrm{C}; 2p)$ were taken as the self-consistent functions for the carbon atom given by Torrance (1934) and λ_s/μ_s, λ_t/μ_t as given above.

This procedure was very effective in securing rapid convergence to self-consistency. Thus the $P(2p)$ function resulting from integration of (2) with the Z_p values given from (5) was found to be already self-consistent to the desired accuracy. The Z_p values which it gave on substitution in (3) differed from the initial values by no more than 0·002 at any point. The $P(2s)$ function, given by the first integration of (2), was not quite so satisfactory, but one further approximation sufficed to give it to the same accuracy as $P(2p)$. One approximation was sufficient for $P(1s)$ which does not differ very much from $P(\mathrm{C}; 1s)$.

The final functions obtained, together with the corresponding ϵ and Z_p values, are given in table 1.

CHARGE DISTRIBUTION

The radial charge distribution for two-quantum electrons in the molecule is given by $\frac{1}{4}P^2(2s)+\frac{3}{4}P^2(2p)$. This is illustrated in figure 1, which also includes the corresponding distribution for carbon atoms,

$$\tfrac{1}{2}P^2(\mathrm{C}; 2s)+\tfrac{1}{2}P^2(\mathrm{C}; 2p),$$

obtained from the functions given by Torrance (1934). The effect of the surface distribution of positive charge at $r = 2a_0$ is apparent in producing an outward shift of electron density. From the evidence derived from diamagnetic susceptibility, polarizability and electron scattering, discussed below, it is probable that this shift should be less marked, at least in the region beyond the maximum.

ENERGY OF THE MOLECULE

The energy of the system may be calculated from the wave functions by the method described by Hartree and Black (1933). We employ the same notation as in their paper and list the various contributions to the energy in table 2*. In calculating these contributions rigorously the 2s wave function

---

* The quantities I, F, G are defined by

$$I(\alpha) = -\frac{1}{2}\int P(\alpha \mid r)\left[\frac{d^2}{dr^2} - V_n - \frac{l_\alpha(l_\alpha+1)}{r^2}\right]P(\alpha \mid r)\,dr,$$

$$F_k(\alpha\beta) = \iint P^2(\alpha \mid r)\,P^2(\beta \mid r_1)\,\frac{r_a^k}{r_b^{k+1}}\,dr\,dr_1,$$

$$G_k(\alpha\beta) = \iint P(\alpha \mid r)\,P(\alpha \mid r_1)\,P(\beta \mid r)\,P(\beta \mid r_1)\,\frac{r_a^k}{r_b^{k+1}}\,dr\,dr_1,$$

where r_a and r_b are respectively the smaller and larger of r and r_1, V_n is the potential energy due to the nuclei above.

TABLE 1. SELF-CONSISTENT WAVE FUNCTIONS AND Z_p VALUES

	Unnormalized wave functions			Contributions to Z_p		
r	$P(1s)$	$P(2s)$	$P(2p)$	1s*	2s	2p
0·01	0·0942	−0·0565	0·0005	0·0564	0·0082	0·0061
0·02	0·1774	−0·1064	0·0019	0·1122	0·0163	0·0122
0·03	0·2507	−0·1502	0·0041	0·1668	0·0244	0·0183
0·04	0·3150	−0·1884	0·0071	0·2198	0·0325	0·0244
0·05	0·3711	−0·2215	0·0108	0·2709	0·0405	0·0305
0·06	0·4198	−0·2499	0·0151	0·3200	0·0483	0·0367
0·07	0·4618	−0·2740	0·0200	0·3667	0·0561	0·0428
0·08	0·4977	−0·2941	0·0254	0·4112	0·0639	0·0489
0·09	0·5281	−0·3106	0·0313	0·4533	0·0715	0·0550
0·10	0·5535	−0·3238	0·0376	0·4930	0·0790	0·0611
0·12	0·5913	−0·3414	0·0514	0·5655	0·0938	0·0733
0·14	0·6145	−0·3487	0·0665	0·6292	0·1083	0·0855
0·16	0·6261	−0·3475	0·0827	0·6846	0·1224	0·0977
0·18	0·6282	−0·3391	0·0997	0·7325	0·1364	0·1099
0·20	0·6229	−0·3247	0·1175	0·7738	0·1501	0·1221
0·22	0·6118	−0·3053	0·1359	0·8091	0·1636	0·1342
0·24	0·5962	−0·2818	0·1547	0·8393	0·1770	0·1464
0·26	0·5771	−0·2549	0·1738	0·8649	0·1903	0·1585
0·28	0·5556	−0·2253	0·1931	0·8867	0·2035	0·1706
0·30	0·5324	−0·1935	0·2125	0·9051	0·2166	0·1826
0·32	0·5081	−0·1600	0·2319	0·9206	0·2297	0·1947
0·36	0·4581	−0·0895	0·2706	0·9446	0·2558	0·2186
0·40	0·4084	−0·0166	0·3088	0·9616	0·2819	0·2423
0·44	0·3609	+0·0567	0·3461	0·9734	0·3080	0·2658
0·48	0·3167	0·1289	0·3822	0·9816	0·3340	0·2891
0·52	0·2762	0·1988	0·4168	0·9874	0·3600	0·3120
0·56	0·2398	0·2656	0·4498	0·9913	0·3859	0·3346
0·60	0·2075	0·3288	0·4812	0·9940	0·4117	0·3569
0·64	0·1791	0·3881	0·5109	0·9959	0·4372	0·3789
0·72	0·1331	0·4943	0·5653	0·9981	0·4871	0·4215
0·80	0·0995	0·5837	0·6133	0·9991	0·5352	0·4625
0·88	0·0759	0·6568	0·6553	0·9996	0·5810	0·5018
0·96	0·0603	0·7151	0·6918	0·9998	0·6242	0·5392
1·04	0·0462	0·7602	0·7234	0·9999	0·6645	0·5747
1·12	0·0332	0·7937	0·7506	0·9999	0·7018	0·6083
1·20	0·0225	0·8170	0·7739	1·0000	0·7361	0·6400
1·28	0·0150	0·8315	0·7936	1·0000	0·7673	0·6699
1·44	0·0075	0·8391	0·8233	1·0000	0·8212	0·7240
1·60	0·0036	0·8246	0·8410	1·0000	0·8645	0·7709
1·76	0·0016	0·7936	0·8468	1·0000	0·8985	0·8112
1·92	0·0008	0·7497	0·8402	1·0000	0·9249	0·8454
2·08	$0{\cdot}0005_5$	0·6950	0·8200	1·0000	0·9448	0·8740
2·24	0·0003	0·6336	0·7885	1·0000	0·9579	0·8976
2·40	$0{\cdot}0001_5$	0·5702	0·7497	1·0000	0·9707	0·9171
2·56	—	0·5080	0·7068	1·0000	0·9788	0·9330
2·88	—	0·3949	0·6172	1·0000	0·9889	0·9565
3·20	—	0·3009	0·5300	1·0000	0·9941	0·9719
3·52	—	0·2263	0·4499	1·0000	0·9968	0·9818
3·84	—	0·1686	0·3788	1·0000	0·9982	0·9883
4·16	—	0·1249	0·3169	1·0000	0·9989	0·9924
4·48	—	0·0923	0·2638	1·0000	0·9993	0·9951
4·80	—	0·0682	0·2184	1·0000	0·9996	0·9968
5·44	—	0·0359	0·1480	1·0000	0·9998	0·9986
6·08	—	0·0187	0·0991	1·0000	0·9999	0·9994
6·72	—	0·0096	0·0658	1·0000	1·0000	0·9997
7·36	—	0·0049	0·0482	1·0000	1·0000	0·9998
8·00	—	0·0025	0·0282	1·0000	1·0000	0·9999
8·64	—	0·0013	0·0183	1·0000	1·0000	1·0000
9·28	—	0·0006	0·0118	1·0000	1·0000	1·0000
9·92	—	0·0003	0·0076	1·0000	1·0000	1·0000
Normalizing factor	2·7477	0·9203	0·7692			
2ε	−22·57	−1·366	−0·654			

* The values of $Z_p(1s)$ given here have been derived from the $P(1s)$ function given by Torrance (1934) for carbon. For the applications considered in this paper the departure from the corresponding function for methane is not significant.

should first be made orthogonal to the $1s$ function, but the correction due to this is so small that we have ignored it.

TABLE 2. CONTRIBUTIONS TO TOTAL ENERGY OF METHANE AND C + 4H

	CH_4		C + 4H	
Term	Value	Coefficient	Value	Coefficient
$I(1s)$	−20·34	2	−17·87	2
$I(2s)$	− 5·466	2	− 3·762	2
$I(2p)$	− 4·627	6	− 3·241	2
$F_0(1s, 1s)$	3·468	1	3·440	1
$F_0(1s, 2s)$	0·7408	4	$0{\cdot}791_5$	4
$F_0(1s, 2p)$	0·6078	12	0·713	4
$F_0(2s, 2s)$	0·5217	1	0·548	1
$F_0(2s, 2p)$	0·4667	12	0·513	4
$F_0(2p, 2p)$	0·4241	15	0·484	1
$F_2(2p, 2p)$	—	0	0·178	$-\frac{1}{5}$
$G_0(1s, 2s)$	0·0546	−2	0·05	−2
$G_0(1s, 2p)$	0·0510	−2	0·05	$-\frac{2}{3}$
$G_0(2s, 2p)$	0·4197	−2	0·456	$-\frac{2}{3}$
Nuclear repulsions	13·84	1	—	—
$E(H)$	—	—	− 0·5000	4
Total energy	$-40{\cdot}37_5$	—	−39·68	—

To examine whether our model is capable of giving a positive binding energy we have also evaluated the energy of the system C + 4H from the self-consistent functions given for carbon by Torrance (1934). The separate contributions are also given in table 2. Comparing the calculated energy of CH_4 with that for C + 4H shows that our model gives a binding energy of 0·70 atomic units, i.e. 19 eV, to be compared with the observed value 20 eV. The exact value is difficult to calculate, as it appears as a small difference between two large quantities. Further, in evaluating the contributions I, the values given for the molecule and for the carbon atom are not exactly comparable; those for CH_4 include a correction for the wave functions not being exactly self-consistent which we could not easily determine for C without further information than that given in Torrance's paper (1934). Too much significance should not, therefore, be attached to the closeness of numerical agreement between the calculated and observed binding energies. It does, however, indicate that the method we have used is a very useful one and that the calculated charge distribution, which is much less sensitive than the binding energy to the detailed form of the wave functions, is reasonably near the truth. Further, it suggests that the wave functions given in table 1 could profitably be employed as first approximations in a more elaborate attempt to evaluate the binding energy. We hope, if circumstances permit, to carry out such an investigation together with an attempt to determine the carbon-hydrogen nuclear separation a priori by calculating the energy for different values of this distance.

DIAMAGNETIC SUSCEPTIBILITY

The molecular susceptibility for a spherically symmetrical system is given in electromagnetic units by (Stoner 1934)

$$-\chi \times 10^6 = 0{\cdot}790\int_0^\infty r^2[\Sigma_{nl}\, 2(2l+1)\, P^2(nl/r)]\, dr. \tag{6}$$

The values of the separate contributions calculated from the functions of table 1 by numerical integration are given in table 3.

TABLE 3. INTEGRALS OCCURRING IN THE EVALUATION OF DIAMAGNETIC SUSCEPTIBILITY AND POLARIZABILITY

Integral	Atomic units	Integral	Atomic units
$(r^2)_{1s,1s}$	0·102	$(r)_{2s,2p}$	1·830
$(r^2)_{2s,2s}$	3·577	$(r)_{2p,2p}$	2·156
$(r^2)_{2p,2p}$	5·788	$(r)_{2s,2s}$	1·732
$(r^2)_{2s,2p}$	4·221	$(r^3)_{2s,2s}$	8·494
—	—	$(r^3)_{2p,2p}$	18·68

We find $\chi = -33{\cdot}2 \times 10^{-6}$ e.m.u. The observed value for methane (Bitter 1929) is $-12{\cdot}2 \times 10^{-6}$ e.m.u., which is very considerably smaller. The discrepancy is in the same sense as, though somewhat greater than, that which occurs for atoms. Part of it is undoubtedly due to the fact that for molecules, which do not possess exact spherical symmetry, a negative term must be included on the right-hand side of (6) (van Vleck 1932), but it is unlikely that this is very large for methane. Allowing for this it is probable that the calculated value is between 2 and 2½ times too large. For atomic fields, calculated without inclusion of exchange, the discrepancy is not usually as large as a factor of 2, so some additional error can be traced to the approximation of averaging the proton distribution. On the other hand, it is probable that the introduction of exchange by the Fock method would greatly improve matters, as for atoms. There is little doubt that the calculated electron distribution is not sufficiently concentrated, the protons claiming less of the electron charge cloud than figure 1 indicates. Further evidence in the same sense is afforded by a study of the polarizability.

POLARIZABILITY

The theory of the polarization of atomic systems in a uniform electric field is not on such certain foundations as that of atomic susceptibility. Conclusions derived from comparison between observed and calculated polarizabilities are therefore not so well founded.

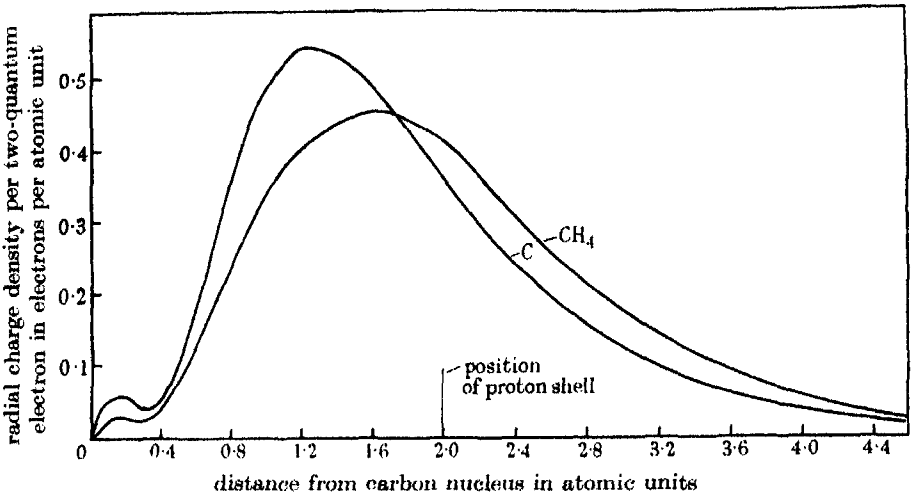

FIGURE 1. Comparison of radial charge distributions for normal carbon and for the spherically symmetrical model of methane, calculated by the self-consistent field method. (Contributions from κ electrons are omitted.)

The most elaborate approximate formula for the polarizability is one which can be derived by the method of Baber and Hassé (1937). According to this the polarizability α is given in atomic units by

$$\alpha = \tfrac{4}{9}\{A \sum_{\rho} (R^2)_{\rho\rho} + B \sum (R^3)_{\rho\rho}\}/C,$$

where

$$\left.\begin{aligned} A &= 2\{\Sigma(r^2)_{\rho\rho}\}\{\Sigma(R^2)_{\rho\rho}\} - \tfrac{4}{3}\{\Sigma(r)_{\rho\rho}\}\{\Sigma(R^3)_{\rho\rho}\}, \\ B &= N\,\Sigma(R^3)_{\rho\rho} - \tfrac{4}{3}\{\Sigma(r)_{\rho\rho}\}\{\Sigma(R^2)_{\rho\rho}\}, \\ C &= 2N\,\Sigma(r^2)_{\rho\rho} - \tfrac{16}{9}\{\Sigma(r)_{\rho\rho}\}^2. \end{aligned}\right\} \tag{7}$$

N is the total number of electrons, and in our case

$$(R^2)_{2s,2s} = (r^2)_{2s,2s} - (r)^2_{2s,2p}, \quad (R^3)_{2s,2s} = (r^3)_{2s,2s} - (r^2)_{2s,2p}(r)_{2s,2p},$$

$$(R^2)_{2p,2p} = (r^2)_{2p,2p} - \tfrac{1}{3}(r)^2_{2s,2p} - \tfrac{1}{3}(r)^2_{1s,2p},$$

$$(R^3)_{2p,2p} = (r^3)_{2p,2p} - \tfrac{1}{3}(r^2)_{2s,2p}(r)_{2s,2p} - \tfrac{1}{3}(r^2)_{1s,2p}(r)_{1s,2p}.$$

The suffix notation is such that

$$\{f(r)\}_{\rho,\sigma} = \int_0^\infty P(\rho|r) f(r)\, P(\sigma|r)\, dr. \tag{8}$$

The integrals involved in (7) are given in table 2. Using them we find

$$\alpha = 7 \cdot 60 \times 10^{-24}\,\text{cm.}^3.$$

In comparing this with observed values we must remember that the measured dielectric constant includes 'atomic' as well as electronic polarization, whereas (7) refers only to the latter. On the other hand, the extrapolated value of $n_\infty^2 - 1$, where n_∞ is the refractive index for infinite wavelength, does not include atomic polarization. The value of $n_\infty^2 - 1$ for methane given by C. and M. Cuthbertson (1914) is $8 \cdot 6 \times 10^{-4}$, while the dielectric constant as measured by Sänger (1926) is greater than unity by $9 \cdot 6 \times 10^{-4}$. These give respective values of 2·5 and $2 \cdot 8 \times 10^{-24}\,\text{cm.}^3$ for α. Taking the lower of these as representing true electronic polarization, we see that the calculated value is three times too large. Although this is a considerable discrepancy, it is not much greater than those met with in comparing theoretical and observed polarizabilities for atoms. Thus for argon the corresponding approximation to (7), using self-consistent wave functions without exchange, gives rather more than twice the observed result. It is of interest to note, however, that the sense of the discrepancy indicates that the calculated electron distribution is too diffuse, in agreement with evidence from diamagnetic susceptibility. How much of this is due to inaccuracy of the theory of polarizability, to the approximation of averaging the proton distribution and to inaccurate experimental information will require further investigation.

VAN DER WAALS FORCES BETWEEN METHANE MOLECULES

The constant C in the asymptotic form $-C/r^6$ of the interaction energy between two spherically symmetrical systems at distance r apart may be related approximately to the polarizabilities by the formula (Buckingham 1937)

$$C = \frac{3}{8}\frac{eh}{\pi}\left(\frac{\alpha^3 n}{m}\right)^{\frac{1}{2}},$$

where n is the number of electrons contributing appreciably to the polarizability (in our case these are the six $2p$ electrons which contribute over 90% of α).

Substituting the theoretical value for α, we find

$$C = 6{\cdot}4 \times 10^{-58}\,\text{erg cm.}^6. \tag{9}$$

The only available value of this constant derived largely from experimental material may be obtained from a paper by Corner (1939). Writing the interaction between two molecules in the form

$$V = \phi_0\left[\frac{1}{n}\left(\frac{r_0}{r}\right)^n - \frac{1}{6}\left(\frac{r_0}{r}\right)^6\right]\Big/\left(\frac{1}{6}-\frac{1}{n}\right), \tag{10}$$

and taking $n = 12$, he determines ϕ_0 from the theoretical relation

$$\phi_0 = 1{\cdot}029 \times 10^{-16}T_c,$$

where T_c is the critical temperature (Lennard-Jones and Devonshire 1937), and r_0 from the observed lattice constant a_0 of solid methane. Using Corner's values $\phi_0 = 1{\cdot}96 \times 10^{-14}$ erg, $a_0 = 4{\cdot}16 \times 10^{-8}$ cm., $r_0/a_0 = 1{\cdot}01$, we find

$$C = 2{\cdot}2 \times 10^{-58}\,\text{erg cm.}^6. \tag{11}$$

This value is likely to be an overestimate, as it includes contributions from higher inverse power interactions which, though present in fact, have not been explicitly included in (10).

Comparison with (9) shows that the theory gives results at least three times too large. This would be expected from the comparison of observed and calculated polarizabilities, as the van der Waals constant is roughly proportional to the $\frac{3}{2}$th power of the polarizability. It is of interest to note that the value of C derived by Margenau (1939) by insertion of the observed value of the polarizability in the formula

$$C = \tfrac{3}{4}\alpha^2 h\nu,$$

where ν is the predominant absorption frequency, is $1{\cdot}12 \times 10^{-58}$ erg cm.^{6}, only half the 'observed' value (11).

THE SCATTERING OF SLOW ELECTRONS BY METHANE

The variation of the effective collision area of methane molecules with electron energy for slow electrons has been measured by several authors (Kollath 1930), as have also the distributions in angle of electrons of various energies scattered elastically by the molecules (Bullard and Massey 1931; Arnot 1931; Mohr and Nicoll 1932; Hughes and McMillen 1933). A striking feature of the results is that, for electrons with energies less than 20 eV, there is a marked similarity in behaviour between methane and argon both as to the magnitude and velocity variation of the total cross-section and the form of the angular distributions. At higher energies the similarity in the angular distributions disappears, those for methane resembling those obtained from lighter atoms such as carbon.

The theory of the scattering of slow electrons by argon has been worked out by Holtsmark (1929), who modified the self-consistent field (without exchange) of the argon atom by including an empirical polarization potential. In this way satisfactory agreement is obtained with the observed cross-section velocity variation. The observed angular distributions are also well represented except for very slow electrons (energies less than 1 eV) (Mott and Massey 1933, p. 145), where a marked discrepancy exists. On the other hand, Buckingham and McDougall (1937) have calculated collision cross-sections and angular distributions, using the unmodified self-consistent field (without exchange), and do not find agreement with experiment for electrons with energies below 10 eV. From our point of view, however, the interesting thing is that their results for argon are very similar to those which we derive below using our self-consistent field for methane (also without exchange), provided the electron energy is less than 25 eV. For higher energies we find behaviour similar to that of a lighter atom than argon. This is just what is observed and it appears that a theory which treats both argon and methane on the same basis reveals the similarities and contrasts which do exist. At the same time it strongly suggests that our self-consistent field for methane is not more markedly in error than the corresponding field for argon. We now consider the details of the theory of the scattering which provide the basis of the above remarks.

The intensity of elastic scattering of electrons of wave number k into the solid angle $d\omega$ about the direction θ is given by

$$I(\theta)\,d\omega = \frac{1}{4k^2}\left|\sum_{l=0}^{\infty}(2l+1)\,(e^{2i\delta_l}-1)\,P_l(\cos\theta)\right|^2, \tag{12}$$

where the phases δ_l are such that the asymptotic form of the solution of the equation for electrons of angular momentum $l(l+1)\hbar$ in the methane field, viz.

$$\frac{d^2}{dr^2}(rF_l)+[k^2-l(l+1)/r^2-2V_n-2\{2Z_p(1s)-2Z_p(2s)-6Z_p(2p)\}/r](rF_l) = 0,$$

is

$$r^{-1}\sin(kr-\tfrac{1}{2}l\pi+\delta_l). \tag{13}$$

The total collision area for elastic collisions is given by

$$Q = \frac{4\pi}{k^2}\Sigma(2l+1)\sin^2\delta_l. \tag{14}$$

Using the Z_p values given in table 1, the phases δ_l necessary for the evaluation of $I(\theta)$ and Q were calculated for a range of electron energies. δ_0 and δ_1 were evaluated by direct numerical integration of (13), δ_2, δ_3, δ_4 and δ_5 by use of Langer's modification (1937) of Jeffreys's approximation (Mott and Massey 1933, p. 92). The values found are given in table 4. Values calculated for argon, using the Z_p values for that atom neglecting exchange (Buckingham and McDougall 1937), are given in brackets.

TABLE 4. PHASES CONCERNED IN CALCULATION OF ELECTRON SCATTERING BY METHANE. CORRESPONDING PHASES CALCULATED FOR ARGON ARE GIVEN IN BRACKETS

ka_0	0·5	0·7	1·0	1·5	2·0
δ_0	5·020 $(\pi+5·253)$	4·665	4·264 $(\pi+4·477)$	3·831	3·494 $(\pi+3·46)$
$\delta_1-\pi$	−0·992 $(\pi-0·887)$	−1·100	−1·242 $(\pi-1·224)$	−1·327 $(\pi-1·56)$	−1·388 $(\pi-1·85)$
δ_2	0·014 (0·020)	0·112	0·595 (0·409)	0·690 (1·28)	0·766 (1·90)
δ_3	—	—	0·071 (0·035)	0·396	0·450 (0·42)
δ_4	—	—	0·013 (0·006)	0·103	0·286 (0·13)
δ_5	—	—	—	—	0·110

To convert from ka_0 to energy, $13·54k^2a_0^2$ = energy in electron-volts.

It will be seen that, for ka_0 less than 1·5 (electron energy less than 30 eV) the δ_0, δ_1 and δ_2 phases for argon and methane are very nearly the same except for integral multiples of π. As the addition of an integral multiple of π to a phase has no effect on the scattering, and as the δ_0, δ_1, δ_2 phases are by far the most important for $ka_0 < 1·5$, it follows that the calculated cross-sections and angular distributions for electrons of energy less than 30 eV will be very similar. The significance of the extra multiple of π appearing for argon is that the field at distances close to the origin is so much larger than for methane that an additional node is introduced in the wave functions for $l = 0$ and $l = 1$. The heavier rare gases, krypton and xenon, have inner fields which are in turn stronger than for argon, and the δ_0, δ_1, δ_2 phases calculated for these atoms and slow electrons differ mainly from those for argon in including extra multiples of π. The result is that for the series methane, argon, krypton, xenon the shape of the angular distribution and cross-section velocity curves for slow electrons are very similar, and methane plays the role which might have been supposed filled by neon. As the δ_0, δ_1 phases for neon do not differ from those for argon merely by a multiple of π, it does not fit into the sequence.

For $ka_0 \geqslant 1{\cdot}5$ it is clear from table 4 that substantial differences begin to appear between the methane and argon phases. In particular δ_2 rises to a much higher value for argon and produces angular distributions typical of $\{P_2(\cos\theta)\}^2$ (Bullard and Massey 1931; Mott and Massey 1933*a*). For methane δ_2 is never sufficiently large to dominate the angular distributions which are more of the $\{P_1(\cos\theta)\}^2$ type even for $ka_0 = 2$ (see figure 3).

Using the phases given in table 4, the cross-sections Q and angular distribution functions $I(\theta)$ may be calculated. The number of terms is sufficient except for $ka_0 = 2$, where the influence of δ_6 and δ_7 on $I(\theta)$ is appreciable and was estimated by extrapolation.

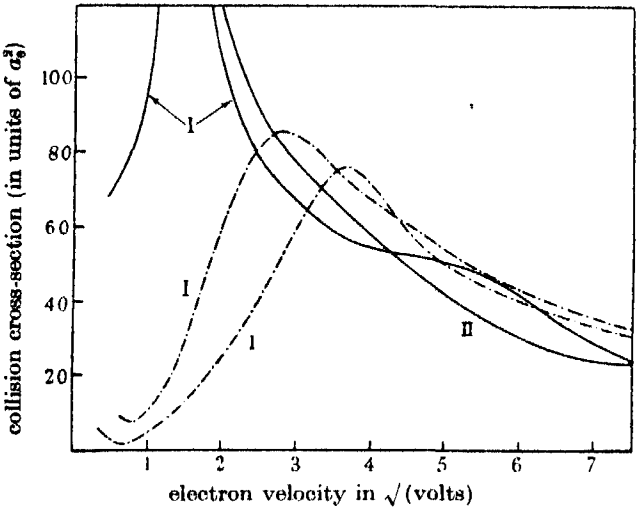

FIGURE 2. Comparison of observed and calculated cross-sections for collision of electrons with argon and methane molecules. —·—·—· observed total collision cross-section. I for argon. ——— calculated elastic collision cross-section. II for methane.

In figure 2 curves illustrating calculated and observed values of Q are given. Corresponding curves for argon are included for purposes of comparison. There is no evidence of any appreciable failure of the theory for either molecule for electrons with energy greater than 10 eV, as the fact that the calculated cross-section falls below the observed at the larger energies can be attributed to the contribution from inelastic collisions included in the measurements. At energies below 10 eV the theory fails for both cases in the same way, the calculated values becoming much too great. This is due to the behaviour of δ_1. The values of this phase remain in the neighbourhood of $\frac{1}{2}\pi$ ($\frac{3}{2}\pi$ for argon) down to quite low energies, so $\sin^2\delta_1/k^2$ becomes very large. This would not arise if δ_1 tended more rapidly to 0 or π (π or 2π for argon) as $k \rightarrow 0$, and this in turn could be brought about by decrease or increase of the distant field respectively. Thus Holtsmark (1929) succeeded in obtaining

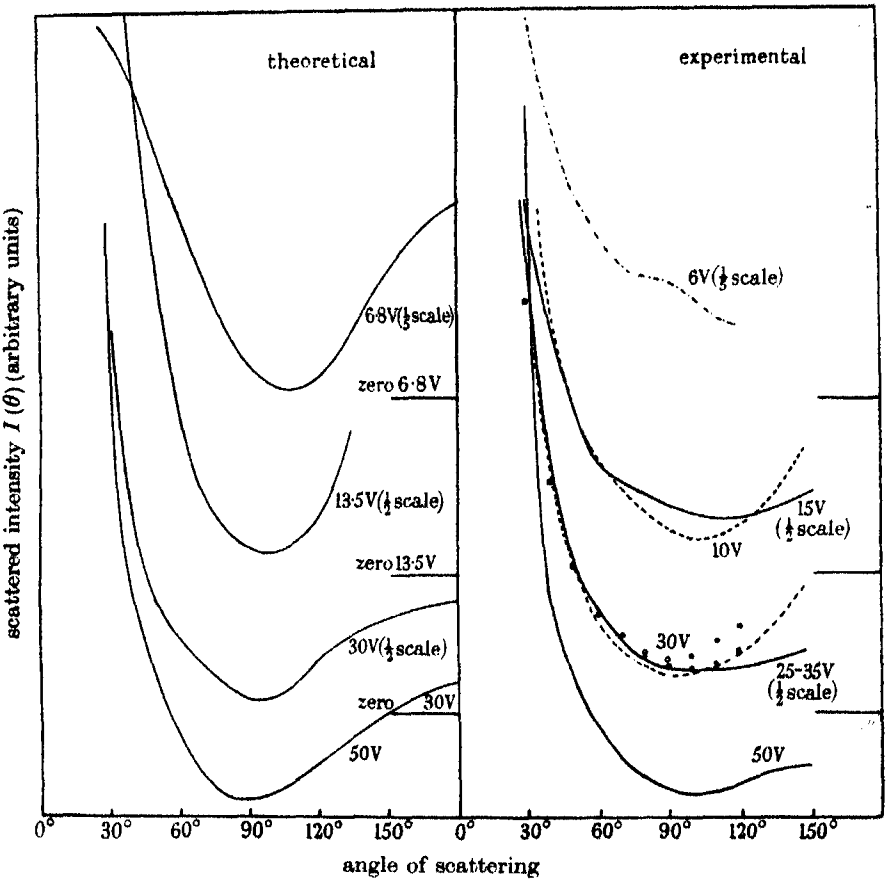

FIGURE 3. Comparison of calculated and observed angular distributions of electrons scattered by methane molecules. Experimental results: ——— Hughes and McMillen (1933), - - - - - Mohr and Nicoll (1932), • Arnot (1931), o Bullard and Massey (1931) 30 eV, —•—•—• Bullard and Massey (1931) 6 eV. The adjustment of scales is as follows. Hughes and McMillen's curves are adjusted so that the intensity for 50 V electrons at 50° agrees with the calculated value. The results of Arnot, Mohr and Nicoll, Bullard and Massey for 30 V electrons are then adjusted to give coincidence with Hughes and McMillen's mean curves for 25–35 V electrons at 50°.

agreement by adding the polarization term which increases the distant field. It is by no means certain that the same result may not have been achieved by inclusion of exchange effects, both in modifying the self-consistent field and in affecting the motion of the incident electron. Whichever effects are responsible, however, in the case of argon are very likely to be effective also for methane, as it is clear from figure 2 that the behaviour of both atoms in experiment and according to our theory is very nearly the same.

The calculated and observed angular distributions are compared in figure 3. In some cases the results of different observers do not agree very well, and it is difficult to introduce a completely satisfactory mode of comparison. The procedure adopted was as follows. The arbitrary constant in the observed values of $I(\theta)$ given by Hughes and McMillen (1933) was adjusted, so theory and observation agreed for 50 eV electrons at 50°. For 30 eV electrons the scales of the observed curves obtained by Arnot (1931), Bullard and Massey (1931) and Mohr and Nicoll (1932) respectively were adjusted so that each agreed at 50° with the mean of the curves for 25 and 35 eV electrons observed by Hughes and McMillen. For comparison with the theoretical curve for 13·5 eV electrons the observed curves found by Mohr and Nicoll for 10 and Hughes and McMillen for 15 eV electrons are given. Finally, the observations of Bullard and Massey for 6 eV electrons are given for comparison with the calculated 6·8 eV curve. In this way only a single adjustment has been made bringing theory and observation into agreement at a fixed angle and electron energy. In view of this it is clear that there is quite good agreement between theory and observation for the higher energies, but the two begin to differ markedly at the lowest energy illustrated. This is to be expected from the comparison of total cross-sections and lends additional weight to the conclusions derived above.

Summarizing, it appears that the study of scattering phenomena indicates that our self-consistent field for methane is not much less satisfactory than the corresponding one for argon. In fact, the agreement with the observed angular distributions at the higher energies and the theoretical reproduction of the similarity in behaviour of argon and methane towards slow electrons encourages the belief that no very serious error has been introduced by averaging the proton distribution.

Concluding remarks and discussion

We have applied our methane field to the investigation of a variety of properties of that molecule, and from only one of these, the diamagnetic susceptibility, is there any evidence that the method is less satisfactory than for atoms. It appears to be in error in the same sense—the calculated electron distribution is too diffuse. This would be improved by the introduction of exchange as in the Fock method for atoms, and the considerable success attained already in the calculation of the energy and of scattering phenomena (including the relation to argon) suggests that such extension would be worth while. The application of the method to other molecules possessing tetrahedral or octahedral symmetry is also likely to lead to results of interest.

We are indebted to the Department of Scientific and Industrial Research for a grant without which it would have been impossible to carry out this investigation after the outbreak of war. It is a pleasure also to acknowledge the award to one of us (R. A. B.) of a Senior Studentship of the Royal Commission for the Exhibition of 1851, the continuance of which during the war period was of great assistance. Finally, we must thank Dr J. McDougall of Leeds University for allowing some results of unpublished work, carried out by him in conjunction with one of us (R. A. B.), to be included in this paper.

REFERENCES

Arnot 1931 *Proc. Roy. Soc.* A, **133**, 615.
Baber and Hassé 1937 *Proc. Camb. Phil. Soc.* **33**, 253.
Bitter 1929 *Phys. Rev.* **33**, 388.
Buckingham 1937 *Proc. Roy. Soc.* A, **160**, 94.
Buckingham and McDougall 1937 Unpublished (Buckingham, Ph.D. Thesis, Cambridge).
Bullard and Massey 1931 *Proc. Roy. Soc.* A, **133**, 637.
Corner 1939 *Trans. Faraday Soc.* **35**, 711.
Coulson 1937 *Trans. Faraday Soc.* **33**, 388.
Cuthbertson, C. and M. 1914 *Proc. Roy. Soc.* A, **97**, 152.
Hartree and Black 1933 *Proc. Roy. Soc.* A, **139**, 321.
Holtsmark 1929 *Z. Phys.* **55**, 436.
Hughes and McMillen 1933 *Phys. Rev.* **44**, 876.
Kollath 1930 *Phys. Z.* **31**, 985.
Langer 1937 *Phys. Rev.* **51**, 669.
Lennard-Jones and Devonshire 1937 *Proc. Roy. Soc.* A, **163**, 53.
Margenau 1939 *Rev. Mod. Phys.* **11**, 1.
Mohr and Nicoll 1932 *Proc. Roy. Soc.* A, **138**, 469.
Mott and Massey 1933 *Theory of atomic collisions.* Clarendon Press.
Sänger 1926 *Phys. Z.* **27**, 556.
Stoner 1934 *Magnetism and matter*, ch. 9, p. 234.
Torrance 1934 *Phys. Rev.* **46**, 388.
van Vleck 1932 *Electric and magnetic susceptibilities*, ch. 10, p. 275. Clarendon Press.
van Vleck and Sherman 1935 *Rev. Mod. Phys.* **7**, 167.

Bose-Einstein statistics and degeneracy

By D. S. Kothari and B. N. Singh
University of Delhi

(*Communicated by M. N. Saha, F.R.S.—Received* 17 *May* 1940)

The thermodynamic properties of degenerate and non-degenerate Bose-Einstein gas in the completely non-relativistic and the completely relativistic cases are derived. The relativistic degenerate case of Bose-Einstein statistics corresponds to black-body radiation. The properties and the possibility of the existence of non-degenerate radiation are discussed.

Recently the theory of the Bose-Einstein (1924) non-relativistic degenerate gas has been revived by London (1938–9) in connexion with its possible applications to liquid helium II. In a non-degenerate (i.e. classical) gas the pressure depends upon the product of the temperature and the concentration, where—as in degeneracy the pressure is (almost) independent of the temperature for a Fermi-Dirac gas, and independent of the concentration for a Bose-Einstein gas, i.e. one of the variables, temperature or volume, is relegated to the background. The properties of a Fermi-Dirac gas, because of its numerous physical and astrophysical applications, have been studied in considerable detail taking account of the effect of relativistic mechanics. The Bose-Einstein gas has so far received much less attention. London in his interesting paper dealing with the relation between liquid helium II and Bose-degeneracy has naturally confined himself to the completely non-relativistic statistics. The present paper is concerned with a detailed discussion of the properties of degenerate and non-degenerate Bose-Einstein gas in the completely non-relativistic and the completely relativistic cases.† The first section deals with the distribution law in non-degeneracy and degeneracy, and related series-expansions of general utility. The physical properties, viz. energy, pressure, free-energy, entropy and specific heats, are dealt with in the second section. The third section deals with the correspondence between black-body radiation and the relativistic Bose-Einstein degenerate case. The properties and the possibility of the existence of non-degenerate radiation are discussed.

1. Let us consider an assembly of N similar particles occupying a volume V. Let ϵ represent the eigen-value for the (translational) kinetic

---

† The statement that there can be no relativistic case in Bose-Einstein statistics has been sometimes made. This is obviously incorrect.

energy of a particle in the assembly. Then, the energy-distribution law states that the number $N(\epsilon)$ of particles possessing kinetic energy ϵ is given by

$$N(\epsilon) = \frac{a(\epsilon)}{1/A\, e^{u}+\beta}; \quad u = \frac{\epsilon}{kT}, \tag{1}$$

where $a(\epsilon)$ is the number of wave functions or states of the particle with eigen-value ϵ of the kinetic energy. The distribution parameter A is independent of ϵ. In fact $kT \log A$ is the Gibbs free energy per particle (chemical potential). In the case of Bose-Einstein statistics $\beta = -1$ and for the Fermi-Dirac statistics $\beta = +1$.

The wave function describing a stationary state of a free particle (of rest mass m) confined in a cubical volume of linear dimensions L is

$$\psi = 2\left(\frac{2}{L^3}\right)^{\frac{1}{2}} \sin\frac{\alpha\pi x}{L} \sin\frac{\beta\pi y}{L} \sin\frac{\gamma\pi z}{L}, \tag{2}$$

where α, β, γ may be any three positive integers (not zero). Taking account of the effect of relativistic mechanics, the eigen-value $\epsilon(\alpha, \beta, \gamma)$ of the kinetic energy characterizing the wave function is given by

$$\epsilon\left(\frac{\epsilon}{2mc^2}+1\right) = \epsilon_0 \rho^2, \tag{3}$$

or

$$\epsilon = mc^2\left[\sqrt{\left(1+\frac{2\epsilon_0\rho^2}{mc^2}\right)}-1\right], \tag{4}$$

where

$$\epsilon_0 = \frac{h^2}{8mL^2}, \quad \rho^2 = (\alpha^2+\beta^2+\gamma^2). \tag{5}$$

The number of wave functions, therefore, for $\rho^2 = 3$ ($\alpha = \beta = \gamma = 1$) is g, for $\rho^2 = 6$ is $3g$, and so on, where g is the weight factor for the particle by virtue of its internal structure (i.e. the number of distinct states associated with each eigen-value of the kinetic energy). For large values of ρ the total number $C(\epsilon)$ of states of energy less than $\epsilon(\rho)$ is 2^{-3} times the volume of a sphere of radius ρ;

$$\begin{aligned} C(\epsilon) &= \frac{\pi}{6}\rho^3 g \\ &= \frac{\pi g}{6}\left[\frac{\epsilon}{\epsilon_0}\left(\frac{\epsilon}{2mc^2}+1\right)\right]^{\frac{3}{2}} \\ &= \frac{4\pi}{3}\frac{Vg}{(ch)^3}(\epsilon^2+2mc^2\epsilon)^{\frac{3}{2}}. \end{aligned} \tag{6}$$

The number of states lying between ϵ and $\epsilon+d\epsilon$ is

$$a(\epsilon)\,d\epsilon = \frac{dC(\epsilon)}{d\epsilon} = \frac{V4\pi g}{(ch)^3}(\epsilon^2+2mc^2\epsilon)^{\frac{1}{2}}\,(\epsilon+mc^2)\,d\epsilon. \tag{7}$$

Instead of dealing with (7) as it stands it becomes much simpler to discuss two limiting cases, which are usually called the non-relativistic and the relativistic cases. In the non-relativistic case the average energy per particle is negligible compared to its rest mass energy, and it is vice versa in the relativistic case. In the completely non-relativistic case, i.e. to the zeroth approximation in $\frac{\epsilon}{mc^2}$, (7) gives

$$a(\epsilon)\,d\epsilon = Vg\frac{2\pi(2m)^{\frac{3}{2}}\,\epsilon^{\frac{1}{2}}}{h^3}\,d\epsilon, \tag{8}$$

and in the completely relativistic case, i.e. to the zeroth approximation in $\frac{mc^2}{\epsilon}$, we have

$$a(\epsilon)\,d\epsilon = Vg\frac{4\pi}{(ch)^3}\epsilon^2\,d\epsilon, \tag{9}$$

and substituting (9) in (1) we obtain

$$N = 4\pi g\left(\frac{kT}{ch}\right)^3 V\int_0^\infty \frac{u^2}{1/A\;e^u-1}\,du. \tag{10†}$$

In the Bose-Einstein statistics the distribution parameter A cannot be greater than unity, for otherwise some of $N(\epsilon)$ would be negative, which of course is not admissible, and thus we have

$$A_0^R = \frac{1}{\Gamma(3)}\int_0^\infty \frac{u^2\,du}{1/A\;e^u-1} = \sum_{n=1}^{n=\infty}\frac{A^n}{n^3}, \tag{11}$$

where A_0^R is a dimensionless number, called the degeneracy discriminant,‡ defined by

$$A_0^R = \frac{N}{8\pi gV}\left(\frac{ch}{kT}\right)^3. \tag{12}$$

---

† The limits of integration 0 to ∞ appear to contradict the assumption $mc^2/\epsilon \to 0$. Such a contradiction also appears in the non-relativistic case. This only means that the results obtained for the relativistic case are valid so long as the average energy is very large compared to the rest-mass energy and the opposite holds in the non-relativistic case.

‡ The appropriateness of the name will be clear in the sequel.

Equation (11) imposes an upper limit on the value of A_0^R, for as A does not exceed unity, A_0^R cannot exceed $\zeta(3) = 1{\cdot}202$, i.e. N cannot be greater than N^*, where

$$N^* = 8\pi g V\left(\frac{kT}{ch}\right)^3 \zeta(3), \tag{13}$$

or T cannot be less than T_0, where

$$T_0 = \frac{ch}{k}\left[\frac{N}{8\pi g V\,\zeta(3)}\right]^{\frac{1}{3}}. \tag{14}$$

T_0 is called the "degeneracy temperature".

This limitation on the value of A_0^R has no physical basis and its presence is easily explained. It arises due to our substitution for $a(\epsilon)$ in (1) the expression (9) which is incorrect for small values of ρ, i.e. for levels in the neighbourhood of the lowest energy state, and as London has shown for the case of $A \to 1$, the particles in excess of the number N populate just these levels: they possess (almost) zero energy and constitute the so-called "condensed" phase. If N_0 denotes the number of particles in the condensed phase (sometimes called the "non-energetic" particles), then using (12), (13) and (14), we have

$$N_0 = N - N^* = N\left(1 - \frac{\zeta(3)}{A_0^R}\right) = N\left[1 - \left(\frac{T}{T_0}\right)^3\right]. \tag{15}$$

Thus we are led to distinguish between two entirely different cases:

(i) *Non-degenerate case*, $A_0^R < \zeta(3)$: When A_0^R is less than $\zeta(3)$, A is less than unity, and the distribution law in this case is

$$N(\epsilon)\,d\epsilon = \frac{4\pi g V}{(ch)^3}\,\frac{\epsilon^2\,d\epsilon}{1/A\;e^{\epsilon/kT} - 1}. \tag{16}$$

(ii) *Degenerate case*: When A_0^R is greater than $\zeta(3)$, A is effectively unity, and the distribution law is

$$\text{for } \epsilon = 0, \quad N_0 = N\left[1 - \frac{\zeta(3)}{A_0^R}\right], \tag{17}$$

and

$$\text{for } \epsilon > 0, \quad N(\epsilon)\,d\epsilon = \frac{4\pi g V}{(ch)^3}\,\frac{\epsilon^2}{e^{\epsilon/kT} - 1}\,d\epsilon. \tag{18}$$

For the degenerate case $A = 1$, hence the Gibbs free-energy $G = NkT \log A$ is zero, i.e. *the Bose-Einstein degeneracy is characterized by zero Gibbs free energy*.

It may be noted here that it is not correct to assign zero energy to the lowest state, for in accordance with the uncertainty principle the kinetic energy of a particle confined in a space of finite dimensions can never be exactly zero. The uncertainty in the energy of a particle is $hc/2\pi L$ in the relativistic case and $h^2/8\pi^2 mL^2$ in the non-relativistic case, and the results obtained here are only valid so long as the average energy per particle of the assembly is much greater than the former value in the relativistic case and the latter value in the other case.

Taking the non-relativistic case, for temperature T less than T_0, the kinetic energy per particle is, from (20) and (44), given by

$$\tfrac{3}{2}k\left(\frac{2\pi mk}{h^2}\right)^{\frac{3}{2}}\frac{\zeta(\frac{5}{2})}{n}T^{\frac{5}{2}},$$

and for this to exceed the uncertainty value it is necessary that

$$L > \frac{h^{\frac{5}{2}}n^{\frac{1}{2}}}{6^{\frac{1}{2}}(2\pi mk)^{\frac{5}{4}}[\zeta(\frac{5}{2})]^{\frac{1}{2}}T^{\frac{5}{4}}}.$$

For the case of liquid helium at $T = 1°\,\mathrm{K}$, this gives

$$L > 1{\cdot}15\times 10^{-7}\,\mathrm{cm}.$$

The preceding results (equations 12 to 18) can be immediately generalized† when the distribution law (1) is of the type

$$N(\epsilon)\,d\epsilon = \frac{VC\epsilon^{s-1}}{1/A\;e^{\epsilon/kT}-1}\,d\epsilon, \tag{19}$$

where $s > 1$. In the non-relativistic case $s = \frac{3}{2}$ and C will be given by (8)

$$C = \frac{2\pi g(2m)^{\frac{3}{2}}}{h^3}. \tag{20}$$

In the relativistic case $s = 3$ and C will be given by (9)

$$C = \frac{4\pi g}{(ch)^3}. \tag{21}$$

The degeneracy discriminant A_0 in the general case will be defined by

$$A_0 = \frac{N}{\Gamma(s)\,C(kT)^s V} = \frac{1}{\Gamma(s)}\int_0^\infty \frac{u^{s-1}}{1/A\;e^{u}-1}\,du = \sum_{n=1}^{\infty}\frac{A^n}{n^s}, \tag{22}$$

with $A_0 < \zeta(s)$ for the non-degenerate case ($A < 1$) and $A_0 > \zeta(s)$ for the degenerate case ($A = 1$). The distribution law in the latter case being, for $\epsilon = 0$,

---

† London (1939) has also discussed this general case and has given general expressions for the specific heat at constant volume. These expressions are included here for the sake of completeness—the non-degenerate expression is given here to a higher approximation.

$$N_0 = N\left[1 - \frac{\zeta(s)}{A_0}\right] = N\left[1 - \left(\frac{T}{T_0}\right)^s\right], \tag{23}$$

where the degeneracy temperature† T_0 is defined by

$$T_0 = \frac{1}{k}\left[\frac{N}{\Gamma(s)\,CV\zeta(s)}\right]^{1/s}, \quad \text{or} \quad \left(\frac{T_0}{T}\right)^s \zeta(s) = A_0; \tag{24}$$

and for $\epsilon > 0$ the distribution law is

$$N(\epsilon)\,d\epsilon = \frac{VC\epsilon^{s-1}\,d\epsilon}{e^{\epsilon/kT} - 1}. \tag{23a}$$

The distribution law being known, the thermodynamic properties of the assembly can be calculated in the usual way. This is done in the next section. We shall first note some series-expansions which will be useful in the sequel.

We begin with equation (22). Inverting the series in (22), we have

$$A = A_0 - a_2 A_0^2 - a_3 A_0^3 - a_4 A_0^4 - a_5 A_0^5 - \ldots, \tag{25}$$

and
$$\frac{A^0}{A} = 1 + a_2 A_0 + (a_3 + a_2^2)\,A_0^2 + (a_4 + 2a_3 a_2 + a_3^2)\,A_0^3 + \ldots, \tag{26}$$

where
$$\left.\begin{aligned} a_2 &= \frac{1}{2^s}, \\ a_3 &= \frac{1}{3^s} - \frac{2}{4^s}, \\ a_4 &= \frac{1}{4^s} - \frac{5}{6^s} + \frac{5}{8^s}, \\ a_5 &= \frac{1}{5^s} - 3\left(\frac{1}{9^s} + \frac{2}{8^s}\right) + \frac{21}{12^s} - \frac{14}{16^s}. \end{aligned}\right\} \tag{27}$$

We require later an expansion of $\Sigma A^n/n^l$ as a power series in A_0. We obtain, using (25),

$$\Sigma\frac{A^n}{n^l} = A_0 - A_0^2\left(a_2 - \frac{1}{2^l}\right) - A_0^3\left(a_3 + \frac{a_2}{2^{l-1}} - \frac{1}{3^l}\right)$$
$$- A_0^4\left(a_4 + \frac{a_3}{2^{l-1}} + \frac{a_2}{3^{l-1}} - \frac{a_2^2}{2^l} - \frac{1}{4^l}\right) - \ldots. \tag{28}$$

---

† In the non-degenerate case $T > T_0$, and in degeneracy $T < T_0$.

For $t = s+1$, this gives

$$\Sigma \frac{A^n}{n^{s+1}} = A_0 - b_2 A_0^2 - b_3 A_0^3 - b_4 A_0^4 - \ldots, \tag{29}$$

where

$$\left.\begin{aligned} b_2 &= a_2 - \frac{1}{2^{s+1}} = \frac{1}{2^{s+1}}, \\ b_3 &= a_3 + \frac{a_2}{2^s} - \frac{1}{3^{s+1}} = \frac{2}{3^{s+1}} - \frac{1}{4^s}, \\ b_4 &= a_4 + \frac{a_3}{2^s} + \frac{a_2}{3^s} - \frac{a_2^2}{2^{s+1}} - \frac{1}{4^{s+1}} = \frac{3}{4^{s+1}} + \frac{5}{2\,.\,8^s} - \frac{3}{6^s}. \end{aligned}\right\} \tag{30}$$

Further, we have

$$\begin{aligned} \frac{A_0}{\Sigma A^n/n^t} = 1 &+ A_0\left(a_2 - \frac{1}{2^t}\right) + A_0^2\left(a_3 + a_2^2 - \frac{1}{3^t} + \frac{1}{4^t}\right) \\ &+ A_0^3\left(-a_4 - 2a_2 a_3 - a_2\left(\frac{1}{3^t} - \frac{1}{4^t}\right) - a_2^3 - \frac{2}{6^t} + \frac{1}{4^t} + \frac{1}{8^t}\right) + \ldots. \end{aligned} \tag{31}$$

For $t = (s-1)$, this gives†

$$\frac{A_0}{\Sigma A^n/n^{s-1}} = 1 - 2b_2 A_0 - 3b_3 A_0^2 - 4b_4 A_0^3 - \ldots. \tag{32}$$

It is to be noted that a power series in A_0 can be written as a power series in $(T_0/T)^s$, for from (24), $A_0 = (T_0/T)^s \zeta(s)$, and therefore the coefficient of $(T_0/T)^{sr}$ is $(\zeta(s))^r$ times the coefficient of A_0^r. The values of the coefficients a, b for the special cases of $s = \frac{3}{2}$ and $s = 3$ are given in table 1.

TABLE 1

	$s = \frac{3}{2}$	$s = 3$		$s = \frac{3}{2}$	$s = 3$
$a_2 =$	0·35354	0·12500	$a_2\zeta(s) =$	0·92348	0·15025
$a_3 =$	−0·05755	0·00579	$a_3[\zeta(s)]^2 =$	−0·39264	0·00836
$a_4 =$	0·00576	0·00224	$a_4[\zeta(s)]^3 =$	0·10272	0·00389
$b_2 =$	0·17677	0·06250	$b_2\zeta(s) =$	0·46174	0·07513
$b_3 =$	0·00330	0·00907	$b_3[\zeta(s)]^2 =$	0·02251	0·01310
$b_4 =$	0·000111	0·00271	$b_4[\zeta(s)]^3 =$	0·001983	0·00471

Differentiating A with respect to A_0 we have from (22)

$$\frac{dA}{dA_0} = \frac{A}{\Sigma A^n/n^{s-1}}, \tag{33}$$

---

† Equation (32) also follows immediately by differentiating (29) with respect to A_0 and using (33).

and noting that $$\left(\frac{\partial A_0}{\partial T}\right)_V = -\frac{sA_0}{T}; \quad \left(\frac{\partial A_0}{\partial V}\right)_T = -\frac{A_0}{V}, \tag{34}$$

we obtain, $$-\frac{T}{s}\left(\frac{\partial A}{\partial T}\right)_V = -V\left(\frac{\partial A}{\partial V}\right)_T = \frac{A_0}{\Sigma A^{n-1}/n^{s-1}}. \tag{35}$$

If we denote the values corresponding to $A_0 = \zeta(s) - 0$ by inserting the suffix $+1$, we have

$$\left(\frac{dA}{dA_0}\right)_{+1} = \frac{1}{\zeta(s-1)}, \tag{36}$$

$$\frac{T_0}{s}\left(\frac{\partial A}{\partial T}\right)_{+1} = V\left(\frac{\partial A}{\partial V}\right)_{+1} = -\frac{\zeta(s)}{\zeta(s-1)}, \tag{37}$$

which is equal to zero for $s = \frac{3}{2}$, and $\dfrac{\zeta(\frac{3}{2})}{\zeta(2)} = 0{\cdot}731$ for $s = 3$.

Similarly, we find $$\left(\frac{d^2A}{dA_0^2}\right)_{+1} = \frac{\zeta(s-1) - \zeta(s-2)}{[\zeta(s-1)]^3}, \tag{38}$$

or $$T_0^2\left(\frac{\partial^2 A}{\partial T^2}\right)_{+1} = s\zeta(s)\left[\frac{s+1}{\zeta(s-1)} + \frac{s\zeta(s)}{[\zeta(s-1)]^2} - \frac{s\zeta(s)\,\zeta(s-2)}{[\zeta(s-1)]^3}\right]. \tag{39}$$

This is equal to $-\frac{9}{8\pi}[\zeta(\frac{3}{2})]^2 = -2{\cdot}441$ for† $s = \frac{3}{2}$, and minus infinity for $s = 3$.

---

† When $1 + p > 0$, $\zeta(p) \equiv \Sigma n^p$ tends to infinity as $\lim\limits_{A \to 1} \Gamma(1+p)\,(1-A)^{-(1+p)}$. This is easily seen as follows (Fowler and Jones 1938):

$$(1-A)^{-(1+p)} = \sum_{n=0}^{n\to\infty} A^n \Gamma(1+p+n)/\Gamma(1+p),\ \Gamma(1+n).$$

For large x, Stirling's theorem gives

$$\Gamma(x) \sim \left(\frac{2\pi}{e}\right)^{\frac{1}{2}} \left(\frac{x}{e}\right)^{x-\frac{1}{2}},$$

hence we have for large n

$$\Gamma(1+p+n)/\Gamma(1+n) \sim \left(\frac{1+p+n}{1+n}\right)^{p+n+\frac{1}{2}} (1+n)^p\, e^{-p} = n^p,$$

or when A tends to unity, $$(1-A)^{-1-p} = \Sigma\,\frac{n^p}{\Gamma(1+p)},$$

that is $$\Sigma n^p = \Gamma(1+p)\,(1-A)^{-1-p}.$$

This gives $$\Sigma n^{\frac{1}{2}}/[\Sigma n^{-\frac{1}{2}}]^3 = \frac{\Gamma(\frac{3}{2})}{[\Gamma(\frac{1}{2})]^3} = \frac{1}{2\pi},$$

a result which is required in evaluating (39) for $s = \frac{3}{2}$.

2. We shall now calculate the energy E and pressure p of the assembly,

$$E = \int \epsilon N(\epsilon)\, d\epsilon. \tag{40}$$

Introducing a dimensionless number B_0 defined by

$$B_0 = \frac{E}{\Gamma(s+1)\, CV(kT)^{s+1}} = \frac{E}{NskT} A_0, \tag{41}$$

we have from (19) and (40) $\qquad B_0 = \Sigma \dfrac{A^n}{n^{s+1}}$. $\qquad$ (42)

In the non-degenerate case A is less than unity, i.e. $B_0 < \zeta(s+1)$ and using (29) we have the power series (denoting the value of E in non-degeneracy by E_+)†

$$E_+/sNkT = \frac{B_0}{A_0} = 1 - b_2 A_0 - b_3 A_0^2 - b_4 A_0^3 - \dots. \tag{43}$$

In the degenerate case‡ $A = 1$, $B_0 = \zeta(s+1)$, and we have for the energy per particle of the assembly, from (41),

$$E_-/N = \frac{\Gamma(s+1)\, CV(kT)^{s+1} \zeta(s+1)}{N} = \frac{\zeta(s+1)\, skT}{A_0}. \tag{44}$$

We shall denote the values corresponding to $A_0 = \zeta(s) - 0$ by the suffix $+1$, and those corresponding to $A_0 = \zeta(s) + 0$ by the suffix -1. In the former case the limit $A_0 = \zeta(s)$ is approached from the side of non-degeneracy and in the latter case from the degenerate side. Equations (43) and (44) show that at $A_0 = \zeta(s)$, $E_{+1} = E_{-1}$, i.e. there is no discontinuity in the value of the energy at $A_0 = \zeta(s)$.

The number $(N - N_0)$ of 'energetic particles', i.e. particles excluding the zero state, is given by (23), and thus the energy per energetic particle becomes

$$\frac{E_-}{N - N_0} = \frac{s\zeta(s+1)}{\zeta(s)} kT = \left.\begin{matrix} 0{\cdot}770kT & \text{for } s = \frac{3}{2}, \\ 2{\cdot}701kT & \text{for } s = 3. \end{matrix}\right\} \tag{45}$$

The pressure of the assembly in the non-relativistic case is

$$p = \frac{2}{3}\frac{E}{V},$$

---

† We use the suffix + to denote the non-degenerate case and suffix − to denote the degenerate case.

‡ It should be noted that in contrast to the case of Fermi statistics 'exact expressions' (instead of series expansions) can be obtained for the various physical quantities in Bose degeneracy.

and in the relativistic case $p = \frac{1}{3}\frac{E}{V}$. The two cases are included in the expression

$$p = \frac{E}{sV}. \tag{46}$$

For non-degeneracy substituting for E_+ from (43) we have

$$p_+ = C\Gamma(s)\,(kT)^{s+1}\,\Sigma\frac{A^n}{n^{s+1}}, \tag{47}$$

or

$$p_+ = nkT[1 - b_2A_0 - b_3A_0^2 - b_4A_0^3 \dots], \tag{47a}$$

n being the number of particles per unit volume.† In degeneracy (44) gives

$$p_- = C\Gamma(s)\,\zeta(s+1)\,(kT)^{s+1}, \tag{48}$$

p_- depends only on temperature and is independent of volume. For $A_0 = \zeta(s)$, $p_{+1} = p_{-1}$.

We can now obtain expressions for the different specific heats.

Differentiating (41) with respect to T and using (35) we have for the specific heat (C_V) at constant volume in the non-degenerate case

$$\begin{aligned}\frac{C_{V+}}{Nk} &= \frac{s(s+1)\,B_0}{A_0} + \frac{sT}{A_0}\left(\frac{\partial A}{\partial T}\right)_V \Sigma\frac{A^{n-1}}{n^s}\\ &= \frac{s(s+1)\,B_0}{A_0} - \frac{s^2A_0}{\Sigma A^n/n^{s-1}}.\end{aligned} \tag{49}$$

Substituting from (43) and (32) we obtain the power series

$$\frac{C_{V+}}{sNk} = 1 + (s-1)\,b_2A_0 + (2s-1)\,b_3A_0^2 + (3s-1)\,b_4A_0^3 + \dots. \tag{50}$$

For $A_0 = \zeta(s) - 0$, (49) reduces to

$$\frac{C_{V+1}}{Nk} = \frac{s(s+1)\,\zeta(s+1)}{\zeta(s)} - \frac{s^2\zeta(s)}{\zeta(s-1)}. \tag{51}$$

In the case of degeneracy (44) gives

$$\frac{C_{V-}}{Nk} = \frac{s(s+1)\,\zeta(s+1)}{A_0}, \tag{52}$$

and for $A_0 = \zeta(s) + 0$,

$$\frac{C_{V-1}}{Nk} = \frac{s(s+1)\,\zeta(s+1)}{\zeta(s)}. \tag{53}$$

---

† It is hardly necessary to mention that n in the summations as in (47) denotes any positive integer, and this is not to be confused with n in (47a).

The discontinuity in the value of the specific heat at $A_0 = \zeta(s)$ is therefore

$$\frac{C_{V-1}-C_{V+1}}{Nk} = \frac{s^2\zeta(s)}{\zeta(s-1)}, \tag{54}$$

and this vanishes when $\zeta(s-1) \to \infty$, i.e. for $s-1<1$. In the non-relativistic case

$$C_{V-1}-C_{V+1} = 0, \tag{55}$$

and in the relativistic case

$$\frac{1}{Nk}[C_{V-1}-C_{V+1}] = \frac{9\zeta(3)}{\zeta(2)} = 6{\cdot}576. \tag{56}$$

For the temperature derivative of the specific heat at $A_0 = \zeta(s)-0$ we find after a little algebra that

$$\begin{aligned}\left[\frac{d(C_{V+}/Nk)}{dT/T_0}\right]_{+1} &= \frac{s^2(s+1)\,\zeta(s+1)}{\zeta(s)} - \frac{s^2\zeta(s)}{\zeta(s-1)} - \frac{s^3[\zeta(s)]^2\zeta(s-2)}{[\zeta(s-1)]^3},\\ &= 2{\cdot}888 - 3{\cdot}665 = -0{\cdot}777 \quad \text{for } s = \tfrac{3}{2}\\ &= -\infty \quad \text{for } s = 3,\end{aligned} \tag{57}$$

and for $A_0 = \zeta(s)+0$, we have immediately from (52)

$$\left[\frac{d(C_{V-}/Nk)}{dT/T_0}\right]_{-1} = \frac{s^2(s+1)\,\zeta(s+1)}{\zeta(s)} = \left.\begin{matrix}2{\cdot}888 & \text{for } s = \tfrac{3}{2}\\ 32{\cdot}41 & \text{for } s = 3\end{matrix}\right\}. \tag{58}$$

We shall now proceed to calculate the specific heat (C_p) at constant pressure. The well-known thermodynamic relation connecting C_p and C_V is

$$C_p - C_V = T\left(\frac{\partial p}{\partial T}\right)_V\left(\frac{\partial V}{\partial T}\right)_p = -T\left(\frac{\partial p}{\partial T}\right)_V^2\Big/\left(\frac{\partial p}{\partial V}\right)_T. \tag{59}$$

In the case of *degeneracy* the pressure is independent of volume,

$$\left(\frac{\partial p}{\partial V}\right)_T = 0,$$

and thus the constant pressure specific heat is infinite. In non-degeneracy from (47) and (35) we obtain for the compressibility

$$\kappa_+ = -V\left(\frac{\partial p}{\partial V}\right)_T = -C\Gamma(s)\,(kT)^{s+1}\,V\left(\frac{\partial A}{\partial V}\right)_T \Sigma\frac{A^{n-1}}{n^s} = \frac{NkTA_0}{V\Sigma A/n^{s-1}}, \tag{60}$$

and hence using (32), we have,

$$\kappa_+ = \frac{NkT}{V}\{1-2b_2A_0-3b_3A_0^2-4b_4A_0^3\ldots\}. \tag{60a}$$

For $A_0 = \zeta(s) - 0$, the compressibility is from (60)

$$\kappa_{+1} = \frac{NkT}{V}\frac{\zeta(s)}{\zeta(s-1)}$$

$$= 0 \quad \text{for } s = \tfrac{3}{2},$$

$$= \frac{NkT}{V} 0{\cdot}731 \quad \text{for } s = 3. \tag{61}$$

Substituting (60) in (59), and noting that

$$p_+ = \frac{E_+}{sV}$$

we have, using (49), $\gamma_+ = \dfrac{C_{p+}}{C_{V+}} = \dfrac{s+1}{s}\dfrac{B_0}{A_0}\dfrac{\Sigma A^n/n^{s-1}}{A_0}$, (62)

which reduces to the power series

$$\gamma_+ = \frac{s+1}{s}\{1 + b_2 A_0 + 2(b_3 + b_2^2) A_0^2 + (3b_4 + 7b_2 b_3 + 4b_2^3) A_0^3 + \ldots\}. \tag{62a}$$ †

For $A_0 = \zeta(s) - 0$, (62) gives

$$\gamma_{+1} = \frac{s+1}{s}\frac{\zeta(s+1)\,\zeta(s-1)}{[\zeta(s)]^2},$$

$$= \infty \quad \text{for } s = \tfrac{3}{2},$$

$$= 1{\cdot}645 \quad \text{for } s = 3. \tag{63}$$

Besides the specific heats at constant volume and pressure, we can define the specific heat (C_s) at constant N_0, i.e. keeping the amount of the condensed phase constant.‡ In non-degeneracy $N_0 = 0$, and C_s is indeterminate; it can be given any value in the range C_V to C_p. In degeneracy, to maintain N_0 constant an increase in the temperature of the assembly must be accompanied by a decrease in volume according to the relation

$$dN_0 = 0 = TdV + sVdT, \tag{64}$$

which follows from (23*a*). We have

$$C_{s-} = \left(\frac{\partial E}{\partial T}\right)_V + \left(\frac{\partial E}{\partial V}\right)_T \left(\frac{\partial V}{\partial T}\right)_{N_0} + p\left(\frac{\partial V}{\partial T}\right)_{N_0}, \tag{65}$$

---

† As already mentioned $\gamma_- = \infty$.

‡ In the case of a liquid-saturated vapour system C_s corresponds to the specific heat when the amount of the liquid and the saturated vapour are separately kept constant—the specific heat of saturated vapour.

which with the help of (44), (52) and (64) gives

$$C_{s-} = 0, \tag{66}$$

and thus during an adiabatic change N_0 and also A_0 remains constant. The constancy of A_0 during an adiabatic process is not confined to the degenerate case only but holds generally as entropy† is a function of A_0 only.

We shall now evaluate the basic thermodynamic functions. The Gibbs free energy G and the Helmholtz free energy F are defined by

$$G = H - ST, \tag{67}$$

$$F = E - ST, \tag{68}$$

where S is the entropy and H is the enthalpy (total heat),

$$H = E + PV. \tag{69}$$

As already mentioned G and A are connected by the simple relation

$$G = kNT \log A. \tag{70}$$

In degeneracy $A = 1$, and therefore $G = 0$: and as already remarked *the Bose-Einstein degeneracy is characterized by zero Gibbs free energy.* This markedly simplifies the expression for other thermodynamic functions in degeneracy. Noting that $p_-V = E_-/s$, E_- being given by equation (44), we have in the degenerate case,

$$G_- = 0. \tag{71}$$

$$\begin{aligned} S_-T = H_- &= -(s+1)\,F_- = (s+1)\,p_-V = \left(\frac{s+1}{s}\right) E_- \\ &= \frac{CV(kT)^{s+1}}{s}\,\Gamma(s+2)\,\zeta(s+1) = \frac{(s+1)\,NkT}{A_0}\,\zeta(s+1). \end{aligned} \tag{72}$$

For $A_0 = \zeta(s) - 0$, we obtain

$$\begin{aligned} S_{-1}T_0 = H_{-1} &= -(s+1)\,F_{-1} = (s+1)\,p_{-1}V = \frac{s+1}{s}\,E_{-1} \\ &= \frac{(s+1)\,NkT_0\,\zeta(s+1)}{\zeta(s)}, \end{aligned} \tag{73}$$

and, in particular,

$$\frac{S_{-1}}{Nk} = (s+1)\frac{\zeta(s+1)}{\zeta(s)} = \left.\begin{matrix} 1{\cdot}284 & \text{for } s = \tfrac{3}{2}, \\ 3{\cdot}602 & \text{for } s = 3. \end{matrix}\right\} \tag{74}$$

---

† See equations (72) and (78).

In the non-degenerate case the expression for G_+ is easily obtained when we note that

$$\int_0^A \frac{dB_0}{dA}\frac{dA}{dA_0}\,dA_0 = \int_0^A \frac{A_0}{A}\frac{dA}{dA_0}\,dA_0,$$

or

$$\Big[\log A\Big]_{\rho\to 0}^{A} = \int_{\rho\to 0}^{A} \frac{1}{A_0}\frac{dB_0}{dA_0}\,dA_0, \tag{75}$$

where B_0 is defined by the equation (42). Substituting the series expansion (43) for B_0 in (75) we have

$$\frac{G_+}{NkT} = \log A = \log A_0 - 2b_2A_0 - \tfrac{3}{2}b_3A_0^2 - \tfrac{4}{3}b_4A_0^3 \ldots, \tag{76}$$

The series expansions for F_+ and S_+ can be at once written down by substituting in (67) and (68) for $H_+ = \left(\frac{s+1}{s}\right)E_+$ from equation (43) and for G_+ from the above equation. We have

$$\frac{F_+}{NkT} = -1 + \log A_0 - b_2A_0 - \frac{b_3}{2}A_0^2 - \frac{b_4}{3}A_0^3 \ldots, \tag{77}$$

$$\frac{S_+}{Nk} = -\log A_0 + (s+1) - (s-1)\,b_2A_0 - \frac{(2s-1)}{2}b_3A_0^2 - \frac{(3s-1)}{3}b_4A_0^3 \ldots \tag{78}$$

3. It now remains to examine some properties of the distribution function itself. The contribution to the energy of the assembly by particles which have their energies lying in an *energy range* of unit extension about the energy value ϵ is by the distribution law (19)

$$\epsilon N(\epsilon) = \frac{C\epsilon^s}{1/A\;e^{\epsilon/kT} - 1}, \tag{79}$$

and is therefore maximum for $\epsilon = \epsilon_m$, where ϵ_m is given by

$$e^{u_m}\left(1 - \frac{u_m}{s}\right) = A, \tag{80}$$

where,

$$\frac{\epsilon_m}{kT} = u_m. \tag{81}$$

In figure 1 the dotted curve marked *EN* shows the relation between u_m and A in the non-relativistic case ($s = \frac{3}{2}$). The variation of A is from zero to unity. The dotted curve *ER* corresponds to the relativistic case ($s = 3$).

Let λ denote the de Broglie wave-length associated with a particle having energy ϵ, then

$$\lambda = \frac{b(s)}{\epsilon^{s/3}}, \tag{82}$$

where, for the non-relativistic case $b(\frac{3}{2}) = h/(2m)^{\frac{1}{2}}$, m being the rest mass, and in the relativistic case $b(3) = hc$. The contribution to the energy of the assembly by particles which have their wave-lengths lying in a *wave-length range* of unit extension about the value λ is

$$\epsilon N(\epsilon)\frac{d\epsilon}{d\lambda} = \frac{3C}{b(s)}\left(\frac{kT}{x}\right)^{1+\frac{4}{3}s}\frac{1}{e^{1/x}/A-1}, \tag{83}$$

where

$$x = kT\left(\frac{\lambda}{b(s)}\right)^{3/s}. \tag{84}$$

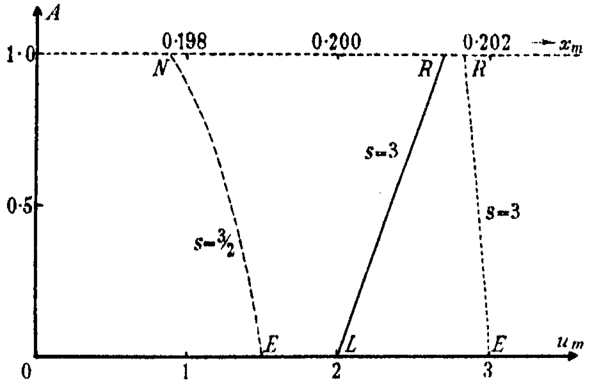

FIGURE 1. $u_m = \frac{\epsilon_m}{kT}$, $x_m = \frac{\lambda_m kT}{hc}$. EN shows the variation of u_m with A in the non-relativistic case and ER in the relativistic case. LR shows the variation of x_m with A in the relativistic case.

The energy contribution is maximum for $\lambda = \lambda_m$, where λ_m is given by

$$e^{1/x_m}\left(1 - \frac{3}{(4s+3)\,x_m}\right) = A, \tag{85}$$

$$x_m = kT\left(\frac{\lambda_m}{b(s)}\right)^{3/s}. \tag{86}$$

In figure 1 the curve LR shows the relation between x_m and A in the relativistic case.

It will be noticed that Wien's displacement law for black-body radiation, i.e. radiation in thermal equilibrium with matter is *only a particular case* *of* (80) *or* (85). ***For, black-body radiation is characterized by zero Gibbs free energy*** ($A = 1$, $G = 0$), ***and represents the degenerate case of relativistic Bose-Einstein statistics.*** In the case of radiation B_0 is defined by

$$\Sigma \frac{A^n}{n^4} = B_0 = \frac{(hc)^3 E}{8\pi \Gamma(4) V (kT)^4} \tag{87}$$

which is obtained from (41) on substituting

$$s = 3 \quad \text{and} \quad C = \frac{8\pi}{(hc)^3}, \tag{88}$$

and as in degeneracy ($A = 1$) $B_0 = \zeta(4) = \pi^4/90$, (87) gives the Stefan's law for black-body radiation

$$\frac{E_-}{V} = \frac{48\pi (kT)^4}{(hc)^3} \frac{\pi^4}{90}. \tag{89}$$

We now ask the question: is it possible to realize the non-degenerate case for radiation? In non-degeneracy

$$B_0 = \frac{(hc)^3 E_+}{48\pi V (kT)^4} < \zeta(4), \tag{90}$$

i.e. the energy density for a given temperature will be smaller than for black-body radiation, and A will be expressed in terms of B_0 by the power series which is obtained on the inversion of (42):[†]

$$\begin{aligned} A &= B_0 - \frac{1}{2^4} B_0^2 - \left(\frac{1}{3^4} - \frac{2}{4^4}\right) B_0^3 - \left(\frac{1}{4^4} - \frac{5}{6^4} + \frac{5}{8^4}\right) B_0^4 - \dots \\ &= B_0 - 0{\cdot}0625 B_0^2 - 0{\cdot}00453 B_0^3 - 0{\cdot}00127 B_0^4 - \dots. \end{aligned} \tag{91}$$

At first sight it might appear that when the energy density of radiation is decreased below its black-body value, say by allowing black-body radiation to escape into a large vacuum chamber (devoid of matter) with perfectly reflecting walls or in other ways, it becomes non-degenerate radiation. This, however, is not correct, for when black-body radiation becomes dilute, there takes place no redistribution of energy in the different frequencies, but the energy in the different frequencies is merely lowered by a constant factor.[‡] The *relative* distribution of energy in the different frequencies is the same as for black-body (degenerate) radiation, only the *absolute* amount of energy for each frequency is smaller. ***Dilute radiation***

[†] This is immediately written down from (25) by putting $s = 4$, and writing B_0 in place of A_0.

[‡] Dilute radiation is not an equilibrium radiation in the thermodynamic sense.

is, therefore, not non-degenerate radiation, for, in non-degeneracy the relative distribution of energy in the different frequencies depends on the actual value of the distribution parameter A, and is not the same as in the case of degeneracy (black-body radiation) which is characterized by $A = 1$. In figure 2 the dotted curve represents the energy distribution for black-body radiation (Planck's formula), i.e. A equal to unity; and the continuous curve is for the non-degenerate case with $A = \frac{1}{10}$. The variation with change in the value of A from zero to unity in the frequency and wavelength which corresponds to the maximum in the energy distribution curve is given by equations (80) and (85), and is shown in figure 1.

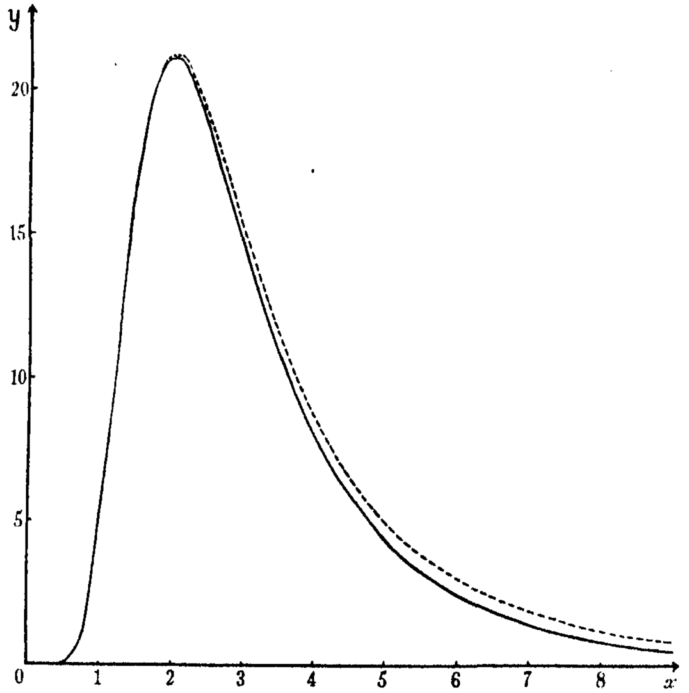

FIGURE 2. $x = \frac{\lambda kT}{ch}$, $y = \frac{1}{x^5}\frac{1}{e^{1/x}/A - 1}$. The dotted curve is for degenerate (black-body) radiation and the continuous curve for non-degenerate radiation with $A = \frac{1}{10}$. In the latter case the ordinates have been multiplied by 10.

The transformation of dilute black-body radiation into non-degenerate radiation requires a redistribution of energy in the different frequencies, but this cannot take place because of the linear character of the electromagnetic equations.[†] The realization of non-degenerate radiation is dependent upon the possibility of direct interaction between photons, and is thus connected with the non-linear developments in the electromagnetic field theory as in the investigations of Born, and Euler and Heisenberg. It is possible that the existence of non-degenerate radiation will be found to be partly responsible for the departure from black-body radiation met with in astrophysical studies, but at the present stage of the theory it is an open question.

It is a pleasure to thank Professor M. N. Saha for his interest in our work.

REFERENCES

Bose, S. N. 1924 *Z. Phys.* **26**, 178.
Einstein, A. 1924 *S.B. preuss. Akad. Wiss.* p. 261.
— 1925. *S.B. preuss. Akad. Wiss.* p. 3.
Fowler, R. H. and Jones, H. 1938 *Proc. Camb. Phil. Soc.* **34**, 573.
London, F. 1938 *Phys. Rev.* **54**, 971.
— 1939. *J. Phys. Chem.* **43**, 49.

[†] Dilute radiation implies the absence of thermal contact with matter, for otherwise it will become black-body radiation at the temperature of matter.

The production of waves by the sudden release of a spherical distribution of compressed air in the atmosphere

By J. J. Unwin, M.Sc.
Christ's College, Cambridge

(*Communicated by G. I. Taylor, F.R.S.—Received* 27 *July* 1940)

An attempt has been made to develop a method for dealing with solutions of problems connected with the production of waves by spherical concentrations of compressed air. Starting from the general equations for three-dimensional spherically symmetrical flow in a homogeneous compressible medium having constant entropy everywhere, a process has been devised to apply step-by-step calculations over small intervals of time to investigate the general features of such a motion. A complete solution has been worked out in one particular case for a not very intense initial distribution of pressure, and various indirect checks have indicated that the results are reasonably accurate. These results show many features of definite interest. As distinct from plane or spherical sound wave theory, it is found that a train of waves passes away from the centre of disturbance, the amplitudes and wave lengths falling off from wave to wave. Furthermore, as distinct from finite amplitude plane wave theory which shows that any wave must eventually become a shock wave, the waves obtained in the finite amplitude spherical wave case show no indication of becoming shock waves, and indeed show towards the closing stages of the calculation a similarity to sound wave propagation. The method is applicable to any spherically symmetrical motion up to such a time as the formation of a shock wave takes place and then fails owing to the assumption of constant entropy.

1. Introduction

Recent experimental work has revealed the nature of air or 'blast' waves which are produced by explosions. Though the theory of sound is of some assistance in developing a dynamical representation of the phenomena observed the limitation imposed in the theory by the assumption that the disturbance is small prevents any quantitative comparison between theory and observation from being made. Indeed, it is shown in the present work that, quite apart from the possible formation of shock waves, phenomena occur in spherical waves of finite amplitude the existence of which is not predicted even qualitatively by the theory of sound.

There are important difficulties to be faced in the application of theoretical methods to this type of phenomenon. In the first place it is necessary to formulate a set of mathematical assumptions which approximate as closely as possible to the conditions actually prevailing in an explosion, and at the same time are not too involved for mathematical development. In the case of an actual explosion a volume of gas is produced during a short time interval by chemical action. This expands at high pressure and compresses the surrounding air, thus forming a wave which is propagated outwards. The outward movement of the air in this wave is necessarily associated with reduction of density, and consequently of pressure, in the region of the explosion. This reduction of pressure will stop outward movement and even reverse it. The ultimate aim of theoretical researches on the formation of air waves from explosions must be to include the action and reaction between the gas formed by the explosive and the surrounding air. It has, however, been suggested by Professor G. I. Taylor that in the first instance a theoretical approach to the problem can be made by regarding this process as a combination of two occurrences, each leading to a separate investigation from a mathematical point of view. The first problem to be considered is the effect produced in a uniform compressible fluid medium such as the atmosphere when a solid sphere rapidly expands from a point to some finite radius. The second problem is concerned with the motion produced when a compressed sphere of fluid localized at rest within the atmosphere is suddenly released. The problem of the expanding sphere has now been fully investigated and the results are shortly to be published. The present paper deals with the solution of the second problem in a particular case, and indicates some of the interesting possibilities that may arise.

To deal with the problem of the compressed sphere of fluid the following assumptions have been adopted. The sphere is such that it could have been formed by an adiabatic compression within the atmosphere; that is to say, the spherical distribution of pressure is itself part of the homogeneous compressible atmosphere, and the pressure, density and temperature conditions at any point could be obtained from an adiabatic compression of the uniform atmosphere at that point. The entropy is thus everywhere constant. The distribution of density is a spherically symmetrical one. Density is assumed to decrease with increasing radius from the centre in such a way that $\partial \rho/\partial r$ is continuous, in order to avoid awkward discontinuities, and finally to approach the uniform density of the atmosphere outside the central disturbance. The initial velocity is everywhere zero. The problem is thus reduced to one of calculation of finite amplitude spherical waves resulting from given initial conditions.

So far as is known at present, no general theory of finite amplitude spherical waves is available. Indeed, the equations which govern such a motion are of so complicated a nature that the attainment of a general solution to cover all initial conditions would appear to be a matter of great difficulty. It was therefore decided that in the first place step-by-step calculations should be carried out, starting from a given set of initial conditions. It was hoped that such a calculation might reveal any important differences that occurred in the formation and behaviour of finite amplitude spherical waves as compared with finite amplitude plane waves or spherical sound waves. This hope has turned out to be fully justified.

The general solutions for small plane and spherical disturbances are well known (Lamb 1916, chap. 10). The small plane disturbance breaks up into two plane sound waves moving outwards in opposite directions, each having half the amplitude of the original disturbance. The small spherical disturbance gives a spherical sound wave which is propagated outwards from the centre of the disturbance. The wave consists of a single crest followed by a single depression, and the amplitude falls off inversely as the distance of the wave from the centre of the disturbance.

The general solutions for finite amplitude plane waves have been obtained by Earnshaw and Riemann (see Lamb 1916) working independently. It was found that any plane wave of finite amplitude must necessarily suffer a change of shape as it moves along. From a graphical viewpoint, those portions of the wave where the density decreases in the direction of propagation become steeper, whereas the portions where density increases tend to become less steep (Taylor and MacColl 1935, p. 215). As a result, any plane wave of finite amplitude must eventually assume the characteristics of a shock wave. Working on these lines it is found that a compressed slab of fluid breaks up into two waves travelling in opposite directions, both of which eventually develop one or more shock wave surfaces.

With regard to finite amplitude spherical waves, it is to be expected that amplitude again will approximately fall off inversely as the distance of the wave from the centre of the disturbance, as with the spherical sound wave. This diminution in amplitude will tend to oppose any tendency there may be for the front wave to become steeper, that is, the wave may fail to assume the characteristics of a shock wave. The results of the calculations have confirmed this conjecture in one case, and have also brought to light other important relative differences in the properties of the finite amplitude spherical waves. Thus, whereas in all three cases previously there is a single wave crest propagated outwards, the finite amplitude spherical disturbance gives rise to a train of waves of diminishing amplitude, rather similar to a train of ripples moving outwards from a disturbance on a liquid surface. The results obtained from these calculations and consideration of various possibilities which arise from them will be dealt with in more detail in later sections.

2. THE METHOD

The motion is a spherically symmetrical one throughout, so that both density ρ and velocity u are functions of radius r and time t only. Also, since the entropy is the same everywhere, the pressure p can be expressed in the form $k\rho^\gamma$ at all points, k and γ being constants. If p_0, ρ_0 are pressure and density conditions within the uniform surrounding medium, or atmosphere, we have

Velocity of sound in the atmosphere $= c_0 = (\gamma p_0/\rho_0)^{\frac{1}{2}} = (\gamma k \rho_0{}^{\gamma-1})^{\frac{1}{2}}$. (1)

Now the equation of motion is

$$\frac{\partial u}{\partial t}+u\frac{\partial u}{\partial r} = -\frac{1}{\rho}\frac{\partial p}{\partial r} = -k\gamma\rho^{\gamma-2}\frac{\partial \rho}{\partial r}, \tag{2}$$

and the equation of continuity is

$$\frac{\partial \rho}{\partial t}+u\frac{\partial \rho}{\partial r} = -\rho\left(\frac{\partial u}{\partial r}+\frac{2u}{r}\right). \tag{3}$$

To reduce these to a non-dimensional form, take new variables defined by

$$u' = \frac{u}{c_0}, \quad r' = \frac{r}{a}, \quad \rho' = \frac{\rho-\rho_0}{\rho_1-\rho_0}, \quad t' = t\Big/\frac{a}{c_0},$$

where a is a length, so far undefined, chosen to represent the linear dimensions of the initial disturbance, and ρ_1 is the density at the centre of the initial disturbance. The last relationship defines a new time unit as the time taken for a sound wave to travel under atmospheric conditions a distance equal to the chosen reference length a.

Substituting for u, ρ, r, and t, and making use of equation (1), we have after some reduction

$$\frac{\partial u'}{\partial t'}+u'\frac{\partial u'}{\partial r'} = -(1+\eta\rho')^{\gamma-2}\frac{\partial}{\partial r'}(1+\eta\rho'), \tag{4}$$

$$\frac{\partial \rho'}{\partial t'}+u'\frac{\partial \rho'}{\partial r'} = -\left(\rho'+\frac{1}{\eta}\right)\left(\frac{\partial u'}{\partial r'}+\frac{2u'}{r'}\right), \tag{5}$$

where $\eta = \dfrac{\rho_1-\rho_0}{\rho_0}$; thus η represents the initial central condensation at the centre of the disturbance, and is a constant throughout a given motion.

The left-hand sides of equations (4) and (5) are total derivatives. If the conditions at a point moving with the fluid are to be discussed, the equations can be written in the final non-dimensional form, dropping the accents,

$$\frac{Du}{Dt} = -(1+\eta\rho)^{\gamma-2}\frac{\partial}{\partial r}(1+\eta\rho), \tag{6}$$

$$\frac{D(1+\eta\rho)}{Dt} = -(1+\eta\rho)\left(\frac{\partial u}{\partial r}+\frac{2u}{r}\right). \tag{7}$$

Unless stated otherwise, all symbols appearing hereafter will be of the non-dimensional forms.

As the expression $(1+\eta\rho)$ is actually equal to the ratio of the absolute density at any point to absolute atmospheric density, it is at once obvious by inspection that these last equations are equivalent to the equations (2) and (3); for the new variables are so defined as to make the velocity of sound in atmospheric conditions unity. At the same time, the new forms have certain advantages. As they give rate of change of velocity and density at a point moving with the fluid, the displacement of a given shell moving with the fluid can be followed. The mass of fluid enclosed by such a shell can be evaluated by a simple integration from the density distribution within it (absolute densities must be used for this purpose), and as this mass should remain constant, the process provides an indirect check on the reliability of the results. Furthermore, initial disturbances having the same density distribution but of various degrees of violence and size can be treated at once by altering the value of the constant η alone, and the results, from a graphical point of view, all begin with the same curve for density distribution. The comparative effects of increased initial pressures on the course of the motion will thus be clearly indicated. It must be emphasized, however, that a complete repetition of the step-by-step process is required for each new set of initial conditions.

A number of shells initially positioned at r_1, r_2, r_3, ... will move with the fluid. Their positions at a time t can be represented by a displacement function of the form $s_t(r)$, this being the position radius of a shell which initially had a position radius r. Suppose now that at a time t the displacement, velocity and density distributions are known, together with the function $D\rho/Dt$. Then the new distributions at the end of a short time interval δt can be found in the following way. From $\rho_t(r)$ the right-hand side of equation (6) can be evaluated, giving the rate of change of velocity for a point moving with the fluid, whence the velocity increments can be found. The mean velocity of the fluid taken from its velocities at the beginning and end of the interval yields the displacement during the interval. Hence the new distributions of velocity and total displacement are known, and can be used in equation (7). It is convenient and sufficiently accurate to evaluate the right-hand side of equation (7) as it stands, using the density distribution for time t. This gives a value for $D\rho/Dt$ at the end of the interval, and the mean $D\rho/Dt$ for the interval can be calculated, after which the density increments are easily found. Consequently the new distributions at time $t+\delta t$ are available. This group of operations constitutes one stage of the step-by-step calculation.

The equations can be solved in this way for a set of initial conditions as described in § 1. The initial distribution of density can be defined by a relation of the form $\rho = f(r)$, and the function $f(r)$ must assume the value unity at the centre ($r = 0$) and must approach zero for large values of r. Finally $f'(r)$ is assumed to approach zero for large values of r, and also at the centre, and it is assumed in addition to be continuous. This last restriction is imposed in order to avoid trouble arising from discontinuous functions in the equations and to eliminate any possibility of the formation of a shock wave at the outset. It is clear that the motion of a shock wave cannot be handled within the limits of the present method owing to the assumption that entropy remains constant everywhere.

At time $t = 0$ then, $\rho = f(r)$. Velocity is zero everywhere. The displacement function $s_0(r)$ is simply equal to r, and $D\rho/Dt$ is zero everywhere. The step-by-step process can be commenced at once over a chosen range of values of r, the operations being carried out at each of a number of reference points spaced over the required range. If these points are sufficiently close to one another the slopes $\partial\rho/\partial r$ and $\partial u/\partial r$ can be calculated with sufficient accuracy at each point by finding the slope of the chord joining adjacent points on either side. A time interval must be chosen which is small enough to reduce errors due to approximations to as low a level as possible, otherwise it is found that the curves become so untidy and unreliable after the application of several stages that it is impossible to carry the process further. On the other hand, too small a time interval makes the calculations very laborious. Experience has shown that in the present case a time interval of 0·05 unit is suitable for the early stages of the motion. In later stages when the slopes of the curves increase, leading to more rapid changes in density and velocity, it is necessary to reduce the interval to 0·01 unit or even less. The distribution of points over the range must be sufficiently dense to facilitate estimations of slope and the construction of accurate curves from the results obtained stage by stage for extrapolation and interpolation purposes. Intervals of 0·01 are convenient, but it is advisable to have points closer together than this near the centre, and in the neighbourhood of peaks of waves. Points may be inserted as required by making graphical interpolations on the ρ and u curves, the appropriate values of r being taken from a plot of the displacement function $s_t(r)$ against r.

When slopes are calculated by taking chords, the two outside and the two inside points will be 'lost' at the conclusion of each stage, since each stage involves the estimation of two slopes. These points can be replaced with the aid of certain physical assumptions as to the character of the boundary motion at each end of the range. Thus it may be assumed that no disturbance is travelling inwards from outer regions of space to interfere with the motions set up by the sphere of initial disturbance considered, and it will then follow that a wave formation will be propagated outwards, and that the extreme front of the disturbance will either take the form of a shock wave or of a progressive sound wave. In the calculations presently to be described it was possible to apply the equations for a progressive sound wave to the outer boundary of the disturbance and so to recover the boundary points. Since we are not concerned in the present problem with any possibility of a source or sink at the centre of disturbance, it is also reasonable to assume on physical grounds that u and $\partial\rho/\partial r$ both approach zero as r approaches zero. If the points of reference are chosen close together near the centre, the velocity curve may be produced into the origin and the density curve may be faired in graphically to a horizontal tangent at $r = 0$.

An extract from the actual calculations, which are described in detail in the next section, is set out in table 1. This table shows one complete stage of the calculation, illustrating how the conditions at a time $t = 0{\cdot}20$ are derived from those at a time $t = 0{\cdot}15$.

3. THE CALCULATIONS

The above method has been applied to obtain a solution in a particular case. In order to avoid any complications arising from the early formation of shock waves a low value was chosen for η, namely, $\eta = 2$. The initial density distribution was defined by the relation $\rho = e^{-4r^2}$. The whole initial disturbance is roughly contained in a sphere of radius unity. The initial central density will be three times atmospheric density, and $\rho = -\frac{1}{2}$ will correspond to zero density (absolute). For air, $\gamma = 1{\cdot}405$.

The variations of $s_t(r)$, ρ and u have been calculated from time $t = 0$ to time $t = 1{\cdot}45$ over an initial range $r = 0$ to $r = 1{\cdot}5$.

The results obtained for the early stages of the motion are tabulated in tables 2 A and 2 B, and the density distributions are shown graphically in figure 1. In this figure density is shown plotted against radius at time

TABLE 1. EXTRACT FROM THE CALCULATIONS

r	$u_{0\cdot15}$	$s_{0\cdot15}(r)$	$\left(\frac{D\rho}{Dt}\right)_{0\cdot15}$	$\rho_{0\cdot15}$	$-2\left(\frac{\partial\rho}{\partial r}\right)_{0\cdot15}$	$\left(\frac{Du}{Dt}\right)_{0\cdot15}$	δu	$u_{0\cdot20}$	$s_{0\cdot20}(r)$	$\frac{\partial u}{\partial r}+\frac{2u}{r}$	$\left(\frac{D\rho}{Dt}\right)_{0\cdot20}$	$\rho_{0\cdot20}$
0	0	0		0·640			0	0	0			0·437
0·05	0·0531	0·0543	−3·904	0·639	0·331	0·203	0·0102	0·0633	0·0572	3·352	−3·813	0·436
0·10	0·1089	0·1087	−3·810	0·622	0·683	0·422	0·0211	0·1300	0·1147	3·345	−3·754	0·433
0·15	0·1594	0·1626	−3·524	0·602	0·856	0·535	0·0268	0·1862	0·1712	3·109	−3·424	0·428
0·20	0·1981	0·2159	−3·128	0·576	1·162	0·736	0·0368	0·2349	0·2267	2·932	−3·152	0·419
0·30	0·2678	0·3238	−2·381	0·497	1·665	1·103	0·0551	0·3229	0·3386	2·542	−2·535	0·374
0·40	0·3031	0·4237	−1·523	0·403	1·924	1·357	0·0678	0·3709	0·4406	1·894	−1·713	0·322
0·50	0·2956	0·5229	−0·759	0·304	1·824	1·377	0·0688	0·3644	0·5394	1·101	−0·887	0·263
0·60	0·2591	0·6199	−0·252	0·217	1·567	1·265	0·0633	0·3224	0·6344	0·428	−0·306	0·203
0·70	0·2016	0·7154	0·057	0·1414	1·212	1·047	0·0524	0·2540	0·7268	−0·110	0·0705	0·1446
0·80	0·1348	0·8102	0·1623	0·0899	0·868	0·785	0·0393	0·1741	0·8179	−0·336	0·1985	0·0989
0·90	0·0850	0·9062	0·1451	0·0503	0·610	0·576	0·0288	0·1138	0·9112	−0·331	0·1822	0·0585
1·00	0·0470	1·0034	0·1151	0·0268	0·364	0·354	0·0177	0·0647	1·0062	−0·288	0·1520	0·0335
1·10	0·0236	1·1017	0·0791	0·0130	0·207	0·204	0·0102	0·0338	1·1031	−0·189	0·0970	0·0175
1·20	0·0106	1·2007	0·0396	0·0058	0·105	0·105	0·0053	0·0159	1·2014	−0·112	0·0564	0·0082
1·30	0·00450	1·3003	0·0188	0·0025	0·0485	0·0484	0·0024	0·00692	1·3006	−0·0548	0·0276	0·0037
1·40	0·00178	1·4001	0·0083	0·0010	0·0214	0·0214	0·00107	0·00285	1·4002	−0·0248	0·0124	0·0015
1·50	0·00068	1·5000	0·0035	0·0004	0·0092	0·0092	0·00046	0·00114	1·5001	−0·0105	0·0053	0·0006

intervals of 0·2, and in order to provide a better picture of the motion the axes for each successive curve are displaced downwards through a corresponding distance of 0·2, the scales being kept the same. At time $t = 0 \cdot 8$ it was found that the density distributions in the outer regions of the range were conforming very closely to distributions calculated from sound wave theory and henceforth much labour was eliminated by making free use of the laws of sound wave theory in place of the step-by-step processes (Lamb 1916, p. 485). As the motion proceeds it turns out that the sound wave theory becomes applicable at distances nearer to the centre. Density distributions deduced by this alternative method have been tabulated in table 4.

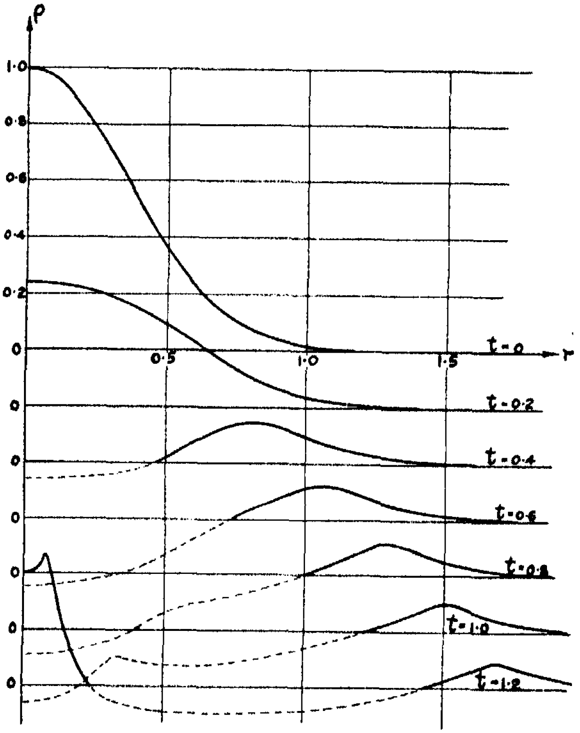

FIGURE 1

In the later stages of the calculations, the variations near the centre begin to take place more rapidly, and density and velocity gradients become steeper. It was therefore necessary gradually to decrease the time interval from 0·05 to 0·01 and extra points of reference were inserted near the centre. At time $t = 1 \cdot 35$ it became difficult to control the operations, and at time

TABLE 2A. VARIATION OF $s_t(r)$, ρ AND u FROM $t = 0$ TO $t = 1·0$ OVER THE RANGE $r = 0$ TO $r = 0·60$

Initial radii …		0	0·05	0·10	0·15	0·20	0·30	0·40	0·50	0·60
t										
0	$s_t(r)$	0	0·05	0·10	0·15	0·20	0·30	0·40	0·50	0·60
	ρ	1·000	0·990	0·961	0·914	0·852	0·698	0·527	0·365	0·237
	u	0	0	0	0	0	0	0	0	0
0·1	$s_t(r)$	0	0·052	0·104	0·156	0·207	0·312	0·411	0·510	0·609
	ρ	0·822	0·818	0·796	0·762	0·718	0·602	0·469	0·337	0·228
	u	0	0·039	0·078	0·114	0·143	0·191	0·213	0·206	0·179
0·2	$s_t(r)$	0	0·057	0·115	0·171	0·227	0·339	0·441	0·539	0·634
	ρ	0·437	0·436	0·433	0·428	0·419	0·374	0·322	0·263	0·203
	u	0	0·063	0·130	0·186	0·235	0·323	0·371	0·364	0·322
0·3	$s_t(r)$	0	0·064	0·128	0·190	0·252	0·374	0·481	0·580	0·671
	ρ	0·128	0·128	0·130	0·137	0·139	0·143	0·157	0·168	0·166
	u	0	0·065	0·133	0·195	0·256	0·361	0·419	0·423	0·389
0·4	$s_t(r)$	0	0·070	0·141	0·210	0·277	0·409	0·522	0·621	0·710
	ρ	−0·057	−0·057	−0·055	−0·049	−0·042	−0·018	0·030	0·081	0·123
	u	0	0·063	0·129	0·186	0·243	0·337	0·383	0·393	0·381
0·5	$s_t(r)$	0	0·076	0·153	0·227	0·300	0·439	0·555	0·656	0·745
	ρ	−0·172	−0·170	−0·166	−0·157	−0·147	−0·110	−0·048	0·015	0·072
	u	0	0·060	0·114	0·163	0·214	0·266	0·282	0·290	0·302
0·6	$s_t(r)$	0	0·082	0·164	0·242	0·318	0·461	0·577	0·678	0·769
	ρ	−0·241	−0·238	−0·231	−0·220	−0·205	−0·153	−0·086	−0·028	0·022
	u	0	0·047	0·089	0·127	0·159	0·170	0·157	0·166	0·191
0·7	$s_t(r)$	0	0·085	0·171	0·252	0·331	0·472	0·586	0·689	0·784
	ρ	−0·278	−0·273	−0·265	−0·253	−0·231	−0·163	−0·101	−0·053	−0·027
	u	0	0·026	0·055	0·076	0·081	0·046	0·028	0·052	0·127
0·8	$s_t(r)$	0	0·087	0·174	0·256	0·333	0·470	0·584	0·690	0·792
	ρ	−0·288	−0·285	−0·277	−0·261	−0·228	−0·149	−0·102	−0·081	−0·064
	u	0	0·005	0·007	0·004	−0·032	−0·094	−0·073	−0·018	0·040
0·9	$s_t(r)$	0	0·086	0·172	0·252	0·322	0·484	0·574	0·686	0·794
	ρ	−0·285	−0·280	−0·267	−0·238	−0·190	−0·126	−0·113	−0·106	−0·084
	u	0	−0·018	−0·045	−0·104	−0·185	−0·212	−0·124	−0·056	−0·010
1·0	$s_t(r)$	0	0·082	0·163	0·233	0·296	0·430	0·561	0·679	0·790
	ρ	−0·262	−0·248	−0·220	−0·163	−0·114	−0·112	−0·125	−0·116	−0·089
	u	0	−0·062	−0·142	−0·264	−0·344	−0·254	−0·138	−0·085	−0·062

TABLE 2B. VARIATION OF $s_t(r)$, ρ AND u FROM $t = 0$ TO $t = 0{\cdot}8$ OVER THE RANGE $r = 0{\cdot}70$ TO $r = 1{\cdot}50$

Initial radii ...	0·70	0·80	0·90	1·00	1·10	1·20	1·30	1·40	1·50
t									
0	0·70	0·80	0·90	1·00	1·10	1·20	1·30	1·40	1·50
0	0·138	0·0775	0·0391	0·0183	0·0079	0·0032	0·0012	0·0004	0·0001
	0	0	0	0	0	0	0	0	0
0·1	0·707	0·805	0·903	1·002	1·101	1·200	1·300	1·400	1·500
	0·139	0·0831	0·0442	0·0220	0·0099	0·0042	0·0017	0·0006	0·0002
	0·137	0·0909	0·0554	0·0301	0·0148	0·0066	0·0027	0·0010	0·0004
0·2	0·727	0·818	0·911	1·006	1·103	1·201	1·301	1·400	1·500
	0·145	0·0989	0·0585	0·0335	0·0175	0·0082	0·0037	0·0015	0·0006
	0·254	0·174	0·114	0·0647	0·0338	0·0159	0·0069	0·0029	0·0011
0·3	0·756	0·839	0·926	1·015	1·108	1·205	1·302	1·401	1·500
	0·149	0·123	0·0866	0·0575	0·0328	0·0176	0·0086	0·0038	0·0016
	0·322	0·246	0·165	0·0972	0·0543	0·0273	0·0127	0·0055	0·0023
0·4	0·789	0·865	0·944	1·026	1·114	1·208	1·303	1·402	1·501
	0·144	0·140	0·115	0·0822	0·0492	0·0282	0·0145	0·0069	0·0031
	0·339	0·286	0·216	0·143	0·0885	0·0483	0·0249	0·0118	0·0051
0·5	0·822	0·895	0·969	1·044	1·126	1·215	1·307	1·403	1·502
	0·111	0·135	0·131	0·109	0·0726	0·0453	0·0248	0·0130	0·0071
	0·308	0·305	0·282	0·215	0·148	0·0873	0·0493	0·0249	0·0108
0·6	0·849	0·924	0·998	1·069	1·145	1·227	1·314	1·407	1·503
	0·0556	0·0830	0·1154	0·1270	0·1049	0·0731	0·0430	0·0241	0·0115
	0·227	0·264	0·288	0·272	0·217	0·143	0·0861	0·0453	0·0234
0·7	0·868	0·947	1·024	1·096	1·169	1·245	1·325	1·413	1·507
	0·002	0·0304	0·0648	0·0921	0·1167	0·1018	0·0744	0·0415	0·0216
	0·157	0·190	0·222	0·261	0·262	0·218	0·140	0·0834	0·0476
0·8	0·880	0·962	1·042	1·118	1·195	1·268	1·342	1·425	—
	−0·037	−0·009	0·0140	0·0409	0·0761	0·1137	0·1062	0·0713	0·0388
	0·091	0·122	0·148	0·169	0·227	0·243	0·209	0·150	—

For further variations occurring after $t = 0{\cdot}8$ see table 4.

TABLE 3. VARIATION OF $s_t(r)$, ρ AND u IN THE NEIGHBOURHOOD OF THE CENTRE OF THE DISTURBANCE DURING THE LATER STAGES OF THE MOTION

Initial radii ... t		0	0·025	0·050	0·075	0·100	0·125	0·150	0·175	0·200	0·250	0·500
1·10	$s_t(r)$	0	0·035	0·070	0·105	0·140	0·171	0·195	0·229	0·257	—	—
	ρ	−0·155	−0·150	−0·133	−0·110	−0·070	−0·015	0·005	−0·002	−0·030	—	—
	u	0	−0·073	−0·149	−0·244	−0·335	−0·432	−0·464	−0·442	−0·398	—	—
1·20	$s_t(r)$	0	0·023	0·048	0·071	0·097	0·125	0·155	0·192	0·225	0·306	0·655
	ρ	0·400	0·406	0·426	0·470	0·422	0·286	0·170	0·072	0·011	−0·055	−0·094
	u	0	−0·176	−0·329	−0·458	−0·484	−0·365	−0·234	−0·219	−0·211	−0·166	−0·153
1·25	$s_t(r)$	0	0·015	0·031	0·052	0·081	0·116	0·149	0·186	0·219	0·300	0·647
	ρ	2·000	1·922	1·610	1·098	0·571	0·266	0·187	0·085	0·014	−0·036	−0·089
	u	0	−0·109	−0·207	−0·176	−0·047	0·025	0·072	−0·005	−0·045	−0·099	−0·164
1·28	$s_t(r)$	0	0·017	0·034	0·056	0·087	0·120	0·152	0·188	0·220	—	—
	ρ	0·940	0·953	1·048	0·750	0·426	0·212	0·174	0·077	0·013	—	—
	u	0	0·213	0·398	0·465	0·432	0·262	0·136	0·126	0·120	—	—
1·30	$s_t(r)$	0	0·020	0·043	0·067	0·098	0·127	0·155	0·192	0·224	0·298	0·639
	ρ	−0·020	0·014	0·080	0·241	0·289	0·224	0·177	0·077	0·012	−0·015	−0·078
	u	0	0·068	0·395	0·633	0·612	0·375	0·204	0·159	0·143	0·042	−0·166
1·32	$s_t(r)$	0	0·020	0·049	0·079	0·110	0·135	0·160	0·196	0·227	—	—
	ρ	−0·090	−0·103	−0·241	−0·076	0·149	0·232	0·179	0·073	0·020	—	—
	u	0	−0·021	0·250	0·457	0·565	0·419	0·283	0·217	0·163	—	—
1·35	$s_t(r)$	0	0·023	0·058	0·086	0·122	0·146	0·170	0·204	0·232	0·302	0·631
	ρ	−0·220	−0·257	−0·350	−0·187	−0·034	0·138	0·130	0·068	0·041	0·003	−0·067
	u	0	0·235	0·321	0·024	0·234	0·348	0·412	0·347	0·230	0·085	−0·159
1·39	$s_t(r)$	0	0·032	0·065	0·080	0·126	0·157	0·187	0·219	0·242	0·306	—
	ρ	−0·480	−0·450	−0·344	−0·124	−0·179	−0·102	−0·035	0·056	0·081	0·019	—
	u	0	0·095	−0·109	−0·166	0·124	0·225	0·375	0·338	0·247	0·130	—
1·43	$s_t(r)$	0	0·020	0·039	0·069	0·126	0·164	0·200	0·231	0·252	0·312	—
	ρ	−0·400	−0·359	−0·157	−0·139	−0·237	−0·214	−0·129	0·026	0·088	0·029	—
	u	0	−0·798	−1·12	−0·347	−0·047	0·228	0·407	0·376	0·262	0·130	—
1·45	$s_t(r)$	—	0?	0·014	0·062	0·126	0·167	0·207	0·237	0·258	0·315	—
	ρ	—	Large	0·293	−0·140	−0·259	−0·263	−0·168	0·017	0·088	0·029	—
	u	0	−1·23	−1·35	−0·302	−0·032	0·154	0·273	0·214	0·237	0·156	—

$t = 1{\cdot}45$ the calculations were finally given up. Fortunately by that time a satisfactory amount of information had been obtained. A selection of the results may be found tabulated in tables 2 A and 3, and the density distributions near the centre for the later stages of the motion are shown graphically in figure 2. In this diagram density distributions have been plotted at time intervals of 0·05 and the axes have been displaced to the left as well as vertically downwards, giving in effect a perspective view of the motion. In order to identify the axes corresponding to each curve, the curves have in all cases been plotted in continuous line where ρ is positive, and in broken line where ρ is negative.

TABLE 4. VARIATIONS OF ρ DERIVED BY SOUND WAVE THEORY, GIVING THE MOTION OF THE FRONT WAVE

Radius	$t = 0{\cdot}7$	0·8	0·9	1·0	1·1	1·2	1·3	1·4
0·7	—	—	—	−0·112	−0·105	−0·096	−0·085	−0·070
0·8	—	—	—	−0·097	−0·096	−0·096	−0·085	−0·073
0·9	—	—	—	−0·076	−0·079	−0·097	−0·085	−0·076
1·0	—	0·0060	—	−0·051	−0·068	−0·072	−0·085	−0·076
1·1	—	0·0330	0·0055	−0·026	−0·046	−0·062	−0·066	−0·076
1·2	—	0·0800	0·030	0·005	−0·024	−0·042	−0·056	−0·060
1·3	—	0·1120	0·074	0·028	0·005	−0·022	−0·039	−0·051
1·4	0·0456	0·0770	0·114	0·068	0·026	0·004	−0·020	−0·036
1·5	0·0229	0·0430	0·072	0·106	0·064	0·024	0·004	−0·019
1·6	0·0112	0·0210	0·040	0·067	0·099	0·060	0·023	0·004
1·7	—	0·0110	0·020	0·038	0·063	0·093	0·056	0·022
1·8	—	—	0·010	0·019	0·036	0·060	0·088	0·053
1·9	—	—	—	0·010	0·018	0·034	0·057	0·083
2·0	—	—	—	—	0·009	0·017	0·032	0·054
2·1	—	—	—	—	—	0·009	0·016	0·031
2·2	—	—	—	—	—	—	0·008	0·015
2·3	—	—	—	—	—	—	—	0·008

All values below the dotted lines are results calculated by sound wave theory; all values above are taken from the results of step-by-step calculations by interpolation.

The results are of considerable interest. The initial stages of the motion are similar to those derived by sound wave theory, the main difference being that $\partial\rho/\partial r$ remains zero at $r = 0$. A wave is formed at time $t = 0{\cdot}4$ and begins to move outwards. It is at this point that a completely new phenomenon appears. As this front wave advances it sheds a recoil wave. The first traces of this appear at time $t = 0{\cdot}6$, and its formation can be clearly followed in the diagrams. Both waves move approximately with the speed of sound, and the front wave takes on the full characteristics of a sound wave from time $t = 0{\cdot}8$. Meanwhile the recoil wave moves inwards, and its approach to the centre is accompanied by a violent rise in density shown in the curves for $t = 1{\cdot}10$ onwards. For reasons shortly to be discussed it is impossible to state the value of the maximum density attained during this recondensation with any certainty, but it would seem that highest pressure will be reached at a time $t = 1{\cdot}26$ approximately and that ρ is then about 2·3. Thus *the new central density is some 85 % greater than the initial central density.*

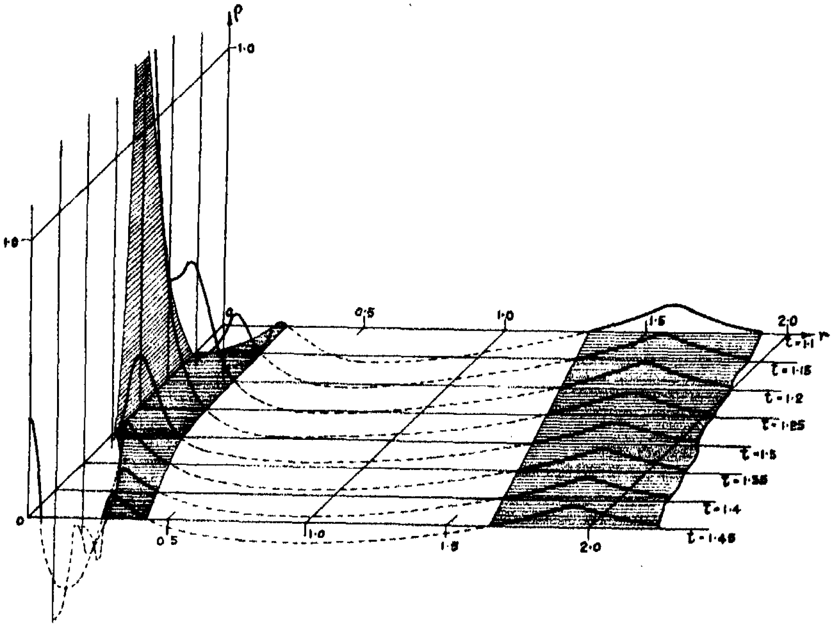

FIGURE 2

As would be expected, the new disturbance quickly breaks up and a second wave is formed at $t = 1{\cdot}30$. The changes of shape assumed during its motion outwards may or may not be due to calculation errors, but it is quite definite that at time $t = 1{\cdot}35$ another recoil wave is formed. At the conclusion of the calculation density is once more rising rapidly at the centre and it is clear that a third concentration of pressure will take place, forming yet another wave. From the results at time $t = 1{\cdot}35$ it has been found possible by sound wave theory to calculate the form of the wave at large distances from the centre with special reference to the first and second waves. A trace of the third wave also appears. From this curve it is possible to derive a reasonably clear picture of what the whole wave train will look like, and a diagram of the wave train obtained in this way is shown in figure 3. In this diagram the form of the wave, after advance to a large distance

R from the centre of disturbance, is shown by plotting density ρ against distance d measured back from the wave front. The calculations thus indicate that a train of waves moves outwards from the initial disturbance. The successive waves are of diminishing amplitude and the distance from peak to peak also falls off with each successive wave.

It is not easy to estimate the accuracy of the results, particularly on the later stages. In the course of the complete calculation there were no less than 42 applications of the process, and it seems unlikely that approximation errors should remain unimportant throughout. There is reason to hope, however, that the results are reasonably accurate up to $t = 1{\cdot}35$ at least. As has already been mentioned the results obtained by the step-by-step process agree with those obtained from sound wave theory in those regions where ρ and u are small. Furthermore, it is possible to apply a sound wave expansion at any stage, taking the existing velocity and density distributions into account. It is then found that for short time intervals after such application the results obtained by the two methods agree remarkably well.

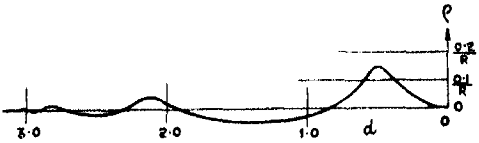

FIGURE 3

An indirect verification can be provided by integrating the density curves as mentioned in the introduction. Two types of integral are available for this purpose. In the first place the total mass of gas within a given reference shell should remain constant. At a time t a given shell, originally at radius r_1, will have a radius $s_t(r_1)$. The absolute density at any point is given by $\rho_A = \rho_0(1+2\rho)$. Hence the total mass of gas within the shell is given by the integral

$$M = \int_0^{s_t(r_1)} \rho_0(1+2\rho)\,4\pi r^2\,dr = 4\pi\rho_0 \int_0^{s_t(r_1)} (1+2\rho)\,r^2\,dr,$$

which should remain constant for all t. Another integral that can be used is an integral for 'excess density'. Clearly the mass of gas contained in the entire atmosphere over and above that required to make the density atmospheric everywhere should also remain constant. The excess density at any point is given by $(\rho_A - \rho_0)$ so that the excess density integral

$$E = \int_0^{\infty} (\rho_A - \rho_0)\,4\pi r^2\,dr = 4\pi\rho_0 \int_0^{\infty} 2\rho r^2\,dr,$$

which should also remain constant. These integrals have been evaluated by numerical methods for various reference shells and at various times and the results are shown in table 5. For reference purposes the number of stages completed up to the particular solution is also given.

TABLE 5. CALCULATIONS OF THE INTEGRALS $M/4\pi\rho_0$ AND $E/4\pi\rho_0$ FOR VARIOUS VALUES OF r AND t

Initial radius ...	$r = 0\cdot 1$		$r = 0\cdot 25$		$r = 0\cdot 5$		$r = 0\cdot 8$			
Time	$s_t(r)$	$M/4\pi\rho_0$	$s_t(r)$	$M/4\pi\rho_0$	$s_t(r)$	$M/4\pi\rho_0$	$s_t(r)$	$M/4\pi\rho_0$	$E/4\pi\rho_0$	No. of stages
0	0·1	0·00098	0·25	0·0142	0·5	0·0903	0·8	0·2616	0·1100	—
0·4	0·141	0·00083	0·343	0·0121	0·621	0·0822	0·865	0·2535	0·1039	8
0·8	0·174	0·00078	0·402	0·0114	0·690	0·0794	0·962	0·2544	0·0945	16
1·2	0·097	0·00056	0·306	0·0107	0·655	0·0753	0·960	0·2526	0·0656	26
1·35	0·122	0·00034	0·302	0·0099	0·631	0·0762	0·954	0·2498	0·0559	37

Near the centre of disturbance the integral M falls off considerably in the course of the calculation. Further out the values of M become more consistent although slight drops are still recorded. Thus the shells take up positions inside those consistent with the density distributions recorded. It is as though each shell slipped slightly in the course of each stage. Now if the shell at $r = 0\cdot 122$ at time 1·35 is displaced to a position in the neighbourhood of $r = 0\cdot 165$, consistency is attained; hence in the worst case the error in shell position at the end of 37 stages amounts only to 0·045* approximately. It is also found that if a given stage is repeated in smaller time intervals, this slipping effect is reduced while the results for density and velocity distributions are not seriously affected. Thus the discrepancies are not to be regarded as serious except perhaps in the immediate neighbourhood of $r = 0$. Owing to the term $2u/r$ appearing in equation (7) it is obvious that calculated values near the centre may not be reliable, and it is for this reason that the height of the peak at the second condensation cannot be stated with certainty.

The integral E is extremely sensitive to small errors. Thus, if the ordinates in the front wave alone were to be increased by so little as 20 %, the value of E at time $t = 1\cdot 35$ at once becomes of the same order as the initial value.

Although these considerations cannot prove that the results are reasonably accurate, it can at least be said that no indication is given that the results may be seriously wrong. The good agreement obtained by the applications of general sound wave theory therefore justify the conclusion that the position is satisfactory with regard to quantitative accuracy, and that there can be little doubt that the results are correct from a qualitative point of view.

---

* The corresponding displacement errors at $r = 0\cdot 25$, 0·5, 0·8 are respectively 0·040, 0·035, 0·015.

4. CONCLUSION

The train of waves which is found as the form of disturbance propagated to infinity bears some similarity to the train of circular ripples moving outwards from a slight disturbance on a liquid surface. Disturbances resulting from more violent initial motions on a liquid surface are characterized by more complicated forms, and something of the same sort of modification of form will certainly take place with the finite amplitude spherical waves when the initial central condensation is increased to values comparable with those attained at the centres of explosions. In particular severe practical difficulties are to be expected in the introduction of the theory to deal with the resulting shock waves. Another difficulty which may prove to be troublesome is the choice of an initial density distribution to correspond with conditions inside an explosion, although it would seem likely that the final wave form will not be so dependent on the density distribution as on the dimensions and violence of the original disturbance. The present methods can in any case deal in some measure with the initial stages of the motion prior to the formation of shock waves, and application of the method in its present form to higher initial central condensations is obviously the next step forward.

Meanwhile, in spite of the low intensity of the disturbance chosen for the first test of the method, the calculation has brought out one or two very interesting points in relation to experimental data. It has, for instance, indicated that more than one wave can come from a single region of condensation. Further, it has also been found that the zones of compression are of small length as compared with the rarefied zones separating them. These facts fit in with some of the experimental information already available, and however unimportant these points may be in themselves they do at least suggest favourable possibilities for the future in the application of this method.

The results obtained give rise to many interesting conjectures. The front wave will at some stage become a shock wave when the initial disturbance reaches a certain intensity, and the question at once arises as to whether it will then remain a shock wave, or whether it will in the course of its motion revert to a normal wave form. The formation of a second wave raises the possibility of a second shock wave being formed, and this in turn raises the possibility of the second shock wave overtaking the front wave, leading to a sudden intensification and perhaps an acceleration of the front wave. The resolution of such problems as these will be a test of the efficacy and the adaptability of the present methods.

I should like in conclusion to record my sincere thanks to Professor G. I. Taylor for much valuable advice and for the continual and sympathetic encouragement which I have received from him while carrying on this work.

REFERENCES

Lamb, H. 1916 *Hydrodynamics*, 4th ed. Camb. Univ. Press.
Taylor and MacColl 1935 Mechanics of compressible fluids. *Aerodynamic Theory* (ed. Durand), 3, div. H. Berlin: Julius Springer.

Precise measurements of the energies of β-rays from radium (B+C)

By A. F. A. HARPER, M.Sc. AND N. F. ROBERTS, M.Sc.
University of Sydney

(*Communicated by C. D. Ellis, F.R.S.—Received* 20 *November* 1940)

Precise measurements of the $H\rho$ values of β-rays from radium B have been made by Ellis and Skinner, Ellis, Scott and Rogers. Except for Rogers and Scott, who used the same methods, the results have differed from one another by amounts considerably in excess of the estimated probable errors.

Measurements have been made by the authors of the $H\rho$ of eleven β-rays of radium B and of one of radium C. The values are based on eleven photographs of the spectra taken with a spectrograph of the type used by Ellis, and ten photographs with a spectrograph of the type introduced by Scott, the field strengths used ranging from 190 to 1050 G. The values obtained agree closely with those of Rogers for the lines measured by him; Rogers's values being 1931·7, 1671·3 and 1406·2 G-cm., and our values 1931·9, 1671·6 and 1406·2 G-cm. These values are considered correct to 1 part in 10^4.

The energies corresponding to the $H\rho$ values have been calculated using weighted mean values of e/m and c given respectively by Bearden and von Friesen. The error in the energies is approximately 1 part in 10^3.

Measurement of the $H\rho$ of the same line for a number of widely differing values of H was a valuable check on the presence of systematic errors which had not been made by previous workers. An appreciable apparent increase of $H\rho$ with H was found, and a comparison of the calculated and observed line forms showed that this apparent increase was to be attributed to scattering of electrons in the emulsion. This effect appears to be one of the most important now limiting the accuracy obtainable by the present method.

1. INTRODUCTION

Measurement of the lines in the β-ray spectrum of an atom affords a method of determining accurately the energies of its γ-rays. These energies are equal to the differences between energy levels of the nucleus, and a knowledge of the γ-ray energies together with certain other evidence has allowed the determination of levels in a number of nuclei (Ellis 1934*a*; Surugue 1937; Gamow 1936). When the atom results from a disintegration in which groups of short range α-particles are ejected, or disintegrates with the ejection of groups of long range α-particles, nuclear levels can be determined by measuring the energies of these α-particle groups (Gamow 1936). For such atoms measurements of the groups of β-particles corresponding to transitions between nuclear levels are a valuable check on the accuracy of the α-ray measurements.

A number of attempts have been made to measure accurately the absolute energies of β-particle groups, but unfortunately the results obtained have been inconsistent. Owing to the ease with which strong sources of radium (B + C) can be prepared, most absolute measurements have been of the energies of the intense groups of these bodies—the energies of groups from most other bodies being determined by relative measurements. The first precise absolute measurements were made by Ellis and Skinner (1924) working on the strong groups of radium B. It was considered that the $H\rho$ values (these are proportional to the velocities and are precisely defined in § 2) were accurate to better than 20 in 10^4; the value obtained for the most intense line being 1938 G-cm. The values obtained were used for some years as standards for determining the absolute energies of other groups. In 1934 Ellis made fresh measurements of the groups from radium (B + C) using new apparatus. The errors in these results for $H\rho$ were considered to be less than 10 in 10^4. The values obtained in 1934 differed from the earlier values by 50 in 10^4—the value for the strongest line being 1925·5 G-cm. In 1934 Scott also published measurements of the $H\rho$ of the strongest line of radium B. The value of 1931·8 G-cm. was obtained, and this was considered accurate to 1 in 10^4. It will be observed that Scott's value lies almost midway between Ellis's two results, differing from each by about 30 in 10^4. Rogers (1936, 1937) checked and substantially confirmed Scott's measurements, and measured the $H\rho$ of the two lines next in intensity also. He considered, however, that the order of accuracy was only 3 in 10^4.

This communication presents measurements of the $H\rho$'s of 11 lines from radium B, and of the line of lowest energy from radium C. Field measurements were made by the method developed by Briggs and Harper (1936), and used by Briggs for α-particle measurements (1936). Measurements of ρ were made using a spectrograph of the type used by Ellis, and also using the type introduced by Scott. To assist in the detection of systematic errors the $H\rho$'s of the same lines were measured with a number of different fields ranging in strength from 270 to 1000 G. An approximately constant positive error in ρ was revealed, and a comparison of the observed and calculated line forms indicated that this error was caused by scattering of the electrons in the emulsion. The probable error in the values obtained for the $H\rho$ of seven of the lines, including the line from radium C, is considered to be not more than 1 in 10^4, and for the other lines not more than 3 in 10^4. Our values agree very closely with those of Rogers for the lines he measured.

2. THE β-RAY SPECTROGRAPH

2·1. *Principle of operation*

The β-ray spectrographs were similar in principle to that introduced by Danysz (1913) and developed by Rutherford and Robinson (1913), in which a beam of β-radiation is focused to form a velocity spectrum on a photographic plate by a magnetic field which is perpendicular to the beam.

The velocity of a group is given by

$$v = \frac{H\rho e/m_0}{\left\{1+\left(\frac{H\rho e}{m_0 c}\right)^2\right\}^{\frac{1}{2}}}, \tag{1}$$

where H = strength of the magnetic field (assumed uniform) in gauss,
ρ = radius of curvature (in cm.) of those particles of the group moving at right angles to the field,
m_0 = rest mass of an electron,
e = charge of an electron,
c = velocity of light.

Measurement of H and ρ, and knowledge of the values of e/m_0 and c therefore allows the determination of v. The energy is given by

$$E = \frac{m_0c^2}{e}\left\{\left(1-\frac{v^2}{c^2}\right)^{-\frac{1}{2}}-1\right\}\times 10^{-8}$$

$$= \frac{m_0c^2}{e}\left[\left\{1+\left(\frac{H\rho e}{m_0c}\right)^2\right\}^{\frac{1}{2}}-1\right]\times 10^{-8}\ \text{eV}. \qquad (2)$$

Two designs of spectrograph were used, the first, spectrograph A, being of the same general form as that of Rutherford and Robinson but with some modifications, and the other, spectrograph B, being similar to that introduced by Scott. Spectrograph A was used in obtaining most of the results in this paper. With spectrograph B an investigation was made of possible causes of the differences between the results of Scott and Rogers and those of other workers.

The fields used in this work were obtained from the permanent magnet described by Briggs (1932). The pole faces were 30 by 30 cm. and the air gap 4 cm. The field was produced by cobalt steel bar magnets, and the strength and uniformity were varied by adjustment of the number and position of these magnets and of the inclination of the pole pieces. Fields of from 190 to 1000 G were used. The vacuum box between the poles was of aluminium.

2·2. *Spectrograph A*

Spectrograph A is shown in figure 1. The source of radiation is at S, and the beam is defined by an aluminium 'ray' slit R, which is screwed against the ground surface of the upper aluminium block M. A slot LL allows the β-rays to pass through to the photographic plate which fits into the slit PP and is pressed against the same ground surface by means of small blocks W. In this way it was assured that the slit and emulsion were in the same plane. The position of the plate relative to the rest of the apparatus was defined by means of two fine slits A, B, each 0·03 mm. wide, which produced templet lines K_1, K_2 on the plate when illuminated from above with a pea lamp. It was a simple matter to make measurements to the edges of the slits with a travelling microscope when the dimensions of the apparatus were being determined. The templet lines obtained on the photographic plates were always sharp and symmetrical and revealed a well-marked peak when microphotometered.

The source used was a flattened platinum wire which fitted in a channel behind a pair of aluminium jaws. The jaws had a separation of 0·090 mm., and were pinned to an aluminium block J. This block was positioned on the main holder by two brass pins and could be simply removed for insertion of sources. The greatest possible lateral movement of the block on the pins was 0·008 mm. and the probable error in positioning was ± 0·001 mm., introducing an error of not more than 1·6 parts in 10^5 in the least radius of curvature which can be measured with this apparatus ($\rho = 3{\cdot}5$ cm.).

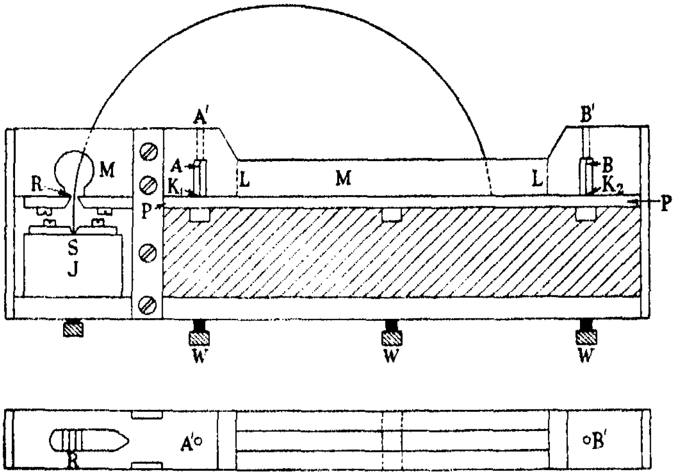

FIGURE 1. Side elevation and plan of spectrograph A.

By using for the source a slit and flat wire, rather than the usual wire or fibre, several advantages resulted.

(*a*) Errors due to source contamination are considerably less than for a cylindrical source, since with a cylindrical source that portion of the β-ray lines used for determining the velocity of the β-rays, viz. the fronts, is formed by particles leaving the source almost tangentially, and is thus markedly affected by any contamination present.

(*b*) The precision with which the effective source, i.e. the source slit, can be positioned, is considerably greater than that with most fibre or wire sources.

(*c*) Measurement of the widths of individual sources is not necessary.

(*d*) Since the position of the source and its effective width is in all cases the same, several successive sources may be used for the one photographic plate. This was of value when only weak radon sources were available. The procedure constituted a delicate check on the accuracy of positioning the source block and main plate-holder in the magnetic field, and on the constancy of the latter. Irregularities in the microphotometered lines of the β-ray spectra could in no cases be ascribed to any of the possible causes mentioned, though the use of two sources for one plate was common and in some cases three, or even four were used.

(*e*) Trouble with sag and lack of linearity of sources was eliminated.

The active deposits of Ra (A + B + C) were collected on the source wires by exposing these to radon at atmospheric pressure through a mercury seal. The radon sources were usually about 100 millicuries and the γ-ray activity of the active deposit was equivalent to that of about 10 mg. Radium in equilibrium with its products when first removed from the radon. The wires were left in the radon for about 30 min., then washed in alcohol and heated in a small vacuum furnace before mounting. Longer exposures to the radon would sometimes result in mercury adhering to the source wire. Contamination on the source has been estimated to have reduced the velocities of the main β-ray groups from Ra B by not more than 6 parts in 10^5 and probably by considerably less.

2·3. *Spectrograph B*

Spectrograph B is illustrated in figure 2. The emulsion surfaces S_1 and S_2 of the photographic plates P_1 and P_2 are in the same plane. A vertical cylindrical hole allows the β-particles to pass through the slits L_1 and L_2 and produce spectra on the photographic plates. The plates were developed and the distances between the lines measured while the plates were attached to the holder, the lines on one plate being viewed directly, and the lines on the other plate viewed through the glass. The source was a quartz

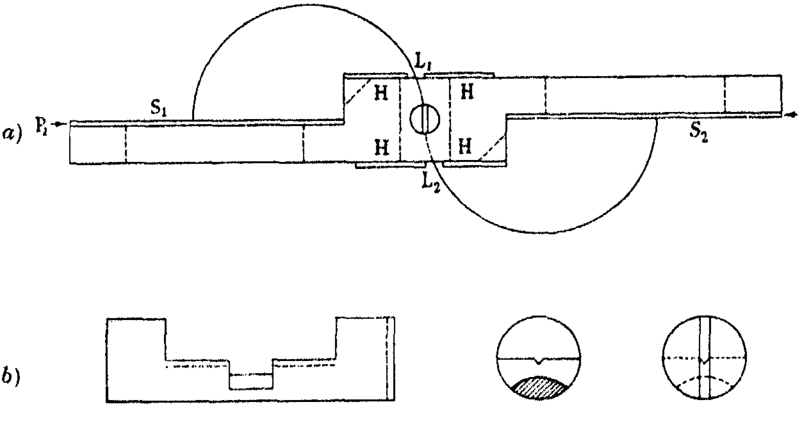

side elevation central section end elevation

FIGURE 2. Spectrograph B. (*a*) Side elevation, (*b*) source-holder.

fibre which was held by a trace of vaseline in a V-cut in the source-holder, figure 2. The diameter of the source was measured with a micrometer screw gauge. As the diameter was only 0·1–0·2 mm., the error thus introduced into the measurement of ρ is not more than 5 in 10^5.

This spectrograph has the important advantage of eliminating the necessity of measuring certain of the plate-holder dimensions as must be done when the conventional type of plate-holder is used. The plate-holder has the disadvantage, however, that the ray slits L_1 and L_2 must be broad if they are to pass β-particle groups which differ considerably in velocity.

2·4. *Pumping system*

The aluminium box, in which the plate- and source-holder was suspended by rigid rods, was sealed by a ground-glass plate and the whole exhausted by a Gaede mercury-vapour diffusion pump backed by a Cenco rotary oil pump. With this system an X-ray vacuum could be obtained in about 7 min. It can readily be shown that with a residual air pressure of 0·05 mm. Hg, the decrease in the velocity of β-particles would amount to only about 1·4 parts in 10^6 and scatter would be correspondingly small. Since the average pressure was always much less than this, this form of error may be neglected.

2·5. *Plates and development*

Several types of photographic plate were tried. Ilford X-ray plates were used for most of the work as they gave good contrast, and with them the Eberhard Effect was not troublesome. Strips about an inch wide were cut from half plates. The development of plates taken with spectrograph A was performed in a test-tube in two-thirds normal strength developer at 14° C and usually took about 20 min., the plate and developer being constantly agitated until development was complete. These methods were adopted to provide uniform development. Errors due to movements of the emulsion on the plates (Briggs 1936) were negligible as these were dried uniformly by a special fan, and there was a margin of at least one-quarter of an inch between the edges of the spectra and the plates.

The Eberhard Effect (Eberhard 1912), i.e. the retardation of the development of the edges of lines on photographic plates, decreases with agitation of the developer, and with lengthening of the period of development. Plates made with spectrograph B had their developmental conditions varied in order to determine the conditions under which the effect caused an appreciable error in ρ. It was established that the error was negligible under the conditions used by Scott, viz. ordinary Kodak plates developed for 4–5 min. in full strength developer, but that, if the development time was appreciably shorter than this and agitation omitted, the frontal point of the edge of a β-ray line could be set back 0·0025 cm. which corresponds to an error of 1 in 10^3 for a line of $H\rho$ equal to 1400 G-cm. measured when the field strength is 1000 G.

3. MEASUREMENT OF β-PARTICLE RADIUS OF CURVATURE

The major measurements required for the determination of ρ are: for spectrograph A—the distance between the outer edge of the line made by the β-rays on the photographic plate to the templet lines K_1 and K_2 (figure 1) and the position of these relative to the source; for spectrograph B—from the outer edge of the β-ray line on one photographic plate to the outer edge of the corresponding line on the other plate. In addition to these the effective source widths must be determined. Distances on the photographic plates were measured with a microphotometer, and the dimensions of spectrograph A with a travelling microscope, the same screw being used for both measurements.

3·1. *Measurement of dimensions of spectrograph A*

The dimensions of spectrograph A required in the determination of ρ were obtained by measurements on both sides of the instrument of the distances indicated in figure 3*a*. In this figure, A and B are the ends of the slits used to produce templet lines on the photographic plates, P is one end of a doubly pointed cylindrical steel rod which is pressed into the V of the jaws of the source slit, and R is the foot of the perpendicular from P to the

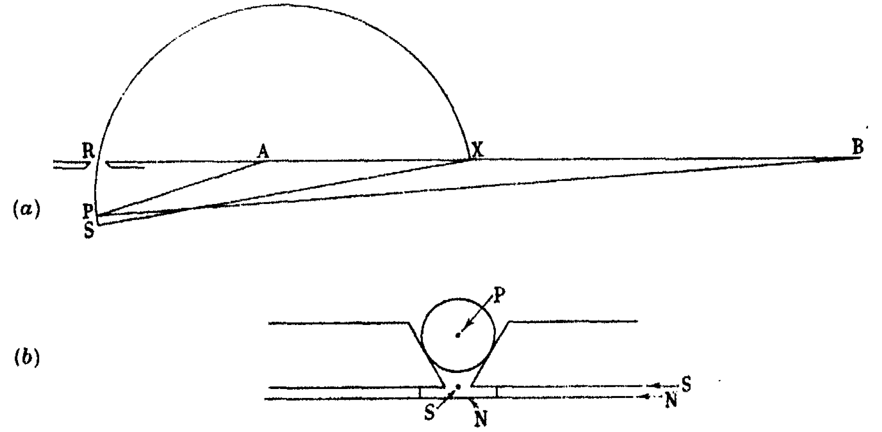

FIGURE 3

line AB. The rod was used because it was undesirable to make the source slit the full width of the spectrograph, and the ends of the rod provided good reference points. The distance PS from the rod point to the centre of the source was obtained from measurements of PN and NS (figure 3*b*). As it is actually the distance from the front edge of the source to the front of the β-ray line (X) which is required, the width of the source slit had also to be measured.

The probable errors in the distances AB, RA, RS and the source slit width ξ have been estimated from the consistency between values obtained from different sets of measurements. The magnitudes of these distances and their probable errors are:

AB	$12{\cdot}9521 \pm 0{\cdot}0002$ cm.
RA	$4{\cdot}4743 \pm 0{\cdot}0005$ cm.
RS	$1{\cdot}2350 \pm 0{\cdot}0005$ cm.
ξ	$0{\cdot}0090 \pm 0{\cdot}0003$ cm.

The radius of curvature ρ of the β-particles producing a given line is calculated from the microphotometrically determined distance BX (or AX), and the distances RB (or RA).

The errors in measurement of the dimensions of the spectrograph contribute an error of 1 in 10^4 to the estimate of the least ρ.

3·2. *Microphotometry*

For the microphotometric work an image of a small central portion of the plate was thrown on to a screen in which there was a fine slit parallel to the edges of the β-ray lines. The light entering this slit fell upon a photoelectric cell connected in series with another cell on which fell light of steady but adjustable intensity. The potential of the common point of these cells, which was measured with a Wilson double-tilted electroscope, was substantially linearly proportional to the density of the portion of the plate whose image was over the slit. The magnification of the lens system was about eight times so that, since the β-ray lines were 0·2–0·4 mm. wide, the intensity was substantially uniform over the slit when this was less than 0·1 mm. wide. When the width was made greater than this, in order to improve the sensitivity, a correction was applied.

Curves III in figures 4*a* and 4*b* are the microphotometer curves of typical β-ray lines in spectrographs A and B respectively. The line has a fairly definite peak and the 'front' is substantially straight throughout the greater part of its length. Point F, where this line meets the average background level, will be referred to as the frontal point.

3·3. *β-Ray line forms*

Calculations of the intensity variation in the beam of electrons incident on the photographic plate have been made for our spectrographs using the methods of Wooster (1927). Differences between the theoretical and experimental curves are to be attributed mainly to (1) the effects of gas present in the initial stages of pumping, (2) non-linearity of photographic response to electronic exposure and (3) scatter of electrons in the emulsion.

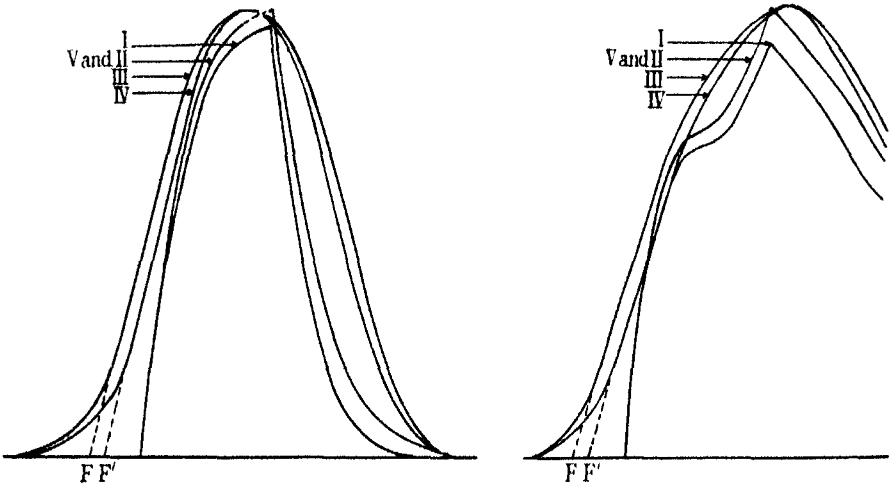

(*a*) (*b*)

Figure 4. (*a*) Curves for spectrograph A, (*b*) curves for spectrograph B. Curve I. Form of variation of intensity of incident beam. Curve II. Form of variation of exposure allowing for effects of gas present in the initial stages of pumping. Curve III. Form of photometer curve of *β*-ray line. Curve IV. Form of photometer curve after correcting for non-linearity of plate response. Curve V. Variation of exposure obtained by correcting curve IV for scattering of electrons in the emulsion.

In figures 4*a* and 4*b* curves I represent the calculated variations of the incident beams in spectrographs A and B respectively, uncorrected for the effects mentioned. The curve I for spectrograph A differs somewhat from that given by Wooster (1927) and Li (1937). This is due mainly to the narrowness of the ray slit used (*R* in figure 1).

Curves II represent the variation when effect (1) is taken into account.

Curves IV are obtained by correcting the microphotometer curves III for the response of the plate. This correction is based on the empirical relationship between the photographic density and the factors determining it (including, of course, the exposure) obtained by Ellis and Wooster (1927) for Ilford X-ray plates. In the plates used the difference between the density of the background and the peak of the lines was usually between 0·5 and 1·5 for the three strong lines of radium B. The resulting correction corresponds to an inwards shift of 0·001 ± 0·0005 cm. in the position of the frontal points.

There is little quantitative data on the scattering of high energy electrons in photographic emulsions. Ellis and Wooster (1927) mention that a line which should have been infinitely fine was in fact 0·2 mm. wide. This statement together with a comparison of our own microphotometer and theoretical curves has led us to estimate the photographic effect of the scattered electrons to be appreciable up to about 0·1 mm. Using this estimate, and assuming an exponential decrease of the photographic action with distance, we have prepared from curves IV, the photometer curves corrected for the response of the plate, curves V to represent the incident electron distribution. The curves thus obtained agree closely in form with the theoretical curves II which have therefore been set in the position in which curves V are obtained when the above corrections are applied to the initial photometer curves III. The corresponding movement in the frontal point amounts to 0·002 ± 0·001 cm.

This correction for scattering has been evaluated by a method which relied partly on trial. An exact but more arduous method, using a Fourier integral representation of the microphotometer curve, has been developed for us by Dr W. G. Baker, but more exact information is required about the effect of the scattering of electrons in photographic emulsions before this method can usefully be applied.

The advancement of the frontal points causes a linear increase with H of the apparent $H\rho$'s estimated from the uncorrected frontal points of microphotometer curves, and the advancement calculated from this increase agrees with the advancement 0·003 ± 0·0015 cm. for response and scattering arrived at from a consideration of line forms. Instead of making a separate estimate of the advancement of the frontal point of each line by measuring its density and comparing its photometer curve with the calculated line form, the mean correction to the frontal points of the lines produced by each β-ray group was obtained from the apparent increase of $H\rho$ with H for these lines. For lines measured with only one field strength the mean of corrections found for other similar lines was used.

3·4. *Order of accuracy of* ρ

Several errors, most of which have already been discussed in the relevant sections, must be combined in estimating the probable error of ρ for each spectrograph. The main sources of these are:

(*a*) the determinations of the frontal points of spectral lines (3·3).

(*b*) movements of the photographic emulsion (2·5).

(*c*) thermal expansion of the components of the spectrographs, photographic plates and microphotometer screw.

(*d*) non-uniformity in the pitch of the measuring screw (4).

(*e*) measurement of the source width (2·3, 3·1).

(*f*) movements of the source block of spectrograph A relative to the other parts of this spectrograph (2·2).

(*g*) the determination of dimensions of spectrograph A (3·1).

Of the above sources of error, all but (*f*) and (*g*) occur with both spectrographs.

An analysis has shown that the probable error introduced into the values of $H\rho$ by thermal effects (*c*), including those on the glass frame used for measurements of the magnetic fields (4·1), does not exceed 5 parts in 10^5 with the maximum temperature variation.

For spectrograph A, table 1 sets out the resultant order of accuracy for frontal point errors of 0·0005, 0·0010 and 0·0020 cm., the magnitude of the other errors entering into the calculation being as specified in the relevant sections. This has been done for the maximum and minimum ρ's obtainable on this apparatus.

TABLE 1. ORDER OF ACCURACY OF ρ (SPECTROGRAPH A) FOR DIFFERENT ERRORS IN FRONTAL POINTS

ρ	Error in frontal point (cm.)		
cm.	0·0005	0·0010	0·0020
3·5	1·1 in 10^4	1·7 in 10^4	3·3 in 10^4
8·3	0·5 in 10^4	0·7 in 10^4	1·3 in 10^4

Since errors (*b*), (*c*) and (*d*) listed above are negligible, the accuracy of ρ for spectrograph B will depend only on the errors in the determination of the source width and frontal points. These errors vary slightly from plate to plate, but the error in the diameter of the source is usually about 0·0002 cm. and the error in the position of the frontal point about 0·0015 cm. The average order of accuracy of ρ as determined with spectrograph B is therefore as follows.

TABLE 2. ORDER OF ACCURACY OF ρ'S MEASURED WITH SPECTROGRAPH B

	Line		
Field	F	G	H
679 G	$3 \cdot 9 \times 10^{-4}$	$3 \cdot 1 \times 10^{-4}$	$2 \cdot 8 \times 10^{-4}$
1050 G	$6 \cdot 0 \times 10^{-4}$	$5 \cdot 0 \times 10^{-4}$	$4 \cdot 4 \times 10^{-4}$

4. MEASUREMENT OF FIELD

The method used for determining the magnetic field has been described by Briggs and Harper (1936) and is similar in principal to the Cotton electromagnetic balance (Cotton 1900) and to the method used by Scott (1934). A flat rectangular coil was hung from one arm of a balance with its plane parallel to the pole faces and measurements made of the force acting on the coil due to the passage of a current i in it. The force mg is equal to $Hinl$, where n is the number of turns of the coil and l is the mean horizontal distance between the wires of the coil, the distances being weighted in proportion to the rate of change of the horizontal component of the field H. By taking the change in force when approximately equal currents are passed through the coil successively in opposite directions, many sources of error are eliminated. The method measures the component of the field perpendicular to the pole faces, and this is the component producing the measured deflexion of the β-particles.

The assemblage of frame and balance was mounted on a platform which could be lowered so that the bottom of the frame was in the part of the field traversed by the β-rays, or raised well above the magnets.

Two coil assemblies were used, one was a well-seasoned cedar frame 18 by 75 cm. of lathes 0·3 cm. thick carrying 35 turns of copper wire, and the other consisted of a glass frame 18 by 85 cm., with 10 turns of wire. This latter was used by Briggs (1936) for the measurements of the absolute velocity of β-particles for radium C′. With the former the weight necessary to balance the change in force on the frame when a current of approximately 1 A was reversed in it was 11·6 g. weight for a field of 125 G, the least field used with the wooden frame. With the glass frame the least field was 190 G, and this corresponded to a change in weight of 6·2 g. The fields for plates 3–12 inclusive (table 4) were measured using the wooden frame, and those for the other plates using the glass frame. The distances between the wires of the frames were measured by a travelling microscope. The screw of this instrument, described by Briggs (1936), was the same as that used for the microphotometry of the β-ray spectral lines, and for measurements on spectrograph A. By using the same screw for all measurements a knowledge of the absolute pitch of the thread is unnecessary. Lack of uniformity of this pitch was not sufficient to introduce errors of importance.

TABLE 3. ESTIMATED ERRORS IN H

$$H=\frac{mg}{il}=\frac{mgR_2R_s}{R_1el},$$

where H = magnetic field
l = weighted mean horizontal distance between the wires of the coil
i = current through the coil
e = e.m.f. of standard cell
mg = weight required to counterbalance force Hil on the coil
R_s = standard 1 ohm resistance
R_1 = reading of potentiometer when balanced against $R_s i$
R_2 = reading of potentiometer when balanced against e

Systematic errors

1.	Error in the determination of l	3 in 10^5
2.	Error in the calibration of the masses	2 in 10^5
3.	Error in the determination of g	1 in 10^5
4.	Error in the calibration of e	1 in 10^5
5.	Error in the calibration of R_s	1 in 10^5
6.	Conversion of international ampere to absolute ampere	3 in 10^5

The square root of the sum of the squares gives the probable systematic error in H as being 5 in 10^5.

Observational errors

7.	Error on adjusting i to counterbalance mg	4 in 10^5
8.	Error caused by frame (of Cotton Balance) being out of position	7 in 10^5
9.	Error in field search + error in Hartree correction	6 in 10^5
10.	Error in setting R_1	7 in 10^6
11.	Error in setting R_2	7 in 10^6
12.	Possible variations in l for wooden frame	1·5 in 10^4

The square root of the sum of the squares gives the probable observational error as 1·0 in 10^4 for measurements with the glass frame, and 1·8 in 10^4 for measurements with the wooden frame.

Hence total probable error is 1·1 in 10^4 for determinations with the glass frame, and 1·9 in 10^4 for determinations with the wooden frame.

In order to determine the absolute field intensity at any chosen point, it is necessary to know the residual field at the geometric centre of the top of the frame and to explore the field between the poles. At 60 cm. above the pole pieces the component of the residual field perpendicular to the plane of the frame is 0·4 G with a field of 125 G, and this could be determined to an accuracy of 5 in 10^4, introducing an error in H of only 2 parts in 10^5. To allow for inhomogeneities of the field between the poles both in their effect on the β-particles (Hartree 1923) and on the frame measurements, a coil of 11,000 sq. cm. turns was used, giving a sensitivity of 0·17 G per cm. deflexion of the galvanometer. The field variations were usually regular and were plotted for an area of 10 by 20 cm. Inaccuracies in the field search and small uncertainties in the positions of the frame and of the spectrograph yield altogether a maximum probable error of 1 in 10^4.

The values of the standard cells and resistances have been measured and re-checked at the National Physical Laboratory and are believed to be known to within 1 in 10^5 in terms of the N.P.L. Standards. One N.P.L. international ampere has been taken as 0·99986 absolute ampere and an error of 3 in 10^5 was allowed for the conversion of international to absolute amperes. Any irregularities in the Wolff potentiometer introduced negligible error. The masses used had been calibrated against N.P.L. standards and the error introduced by them was not greater than 2 in 10^5.

The errors in determining the field H are set out in table 3. Owing to some doubt about the interpretation of one set of divergent readings for l for the wooden frame the possibility of a slight variation of the position of the wires of this frame with temperature and humidity has been allowed for by inserting an error of 1·5 in 10^4 in the observational errors with this frame. The total errors in H thus derived are 1·1 in 10^4 for determinations made using the glass frame and 1·9 in 10^4 for determinations with the wooden frame.

5. RESULTS

In table 4 are measurements of $H\rho$ made with spectrographs A and B of lines of $H\rho$ value equal to and greater than 1406 G-cm. The letters used to designate the lines are those introduced by Ellis (1932).

Only measurements on one plate of lines of $H\rho$ less than 1406 G-cm. are presented. These are given in table 5. In this table are given also the weighted means of the various measurements of each $H\rho$ of table 4, the means being obtained by weighting each measurement inversely as the square of its theoretical probable error.

The probable observational error to be expected in each weighted mean because of the differences between the various measurements was calculated using the formula (Bond 1935, p. 83)

$$e = c_n\sqrt{\frac{(v_1/r_1)^2+\ldots+(v_n/r_n)^2}{(1/r_1^2+\ldots+1/r_n^2)\,(n-1)}},$$

where r_n is the theoretically estimated error in the $H\rho$ value which differs from the weighted mean by an amount v_n, and c_n is Jeffreys's constant, which is a function of n, decreasing from unity to 0·645 as n increases from unity to infinity. The errors calculated in this way are given in the second column of table 5.

In the third column of table 5 are the systematic errors to be expected in the weighted means because of the systematic errors in H and ρ.

In the last column are the total probable errors obtained as the square roots of the sums of the squares of the observational and systematic errors. They are in good accord with those to be expected from the previously estimated errors in H and ρ (3·4 and table 3). It should be repeated here, however, that the determinations of $H\rho$, and of the errors, depend to a considerable extent upon the interpretation of microphotometer curves and that further work on scattering is desirable.

TABLE 4. MEASUREMENT OF $H\rho$.

Plate	Field	Line						
no.	G	F	G	Ga	H	Ha	I	O
3	417·451	—	1672·4	1770·1	1932·2	2009·2	2251·8	2972·6
5	417·451	—	1673·4	1769·6	1932·9	2009·4	2251·6	2972·9
9	418·411	—	1671·8	—	1931·9	—	—	2972·1
10	418·411	—	1671·9	1770·0	1931·9	2008·8	2251·8	2972·0
12	418·305	—	1671·9	1769·1	1931·6	2008·2	2250·2	2971·8
13	418·319	—	1671·6	1769·0	1931·6	2008·6	2250·4	—
14	418·319	—	1671·8	1769·5	1932·3	2008·9	2250·7	—
15	273·096	1406·1	1671·0	—	1931·1	—	—	—
16	273·096	1406·0	1671·3	—	1931·3	—	—	—
17	273·096	1406·1	1671·3	1768·9	1931·6	2008·6	2250·7	—
18	190·095	1406·6	—	—	—	—	—	—
1B	679·487	1406·2	—	—	—	—	—	—
2B	679·487	1406·8	1671·7	—	1931·8	—	—	—
3B	679·487	—	1671·4	—	1931·6	—	—	—
4B	679·480	—	1671·5	—	1931·9	—	—	—
5B	679·480	—	—	—	1931·8	—	—	—
6B	1054·06	—	—	—	1932·2	—	—	—
7B	1054·06	—	—	—	1931·6	—	—	—
8B	1054·06	1406·4	1671·7	—	1932·0	—	—	—
9B	1054·06	—	—	—	1932·0	—	—	—

Table 6 gives the energies corresponding to the $H\rho$ values in table 5. The calculations are made by means of equation (2), using for e/m the value $1{\cdot}7591 \pm 0{\cdot}0008 \times 10^7$ e.m.u. recommended by Bearden (1939), and for c the value $2{\cdot}9978 \pm 0{\cdot}0002 \times 10^{10}$ cm. sec.$^{-1}$ recommended by von Friesen (1937). In the last column of this table are the probable errors computed as the square root of the sum of the squares of the probable errors in e/m_0, c^2, and the quantity $\left\{1+\left(\dfrac{He}{m_0c}\right)^2\right\}^{-\frac{1}{2}}-1.$

TABLE 5. FINAL RESULTS FOR $H\rho$

Line	$H\rho$ G-cm. abs. e.m.u.	Probable observational error parts in 10^5	Probable systematic error parts in 10^5	Total probable error parts in 10^5
A	658·9	—	—	26
Aa	665·0	—	—	26
B	766·1	—	—	22
Ba	768·4	—	—	22
C	790·4	—	—	22
F	1406·2	9	5	10
G	1671·7	8	5	9
Ga	1769·4	6	7	9
H	1931·9	3	5	6
Ha	2008·8	5	6	8
I	2251·1	6	6	9
O	2972·3 (radium C)	6	6	9

TABLE 6. ENERGIES OF β-RAYS

Line	Disintegrating nucleus*	$H\rho$ G-cm.	Energy eV	Probable error parts in 10^3
A	Radium B	658·9	$0{\cdot}3686\times10^5$	1
Aa	,,	665·0	$0{\cdot}3752\times10^5$	1
B	,,	766·1	$0{\cdot}4925\times10^5$	1
Ba	,,	768·4	$0{\cdot}4953\times10^5$	1
C	,,	790·4	$0{\cdot}5227\times10^5$	1
F	,,	1406·2	$1{\cdot}515\times10^5$	0·85
G	,,	1671·7	$2{\cdot}048\times10^5$	0·7
Ga	,,	1769·4	$2{\cdot}255\times10^5$	0·7
H	,,	1931·9	$2{\cdot}614\times10^5$	0·7
Ha	,,	2008·8	$2{\cdot}799\times10^5$	0·7
I	,,	2251·1	$3{\cdot}336\times10^5$	0·7
O	Radium C	2972·3	$5{\cdot}162\times10^5$	0·7

* The β-rays shown here as being associated with the disintegration of radium B are usually referred to as the β-rays of radium B, but actually they are emitted by the following body. The term β-rays of radium C or other body has a similar meaning.

To say that these β-rays are emitted by the excited nucleus of radium C is misleading.

6. COMPARISON WITH RESULTS OF OTHER WORKERS

Other measurements of the $H\rho$ values of β-ray lines with which the results given in table 5 are to be compared are those of Ellis and Skinner (1924), Ellis (1934*b*) and of Scott and Rogers (1934, 1936, 1937). Values obtained by these workers for the three lines measured by Rogers are given in table 7, together with those obtained by the authors.

TABLE 7

Harper and Roberts	Rogers* (1937)	Scott (1934)	Ellis (1934*b*)	Ellis and Skinner (1924)
1406·2	1406·2	—	1400·4	1410 G-cm.
1671·6	1671·3	—	1665·9	1677 ,,
1931·9	1931·7	1931·8	1925·5	1938 ,,
1 in 10^4	3 in 10^4	1 in 10^4	10 in 10^4	20 in 10^4

* Rogers values of 1406·1, 1671·1 and 1931·5 have been corrected for an error which appears to have been made (1936, p. 512) in converting international amperes to absolute amperes.

The numbers in the bottom row of this table are the errors given by the workers for their results. Rogers's method of estimating errors, however, leads to a quantity larger than the probable error, so that the figure of 3 in 10^4 is not directly comparable with the others. The figure of 10 in 10^4 for Ellis's 1934 results is deduced from his statement that the energy values are correct to better than 1/500.

Scott and Rogers measured the distance 4ρ between the edges of corresponding β-ray lines on either plate of their spectrograph with a travelling microscope; but we have found this measurement of the distance to be always less than that obtained with a microphotometer incorporating the same measuring screw as the microscope. Consistent results with the microscope method were obtained by a number of skilled observers and from experiments on a number of different β-ray lines it was found that the cross-hair of the microscope was set in from the edge of the line about a quarter of the distance from the frontal point of the line to its peak. This latter distance is about 0·2 mm. An effect such as this is to be expected from the known systematic errors usual in setting on an asymmetrical object of this type. Under our experimental conditions, the error made in setting the microscope almost exactly counterbalanced the advancement of the front caused by scattering of the electrons in the emulsion. This may indicate that the closeness of agreement between our results and those of Scott and Rogers is to a certain extent fortuitous.

We are indebted to the Cancer Research Department, University of Sydney, for radon supplies. We take pleasure in thanking Dr G. H. Briggs, then Assistant Professor of Physics, University of Sydney, for suggesting the work here described, and for much valuable assistance and advice throughout the investigation.

REFERENCES

Bearden, J. A. 1939 *Phys. Rev.* **55**, 584.
Bond, W. N. 1935 *Probability and random errors.* London: Edward Arnold.
Briggs, G. H. 1932 *J. Sci. Instrum.* **9**, 5.
Briggs, G. H. 1936 *Proc. Roy. Soc.* A, **157**, 183.
Briggs, G. H. and Harper, A. F. A. 1936 *J. Sci. Instrum.* **13**, 119.
Cotton, A. 1900 *L'éclairage éléctrique.*
Danysz 1913 *Ann. Phys., Paris,* **30**, 241.
Eberhard 1912 *Phys. Z.* **13**, 288.
Ellis, C. D. 1932 *Nature, Lond.*, **129**, 276.
Ellis, C. D. 1934*a* *Int. Conf. Physics*, **1**. London: Physical Society.
Ellis, C. D. 1934*b* *Proc. Roy. Soc.* A, **143**, 350.
Ellis, C. D. and Skinner, H. W. B. 1924 *Proc. Roy. Soc.* A, **101**, 1.
Ellis, C. D. and Wooster, W. A. 1927 *Proc. Roy. Soc.* A, **114**, 266.
v Friesen, S. 1937 *Proc. Roy. Soc.* A, **160**, 424.
Gamow, G. 1936 *Atomic nuclei and nuclear transformations.* Oxford.
Hartree 1923 *Proc. Camb. Phil. Soc.*
Li, K. T. 1937 *Proc. Camb. Phil. Soc.* **33**, 164.
Rogers, F. T. 1936 *Phys. Rev.* **50**, 515.
Rogers, F. T. 1937 *Phys. Rev.* **51**, 588.
Rutherford, E., Chadwick, J. and Ellis, C. D. 1930 *Radiations from radioactive substances.* Cambridge.
Rutherford, E. and Robinson, H. 1913 *Phil. Mag.* **26**, 717.
Scott, F. A. 1934 *Phys. Rev.* **46**, 633.
Surugue, J. 1937 *Ann. Phys., Paris,* **8**, 484.
Wooster, W. A. 1927 *Proc. Roy. Soc.* A, **114**, 729.

The γ-ray transition of radio-bromine

By R. E. Siday, B.Sc., Birkbeck College

(Communicated by P. M. S. Blackett, F.R.S.—
Received 4 December 1940—Revised 7 March 1941)

The disintegration by the emission of γ-rays of the metastable isotope of radio-bromine was investigated by the method of the cloud chamber. The principal γ-ray was found to have an energy of 47 kV and a coefficient of internal conversion in the K shell of 0·43. Confirmation of a weaker γ-ray of 37 kV was also obtained.

1. Introduction

Although there are only two isotopes of bromine, the bombardment of this element by slow neutrons produces three radioactive forms which disintegrate with the periods 18 min., 4·4 and 34 hours respectively.

The 34 hr. period has been shown to belong to an active isotope Br^{82}, leaving the other two forms to be associated with the isotope Br^{80}. The Br^{80} nucleus is formed from Br^{79} by the capture of a neutron and decays with the emission of β-rays with a period of 18 min. It has become clear, however, that the neutron may alternatively be captured into an excited level, leaving the Br^{80} in a metastable state which returns to its normal 18 min. form by the emission of γ-rays with the period of 4·4 hr.

In this paper an account is given of experiments by the cloud chamber method. As indicated in a previous note, the results will be shown to indicate homogeneous energy groups of electrons due to the internal conversion of the γ-rays of the metastable nuclei, superimposed on the continuous β-ray spectra of the 18 min. and 34 hr. isotopes.

It was found necessary only to measure electron energies up to about 50 kV, and this was accomplished by measuring the lengths of the tracks. The conversion of ranges into energies was made, using the known relation between energy and range in oxygen, which was the gas used in the cloud chamber (Williams 1931) and corrections for vapours present were made on the assumption that the mean range of a slow β-ray passing through matter is inversely proportional to the number of electrons per cubic centimetre of the matter.

The energy spectrum of the β-rays above 50 kV has already been determined (Alichanov, Alichanian and Dzelepow 1936).

Two sets of experiments were made. In one set the lengths of tracks of electrons, starting from especially prepared thin films of radio-bromine compounds suspended in the chamber, were measured. Under the experimental conditions valid energy determinations down to 20 kV were made.

In the second set of experiments radioactive ethyl bromide was introduced into the chamber and the tracks of electrons starting in the gas of the chamber were observed. In these experiments energies down to 20 kV were measured.

Many of the tracks starting in the gas were found to be accompanied by other very short tracks starting at the same points. The internal conversion of the γ-rays of the metastable nuclei gives rise to the characteristic K and L X-rays of bromine. The very short tracks were then the Auger electrons due to the K X-rays of bromine. The Auger electron tracks corresponding to the L X-rays would be too short to be observed.

2. Preparation of the foils

A technique was devised whereby thin layers of radio-bromine compounds of very high concentration were formed on inert surfaces suitable for suspension in the cloud chamber.

The following behaviour characteristic of the radioactive halogens was observed in the course of some preliminary experiments and was utilized as a technique for obtaining very thin radioactive deposits.

If ethyl bromide, say, is activated by slow neutrons the radio-bromine, in whatever form it may be, can largely be removed from the liquid simply by immersing metal foils in it. This effect is independent of the nature of the metal surface and roughly equal concentrations are obtained on platinum, stainless steel, silver and copper. On the other hand, non-metallic surfaces are not activated in this way. Experiments with Geiger counters showed that the activity of these foils decayed with time in the same way as the radioactive ethyl bromide, and that the activity was clearly due to radioactive bromine atoms.

Accordingly very thin cellophane was sputtered with silver on one side, and immersed in ethyl bromide that had been activated by bombardment with slow neutrons during a period of 13 hr. Since there is no appreciable transfer of activity to cellophane surfaces, in this way thin foils radioactive only on one side were prepared.

Two essential uncertainties arise in the determination, by range measurements, of the energies of electrons starting from the radioactive surfaces of these foils.

The first is due to the finite thickness of the radioactive layer of material on the cellophane foils. However, the total stopping power of the sputtered silver and the radioactive layer that it picked up could easily be reduced to the equivalent of a few tenths of a millimetre of air, while the activity of the surface was still intense enough to give 2–3 tracks per expansion. The radon-beryllium sources used in the activation of the ethyl bromide were 50–80 millicuries strong.

The second type of error arose because tracks starting from the foils did not quite join up to them. The number of tracks from a given foil observed in each expansion depends directly on the time for which the chamber is supersaturated before illumination. The longer this is, the larger is the number of tracks observed but they were found to have greater separation from their surfaces of origin.

With the available radon-beryllium sources, it was found that to reduce this separation below a maximum of about 3 mm., too great a reduction in the average number of tracks per expansion would have been necessary.

The effect of these uncertainties on the accuracy of electron energies determined by range measurements, while important at low energies, is small at higher energies. The error in the energy estimation of a 20 kV electron by range measurements *uncorrected* for these two causes of inaccuracy is about 10 %, so that in these experiments energy spectra were only traced down to 20 kV. Energy measurements below this were made on electrons starting in the gas of the chamber.

3. RADIOACTIVE ETHYL BROMIDE IN THE CHAMBER

In these experiments up to 1·5 c.c. of radioactive ethyl bromide was squirted into the chamber. Alcohol and water was the condensing agent, and it was found that the best yield of tracks starting in the gas was obtained by using as little as possible of this mixture.

Ethyl bromide directly activated by slow neutrons could not be used as the yield of tracks starting in the gas was in this case always very low. Probably this was due to that transfer of activity to the metal surface of the chamber described above.

Some experiments were made in an attempt to influence the adsorption of activity on metal surfaces by simple physical and chemical means. The application of electrostatic fields was found to have no effect. Neither did the distillation of the liquid. Free bromine added to the liquid completely stopped the adsorption to those metals such as platinum, which are not attacked by bromine.* But, of course, free bromine could not be introduced into a cloud chamber. The way adopted out of this difficulty was to prepare the ethyl bromide from radioactive bromine. This ethyl bromide did not lose its activity to metal surfaces.

For this purpose radio-bromine was prepared by the method of Szilard and Chalmers. A little bromine dissolved in a large bulk of *n*-butyl bromide was irradiated by slow neutrons for 13 hr., and after the irradiation the bromine was extracted by caustic soda, recovered by distillation with hydrochloric acid, and converted into ethyl bromide by distillation with alcohol and red phosphorus. After shaking the distillate of ethyl bromide with sodium carbonate to remove any free acid, and then re-distilling it in vacuo, it was sufficiently pure for introduction into the Wilson chamber. That is to say, that, after its introduction, the chamber could rapidly be cleaned after the expansion had been adjusted to its new correct value. This value depended on the amount of ethyl bromide introduced, but was usually about 1·19. The use of larger amounts of ethyl bromide and higher ratios made the cleaning of the chamber difficult and uncertain. The whole time involved from the end of the irradiation to the commencement of the photography was less than two hours, while the half life of the metastable nucleus is 4·4 hr.

4. Construction of energy spectra

The tracks of the electrons were reprojected on to a screen through the stereoscopic pair of lenses which photographed them, and their lengths were found from co-ordinate measurements at various points throughout their paths.

It is clear that such energy determinations could only be made on tracks which begin, end, and have their entire paths in the illuminated part of the chamber.

The observed number of tracks of any particular length must be multiplied by a factor or weight to give the number of tracks which would be observed in the whole solid angle.

---

* This observation gives rise to an alternative way of preparing thin active foils, which was, in fact, used in some of the experiments. The silver sputtered cellophane was attached to a rhodium plated frame and together with the frame was immersed in the activated ethyl bromide to which a little free bromine had been added. Active deposit was formed on the silver but not on the frame or the unsilvered side of the cellophane. While greater strengths could be obtained, it was necessary to use greater thicknesses of sputtered silver.

Owing to atomic impacts, tracks of electrons in the energy range measured are by no means straight, and in calculating the weight to be ascribed to a track, the linear separation of its end-points was taken as a measure of its length.

Thefactor was then given by the ratio of the total solid angle to the solid angle available for the track to lie in the illuminated part of the chamber.

The factor to be applied to a track of given length as defined above depends on the position of the origin of the track. In the first set of experiments the origins of the tracks were confined to the centre of the chamber where the foils were suspended, and as the range of the fastest electrons measured was less than the radius of the chamber, the solid angle was defined only by the depth of the light beam illuminating the chamber. The origins of the tracks starting in the gas of the chamber are, however, distributed at random throughout the chamber and many lie near the walls, so that tracks starting at these points are cut off by the walls as well as by passing out of the light. This materially reduced the number observed and so increases the factors to be applied to the higher energy tracks. Owing to statistical fluctuation of the reduced number of these tracks, little reliance could be placed on their calculated total number; for this reason the energy spectrum of the electrons starting in the gas, while it could be traced down to 10 kV, was not extended above about 40 kV.

5. THE ENERGY SPECTRA

Figure 1 gives the energy distribution of the electrons up to about 50 kV, and was constructed from the experiments in which tracks start from the foils. It shows two peaks at 33 and 46 kV, and although the latter contains relatively few tracks its position agrees with the existence of a single γ-ray line, the two peaks corresponding to the conversion of this γ-ray in the *K* and *L* shells of the bromine atom.

In figure 2 is traced the same curve derived from the electrons starting in the gas of the chamber. This curve only exhibits the *K* conversion peak, since, because of the statistical fluctuation explained above, it was not possible to extend the curve much above 40 kV.

The three results obtained together agree with the existence of a single γ-ray line of about 47 kV, the value previously reported (Siday 1939) being 10 % too low.

Valley and McCreary (1939) have also reported the existence of this line, their more recent value being nearly 49 kV. Their results were based on magnetic methods and should, without question, be more accurate than those based on cloud chamber methods as, owing to straggling, peaks obtained by the latter method are essentially broader. The shape of the *K* conversion peak in figure 1 agrees fairly well, in fact, with the theoretical distribution due to straggling, so that its very considerable breadth arises largely from this cause.

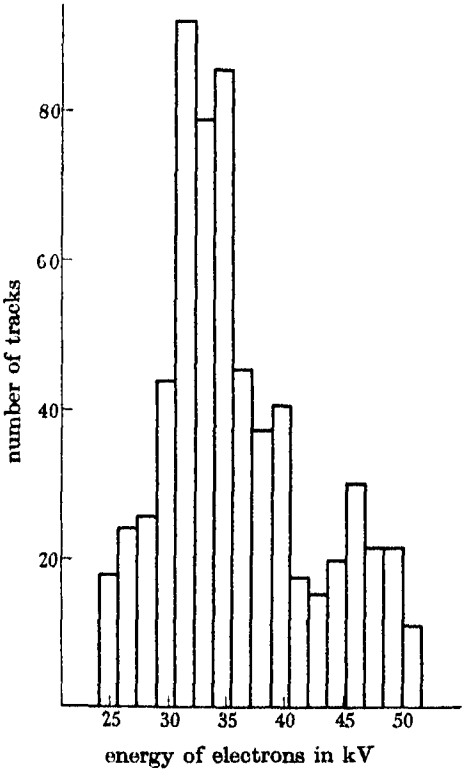

FIGURE 1

Valley and McCreary have also reported the existence of a very much weaker γ-ray line whose energy they now give as either 25 or 37 kV, the ambiguity arising from the uncertainty of the origin of the electrons they observed, i.e. whether they arose from a *K* or an *L* conversion. However, Grinberg and Rossinow (1940) have observed this ray directly, and shown it to be of 37 kV energy.

In figure 2 the presence of these would be masked by the background of the slow β-rays of the continuous β-ray spectrum of the 18 min. isotope, and by statistical fluctuation.

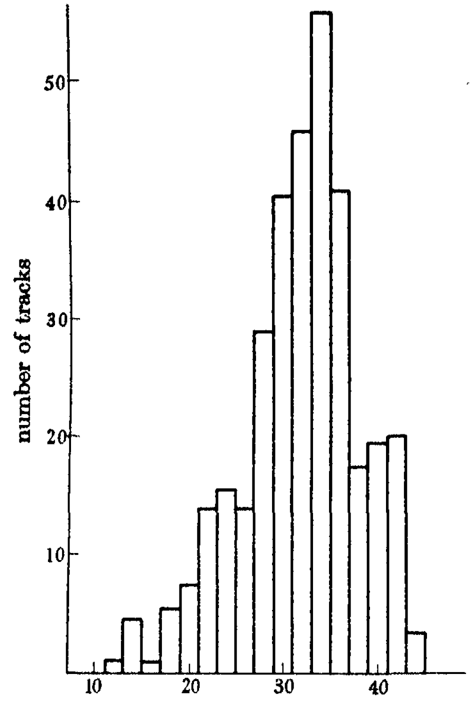

FIGURE 2

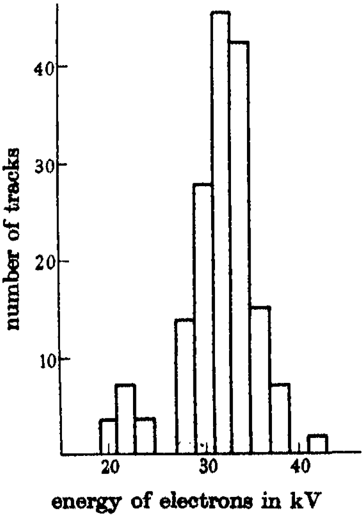

FIGURE 3

In order to investigate this point, a larger number of tracks starting in the gas were observed and measured, and an energy spectrum was constructed of those tracks which had Auger electrons at their origins, and were therefore unambiguously due to *K* conversion electrons.

The spectrum is shown in figure 3. The small peak is sufficient to identify the β-ray line of Valley and McCreary as due to a *K* conversion confirming that it arises from a 37 kV γ-ray.

6. THE COEFFICIENT OF INTERNAL CONVERSION

From a study of the number of β-rays emitted by the 18 min. isotope in a particular set of experiments, and their rate of decay, it is possible to calculate the number of metastable 4·5 hr. nuclei disintegrating in the same set of experiments. Were there only one γ-ray emitted by the metastable nucleus, the number of these nuclei disintegrating would be equal to the number of these γ-rays emitted, and their coefficient of internal conversion would be given by the ratio of the number of conversion electrons emitted in these experiments to the calculated number of metastable nuclei disintegrating.

A particular difficulty arises from the existence of two γ-rays. This indicates alternative methods of disintegration of the metastable nucleus. Figure 3 shows that the *K* conversion spectrum of the 37 kV line is very much weaker than that of the 47 kV line. Now it is most likely that the coefficients of conversion of these two γ-rays in the *K* shell are of the same order of magnitude. In fact it is to be expected that the 37 kV γ-ray has a higher coefficient than the 47 kV γ-ray. Figure 3 shows that unless the 37 kV γ-ray has a very much *smaller* coefficient than the 47 kV γ-ray, the metastable nucleus has a very much higher probability of emitting a 47 kV γ-ray, so that the total number of these nuclei disintegrating can be taken as the total number of γ-rays emitted.

In order to calculate the coefficient of internal conversion of the 47 kV γ-ray, it is clearly necessary to distinguish experimentally between the β-rays, derived from the 18 min. isotope, and the conversion electrons. By inspection, the electron tracks can be divided into two groups, one belonging to electrons having energies greater than 50 kV, and the other to electrons having energies less than this. The former consists entirely of β-rays derived from the 18 min. isotope, while the latter consists partly of these β-rays, but mainly of conversion electrons.

Figure 1 shows that the electrons up to 50 kV fall under two peaks at the *K* and *L* conversion energies of the 47 kV γ-ray; and that owing to straggling these peaks extend up to about 40 and 50 kV respectively. The bulk of the tracks lie in the K peak and these can be separated into β-rays and conversion electrons as follows.

In the experiments in which tracks start in the gas of the chamber, about 40 % of the tracks falling in the K peak were found to have associated with them the Auger electrons derived from the K X-rays of bromine. Since the probability of an Auger conversion for the K X-rays of bromine is 0·55 it follows that about three-quarters of the electrons on the K peaks are conversion electrons.

It is not possible to observe the very short tracks belonging to the L Auger conversion of the L X-rays of bromine and so the proportion of conversion electrons to β-rays in the L peak could not be accurately determined. Assuming that the continuous β-ray spectrum of the 18 min. isotope does not show any sharp maximum below 50 kV, however, about one-third of the tracks in this peak are conversion electrons. The number concerned is, however, small compared with the number in the K peak.

The estimation of the coefficient of internal conversion was made therefore in the following steps:

(1) Calculation of the total number of conversion electrons emitted in a particular set of experiments.

(2*a*) Calculation of the total number of 18 min. nuclei disintegrating in the same set of experiments from the number of β-rays observed.

(2*b*) Calculation of the number of metastable nuclei disintegrating from the number of 18 min. β-rays and their rate of decay.

The coefficient of internal conversion was then given by the ratio of the number of conversion electrons to the number of metastable nuclei disintegrating.

(1) *The total number of conversion electrons*

In the chosen set of experiments the total number of tracks emitted from the radioactive side of the foil was 256 in the K peak, and 48 in the L peak. These numbers were calculated from the observed numbers by multiplying by the factor or weight described above.

The number of K conversion electrons emitted from both sides of the foil was therefore given by

$$\tfrac{3}{4}\,.\,256 \times 2 = 384,$$

and the number of L conversion electrons by

$$\tfrac{1}{3}\,.\,48 \times 2 = 32.$$

Also, the total number of primary β-rays in both groups is

$$512-(384+32) = 96.$$

(2*a*) *The total number of β-rays*

The total number of primary β-rays of energies up to 50 kV is, then, 96. All the rays of greater energy are primary β-rays. The total number of these could not be found by directly counting all those that could be distinguished on the photographs. The number obtained from such a count would be low because tracks steeply inclined to the vertical foils have very short lengths projected on the plane of the chamber and are easily missed, especially among the more heavily ionizing low energy electrons.

From the apparent length of a track of a β-ray the angle this track makes with the plane of the chamber can be calculated, since the observed length is determined by the configuration of the illuminated part of the chamber.* Accordingly, by measuring tracks whose projected lengths are not less than some value l, only tracks confined to an angle θ with the plane of the chamber are counted. Table 1 gives the number N of tracks whose projected lengths are not less than l, and the calculated angle θ with the plane of the chamber in which they are confined. Assuming uniform angular emission of the tracks emitted from the foils the ratio $N/\sin\theta$ should be constant and equal to the total number of tracks emitted into the full solid angle.

TABLE 1

Projected length l of track (cm.)	1·5	3·0	4·5	6·0	7·5
No. of tracks N not shorter than l	737	480	330	230	110
Angle of emission θ	60·0	31·2	21·6	16·2	12·8
Ratio: $N/\sin\theta$	1474	1780	1740	1640	1000

The values of the ratio $N/\sin\theta$ in table 1 show how the number of short tracks counted was low, the value in the first column being small. The values in the last columns are also low as tracks of this length begin to be cut off by the walls of the chamber. The total number of tracks taken from the second and third columns is 1760, which, together with the 96 β-rays of energy less than 50 kV, brings the total number of β-rays emitted in these experments to 1850.

---

* The tracks in this energy range are considerably longer than the radius of the chamber.

(2*b*) *Calculation of the number of metastable atoms disintegrating*

The 18 min. isotope which emits the continous β-ray spectrum is formed in two ways. First, it is formed by neutron capture in the irradiation of bromine by neutrons; and secondly, it is formed through the decay of the metastable 4·4 hr. form.

The foils were activated for three times the period of the metastable nucleus. If m atoms of the 18 min. isotope were formed per minute of the activation, the number of primary β-rays emitted from a time t to a time T after the irradiation had stopped is given by

$$\frac{m}{\lambda_1}\left[e^{-\lambda_1 t} - e^{-\lambda_1 T}\right], \tag{1}$$

where λ_1 is the decay constant corresponding to 18 min. and is equal to 0·69/18 min.$^{-1}$.

Again, if n_0 atoms of bromine are excited into the metastable state per minute of the irradiation, these will produce during the same period of time a number of β-rays given by

$$\int_t^T P\,dT, \tag{2}$$

where $$P = \frac{n}{\lambda_2 - \lambda_1}\left[\lambda_2 e^{-\lambda_1 t} - \lambda_1 e^{-\lambda_2 t}\right]$$

to sufficient accuracy, and $$n = \tfrac{7}{8} n_0.$$

Table 2 gives the number of β-ray tracks on the photographs covering different periods of time $t - T$ after the irradiation had been completed together with the corresponding values of 1 and 2 which were calculated in terms of m and n.

The numbers of tracks appearing in table 2 have been corrected for the tracks which belong to the 34 hr. isotope. The relative intensity of these rays to those belonging to the 4·4 hr. period form is 0·6 (Snell 1934). This correction amounts to about 20 % of the observed number of tracks, and it was assumed that three-quarters of these had energies above 50 kV.

TABLE 2

No. of photos	1–20	21–40	41–60	61–80	81–100	101–120
Time $T - t$ min.	40–55	55–70	70–85	85–100	100–115	115–130
No. of tracks	159	125	110	94	81	78
No. given by 1	2·30m	1·40m	0·80m	0·46m	0·23m	0·12m
No. given by 2	18·3n	18·0n	17·1n	16·4n	14·6n	13·9n

Neglecting the last column, the following equations in m and n result:

$$159 = 18{\cdot}3n + 2{\cdot}3m, \qquad 94 = 16{\cdot}4n + 0{\cdot}46m,$$
$$125 = 18{\cdot}0n + 1{\cdot}4m, \qquad 81 = 14{\cdot}6n + 0{\cdot}23m.$$
$$110 = 17{\cdot}1n + 0{\cdot}80m,$$

The values of m and n* derived from these equations by the method of least squares are

$$n = 5{\cdot}1, \quad m = 26.$$

The last column was neglected, as the contribution of the m term in it to the total number of tracks is only three tracks, so that no reliable estimate of m could be derived from it.

The total number of β-rays observed on the photographs throughout the whole time of the experiment was 647 (excluding those belonging to the 34 hr. isotope), and the number of metastable atoms decaying corresponding to these is given by

$$\frac{n}{\lambda_2}\left(e^{-\lambda_2 40} - e^{-\lambda_1 130}\right) = 357.$$

The numbers used in these equations are the numbers of observed β-rays, and it has been shown that the total number of β-rays is obtained by multiplying by the factor $\frac{1856}{737}$.

The number of 18 min. atoms decaying over the period represented by the photographs is then

$$\tfrac{1856}{737} \times 357 = 900.$$

The number of K electron tracks is 384, so that the K-shell internal conversion coefficient is

$$384/900 = 0{\cdot}43,$$

and the coefficient in the L shell is about one-tenth of this.

I wish to record here my appreciation of the advice and guidance of Prof. P. M. S. Blackett, and of the continued support of Prof. J. D. Bernal. Dr L. Simons has also been helpful, and I should like to thank Prof. S. Sugden for his assistance especially on chemical matters.

---

* While the value of n derived in this way is reliable, the ratio of m/n obtained is not accurate, as a small change in n produces a large one in m.

REFERENCES

Alichanov, Alichanian and Dzelepow 1936 *Phys. Z. Sowjet.* **10**, 1, 78.
de Vault, D. C. and Libby, W. F. 1939 *Phys. Rev.* **55**, 322.
Grinberg and Rossinow 1940 *Phys. Rev.* **58**, 181.
Segre, E., Halford, R. S. and Seabourg, G. T. 1939 *Phys. Rev.* **55**, 321.
Siday, R. E. 1939 *Nature, Lond.*, **143**, 681.
Snell, A. H. 1934 *Phys. Rev.* **52**, 1016.
Valley, G. E. and McCreary, R. L. 1939*a* *Phys. Rev.* **55**, 666.
Valley, G. E. and McCreary, R. L. 1939*b* *Phys. Rev.* **56**, 863.
Williams, E. J. 1931 *Proc. Roy. Soc.* A, **130**, 310.

On transition from laminar to turbulent flow in the boundary layer

BY A. FAGE, A.R.C.S. AND J. H. PRESTON, B.SC., PH.D.

(*Communicated by E. F. Relf, F.R.S.—Received* 10 *December* 1940)

[Plate 5]

Information on transition from laminar to turbulent flow in boundary layers on streamline bodies of revolution in a water stream is obtained from visual and photographic observation of the movements of small particles and filament bands. The cases considered are transition caused by isotropic turbulence in the free stream, by a falling velocity in a stream substantially free from turbulence, and by flow disturbances from surface wires.

A non-dimensional number, specified in terms of the intensity and scale of turbulence, the boundary-layer thickness, and the mean velocity just outside the layer, is found to be representative of the conditions of flow in the boundary layer of a body in a turbulent stream: and values of this number at transition obtained from observations made for a body of revolution have the same order of magnitude as those calculated for a flat plate from measurements taken by Hall and Hislop.

Transition in a region of falling velocity in a steady stream arises from a separation of the laminar boundary layer from the surface; and after separation, the flow in the layer becomes turbulent and then rejoins the surface. The observed position of transition is near the position of separation given by a solution of the momentum equation for laminar flow and for the observed distribution of velocity just outside the layer.

Flow disturbances from a surface wire placed in a laminar boundary layer cause fully developed turbulent flow to be established at the wire when $u_s d/\nu > 400$, where d is the wire diameter, u_s is the velocity in the laminar layer at a distance d from the surface, and ν is the kinematic viscosity.

The measured maximum value of the downstream component of turbulent velocity in the stream behind a grid is about 3·3 times the root-mean-square value.

INTRODUCTION

(1) The behaviour of flow in the boundary layer of a streamline body in the region where transition from laminar to turbulent flow takes place depends on the conditions responsible for the transition. When transition is caused by disturbances of flow in the stream outside the layer, the fluctuating pressure gradients within the layer associated with those without cause spasmodic and transient separations of the layer from the surface over a downstream region whose length depends on, and increases with, the intensity of the disturbances. When the stream is steady and transition is caused by the retarding influence of a falling stream velocity, the layer separates from the surface, becomes unstable, breaks down, and eventually rejoins the surface as a turbulent layer. The position of separation is fixed by the velocity gradient in the stream, and the separated layer soon breaks down, so that transition extends over a shorter region than when caused by turbulence outside the layer. Transition can also be caused by surface obstructions, and then the disturbances of flow responsible for the transition are directly introduced into the layer by the obstructions themselves.

The present experiments* are concerned with transition phenomena on long streamline bodies of revolution caused by isotropic turbulence in the free stream, by a falling velocity in a steady free stream, and by surface wires. An analysis of observations taken in isotropic turbulent streams behind square-mesh grids is also included.

Investigations on problems of fluid motion which are based on the visual observation of the movements of particles are more conveniently made in water than in air, for particles move appreciably slower in water than in air (about 1/13th) for the same flow pattern given by the same body, and the choice of particles suitable for observation in water is less restricted than it is for air. Observation is facilitated if the body is held fixed in a tunnel stream than if moved through a stationary fluid: and the utility of a tunnel is enhanced if its stream is substantially free from turbulence, for then observation of flow can be made for a body either in the steady free stream or in a stream into which turbulence of known intensity and scale has been introduced by a grid. The water tunnel used in the present work incorporated in its design those features known to be favourable to the production of a steady stream, and was equipped with instruments specially designed for observation of flow.

---

* The work was carried out in the Aerodynamics Department of the National Physical Laboratory, and it is presented on the recommendation of the Aeronautical Research Committee and by permission of the Director of the Laboratory.

APPARATUS*

(*a*) *Water tunnel*

(2) A sketch of the water tunnel is given in figure 1. The tunnel is of the closed-return type, and it is particularly suitable for observation of flow near the surface of long streamline bodies of revolution. The observation chamber is circular in cross-section and has two semicircular perspex windows. To eliminate astigmatic distortion of view, the windows are enclosed in water cells having vertical perspex sides and free water surfaces. The water flows from the inlet chamber to the observation chamber through a fine honeycomb, a settling chamber and a contracting entrance nozzle. The honeycomb straightens the flow and reduces both the scale and intensity of the disturbances in the inflowing stream, the settling chamber gives the water time to dissipate the turbulent energy of the smaller eddies by the action of viscosity, and the contraction of flow in the entrance nozzle reduces the fractional intensity of turbulence. The water flowing out of the observation chamber is deflected downwards by vanes in the outlet chamber and returns to the inlet chamber through a divergent duct having a circular cross-section. The average speed of flow through the inlet chamber is small, and unevenness in this flow is smoothed out by horizontal and vertical baffle plates. The screw circulating the water is belt-driven by a $\frac{1}{2}$ h.p. motor, regulated by a potentiometer control on a 100 V battery supply. Stroboscope disks on the screw shaft are viewed by a Neon lamp on 50 cycle a.c. mains to measure

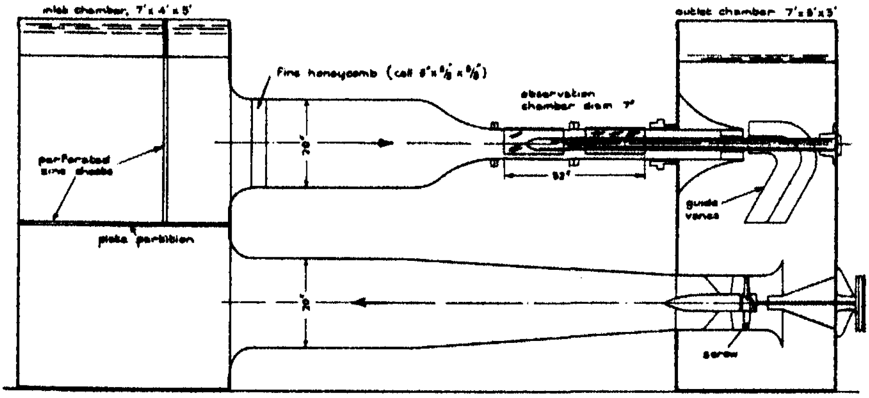
inlet chamber, 7' x 4' x 5'
outlet chamber 7' x 5' x 3'
fine honeycomb (cell 6" x ⅛" x ⅛")
observation chamber diam 7"
perforated zinc sheets
plate partition
20"
20"
52"
guide vanes
screw

FIGURE 1. Water tunnel (elevation)

---

* Only a brief description of the apparatus is given. A full description is published in the *Journal of the Royal Aeronautical Society* (Fage and Preston 1941).

the speed and to indicate steady running conditions. The stream in the observation chamber is substantially free from turbulence at all speeds and throughout the entire length, except near the wall.

(b) *Fluid-motion microscope**

(3) A photograph of this instrument is given in figure 2: and a sketch of the instrument and the illumination system arranged for flow observation in figure 4. This instrument is designed in the light of experience gained in earlier experiments with apparatus* of the same kind (Fage and Townend 1932; Fage 1936*a*) and allows the movements of small particles in a beam of light to be observed and measured. There is an optimum size and number of particles which gives, for a given brightness of illumination, the best condition for observation. This condition is obtained when bright particles are seen against a dark background: and if too many particles are present the diffused light scattered from them gives a background too bright for sharp contrast.

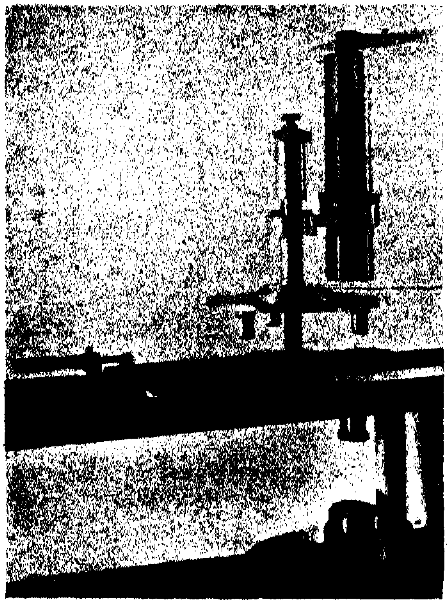

Figure 2. Fluid-motion microscope.

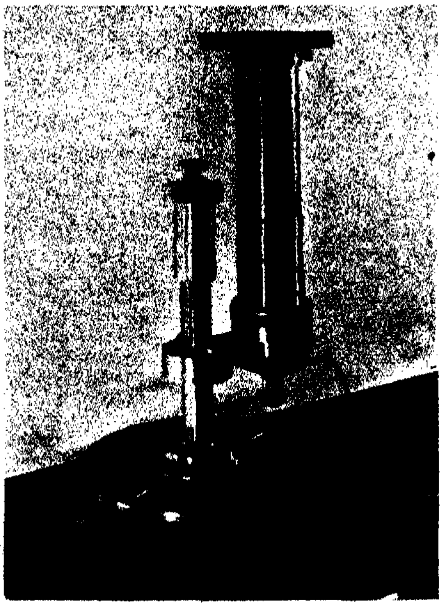

Figure 3. Microscope with interrupter.

---

* The name fluid-motion microscope now introduced is more appropriate than the name ultramicroscope used formerly.

Suitable particles for observation are those from fine aluminium powder, sifted to obtain a fairly uniform size (0·0015 in.). The field of flow is illuminated by a horizontal beam of light at right angles to the axis of the optical system. The illumination system shown in figure 4 gives a light beam of rectangular cross-section (0·40 in. wide and 0·15 in. deep) at the point of observation. The principle of velocity measurement with the fluid-motion microscope depends on the fact that a particle appears to be stationary when viewed through an instrument moving at the same speed, and as a streak, when viewed at a different speed. Movement of the entire microscope is not necessary, for relative movement can be simulated by a rotation of the objective about an offset axis, the tube and eyepiece remaining fixed. The speed of a particle brought to apparent rest is determined from the measured rotational speed of the objective and a calibration factor. The field of flow is visible for only a small part of each revolution, and the time interval between successive views is shortened by mounting three identical objectives on the rotating disk. The maximum speed at a point of observation in turbulent flow is determined from the highest rotational speed, and the minimum speed from the lowest rotational speed, for which particles appear

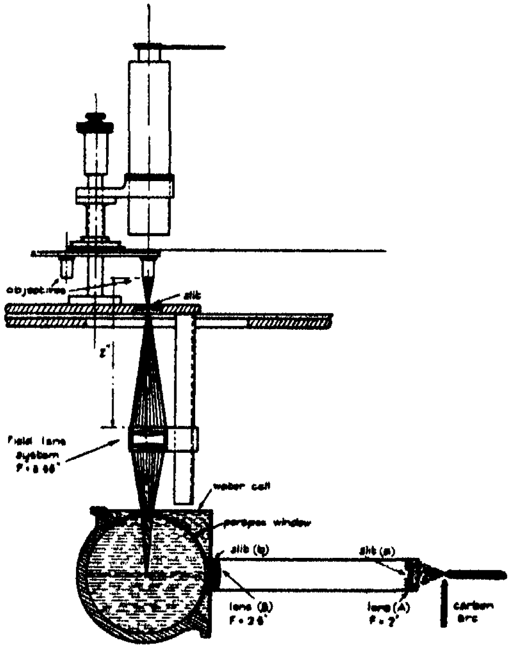

FIGURE 4

as points or short cross-stream streaks. The mean speed of flow is given with good accuracy by the mean of the maximum and minimum speeds: and the maximum value of the downstream component of turbulent velocity by one-half the difference between the maximum and minimum speeds. As mentioned previously, reference should be made to the paper in the *Journal of the Aeronautical Society* (Fage and Preston 1941) for a full description of the fluid-motion microscope and of the way in which it was used in the present work.

(c) *Speed measurement from photographs of particle tracks*

(4) The fluid-motion microscope fitted with an interrupter disk and photographic plate and used at a low magnification (about 6 : 1) allows the speed of a particle to be determined from a measurement of the length of its streak recorded for a known time of exposure. The photographic plate is placed in the position normally occupied by the eyepiece, as shown in figure 3, and particle images on the plate are obtained by the field lens and the objective lens (stationary) of the microscope. The time of exposure is fixed by the interrupter disk (shutter) rotating at a constant speed, and with the sharp radial edges of the teeth cutting the axis of the image beam as they move at right angles to the direction of motion of the particles. The disk is rotated at a speed which allows at least two complete streaks of a particle to be recorded on the photographic plate, and the lengths measured on the plate are from the beginning of one streak to the beginning of the next, so that the measurements are not affected by particle size. Velocity can be measured with an accuracy within ± 1 %, and the distribution of mean velocity in a boundary layer down to a distance of about 0·004 in. from the surface can be determined. A representative photograph of particle tracks in a boundary layer is given in figure 5 (plate 5).

TRANSITION CAUSED BY ISOTROPIC TURBULENCE IN FREE STREAM

(5) Experiments were made on a smooth streamline body of revolution, model I, in turbulent streams produced by square-mesh grids upstream of the model. Model I is a long circular cylinder of external diameter 3 in., to which a semi-ellipsoidal nose-piece of diameter 3 in. and length 6 in. is screwed (figure 6*a*). The model was aligned with its axis along that of the observation chamber, and supported at the tail in a rigid housing, about 16 in. beyond the downstream end of the chamber. The model was hollow and watertight, and the shell thickness was such that the overhung weight

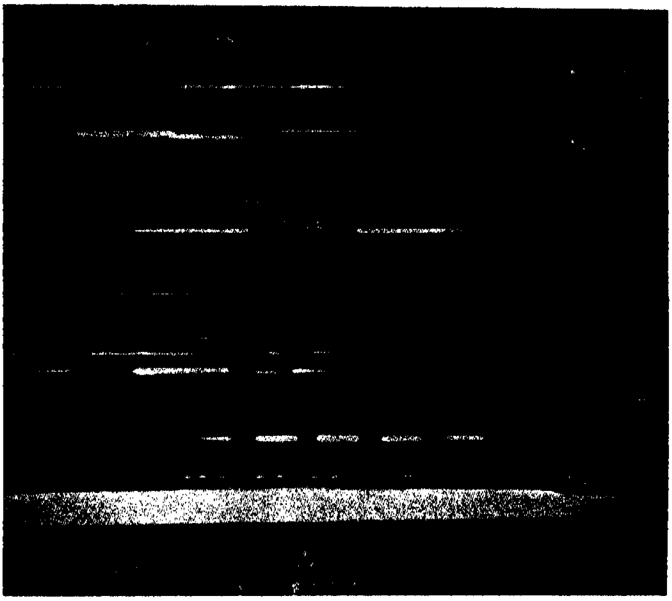

Figure 5

of the model was just balanced by the buoyancy of the displaced water. There was therefore no distortion of shape due to the weight, and no interferences with the flow arising from the method of support. Two grids, designated I and II, were used. The mesh, M, of grid I was 0·5 in., and of grid II 0·25 in. Each grid was constructed of two sets of equally spaced circular rods, the rods of one set touching and being at right angles to those of the other set. The rods were held rigidly in a thin circular ring, made to fit the entrance to the observation chamber, at a section 7·4 in. upstream of the nose of the model. The experiments were framed to obtain data which would show whether a number representative of the conditions in the boundary layer at the transition point could be obtained in terms of the intensity and scale of the turbulence in the stream outside the layer, the velocity at the outer edge of the layer and the thickness of the layer; and for this purpose measurements of the position of transition, of turbulence, and of normal-pressure were made.

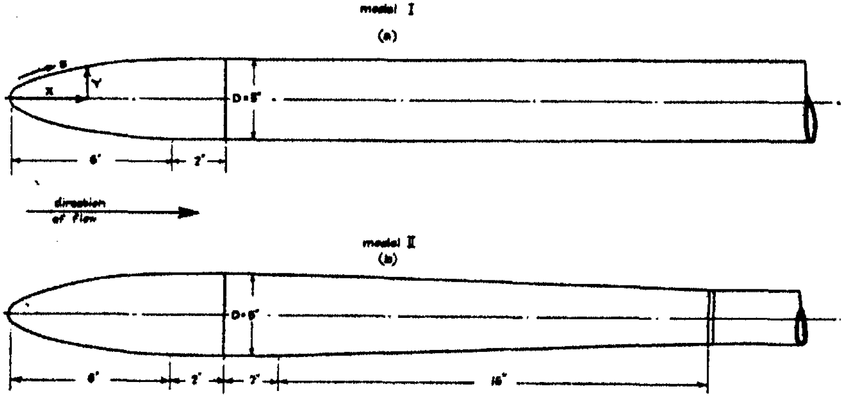

FIGURE 6

(a) *Experiments*

(6) The position of transition was determined from observations of the behaviour of a fine filament band of white ink flowing into the laminar boundary layer from a surface hole at an axial distance of about 0·25 in. from the nose. At first, a filament band flowed steadily along the surface without perceptible change in breadth, but eventually an abrupt transient thickening having the appearance of a puff occurred. The puffs were emitted spasmodically over an appreciable length of the model, with an intensity and frequency increasing with the distance downstream, and ultimately the filament band diffused rapidly into the surrounding water. The transition region is taken to be the region within which puffs are seen, and the transition

point to be the point nearest the nose at which puffs are seen. A filament band is therefore rarely broken at a transition point and rarely seen beyond the end of a transition region. The positions of transition point obtained from filament observations on the model in the turbulent streams behind the two grids are plotted against datum stream velocity in figure 7, where X is the axial distance from the nose, and U_0 is the datum velocity measured just outside the boundary layer at $X = 24{\cdot}3$ in. The transition point moves towards the nose as the stream velocity increases, and occurs earlier in the turbulent stream behind grid I than in that behind the finer grid II.

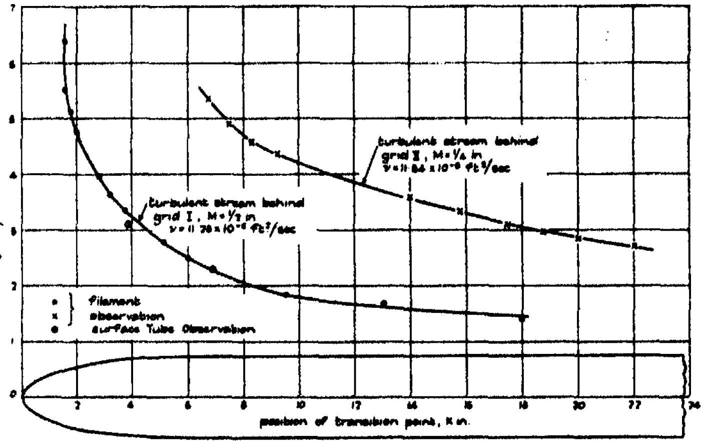

FIGURE 7

The standard method of locating transition in a boundary layer is from the reading of a small total-head tube on the surface: the stream velocity for which the transition point coincides with the position occupied by the mouth of the tube being that for which the pressure given by the tube changes abruptly with an increase in stream velocity. Pressure observations were taken with two surface tubes of the Stanton type (figure 8), one tube being mounted at $X = 6{\cdot}9$ in. with its upper lip about 0·02 in. from the surface, and the other at $X = 3{\cdot}91$ in. with its upper lip about 0·01 in. from the surface. The results obtained are plotted in figure 7, and they lie close to the curve obtained from filament observations. The present method of observing the position of transition point from the behaviour of a filament band

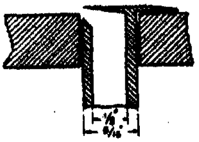

FIGURE 8. Surface tube. Cross-stream width = 0·1 in.

therefore gives results consistent with those given by the surface-tube method*.

(7) Values of the ratio of the maximum value of the component of turbulent velocity in the direction of mean flow, denoted by u_T, to the local mean velocity at the outer edge of the boundary layer, denoted by u_1, were measured with the fluid-motion microscope. The values of u_T/u_1 measured at a given point at several values of U_0 did not differ from each other by more than the probable individual error of measurement. The mean values of u_T/u_1 obtained from measurements taken at several velocities are plotted against X in figure 9.

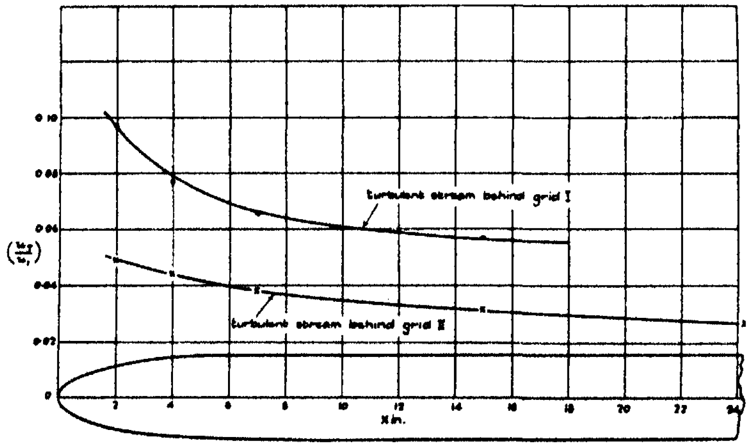

FIGURE 9

(8) Normal pressures p at small holes on a generator line of the model were measured on a Chattock ethylene di-bromide gauge (13 in. or 26 in. cup centres) against a datum pressure, p_0, taken at the hole $X = 24{\cdot}3$ in. Values of the non-dimensional coefficient $(p-p_0)/\frac{1}{2}\rho U_0^2$ calculated from these pressure measurements changed with the stream velocity, but the change was quite small. The difference in the values for the two turbulent streams was also small. Mean values of $(p-p_0)/\frac{1}{2}\rho U_0^2$ taken for the two streams and for several velocities ($U_0 = 3$ to 5 ft./sec.) are given in table 1. From these pressure coefficients the velocity just outside the outer edge of the boundary, u_1, was calculated on the assumptions that the pressure in the layer is constant and equal to the value on the surface, and that the total head in the stream just outside the layer is constant. These values of u_1/U_0 are given in

---

* For applications of this method see Jones (1938), Hall and Hislop (1938), Stephens and Haslam (1938), Fage and Falkner (1930).

table 1. The value of u_1/U_0 increases continuously with X over the entire length of the model. The increase on the parallel part ($X > 6$ in.) arises from the constriction of flow due to the boundary layers on the model and the tunnel wall.

TABLE 1. WATER TEMPERATURE = 66° F

($\nu = 11{\cdot}12 \times 10^{-6}$ ft.^{2}/sec.)

X in.	$(p-p_0)/\frac{1}{2}\rho U_0^2$	u_1/U_0
0·0	1·0	0·0
0·24	0·547	0·673
1	0·295	0·840
2	0·175	0·908
4	0·088	0·955
7	0·079	0·960
12	0·050	0·975
20	0·012	0·994
24·3	0·0	1·0

Values of the momentum thickness of the boundary layer, denoted by ϑ, required for the analysis below were calculated from the distribution of u_1/U_0 given in table 1 by the method given in § 24. The momentum thickness ϑ is given by $\int_0^\delta \frac{u}{u_1}\left(1-\frac{u}{u_1}\right)dy$, where δ is the thickness of the boundary layer, and u is the tangential component of the velocity in the boundary layer at a normal distance y from the surface.

Calculated values of $\frac{\vartheta}{D}\left(\frac{U_0 D}{\nu}\right)^{\frac{1}{2}}$, and of $\frac{\delta^2}{\nu}\frac{du_1}{ds}$, denoted by Λ, where D is the diameter of the maximum cross-section of the body, and s is the peripheral distance from the nose of the body, are given in table, 5.

(b) *Analysis of experimental data*

(9) Transition due to turbulence in the free stream is considered to arise from transient separations of the boundary layer from the surface caused by the pressure gradients within the layer associated with those without. The disturbing effect within the layer of the pressure gradients without depend on $\sqrt{\overline{\left(\frac{\partial p'}{\partial s}\right)^2}}$, where $\frac{\partial p'}{\partial s}$ is the value of the pressure gradient at any instant, on the thickness of the layer δ, on the velocity at the outer edge of the layer u_1 and on the viscosity μ. Taylor (1936) has suggested that according to the Kármán-Pohlhausen theory it would be expected, when transition is caused solely by turbulence in the free stream, that the instantaneous

distribution of velocity in the layer would depend on the value of $-\dfrac{\delta^2}{\mu u_1}\dfrac{\partial p'}{\partial s}$. It follows that the non-dimensional number $-\dfrac{\delta^2}{\mu u_1}\sqrt{\overline{\left(\dfrac{\partial p'}{\partial s}\right)^2}}$ should tend to have a definite value at transition. In the same paper the relation

$$\sqrt{\overline{\left(\frac{\partial p'}{\partial s}\right)^2}} = \frac{2\sqrt{2}}{AM^{\frac{1}{2}}}\frac{\rho}{\nu^{\frac{1}{2}}}\left(\sqrt{\overline{u_t^2}}\right)^{\frac{5}{2}}$$

is derived for isotropic turbulence in the stream behind a grid of mesh $M\left(\dfrac{M\sqrt{\overline{u_t^2}}}{\nu} > 60\right)$, where $\sqrt{\overline{u_t^2}}$ is the root-mean-square of the downstream component of turbulent velocity, and A is a universal constant for grids of the same type. On substitution of this relation for $\sqrt{\overline{\left(\dfrac{\partial p'}{\partial s}\right)^2}}$, the number $-\dfrac{\delta^2}{\mu u_1}\sqrt{\overline{\left(\dfrac{\partial p'}{\partial s}\right)^2}}$ becomes

$$\frac{2\sqrt{2}}{A}\left(\frac{\delta\sqrt{\overline{u_t^2}}}{\nu}\right)^{\frac{5}{2}}\left(\frac{\delta}{M}\right)^{\frac{1}{2}}\left(\frac{\nu}{\delta u_1}\right),$$

which can be written

$$\frac{2\sqrt{2}}{A}\left(\frac{\delta}{\vartheta}\right)^{2}\left(\frac{\sqrt{\overline{u_t^2}}}{u_T}\right)^{\frac{5}{2}}\left(\frac{\vartheta u_T}{\nu}\right)^{\frac{5}{2}}\left(\frac{\vartheta}{M}\right)^{\frac{1}{2}}\left(\frac{\nu}{\vartheta u_1}\right),$$

where u_T is the maximum value of u_t. The values of $\dfrac{\sqrt{\overline{u_t^2}}}{u_T}$ and of $\left(\dfrac{\delta}{\vartheta}\right)$ can be taken to be constant (see §§ 26 and 24). Taking the $(\frac{5}{2})$th root and ignoring the constant we get the non-dimensional number $\left(\dfrac{\vartheta u_T}{\nu}\right)\left(\dfrac{\vartheta}{M}\right)^{\frac{1}{5}}\left(\dfrac{\nu}{\vartheta u_1}\right)^{\frac{2}{5}}$, and on the present argument this number should tend to have a constant value at transition. For convenience of reference this number will be denoted by the symbol ξ_M.

Values of ξ_M at transition calculated from the experimental data for the model in the turbulent streams behind the two grids are plotted against the value of $\vartheta u_1/\nu$ at transition in figure 10. The values of ξ_M for grid I increase progressively from 0·60 to 0·86 $\left(100 < \dfrac{\vartheta u_1}{\nu} < 260\right)$, those for grid II from 0·55 to 0·62 $\left(260 < \dfrac{\vartheta u_1}{\nu} < 400\right)$; and although the values are not constant[*]

---

[*] Some differences are to be expected because the experimental values of dp/ds although small are not zero, as assumed in the derivation of the number ξ_M.

they have the same order of magnitude. The average value for the two streams is 0·65.

It is here of interest to mention that it can be shown that the non-dimensional number $\vartheta u_T/\nu$ tends to have a constant value at transition. The value of this number for the model behind grid I rises from 11·0 to 14·4 $\left(100 < \frac{\vartheta u_1}{\nu} < 260\right)$, and behind grid II from 10·4 to 11·2 $\left(260 < \frac{\vartheta u_1}{\nu} < 400\right)$.

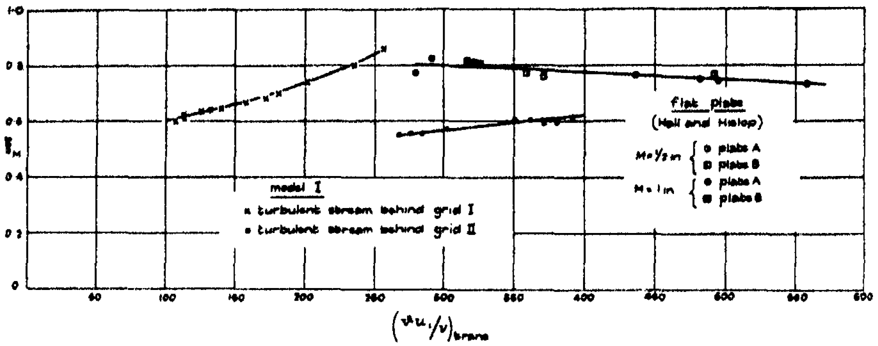

FIGURE 10

The values of non-dimensional numbers involving ϑ will depend on whether the measured value or the value calculated from a solution of the boundary layer equations for steady flow is taken, for there is reason to believe (Dryden 1936) that when the flow in the free stream is turbulent the actual value of ϑ is greater than the theoretical value.

(10) Experiments on transition from laminar to turbulent flow in the boundary layer of a flat plate in isotropic turbulent streams behind two square-mesh grids, $M = 0{\cdot}5$ and 1 in. respectively, have been made by Hall and Hislop (1938). For a laminar boundary layer on a flat plate

$$\frac{u_1\vartheta}{\nu} = 0{\cdot}664\left(\frac{u_1 X}{\nu}\right)^{\frac{1}{2}}, \quad \text{and} \quad \xi_M = (0{\cdot}664)^{\frac{1}{5}}\frac{u_T}{u_1}\left(\frac{X}{M}\right)^{\frac{1}{5}}\left(\frac{u_1 X}{\nu}\right)^{-\frac{1}{10}},$$

where X is the distance along the plate measured from the leading edge. Values of ξ_M at transition calculated from values of $\frac{\sqrt{\overline{u_1'^2}}}{u_1}\left(\frac{X}{M}\right)^{\frac{1}{5}}$ and $\left(\frac{u_1 X}{\nu}\right)$ given in the paper by Hall and Hislop, and for the experimental relation

$u_T = 3\cdot3\sqrt{\overline{u^2}}$ derived in § 26, are plotted against $\left(\frac{\vartheta u_1}{\nu}\right)_{\text{trans.}}$ in figure 10. The value of ξ_M falls slowly from

$$0\cdot80 \text{ at } \left(\frac{\vartheta u_1}{\nu}\right)_{\text{trans.}} = 280 \text{ to } 0\cdot73 \text{ at } \left(\frac{\vartheta u_1}{\nu}\right)_{\text{trans}} = 560.$$

The average value is 0·76. This value has the same order of magnitude as the average value 0·65 obtained from the present experiments on model I, so that ξ_M for the flat plate and model I tends to have the same value at transition.

(11) The non-dimensional number

$$\left(\frac{\vartheta u_T}{\nu}\right)\left(\frac{\vartheta}{L}\right)^{\frac{1}{5}}\left(\frac{\nu}{\vartheta u_1}\right)^{\frac{2}{5}},$$

denoted by ξ_L and obtained by the substitution of L for M in ξ_M, where L is the Taylor scale of turbulence given by $\int_0^\infty R_l dl$, and R_l is the correlation coefficient for u-velocity fluctuations at two points separated a lateral distance l, is more likely to be representative of the conditions in the boundary layer than ξ_M, when the value taken for L is that in the stream at the station considered. Measurements of L were not made, but rough values have been calculated from relations for L obtained by Dryden and others (1937) for isotropic turbulent streams behind ½ and ¼ in. grids. For these values of L, the value of ξ_L for the model rises from 0·83 to 1·12 over the range of $(\vartheta u_1/\nu)_{\text{trans.}}$ covered for the model behind grid I, and the value is practically constant at 0·70 for grid II.

Transition caused by a falling velocity in the free stream

(*a*) *Model II*

(12) Model II (figure 6*b*) was formed by a semi-ellipsoidal nose-piece of diameter 3 in. and length 6 in., a cylindrical part of diameter 3 in. and length 4 in., and a tail tapering in diameter from 3 to 2 in. over a length of 16 in. The shape of the tail generator is given by $75\cdot8\,(1\cdot5 - Y) = (X - 10)^{1\cdot31}$, where Y is the radius in inches at an axial distance X inches from the nose. The model was supported in the free stream of the tunnel by a spindle at the tail (see remarks for Model I, § 5), and transition caused by the falling velocity arising from the taper of the tail was observed.

(13) Non-dimensional pressure coefficients obtained from measurements at a number of small holes on a generator of the model, and for a datum velocity U_0 and pressure p_0 taken at a point just outside the boundary layer at $X = 22$ in., are given in table 2. The last column of the table gives values of u_1/U_0 for $U_0 = 3{\cdot}03$ ft./sec., determined from the measured pressure (see § 8). The value of u_1/U_0 rises from zero on the nose to a maximum at $X = 8{\cdot}1$ in., and then falls continuously on the tail.

TABLE 2. WATER TEMPERATURE = 58·5° F

($\nu = 12{\cdot}4 \times 10^{-6}$ ft.²/sec.)

	$(p-p_0)/\frac{1}{2}\rho U_0^2$			u_1/U_0
X in.	$U_0 = 1{\cdot}66$	$U_0 = 3{\cdot}03$	$U_0 = 5{\cdot}16$	$U_0 = 3{\cdot}03$ ft./sec.
0·0	1·000	1·000	1·000	0·0
0·24	0·504	0·505	0·511	0·703
1	0·186	0·173	0·176	0·909
2	+0·062	+0·041	+0·047	0·980
4	−0·063	−0·078	−0·071	1·038
7	−0·081	−0·092	−0·083	1·045
10	−0·117	−0·130	−0·122	1·062
14	−0·087	−0·091	−0·085	1·045
18	−0·047	−0·043	−0·042	1·021
22	0·0	0·0	0·0	1·000
26	+0·040	+0·067	+0·092	0·966

(14) Observations of the behaviour of filament bands and of particles in the boundary layer were made for a number of stream velocities within the range 1–5·2 ft./sec. at a water temperature 60° F ($\nu = 12{\cdot}1 \times 10^{-6}$ ft.²/sec.). The observations for velocities below 1·6 ft./sec. indicated that the flow was laminar over the entire length of the model, and that the layer separated from the surface at the junction with the supporting spindle. For the velocity range $U_0 = 1{\cdot}6$–$2{\cdot}3$ ft./sec., filament bands thickened and oscillated near the end of the tail and then separated from the surface, the separation becoming more definite with an increase in velocity; also particles on the surface were brought to rest as the separation point was approached, and beyond they exhibited the to-and-fro movements associated with reversal of flow. The position of separation changed from about $X = 24{\cdot}7$ in. for $U_0 = 1{\cdot}6$ ft./sec. to $X = 23{\cdot}5$ in. for $U_0 = 2{\cdot}3$ ft./sec. From $U_0 = 2{\cdot}3$ to 3·7 ft./sec. filament bands separated from the surface ($X = 23{\cdot}5$ to 25·5 in.), became very unsteady after separation, and soon broke down into discrete eddies: and particles arrived with a steady slow velocity at the separation point and were then swept rapidly away. Above $U_0 = 3{\cdot}7$ ft./sec., the characteristic feature was a sudden breakdown of the laminar boundary

layer and the emission of puffs of diffused turbulence ($X = 23$ in.). The puffs were definite and they occurred spasmodically, and resembled those emitted when transition is caused by turbulence in the free stream. In brief, the observations showed a definite separation of the laminar boundary layer from the surface at the lower velocities, a breakdown from laminar to turbulent flow in the separated layer at the medium velocities, and a fairly sudden but not stationary transition from laminar to turbulent flow at the higher velocities: and it would seem from the sequence of these changes with speed and their occurrence on the same part of the model that transition at the higher speeds is due to a separation of the laminar boundary layer from the surface.

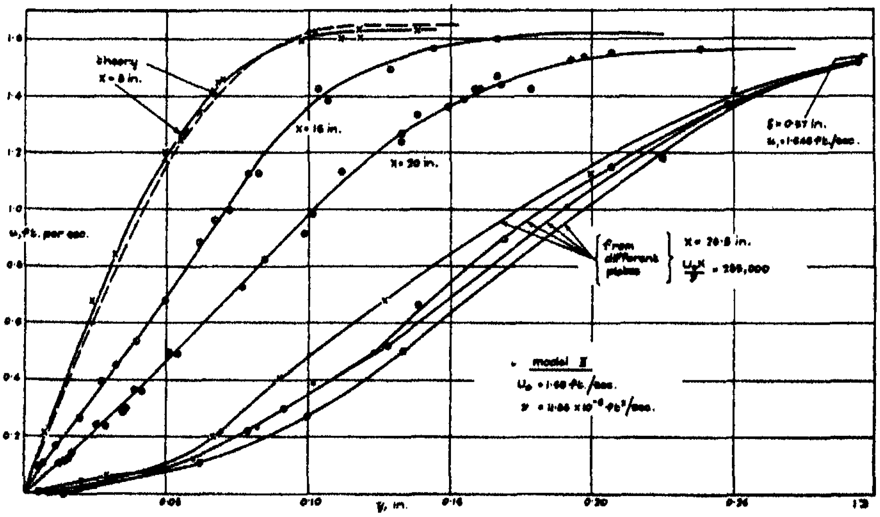

FIGURE 11

(15) Distributions of velocity in the boundary layer, u against y, determined from photographs of particle streaks (see § 4) are given in figure 11. The length of the surface covered is from the position of maximum velocity to near the position of boundary-layer separation: and the curves show for this region the change in velocity distribution, and the fall in the velocity gradient at the surface to the zero value at separation. The velocity distributions plotted for the station $X = 25{\cdot}8$ in. were obtained from four plates. The values of u measured on each plate fall on a smooth curve, but the curves differ from plate to plate. The velocity distribution in the region of separation therefore changes with time, and separation does not occur at a fixed position. The dotted curve in figure 11 ($X = 8$ in.) gives the distribution of

u calculated by the Kármán-Pohlhausen method (§ 24). This theoretical distribution is in close agreement with the measured distribution.

(16) It would be possible to obtain a check on the observed position of separation by a comparison with the position obtained, for the measured distribution of u_1, from a solution of the boundary layer equations by a method due to Howarth (1938). To apply this method to the region of falling velocity on the tapering tail of the model would necessitate the calculation of a new set of coefficients (see Howarth's paper), and this calculation did not seem to be worth while because of the labour which would be involved, and because the coefficients would be applicable only to the particular body for which they were calculated. There is, however, reason to believe that the observed position of separation is near the position which would be given by calculation (see § 21).

(*b*) *Model I*

(17) The position of separation of the laminar boundary layer on a body of revolution in a stream in which the velocity falls in the direction of flow can be determined by the method and for the coefficients given in Howarth's paper, provided the body has a constant cross-section and the thickness of the boundary layer is small compared with the radius of the cross-section, so that the flow in the layer approximates to the two-dimensional type. These conditions hold for model I, and to obtain data needed for a comparison between theory and observation, experiments were made on this model in a divergent stream, obtained by fitting a divergent sleeve with a faired entry into the tunnel. The sleeve was made in three parts: the first was 18·5 in. long and had a uniform diameter of 5·8 in.; the second tapered in diameter from 5·8 to 6·2 in. over a length of 21 in.; and the third was 14·5 in. long and had a uniform diameter of 6·2 in. The first and third parts were made of thin brass tubes and the tapered part of perspex. The model was supported in a housing well beyond the observation chamber, and the taper began 9 in. beyond the nose of the model.

(18) Distributions of pressure measured on a generator of the model are given in table 3, in terms of non-dimensional coefficients and for a datum velocity U_0 and pressure p_0 taken just outside the boundary layer at $X = 20$ in. Distributions of u_1/U_0 calculated from the pressure distributions for $U_0 = 1{\cdot}7$ and $3{\cdot}0$ ft./sec. are given in the last two columns of the table. The value of u_1/U_0 reaches a maximum value at $X = 9{\cdot}17$ in., and then falls continuously with an increase in X.

TABLE 3. WATER TEMPERATURE = 56° F

($\nu = 12{\cdot}85 \times 10^{-6}$ ft.²/sec.)

	$(p-p_0)/\frac{1}{2}\rho U_0^2$				u_1/U_0	
X in.	$U_0 = 1{\cdot}7$	$U_0 = 3{\cdot}0$	$U_0 = 4{\cdot}5$	$U_0 = 6{\cdot}0$	$U_0 = 1{\cdot}71$	$U_0 = 3{\cdot}0$
0·0	1·0	1·0	1·0	1·0	0·0	0·0
0·25	0·576	0·566	0·557	0·551	0·652	0·659
1	0·309	0·292	0·278	0·268	0·832	0·842
2	0·177	+0·159	+0·147	+0·136	0·907	0·917
4	+0·013	−0·004	−0·016	−0·025	0·994	1·002
7	−0·043	−0·052	−0·064	−0·073	1·022	1·026
12	−0·046	−0·052	−0·061	−0·066	1·023	1·026
16	−0·017	−0·025	−0·028	−0·030	1·008	1·0125
20	0·0	0·0	0·0	0·0	1·0	1·0
24	+0·020	+0·025	+0·029	+0·030	0·990	0·9875

(19) Observations of the behaviour of filament bands on the surface of the model were made at $U_0 = 1{\cdot}7$ and 3·0 ft./sec. (water temperature 61·5° F, $\nu = 11{\cdot}8 \times 10^{-6}$ ft.²/sec.). At the lower velocity, the filament bands were steady and straight from the nose to about $X = 18$ in.: but beyond this station they were either steady and straight, or else they curved slowly on the surface, and, after straightening again at about $X = 24$ in., waved slightly and spread laterally. No separation of filament bands from the surface was observed. At the higher velocity, filament bands were steady and straight as far as $X = 18$ or 19 in., and then spread spasmodically in a fan-like fashion. Puffs having the appearance of a break in the band occurred infrequently in the region near $X = 18{\cdot}5$ in., and frequently near $X = 25$ in. No separation of filament bands was observed. The position of transition could not be observed with precision, but it was probably beyond $X = 18{\cdot}5$ in., where puffs were occasionally seen, and not so far back as $X = 25$ in., where puffs were frequent.

(20) Theoretical distributions of u in the boundary layer calculated from the mean measured distribution of u_1 for $U_0 = 1{\cdot}71$ and 3·0 ft./sec. (§ 25) are compared with distributions measured by the photographic method in figure 12. For stations $X = 15{\cdot}3$ and 19·45 in. the calculated and measured distributions are in fair agreement, but this is not so for station $X = 23{\cdot}6$ in. where the calculated slope at the surface is smaller than the measured slope. The calculated and measured distributions of u are, however, consistent with each other in so far as they support the filament-band observations that there is no separation of the boundary layer from the surface. It would seem therefore that the observed transition cannot be caused solely by the

gradient in u_1, but must arise from this gradient assisted by irregularities of flow introduced into the tunnel stream by the divergent sleeve.

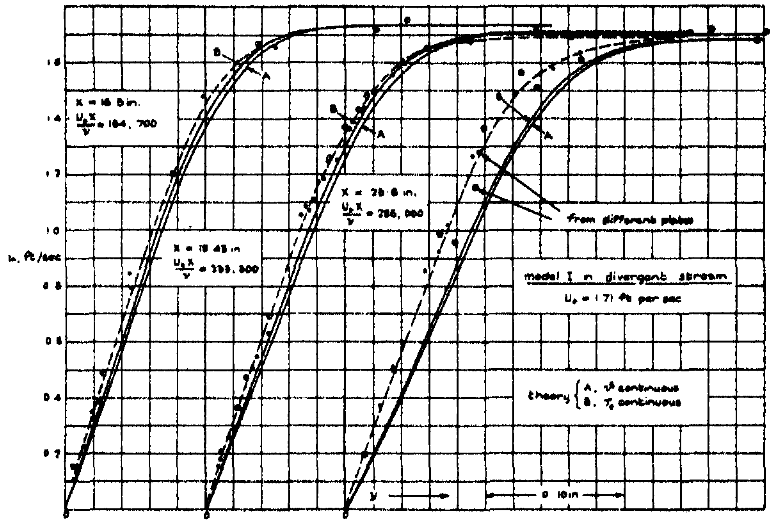

FIGURE 12

(21) The measured negative gradient of u_1 on model II in the free stream of the tunnel is double the gradient on model I in the tunnel with the divergent sleeve. The position of separation on model I which would be calculated by the method of § 25 for double the gradient is $X = 23{\cdot}7$ in. The observed position of separation on model II ($X = 24$ in.) is therefore about the same as the calculated position on model I for the same gradient of u_1. It is not to be expected that the conditions of flow in the boundary layers of the two models would be the same for the same gradient of u_1, since model II has a tapering tail whereas model I has a tail of uniform cross-section, but it would seem justifiable to draw the conclusion that the observed position of separation on model II is probably not far from the position which would be obtained by calculation.

TRANSITION CAUSED BY SURFACE WIRES

(22) Local disturbances of flow due to a surface wire placed in a laminar boundary layer at right angles to the direction of flow depend on the diameter of the wire and on the conditions of flow in the region where the wire is placed: and the forward movement of transition due to a wire depends on the local disturbances created by the wire and on the conditions which

existed in the boundary layer beyond the wire before it was introduced into the layer. Local disturbances of flow due to surface wires and their effect on the position of transition were observed on models I and II in the water tunnel (uniform cross-section) by means of fine filament bands of white ink flowing smoothly out of a small surface hole in front of the wire. Each wire was mounted on the surface of a model in the form of a ring with its plane normal to the model axis. Special consideration was given to the case for which the disturbances created by a wire were sufficient to bring transition to the wire itself. Observation was made for wires of diameter 0·007–0·048 in. and for a range of U_0 from 1–6 ft./sec. For model I the datum velocity U_0 was taken at a point just outside the boundary layer at $X = 24{\cdot}3$ in., and for model II at $X = 22{\cdot}0$ in.

The changes of flow in the boundary layer at and beyond a wire revealed by the behaviour of filament bands follow the same general sequence with increase in stream velocity; but the velocity at which a particular manifestation occurs depends on the diameter and position of the wire. At a low velocity, a filament band flowed steadily and smoothly over a wire without forming a wake, and, with an increase in speed, local standing vortices behind the wire were formed. At first, these vortices were fairly steady, but with an increase in velocity, the ink entrained within them spread with a spiral motion circumferentially along the wire, either on one or on both sides of the main filament, and either in a continuous or in a periodic manner. Sometimes the ink was carried far around the model in the form of a tight spiral and then discharged, continuously or intermittently, into the boundary layer in the form of a secondary weak filament band. Transition in the secondary band sometimes occurred earlier than in the main band. At higher velocities, the circumferential movement disappeared, the standing vortex drew out, and opened at its downstream end in the form of a vortex sheet. This sheet eventually broke down, formed a turbulent wake, and carried downstream a highly diffused band of ink.

With the approach to a transition region some distance downstream from a wire, a filament band tended to wave slightly and occasionally to lift from the surface. Within the transition region, puffs of white ink were emitted from the filament in a spasmodic manner, both the strength and the frequency of appearance of the puffs increasing with the distance downstream. Beyond the transition region, a filament band became widely diffused and spread rapidly into the stream. The position nearest the nose of a model at which puffs were seen was taken to be the transition point. As the velocity increased and the transition point approached a wire, the length of the transition region over which puffs were seen tended to become shorter, and, when transition at the wire was just completed, no trace of the filament band was visible.

With fine wires, the wire disturbances in a slow stream were damped out before the region of retarded flow was reached. With medium wires and for medium stream velocities, transition appeared to be due to eddies and to separation of the boundary layer. With larger wires and higher velocities, a filament band behaved in the same manner as when transition is caused by turbulence. On model II, transition arose from the combined effect of the velocity gradient in the free stream and the wire disturbances, but on model I, from the wire disturbances only: and the additional effect of the velocity gradient made transition more definite.

(23) The transition point on a model moved forward with an increase in diameter and in stream velocity: and the forward movement was greater the nearer the wire to the nose. Curves showing how the position of transition, $X_{\text{trans.}}$, depends on stream velocity, U_0, and wire diameter, d, are given in figure 13. These curves are for wires at $X = 8$ in. on model II, and they are

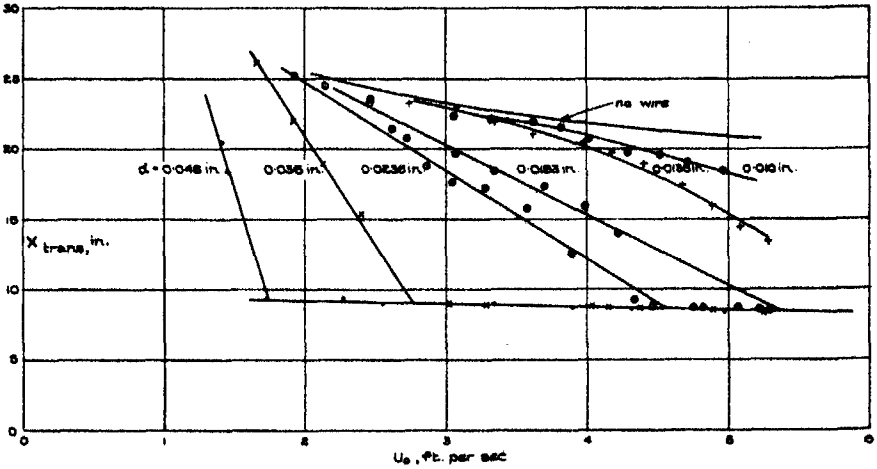

FIGURE 13. Model II, wires at $X = 8$ in., $\nu = 13{\cdot}05 \times 10^{-6}$ ft.^{2}/sec.

representative of the results obtained for model I, except that in a few cases the position of transition could not be located with the same precision. The lowest value of U_0 which brings transition to a wire was found from curves such as those in figure 13. These values for the two stations on each model are given in table 4.

The velocity in the boundary layer (without a wire) at $y = d$, denoted by u_d, obtained from solutions of the momentum equation of the boundary layer for the measured distributions of u_1 (§ 24) are given in the table. The last column gives values of $u_2 d/\nu$, and it is seen that the magnitude of these values for wires at the two stations on each model is (with two exceptions) of the order 400. Turbulence in the boundary layer behind a wire therefore becomes fully established at the wire when $u_2 d/\nu > 400$. The range of d/δ covered in the experiments is 0·2–1·2 (see table).

TABLE 4

	d in.	U_0 ft./sec.	d/δ	u_2 ft./sec.	$u_2 d/\nu$
Model II					
Wire position, $X = 8$ in.	0·048	1·74	0·40	1·27	390
$u_1 = 1{\cdot}056 U_0$	0·036	2·76	0·37	1·89	435
$\nu = 13{\cdot}05 \times 10^{-6}$ ft.²/sec.	0·0235	4·58	0·31	2·72	410
$\delta = 0{\cdot}164/\sqrt{U_0}$ in.	0·0193	5·37	0·27	2·92	360
Model II					
Wire position, $X = 1$ in.	0·048	1·62	1·22	1·47	450
$u_1 = 0{\cdot}909 U_0$	0·022	3·38	0·81	3·04	427
$\nu = 13{\cdot}05 \times 10^{-6}$ ft.²/sec.	0·016	4·74	0·70	4·14	423
$\delta = 0{\cdot}050/\sqrt{U_0}$ in.					
Model I					
Wire position, $X = 8$ in.	0·048	2·13	0·40	1·42	420
$u_1 = 0{\cdot}963 U_0$	0·022	3·52	0·23	1·51	205
$\nu = 13{\cdot}45 \times 10^{-6}$ ft.²/sec.	0·019	5·16	0·24	2·31	270
$\delta = 0{\cdot}177/\sqrt{U_0}$ in.					
Model I					
Wire position, $X = 1$ in.	0·0225	3·49	0·81	2·94	425
$u_1 = 0{\cdot}851 U_0$	0·019	3·97	0·73	3·28	400
$\nu = 13{\cdot}05 \times 10^{-6}$ ft.²/sec.	0·014	6·09	0·67	4·93	440
$\delta = 0{\cdot}052/\sqrt{U_0}$ in.					

SOLUTION OF THE MOMENTUM EQUATION FOR STEADY FLOW IN THE BOUNDARY LAYER

(24) The momentum equation for steady flow in the boundary layer of a solid of revolution obtained by Kármán and Pohlhausen on the assumption that the distribution of velocity in the boundary layer can be represented by a polynomial of the fourth degree is

$$\frac{dz}{ds} = \frac{g(\Lambda)}{u_1} + z^2 \frac{d^2u_1}{ds^2} h(\Lambda) - \frac{1}{Y}\frac{dY}{ds}\frac{1}{du_1/ds} h^*(\Lambda),$$

where $z = \frac{\delta^2}{\nu}$, $\Lambda = \frac{\delta^2}{\nu}\frac{du_1}{ds}$, s is the peripheral distance from the nose, Y is the radius of the cross-section and $g(\Lambda)$, $h(\Lambda)$ and $h^*(\Lambda)$ are known functions of Λ (see Goldstein 1938).

Solutions of this equation for the front parts of models I and II over which u_1 is rising in the direction of flow were obtained, for the measured distributions of u_1, by step-by-step integration. The values of u_1, du_1/ds and d^2u_1/ds^2 taken in the solutions were obtained from simple algebraic relations closely representing the measured distributions of u_1. The values of u_1/U_0 taken in the solutions of the momentum equation, and the values of $\frac{\vartheta}{D}\left(\frac{U_0D}{\nu}\right)^{\frac{1}{2}}$ and Λ obtained for the two models are given in table 5.

TABLE 5

			Model I in turbulent streams behind grids I and II			Model II in tunnel with uniform cross-section			Model I in tunnel with divergent sleeve		
$\frac{X}{D}$	$\frac{s}{D}$	$\frac{D}{Y}\frac{dY}{ds}$	$\frac{u_1}{U_0}$	$\frac{\vartheta}{D}\left(\frac{U_0D}{\nu}\right)^{\frac{1}{2}}$	Λ	$\frac{u_1}{U_0}$	$\frac{\vartheta}{D}\left(\frac{U_0D}{\nu}\right)^{\frac{1}{2}}$	Λ	$\frac{u_1}{U_0}$	$\frac{\vartheta}{D}\left(\frac{U_0D}{\nu}\right)^{\frac{1}{2}}$	Λ
0·0	0·0	∞	0·0	0·089	4·716	0·0	0·088	4·716	0·0	0·092	4·716
0·0060	0·04	24·3	0·270	0·094	4·39	0·293	0·093	4·302	0·270	0·097	4·32
0·0228	0·08	11·3	0·464	0·109	3·81	0·498	0·109	3·625	0·460	0·107	4·15
0·0470	0·12	7·1	0·586	0·129	3·17	0·614	0·127	3·297	0·568	0·128	3·05
0·0750	0·16	4·9	0·665	0·150	2·67	0·700	0·145	2·760	0·647	0·145	2·55
0·1045	0·20	3·8	0·718	0·170	2·30	0·759	0·164	2·44	0·700	0·168	2·38
0·1733	0·28	2·45	0·779	0·206	1·93	0·828	0·198	2·02	0·765	0·206	2·00
0·2450	0·36	1·74	0·819	0·239	1·77	0·873	0·230	1·76	0·804	0·240	1·80
0·3185	0·44	1·35	0·847	0·270	1·64	0·904	0·260	1·63	0·834	0·270	1·70
0·3940	0·52	1·05	0·868	0·298	1·52	0·927	0·287	1·55	0·857	0·298	1·65
0·4700	0·60	0·89	0·884	0·324	1·44	0·946	0·313	1·48	0·876	0·323	1·66
0·5470	0·68	0·75	0·898	0·349	1·35	0·961	0·336	1·48	0·892	0·344	1·74
0·625	0·76	0·65	0·909	0·373	1·27	0·974	0·358	1·46	0·906	0·366	1·81
0·703	0·84	0·55	0·918	0·397	1·18	0·985	0·379	1·44	0·920	0·385	1·81
0·781	0·92	0·49	0·925	0·420	1·09	0·994	0·399	1·42	0·932	0·402	1·83
0·860	1·00	0·42	0·931	0·442	1·02	1·004	0·419	1·40	0·944	0·420	1·82
0·939	1·08	0·37	0·936	0·464	0·96	1·012	0·437	1·35	0·956	0·437	1·82
1·018	1·16	0·325	0·940	0·485	0·89	1·018	0·457	1·31	0·966	0·455	1·79
1·097	1·24	0·285	0·944	0·506	0·83	1·026	0·475	1·27	0·975	0·473	1·77
1·256	1·40	0·215	0·948	0·547	0·70	1·035	0·513	1·11	0·991	0·506	1·61
1·416	1·56	0·155	0·952	0·591	0·53	1·042	0·554	0·89	1·002	0·543	1·43
1·575	1·72	0·105	0·955$_5$	0·637	0·40	1·047	0·596	0·65	1·011	0·583	1·21
1·635	1·88	0·060	0·956	0·683	0·31	1·050	0·640	0·50	1·018	0·624	0·98
1·895	2·04	0·025	0·957	0·729	0·28	1·052	0·684	0·39	1·023	0·669	0·75
2·055	2·20	0·0	0·958$_5$	0·775	0·32	1·054	0·728	0·31	1·026	0·712	0·56
2·255	2·40	—	0·960	0·833	0·36	1·055	0·784	0·20	1·028	0·770	0·35
2·455	2·60	—	0·961$_5$	0·885	0·41	1·055$_5$	0·837	0·12	1·029	0·823	0·20
2·655	2·80	—	0·963	0·937	0·46	1·056	0·887	0·0	1·0295	0·874	0·11
2·855	3·00	—	0·964$_5$	0·982	0·50	—	—	—	1·0299	0·924	+0·06
3·055	3·20	—	0·966	1·026	0·55	—	—	—	1·0300	0·970	0·0
3·255	3·40	—	0·967$_5$	1·066	0·60	—	—	—	1·0298	1·020	−0·15
3·455	3·60	—	0·969	1·106	0·64	—	—	—	1·0292	1·056	−0·49
3·655	3·80	—	0·970$_5$	1·143	0·69	—	—	—	1·0278	1·112	−0·75
3·855	4·00	—	0·972	1·180	0·73	—	—	—	1·0262	1·158	−0·91
4·655	4·80	—	0·977	1·314	0·91	—	—	—	See table 6		
5·455	5·60	—	0·983	1·428	1·08	—	—	—			
6·255	6·40	—	0·989	1·527	1·24	—	—	—			
7·055	7·20	—	0·994	1·618	1·40	—	—	—			
7·855	8·00	—	1·00	1·700	1·55	—	—	—			

(25) The velocity distribution beyond $s = 4D$ on model I in the tunnel with the divergent stream is given by $u_1/U_0 = 1{\cdot}0262 - 0{\cdot}0095\,(s/D - 4)$, and the solution of the momentum equation for this case of falling u_1 in the direction of flow was found by the method due to Howarth (1938), on the assumption that the flow in the boundary layer on the model beyond $s = 4D$ is the same as that on a flat plate beyond a point $s = s_0$, when the values of u_1, du_1/ds and ϑ (or frictional intensity τ_0) for the plate at $s = s_0$ are the same as those obtained from the Kármán-Pohlhausen solution for the model at $s = 4D$. For continuity in ϑ at $s = 4D$ there is discontinuity in τ_0, and vice versa. Separation occurs at $s = 14{\cdot}4D$ for continuity in ϑ, and at $s = 14{\cdot}7D$ for continuity in τ_0. The results of the calculations for this case are given in table 6.

TABLE 6. $\dfrac{u_1}{U} = 1{\cdot}0262 - 0{\cdot}0095\left(\dfrac{s}{D} - 4\right)$

		Continuity of ϑ		Continuity of τ_0	
$\dfrac{X}{D}$	$\dfrac{s}{D}$	$\dfrac{\vartheta}{D}\left(\dfrac{U_0D}{\nu}\right)^{\frac{1}{2}}$	$\dfrac{\tau_0}{\rho U_0^2}\left(\dfrac{U_0D}{\nu}\right)^{\frac{1}{2}}$	$\dfrac{\vartheta}{D}\left(\dfrac{U_0D}{\nu}\right)^{\frac{1}{2}}$	$\dfrac{\tau_0}{\rho U_0^2}\left(\dfrac{U_0D}{\nu}\right)^{\frac{1}{2}}$
3·855	4·0	1·158	0·176	1·076	0·194
4·355	4·5	1·273	0·157	1·190	0·170
4·855	5·0	1·365	0·142	1·292	0·153
5·355	5·5	1·468	0·127	1·384	0·137
5·855	6·0	1·560	0·115	1·476	0·123
6·355	6·5	1·642	0·106	1·568	0·113
6·855	7·0	1·724	0·096	1·660	0·103
7·355	7·5	1·819	0·089	1·752	0·094
7·855	8·0	1·900	0·081	1·845	0·085
8·355	8·5	1·991	0·074	1·928	0·079

VALUE OF $u_T/\sqrt{\overline{u_t^2}}$ FOR ISOTROPIC TURBULENCE

(26) Values of the ratio of the maximum value of the downstream component of turbulent velocity, u_T, to the local mean velocity, U, were measured with the fluid-motion microscope at a number of points on the centre line of the tunnel in the isotropic-turbulent streams behind grids I and II. Values of the reciprocal of this ratio, U/u_T, are plotted against x/M, where x is the downstream distance behind a grid, in figure 14.

For each grid they lie closely on a straight line for the range of x/M covered. The values of $d(U/u_T)/d(x/M)$, obtained from the slopes of these lines are 0·32 (grid I) and 0·30 (grid II). The mean value is 0·31.

Hot-wire measurements of $U/\sqrt{\overline{u_t^2}}$ in airstreams behind square-mesh grids of the same type as those used in the present experiments have been made by Dryden and others (1937), by Simmons and Salter (see Taylor 1935) and by Hall and Hislop (1938). These experimenters found that the measurements of $U/\sqrt{\overline{u_t^2}}$ for the range $x/M = 20$ to 60 fall on a straight line.* Representative lines obtained when $U/(3{\cdot}3\sqrt{\overline{u_t^2}})$ is plotted against x/M are given in figure 14. The values of $d\,(U/3{\cdot}3\sqrt{\overline{u_t^2}})\Big/d\!\left(\dfrac{x}{M}\right)$ obtained from these lines are 0·28 (Dryden), 0·31 (Simmons) and 0·34 (Hall). The average value is 0·31. This value is equal to that of $d\!\left(\dfrac{U}{u_T}\right)\Big/d\!\left(\dfrac{x}{M}\right)$ given above, so that $u_T = 3{\cdot}3\sqrt{\overline{u_t^2}}$.

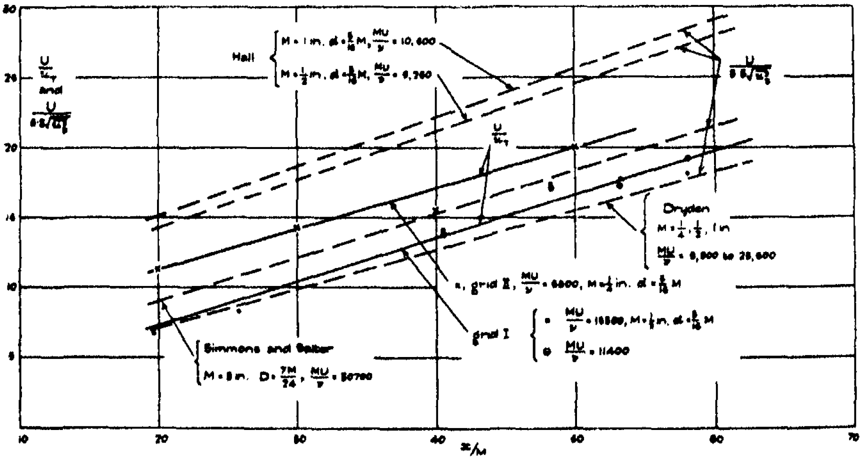

FIGURE 14

(27) An analysis of a cinematograph film of the turbulent velocities in the wake behind a long circular cylinder gives the same relation between u_T and $\sqrt{\overline{u_t^2}}$. The film was taken by Dr Townend to obtain information needed for an investigation made some years ago by one of the present writers (Fage 1936b), and records the movements of a succession of small masses of air, heated by a continuous series of sparks and made visible in a bright beam of light by the Schlieren method, at a point in the wake (28·5 diameters behind a $\frac{3}{8}$ in. cylinder, $U_0 = 35{\cdot}1$ ft./sec.) where the turbulence in the stream closely resembles the isotropic type. From this film 670 measurements of the downstream component of the turbulent velocity u_t were made. A histogram constructed from them for a group interval 0·057 of u_t/U, and also the

---

* Actually, $d(U/\sqrt{\overline{u_t^2}})/d(x/M)$ falls with the distance downstream (see Kármán and Howarth 1938), but for the range of x/M here considered the change from the theoretical value $5/A^2$, where A is a universal constant (see Taylor 1935), is small.

'normal' distribution curve for this group interval and the value 0·1465 of $\sqrt{\overline{u_t^2}}/U$ calculated from the measurements, are given in figure 15. The 'normal' curve passes evenly through the tops of the rectangles of the histogram so that the distribution of u_t/U is closely an ideally random one. The value of u_T/U recorded on the film was 0·482, so that $u_T = 3{\cdot}3\sqrt{\overline{u_t^2}}$. It is of interest to add that Townend (1934) has shown that $u_T = 2{\cdot}9\sqrt{\overline{u_t^2}}$, for fully developed turbulent flow in a square pipe, and that Simmons and Salter (1934) have obtained the relation $u_T = 2{\cdot}8\sqrt{\overline{u_t^2}}$ for flow behind a grid by a photometric method involving the use of a fine hot-wire anemometer.

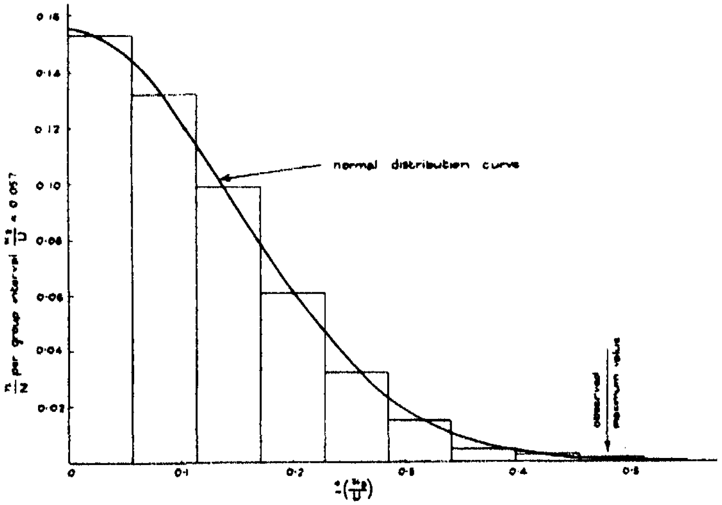

FIGURE 15

(28) The conclusion that $u_T = 3{\cdot}3\sqrt{\overline{u_t^2}}$ needs further consideration. For a 'normal' distribution of u_t the value of u_T observed would increase with the number of particles under observation and so with the time of observation. The 'normal' relation is $\frac{n}{N} = \left(\frac{n}{N}\right)_0 e^{-(u_t/U)^2/2\sigma^2}$, where N is the total number of observations, n is the number of observations per group interval, $\left(\frac{n}{N}\right)_0 = \frac{\text{group interval}}{\sigma 2\pi}$ and $\sigma = \sqrt{\overline{u_t^2}}/U$. If $(u_T/U)_1$ be the maximum value of u_t/U observed during a standard time of observation t_1, and $(u_T/U)_2$ the value in a time t_2 ($t_2 > t_1$), then on the assumption that the maximum velocity $(U+u_T)$ and the minimum velocity $(U-u_T)$ occur only once during the time

of observation, and that the number of particles seen is proportional to the time of observation, we have

$$\frac{1}{at_1} = \left(\frac{n}{N}\right)_0 e^{-(u_T/U)_1^2/2\sigma^2}$$

and

$$\frac{1}{at_2} = \left(\frac{n}{N}\right)_0 e^{-(u_T/U)_2^2/2\sigma^2},$$

where a is the number of particles seen in unit time.

From these relations we get

$$\left(\frac{u_T}{U}\right)_2 = \left(\frac{u_T}{U}\right)_1 \left[1 + \frac{2\sigma^2}{(u_T/U)_1^2} \log_e \frac{t_2}{t_1}\right]^{\frac{1}{2}},$$

and, on substitution of the experimental relation $(u_T/U)_1 = 3{\cdot}3\sigma$,

$$\left(\frac{u_T}{U}\right)_2 = \left(\frac{u_T}{U}\right)_1 \left[1 + 0{\cdot}423 \log_{10} \frac{t_2}{t_1}\right]^{\frac{1}{2}}.$$

If $t_2/t_1 = 3, \quad (u_T/U)_2 = 1{\cdot}1(u_T/U)_1,$

and if $t_2/t_1 = 11, \quad (u_T/U)_2 = 1{\cdot}2(u_T/U)_1,$

so that the standard time of observation with the fluid-motion microscope is such that no appreciable increase in the value of u_T/U is to be expected if observation were made for a much longer time.

It is unlikely that an ideally random distribution of u_t can exist, for this implies that extremely large values of u_T/U would be observed if observation were made over a very long time. Although the present experiments were concerned with observation of the movements of particles, it is really the movements of small masses of water which are involved, and it is difficult to believe that these small viscous masses can have very large values of u_T.

(29) Mr W. S. Walker assisted the writers with the experiments.

REFERENCES

Dryden, H. L. 1936 *Rep. Nat. Adv. Comm. Aero., Wash.*, pp. 339–364.

Dryden, H. L., Schubauer, G. B., Mock, Jr., W. C. and Skramstad, H. K. 1937 *Rep. Nat. Adv. Comm. Aero., Wash.*, pp. 109–140.

Fage, A. 1936*a* *Phil. Mag.* **21**, 80–105.

Fage, A. 1936*b* *Proc. Roy. Soc.* A, **155**, 576–596.

Fage, A. and Falkner, V. M. 1930 *Proc. Roy. Soc.* A, **129**, 378–410.

Fage, A. and Preston, J. H. 1941 *J. R. Aero. Soc.* **45**, 124.

Fage, A. and Townend, H. C. H. 1932 *Proc. Roy. Soc.* A, **135**, 656–684.

Goldstein, S. 1938 *Modern developments in fluid dynamics*, **1**, chap. 4. Oxford Univ. Press.
Hall, A. A. and Hislop, G. S. 1938 *Rep. Memor. Aero. Res. Comm., Lond.*, no. 1843.
Howarth, L. 1938 *Proc. Roy. Soc.* A, **164**, 547–579.
Jones, B. M. 1938 *J. Aero. Sci. Amer.* **5**, 81–101.
Kármán, de T. and Howarth, L. 1938 *Proc. Roy. Soc.* A, **164**, 192–215.
Simmons, L. F. G. and Salter, C. 1934 *Proc. Roy. Soc.* A, **145**, 212–234.
Stephens, A. V. and Haslam, J. A. G. 1938 *Rep. Memor. Aero. Res. Comm., Lond.*, no. 1800.
Taylor, G. I. 1935 *Proc. Roy. Soc.* A, **151**, 421–454.
Taylor, G. I. 1936 *Proc. Roy. Soc.* A, **156**, 307–317.
Townend, H. C. H. 1934 *Proc. Roy. Soc.* A, **145**, 180–211.

Further investigations of solid *n*-paraffins

(Repulsion potential and compressibility)

BY ALEX MÜLLER

(*Communicated by Sir William Bragg, F.R.S.—Received* 30 *January* 1941)

Experiments are made on the compressibilities of solid *n*-paraffins. The lattice deformations due to pressure are measured with the aid of X-rays, the pressures ranging between 700 and 1500 atm. It is found that the linear compressibilities in a plane normal to the chain axes are of the order of 3 to 12×10^{-12} cm.^{2}/dyne. The compressibility in the direction of the chain is less than 3×10^{-13} cm.^{2}/dyne.

Numerical estimates show that the repulsive forces between paraffin chains have their origin essentially in the hydrogen shells that surround the carbon chain. The forces are of the same order as those existing between helium atoms.

The mutual attraction between the chain molecules in a paraffin crystal is essentially due to polarization forces of the van der Waals type. Previous calculations (Müller 1936*a*) show that the lattice energy of a hydrocarbon crystal is accounted for by these forces within reasonable limits.

In the present paper an attempt is made to obtain more information about the forces acting between paraffin molecules, attention being concentrated chiefly on the repulsive forces.

The paper is in two parts. The first deals with experiments on the compressibility, the second with the nature and magnitude of the forces which hold the molecules together in the lattice.

Owing to the peculiar structure of the chain molecules, it is to be expected that the linear compressibilities vary considerably with the direction. The measurement of the total volumetric change with pressure is therefore ruled out in this investigation. The method adopted here relies upon the direct determination of the changes in the lattice dimensions with the aid of X-rays. The technical difficulties connected with this method are also discussed.

The compressibilities to be measured are of the order of 10^{-6}–10^{-5} $\text{cm.}^2/\text{kg.}$ A pressure of say 1000 atm. produces therefore a change of $\frac{1}{10}$–1% in the lattice dimensions. It is found that an effect of this order has to be aimed at, otherwise the uncertainties due to the reading errors in the position of the X-ray lines become too large. A change of this magnitude can under normal conditions be measured with a fair degree of accuracy. Under the present conditions there are unfortunately circumstances which reduce the accuracy; for instance, no focusing can be obtained owing to the small size of the specimen. The size has to be kept small for the following reason. The material is enclosed in a container which has to stand a pressure of at least 1000 atm. and the walls of the container must be kept as thin as possible in order to avoid heavy absorption of the X-rays. It is easily seen that this can be achieved only by keeping the volume of the specimen as small as possible. In the present work the actual volume irradiated by X-rays is a few cubic millimetres. This is not much considering that the distance between the specimen and the film is not less than 30 cm. and reaches 100 cm. in some of the experiments. Even under the most favourable conditions the absorption in the walls of the containers is large, and without the powerful X-ray sources available in the laboratory the work could not have been carried out. A large number of experiments were made to find the best material for the container and the most suitable design of the apparatus. It is not intended to give a record of the various designs, but a few may be mentioned which gave the best results.

In the first set of experiments the K_α lines of silver are used. They have a comparatively high penetrating power but have the disadvantage of giving small reflecting angles and poor photographic yield. The container is a small electron-metal tube of 2 mm. external diameter and 1 mm. bore. Another type of container has a thicker tube which is thinned down in two places so as to leave a thickness of about 1·5 mm. for the passage of the X-rays. The first stood up to a pressure of about 1000, the second to 1500 atm.

The second set of experiments is made with the far less penetrating copper rays. The electron metal has to be abandoned and the best results are obtained with beryllium containers backed by a surrounding steel tube with suitably drilled holes for the passage of the X-rays.

These containers are made in the following way. A heavy walled steel container with a fairly wide bore is filled with a stiff paste of powdered beryllium (grain size about 120 to an inch) and bakelite varnish. The volatile constituent of the paste is first removed by moderate heating. After this a tight-fitting piston rod of hardened steel is pushed down on the paste under high pressure and the material is baked at about 140° C while the pressure is on. The beryllium-bakelite plug in the steel container is now a solid mass which can be worked with a tool. A central hole of about 1 mm. diameter is drilled, just reaching slightly beyond a set of radial holes in the outer steel cylinder. These holes are of ample width to allow for the small variations in angle of the reflected beams. These containers are not always pressure-tight after the first baking. A leaky container can often be made tight by the addition of bakelite varnish and subsequent heating. A carefully made container with a 1 mm. hole and 1 mm. wall stands up to a pressure of 1000–1500 atm. The bore of the inlet and outlet holes for the X-rays is about 1·5 mm.

The containers described so far are suitable for experiments in which the rays are transmitted through the specimen. A pattern which is particularly suited for large-angle reflexions is built on slightly different lines. This container has a 1 cm. diameter hole with a flat portion at the closed end. Two slots 1 mm. wide are cut on the outside at right angles to each other and each along a diameter of the circular steel container. Near the centre at the bottom of one of the slots the material is removed so as to form a narrow window of about 5 mm. length and the same width as the slot. The beryllium treated in the same way as before covers the whole inside in a flat sheet 0·5 mm. thick. The paraffin is put on top of the beryllium layer. The X-rays pass along the slot, penetrate through the beryllium window and are reflected by the paraffin. A slight focusing effect is obtained here on account of the extension of the material. A thin sheet of lead is placed in the right-angle slot with its edge a few millimetres from the window. The opening acts as a slit of the type used in the Seemann X-ray spectrograph.

The substances investigated are

n-$C_{17}H_{36}$ m.p. 22° C, n-$C_{23}H_{48}$ m.p. 47° C, commercial wax m.p. 58° C
and n-$C_{29}H_{60}$ m.p. 64·5° C.

The deformation of the lattice in a plane perpendicular to the chain axes is obtained from measurements of the pressure shift of the two strongest reflexions 110 and 200. These two spacings are practically independent of the chain length; in other words, the two reflecting angles are the same for all the substances. The angles depend of course upon the wave-length of the X-rays. The linear compressibilities along the *a* and the *b* axes are calculated from the observed shift of the two lines. The changes of the *c* axes are derived from measurements of high orders of the long spacings. The corresponding reflexion angles are large and the intensities are smaller than those obtained from the 110 and 200 planes. The observations are made with the aid of the reflexion method.

Transmission photographs are taken with Ag and Cu radiation from a 5 kW generator with rotating anode. The distances between film and specimen are 50 and 100 cm. for Ag radiation and 30 cm. for Cu radiation. The times of exposure vary between 1 and 2½ hr.

Reflexion photographs are made with Cu radiation from the 50 kW generator. The absorption in the window is high and the reflected beam weak, so that in spite of the increased primary intensity the time of exposure remains the same as before.

The high pressure to which the specimen is subjected is produced by a hydraulic press. A thick-walled steel cylinder with a sliding piston of 1 cm.^{2} section is placed between the ram blocks of the press. The cylinder space is filled with oil and communicates through a steel capillary with the specimen container. Direct contact between the oil and the specimen is eliminated with the aid of a small steel plunger placed on top of the material. The pressure is read on a Bourdon gauge connected to the hydraulic press. The readings are corrected for the friction loss in the piston packing; they amount to about 25–30 % at 1000 atm.

The actual experiment is carried out as follows: A few cubic millimetres of the substance are put into the narrow hole of the specimen container with the small plunger on top. The container and the capillary are filled with oil and screwed together tightly. The oil-filled cylinder with its piston are placed between the ram blocks and the pressure is raised slowly up to its final value. A photograph is taken and after finishing the exposure the pressure is released. The second photograph is taken with the specimen at normal pressure. Both photographs are recorded side by side on the same piece of film. The shifts of the lines are small, usually between 1 and 3 mm. They are measured with a screw of known pitch and pointer, or directly with a ruler. The accuracy of these measurements is not high, the error being of the order of ± 10 %. Variations in the readings between successive experiments are of the same order. Table 1 gives an example of the magnitude of these variations.

The shifts of the spacings are calculated with the well-known expression

$$\frac{\Delta D}{D} = \frac{1}{2\tan\theta}\frac{\Delta l}{R},$$

$\Delta D/D$ = relative change of spacing, θ = glancing angle, Δl = observed shift of line, R = distance specimen film.

Table 2 gives the summary of the observed changes of the spacings 110 and 200 They are all reduced to a pressure difference of 1000 kg./cm.^{2} under the assumption that the changes are proportional to the pressure.

TABLE 1

Material	Pressure kg./cm.^{2}	Distance cm.	Shift 110 mm.	Shift 200 mm.	Radiation
$C_{23}H_{48}$	1200	100	2·7	2·3	Ag
	1200	100	2·0	1·8	Ag
Commercial	1400	30	1·6	2·0	Cu
wax	1400	30	2·0	2·0	Cu
	1400	30	2·0	2·7	Cu

TABLE 2. OBSERVED $\Delta D/D$ FOR A PRESSURE OF 1000 KG./CM.^{2}

Index	$C_{17}H_{36}$	$C_{23}H_{48}$	Commercial wax	$C_{29}H_{60}$
110	0·015	0·015	0·009	0·004
200	—	0·011	0·010	0·003

The changes of the *a* and the *b* axes are obtained from these observations with the aid of a simple geometrical analysis. They are given in table 3.

TABLE 3. RELATIVE CHANGES OF THE *a* AND THE *b* AXES DUE TO A PRESSURE OF 1000 KG./CM.^{2}

(Substances at room temperature)

	$\Delta a/a$	$\Delta b/b$
n-$C_{23}H_{48}$	$1{\cdot}1 \times 10^{-2}$	$1{\cdot}3 \times 10^{-2}$
Commercial wax	$1{\cdot}0 \times 10^{-2}$	$0{\cdot}9 \times 10^{-2}$
n-$C_{29}H_{60}$	$0{\cdot}3 \times 10^{-2}$	$0{\cdot}3 \times 10^{-2}$

There was only one photograph taken with $C_{17}H_{36}$. This substance being rather close to its melting-point at room temperature, the reflexions are weaker than those of the others. The 200 line was too faint to be measured with certainty. This is the reason why the data for this substance are not given in table 3. The fact that the displacement of the 110 line is of the same order as that observed with $C_{23}H_{48}$ suggests that the axial changes of

$C_{17}H_{36}$ are similar to those of the other paraffins. It will be noted that the figures in table 3 show a tendency to become smaller with increasing chain length, or, what amounts to the same, with increasing melting-point. This is likely to have a physical significance since the differences are just outside the error limit.

No change of the third or c axis is obtained within the present limits of accuracy. The observations of the 00(60) and 00(62) plane of $C_{29}H_{60}$ show no signs of a shift with pressure, in spite of the fact that the reflecting angles of these planes are more than three times as large as that of the 110 plane. From this it is estimated that the compressibility in the direction of the C axis is less than one-tenth of that of the other two.

There is an obvious similarity between this and an earlier observation (Müller 1932) dealing with the thermal expansion of paraffins. The expansion of the long axis is much smaller than that of the two axes perpendicular to it. Both phenomena have the same origin. Changes in the direction of the long axes are opposed by chemical binding forces; those perpendicular to this direction are counteracted by the much weaker polarization forces. The observations made with $C_{29}H_{60}$ can therefore be assumed to hold for all long-chain paraffins. The situation alters only when the chain length becomes of the same order as the gap between successive chains.

Table 4 gives a summary of the experiments dealt with in the first part of this paper.

TABLE 4. LINEAR COMPRESSIBILITIES IN THE DIRECTION OF THE MAIN AXES FOR SUBSTANCES AT ROOM TEMPERATURE

	$\frac{1}{\Delta p}\frac{\Delta a}{a}$ cm.²/dyne	$\frac{1}{\Delta p}\frac{\Delta b}{b}$ cm.²/dyne	$\frac{1}{\Delta p}\frac{\Delta c}{c}$ cm.²/dyne
n-$C_{23}H_{48}$	10×10^{-12}	11×10^{-12}	$< 3 \times 10^{-13}$
Commercial wax	9×10^{-12}	8×10^{-12}	$< 3 \times 10^{-13}$
n-$C_{29}H_{60}$	$2{\cdot}5 \times 10^{-12}$	3×10^{-12}	$< 3 \times 10^{-13}$

The object of the second part of this paper is to gain information about the repulsive forces acting between paraffin molecules. It is clear that the present enquiry can only deal with the order of magnitude of the forces.

A suggestion has already been made in a previous paper (Müller 1936*a*) about the lattice potential of paraffins, and subsequent calculations were published in the same year (Müller 1936*b*). For the sake of completeness some of the items are repeated here in slightly more detail. They are preliminary to a discussion involving the new experiments on compressibilities given in the first part of this paper.

The calculation of the compressibility from a potential function involves, as is well known, the second derivative of the potential, and is consequently a very stringent test. Before attempting such a test it seems to be advisable to proceed first with a less exacting enquiry. This will be done in the first part of the following discussion.

The suggestion made previously is this. The repulsion between paraffin molecules is governed by forces of the same type and the same magnitude as those existing in helium. Here is the argument in favour of this hypothesis.

The hydrogen atoms in a paraffin molecule form an envelope round the carbon chain. These hydrogen envelopes are in contact with each other in the crystal, and since the repulsion forces are known to be of a very short range it seems very likely that the main contribution to the repulsion potential originates from the hydrogen atoms. We now take a single CH_2 group and approach one of the hydrogen atoms in the direction of C—H bond from the outside. The spin of the hydrogen atom being compensated by the chemical binding and the electron density being similar to that of a helium atom, it is to be expected that the repulsive force of a combination CH ↔ HC is of the same order as that acting between a pair of helium atoms. This conclusion is supported by chemical evidence, for it is well known that the saturated paraffins are not attacked by strong chemical reagents and that they resemble in this respect the inert helium.

The repulsion potential of helium has been calculated from first principles by Slater (Slater 1928). He finds for one pair of helium atoms

$$\phi_a = 7{\cdot}70 \times 10^{-10} \times e^{-2{\cdot}43R/a_0}\,\text{erg},$$

where R is the distance between the nuclei and a_0 the Bohr radius 0·528 A.

(It happens that owing to a numerical coincidence

$$e^{-2{\cdot}43/0{\cdot}528} = 10^{-1{\cdot}999} \sim 10^{-2{\cdot}00}.$$

Slater's formula can therefore be written in the following simple form:

$$\phi_a = 7{\cdot}70 \times 10^{-10} \times 10^{-2{\cdot}00R}\,\text{erg},$$

R in A.)

Applying Slater's expression to our problem, we have to introduce for R the actual distances between the hydrogen centres in the paraffin lattice. Only those atoms that are closest together give an appreciable contribution towards the potential. This distance is known from previous work on the structure of paraffin. It is found to be 2·4 A. Taking into account the correct number of co-operating pairs of hydrogen atoms, this results in a repulsion potential of about 2×10^{-14} erg per CH_2 group. The van der Waals attraction potential is about $1{\cdot}5 \times 10^{-13}$ erg. This shows at once that the repulsion potential is not only of the right order of magnitude but leaves an excess of attraction energy that agrees quite well with the directly observed sublimation energy of a paraffin crystal.

In fact the hypothesis of the approximate identity of the repulsion in helium and paraffin goes even further. In a paper dealing with certain physical properties of solid hydrocarbons (Müller 1936*b*), a set of figures is given representing the values of the van der Waals and the repulsion potential as a function of the setting angle of the chain molecules in the lattice. The physical meaning of this setting angle ϕ as shown on figure 3 (Müller 1936*a*) is briefly the following: Assuming the chain axes in a paraffin crystal are kept parallel at a fixed distance from each other in conformity with structure data, the molecules have still one degree of freedom left, namely, the rotation round their long axes. There is only one degree on account of the symmetry of the system. The angle related to this degree of freedom is called the setting angle ϕ. Any variation of this angle alters the distances between the atoms of neighbour molecules and therefore affects the lattice potential. We give first the variations of the attraction potential (table 5).

TABLE 5. VAN DER WAALS POTENTIAL OF 1 CH_2 GROUP IN SOLID PARAFFIN AS A FUNCTION OF THE SETTING ANGLE ϕ

ϕ	Calculated with polarization and ionization potential erg	Calculated with polarization and susceptibility erg
0°	$-1{\cdot}86 \times 10^{-13}$	$-3{\cdot}10 \times 10^{-13}$
30°	$-1{\cdot}52 \times 10^{-13}$	$-2{\cdot}58 \times 10^{-13}$
60°	$-1{\cdot}48 \times 10^{-13}$	$-2{\cdot}55 \times 10^{-13}$
90°	$-1{\cdot}75 \times 10^{-13}$	$-3{\cdot}00 \times 10^{-13}$

The way these figures are calculated is explained in Müller (1936*a*). Atomic centres are used. The first set of figures involves the use of ionization potential and polarization of the atomic centres, the second their polarization and susceptibility. The second set has already been published in a previous paper (Müller 1936*b*). Both methods of calculation are equally justifiable. It is found, however, that the figures in the first column agree better with the latest experimental data on the heat of sublimation given by Ubbelohde (1938).

Table 6 gives the repulsion potential calculated with Slater's helium potential

TABLE 6. REPULSION POTENTIAL OF 1 CH_2 GROUP IN SOLID PARAFFIN AS FUNCTION OF THE SETTING ANGLE ϕ

ϕ	n	D_1 A	I, repulsion potential erg	n	D_2 A	II, repulsion potential erg
0°	4	2·11	$0{\cdot}93 \times 10^{-13}$	8	3·18	$0{\cdot}013 \times 10^{-13}$
30°	4	2·41	$0{\cdot}23 \times 10^{-13}$	4	2·94	$0{\cdot}020 \times 10^{-13}$
60°	2	2·24	$0{\cdot}25 \times 10^{-13}$	2 2	2·57 2·99	$0{\cdot}067 \times 10^{-13}$
90°	2	1·95	$0{\cdot}99 \times 10^{-13}$	4	3·07	$0{\cdot}011 \times 10^{-13}$

Total repulsion

ϕ	Erg
0°	$0{\cdot}94 \times 10^{-13}$
30°	$0{\cdot}25 \times 10^{-13}$
60°	$0{\cdot}31 \times 10^{-13}$
90°	$1{\cdot}00 \times 10^{-13}$

n = number of H atoms in the lattice having the same distance from either of the two hydrogens in the CH_2 group.

D_1 = minimum distances between the H atoms in the CH_2 group and the surrounding H atoms in the lattice.

D_2 = second nearest distances.

Comparison between the figures in I and II show the very rapid decrease of the potential with increasing distance. The next smallest terms are negligible. (The figures for the total repulsion differ slightly from those given in the previous paper (Müller 1936*b*). The differences are due to small errors in the earlier calculations.)

We now come to the second point in the argument. The minimum energy of the van der Waals potential as shown in table 5 occurs when the setting angles are either 0° or 90°. This is in contradiction with X-ray observations, for it is found that the setting angle lies definitely between these two extremes. This discrepancy vanishes if the repulsive forces are taken into account as is shown in table 7.

TABLE 7. TOTAL POTENTIAL (VAN DER WAALS + REPULSION) OF 1 CH_2 GROUP IN SOLID PARAFFIN

ϕ	Erg
0°	$-0{\cdot}92 \times 10^{-13}$
30°	$-1{\cdot}27 \times 10^{-13}$
60°	$-1{\cdot}17 \times 10^{-13}$
90°	$-0{\cdot}75 \times 10^{-13}$

The minimum potential is now shifted to a region between the two extremes $\phi = 0°$ and $\phi = 90°$ and the results of the calculation agree with experimental evidence. The lower absolute values of the van der Waals potential in table 5 are used in the calculation of the data in table 7. The conclusion as regards the position of minimum energy is not altered if the other set of figures is introduced. The first gives the best agreement with the latest experimental data on the heat of sublimation (Ubbelohde 1938). They are -1 to $-1\cdot3 \times 10^{-13}$ erg per CH_2, whereas the calculated minimum energy in table 7 is $-1\cdot27 \times 10^{-13}$ erg.

The present argument is carried a step farther if we take into account the difference between the maximum and the minimum energies in table 7. This difference is about 3×10^{-14} erg per CH_2 and measures the size of the potential barrier that has to be surmounted when the molecules rotate round their long axes. It must be remembered that the figures in table 7 refer to any hydrocarbon whose melting-points are at least 15–20° C above room temperature. These substances have a chain length of not less than say 20 carbon atoms. The total barrier for such a molecule is $20 \times 3 \times 10^{-14}$ erg $= 6 \times 10^{-13}$ erg. The kinetic energy of a rigid rotator at room temperature is approximately $300 \times \frac{1}{2}k = 2 \times 10^{-14}$ erg or only $\frac{1}{30}$ of the potential barrier. Free rotation of the molecule as a whole is therefore infrequent at room temperature, as is shown directly by observations of the dielectric constants of long-chain monoketones (Müller 1937). This holds no longer when the substance is kept at a temperature just below the melting-point. Previous experiments (Müller 1932) show that these substances increase their volume considerably in a range of 15–20° C below their melting-points. This increase lowers the height of the potential barrier to such an extent that it becomes comparable in magnitude with the kinetic energy of free rotation. The calculation is very simple. The minimum distance between hydrogen atoms is, according to table 6, 2·41 A (setting angle 30°); this holds for room temperature. At the melting-point the corresponding distance as obtained from direct lattice measurements is 3·15 A. The ratio of the corresponding repulsion potentials calculated with Slater's formula (simplified form) is therefore $10^{-2(2\cdot41-3\cdot15)} \sim 30$, which substantiates the above statement. Free rotation is therefore to be expected near the melting-point, and this is again in agreement with the observations on ketones mentioned before. Concluding the first part of the discussion it can be said that the proposed potential function gives a good account of the energy and energy changes of the hydrocarbon crystal.

The analogy between helium and paraffin cannot be expected to go much further. A rough calculation of the compressibility illustrates this clearly, since it is found that the result has the wrong sign.

For the purpose of further comparison it seems reasonable, however, to assume that the general law of repulsion in paraffin has the same form as Slater's helium potential, i.e.

$$V_R = Me^{-\epsilon r}.$$

The constants in this formula are to be determined with the aid of experimental data such as energy and compressibility. It is to be expected that the figures obtained in this way should not differ very much from those in the helium potential. This holds in particular for the constant ϵ.

A rigorous treatment, apart from being very tedious, is barred by the fact that the system we are dealing with is at room temperature and therefore not static. Too little is known about the thermal effect upon the compressibility in this particular problem. It is neglected in the following approximate calculations. An accurate treatment would further be rendered illusory by the inaccuracy of the present experiments.

The calculation of the compressibility requires the knowledge of the second derivative of both the van der Waals and the repulsion potential. The rigorous calculation of this quantity is tedious, particularly in the case of the van der Waals potential. The present approximate calculations are made with 50 terms of the Σ'/R^6 series. The numerical values of R and the angles between these vectors and the crystal axes are taken from the structure model. The angles enter into the derivatives of the potential. A rough estimate is made of the error due to the breaking off of the series and the figures are corrected for this error. The result of the numerical calculations is given in table 8.

TABLE 8. VAN DER WAALS POTENTIAL V_A AND TOTAL DERIVATIVES OF V_A FOR 1 CH_2 GROUP IN EQUILIBRIUM POSITION. SETTING ANGLE 30°

Potential	First total derivative	Second total derivative
V_A	$\frac{\partial V_A}{\partial a} + \frac{\partial V_A}{\partial b}\frac{\Delta b}{\Delta a}$	$\frac{\partial^2 V_A}{\partial a^2} + 2\frac{\partial^2 V_A}{\partial a \partial b}\frac{\Delta b}{\Delta a} + \frac{\partial^2 V_A}{\partial b^2}\left(\frac{\Delta b}{\Delta a}\right)^2$
Calculated with ionization potential and polarization		
erg	dyne	dyne/cm.
$-1{\cdot}52 \times 10^{-13}$	$2{\cdot}60 \times 10^{-5}$	$-5{\cdot}5 \times 10^{3}$
Calculated with polarization and susceptibility		
$-2{\cdot}57 \times 10^{-13}$	$4{\cdot}26 \times 10^{-5}$	$-8{\cdot}3 \times 10^{3}$

$\partial V_A/\partial a$, $\partial V_A/\partial b$, $\partial^2 V_A/\partial a^2$, $\partial^2 V_A/\partial b^2$ and $\partial^2 V_A/\partial a \partial b$ are the partial derivatives of V_A, and Δa and Δb the increments of the a and the b axes. The increment of the c axis, being much smaller than the two others, is assumed to be zero.

The ratio $\Delta b/\Delta a$ is $\frac{2}{3}$. The experimental data in table 3 show that $\Delta a/a$ is equal to $\Delta b/b$ within the limits of error, and since the axial ratio b/a is $\frac{2}{3}$ it follows that $\Delta b/\Delta a = \frac{2}{3}$.

The calculation of the repulsion potential is much simpler. Only four terms are taken into account. They are all due to those hydrogen atoms that are closest to the two hydrogens in the CH_2 group for which the potential is calculated. The higher terms are much smaller. They are neglected here.

TABLE 9. REPULSION POTENTIAL V_R AND DERIVATIVES FOR 1 CH_2 GROUP IN EQUILIBRIUM POSITION. SETTING ANGLE 30°

V_R erg	First derivative dyne	Second derivative dyne/cm.
$2Me^{-2 \cdot 41\epsilon}$	$-2 \times 1 \cdot 005 \times 10^8 M\epsilon e^{-2 \cdot 41\epsilon}$	$2 \times 10^{16} Me^{-2 \cdot 41\epsilon} \quad (1 \cdot 010\epsilon^2 - 0 \cdot 180\epsilon)$
	$= -1 \cdot 005 \times 10^8 \epsilon V_R$	$= 10^{16} (1 \cdot 01\epsilon^2 - 0 \cdot 18\epsilon) V_R$

ϵ is measured in $10^8 \times 1$/cm. units (A^{-1}).

Here again the angles between the radii and the axes enter into the calculation. 2·41 A is the equilibrium distance between the nearest hydrogen atoms. The factor 2 is obtained as follows: The potential of one pair of hydrogen atoms is

$$Me^{-\epsilon r}.$$

The lattice potential is $\qquad V_R = \frac{1}{2} \Sigma \kappa M e^{-\epsilon r_\kappa},$

and since we have four atoms of the same kind the potential is equal to

$$V_R = \tfrac{1}{2} \times 4 \times Me^{-\epsilon r}.$$

We have now all the data necessary for the evaluation of the constants M and ϵ and of the compressibility.

The calculation is again carried out with the two sets of figures given in table 8.

The lattice energy of a CH_2 group is about 1×10^{-13} erg according to the latest experiments. The van der Waals potential calculated with the first set of constants is $-1 \cdot 52 \times 10^{-13}$ erg. Therefore

$$V_R = 0 \cdot 52 \times 10^{-13} \text{ erg} = 2Me^{-2 \cdot 41\epsilon}.$$

With the second set of constants it is

$$V_R = 1 \cdot 57 \times 10^{-13} \text{ erg}.$$

These values are now substituted in the expressions given in table 9.

Since the system is in equilibrium we have

$$\text{First derivative of } (V_A + V_R) = 0,$$

and therefore from tables 8 and 9

$$\epsilon = \frac{2{\cdot}60 \times 10^{-5}}{1{\cdot}005 \times 0{\cdot}52 \times 10^{8} \times 10^{-13}} = 5{\cdot}0 \text{ A}^{-1},$$

or with the second set

$$\epsilon = \frac{4{\cdot}26 \times 10^{-5}}{1{\cdot}005 \times 1{\cdot}57 \times 10^{8} \times 10^{-13}} = 2{\cdot}7 \text{ A}^{-1}.$$

We simplify the calculation of the compressibility assuming the substance to be isotropic in a plane normal to the chain axes. The error thus introduced is unimportant. It does not affect the order of magnitude of the resulting figure. Under these conditions we have

$$\text{Linear compressibility} = \frac{q}{l} \times \frac{1}{\text{second derivative of total potential}},$$

where q is the cross-section of one CH_2 group measured in a plane parallel to the chain axes and l the distance between successive planes containing the axes of the chains and being parallel either to the a or the b axes of the crystal. If q is measured in a plane containing the a and the c axis, its numerical value is $1{\cdot}27 \times 7{\cdot}4$ A^2, and the corresponding distance $l = 2{\cdot}5$ A; if it is measured in the bc plane, we have $q = 1{\cdot}27 \times 4{\cdot}95$ A^2 and $l = 3{\cdot}7$ A. These data are taken directly from the structure model of the paraffin crystal. The q/l obtained with these data differ from each other. The average q/l is $2{\cdot}7_3$ A.

Table 10 gives the second derivatives of the total potential. These are calculated with the two sets of figures for ϵ and V_R given above and the data in tables 8 and 9.

TABLE 10. CALCULATED SECOND DERIVATIVES OF THE TOTAL POTENTIAL $V_A + V_R$

With $\epsilon = 5{\cdot}0$ A^{-1} and $V_R = 0{\cdot}52 \times 10^{-13}$ erg	$7{\cdot}2 \times 10^3$ dynes/cm.
With $\epsilon = 2{\cdot}7$ A^{-1} and $V_R = 1{\cdot}57 \times 10^{-13}$ erg	$2{\cdot}5 \times 10^3$ dynes/cm.

The calculated compressibilities are therefore

$$2{\cdot}7 \times 10^{-8}/7{\cdot}2 \times 10^3 = \underline{3{\cdot}8 \times 10^{-12}} \text{ cm.}^2\text{/dyne}$$

with the first and

$$2{\cdot}7 \times 10^{-8}/2{\cdot}5 \times 10^{3} = \underline{10{\cdot}8 \times 10^{-12}} \text{ cm.}^2/\text{dyne}$$

with the second value in table 10.

The experimental data vary between $2{\cdot}5 \times 10^{-12}$ and 11×10^{-12} cm.^{2}/dyne according to table 4, i.e. the calculation gives the right order of magnitude.

The present calculations neglect the effect of the thermal motion. In comparing calculations and experiment it is consistent to select those values of the compressibilities that are least affected by temperature; in other words, the measurement on the substance with the longest chain and the smallest compressibility. Doing so it appears that the first set of figures in table 10 give the best agreement between calculation and observation.

The repulsion potential of one pair of hydrogen atoms in the paraffin crystal is therefore

$$44 \times 10^{-10} \times e^{-5{\cdot}0R} \text{ erg per H—H,}$$

whereas the Slater potential for helium is

$$7{\cdot}7 \times 10^{-10} \times e^{-4{\cdot}6R} \text{ erg per He—He.}$$

R = distance in A units.

The factors of R in the exponentials differ by about 10 %. The value of the equilibrium potential at $R = 2{\cdot}4$ A is $0{\cdot}52 \times 10^{-13}$ erg for H—H and about half this figure for He—He.

It is possible that the repulsion effect may not be entirely due to the hydrogens and that the effect of the next nearest C—H combinations ought to have been taken into account. This might possibly make the similarity between the helium and the paraffin hydrogens still closer. Attempts to discuss this matter have to be postponed until better experimental data are available. The preceding calculations indicate that the present assumptions are essentially correct.

In conclusion, the writer wishes to thank Mr H. Smith for his untiring help and for many valuable technical suggestions in connexion with the design of the beryllium pressure containers. He also expresses his appreciation to the director and the managers of the Royal Institution for their kind interest in this work.

References

Müller, A. 1932 *Proc. Roy. Soc.* A, **138**, 514.
Müller, A. 1936*a* *Proc. Roy. Soc.* A, **154**, 624.
Müller, A. 1936*b* *Helv. Phys. Acta*, **9**, 626.
Müller, A. 1937 *Proc. Roy. Soc.* A, **158**, 403.
Slater, J. C. 1928 *Phys. Rev.* **32**, 349.
Ubbelohde, A. R. 1938 *Trans. Faraday Soc.* **34**, 282.

The electronic charge

By V. D. Hopper, M.Sc. and T. H. Laby, F.R.S.
University of Melbourne

(*Received* 3 *March* 1941)

[Plate 6]

The determination of e by a new oil-drop method in which the electric field is horizontal has been described. The expression for e in terms of quantities measured is similar to that which applies to H. A. Wilson's method. The correction for the departure from Stokes's law is obtained from Millikan's relation

$$e_1^{\frac{2}{3}} = e^{\frac{2}{3}} + m/pa,$$

where e_1 is the uncorrected value of e, p cm. of mercury is the pressure and a cm. the radius of the drop. The oil drops used are larger than those used by previous experimenters, and their velocity of fall and the velocity in the direction of the electric field could be estimated with satisfactory accuracy.

Assuming $\eta_{23} = 1830 \times 10^{-7}$ c.g.s. unit, the value of e obtained is $(4{\cdot}8020 \pm 0{\cdot}0013) \times 10^{-10}$ e.s.u. The probable error calculated by the least squares is about one-third of that obtained by Millikan, whose result becomes $(4{\cdot}7992 \pm 0{\cdot}0037) \times 10^{-10}$ e.s.u., when the above value of η_{23} is assumed. The errors in the determination of η_{23} by the rotating cylinder and the capillary tube method are discussed and the final mean

$$\eta_{23} = (1830{\cdot}06 \pm 2{\cdot}5) \times 10^{-7} \text{ c.g.s. unit.}$$

is derived. This contributes an error of 1 in 500 in e and is its major uncertainty by the oil-drop method. Recent determinations of the electronic charge by the X-ray method have been analysed. The mean value of e by this method is deduced to be $(4{\cdot}8044 \pm 0{\cdot}0007) \times 10^{-10}$ e.s.u., and this result differs from the mean of the determinations of Millikan and the authors $(4{\cdot}8007 \pm 0{\cdot}002) \times 10^{-10}$ e.s.u., by $0{\cdot}0037 \times 10^{-10}$ e.s.u., which is less than the error due to the viscosity of air. Assuming the X-ray value of e, the viscosity of air can be deduced and is found to be $(1830{\cdot}9 \pm 0{\cdot}5) \times 10^{-7}$ c.g.s. unit at 23° C.

INTRODUCTION

The values of three of the general constants of physics, e, h and e/m, have been the subject of much discussion and experiment. Discrepancies exist such as the disagreement in the value of e as found by the drop and the X-ray methods, and the disagreement between the value of Rydberg's constant calculated from e, h and e/m and its observed value.

It would appear that these discrepancies can only be removed by improvements in the methods which are used in the determination of the constants. Of the many methods which have been used to determine the electronic charge, the oil-drop and the X-ray methods are accepted as the more reliable. It is true that the reliability of the drop method has been questioned, and one of the authors believed, until he had carried out experiments by the X-ray method, that it would be the more accurate of the two methods. The conclusions which we have reached in the course of the experiments described below is that the highest accuracy attainable by the drop method has not yet been reached, that the uncertainty as to the correct value of the viscosity (η) of air is the major error in the value of e by this method, and that when the uncertainty as to the value of η is removed the accuracy of the drop method will equal that of the X-ray method as it has so far been developed.

ASSUMPTIONS OF THE DROP METHOD

The drop method, introduced by H. A. Wilson and used by him with water, was improved by Millikan by the use of oil drops. Millikan and his co-workers in experiments from 1906 to 1917 established that Stokes's law in a corrected form applied to a drop of liquid falling through a gas, and that Einstein's theory of the Brownian motion applied too. Cunningham in 1910 gave a theoretical deviation for the correction to be applied to Stokes's law for a sphere moving in a gas. These brilliant investigations placed the assumptions made in the drop method on a sound foundation of experimentally verified theory, and are the justification of an attempt to improve the experimental application of those principles in the measurement of e. (This symbol is used as an abbreviation for 'value of the electronic charge'.)

In the method to be described here there is a departure from the principle of H. A. Wilson's experiment in which the electric and gravitational fields are parallel, and the electric field changes the speed of fall without changing its direction.

In the method of the authors the electric field is horizontal and it changes the direction of fall. This, when combined with a photographic method of measuring the velocity of the drop, has the advantage that departures from Stokes's law, the presence of convection currents in the air, a change in the charge of the drop, and any error in the direction of the electric field can be detected.

The accuracy with which e can be measured by the drop method is limited by the accuracy with which the viscosity of air, η, and its variation with temperature are known, since $e \propto \eta^{\frac{3}{2}}$. Some forty determinations of η have been made, and the value of η to be accepted is discussed later.

Criticisms of drop measurements of e. Millikan (1913–30) made two series of measurements of e, one of which gave fifty-eight values of e and the other twenty-five values. Ishida, Fukushina and Suetsuga (1937) and Bäcklin and Flemberg (1936) have also measured e by the drop method. Table 1 contains the range of values of a cm., the radius, and t sec., the times of fall, of the ten largest drops used in previous measurements of e by the drop method.

TABLE 1

a cm.	t sec.	Observers
$1{\cdot}7 - 4{\cdot}3 \times 10^{-4}$	$3{\cdot}7 - 22$	Ishida, Fukushina and Suetsuga
$2{\cdot}4 - 5{\cdot}8 \times 10^{-4}$	$4{\cdot}4 - 15$	Millikan (1913)
$1{\cdot}65 - 2{\cdot}3 \times 10^{-4}$	$14{\cdot}1 - 26{\cdot}8$	Millikan (1917)
$0{\cdot}83 - 1{\cdot}8 \times 10^{-4}$	—	Bäcklin and Flemberg

In the above measurements the time t has been measured by an 'eye and hand' method closely similar to that used in meridian observations of stars with a fixed wire micrometer and tapping key. The errors to which such observations are subject have been discussed by Spencer Jones (1938).

Table 2 of this reference (Spencer Jones 1938) shows that the personal equation of two observers may differ by as much as 0·47 sec., and this is evidence that the personal error must be considered in the timing of drops.

We conclude from data given in Millikan's paper that:

(1) his Hipp chronoscope had a rate of $+0{\cdot}2\,\%$;

(2) the combined personal and chronoscope error

$$\text{start} - \text{stop} \doteq +0{\cdot}023 \text{ sec.};$$

(3) the mean departure from the mean $= \pm 0{\cdot}05$ sec.

Millikan corrects for the systematic error (1), and possibly for the systematic error (2). The random error (3) necessarily enters into the value of e derived from the experiments. Insufficient data are available to evaluate the effect of this timing error on Millikan's value of e, but the following indicates its magnitude. If the time of free fall is $30 \pm 0{\cdot}05$ sec., and of ascent in the electric field is $80 \pm 0{\cdot}05$ sec., the error in $(1/t_g + 1/t_F)(1/t_g)^{\frac{1}{2}}$ is $\pm 0{\cdot}20\,\%$, and this is the error in e. If $t_g = 4{\cdot}4 \pm 0{\cdot}05$ sec., the minimum resulting error in e is over 1 %. Thus the eye-and-hand method of timing cannot be used with large drops. A large number of observations will of course reduce the random error of their mean, but the systematic personal error ((2) in above list) cannot be so eliminated.

We have timed drops by photographing them with an exposure of 0·00067 sec. at intervals of 0·04 sec. In the case of the drop of maximum velocity of 1 cm./sec. the image velocity on the photographic plate is 12 cm./sec., and the position of the image could be measured in some cases to better than 0·0007 cm., which is equivalent in time to 0·00006 sec. This estimate gives the error in timing due to the error in measuring the photographic plates as 1 in 10,000. The error in the speed of the timing disk is discussed later.

Optimum size of drop. Errors of timing are least for slowly moving and therefore for small drops, but the errors due to Brownian motion and to Stokes's law correction both increase as the drop radius, a, decreases. In the previous determinations it will be seen from the above table that the 10 drops which are most important to Millikan's 1913 value of e were timed for a period of from 4·4 to 15 sec., and the error of timing for these drops is larger than the Brownian or Stokes errors. Millikan in his 1917 measurements used smaller drops than in 1913, and while this decreases the timing error it increases that due to Brownian motion, and the error of extrapolation required in the Stokes correction.

With photographic timing the use of drops larger than the largest we used (radius $9{\cdot}6\mu$) would have reduced the already small Stokes correction of our experiments. An unexpected difficulty arises in the use of larger drops. Oil drops when formed have a charge $\pm ne$, where n is roughly proportional to a^3 for a given oil. n was so large for castor oil that only a few measurements with that oil could be used. Even for apiezon oil one drop gave

$$n = 276\,(a = 7{\cdot}4\mu),$$

which was as large as was desirable in these experiments. The precision of the measurement of e limits the maximum value of n which can be used if ambiguity in the choice of n is to be avoided.

Brownian motion. The mean displacement $\overline{\Delta x}$ of a drop in a time τ in a medium of viscosity η is

$$(\overline{\Delta x})^2 = RT\tau/(3\pi\eta Na), \tag{1}$$

where R, N are the gas and Avogadro's constants, and T the absolute temperature. The velocity of free fall is

$$v = 2\rho g a^2/9\eta. \tag{2}$$

Putting $x = v\tau$, where x is the distance moved by the drop in time τ, then

$$\overline{\Delta x}/x = c/a^{\frac{5}{2}}\tau^{\frac{1}{2}}, \tag{3}$$

where c is a constant. Thus the Brownian motion error $\Delta\bar{x}/x$ is proportional to $a^{-\frac{3}{2}}$.

$$\text{For } a = 1{\cdot}7\times 10^{-4} \text{ cm. and } \tau = 29 \text{ sec.,} \quad \overline{\Delta x}/x = 2{\cdot}0\times 10^{-3},$$

$$\text{For } a = 10\times 10^{-4} \text{ cm. and } \tau = 0{\cdot}5 \text{ sec.,} \quad \overline{\Delta x}/x = 1{\cdot}8\times 10^{-4}.$$

The first line applies to a drop used by Millikan, and the second line to a drop used in our experiments.

Correction to Stokes's law. Millikan, to correct for the effect of the discontinuity of the medium, plotted $e_1^{\frac{2}{3}}$ against $1/pa$, where e_1 is the uncorrected value of e obtained from the observations and p is the pressure of the gas in which the drop moves. The points fell on a straight line, given by the equation

$$e_1^{\frac{2}{3}} = m/pa + e^{\frac{2}{3}}. \tag{4}$$

Extrapolating to $1/pa \rightarrow 0$, the value of $e^{\frac{2}{3}}$ for $pa \rightarrow \infty$ is found. The accuracy of $e^{\frac{2}{3}}$ calculated from the observations will depend on the range of the values of $1/pa$ covered and upon the observations being accurate at both ends of the range. It is to be noticed, however, that when $1/pa$ is small with visual observations the timing error is large, and when $1/pa$ is large Brownian motion displacements are large. These considerations require the use of drops with a sufficiently large range of values of a, and that for the smallest drop used the Brownian motion error should not be large.

PRINCIPLE OF METHOD

The drop first falls under gravity between two vertical plates, is illuminated intermittently, and appears as a series of bright stars on a black background. Then a horizontal electric field is applied and the drop is deflected laterally along a straight path inclined at an angle θ to the vertical. The photographic plate shows a series of black dots on a light background (see figure 1, plate 6).

Let v_g be the vertical velocity of the drop when no electric field is applied. Applying Stokes's law we have

$$mg = 6\pi\eta a v_g, \tag{5}$$

where m is the mass of the drop. Thus

$$\tfrac{4}{3}\pi a^3(\rho-\sigma)\,g = 6\pi\eta a v_g$$

(ρ being the density of the oil and σ that of the air), and

$$a^2 = \tfrac{9}{2}\eta v/(\rho-\sigma)\,g. \tag{6}$$

When an electric field of strength X is applied, the drop quickly reaches a terminal velocity of r at an angle θ to the vertical. If v_x is the velocity of the drop in the direction of the field then, applying Stokes's law,

$$Xne = 6\pi\eta a v_x. \tag{7}$$

Substituting for a we have

$$Xne = 9\sqrt{2}\,\pi\eta^{\frac{3}{2}}(\rho-\sigma)^{-\frac{1}{2}}g^{-\frac{1}{2}}v_g^{\frac{1}{2}}v_x. \tag{8}$$

v_g was measured directly, and v_x can be calculated from a measurement of two of the three quantities r, θ and v_g' (v_g' being the vertical velocity of the drop after deflexion). In the tabulated results v_x is calculated from the expression

$$v_x = \frac{r\sin\theta}{\cos\delta}, \tag{9}$$

where δ is the direction of the field from the horizontal and is calculated from the expression

$$\tan\delta = \frac{v_g - v_g'}{r\sin\theta}. \tag{10}$$

It is not necessary to measure v_g, v_g' and r for other oil drops, as only two of these measurements are necessary, but in general all three were measured to check the value of δ.

Time to reach terminal velocity. The time taken for a drop to reach terminal velocity after deflexion can be derived as follows:

Assuming the electric field to be horizontal and to act in the z direction, the equation of motion of the drop is given by the equations

$$Xne - 6\pi\eta a\dot{z} = m\ddot{z} \tag{11}$$

and

$$mg - 6\pi\eta a\dot{y} = m\ddot{y}. \tag{12}$$

Consider equation (11) and let $k = (6\pi\eta a/m)$ and $(Xne/m) = L$, i.e. the equation becomes

$$L - k\dot{z} = \ddot{z}.$$

The solution of this is $z = c_1 + c_2 e^{-kt} + (L/k)\,t$,

where c_1 and c_2 are constants. Initially

$$t = 0, \quad z = 0, \quad \dot{z} = 0, \quad c_1 + c_2 = 0, \quad \text{and} \quad c_2 = L/k^2,$$

i.e.

$$\dot{z} = -(L/k)(e^{-kt} - 1).$$

Let $\dot{z}_e$ be the terminal velocity (i.e. $\dot{z}$ when $t \to \infty$), then $\dot{z}_e/\dot{z} = (1 - e^{-kt})$.

When $$(\dot{z}_c - \dot{z})/\dot{z}_c = 1/10{,}000 \quad \text{and} \quad a = 5\mu,$$

$$t < 0{\cdot}003 \text{ sec.}$$

Thus a drop (radius 5μ) takes less than 0·003 sec. to reach within 1 part in 10,000 of its terminal velocity.

MICROPHOTOGRAPHY OF MOVING DROPS

Accuracy in the calculation of the electric field requires the condenser plates between which the oil drops move to be several times as wide as their distance apart. The plates are 0·4985 cm. apart, and a microscope objective of focal length 3·8 cm. was chosen to enable the plates to be made sufficiently wide.

The photography of small drops moving with a velocity of about 1 cm./sec. with an exposure of 1/1500 sec. using an objective of small numerical aperture requires some departure from normal photographic method.

As it was desired to improve the definition of the image by the use of a fine-grained plate, a high intensity of illumination on a dark background is necessary. A condenser was designed to give a hollow cone of light, the apex of which was at the drop. The angle of the cone of light was sufficiently large for none of its light to enter the objective. A 20 amp. mirror arc gave ample illumination. A system of filters and shutters reduced the radiation from the arc absorbed in the enclosure in which the drops fell to such a small amount that no convection currents were set up in the air surrounding the drops.

The details of the above-mentioned arrangements are shown in figures 2*a* and 2*b* and are described below under the headings: optical system, illumination, shutters, photography, magnification, etc.

Optical system. Light from the arc (see figure 2) is focused by its mirror on the dark-ground condenser, and is refracted by it to form a hollow cone of angle of about 40°. This gives with the objective used dark-ground illumination. Refracted and scattered light from the drop is focused by the Zeiss 1½ in. objective on the photographic plate, at such a distance as to give a magnification of × 12·001. A reflecting prism can be turned to throw the light beam into a focusing microscope which is adjusted to be in focus when the camera is exactly focused. It enables visual observations to be made of the field to be photographed; its prism is turned out just before exposures are made.

The Leitz microscope, from which the apparatus is constructed, is supported on a microcamera stand, which is levelled to make the direction of the electric field horizontal. The microcamera and the copper box containing the

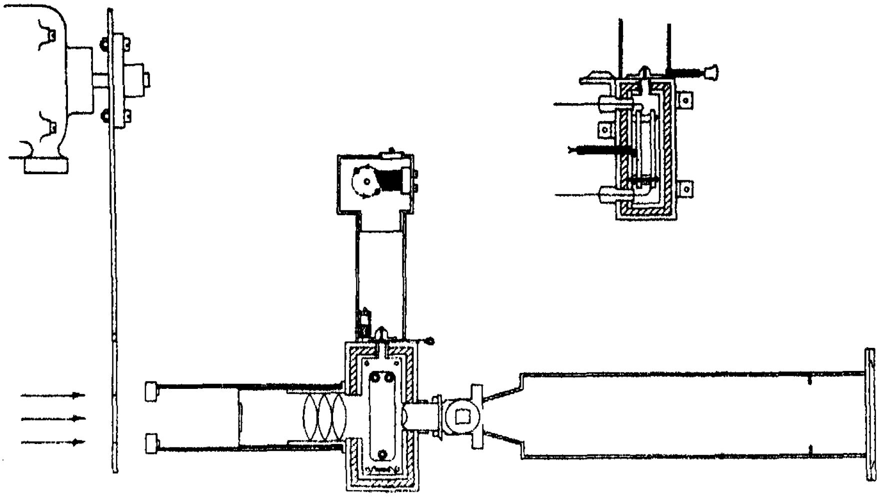

FIGURE 2a. Design of apparatus.

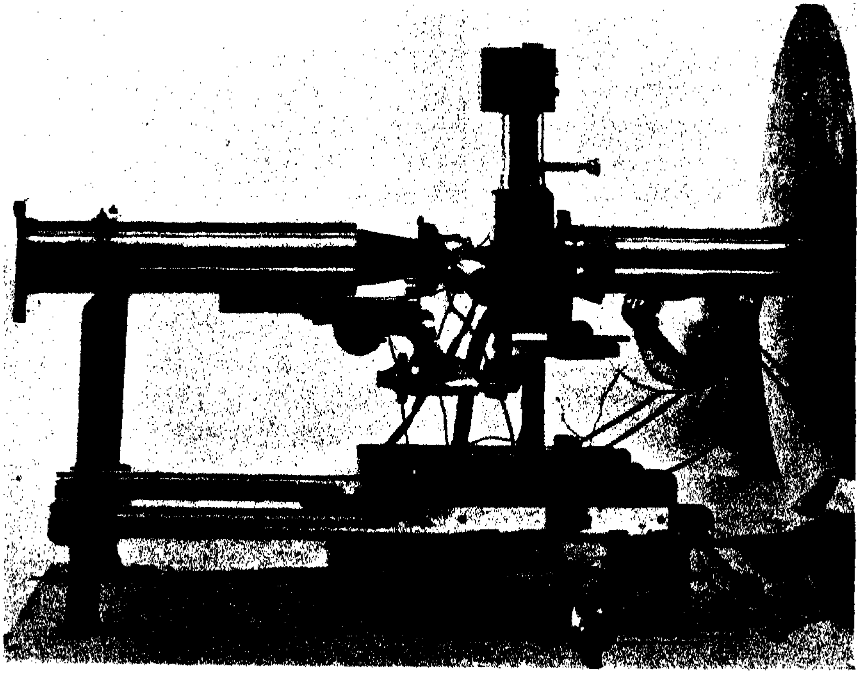

FIGURE 2b. Photograph of apparatus.

condenser were carefully designed to be rigid and retain adjustments once made.

The dark-ground condenser is shown in figure 2. Its design was reached after many other systems had been tested. It consists of three achromatic lenses of 10 cm. focal length, an exit stop of 1 in. diameter placed about 1 in. from the last lens, and a compur shutter with iris diaphragm which covers the entrance to the condenser. This stop and iris diaphragm are carried by telescoping tubing for their adjustment relative to the condenser.

The objective. A Zeiss objective of $1\frac{1}{2}$ in. focal length was chosen for its definition after comparison with a few other lenses.

Illumination. The carbons of the arc are horizontal and in the direction of the axis of the optical system. Complete mechanical adjustments for the carbons and parabolic mirror enabled an image of the arc crater to be formed on the condenser.

Shutters and filters. Three glass boxes filled with water are placed in the beam from the arc to reduce the heat rays; their effectiveness is shown by the water boiling in the first box if the arc remains on for some time.

A large metal shutter protects the apparatus from radiation when observations are not being taken. A rotating disk of aluminium 25 cm. in radius mounted on the axle of a 50 cyc./sec. synchronous motor with a window cut in it near its edge 6° in angular aperture allows the light to pass 25 times per sec. for $\frac{1}{1500}$ sec. It cuts off $\frac{59}{60}$ of the radiation which would enter the condenser. The compur shutter at the entrance to the condenser, normally closed, is open for 2 sec. when exposures are made. Fifty exposures are made of a total duration of $\frac{1}{30}$ sec. All photographic plates used to measure e were examined for evidence of convection currents, but no evidence of convection due to the illumination was found. Good definition in all the images of a drop on a plate is evidence of the absence of convection.

Photography. Kodak ordinary plates developed in Agfa fine-grain developer at 18° C gave a well-defined image free from grain and background fog of even the fastest moving drop. To prevent distortion of the emulsion the plates were kept horizontal while in a wet condition. Using a microscope magnification of about × 17 when measuring the resulting plates, accurate settings of micrometer eyepiece wire could be made. The initial magnification being × 12, the total is 204 in these measurements.

Magnification. The initial magnification is determined by the focal length of the microscope objective and the camera length. Tests showed that when the image on the photographic plate is well defined the magnification is constant to 1 in 20,000. It was measured by photographing a Grayson ruling on glass and measuring the ratio of the distance between two consecutive lines on the photographic plate to the distance between them on the ruling. These measurements given in the attached table were made by means of the Zeiss travelling microscope used for all plate measurements, the screw of which had been carefully calibrated.

TABLE 2

Plate	No. of obs.	Magnification
1	5	(42·009 ± 0·002)/(3·5004 ± 0·0003)
2	5	(42·005 ± 0·002)/(3·5004 ± 0·0003)
	Mean	12·001 ± 0·001*

* ± 0·001 in the above table is the mean departure from the mean and not the probable error of the mean.

VISCOSITY OF THE AIR

In the expression for e, $e \propto \eta^{\frac{3}{2}}$. This means that the air in which the drops fall must be dry air, that its temperature must be maintained constant and be known to an accuracy of 0·026° C if $\eta^{\frac{3}{2}}$ is to be known to 1 in 10,000. The measures taken for keeping the temperature constant, measuring it, and the value to be assumed for η are discussed below.

Thermostat (Laby and Hopper 1939*a*). To attain uniformity of temperature, the air in which oil drops fall is enclosed in an inner copper box of wall thickness 0·15 cm., surrounded by 0·5 cm. of thin sheets of synthetic cork. The outermost wall is of copper 0·15 cm. thick. To obtain constancy of temperature in this box and the metal and glass parts connected to it, a thermostatic device was devised which proved convenient and very effective. A resistance thermometer of 100 Ω resistance was made by tightly winding no. 45 gauge cotton-covered copper wire round the brass tube of the microscope condenser which is in thermal contact with the copper box. This coil formed one arm of an equal-armed Wheatstone bridge, the other arms being of manganin. With the dissipation of 0·01 W in the copper coil, a change of temperature of 0·001° C caused a galvanometer deflexion of 0·25 cm. The galvanometer spot moved across the window of a gas-filled photoelectric cell when deflected slightly from its equilibrium position. The current from the cell was amplified by a 2A3 triode valve, the plate current of which operated a polarized relay which lit two 20 W 230 V lamps placed on opposite sides of the copper box, each of them being about 45 cm. from it. All sides of the box were heated by the radiant heat of the lamps.

This device kept the box at a constant temperature T, a few degrees above the room temperature, t. T must of course be greater than t. Its effect on the temperature of the box is shown in figure 3. It proved most convenient and effective.

Temperature measurement. Although it is not in general a good practice to use base metal thermocouples for accurate temperature measurement, a copper-constantan couple was used to measure the air temperature. The constantan wire of the couple was selected for its freedom from inhomogeneities. The cold junction was placed in a mixture of ice and distilled water stirred by a slowly reciprocating vertical plunger, and the other junction was in the air in the copper box adjacent to where the drops fell. A three-dial 'thermokraftfrei' low-resistance potentiometer by Wolff with a galvanometer reading to 0·1 μV (i.e. 0·002° C) was used with the thermocouple.

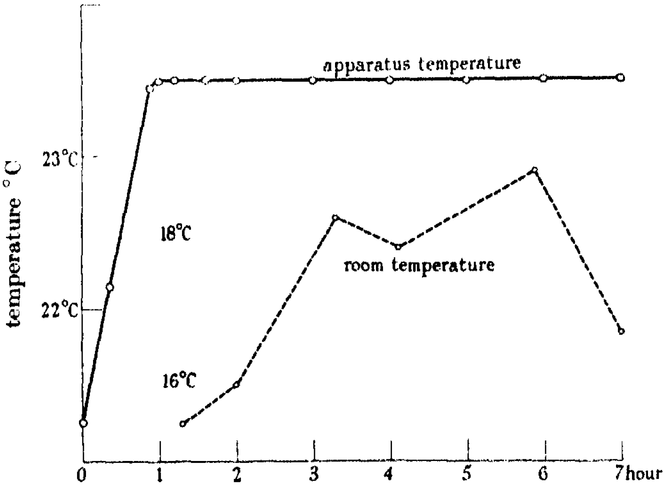

FIGURE 3. Temperature inside apparatus, controlled by radiant heat method.

Viscosity of air. The uncertainty which exists as to the value of the viscosity of air to be accepted sets a limit to the accuracy with which e can be determined by the drop method.

In deriving from the many available values of η for air a 'best' value to be used in calculating e, no procedure is free from arbitrary assumptions. Only two methods of determining the viscosity of a gas will be considered, which are

(1) the steady deflexion of a cylinder, and
(2) flow through a cylindrical tube.

Methods in which the air is accelerated are rejected as not having a valid theory. Fabry and Perot's interference fringe method, in which a plane circular disk is lifted from another plane surface while theoretically sound, and possibly capable of yielding high accuracy, does not appear to have been used in measurements of the highest precision.

Rotating cylinder method. Determinations of η by the deflexion of a cylinder have been made by Kellström, Houston, Harrington and Gilchrist. The last three of these form a connected investigation which Gilchrist began in Professor Millikan's laboratory, and Harrington continued using the same apparatus. Houston used improved apparatus, and has discussed in detail the theory of the method. Kellström's measurements of the constants of his apparatus are of great precision, but he does not mention having made a correction to the length of the inner cylinder, which is to be regarded as extending into the air gaps at its two ends. Further, the moment of inertia of the inner cylinder as observed by Kellström is too large by the moment of inertia of the air which it carries with it as it rotates. (Harrington and Houston use a vacuum to eliminate this error.) Both these corrections would reduce Kellström's value for η. The air inertia correction cannot be estimated, but the air gap one can be. It is half the two air gaps, i.e. 0·11 mm. on 99·98 mm., and it decreases η from 1834·62 to $183·6 \times 10^7$. The major experimental difficulty of the deflexion method is in the measurement by means of a suspension filament of the torsion couple which acts on the deflected cylinder.

Bearden's measurement. Since writing the above Bearden (1939) has published a determination of η by this method in which the outer cylinder is deflected. A tungsten wire, heat treated at 1200° C, was used as filament and the law of its elastic properties investigated. The value of η_{23} given is $1834·12 \times 10^{-7}$, but using a temperature correction of $4·83 \times 10^{-7}$ per ° C at 23° C, for reasons given below, we will use $\eta_{23} = (1833·8 \pm 0·06) \times 10^{-7}$.

External consistency of viscosity observations. There are nine values of η_{23} in table 3, and the errors of these values can be estimated both from internal and external consistency.

How are the observed values and their probable errors (calculated by internal consistency) to be reconciled? Consider the values 1833·8 ± 0·06, 1830 ± 0·7, 1822·6 ± 0·7. The chance of an observation with a probable error of ± 0·06 having an error of 3·8 or more is vanishingly small, and one with a probable error of ± 0·7 having an error of 3·8, that is, 5 times its probable error is $\frac{1}{1340}$, and an error of 11·2 vanishingly small. We conclude that either the random errors of most of the observations of η have been underestimated or that the observations are subject to systematic error. The error of the mean of these values, 1828·7, is $\pm 0·67\{\Sigma v^2/(n-1)\}^{\frac{1}{2}} = \pm 3$, that is, the external consistency error includes both their systematic and random errors. As it is larger than all but one of the internal consistency errors of the observations, we conclude the systematic error is larger than the random error.

In the case of Bearden's value the error ± 0·06 may be an underestimate. It is calculated by means of the partial derivative of

$$\eta = F(b^2 - a^2)\,\phi t/8\pi L b^2 a^2,$$

and the errors of a, b, ... are estimated from their internal consistency. In calculating it the error in $(b^2 - a^2)$ is taken to be $\pm 0{\cdot}45$ in 10,000 for one pair of cylinders, and $\pm 0{\cdot}2$ for another pair. Other figures given by the author show, however, an error of from 4 to 7 in 10,000 in $(b^2 - a^2)$ equivalent to $\pm(0{\cdot}7 \text{ to } 1{\cdot}3) \times 10^{-7}$ in η_{23}. This brings the two estimates of error somewhat closer.

In weighting the five values of η obtained by the method account is taken of the interdependence of Harrington and Gilchrist's experiments, and that Kellström's value is not corrected for air inertia in the measurements of I. Using the weights shown in table 3 the weighted mean of η_{23} is $1830{\cdot}6 \times 10^{-7}$.

Capillary tube method. Vogel in 1914 reviewed sixteen determinations of η by this method, and some six have been made since then. In a critical review of the more recent of these experiments it is desirable to know what systematic errors arise in the tube flow method.

Very fine bore glass tubes of less than 0·2 mm. radius have been generally used, but Rapp, Maxwell and Rigden have used somewhat larger bores. The tube is calibrated with a mercury thread, but the methods used to correct the radius are open to experimental and theoretical criticism. The mean velocity of flow may exceed 1000 cm./sec. and approach the velocity for turbulent flow, 8000 cm./sec., as given by Reynolds's criterion. It is evident that the random error in η will be larger the finer the bore of the tube used.

The theory of the flow of gas through a tube assumes the gas follows Boyle's law, that it is at a constant temperature (it expands as it flows), and that there is no loss or gain of kinetic energy at the ends of the tube.

According to Bond's theory these last corrections in η depend on v^2/c^2, where v is the velocity of flow, and c the velocity of sound. Thus these corrections will in general increase as the tube radius decreases. There is evidence that this gives rise to a systematic error in measurements of η by the tube method, and it would account for the higher values found by five earlier observers, who used fine tubes, as compared with the lower values of η found by Rapp, Maxwell and Rigden who used tubes with more than twice the radius of the earlier experimenters. All recent observers have made the same correction for slip at the walls of the tube.

Values of η determined since 1910 are given in table 3. Rigden and Bond used the same apparatus and method of reduction. Their results differ by $4 \cdot 6 \times 10^{-7}$ which is 6 times the error Bond gives for his experiment. Rapp's value for η_{23}, 1822·7, is low. His experiment was repeated by Maxwell using relatively large-bored tubes. Using a steady oil-pressure head and thermostatic temperature control he made 109 measurements of η.

Using the weights shown the mean for the tube method is $1829 \cdot 7 \times 10^{-7}$.

Weighted mean. The final mean of the nine observations with the weights stated is

$$= (1830 \cdot 0_6 \pm 2 \cdot 5) \times 10^{-7} \text{ unit g.cm.}^{-1} \text{ sec.}^{-1}.$$

TABLE 3. VISCOSITY OF AIR

Observer	Date	Temp. °C	η_{23}	Error	Weight
Rotating cylinder:					
Bearden	1939	20	1833·8	0·06	4
Houston	1937	22	1829·2	2·5	3
Kellström (corr.)	1937	20	1832·6	3·0	2
Harrington	1916	23	1822·6	0·7	1
Gilchrist	1913	20·2	1825·7	1·3	1
		Mean	1830·6		
Capillary tube:					
Rigden	1938	17	1830·0	0·69	2
Bond	1938	15	1834·6	0·8	1
Rapp	1913	26	1822·7	1·8	1
Maxwell	1916	22·5	1827·3	—	1
		Mean	1829·7		

Final weighted mean $= (1830 \cdot 0_6 \pm 2 \cdot 5) \times 10^{-7}$.

Temperature variation. The linear relation

$$\eta_{23} = \eta_t + 4 \cdot 93 \times 10^{-7}(23 - t)$$

has been generally used to reduce observations of η to 23° C, but this relation is not sufficiently accurate. Sutherland's expression

$$\eta_\theta = \eta_{273}(273 + c)/(\theta + c)(\theta/273)^{\frac{3}{2}}$$

is accurate over a wide range of temperatures. We conclude from a critical examination of a number of investigations of the temperature variation of η for air that $C = 117$. This value is used in calculating table 3. The value of the temperature coefficient of viscosity at 23° C is then $4 \cdot 83 \times 10^{-7}$ c.g.s./° C.

ELECTRIC FIELD

Parallel conducting plates are used to give the horizontal electric field required for the deflexion of the drops. The question arises as to what shape these plates should be given, and what should the ratio of their width, w, to their distance apart, d, be in order that the field may be calculated.

The known solutions, namely, of the field on the axis of parallel circular plates and Helmholtz solution of the semi-infinite planes with straight opposite boundaries are not practically applicable to our problem beyond that Helmholtz's solution is a guide in estimating whether w/d has been chosen sufficiently large.

In deciding the value of w/d a compromise is made between the electrical and optical requirements. The latter require dark-ground illumination of the drop, and a hollow cone of light of vertical angle of 40° is necessary with the microscope objective chosen. Rectangular plates 2·0 cm. wide and 7 cm. long and 0·5 cm. apart have been used.

Helmholtz in 1868 found the field near the edge of two semi-infinite parallel planes, and his solution is discussed by Maxwell, Rayleigh and later writers.

We may apply this solution to find the ratio of the field for plates d apart at a point midway between the plates and distant $2d$ from the edge, to the field at an infinite distance from the edge. It is found that the difference in the fields is less than 1 in 10^6. This is some justification for believing that we may put $X = V/d$ without error important to the accuracy sought in these measurements.

Construction of condenser. The condenser plates are made of glass silver plated over a middle portion, but unsilvered at the ends, which act as part of the electrical insulation between the two conducting surfaces. The glass plates were tested for flatness against a glass optical flat by means of Newton's rings. They were separated by three lengths of pyrex capillary tubing (see figure 2) which were lapped to be of equal length. Ivory bolts and nuts hold the plates together and they are supported by three short lengths of the pyrex tubing on a steel plate 3 mm. thick. This geometrical system of support by pyrex glass from a steel plate gave rigidity and excellent electrical insulation.

The electrical connexion to the silvering required to be carefully made. The insulating bushes for connexion to terminals are of amber.

Adjustment of condenser plates vertical. Before the results with apiezon oil were obtained, the plates were made nearly vertical, and to do this precision in their adjustment was necessary. A small oil-damped plumb bob with a very fine wire filament was placed close to the surface of one of the condenser plates, the outer copper boxes having been removed. If the glass plate is vertical, the distance (measured by means of a telemicroscope) from the filament to its image in the plate is the same at the top and bottom of the plate. Levelling screws under the platform supporting the microcamera adjusted the condenser plates to be vertical, and the bubble of a circular level attached to the stand of the microcamera is subsequently used to indicate when the plates are vertical.

Distance between plates. The pyrex separating pieces were compared by means of a dial gauge (reading to 1/10,000 in. and by estimation to 1/100,000 in.) with a Pitter 5 mm. steel slip gauge certified by the N.P.L. It was found that

$$\text{Mean length of separating pieces at } 23^\circ\text{ C} = 0{\cdot}49852 \pm 0{\cdot}00006 \text{ cm.}$$

as the mean of 20 measurements. This is taken as the distance between the silvered surfaces of the glass plates.

These condenser plates were not intended for the final measurements of e, and it was intended to construct the equivalent of a Fabry and Perot etalon using, however, three distance pieces, and determine its separation in terms of the wave-length of light. Delay in the construction of the etalon made it necessary to proceed with the condenser measured as described above.

Difference of potential. A difference of potential of 3000 V, which makes X about 6000 V/cm., has been found sufficient to deflect the largest drops we have used. As already explained the large charge found on such drops makes X much less than if the charge on these drops did not increase with their volume.

For the constant potential we have used rectified alternating current from the public supply. We are indebted to Mr T. P. Gill, M.Sc. (1939), for a most effective solution of the design of the stabilizer used. It is a two-stage Evans circuit carefully balanced, and its output potential has the same constancy as has been observed in this laboratory for small storage cells, namely, of about 1 in 10,000. It is very much more convenient than a battery.

The circuit used to connect the stabilizer to the condenser plates and to a potentiometer for measuring, V, the potential applied to the condenser is shown in figure 4.

The potential, V, is given by

$$V = E(R+r)/r,$$

where E is the potential difference across r which is measured on the potentiometer in terms of the e.m.f. of a Weston cell. The potentiometer is a three-

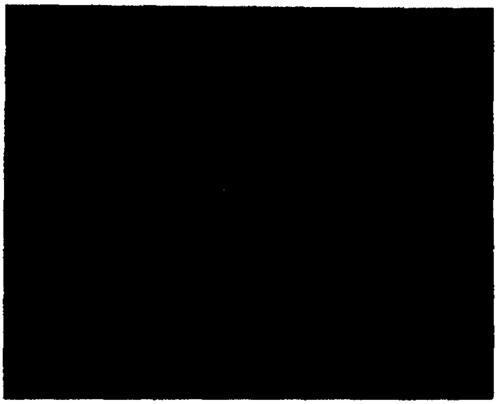

FIGURE 1 A. Deflected drops.

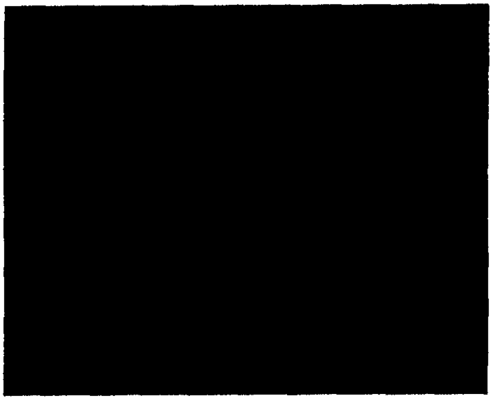

FIGURE 1 B. Undeflected drops.

dial Wolff 'thermokraftfrei' low resistance one in which, as the resistance in the galvanometer circuit is constant, readings of galvanometer deflexions enable the fifth figure in the value of E to be estimated.

V is found in terms of the international volt, but X in the expression for the electronic charge is in electrostatic units. The ratio for these units used is given under calculation of results.

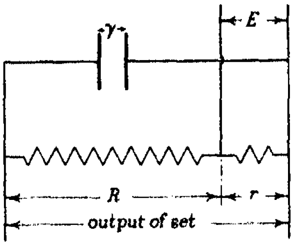

FIGURE 4. Electrical circuit.

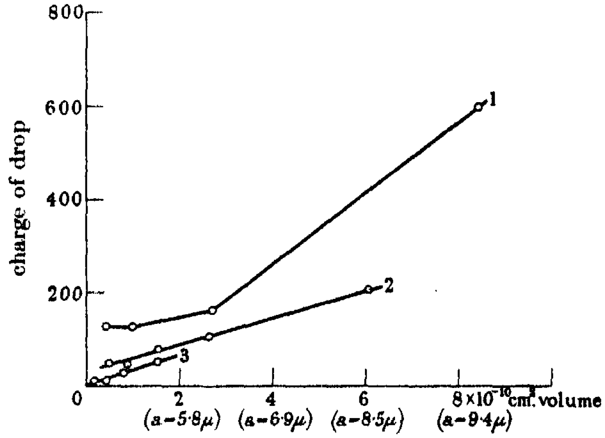

FIGURE 5. Relationship between charge and volume of drops. 1, castor oil; 2, apiezon oil, A; 3, apiezon oil, B.

OILS USED AND THEIR PROPERTIES

We have used in our observations apiezon oil because of its low vapour pressure, and castor oil because it gives drops carrying large charges. We have not observed any evidence of the evaporation of drops as Ishida and his co-workers did. If there is evaporation for apiezon oil it will be less in the following experiments than for the Japanese observations, since the drops used are larger and are under observation for much less time.

In figure 5 the charge $\pm ne$ of a drop on its formation by the method described below is plotted against a^3, where a cm. is the radius of the drop.

The points with some large departures tend to fall on a straight line for each oil, castor oil being more highly charged per unit volume than the other oil.

This property of an oil of forming drops for which n is large is an important one, for it is possible to use proportionately smaller electric fields and potential differences. In one of our experiments $a = 9{\cdot}6 \times 10^{-4}$, $n = 233$, and a potential difference of 2200 V gave a sufficient angle of deflexion. One oil drop was photographed for which n was 1000.

Production of oil drops. An atomizer, and the ejection by air of oil from the fine end of a glass tube, have been tried for producing drops of the radii required of from 3 to 10μ and larger. In the most effective method found after many experiments a drop of oil is placed on the wires of a fine steel brush; a rotating bar first pushes the wires of the brush back and then suddenly releases them with the production of a copious supply of oil drops of about the desired range of sizes. Care was taken to clean the wire brush thoroughly before the oil to be used was dropped on it.

The operation of producing drops is done in a box vertically above the copper box in which the drops are observed. The tube connecting the two boxes is fitted with a tap which serves to separate drops of different sizes, to protect the air in the copper box from external disturbances, and to allow drops to enter so that they are in focus, as they fall past the microscope objective.

Density. This requires to be known, for an accuracy of 1 in 10,000 in e, to 1 in 5000, and to be measured at two temperatures, preferably in the range 15–25° C. A pyrex sinker was weighed in air, in water, and in the oil the density of which is desired. The high viscosity and expansion of the oils make steady and accurately known temperatures necessary for the measurements.

TABLE 4

Oil	Density	Temperature ° C	Coef. of density change per ° C
Castor	0·96166 g./cm.^{3}	17·73	0·000630
Apiezon	0·88762	25·20	0·000641

The densities and temperatures are graphically interpolated from observations over the range 16·85–27·7° C for the first, and 19–29·8° C for the second oil. We are indebted to Mr P. G. Law for taking most of these rather exacting density observations.

VELOCITIES OF DROPS

The distance between consecutive images of a drop taken at intervals of 0·04 sec. are measured with the Zeiss microscope to test if the velocity is uniform. If it is not, the reason for the departure is investigated and the drop is not used for measuring e. If it is uniform the velocity of the drop is

$$v = fs/Mn,$$

where s cm. is distance on the plate between the first and last of $(n+1)$ consecutive images, $1/f$ sec. is interval between successive exposures, and M is the magnification of the camera. f is taken to be 25, a correction being made for the small departures from this value, and $M = 12{\cdot}001$. As v is observed for freely falling drops, their path is vertical and s is measured in the direction of the drops.

In the case of drops deflected by the electric field two methods were tried in the reduction of the observations. In one the angle, θ, between the direction of the path of the freely falling drops and that of the deflected ones was measured by means of a device constructed from the azimuth bearing and circle of a theodolite which read to 20″ of angle.

In the other the successive distances between the images of the deflected drops were measured by means of the Zeiss travelling microscope, and the terminal velocity of the drops could then be determined. This latter method proved the more satisfactory, and was employed for the results with the apiezon oil. With the castor oil, both methods were employed to enable the angle of the plates from the vertical to be calculated.

Frequency of illumination. The rotating disk could have been driven with a synchronous motor supplied by current from an elinvar tuning fork. For the power needed such equipment would be expensive. The disk is actually driven by means of a synchronous motor connected to the a.c. supply which is subject only to small departures from its average frequency of 50 cyc./sec. For that frequency the disk makes 25 rev./sec.

To measure the actual speed of the aluminium disk forty holes 1 mm. in diameter and 9° apart were drilled in a circle concentric with the axis of rotation. A neon lamp supplied by 1000 cyc./sec. a.c. is viewed through the holes. Since the lamp is extinguished 2000 times/sec. the rate of revolution of the disk, f, is given by

$$f = 25 \pm z/(80t),$$

where z is the number of black bands which appear to pass in t sec., t being measured by a stop-watch. It is to be explained that sharp black bands appear to cross the lamp, and the number crossing per second can readily be counted. The determination of f takes about 3 sec. The correction $z/80t$ is rarely greater than $\pm 0{\cdot}02$ sec.$^{-1}$, and z/t is observed whenever photographs are taken to measure drop velocities.

The 1000 cyc./sec. a.c. is obtained from an elinvar valve-maintained tuning fork made by Sullivan. The output from the fork is connected to a power amplifier, the output of which is connected to the neon lamp. We are indebted to Mr Frank Kerr, M.Sc., for designing and constructing the amplifier.

CALIBRATIONS

Screw of measuring microscope. The Zeiss microscope used to measure photographs of oil drops, etc. consists of a microscope with a 3 × objective and 5·5 × eyepiece, which is moved relative to the plate, being measured by a 50 mm. screw of 1 mm. pitch. A telemicroscope was used in calibrating the screw to read the drum to 0·0001 mm. Each millimetre of the pitch was compared with 1 mm. of a Grayson ruling on glass. Some 600 observations were taken. They showed that from 21 to 50 mm. the pitch was most regular, and only this part of the screw was used. Over this section of it

$$\text{Mean pitch of screw} = 0{\cdot}9982,\ \pm 0{\cdot}00026 \text{ mm. (Grayson).}$$

What part of this small error was due to errors of setting and what to errors of pitch could not be distinguished. It is therefore assumed the pitch is constant to $0{\cdot}3\mu$.

The screw was compared with a Nickel metre of H section of the highest quality made by the Société Genèvoise for which there is a certificate of the International Bureau of Weights and Measures. The mean of twelve observations is given in table 5.

TABLE 5

Temp. °C	Nickel metre mm.	Length calculated from certificate cm.	Length read on Zeiss microscope
20	500–525	2·4999	2·5000 ± 0·0002

Standard of potential. As explained above the potential difference, V, applied to the condenser plates is measured in each experiment in terms of the e.m.f. of a Weston cell. The cell used, supplied by the Cambridge Instrument Co., has an N.P.L. certificate No. 57384, which gives for the e.m.f. of the cell

$$e_{25} = 1{\cdot}01805 \text{ international volts.}$$

This cell was compared on 22 November 1938 with two other cells with N.P.L. certificates. Such a comparison only shows whether the relative values of the e.m.f.'s of the cells has remained constant, which it has as set out in table 6.

TABLE 6

N.P.L. certificate cell no.	57380	57384	58504
e_{25} international volt	1·01805	1·01805	1·01815
Relative 22 Nov. 1938	1·01805	(1·01805)	1·01815

These cells were again carefully compared by Mr P. G. Law, in November 1939, and the same results were obtained.

Elinvar electrically driven tuning fork. This 1000 cyc./sec. fork made by Sullivan has an N.P.L. certificate of its frequency when used with a certain valve. The valve having been replaced by another of the same type, Mr Gill confirmed the previous calibration. The fork was connected to a General Radio synchronous motor and counter in the form of a clock, and compared with the hourly wireless time signals over a period of 24 hr. The frequency of the fork and associated valve

$$= 1000{\cdot}041 \pm 0{\cdot}002 \text{ cyc./sec. at } 16^\circ \text{ C.}$$

The N.P.L. certificate gives the temperature coefficient as 4 in $10^6/^\circ$ C.

EXAMPLE OF CALCULATION

The calculation of e for plate 4, which is a general case, is as follows:

$$ne = 9\sqrt{2}\,.\,\pi g^{-\frac{1}{2}}(\rho-\sigma)^{-\frac{1}{2}}\,\eta^{\frac{3}{2}}dc \times 10^{-8}\,pq^{-1}\,i^{-1}\,\Omega^{-1}M^{-\frac{3}{2}}f^{\frac{1}{2}}s_g^{\frac{1}{2}}s_x,$$

where ρ = density of the oil (0·89139 g./cm.^{3}),

σ = density of the air (0·0012 g./cm.^{3}),

η = viscosity of air ($1{\cdot}8163 \times 10^{-7}$ c.g.s.),

d = distance between the plates (0·49852 cm.),

c = ratio of e.s.u. to e.m.u. of potential difference ($2{\cdot}99776 \times 10^{10}$),

q = conversion factor from international to absolute units of potential (1·00034),

i = current through resistance (0·58660 mA),

Ω = resistance in parallel with plates (3, 002, 958 ohms),

M = magnification due to camera (12·001),

f = speed of rotation of disk (24·991 cyc./sec.),

s_g = mean distance between images of the drop—no electric field (0·21636 cm.),

s'_g = mean distance between images of the drop in the vertical direction with electric field (0·21720 cm.),

s_x = mean distance between images of the drop in the direction of the electric field (0·10317 cm.),

s_r = mean distance between images of the drop in the direction of deflexion (0·24031 cm.).

$$s_x = s_r \sin\theta/\cos\delta,$$

where

$$\theta = \arccos s'_g/s_r,$$

and δ is the angle between the direction of the electric field and the horizontal. It is given by

$$\tan\delta = (s_g - s'_g)/s_r \sin\theta,$$

s_r being the mean distance between successive images after deflexion, and s'_g being its vertical component. The observed values of s_g, s_r, s'_g for plate 4 are as follows:

s_g: 0·2164, 0·2166, 0·2162, 0·2163, 0·2164, 0·2163, 0·2163, 0·2164; mean 0·21636 cm.

s_r: 0·2403, 0·2399, 0·2408, 0·2401, 0·2403, 0·2410, 0·2398; mean 0·24031 cm.

s'_g: 0·2175, 0·2170, 0·2170, 0·2178, 0·2171, 0·2170, 0·2169, 0·2166, 0·2174, 0·2177, 0·2172, 0·2174; mean 0·21720 cm.

s_x is calculated from the formula above.

Substituting in formula (15), we have

$$ne = 402{\cdot}552 \times 10^{-10} \text{ e.s.u.}$$

For $n =$	81	82	83
$e_1^{\frac{2}{3}}$	62·742	62·231	61·730 × 10^{-8}
Residual v^2	261,121	0	249,000 × 10^{-22}

The value of n is evidently 82, and for that value $e_1^{\frac{2}{3}} = 62{\cdot}231 \times 10^{-10}$ e.s.u. The values 81 *or* 82 *for* n *give a* v^2 *very much larger than the largest value,* 841, found in table 8.

Discussion of results

In deducing the values of ne given in table 8, the provisional value of η_{23} used was $1834{\cdot}0 \times 10^{-7}$ c.g.s. unit, and the value of η at other temperatures was calculated by Sutherland's formula using $c = 115$. The values of e and m in the expression

$$e_1^{\frac{2}{3}} = e_0^{\frac{2}{3}} + m/pa,$$

which gave the best fit with the values of $e^{\frac{2}{3}}$ and $1/pa$ contained in table 8, were calculated by the method of least squares. Writing the above

$$y = a_{01} + a_{11}x,$$

then
$$a_{01} = \frac{(\Sigma x)(\Sigma xy) - \Sigma y \,.\, \Sigma x^2}{n(\Sigma x^2) - (\Sigma x)^2},$$

and
$$a_{11} = \frac{\Sigma x \,.\, \Sigma y - n\Sigma xy}{n(\Sigma x^2) - (\Sigma x)^2}.$$

These relations give for

$$e_0^{\frac{2}{3}} = 61{\cdot}456 \pm 0{\cdot}0011 \times 10^{-8} \text{ e.s.u.},$$

$$m = 0{\cdot}03790 \pm 0{\cdot}00044 \times 10^{-8} \text{ (p in cm. of mercury, a in cm.).}$$

In calculating e_0 from the above value of $e_0^{\frac{2}{3}}$ it has to be corrected to $\eta_{23} = 1830 \times 10^{-7}$, and the value given by our observations for the electronic charge is

$$e_0 = (4{\cdot}8020 \pm 0{\cdot}0013) \times 10^{-10} \text{ absolute e.s.u.}$$

e by oil-drop method. In the following table the value of e found by other observers assuming that $\eta_{23} = 1830 \times 10^{-7}$ is given. Millikan's value is also corrected to absolute electrostatic units and his value of m is given. Where errors are given against an observer they are calculated by the expression for a_{01} and a_{11} given above.

			Errors		
Observer	$e_0 \times 10^{10}$	$m \times 10^8$	$\times 10^{10}$ e_0	$\times 10^{10}$ mean e_1	$\times 10^8$ m
Authors	4·8020	0·03777	± 0·0013	± 0·00036	± 0·00044
Millikan	4·7992	0·03784	± 0·0037	± 0·0014	± 0·00013
Bäcklin and Flemberg	4·7811	0·0372	± 0·018	± 0·004	± 0·0014
Ishida and others	4·8350	0·0361			

Our value of e differs from Millikan's by $0{\cdot}0028 \times 10^{-10}$, and this is less than his error. Our and Millikan's value of m only differ by $0{\cdot}00007 \times 10^{-8}$. Bäcklin and Flemberg's e and ours differ by $0{\cdot}021 \times 10^{-10}$, but their error is $\pm 0{\cdot}018 \times 10^{-10}$. Ishida and others value of e is much higher than any of the other three values of e. These investigators assume that the density of their oils changed slowly with time when in the drop form, even before the light from the arc fell on the drops. Their high result is a consequence of this assumption which does not appear to be justified.

X-ray method. In this method of determining the electronic charge, e e.s.u., the wave-length of an X-ray line is measured in cm. and in XU. The ratio of the XU to the cm. is measured. The XU is conventionally defined as 1/3029·45 of the distance at 18° C between adjacent (100) planes of calcite. The wave-length, λ_g cm., is measured by means of a ruled grating.

Bragg's law, $n\lambda = 2d_n\{1 - 4d^2\delta/n^2\lambda^2\} \sin \phi_n$,

is used to calculate λ in terms of d_n and ϕ_n, the angle of 'reflexion' for the nth order. The second term in the bracket corrects for refraction, where $\mu = 1 - \delta$ is the refractive index of the crystal. If $d_\infty = 3029{\cdot}45$ XU, then $d_1 = 3029{\cdot}04$, $d_2 = 3029{\cdot}34$.

The grating space of a crystal, $d_{\infty 18}$, is calculated by means of the following relation, to the mass of the half-molecule which is associated with that cell when it is a rhombohedron:

$$d_{18}^3\phi(\beta)\,\rho_{18} = M/2N = Me/2F,$$

and

$$e = 2d_{18}^3\phi(\beta)\,\rho_{18}F/M,$$

where M is the molecular weight, ρ_{18} g.cm.$^{-3}$ the density of the crystal, $d_{18}\phi(\beta)$ the volume of the unit rhombohedron cell, N the number of molecules per g.mol., and F e.s.u./g. equivalent to the Faraday, e e.s.u. the electronic charge.

In the reduction of the X-ray determinations of e we use the following values of the above constants:

Symbol	ρ_{18}	$\phi(\beta)$	δ	M	c	$F \times 10^{-14}$
Value	2·710467	1·09594	$10{\cdot}2 \times 10^{-6}$	100·09	$2{\cdot}99776 \times 10^{10}$	2·89225
Error in 10^4	±0·1	±0·1	—	±0·5	±0·13	±1·1
	Bearden	Birge	Cooksey	1939 at. wt.	Birge	Int. Bur. W. and M.

F is calculated from the definition of the ampere, i.e. 0·001118 g. of silver per coulomb and 1 int. coulomb = $0{\cdot}99986 \times 10^{-1}$ e.m.u. The third line gives the errors as estimated by Birge and in parts per 10,000. We will calculate, e, the charge for which $d_{\infty 18} = 3{\cdot}02945 \times 10^{-8}$ cm. It is

$$e_0 = 4{\cdot}77306 \times 10^{-10} \text{ e.s.u.}$$

In the expression used to calculate e_0, e_0 is proportional to d^3, it follows from this that

$$e = e_0(\lambda_g/\lambda_c)^3 = 4{\cdot}77306 \times 10^{-10}(\lambda_g/\lambda_c)^3,$$

which is a convenient relation for the reduction of measurements of e by the X-ray method. It is to be noted that the error in e is that contributed by the constants which enter into its calculation. F and M contribute the largest

TABLE 7

Plate	Temp. °C	$\eta \times 10^{-4}$ c.g.s.	ρ_t c.g.s.	p cm. Hg	$a \times 10^{-4}$ cm.	$1/pa$	i mA	Ω ohms resistance	f rev./sec.	M magnification
1	15·27	1·7950	0·96339	75·59	9·570	13·824	0·58183	3,803,608	25·018	11·983
2	22·10	1·8296	0·89161	75·40	7·4124	17·892	0·74110	3,002,799	25·007	12·001
3	16·51	1·8024	0·96242	74·76	7·0678	18·925	0·58045	3,803,552	25·000	11·983
4	19·34	1·8163	0·89139	75·30	6·4925	20·455	0·58660	3,002,958	24·991	12·001
5	12·70	1·7838	0·96482	76·68	6·3267	20·613	0·58653	3,803,724	25·018	11·983
6	19·35	1·8163	0·89138	75·30	6·3264	20·992	0·58900	3,002,957	25·016	12·001
7	18·90	1·8141	0·89167	75·80	6·168	21·390	0·57884	3,002,977	24·991	12·001
8	22·02	1·82925	0·88967	75·25	5·8672	22·650	0·58560	3,002,805	24·992	12·001
9	22·10	1·8296	0·88962	75·40	5·7116	23·220	0·74080	3,002,799	25·022	12·001
10	24·71	1·8422	0·88795	75·50	5·6768	23·332	0·58220	3,002,596	24·985	12·001
11	24·71	1·8422	0·88795	75·50	5·1285	25·826	0·58220	3,002,596	24·985	12·001
12	17·76	1·8086	0·89240	74·80	5·048	26·486	0·60850	3,003,024	25·013	12·001
13	18·70	1·8133	0·89180	75·80	4·3307	30·464	0·57814	3,002,985	25·010	12·001
14	24·71	1·8422	0·88795	75·50	3·973	33·299	0·58220	3,002,596	25·000	12·001
15	15·16	1·7959	0·96327	75·30	3·7873	35·066	0·58163	3,803,613	25·010	11·983
16	17·02	1·8049	0·96210	74·71	3·379	39·607	0·58048	3,803,529	25·003	11·983

TABLE 8

Plate	s_g mm.	s_g' mm.	s_r mm.	θ°	$\times 10^{10}$ e.s.u. ne_1	n	$\times 10^8$ e.s.u. $e_1^{\frac{2}{3}}$	$\times 10^8$ e.s.u. $e_1^{\frac{2}{3}}$ calc.	$\times 10^{22}$ e.s.u. v^2
1	5·1211	5·0286	5·610	26° 19′	1136·58	233	61·968	61·980	144
2	2·7898	2·8132	4·7113	53° 20′	1351·72	276	62·132	62·134	4
3	2·7808	2·7418	3·4937	38° 18′	735·09	150	62·158	62·173	225
4	2·1636	2·1720	2·4031	25° 20′	402·552	82	62·231	62·231	0
5	2·2554	2·3089	2·492	22° 10′	280·023	57	62·261	62·237	576
6	2·0494	2·0541	2·4592	33° 21½′	515·771	105	62·257	62·252	25
7	1·95214	1·9370	2·0058	15° 3′	196·642	40	62·289	62·267	484
8	1·7485	1·7517	1·9725	27° 22′	324·531	66	62·298	62·314	256
9	1·655	1·663	2·5729	49° 44′	541·557	110	62·350	62·336	196
10	1·6196	1·6155	1·7850	64° 52′	265·904	54	62·357	62·340	289
11	1·3551	1·3628	2·562	57° 22′	695·399	141	62·423	62·435	144
12	1·3120	1·3120	1·4382	24° 11′	172·762	35	62·458	62·460	4
13	0·9626	0·9328	1·3860	47° 42′	272·292	55	62·582	62·611	841
14	0·7962	0·7957	1·6046	60° 15½′	342·597	69	62·703	62·717	225
15	0·8018	1·0014	3·787	74° 40′	662·083	133	62·812	62·785	729
16	0·63455	0·65759	7·1280	84° 48′	1153·913	231	62·957	62·957	0

errors, and using Birge's estimates (see table above) the error in e is 1·1 in 10,000.

In the measurements of Söderman and Bäcklin the X-ray line used was the Al $K_{\alpha 12}$ line, and in Bearden's the α_1, α_2 and β lines of the K spectra of Cu and Cr.

Söderman used a concave grating with glancing incidence but with the photographic plate normal to one of the diffracted rays. His value of λ_g is measured by comparing the Al $K_{\alpha 12}$ line (8·34 A) in its 8th, 9th and 10th orders relative to a number of 1st order of certain intense and well-defined Al spark lines, the wave-length of these having been compared by Söderqvist with oxygen lines in the ultra-violet optical spectrum. This is an application of Rowland's method of coincidence in different orders, and its accuracy is only limited by the homogeneity of the lines used, and resolving power of the glancing incidence concave grating spectrometer. Söderman mentions $\lambda/\delta\lambda = 1200$ as estimate of the resolving power of his spectrometer. He found Al $K_{\alpha 12}$ $\lambda_g = 8{\cdot}3401 \times 10^{-8}$ cm. Söderman and Bäcklin use for the crystal wave-length, λ_c, of the Al $K_{\alpha 12}$, the value found by Larsson

$$\lambda\,\mathrm{Al}\,K_{\alpha 12} = 8321{\cdot}35\,\mathrm{XU}$$

using a mica crystal, which did not resolve the $\alpha 12$ doublet.

A comparison of Haglund's (1935) measurements of λ_c for the Al $K_{\alpha 12}$ doublet shows that its width and asymmetrical structure set the limit to the precision of the measurement of λ_c for this doublet. He found, using the crystals stated, the effective wave-length to be

$$\text{Mica} \quad \lambda_c = 8322{\cdot}93\,\mathrm{XU};$$

$$\text{Gypsum} \quad \lambda_c = 8322{\cdot}87\,\mathrm{XU}.$$

A quartz crystal resolved the doublet and gave

$$\lambda_{\alpha_1} = 8322{\cdot}18, \quad \lambda_{\alpha_2} = 8324{\cdot}62\,\mathrm{XU}.$$

Larsson's value is less than the smallest of Haglund's values.

Bearden (1931*a*, 1935) has published two determinations of λ_g/λ_c for K lines of Cu and Cr. In his 1935 paper he describes isolating the Cu $K_{\alpha 1}$ line with a double crystal monochromator, and measuring λ_g with a ruled grating. An accurate circle is used to measure angles of incidence and diffraction in the second order. These ranged from 480″ to 1580″, and the error of reading, etc. was about ±0·25″. Twelve observations gave $\lambda_g = 1{\cdot}5406 \times 10^{-8}$ cm.

The following closely agreeing values of the crystal wave-length of $\lambda \mathrm{Cu}\, K_{\alpha 1}$ are available:

1537·396 XU, Siegbahn,
1537·395 XU, Wennerlof,
1537·399 XU, Bearden and Shaw.

The mean is 1537·397 and

$$\lambda_g/\lambda_c = 1540{\cdot}6/1537{\cdot}397 = 1002{\cdot}08,$$

i.e.

$$1\ \mathrm{XU} = 1{\cdot}00208 \times 10^{-11}\ \mathrm{cm.}$$

and

$$e = 4{\cdot}8029 \times 10^{-10}\ \mathrm{e.s.u.}$$

The author does not reduce his 1935 observations separately, but combines them in a weighted mean with his 1931 measurements and with those of Söderman and Bäcklin. This mean is = 1·00248, which is the mean of his 1931 measurements as given in his 1935 paper. With much hesitation we calculate separately his 1931 and his 1935 values of e, believing the considerable improvements which the author has made in the 1935 measurements justify their separate reduction. In 1931 he used Cu and Cr K_β lines and the Cu and Cr $K_{\alpha 12}$ unresolved doublet and found λ_g/λ_c as a mean (of over 700 observations) for these lines = 1·00222, and therefore

$$e = 4{\cdot}8049 \times 10^{-10}$$

ELECTRONIC CHARGE X-RAY METHOD

Observer	X-ray line	λ_g cm.	λ_c XU	λ_g/λ_c	e e.s.u.
Söderman	Al $K_{\alpha 12}$	8340·1	8321·35	1·00225	$4{\cdot}805_4$
Bäcklin	Al $K_{\alpha 12}$	8339·5	8321·35	1·00218	$4{\cdot}804_4$
Bearden 1935	Cu K_{α_1} etc.	1540·6	1539·397	1·00208	$4{\cdot}802_9$
Bearden 1931	Cu and Cr K	—	—	1·00222	$4{\cdot}804_9$

Mean value $e = (4{\cdot}804_4 \pm 0{\cdot}0007) \times 10^{-10}$.

CONCLUSION

The value of e by the X-ray method is $(4{\cdot}8044 \pm 0{\cdot}0007) \times 10^{-10}$ e.s.u., whilst that obtained by the oil-drop determinations of Millikan and the authors is $(4{\cdot}8007 \pm 0{\cdot}002) \times 10^{-10}$ e.s.u., if η_{23} is assumed to be 1830×10^{-7} c.g.s. units. The main uncertainty in the value of e as found by the drop method is in the value which is used for viscosity of air. The value of η obtained from the weighted mean of nine separate experiments is

$(1830 \pm 2{\cdot}5) \times 10^{-7}$ c.g.s. units, and as it enters to the $\frac{3}{2}$ power in the expression for e the final error in e is 1 in 500. This error far exceeds the difference between the X-ray and oil-drop values of e given above. It will be noticed that the other errors entering into the determination of e by the oil-drop method can be made very small and have been estimated at less than 1 part in 3000 in the experiment described in this paper. A determination of the viscosity of air is being attempted in this laboratory using a method suggested by Fabry and Perot in which there is lamina flow of air between optically flat disks. It is hoped that improved precision will be obtained by this method.

The oil-drop method can be used to determine the viscosity of air if the X-ray value of e is assumed. Thus if e be taken as

$$(4{\cdot}8044 \pm 0{\cdot}0007) \times 10^{-10} \text{ e.s.u.},$$

the mean result of Millikan's and of the authors' experiments gives

$$\eta_{23} = (1830{\cdot}9 \pm 0{\cdot}5) \times 10^{-7} \text{ c.g.s. units},$$

whilst the authors' results alone give

$$\eta_{23} = (1830{\cdot}6 \pm 0{\cdot}4) \times 10^{-7} \text{ c.g.s. units}.$$

It might be of interest to note that if $e = 4{\cdot}802 \times 10^{-10}$, $h/e = 1{\cdot}3765 \times 10^{-17}$ (a mean of h/e determined by the X-ray method and by Wien's law), and $c = 2{\cdot}99774 \times 10^{10}$, then $1/\alpha = 136{\cdot}76$. If, however, Rydberg's constant $R(109{,}737{\cdot}43)$ and $e/m(1{\cdot}7589 \times 10^{7})$ are substituted in the formula $1/\alpha = [c/4\pi R(e/m)\,e]^{\frac{1}{3}}$, it becomes 137·03 which is nearly integral. Also if the above values of e, e/m and R are substituted in Rydberg's formula, then $h/e = 1{\cdot}3792 \times 10^{-17}$ or 1 in 500 larger than the weighted mean of the recent values of h/e. The recent work of Ohlin (1940) indicates that the previously determined values of h/e by the short wave-length limit of the continuous X-ray spectrum might be low owing to the fact that the X-ray tubes had not been evacuated to a sufficiently high degree. If this is so, then it is possible that both Eddington's relation and Rydberg's formula will be experimentally satisfied.

We are grateful to Mr T. P. Gill, M.Sc., Miss E. Parker, B.Sc., and Mr P. G. Law, M.Sc., for the valuable assistance they gave in this investigation. One of the authors (V. D. H.) held the Dixon and Major Research Scholarships of the University of Melbourne. Grants from the Commonwealth Research Fund were received towards the cost of the investigation.

References

Bäcklin 1935 *Z. Phys.* **93**, 450.
Bäcklin and Flemberg 1936 *Nature, Lond.*, **137**, 655.
Bearden 1926 *Proc. Nat. Acad. Sci., Wash.*, **15**, 528.
Bearden 1931*a* *Phys. Rev.* **37**, 1210.
Bearden 1931*b* *Phys. Rev.* **38**, 2089.
Bearden 1935*a* *Phys. Rev.* **48**, 385.
Bearden 1935*b* *Phys. Rev.* **47**, 811.
Bearden 1939 *Phys. Rev.* **56**, 1032.
Bearden and Shaw 1934 *Phys. Rev.* **46**, 761.
Birge, R. R. 1932 *Phys. Rev.* **40**, 228.
Bond 1938 *Phil. Mag.* **25**, 961.
Du Mond and Bollman 1938 *Phys. Rev.* **54**, 1005.
Fabry and Perot 1897 *Ann. Chem. Phys.* **13**, 275.
Gilchrist 1913 *Phys. Rev.* **1**, 124.
Gill, T. P. 1939 *J. Sci. Instrum.* **16**, 345.
Haglund 1935 *Z. Phys.* **94**, 369.
Harrington 1916 *Phys. Rev.* **8**, 738.
Houston 1937 *Phys. Rev.* **52**, 741.
Ishida, Fukushina and Suetsuga 1937 *Phys. Chem. Res., Tokyo*, **32**, 57.
Kellström 1937 *Phys. Rev.* **23**, 313.
Laby and Bingham 1930 *Nature, Lond.*, **126**, 915.
Laby and Hopper 1939*a* *Nature, Lond.*, **143**, 240.
Laby and Hopper 1939*b* *Nature, Lond.*, **143**, 158.
Laby and Hopper 1940 *Nature, Lond.*, **145**, 932.
Maxwell 1916 *Phys. Rev.* **8**, 479.
Millikan, R. A. 1913 *Phys. Rev.* **2**, 109.
Millikan, R. A. 1917 *Phil. Mag.* **32**, 1.
Millikan, R. A. 1930 *Phys. Rev.* **35**, 1231.
Millikan, R. A. 1938 *Ann. Phys., Lpz.*, **32**, **34**.
Ohlin 1940 *Medd. Uppsala Univ. fys. Instn.*
Rapp 1913 *Phys. Rev.* **2**, 364.
Rigden 1938 *Phil. Mag.* **25**, 961.
Robinson 1935 *Rep. Progr. Phys.* **2**, 247.
Robinson 1937 *Rep. Progr. Phys.* **4**, 212.
Söderman 1935*a* *Nova Acta Soc. Sci. Uppsala.* **9**. 1.
Söderman 1935*b* *Nature, Lond.*, **135**, 67.
Spencer Jones 1938 *Rep. Progr. Phys.* **4**, 1.

General classical theory of spinning particles in a Maxwell field

BY H. J. BHABHA, PH.D. AND H. C. CORBEN, PH.D.

(*Communicated by P. A. M. Dirac, F.R.S.—Received* 17 *December* 1940)

The purpose of this paper is to give the complete classical theory of a spinning particle moving in a Maxwell field. The particle is assumed to be a point, and its interaction with the field is described by a point charge g_1 and a point dipole g_2. The Maxwell equations are assumed to hold right up to the point representing the particle. Exact equations are then derived for the motion of the particle in a given external field which are strictly consistent with the conservation of energy, momentum and angular momentum, and hence contain the effects of radiation reaction on the motion of the particle. It is shown that in the presence of a point dipole the energy tensor of the field can and must be redefined so as to make the total energy finite. The mass, the angular momentum of the spin, and the moment of inertia perpendicular to the spin axis appear in the equations as arbitrary mechanical constants. Reasons are given for believing that for an elementary particle the last constant is zero, in agreement with relativistic quantum theory.

In the general theory there is no relation between the electric and magnetic dipole moments of the particle and the state of its translational motion. A procedure is given for deriving from the general equations specialized equations consistent with the condition that the dipole is always a purely magnetic or electric one in the system in which the particle is instantaneously at rest. The radiation reaction terms are very much simpler in the former of these specialized cases than in the general case. The effect of radiation reaction is to make the scattering of light by a rotating dipole *decrease* inversely as the square of the frequency for high frequencies, just as for scattering by a point charge.

The quantum treatment of a point charge and its interaction with quantized fields gives rise to a number of difficulties, for example, those connected with self-energies, which become very much greater when the particle has an *explicit* spin interaction with the field, as in the case of protons or neutrons and their interaction with the meson field. These difficulties are due at least in part to a neglect of the effects of radiation reaction. For a point charge the effects of the radiation reaction can be estimated by a comparison with the classical theory of Lorentz, and it is generally assumed that the quantum theory will give correct results in those energy regions and for those processes where the effects of this radiation reaction are negligible. For a point dipole the position is less satisfactory; for in the absence of a classical theory giving the effects of radiation reaction on the motion of the dipole, it has not been possible to delimit the region in which the quantum theory might be expected to give correct results. In particular, it has been impossible to decide whether the multiple processes and Heisenberg explosions predicted by the quantum theory fall, at least partly, in a region where the theory should be valid and are therefore to be regarded as deserving of credence, or whether they take place entirely in energy regions where the theory loses all claim to validity by its vital neglect of radiation reaction, and are hence to be regarded as entirely spurious. An exact classical theory of spinning particles taking into account the effects of radiation reaction is therefore of considerable physical interest. The purpose of this paper is to supply a complete classical theory of spinning particles moving in a Maxwell field. The extension of this theory to a meson field is carried out in the paper which immediately follows this.

It will be shown in this paper that our classical theory is the parallel of a quantum theory in which the particle has an *explicit* spin interaction with the Maxwell field. It is *not* the classical equivalent of a theory in which the interaction of the particle with the field is expressed only through the potentials, as in Dirac's theory of the electron. All comparisons must therefore be between this theory and a quantum theory in which the particle has an explicit spin interaction with the field, such as could always be introduced mathematically.† It appears, however, that the electron as it occurs in nature does not have such an explicit interaction with the Maxwell field, so that the theory of this paper is not applicable, even in the classical limit, to an electron. On the other hand, protons and neutrons have an explicit spin interaction with the meson field. Our classical theory, or rather the extension of it to a meson field carried out in the following paper, is then applicable to this problem. All the remarks we make below will then only refer to a quantum theory containing an added spin interaction with the Maxwell field of the type mentioned.

It must be demanded of any complete classical theory that it shall be consistent with the principle of relativity, and this almost inevitably requires that the dipole be considered as a point with no extension. For if a particle of finite extension be considered, then it is not possible to specify the distribution of charge and dipole moment over the finite volume occupied by the particle in a relativistically consistent way without introducing a field (other than the Maxwell field) which shall be responsible for preserving the shape of the particle. The introduction of another field for this purpose would be artificial and in any case much more complicated than treating the dipole as a point. We now meet the difficulty that the field energy as usually defined becomes infinite in the immediate neighbourhood of the dipole. This difficulty may be avoided either by modifying Maxwell's equations so that the field remains finite in the immediate neighbourhood of the dipole, or by assuming that the Maxwell equations hold exactly right up to the point singularity representing the dipole, and modifying the definition of field energy when singularities are present in the field. The latter method has been applied successfully by Dirac (1938) and Pryce (1938) to a point electron, and it is the method we shall follow in this paper.

---

† A further interaction term of the type $g_2 F_{\mu\nu} \gamma^\mu \gamma^\nu \psi$ could be added to the Dirac equation, where $F_{\mu\nu}$ are the field strengths, and γ_μ the Dirac matrices as defined by Pauli (1933, p. 220).

The procedures of Dirac and Pryce are different, but lead to the same result, and both amount in essence to adding terms to the usual Maxwellian expression for the field energy which just cancel some of the singular terms and make the total field energy of a point charge finite. We believe that this procedure is not a mere mathematical device but is physically sensible. One can see this at once by going back to the origin of the idea of field energy. Consider the static case. The potential energy of any non-singular distribution of charge or dipole moment, that is, the work done in bringing this distribution of charge and dipole moment from infinity into the actual configuration, can be transformed by using Maxwell's equations into an integral over the whole of space occupied by the field, and hence may be regarded as energy stored in the field. But this transformation is no longer possible if singularities, for example point charges or point dipoles, are present in the field. The self-energy difficulties in the classical theory therefore arise by using a definition of field energy which is no longer valid in the presence of singularities.

It is of course possible to look upon a point electron as the limiting case of a distribution in which the same charge is initially spread over a finite volume. The Maxwellian definition of field energy can be used now, and in the limit when the charge becomes concentrated in a point the total field energy becomes infinite. This infinite field energy has a physical meaning, for it corresponds to the evident fact that the work done against electrostatic force in compressing a charge originally spread over a finite volume into a point is infinite. There are, however, no purely logical or mathematical reasons why a point charge or point dipole should be regarded as limiting cases in this manner. Moreover, it would be contrary to our present views about elementary particles to look upon them as made up in this way. It therefore seems to us logical and physically reasonable to look upon the elementary particles in nature as point charges or point dipoles, and to reformulate the definition of field energy when singularities are present in the field. It will be shown in this paper that this can be done for a point dipole in a way consistent with the principle of relativity.

We treat a particle as a point having an interaction with the field characterized by a charge g_1 and a dipole moment g_2, and we assume that the Maxwell equations are valid right up to the point. We then derive equations for the motion of the particle which are consistent with the conservation of energy, momentum and angular momentum for the system as a whole consisting of the particle and the field. These equations will automatically include the effects of radiation reaction. The conservation of angular momentum has to be demanded explicitly, for it gives the equation for the rotation of the dipole. The mass of the particle, the angular momentum of the spin and the moment of inertia perpendicular to the axis of the spin appear in the equations as arbitrary and independent constants.

In the general classical theory there is no connexion between the translational motion of the dipole and its rotational motion (by rotation is here understood a rotation in the direction of the time axis as well as a space rotation). It would be quite possible theoretically, for example, for an initially pure magnetic dipole with no translational motion to develop in a suitable external field an electric dipole moment at right angles to its magnetic moment while still continuing to be at rest. Dipoles of this sort do not seem to occur in nature. It is possible, however, to impose the condition that a dipole shall always remain a pure electric or magnetic dipole in the rest system, and a procedure is given for deriving from our general equations specialized equations consistent with either of these conditions. The special equations for a dipole which remains a pure magnetic dipole in the rest system have already been derived by a direct method (Bhabha 1940*a*, referred to in this paper as B) and are the same as those which are derived as a particular case of the present general theory. As has been mentioned before (Bhabha 1940*b*), the effect of radiation reaction is very much more complicated in the general than in either of the two special cases mentioned above, but there seems to be no reason within the limits of the classical theory for excluding the general case. It is therefore to be regarded as an achievement of relativistic quantum theory that it automatically demands that an elementary particle shall have only a pure magnetic moment in the system in which it is at rest.

As has been mentioned earlier, the dipole may also have a moment of inertia perpendicular to the axis of the spin, and this enters in the theory as an entirely independent constant. The equations, however, take their simplest form if the moment of inertia perpendicular to the axis of the spin is put equal to zero, that is, when the mechanical properties of the particle are those of a *pure* gyroscope. A comparison of the classical equations with those of the quantum theory, as well as a comparison of the respective cross-sections for the scattering of light, clearly shows that in the quantum theory the particle automatically has the mechanical properties of a pure gyroscope. The quantum theory therefore again appears to be an advance on classical theory in that it allows only the classically simplest case, in conformity with what is found in nature.

Where the present classical theory goes beyond the quantum theory is in being able to treat the effects of radiation reaction exactly, whereas the quantum theory neglects these completely. Our theory shows quite clearly the frequency in the neighbourhood of which radiation reaction first begins to dominate the scattering of light, and hence allows us to fix the region of validity of the quantum theory. It appears that within this region the classical and quantum theories give the same scattering, showing that *quantum* effects have not yet come in, as is to be expected also from quite general arguments. The present classical theory, therefore, apart from being of general theoretical interest, actually allows us to give a scattering formula which should be valid for frequencies far beyond the region of validity of the quantum formula under certain circumstances.

An important point may be noticed. The classical theory shows that for very high frequencies *the scattering of light does not depend either on the charge or on the dipole moment or on the mechanical constants of the particle, but is a pure function of the frequency, decreasing as the inverse square of the frequency.* This is true for both scattering by a pure charge as calculated by Dirac and for scattering by a dipole as calculated below, and appears to be a fundamental property of radiation. It is shown in the following paper that it is also true of a meson field. It is clear that a series in ascending powers of the charge or dipole moment cannot approximate to a behaviour of this sort. The proper treatment of radiation reaction, therefore, will probably require a far-reaching extension of quantum theory. The classical theory developed in this paper gives an exact treatment of radiation reaction, but its quantization appears to present very great difficulties.

GENERAL THEORY

We use tensor notation throughout, and for convenience put the velocity of light equal to unity. The metric tensor $g_{\mu\nu}$ is assumed to have the form $g_{00} = 1, g_{11} = g_{22} = g_{33} = -1$, with all the other components vanishing.

As stated in the introduction, we treat the particle as a point. Its co-ordinates are denoted by z_μ, which may be considered as functions of the proper time τ measured from an arbitrary point on the world line of the particle. A dot over a letter is used to denote differentiation with respect to the proper time τ. The velocity $\dot{z}_\mu$ of the particle is denoted by v_μ. The spin of the particle is described by an antisymmetric tensor $S_{\mu\nu}$ which may also be considered as a function of τ. The particle is assumed to have a charge g_1. The charge and current density P_μ at any point of space x_ρ may then be written with the help of δ-functions in the form

$$\mathrm{P}_\mu = g_1 \int_{-\infty}^{\infty} d\tau \, v_\mu \delta(x_0 - z_0)\, \delta(x_1 - z_1)\, \delta(x_2 - z_2)\, \delta(x_3 - z_3). \tag{1}$$

The dipole moment of the particle is denoted by g_2. It gives rise to a dipole density $\Sigma_{\mu\nu}$ at a point x_ρ which may be written in the form

$$\Sigma_{\mu\nu} = g_2 \int_{-\infty}^{\infty} d\tau \, S_{\mu\nu}(\tau)\, \delta(x_0 - z_0)\, \delta(x_1 - z_1)\, \delta(x_2 - z_2)\, \delta(x_3 - z_3). \tag{2}$$

It is found convenient to adopt the following notation. The invariant formed from any two tensors $X_{\mu\nu}$ and $Y_{\mu\nu}$ is written in the scalar product notation:

$$(XY) \equiv X_{\mu\nu} Y^{\mu\nu}, \quad X^2 \equiv (XX) = X_{\mu\nu} X^{\mu\nu}.$$

The invariant formed by any combination of tensors and two vectors is written in the usual matrix notation; thus

$$(\dot{v} \ddot{S} \dot{S} v) \equiv \dot{v}^\mu \ddot{S}_{\mu\rho} \dot{S}^{\rho\nu} v_\nu, \quad \dot{v}^2 \equiv \dot{v}_\rho \dot{v}^\rho.$$

The antisymmetric tensor formed from *two other antisymmetric* tensors $X_{\mu\nu}$ and $Y_{\mu\nu}$ is sometimes written in the vector product notation

$$[X \, . \, Y]_{\lambda\mu} = X_{\lambda\sigma} Y^\sigma{}_\mu - X_{\mu\sigma} Y^\sigma{}_\lambda.$$

Then if $X_{\mu\nu}$, $Y_{\mu\nu}$ and $Z_{\mu\nu}$ are three antisymmetric tensors, the following identity holds:

$$(X[Y \, . \, Z]) = (Y[Z \, . \, X]). \tag{3}$$

The vector v_μ by definition satisfies the equation

$$v^2 = 1. \tag{4}$$

The equations derived from this by successive differentiation are†

$$(v\dot{v}) = 0, \tag{5a}$$

$$(v\ddot{v}) + \dot{v}^2 = 0, \tag{5b}$$

$$(vv^{\mathrm{iii}}) + 3(\dot{v}\ddot{v}) = 0, \tag{5c}$$

$$(vv^{\mathrm{iv}}) + 4(\dot{v}v^{\mathrm{iii}}) + 3\ddot{v}^2 = 0. \tag{5d}$$

---

† We write v^{iii} and v^{iv} for the third and fourth derivatives with respect to τ.

Now in order that the constant g_2 should have a meaning, the absolute magnitude of the tensor $S_{\mu\nu}$ must remain constant. Thus we must demand that

$$S^2 \equiv S_{\mu\nu}S^{\mu\nu} = \text{constant}. \tag{6}$$

The equations derived from this by successive differentiation are

$$(SS') = 0, \tag{7a}$$

$$(SS'') + S'^2 = 0, \tag{7b}$$

$$(SS''') + 3(S'S'') = 0. \tag{7c}$$

The equations of motion of the dipole must be such as to be consistent with the equations (4), (5), (6) and (7).

If we denote the Maxwell potentials by ϕ_ν and the field strengths by $F_{\mu\nu}$, the Maxwell equations may be written in the form

$$\frac{\partial}{\partial x^\mu}\phi_\nu - \frac{\partial}{\partial x^\nu}\phi_\mu = F_{\mu\nu}, \tag{8a}$$

$$\frac{\partial}{\partial x_\mu}F_{\mu\nu} = 4\pi\,\mathrm{P}_\nu + 4\pi\frac{\partial}{\partial x_\mu}\Sigma_{\mu\nu}. \tag{8b}$$

From (8a) it follows at once that

$$\frac{\partial}{\partial x^\lambda}F_{\mu\nu} + \frac{\partial}{\partial x^\mu}F_{\nu\lambda} + \frac{\partial}{\partial x^\nu}F_{\lambda\mu} = 0. \tag{9}$$

The potentials may be taken to satisfy the equation

$$\frac{\partial}{\partial x_\mu}\phi_\mu = 0, \tag{10}$$

and hence it follows from (8) that

$$\frac{\partial}{\partial x_\rho}\frac{\partial}{\partial x^\rho}\phi_\nu = 4\pi\,\mathrm{P}_\nu + 4\pi\frac{\partial}{\partial x_\mu}\Sigma_{\mu\nu}. \tag{11}$$

The usual energy-momentum density tensor of the field $T_{\mu\nu}$ is given by the expression

$$4\pi T_{\mu\nu} = F_{\mu\rho}F^\rho{}_\nu + \tfrac{1}{4}g_{\mu\nu}F_{\rho\sigma}F^{\rho\sigma}. \tag{12}$$

It satisfies the equation of conservation

$$\frac{\partial}{\partial x_\nu}T_{\mu\nu} = 0 \tag{13}$$

in free space.

As in a previous paper (Bhabha 1939*b*) we introduce a tensor $M_{\lambda\mu\nu}$, antisymmetric in λ and μ, to represent the angular momentum density of the field:

$$M_{\lambda\mu\nu} \equiv x_\lambda T_{\mu\nu} - x_\mu T_{\lambda\nu}. \tag{14}$$

It likewise satisfies the equation of conservation in free space

$$\frac{\partial}{\partial x_\nu} M_{\lambda\mu\nu} = 0. \tag{15}$$

The solutions of (11) giving the retarded and advanced potentials are well known. Our theory is quite symmetrical in retarded and advanced potentials, and we therefore only deal with retarded potentials for simplicity. Due to the two terms on the right-hand side of (11), the retarded potential $\phi_\nu^{\text{ret.}}$ is a sum of two parts:

$$\phi_\nu^{\text{ret.}} = \phi_\nu^{(1)} + \phi_\nu^{(2)}, \tag{16}$$

the first being proportional to g_1, the second to g_2.

We introduce the vector s_μ to represent the distance from the actual point to the retarded point $z_\mu(\tau_0)$:

$$s_\mu \equiv x_\mu - z_\mu(\tau_0). \tag{17}$$

The retarded time τ_0 is defined by the equation

$$s_\mu s^\mu \equiv \{x_\mu - z_\mu(\tau_0)\}\{x^\mu - z^\mu(\tau_0)\} = 0. \tag{18}$$

We introduce the following symbols:

$$\kappa \equiv s_\mu(\tau_0)\, v^\mu(\tau_0), \quad \kappa' \equiv s_\mu(\tau_0)\, \dot{v}^\mu(\tau_0), \quad \kappa'' \equiv s_\mu(\tau_0)\, \ddot{v}^\mu(\tau_0), \tag{19}$$

and

$$\mathcal{S}_\mu = S_{\mu\nu}v^\nu, \quad S'_\mu = \dot{S}_{\mu\nu}v^\nu, \quad S''_\mu = \ddot{S}_{\mu\nu}v^\nu, \quad S'''_\mu = S^{\text{iii}}_{\mu\nu}v^\nu, \quad S''''_\mu = S^{\text{iv}}_{\mu\nu}v^\nu. \tag{20}$$

The retarded potentials may then be written in the well-known forms

$$\phi_\nu^{(1)} = g_1 \frac{v_\nu}{\kappa}, \tag{21}$$

$$\phi_\nu^{(2)} = g_2 \frac{\partial}{\partial x_\rho}\left(\frac{S_{\rho\nu}}{\kappa}\right). \tag{22}$$

All the quantities on the right-hand side are understood to be taken at the retarded time τ_0. In carrying out the differentiation in (22) we must remember that a change in the point x_ρ not only changes the distance s_ρ but also changes the retarded time τ_0. The general method of carrying out the differentiation has been given in an earlier paper (Bhabha 1939*a* referred to here as A). We thus find†

$$\phi_\nu^{(2)} = g_2\left\{\frac{\mathcal{S}_\nu}{\kappa^2}+\frac{s^\rho S_{\rho\nu}}{\kappa^3}, \quad -\frac{s^\rho S_{\rho\nu}}{\kappa^3}\kappa'+\frac{s^\rho \dot{S}_{\rho\nu}}{\kappa^2}\right\}. \tag{23}$$

Now s_μ, κ and κ' are of the same order, so that the first two terms are of order κ^{-2} and the next two of order κ^{-1}.

The retarded field strengths can be calculated at once by using (8*a*). Corresponding to (16) we write

$$F_{\mu\nu}^{\text{ret.}} = F_{\mu\nu}^{(1)} + F_{\mu\nu}^{(2)}. \tag{24}$$

$F_{\mu\nu}^{(1)}$ and $F_{\mu\nu}^{(2)}$ are given in the appendix. The first is the field of a pure point charge and is proportional to g_1. It has terms of order κ^{-2} and κ^{-1}. The second is the field of a pure point dipole and is proportional to g_2. It has terms of order κ^{-3}, κ^{-2} and κ^{-1}. Following Dirac we write the actual field $F_{\mu\nu}$ at any point as the sum of the retarded field $F_{\mu\nu}^{\text{ret.}}$ at that point plus an ingoing field $F_{\mu\nu}^{\text{in.}}$:

$$F_{\mu\nu} = F_{\mu\nu}^{\text{ret.}} + F_{\mu\nu}^{\text{in.}}. \tag{25}$$

The ingoing field $F_{\mu\nu}^{\text{in.}}$ satisfies the Maxwell equations for empty space, i.e. (8) and (9), with the right-hand side of (8*b*) put equal to zero.

We now proceed to find the exact equations of motion for the particle. It is necessary at this stage to introduce the idea of an antisymmetric tensor $X_{\mu\nu}^*$ adjunct (dual) to a given antisymmetric tensor $X_{\mu\nu}$. Its components are connected with those of $X_{\mu\nu}$ by the equations

$$\left.\begin{aligned} X^{*01} &= X_{23}, & X^{*02} &= X_{31}, & X^{*03} &= X_{12}, \\ X^{*23} &= X_{01}, & X^{*31} &= X_{02}, & X^{*12} &= X_{03}. \end{aligned}\right\} \tag{26a}$$

Any of the relations (26*a*) can be deduced from any other by successively changing any three suffices in rotation. Using the tensor $g_{\mu\nu}$, we can deduce from (26*a*) that

$$\left.\begin{aligned} X_{01}^* &= -X^{23}, & X_{02}^* &= -X^{31}, & X_{03}^* &= -X^{12}, \\ X_{23}^* &= -X^{01}, & X_{31}^* &= -X^{02}, & X_{12}^* &= -X^{03}. \end{aligned}\right\} \tag{26b}$$

It follows at once from (26) that

$$(X^*)^* = -X. \tag{27}$$

---

† Following Dirac, we separate terms which correspond (as $\kappa \to 0$) to singularities of different orders by a comma.

If $X_{\mu\nu}$, $Y_{\mu\nu}$ are two antisymmetric tensors, then it can be proved easily that

$$(XY^*) = (X^*Y), \tag{28a}$$

$$[X.Y^*] = [X^*.Y], \tag{28b}$$

and

$$[X.Y]^* = [X.Y^*] = [X^*.Y]. \tag{29}$$

It will appear presently that the six-vector $S^*_{\mu\nu}$ adjunct to $S_{\mu\nu}$ plays an important part in the equations and is on the same footing as $S_{\mu\nu}$. Using (26) we have

$$(SS^*) \equiv S_{\mu\nu}S^{*\mu\nu} = 4(S_{01}S_{23}+S_{02}S_{31}+S_{03}S_{12}), \tag{30}$$

and, by (29),

$$[S.S^*] = [S.S]^* = 0. \tag{31}$$

Now the change $\delta S_{\lambda\mu}$ in the components of the spin due to the most general type of rotation possible (by a rotation we always mean a spatial rotation as well as a rotation involving the time component) can always be written in the form

$$\delta S_{\lambda\mu} = S_{\lambda\rho}\phi^{\rho}{}_{\mu} - S_{\mu\rho}\phi^{\rho}{}_{\lambda},$$

where $\phi_{\rho\mu}$ is an infinitesimal antisymmetric tensor. Thus the most general form for the equation giving the rotation of the spin is

$$\dot{S}_{\lambda\mu} = S_{\lambda\rho}\Theta^{\rho}{}_{\mu} - S_{\mu\rho}\Theta^{\rho}{}_{\lambda}, \tag{32a}$$

$\Theta_{\rho\mu}$ being some six-vector. Θ may itself involve derivatives of S. In our abbreviated notation this equation reads

$$\dot{S} = [S.\Theta]. \tag{32b}$$

This expression for $\dot{S}$ automatically satisfies (7a), for, by (3),

$$(S\dot{S}) = (S[S.\Theta]) = (\Theta[S.S]) = 0; \tag{33}$$

Similarly it follows from (32) and (31) that

$$(S^*\dot{S}) = (S^*[S.\Theta]) = (\Theta[S^*.S]) = 0; \tag{34}$$

whence

$$(S^*S) = \text{constant}. \tag{34a}$$

The equation adjunct to (32) is

$$\dot{S}^* = [S.\Theta]^* = [S.\Theta^*] = [S^*.\Theta]. \tag{35}$$

Multiplying (32) and (35) by arbitrary constants I and I' and adding, we find

$$I\dot{S} + I'\dot{S}^* = [S.\Theta']. \tag{36}$$

We have written Θ' in place of $I\Theta + I'\Theta^*$. This is the most general form that can be taken by the equations of motion for the rotation of the dipole.

It will be seen below that the condition that the rotational equations must have the form (36) takes us a long way towards determining the radiation reaction terms.

Conversely, we can go back from equation (36) to the equations (32) and (35). For the equation adjunct to (36) is

$$I\dot{S}^{*} - I'\dot{S} = [S.\Theta'^{*}]; \tag{37}$$

whence, by (36), we deduce

$$(I^2+I'^2)\dot{S} = [S.(I\Theta' - I'\Theta'^{*})] = (I^2+I'^2)[S.\Theta],$$

which is just equation (32). It follows from this, as can also be proved directly, that it is a necessary consequence of an equation of the type (36) that

$$(S\dot{S}) = 0, \tag{33}$$

$$(S^{*}\dot{S}) = 0. \tag{34}$$

It further follows from the symmetry of the right-hand side of (36) in S and Θ', as also from (32) and (35), that

$$(\dot{S}\Theta) = 0, \tag{38}$$

$$(\dot{S}^{*}\Theta) = 0. \tag{39}$$

Thus two invariant equations are a consequence of the rotational equation (36). As will be seen below, another invariant equation can be deduced from the equations of motion giving the translation of the particle, and the requirement that this equation shall be consistent with (38) gives us further conditions determining the equations of motion.

To proceed further we follow a method first used by Dirac (1938). Consider the world line of the particle to be given, and also the direction of the spin at every point. Now surround this world line by a thin world tube, the radius of which will ultimately be made to tend to zero, and calculate by using the tensors $T_{\mu\nu}$ and $M_{\lambda\mu\nu}$ the flow of field energy, momentum and angular momentum through the three-dimensional surface of a finite length of this tube bounded by the proper times τ_1 and τ_2. For conservation, the flow of energy, momentum and angular momentum through the surface of this length of tube must equal the difference in these quantities at the two ends of the tube. The rate of flow of these quantities must therefore be a perfect differential. This will only be the case if, depending on the ingoing field, the world line has a certain shape and the dipole a certain orientation at each point. In other words, this condition will give the equations of motion of the particle in the given ingoing field.

It is easy to show that our results do not depend on the shape of the tube. For convenience we take the tube defined by

$$\kappa \equiv s_\mu(\tau_0)\, v^\mu(\tau_0) = \epsilon, \tag{40}$$

where ϵ will be treated as a small quantity which will ultimately be made to tend to zero. We fix our attention on some point τ_0 of the world line and consider it in the particular Lorentz system in which the velocity at that point has the special form $v_0 = 1$, $v_1 = v_2 = v_3 = 0$. This will be called the rest system of the point. Then from (40) it follows that in this system $s_0 = \epsilon$, and since $s_\mu s^\mu = 0$, a two-dimensional sphere of radius ϵ with the point τ_0 as centre taken at a time ϵ later forms a section of the tube. All points on the surface of this sphere correspond to the same retarded point τ_0. Thus any integral over the surface of the tube can always be regarded as a two-dimensional integral over the surface of a sphere centred round a point with the proper time τ, and then an integral along the world line with respect to the proper time τ.

If we denote by dS^ν an element of the surface of the tube taken as positive when the normal is directed outwards, then the flow of energy and momentum into a length of the tube whose ends correspond to the proper times τ_1 and τ_2 is

$$\int T_{\mu\nu}\, dS^\nu, \tag{41}$$

which, in view of what has been said above about integration over the surface of the tube, can always be written in the form

$$\int_{\tau_1}^{\tau_2} T_\mu\, d\tau. \tag{42}$$

For conservation of energy and momentum this must only depend on the conditions at the two ends of the tube, so that the integral must be a perfect differential. Therefore we must have

$$T_\mu = \dot{A}_\mu, \tag{43}$$

where A_μ is some tensor which has to be found. Equation (43) determines the translational motion of the particle.

The flow of angular momentum into the tube is given by

$$\int M_{\lambda\mu\nu}\, dS^\nu. \tag{44}$$

By (14) and the definition (17) of s_μ, (44) can be written

$$\int (s_\lambda T_{\mu\nu} - s_\mu T_{\lambda\nu})\,dS^\nu + \int (z_\lambda T_{\mu\nu} - z_\mu T_{\lambda\nu})\,dS^\nu. \tag{44a}$$

The first integral can again be written in the form

$$\int_{\tau_1}^{\tau_2} M_{\lambda\mu}\,d\tau, \tag{44b}$$

while the second becomes

$$\int_{\tau_1}^{\tau_2} (z_\lambda T_\mu - z_\mu T_\lambda)\,d\tau.$$

Thus, by (43),

$$\begin{aligned}\int M_{\lambda\mu\nu}\,dS^\nu &= \int_{\tau_1}^{\tau_2} d\tau \{M_{\lambda\mu} + (z_\lambda \dot{A}_\mu + z_\mu \dot{A}_\lambda)\} \\ &= \int_{\tau_1}^{\tau_2} d\tau \left\{M_{\lambda\mu} - (v_\lambda A_\mu - v_\mu A_\lambda) + \frac{d}{d\tau}(z_\lambda A_\mu - z_\mu A_\lambda)\right\}.\end{aligned}$$

For conservation of angular momentum, the integrand of this must be a perfect differential. Put it equal to $\dot{B}_{\lambda\mu} + \frac{d}{d\tau}(z_\lambda A_\mu - z_\mu A_\lambda)$. This leads to

$$M_{\lambda\mu} - (v_\lambda A_\mu - v_\mu A_\lambda) = \dot{B}_{\lambda\mu}, \tag{45}$$

where $B_{\lambda\mu}$ has to be found. Equation (45) then determines the rotational motion of the dipole.

We now return to T_μ. Owing to the quadratic form (12) of $T_{\mu\nu}$ in the field strengths and the splitting of $F_{\mu\nu}$ into two parts by (25), $T_{\mu\nu}$ can be written as the sum of three parts:

$$T_{\mu\nu} = T^{\text{ret.}}_{\mu\nu} + T^{\text{mix.}}_{\mu\nu} + T^{\text{in.}}_{\mu\nu}.$$

The first contains the retarded field only, the second the product of the retarded and ingoing fields, and the last only the ingoing field. Since $F^{\text{in.}}_{\mu\nu}$ is not singular on the world line, $T^{\text{in.}}_{\mu\nu}$ is also not singular, and hence in the limit $\epsilon \to 0$ will make no contribution to (41). Thus we may write

$$T_\mu = T^{\text{ret.}}_\mu + T^{\text{mix.}}_\mu. \tag{46}$$

Since, according to (24), $F^{\text{ret.}}_{\mu\nu}$ consists of two parts, $T^{\text{ret.}}_\mu$ will contain terms proportional to g_1^2, $g_1 g_2$ and g_2^2, while $T^{\text{mix.}}_\mu$ will contain the ingoing field and terms proportional to g_1 and g_2. Corresponding to this we write A_μ as the sum of three parts:

$$A_\mu = A^{\text{ret.}}_\mu + A^{\text{mix.}}_\mu + A^{\text{mech.}}_\mu. \tag{47}$$

The first only contains terms proportional to g_1^2, $g_1 g_2$ and g_2^2, the second contains the ingoing field and terms proportional to g_1 or g_2, while the third does not contain g_1 or g_2. We call $A_\mu^{\text{mech.}}$ the mechanical part of the energy.

If we write
$$T_\mu^{\text{react.}} \equiv T_\mu^{\text{ret.}} - \dot{A}_\mu^{\text{ret.}}, \tag{48}$$
the translational equation (43) becomes
$$T_\mu^{\text{react.}} + T_\mu^{\text{mix.}} - \dot{A}_\mu^{\text{mix.}} = \dot{A}_\mu^{\text{mech.}}. \tag{49}$$

For the same reasons as lead to (46), $M_{\lambda\mu}$ can also be written as the sum of two parts:
$$M_{\lambda\mu} = M_{\lambda\mu}^{\text{ret.}} + M_{\lambda\mu}^{\text{mix.}}, \tag{50}$$
the first of which contains terms proportional to g_1^2, $g_1 g_2$ and g_2^2, while the second has terms proportional to g_1 and g_2 containing the ingoing field. Corresponding to (50) we write $B_{\lambda\mu}$ as the sum of two parts:
$$B_{\lambda\mu} = B_{\lambda\mu}^{\text{ret.}} + B_{\lambda\mu}^{\text{mech.}}. \tag{51}$$
Here $B_{\lambda\mu}^{\text{ret.}}$ contains all the terms proportional to g_1^2, $g_1 g_2$ and g_2^2, while $B_{\lambda\mu}^{\text{mech.}}$ only contains terms independent of g_1 and g_2, and represents the mechanical properties of the spin, as will be seen below. $B_{\lambda\mu}^{\text{mix.}}$ cannot exist for dimensional reasons. It would have to be a product of g_2 times the ingoing field times a quantity of the dimensions of a length, and no such quantity can be made up of $S_{\mu\nu}$ or v_μ and their derivatives (provided, naturally, that the reciprocals of these quantities are excluded). If we write
$$M_{\lambda\mu}^{\text{react.}} \equiv M_{\lambda\mu}^{\text{ret.}} - (v_\lambda A_\mu^{\text{ret.}} - v_\mu A_\lambda^{\text{ret.}}) - \dot{B}_{\lambda\mu}^{\text{ret.}}, \tag{52}$$
the rotational equation (45) can be written
$$M_{\lambda\mu}^{\text{react.}} + \{M_{\lambda\mu}^{\text{mix.}} - (v_\lambda A_\mu^{\text{mix.}} - v_\mu A_\lambda^{\text{mix.}})\} = \dot{B}_{\lambda\mu}^{\text{mech.}} + (v_\lambda A_\mu^{\text{mech.}} - v_\mu A_\lambda^{\text{mech.}}). \tag{53}$$

The terms $T_\mu^{\text{react.}}$ in (49) and $M_{\lambda\mu}^{\text{react.}}$ in (53), being quadratic in g_1 and g_2, represent the effects of radiation reaction.

The derivation of (53) shows that as far as the conservation laws are concerned $B_{\lambda\mu}^{\text{mech.}}$ is arbitrary. The general arguments given at the beginning show that the rotational equation must be of the form (36). We may therefore put
$$B_{\lambda\mu}^{\text{mech.}} = I S_{\lambda\mu} + I' S_{\lambda\mu}^{*} + B_{\lambda\mu}^{\prime\,\text{mech.}}, \tag{54}$$
where I and I' are arbitrary constants. (53) then becomes
$$\begin{aligned} I\dot{S}_{\lambda\mu} + I'\dot{S}_{\lambda\mu}^{*} &+ \{v_\lambda A_\mu^{\text{mech.}} - v_\mu A_\lambda^{\text{mech.}} + \dot{B}_{\lambda\mu}^{\prime\,\text{mech.}}\} \\ &= \{M_{\lambda\mu}^{\text{mix.}} - (v_\lambda A_\mu^{\text{mix.}} - v_\mu A_\lambda^{\text{mix.}})\} + M_{\lambda\mu}^{\text{react.}}. \end{aligned} \tag{55}$$

Now the reaction and the mixed terms in (55) contain different powers of the fundamental constants g_1 and g_2, while the mechanical terms are independent of them. Each group by itself must therefore have the form of the right-hand side of (36). Hence we must have

$$M_{\lambda\mu}^{\text{react.}} \equiv S_{\lambda}{}^{\rho} C_{\rho\mu}^{\text{react.}} - S_{\mu}{}^{\rho} C_{\rho\lambda}^{\text{react.}}. \tag{56}$$

In other words, $A_{\mu}^{\text{rot.}}$ and $B_{\lambda\mu}^{\text{rot.}}$ must be so chosen that the left-hand side of (56) has the form of the right-hand side of this equation. $C_{\rho\mu}^{\text{react.}}$ is an antisymmetric tensor which is not yet known. Similarly, $A_{\mu}^{\text{mech.}}$ and $B_{\lambda\mu}'^{\text{mech.}}$ must be so chosen that

$$v_{\lambda} A_{\mu}^{\text{mech.}} - v_{\mu} A_{\lambda}^{\text{mech.}} + \dot{B}_{\lambda\mu}'^{\text{mech.}} \equiv S_{\lambda}{}^{\rho} C_{\rho\mu}^{\text{mech.}} - S_{\mu}{}^{\rho} C_{\rho\lambda}^{\text{mech.}}. \tag{57}$$

Consider now the mixed terms. It is shown in the appendix that

$$\begin{aligned} T_{\mu}^{\text{mix.}} = {} & g_1 F_{\mu\sigma}^{\text{in.}} v^{\sigma} \\ & + g_2\left[-\tfrac{1}{2} S^{\rho\sigma} \frac{\partial}{\partial x^{\mu}} F_{\rho\sigma}^{\text{in.}} + \frac{d}{d\tau}\{\tfrac{2}{3} S_{\mu\sigma} F^{\text{in.}\,\sigma\nu} v_{\nu} - \tfrac{2}{3} F_{\mu\sigma}^{\text{in.}} \mathcal{S}^{\sigma} + \tfrac{1}{3} v_{\mu} S^{\rho\sigma} F_{\rho\sigma}^{\text{in.}}\}\right], \end{aligned} \tag{58}$$

$$\begin{aligned} M_{\lambda\mu}^{\text{mix.}} = {} & g_2[S_{\lambda}{}^{\sigma} F_{\sigma\mu}^{\text{in.}} - S_{\mu}{}^{\sigma} F_{\sigma\lambda}^{\text{in.}} + \tfrac{2}{3} v_{\lambda} S_{\mu}{}^{\sigma} F_{\sigma\nu}^{\text{in.}} v^{\nu} \\ & - \tfrac{2}{3} v_{\mu} S_{\lambda}{}^{\sigma} F_{\sigma\nu}^{\text{in.}} v^{\nu} - \tfrac{2}{3} v_{\lambda} F_{\mu\sigma}^{\text{in.}} \mathcal{S}^{\sigma} + \tfrac{2}{3} v_{\mu} F_{\lambda\sigma}^{\text{in.}} \mathcal{S}^{\sigma}]. \end{aligned} \tag{59}$$

Put

$$A_{\mu}^{\text{mix.}} = g_2\{\tfrac{2}{3} S_{\mu}{}^{\sigma} F_{\sigma\nu}^{\text{in.}} v^{\nu} - \tfrac{2}{3} F_{\mu\sigma}^{\text{in.}} \mathcal{S}^{\sigma} - \tfrac{1}{6} v_{\mu} S^{\rho\sigma} F_{\rho\sigma}^{\text{in.}}\}. \tag{60}$$

This at once gives

$$M_{\lambda\mu}^{\text{mix.}} - (v_{\lambda} A_{\mu}^{\text{mix.}} - v_{\mu} A_{\lambda}^{\text{mix.}}) = g_2\{S_{\lambda}{}^{\sigma} F_{\sigma\mu}^{\text{in.}} - S_{\mu}{}^{\sigma} F_{\sigma\lambda}^{\text{in.}}\}, \tag{61}$$

which is just of the required form. In fact, the condition that the mixed terms in (55) must have the form of the right-hand side of (36) uniquely determines the first two terms of $A_{\mu}^{\text{mix.}}$. A term consisting of v_{μ} multiplied by an invariant could always be added to $A_{\mu}^{\text{mix.}}$ without altering the left-hand side of (61). But this term would alter the mixed terms in the translational equation (49). It will appear almost immediately that even a term of this type is uniquely determined, and has to be taken to be the third term of (60). By (58) and (60), the mixed terms in (49) then reduce to

$$T_{\mu}^{\text{mix.}} - \dot{A}_{\mu}^{\text{mix.}} = g_1 F_{\mu\sigma}^{\text{in.}} v^{\sigma} - \tfrac{1}{2} g_2 S^{\rho\sigma} \frac{\partial}{\partial x^{\mu}} F_{\rho\sigma}^{\text{in.}} + \tfrac{1}{2} g_2 \frac{d}{d\tau}(v_{\mu} S^{\rho\sigma} F_{\rho\sigma}^{\text{in.}}). \tag{62}$$

By (62), the translational equation (49) becomes

$$\dot{A}_{\mu}^{\text{mech.}} = g_1 F_{\mu\sigma}^{\text{in.}} v^{\sigma} - \tfrac{1}{2} g_2 S^{\rho\sigma} \frac{\partial}{\partial x^{\mu}} F_{\rho\sigma}^{\text{in.}} + \tfrac{1}{2} g_2 \frac{d}{d\tau}(v_{\mu} S^{\rho\sigma} F_{\rho\sigma}^{\text{in.}}) + T_{\mu}^{\text{react.}}. \tag{63}$$

By substituting (56), (57) and (61) in (55), the rotational equation may be written

$$I\dot{S}_{\lambda\mu} + I'\dot{S}^*_{\lambda\mu} + [S\,.\,C^{\text{mech.}}]_{\lambda\mu} = g_2[S\,.\,F^{\text{in.}}]_{\lambda\mu} + [S\,.\,C^{\text{react.}}]_{\lambda\mu}. \tag{64}$$

The simplest invariant equation which can be deduced from (63) is obtained by contracting it with v^μ. Remembering (4) and (5a), and using the obvious relation

$$v^\mu S^{\rho\sigma}\frac{\partial}{\partial x^\mu}F^{\text{in.}}_{\rho\sigma} = S^{\rho\sigma}\frac{d}{d\tau}F^{\text{in.}}_{\rho\sigma},$$

we find

$$v^\mu \dot{A}^{\text{mech.}}_\mu - \tfrac{1}{2}g_2(\dot{S}F^{\text{in.}}) = v^\mu T^{\text{react.}}_\mu. \tag{65}$$

By the reasoning which leads from (36) to (38) and (39), we see that the rotational equation (64) leads to two invariant equations

$$(\dot{S}C^{\text{mech.}}) - g_2(\dot{S}F^{\text{in.}}) = (\dot{S}C^{\text{react.}}) \tag{66}$$

and

$$(\dot{S}^*C^{\text{mech.}}) - g_2(\dot{S}^*F^{\text{in.}}) = (\dot{S}^*C^{\text{react.}}). \tag{67}$$

The expressions containing the ingoing fields in (65) and (66) are identical, so that consistency requires that

$$(\dot{S}C^{\text{mech.}}) = 2v^\mu \dot{A}^{\text{mech.}}_\mu \tag{68}$$

and

$$(\dot{S}C^{\text{react.}}) = 2v^\mu T^{\text{react.}}_\mu. \tag{69}$$

We now see that the last term of $A^{\text{mix.}}_\mu$ in (60) was uniquely determined. For the addition to $A^{\text{mix.}}_\mu$ of a term consisting of v_μ multiplied by an invariant containing the ingoing field would have left (61) and hence (66) unchanged, while changing (62) and hence the terms in (65) containing the ingoing field. This would have made (65) and (66) inconsistent.

THE MECHANICAL CONSTANTS

We now come to $A^{\text{mech.}}_\mu$ and $B^{\text{mech.}}_{\lambda\mu}$. These may be any expressions which satisfy the condition that the left-hand side of (57) shall be identically of the form of the right-hand side of that equation:

$$v_\lambda A^{\text{mech.}}_\mu - v_\mu A^{\text{mech.}}_\lambda + \dot{B}'^{\text{mech.}}_{\lambda\mu} \equiv S_\lambda{}^\rho C^{\text{mech.}}_{\rho\mu} - S_\mu{}^\rho C^{\text{mech.}}_{\rho\lambda}. \tag{57}$$

They must further satisfy (68).

Expressions which satisfy these conditions are

$$A^{\text{mech.}}_\mu = v_\mu\{M + \tfrac{1}{4}K\dot{S}^2 + \tfrac{1}{4}K'(\dot{S}\dot{S}^*)\} \tag{70}$$

and

$$B'^{\text{mech.}}_{\lambda\mu} = K[S\,.\,\dot{S}]_{\lambda\mu} + K'[S\,.\,\dot{S}^*]_{\lambda\mu}, \tag{71}$$

where M, K and K' are arbitrary constants. M has the dimensions of a mass, and K and K' those of a moment of inertia.

If we introduce (70) into (63),the translational equation can be written in its final form

$$M\dot{v}_{\mu}+\frac{d}{d\tau}v_{\mu}\{\tfrac{1}{4}K\dot{S}^{2}-\tfrac{1}{4}K'(\dot{S}\dot{S}^{*})-\tfrac{1}{2}g_{2}(SF^{\text{in.}})\}$$
$$=g_{1}F^{\text{in.}}_{\mu\sigma}v^{\sigma}-\tfrac{1}{2}g_{2}S^{\rho\sigma}\frac{\partial}{\partial x^{\mu}}F^{\text{in.}}_{\rho\sigma}+T^{\text{react.}}_{\mu}. \qquad (72)$$

By substituting (71) into (64), the rotational equation becomes

$$I\dot{S}_{\lambda\mu}+I'\dot{S}^{*}_{\lambda\mu}+K[S.\ddot{S}]_{\lambda\mu}+K'[S.\ddot{S}^{*}]_{\lambda\mu}=g_{2}[S.F^{\text{in.}}]_{\lambda\mu}+[S.C^{\text{react.}}]_{\lambda\mu}, \qquad (73)$$

and the invariant equation (66) becomes

$$K(\dot{S}\ddot{S})+K'(\dot{S}\ddot{S}^{*})-g_{2}(\dot{S}F^{\text{in.}})=(\dot{S}C^{\text{react.}}). \qquad (74)$$

The substitutions (70) and (71) are not the most general which are possible and they have been chosen for their simplicity. Moreover, the five constants M, I, I', K and K' are capable of simple physical interpretations, and represent the mechanical properties of a spinning particle which are well known from ordinary mechanics. Reasons will be given in the last section for believing that even (70) and (71) lead to equations which are too general, and that for the elementary particles which occur in nature, I', K and K' are zero.

I and I' represent the gyroscopic properties of the particle, and their physical meaning becomes particularly clear in certain special cases which will be investigated in a later section. It will be shown there that when the equations are such that the dipole is always a pure magnetic dipole in the rest system, I is the angular momentum of the spin about the axis of the dipole and K is the moment of inertia about an axis perpendicular to the direction of the dipole. In this case I' is zero. When the equations are such that the dipole is always a pure electric dipole in the rest system, I' represents the angular momentum of the spin about the axis of the *electric* dipole, and K' is the moment of inertia about a perpendicular axis, while I must now be zero.

It should be emphasized that all the five constants M, I, I', K and K' are completely independent and arbitrary, and may be given any positive or negative values. This may seem to be in contradiction with the properties of bodies in ordinary mechanics, where, for example, a non-vanishing value of I, the angular momentum about one axis, necessarily requires that the moment of inertia about a perpendicular axis shall be positive. This contradiction is only apparent, and results from the fact that in ordinary mechanics the mass density is always assumed to be positive at all points of the particle. In general theory, however, the mass density need not be positive at every point any more than the total mass of the particle need be positive, and once the mass density is allowed to take on both positive and negative values, it can easily be seen that a mass distribution can be given in a body of finite size for which the mechanical constants have arbitrarily assigned values, positive or negative. It is therefore not surprising that in our theory, where the particle is treated as a point, the five constants are entirely independent and arbitrary.

It is now easy to see the physical meaning of all the terms on the left-hand side of the *translational equation* (72). The first term just expresses the ordinary mechanical properties of a particle whose rest mass is M. Next, $[S.\dot{S}]$ represents the rate of rotation of the direction of the spin, and the kinetic energy associated with this motion is $\frac{1}{4}K\dot{S}^2$. In conformity with relativistic ideas this appears as an addition to the mass in (70) and (72). The meaning of the next term is similar. Lastly, $-\frac{1}{2}g_2(SF^{\text{in.}})$ is the potential energy of the dipole in the given ingoing field, and this also appears as an addition to the mass of the particle in (72).

The meaning of equation (74) is also clear. It states that $\frac{1}{2}g_2(\dot{S}F^{\text{in.}})$, the rate of decrease of the potential energy of the dipole in the ingoing field *due to a rotation of the dipole*, is equal to the rate of increase of the rotational kinetic energy plus the rate at which energy is radiated away, $-\frac{1}{2}(\dot{S}C^{\text{react.}})$.

To find other possible additions to (70) and (71), we have to find further solutions of (57) and (68). The easiest way to do this is to proceed methodically by taking terms which can combine with each other in groups. We illustrate the method of finding solutions by two examples which will be of use later when we come to discuss the radiation reaction terms. Possible additions to $A_\mu^{\text{mech.}}$ which do not contain the spin $S_{\mu\nu}$ at all have already been investigated in detail in a previous paper (Bhabha 1939*b*). It is shown there that besides the first term of (70) there is only one other solution possible which is reasonably simple, and this would lead to a motion of the particle quite unlike anything that is known in nature.

Now consider all possible additions to $A_\mu^{\text{mech.}}$ which are quadratic in $S_{\lambda\mu}$ and do not contain any differentiations with respect to τ. The most general combination of this type is

$$A''^{\text{mech.}}_\mu = e_1 v_\mu S^2 + e_2 v_\mu \dot{S}^2 + e_3 S_{\mu\rho}\dot{S}^\rho. \tag{75}$$

The e's are arbitrary constants having the dimensions of a mass. By (57), terms of this sort must combine with a certain $\dot{B}''^{\text{mech.}}_{\lambda\mu}$, so that $B''^{\text{mech.}}_{\lambda\mu}$ must contain one differentiation less than $A''^{\text{mech.}}_{\mu}$. This is not possible with the substitution (75), so that in this case $B''^{\text{mech.}}_{\lambda\mu}$ is zero We find

$$\begin{aligned} v_\lambda A''^{\text{mech.}}_{\mu} - v_\mu A''^{\text{mech.}}_{\lambda} &= e_3(v_\lambda S_{\mu\rho}\mathcal{S}^\rho - v_\mu S_{\lambda\rho}\mathcal{S}^\rho) \\ &= -e_3\{S_{\lambda\sigma}(\mathcal{S}^\sigma v_\mu - v^\sigma \mathcal{S}_\mu) - S_{\mu\sigma}(\mathcal{S}^\sigma v_\lambda - v^\sigma \mathcal{S}_\lambda)\}, \end{aligned} \tag{76}$$

which satisfies the condition (57). By (4), (5*a*) and (6), the equation (68) then requires that

$$-e_3(\mathcal{S}S') = 2e_2(\mathcal{S}S') + 2e_2(\mathcal{S}S\dot{v}) - 2e_3(\mathcal{S}S') - e_3(\mathcal{S}S\dot{v}).$$

This gives
$$e_3 = 2e_2.$$

Writing M for e_1 and M' for e_2, we see that possible additions to (70) are given by

$$A''^{\text{mech.}}_{\mu} = Mv_\mu S^2 + M'(v_\mu \mathcal{S}^2 + 2S_{\mu\sigma}\mathcal{S}^\sigma), \tag{77}$$

where M and M' are independent and arbitrary constants. Since S^2 is a constant, the first term has in fact already been included in (70). The second term gives a possible addition to the translational equation. We should expect the elementary particles in nature to obey the simplest possible equation, and therefore we should expect M' to be zero.

Next consider additions to $A^{\text{mech.}}_{\mu}$ which are quadratic in $S_{\lambda\mu}$ or its derivatives and contain one differentiation with respect to τ. It can easily be shown by an analysis similar to that given above that there is only one possible solution of (57) and (68) of this type, namely,

$$\left.\begin{aligned} A'''^{\text{mech.}}_{\mu} &= I''\{2v_\mu(\mathcal{S}S') + \dot{S}_{\mu\sigma}\mathcal{S}^\sigma + S_{\mu\sigma}S'^\sigma\}, \\ B'''^{\text{mech.}}_{\lambda\mu} &= -I''\{v_\lambda S_{\mu\sigma}\mathcal{S}^\sigma - v_\mu S_{\lambda\sigma}\mathcal{S}^\sigma\}. \end{aligned}\right\} \tag{78}$$

I'' is an arbitrary constant having the dimensions of mass times length, i.e. of an angular momentum (since the velocity of light is put equal to unity). The addition (78) is obviously far more complicated than anything in (70) and (71), and we should expect I'' to be zero for an elementary particle.

There appears to be no limit to the number of solutions which can be found satisfying (57) and (68), but they are all very much more complicated than (70) and (71), and we should be justified in believing that they do not occur in the description of an elementary particle.

THE REACTION OF RADIATION

The radiation reaction terms still remain to be determined. $T^{\text{ret.}}_{\mu}$ and $M^{\text{ret.}}_{\lambda\mu}$ are given in the appendix. We have to fix $A^{\text{ret.}}_{\mu}$ and $B^{\text{ret.}}_{\lambda\mu}$. As mentioned before, they have to be so chosen that $M^{\text{react.}}_{\lambda\mu}$ is identically of the form given by (56), that is, by (52),

$$\{M^{\text{ret.}}_{\lambda\mu} - (v_\lambda A^{\text{ret.}}_\mu - v_\mu A^{\text{ret.}}_\lambda) - \dot{B}^{\text{ret.}}_{\lambda\mu}\} \equiv S_\lambda{}^\rho C^{\text{react.}}_{\rho\mu} - S_\mu{}^\rho C^{\text{react.}}_{\rho\lambda}, \tag{79}$$

with $C^{\text{react.}}_{\rho\mu}$ and $T^{\text{react.}}_\mu$ satisfying (69), which, by the definition (48) of $T^{\text{react.}}_\mu$, may be written

$$(\dot{S}C^{\text{react.}}) = 2v^\mu(T^{\text{ret.}}_\mu - \dot{A}^{\text{ret.}}_\mu). \tag{69a}$$

We separate the terms in (79) and (69a) which are proportional respectively to g_1^2, $g_1 g_2$ and g_2^2 into three groups. It is obvious that the terms proportional to g_1^2 will not contain $S_{\lambda\mu}$ or its derivatives, each term proportional to $g_1 g_2$ will contain $S_{\lambda\mu}$ or one of its derivatives once, while $S_{\lambda\mu}$ and its derivatives will appear twice in each term proportional to g_2^2. Each group of terms by itself has to satisfy the equations (79) and (69a). It is convenient at this stage to introduce a notation which will be of use later. We distinguish the symbols containing only terms of the first group by writing a (0) after the symbol, those of the second by a (1), and those of the third by a (2), thus expressing the fact that the groups are respectively independent of, linear and quadratic in $S_{\lambda\mu}$ and its derivatives. Thus, for example,

$$M^{\text{react.}}_{\lambda\mu} \equiv g_1^2 M^{\text{react.}}_{\lambda\mu}(0) + g_1 g_2 M^{\text{react.}}_{\lambda\mu}(1) + g_2^2 M^{\text{react.}}_{\lambda\mu}(2). \tag{80}$$

The general method has already been given in B. Since the retarded field of a point charge or dipole tends to infinity as we approach the dipole, both $T^{\text{ret.}}_\mu$ and $M^{\text{ret.}}_{\lambda\mu}$ will contain terms which tend to infinity as $\epsilon \to 0$. We therefore write

$$T^{\text{ret.}}_\mu = T^{(\epsilon)}_\mu + T^{(0)}_\mu, \tag{81}$$

where $T^{(\epsilon)}_\mu$ contains all the terms which are singular. Similarly, we write

$$M^{\text{ret.}}_{\lambda\mu} = M^{(\epsilon)}_{\lambda\mu} + M^{(0)}_{\lambda\mu}. \tag{82}$$

$T^{(\epsilon)}_\mu$ is given in the appendix by (123), (125) and (127). It appears that it is a perfect differential. It is therefore possible to split $A^{\text{ret.}}_\mu$ into two parts:

$$A^{\text{ret.}}_\mu = A^{(\epsilon)}_\mu + A^{(0)}_\mu, \tag{83}$$

of which $A^{(\epsilon)}_\mu$ alone contains the singular terms and is so chosen that

$$T^{(\epsilon)}_\mu - \dot{A}^{(\epsilon)}_\mu = 0. \tag{84}$$

Thus, remembering (48), we find that

$$T^{\text{react.}}_\mu = T^{(0)}_\mu - \dot{A}^{(0)}_\mu, \tag{85}$$

and is now entirely free from singularities. It remains finite as $\epsilon \to 0$.

$M^{(\epsilon)}_{\lambda\mu}$ is also given in the appendix by (130) and (132) and is not a perfect differential. However, it only appears in the rotational equation (55) in the combination (52):

$$M^{\text{ret.}}_{\lambda\mu} - (v_\lambda A^{\text{ret.}}_\mu - v_\mu A^{\text{ret.}}_\lambda) - \dot{B}^{\text{ret.}}_{\lambda\mu}.$$

(83) shows that $A^{\text{ret.}}_\mu$ also contains singular terms. It now appears that, with $A^{(\epsilon)}_\mu$ determined by (84),

$$M^{(\epsilon)}_{\lambda\mu} - (v_\lambda A^{(\epsilon)}_\mu - v_\mu A^{(\epsilon)}_\lambda)$$

is a perfect differential. It is therefore possible to split $B^{\text{ret.}}_{\lambda\mu}$ into two parts:

$$B^{\text{ret.}}_{\lambda\mu} = B^{(\epsilon)}_{\lambda\mu} + B^{(0)}_{\lambda\mu}, \tag{86}$$

where $B^{(\epsilon)}_{\lambda\mu}$ alone contains the singular terms and is so chosen that

$$M^{(\epsilon)}_{\lambda\mu} - (v_\lambda A^{(\epsilon)}_\mu - v_\mu A^{(\epsilon)}_\lambda) - \dot{B}^{(\epsilon)}_{\lambda\mu} = 0. \tag{87}$$

Hence, by (52),

$$M^{\text{react.}}_{\lambda\mu} = M^{(0)}_{\lambda\mu} - (v_\lambda A^{(0)}_\mu - v_\mu A^{(0)}_\lambda) - \dot{B}^{(0)}_{\lambda\mu}. \tag{88}$$

This is now entirely free from singularities and remains finite as $\epsilon \to 0$. Thus the rotational equation (55) also has no singular terms.

The above analysis shows that it is *possible* to eliminate the singularities which result from taking the energy tensor of the field to have the form (12). The question now arises as to how far this elimination is mathematically *necessary* in order that the conservation laws should hold. Consider the terms of order ϵ^{-3} in $T^{(\epsilon)}_\mu$. These are quadratic in $S_{\lambda\mu}$ and contain one differentiation with respect to τ. The terms of order ϵ^{-3} in $A^{(\epsilon)}_\mu$ must therefore be quadratic in $S_{\lambda\mu}$ and contain no differentiation with respect to τ. The equations (79) and (69a) therefore cannot determine such terms uniquely, because we could always add an expression like (77) with arbitrary M and M', since this satisfies (57) and (68). The same applies to terms of order ϵ^{-2} in $A^{(\epsilon)}_\mu$, since these must be quadratic in $S_{\lambda\mu}$ and contain one differentiation with respect to τ. These and the corresponding terms in $B^{(\epsilon)}_\mu$ must therefore be arbitrary to the extent of a possible addition of the expressions (78) with arbitrary I''. Since there are seven terms of order ϵ^{-2} in $T^{(\epsilon)}_\mu$ and only three in $A'''^{\,\text{mech.}}_\mu$ of (78), it is clear that the elimination of four of the singular terms of this order is *necessary*, while the elimination of the other three is a matter of choice. We may then sum up the position as follows. While the elimination of some of the singular terms is necessary and is achieved automatically by our method, the elimination of others is at our choice. But the non-elimination of such singular terms is merely equivalent to putting one of the arbitrary mechanical constants in our equations, for example, M, I or I'', equal to infinity. To put one of these constants, say M, equal to infinity is equivalent to making a *physical* assumption as definite as giving it some particular finite value, and this can only be decided by comparison with experiment. Reasons will be given in the last section for the belief that in order to describe the elementary particles *as they appear in nature* within the limits of classical theory, all the mechanical constants except M and I have to be put equal to zero. In this sense the conservation laws demand that all the singular terms *must* be eliminated.

It should be noticed that the elimination of the singularities is not trivial. It is easy to see that the coefficients of some of the terms in $T_\mu^{(\epsilon)}$ and $M_{\lambda\mu}^{(\epsilon)}$ might have had such values as to make the simultaneous elimination of all the singular terms impossible. The singularities would then have been inherent in the problem. That this is not the case shows that the singularities introduced by taking the energy tensor to have the form (12) even in the presence of point charges or point dipoles are entirely spurious, for they do not enter into the equations of motion. It would therefore be logical to seek to alter the expression for the energy tensor (12) when point charges and point dipoles are present so as to make the total energy of the field finite. This has already been done by Pryce for a point charge, and the results of this paper show that it must be possible for a point dipole also.

It only remains to determine $A_\mu^{(0)}$ and $B_{\lambda\mu}^{(0)}$. This is done in the appendix. The method is similar to the one we have used in deducing expressions (77) and (78), but is very much more complicated. $T_\mu^{(0)}(2)$ is given in the appendix and has four differentiations with respect to τ. $A_\mu^{(0)}(2)$ must therefore have three differentiations with respect to τ. The number of possible independent terms in $A_\mu^{(0)}(2)$ is therefore very large, and in fact there are fifty-seven terms in $A_\mu^{(0)}(2)$, and twenty-nine terms in $B_{\lambda\mu}^{(0)}(2)$. It is remarkable, however, that the conditions (79) and (69a) are so stringent as to determine the coefficients of all these terms either uniquely or in terms of six arbitrary constants. Thus $T_\mu^{\text{react.}}(2)$ and $M_{\lambda\mu}^{\text{react.}}(2)$ are determined in terms of six arbitrary constants. A considerable simplification can be introduced by giving some of these constants particular numerical values, but we do not need to go deeper into this point. $T_\mu^{\text{react.}}(2)$ contains all derivatives of v_μ and $S_{\lambda\mu}$ up to the fourth, and $M_{\lambda\mu}^{\text{react.}}(2)$ contains all derivatives of these quantities up to the third. Similarly, it is shown in the appendix that $T_\mu^{\text{react.}}(1)$ and $M_{\lambda\mu}^{\text{react.}}(1)$ can be determined entirely in terms of one arbitrary constant. $T_\mu^{\text{react.}}(1)$ and $M_{\lambda\mu}^{\text{react.}}(1)$ respectively contain all derivatives of v_μ and $S_{\lambda\mu}$ up to the third and second. $T_\mu^{\text{react.}}(0)$ is just the usual radiation reaction term for a point charge, while $M_{\lambda\mu}^{\text{react.}}(0)$ is zero. The complete expression for $M_{\lambda\mu}^{\text{react.}}$ is given in the appendix.

This completely determines the translational equation (72) and the rotational equation (73). Since, however, all derivatives of v_μ and $S_{\lambda\mu}$ up to the fourth appear in $T_\mu^{\text{react.}}$ and all derivatives up to the third in $M_{\lambda\mu}^{\text{react.}}$, the conditions under which the solutions of these equations are definite have to be investigated. If $\dot{v}_\mu$, $\ddot{v}_\mu$, v_μ^{iii}, $\dot{S}_{\lambda\mu}$ and $\ddot{S}_{\lambda\mu}$ vanish, then in the absence of an ingoing field all the terms in equation (73) vanish except $M_{\lambda\mu}^{\text{react.}}$, and from the expression for this given in the appendix we see that (73) reduces to

$$[S_{\lambda\rho}\{\tfrac{2}{3}S^{\text{iii}\,\rho}{}_\mu+\tfrac{4}{3}(v_\rho S_\mu''' - v_\mu S_\rho''')\}] = 0. \tag{89}$$

Moreover, the second term of (7*c*) now also vanishes, and hence this equation demands that

$$(SS^{\text{iii}}) = 0. \tag{90}$$

From equations (89) and (90) it can be deduced that $S_{\lambda\mu}^{\text{iii}}$ must vanish. (The easiest way to do this is to introduce two space vectors† for S_{0k}, S_{0l}, S_{0m} and S_{lm}, S_{mk}, S_{kl}, and to consider equation (89) in the rest system.) Thus, as a consequence of the rotational equation (73), $\dot{S}_{\lambda\mu}$ and $\ddot{S}_{\lambda\mu}$ will continue to be zero, and hence all higher derivatives will also vanish, in particular $S_{\lambda\mu}^{\text{iv}}$. Now consider the translational equation (72). When $\dot{v}_\mu$, $\ddot{v}_\mu$, v_μ^{iii}, $\dot{S}_{\lambda\mu}$ and $\ddot{S}_{\lambda\mu}$ vanish, all the terms in (72) vanish in the absence of an ingoing field except $T_\mu^{\text{react.}}$, and hence this equation demands that $T_\mu^{\text{react.}}$ shall vanish. As shown above, it follows from the rotational equation that $S_{\lambda\mu}^{\text{iii}}$ and $S_{\lambda\mu}^{\text{iv}}$ must also vanish, and in these circumstances it follows from (138) in the appendix that $T_\mu^{\text{react.}} = 0$ reduces to

$$v_\mu^{\text{iv}}(\tfrac{2}{5}\dot{S}^2 - \tfrac{1}{15}S^2) + \tfrac{2}{15}v_\mu(\dot{S}Sv^{\text{iv}}) + \tfrac{2}{15}S_{\mu\nu}S^{\nu\rho}v_\rho^{\text{iv}} = 0. \tag{91}$$

Further, (5*d*) now becomes $(vv^{\text{iv}}) = 0$, so that in the rest system $v_0^{\text{iv}} = 0$. Thus in the rest system (91) just reduces to the three equations

$$v_k^{\text{iv}}(\tfrac{2}{5}\dot{S}^2 - \tfrac{1}{15}S^2) + \tfrac{2}{15}S_{k\nu}S^{\nu l}v_l^{\text{iv}} = 0,$$

from which it can be deduced that $v_k^{\text{iv}} = 0$. Hence the particle will continue in a state of uniform motion with its spin pointing in a fixed direction. Thus the solutions of the equations of motion (72) and (73) will be perfectly definite if the initial velocity and direction of the spin are given, and only those solutions are allowed for which $\dot{v}_\mu$, $\ddot{v}_\mu$, v_μ^{iii}, $\dot{S}_{\lambda\mu}$ and $\ddot{S}_{\lambda\mu}$ all vanish after the ingoing field has died down. We may take (72) and (73) to be the exact equations of motion taking radiation reaction into account for a spinning particle moving in a Maxwell field.

---

† We make the convention that Latin suffices only take on the values 1, 2 and 3.

SPECIALIZED EQUATIONS

Although the equations (72) and (73) give a consistent mathematical scheme for the motion of a spinning particle they are in some ways too general to be used for a description of the elementary particles which occur in nature. There is no connexion between the velocity of the particle and the state of its dipole moment. If we introduce a space vector **M** to denote the magnetic dipole moment S_{lm}, S_{mk}, S_{kl} and a space vector **D** to denote the electric dipole moment S_{0k}, S_{0l}, S_{0m}, the equations are such that, according to (6), (30) and (34*a*),

$$\mathbf{M}^2-\mathbf{D}^2 = \text{constant}, \tag{92a}$$

$$(\mathbf{MD}) = \text{constant}. \tag{92b}$$

Except for these two constants of the motion, the magnitudes of **M** and **D** may change without any relation to the velocity. For example, if we had a dipole of the special type which initially had only a magnetic moment but no electric moment in its rest system, an ingoing field could easily be found which after a time brought the dipole to rest again, but this time, without violating (92*a*) and (92*b*), with an electric moment perpendicular to the magnetic moment and a larger value of the magnetic moment. (This is particularly evident when $g_1 = 0$, for then a constant electric field would do this.) The elementary particles in nature do not behave in this way, and the question now arises as to whether it is possible to give a procedure for deriving specialized equations from (72) and (73) which leave a pure magnetic dipole always a pure magnetic dipole in the rest system and a pure electric dipole always a pure electric dipole.

Consider first the case where the dipole is a pure magnetic dipole in the rest system. This is expressed in mathematical form by the equation

$$S_{\mu\nu} v^{\nu} = 0. \tag{93}$$

The equations obtained by differentiating this are

$$S'_{\mu} + S_{\mu\nu}\dot{v}^{\nu} = 0, \tag{94a}$$

$$S''_{\mu} + 2\dot{S}_{\mu\nu}\dot{v}^{\nu} + S_{\mu\nu}\ddot{v}^{\nu} = 0, \tag{94b}$$

$$S'''_{\mu} + 3\ddot{S}_{\mu\nu}\dot{v}^{\nu} + 3\dot{S}_{\mu\nu}\ddot{v}^{\nu} + S_{\mu\nu}v^{\text{iii}\,\nu} = 0, \tag{94c}$$

$$S''''_{\mu} + 4S^{\text{iii}}_{\mu\nu}\dot{v}^{\nu} + 6\ddot{S}_{\mu\nu}\ddot{v}^{\nu} + 4\dot{S}_{\mu\nu}v^{\text{iii}\,\nu} + S_{\mu\nu}v^{\text{iv}\,\nu} = 0. \tag{94d}$$

Suppose the equations of motion as derived previously without the condition (93) are (43) and (64), which we write in the more general form (36):

$$\dot{A}_{\mu} = T_{\mu}, \tag{43}$$

$$I\dot{S}_{\lambda\mu} + I'\dot{S}^{*}_{\lambda\mu} = [S.\Theta]_{\lambda\mu}. \tag{36}$$

We have to find whether, when the constraint (93) is imposed, a procedure can be found within the method used for deducing (43) and (36) which allows (43) and (36) to be so altered as to make them consistent with the equations (93) and (94). The only condition that A_μ has to satisfy is that the two invariant equations (65) and (66) shall be consistent. In our present notation this requires that

$$v^\mu(T_\mu - \dot{A}_\mu) = \tfrac{1}{2}(\dot{S}_{\lambda\mu}\Theta^{\lambda\mu}). \tag{95}$$

Contract (36) with v^μ and replace A_μ by $A_\mu + A'_\mu$, where

$$A'_\lambda = \{I\dot{S}_{\lambda\mu} + I'\dot{S}^*_{\lambda\mu} - [S.\Theta]_{\lambda\mu}\}v^\mu. \tag{96}$$

An addition to A_μ of A'_μ adds according to (45) a term $v_\lambda A'_\mu - v_\mu A'_\lambda$ to the left-hand side of (36). Thus (36) is changed to†

$$\begin{aligned} I\{\dot{S}_{\lambda\mu} + v_\lambda S'_\mu - v_\mu S'_\lambda\} + I'\{\dot{S}^*_{\lambda\mu} + v_\lambda \dot{S}^*_{\mu\nu}v^\nu - v_\mu \dot{S}^*_{\lambda\nu}v^\nu\} \\ = [S_\lambda{}^\rho + \{\Theta_{\rho\mu} - (\Theta_{\rho\nu}v^\nu v_\mu - \Theta_{\mu\nu}v^\nu v_\rho)\}]_-. \end{aligned} \tag{97}$$

In general (97) would not be permissible as the rotational equation because it has not the form (36). But in the special case when (93) and (94) are valid it can be written in the form

$$\begin{aligned} I\dot{S}_{\lambda\mu} + I[S_{\lambda\rho}(\dot{v}^\rho v_\mu - v^\rho \dot{v}_\mu)]_- + I'\{\dot{S}^*_{\lambda\mu} + v_\lambda \dot{S}^*_{\mu\nu}v^\nu - v_\mu \dot{S}^*_{\lambda\nu}v^\nu\} \\ = [S_\lambda{}^\rho\{\Theta_{\rho\mu} - (\Theta_{\rho\nu}v^\nu v_\mu - \Theta_{\mu\nu}v^\nu v_\rho)\}]_-. \end{aligned} \tag{98}$$

This is of the required form (36) *provided* $I' = 0$. Thus (43) and (36) must be replaced by

$$\dot{A}_\mu + \frac{d}{d\tau}\{IS'_\mu - S_{\mu\rho}\Theta^{\rho\nu}v_\nu\} = T_\mu \tag{99}$$

and

$$I\{\dot{S}_{\lambda\mu} + v_\lambda S'_\mu - v_\mu S'_\lambda\} = [S_\lambda{}^\rho\{\Theta_{\rho\mu} - \Theta_{\rho\nu}v^\nu v_\mu\}]_-. \tag{100}$$

(98) with $I' = 0$ leads to the invariant equation

$$-2I\dot{v}^\rho \dot{S}_{\rho\mu}v^\mu + (\dot{S}\Theta) - 2S'^\rho\Theta_{\rho\nu}v^\nu = 0,$$

while (99) leads to

$$v^\mu(T_\mu - \dot{A}_\mu) - S'^\rho\Theta_{\rho\nu}v^\nu - Iv^\mu\dot{S}_{\mu\rho}\dot{v}^\rho = 0.$$

Since, by (94*a*), $$\dot{v}^\rho\dot{S}_{\rho\mu}v^\mu = -\dot{v}^\rho S_{\rho\mu}\dot{v}^\mu = 0,$$

it follows in view of (95) that these two equations are consistent. Contracting (100) with v^μ, we see that it vanishes identically, so that *in the rest system* this equation determines the rotational motion only for $\lambda, \mu \neq 0$. In other words, it only determines $\dot{S}_{kl}$. In this system $\dot{S}_{0k}$ are then determined explicitly by (94a). We have thus given a procedure for deriving from equations (43) and (36) others of the correct form which are consistent with the constraint (93) and satisfy the conservation laws.

---

† The minus sign behind a bracket indicates that the same terms with ν and μ interchanged are to be subtracted.

Let us apply this method to the equations (72) and (73), with $K' = 0$ for simplicity. According to (99) the translational equation (72) is to be replaced by

$$M\dot{v}_\mu + \frac{d}{d\tau}\{IS'_\mu + \tfrac{1}{4}Kv_\mu \dot{S}^2 + KS_{\mu\rho}S''^\rho - \tfrac{1}{2}g_2 v_\mu(SF^{\text{in.}}) - g_2 S^\mu{}_\sigma F^{\text{in.}}_{\sigma\nu} v^\nu\}$$
$$= g_1 F^{\text{in.}}_{\mu\sigma} v^\sigma - \tfrac{1}{2}g_2 S^{\rho\sigma}\frac{\partial}{\partial x^\mu}F^{\text{in.}}_{\rho\sigma} + T^{\text{self}}_\mu, \qquad (101)$$

where we have written

$$T^{\text{self}}_\mu \equiv T^{\text{react.}}_\mu + \frac{d}{d\tau}(S_\mu{}^\rho C^{\text{react.}}_{\rho\nu} v^\nu). \qquad (102)$$

According to (100) the rotational equation (73) must be replaced by

$$I\{\dot{S}_{\lambda\mu} + v_\lambda S'_\mu - v_\mu S'_\lambda\} + K[S_\lambda{}^\rho\{\dot{S}_{\rho\mu} - S''_\rho v^\mu\}]_-$$
$$= g_2[S_\lambda{}^\rho\{F^{\text{in.}}_{\rho\mu} - F^{\text{in.}}_{\rho\nu} v^\nu v_\mu\}]_- + [S.D]_{\lambda\mu}, \qquad (103)$$

where
$$D_{\lambda\mu} \equiv C^{\text{react.}}_{\lambda\mu} - (C^{\text{react.}}_{\lambda\rho} v^\rho v_\mu - C^{\text{react.}}_{\mu\rho} v^\rho v_\lambda). \qquad (104)$$

(101) and (103) are just the equations for this case derived in a previous paper (B, equations (30) and (31)) by a direct method.† The constants g_1 and K were there put equal to zero. It can easily be seen from the expression for $C^{\text{react.}}_{\lambda\mu}(1)$ given by (137b) of the appendix that the $g_1 g_2$ terms vanish in the expression on the right-hand side of (104), so that $D_{\lambda\mu}$ contains only the pure spin reaction terms proportional to g_2^2. In other words, for a dipole which is a pure magnetic one in the rest system, the equations for the rotation of the dipole are the same whether the particle has a charge g_1 or not. Now, as mentioned before, $C^{\text{react.}}_{\lambda\mu}(2)$ given by (140) has six arbitrary constants. When we build the expression on the right-hand side of (104) and use the equations (93) and (94), three of the arbitrary constants drop out, while the remaining three always appear together in a certain combination, so that the resulting expression for $D_{\lambda\mu}$ has in effect but one arbitrary constant. $D_{\lambda\mu}$ is given in the appendix by (142) and is exactly the radiation reaction term given in the previous paper (B, (46)).

---

† Owing to a slip the g_2 terms in B appear with the same sign as here, whereas they should appear with the opposite sign since the field strengths as defined by (8a) are equal to minus the field strengths in B. This is of no physical consequence, for it is merely equivalent to reversing the sign of g_2, which is always possible.

The radiation reaction terms in the translational equation (101) are given in the appendix. $T_\mu^{\text{self}}(0)$ is the same as $T_\mu^{\text{react.}}(0)$ by (102), since $C_{\lambda\mu}^{\text{react.}}(0)$ is zero. It is the well-known expression for a point charge. $T_\mu^{\text{self}}(1)$ has no arbitrary constant in it and is given by (143) in the appendix, while $T_\mu^{\text{self}}(2)$ can be expressed in terms of *one* arbitrary constant and is exactly the radiation reaction term given in the previous paper (B, appendix).

We thus see that, if the radiation reaction terms are neglected, the equations (101) and (103) are formally more complicated than (72) and (73) (with I' and K' equal to zero), but *with the radiation reaction* terms the equations (72) and (73) are vastly more complicated than (101) and (103). Moreover, whereas the damping terms in (101) and (103) have but *one* arbitrary dimensionless constant, those in (72) and (73) have no less than seven arbitrary constants. Thus, although the classical theory cannot exclude the general case treated in the previous section, it at least gives us a reason why the elementary particles in nature might be expected to belong to the specialized case treated in this section. Relativistic quantum theory is an advance on classical theory in that in it the elementary particles automatically and necessarily have only a magnetic moment in their rest system, as is found in nature.

Lastly, we consider the case where the dipole is a pure *electric* dipole in the rest system. This is expressed mathematically by the equation

$$S^*_{\mu\nu}v^\nu = 0. \tag{105}$$

To alter (43) and (36) so as to be compatible with (105) we proceed exactly as before and add (96) to A_μ. The rotational equation then becomes (97), and in order that this should be of the form (36) I must now be put equal to zero, while I' remains arbitrary. By using the identities (27) and (28*b*) and the equation (105) it can easily be shown that the right-hand side of (97) can be brought into the form of the right-hand side of (36), if desired. It is, however, convenient to keep it in the form which it has in (97), with $I = 0$.

THE SCATTERING OF LIGHT BY A DIPOLE

To get an insight into the rotation of the dipole alone we may simplify the problem by putting M equal to infinity. In this case it follows from the translational equation (101) that all the derivatives of the velocity vanish, and we may conveniently consider the particle in the rest system. If we use the space vector $\mathbf{M}$ introduced at the beginning of the previous section to denote the spin, the rotational equation (103) then takes the particularly simple form

$$I\dot{\mathbf{M}} + K[\mathbf{M}\,.\,\ddot{\mathbf{M}}] = g_2[\mathbf{M}\,.\,\mathbf{H}] - \tfrac{2}{3}g_2^2[\mathbf{M}\,.\,\mathbf{M}^{\text{III}}], \tag{106}$$

where the square brackets now denote the usual vector product, and **H** is the magnetic force of the ingoing field. If we put the constant K equal to zero we get just the equation given in the previous paper (B, (51)). As shown there, the last term in (106), which embodies the effects of radiation reaction can be derived quite simply from dimensional arguments and the condition that the work done by an external periodic force on the dipole shall be equal to the energy radiated by the dipole. The general reaction terms in (72) and (73) or (101) and (103) naturally cannot be derived so easily.

We now consider the scattering of light by this dipole. The calculation is but a generalization of the calculation given in the previous paper and is a particular case of the problem of the scattering of meson waves by a dipole dealt with in detail in the paper which immediately follows this. We therefore only give the result. We henceforth write x, y, z for the space coordinates and t for x_0. Let the ingoing light wave of frequency ω be described by

$$\mathbf{H} = \mathbf{H}_0 \cos \omega(z-t), \tag{107}$$

where $\mathbf{H}_0$ lies along the x-axis. We consider the scattering for weak fields, so that the oscillation of the dipole is small and we may write

$$\mathbf{M}(t) = \mathbf{M}_0 + \mathbf{M}_1 \sin \omega t + \mathbf{M}_2 \sin(\omega t + \delta),$$

$\mathbf{M}_0$ being the initial value of $\mathbf{M}$, the length of which may be taken to be unity. Denote by θ the angle between $\mathbf{M}_0$ and $\mathbf{H}$. The vectors $\mathbf{M}_0$, $\mathbf{M}_1$ and $\mathbf{M}_2$ are mutually perpendicular and such that $[\mathbf{M}_0 . \mathbf{M}_1]$ is in the direction $\mathbf{M}_2$. Let η denote the angle between the vectors $[\mathbf{M}_0 . \mathbf{H}]$ and $\mathbf{M}_1$, $\mathbf{M}_1$ lying in such a direction that the angle† between the planes $[\mathbf{M}_0 . \mathbf{M}_1]$ and $[\mathbf{M}_0 . \mathbf{H}]$ is $\frac{1}{2}\pi - \eta$. If we write for brevity

$$\alpha = \frac{3}{2}\frac{I}{g_2^2}, \quad \beta = \frac{3}{2}\frac{K}{g_2^2}, \tag{108}$$

it can be shown that

$$|M_1| = \frac{3}{2}\frac{H_0 \alpha \sin\theta}{g_2^2 \omega \{(\alpha^2 - \beta^2\omega^2 - \omega^4)^2 + 4\alpha^2\omega^2\}^{\frac{1}{2}}}, \tag{109a}$$

$$\left|\frac{M_2}{M_1}\right| = (\beta^2\omega^2 + \omega^4)^{\frac{1}{2}} \alpha^{-1}, \tag{109b}$$

$$\tan\eta = \frac{2\alpha\omega^3}{\alpha^2 - \beta^2\omega^2 - \omega^4}, \tag{109c}$$

$$\tan\delta = -\frac{\beta}{\omega}. \tag{109d}$$

---

† A slight slip has occurred in B. With the angle ϕ as defined there, the sign of the right-hand side of (55b) should be reversed.

Thus, as we should expect, the dipole does not carry out a pure oscillation as in the case investigated in B, but, owing to the presence of the inertial term K, it executes a small elliptic gyration about its original direction.

The scattering cross-section, i.e. the energy scattered divided by the energy carried by the incident light wave per unit area, is

$$6\pi \sin^2\theta \frac{\omega^2(\alpha^2+\beta^2\omega^2+\omega^4)}{(\alpha^2-\beta^2\omega^2-\omega^4)^2+4\alpha^2\omega^4}. \tag{110}$$

For $\beta = 0$ this just goes over into the cross-section given in B, namely,

$$6\pi \sin^2\theta \frac{\omega^2}{\alpha^2+\omega^4}, \tag{111}$$

while for $\alpha = 0$ it reduces to

$$6\pi \sin^2\theta \frac{1}{\beta^2+\omega^2}. \tag{112}$$

The effect of radiation reaction is contained in the *explicit* ω^4 terms in (110). Their effect is twofold. For very high frequencies they cause the scattering to diminish as ω^{-2} quite irrespective of the values of α or β. Moreover, if we neglect these reaction terms, the denominator of (110) becomes zero for a frequency

$$\omega = \frac{\alpha}{\beta} = \frac{I}{K},$$

which gives an infinite scattering for this frequency. As is well known, I/K is the natural precession frequency of the spin for small oscillations, so that we have to do here with a resonance phenomenon. The effect of radiation reaction is to make the scattering finite even for this resonance frequency, as we should expect. It is interesting to note that while the scattering due to a pure gyroscopic spin ($K = 0$) tends to infinity like ω^2 with increasing frequency, the addition of a finite moment of inertia perpendicular to the spin axis ($K \neq 0$) makes the scattering cross-section tend to a finite value for high frequencies, *even in the absence of radiation reaction*. That the effect of radiation reaction on the *rotation* of the dipole is to make the scattering diminish for very high frequencies as ω^{-2}, bears a striking resemblance to the scattering by a point charge calculated by Dirac (1938), the cross-section for which has exactly the dependence on frequency given by (112), where the effect of radiation reaction on the *translation* of the point charge is also to make the scattering decrease as ω^{-2} for high frequencies. Since a point charge and a point dipole are entirely different things and the mechanism of scattering is also different, this leads us to suspect that it may be a fundamental property of radiation that for high frequencies the scattering should decrease as ω^{-2}.

It is of interest to compare our classical theory with the quantum theory for a particle of spin $\frac{1}{2}\hbar$ as described by the Dirac equation. In this quantum theory it is possible to add in addition to the usual interaction which is described by means of the potentials, an explicit spin interaction of the particle with the Maxwell field equivalent to the g_2 term. The calculation of the scattering of light by a particle with this explicit spin interaction, leads, if the mass of the particle is ultimately allowed to tend to infinity, to a scattering cross-section of the form (111) with the absence of the ω^4 term in the denominator. The absence of the ω^4 term is understandable, for it is the result of radiation reaction, and as is well known, this is neglected in the quantum theory. However, the fact that the quantum theory then leads to a cross-section agreeing in form with (111) and not (110), with the *explicit* ω^4 terms omitted in each case, shows clearly that the Dirac equation automatically describes a particle for which β is zero, that is, for which K vanishes. Thus the Dirac equation automatically describes a spinning particle which has the simplest possible mechanical properties, namely those of a pure gyroscope, characterized by $I = \frac{1}{2}\hbar$, $K = 0$. Moreover, the cross-section (111), which correctly contains the effect of radiation reaction, shows that the validity of the quantum theory of an explicit spin interaction would be restricted to frequencies for which the ω^4 term is unimportant, i.e., for frequencies

$$\omega \ll \sqrt{\alpha} = \sqrt{\frac{3I}{2g_2^2}}.$$

If the g_2 term in the quantum theory is put equal to zero, the scattering reduces to just that given by the Klein-Nishina formula and vanishes as the mass of the particle tends to infinity.

The question now arises as to whether the above theory can be applied in the classical limit to an electron or not, for as is well known, the magnetic moment of the electron is a pure quantum effect. The argument of the previous paragraph shows that the magnetic moment of the electron is not to be described in this way for that *would be equivalent to describing the magnetic moment in the quantum theory by an explicit spin interaction term with* $g_2 = e\hbar/2m$. This would not give agreement with nature, as can be seen by comparing the theoretical scattering for an explicit g_2 term with that found experimentally for free electrons. It is justifiable to calculate the theoretical scattering by using (111), for, as has been mentioned before, this completely agrees for frequencies $\omega \ll \sqrt{\alpha}$ with the quantum formula derived with a g_2 term.† The fact that the electron was considered as fixed at a point in calculating (111) is of no account since the scattering due to the rotation of the spin with an explicit g_2 term is far greater than that due to the translation of the dipole. Putting $I = \frac{1}{2}\hbar$, $K = 0$, $g_2 = e\hbar/2m$, thus making $\alpha = 3(\hbar/e^2)(m/\hbar)^2$, we find that the scattering given by (111) for $\omega = 5m/\hbar$ is already about twenty times larger than the scattering given by the Klein-Nishina formula for the same frequency. Since the Klein-Nishina formula has been checked experimentally up to these frequencies (see for example, Heitler 1936), we must conclude that the above scattering cross-section is not applicable to an electron. This is entirely to be attributed to the fact that *to describe the electron and its interaction with the Maxwell field as it occurs in nature we must put $g_2 = 0$ both in the classical and quantum theories.* The equations of the preceding section are naturally applicable to an electron if we specialize them by putting $g_2 = 0$, $K = 0$, $I = \frac{1}{2}\hbar$, in which case (103) shows that the spin continues to point in the same direction in the rest system, while in the limit $\hbar \to 0$ (101) just becomes the well-known Lorentz-Dirac equation. The quantum theory of the electron might therefore be expected to be valid up to energies of $137mc^2$ as hitherto supposed, and contrary to a tentative suggestion recently made by one of us (Bhabha 1940*b*).

For the meson it is not yet known from experiment whether an explicit spin interaction term is necessary to describe its interaction with the Maxwell field or not. If it is found that such a term is required in the quantum description of the meson's interaction with the Maxwell field, then the above theory would certainly be applicable to this case in the classical limit, and (111) shows that the neglect of the effect of radiation reaction on the rotation of the spin would restrict the validity of quantum theory to frequencies such that‡

$$\omega \ll \sqrt{\frac{3I}{2g_2^2}} = \sqrt{\frac{3\hbar}{2g_2^2}}.$$

It is known that the heavy particles have an explicit spin interaction with the meson field, so that the theory of this paper would certainly describe their behaviour in the classical limit, but we shall not consider this problem here as it is treated in detail in the paper which immediately follows this, where the present theory is extended to cover meson fields.

---

† Detailed calculations by Bhabha and Madhava Rao (1941, *Proc. Indian Acad. Sci.* A, **13**, 9–24) have shown that the quantum and classical cross-sections have the same dependence on energy, scattering angle and polarization of the incident and scattered light, but that the former is larger than the latter by a constant factor 3. This factor results from physically understandable differences in the quantum and classical averaging over the initial orientations of the spin of the scattering particle (see footnote on p. 341 of the subsequent paper).

‡ Here g^2 denotes the strength of a possible explicit interaction of the meson with the Maxwell field, and not as usual the strength of the spin interaction of the heavy particles with the meson field.

APPENDIX

The field strengths can be derived according to (8*a*) by differentiating the potentials (21) and (23). The method of differentiation has been given in a previous paper (A). We give only the result:†

$$F^{(1)}_{\mu\nu} = g_1\left[\frac{s_\mu v_\nu}{\kappa^3}, \quad -\frac{s_\mu v_\nu}{\kappa^3}\kappa' + \frac{s_\mu \dot{v}_\nu}{\kappa^2}\right]_- . \tag{113}$$

This is the usual field of a point charge. Further

$$\begin{aligned} F^{(2)}_{\mu\nu} = g_2\Bigg[&\frac{S_{\mu\nu}}{\kappa^3} + 3\frac{s_\mu \mathcal{S}_\nu}{\kappa^4} - 2\frac{v_\mu \mathcal{S}_\nu}{\kappa^3} + 3\frac{s^\rho S_{\rho\nu}}{\kappa^5}(s_\mu - \kappa v_\mu), \\ &+\frac{\dot{S}_{\mu\nu}}{\kappa^2} - \frac{S_{\mu\nu}}{\kappa^3}\kappa' - 3\frac{s_\mu \mathcal{S}_\nu}{\kappa^4}\kappa' + 2\frac{s_\mu S'_\nu}{\kappa^3} + \frac{s_\mu S_{\nu\rho}\dot{v}^\rho}{\kappa^3} - \dot{v}_\mu\frac{s^\rho S_{\rho\nu}}{\kappa^3} \\ &+3\frac{s_\mu s^\rho \dot{S}_{\rho\nu}}{\kappa^4} - 2\frac{v_\mu s^\rho S_{\rho\nu}}{\kappa^3} - 6\frac{s_\mu s^\rho S_{\rho\nu}}{\kappa^5}\kappa' + 3\frac{v_\mu s^\rho S_{\rho\nu}}{\kappa^4}\kappa', \\ &+\frac{s_\mu s^\rho \ddot{S}_{\rho\nu}}{\kappa^3} - 3\frac{s_\mu s^\rho \dot{S}_{\rho\nu}}{\kappa^4}\kappa' + 3\frac{s_\mu s^\rho S_{\rho\nu}}{\kappa^5}\kappa'^2 - \frac{s_\mu s^\rho S_{\rho\nu}}{\kappa^4}\kappa''\Bigg]_- . \end{aligned} \tag{114}$$

We proceed to calculate T_μ and $M_{\lambda\mu}$. For the world tube defined by (40) it was shown in A (formula (54)) that the directed surface element dS^ν of the tube is given by

$$dS^\nu = \{s^\nu(1-\kappa') - \epsilon v^\nu\}\,\epsilon\, d\Omega\, d\tau. \tag{115}$$

Here $d\Omega$ represents an element of solid angle subtended at the point τ of the world line in the rest system of this point by a portion of the sphere of radius ϵ with this point as centre. As mentioned in the text, this sphere taken at a time ϵ later than τ is a section of the world tube. For all points on this sphere, $s_0 = \epsilon$, while $\sum_1^3 s_k^2 = \epsilon^2$. Hence, if A_μ is any vector which is not a function of position on the surface of the sphere,

$$\frac{1}{4\pi\epsilon}\int s^\lambda A_\lambda\, d\Omega = A_0 = v^\lambda A_\lambda, \tag{116a}$$

---

† The minus sign behind a bracket indicates that the same terms with ν and μ interchanged are to be subtracted.

since in the rest system $v_0 = 1$, $v_1 = v_2 = v_3 = 0$. Similarly, if B_μ is another vector which is also not a function of position on the surface of the sphere,

$$\frac{1}{4\pi\epsilon^2}\int s^\lambda A_\lambda s^\mu B_\mu \, d\Omega = A_0 B_0 + \tfrac{1}{3}\sum_1^3 A_k B_k.$$

We can at once write this in tensor form by combining the terms with v_μ; thus

$$\frac{1}{4\pi\epsilon^2}\int (sA)(sB)\, d\Omega = -\tfrac{1}{3}(A_\lambda B^\lambda) + \tfrac{4}{3}(v^\lambda A_\lambda)(v^\mu B_\mu). \qquad (116b)$$

Proceeding in this way we can easily show that

$$\frac{1}{4\pi\epsilon^3}\int (sA)(sB)(sC)\, d\Omega = -\tfrac{1}{3}P(AB)(Cv) + \tfrac{6}{3}(Av)(Bv)(Cv). \qquad (116c)$$

The symbol P denotes that we have to sum over all possible combinations of the vectors occurring in the product, each combination being taken only once; thus

$$P(AB)(Cv) = (AB)(Cv) + (BC)(Av) + (CA)(Bv).$$

The generalization of the formulae (116) is easily found. In these calculations only integrals involving products of not more than eight vectors A, B, C, D, E, F, G and H appear. We have

$$\frac{1}{4\pi\epsilon^4}\int (sA)(sB)(sC)(sD)\, d\Omega = \frac{1}{3.5}P(AB)(CD) - \frac{6}{3.5}P(AB)(Cv)(Dv)$$
$$+ \frac{6.8}{3.5}(Av)(Bv)(Cv)(Dv). \qquad (116d)$$

$$\frac{1}{4\pi\epsilon^5}\int (sA)\dots(sE)\, d\Omega = \frac{1}{3.5}P(AB)(CD)(Ev) - \frac{8}{3.5}P(AB)(Cv)(Dv)(Ev)$$
$$+ \frac{8.10}{3.5}(Av)\dots(Ev), \qquad (116e)$$

$$\frac{1}{4\pi\epsilon^6}\int (sA)\dots(sF)\, d\Omega = -\frac{1}{3.5.7}P(AB)(CD)(EF)$$
$$+ \frac{8}{3.5.7}P(AB)(CD)(Ev)(Fv)$$
$$- \frac{8.10}{3.5.7}P(AB)(Cv)\dots(Fv) + \frac{8.10.12}{3.5.7}(Av)\dots(Fv), \qquad (116f)$$

$$\frac{1}{4\pi\epsilon^7}\int (sA)\dots(sG)\,d\Omega = -\frac{1}{3.5.7}P(AB)(CD)(EF)(Gv)$$

$$+\frac{10}{3.5.7}P(AB)(CD)(Ev)\dots(Gv)$$

$$-\frac{10.12}{3.5.7}P(AB)(Cv)\dots(Gv)+\frac{10.12.14}{3.5.7}(Av)\dots(Gv), \quad (116g)$$

$$\frac{1}{4\pi\epsilon^8}\int (sA)\dots(sH)\,d\Omega = \frac{1}{3.5.7.9}P(AB)(CD)(EF)(GH)$$

$$-\frac{10}{3.5.7.9}P(AB)(CD)(EF)(Gv)(Hv)$$

$$+\frac{10.12}{3.5.7.9}P(AB)(CD)(Ev)\dots(Hv)-\frac{10.12.14}{3.5.7.9}P(AB)(Cv)\dots(Hv)$$

$$+\frac{10.12.14.16}{3.5.7.9}(Av)\dots(Hv). \quad (116h)$$

Introducing (12) and (115) into (41) and remembering that this is equal to (42), we find

$$T_\mu = \frac{1}{4\pi}\int\{F_\mu\rho F_{\rho\nu}+\tfrac{1}{4}g_{\mu\nu}F_{\rho\sigma}F^{\rho\sigma}\}\{s^\nu(1-\kappa')-\epsilon v^\nu\}\,\epsilon\,d\Omega. \quad (117)$$

Consider first $T_\mu^{\text{mix.}}$. Remembering (25), we have

$$T_\mu^{\text{mix.}} = \frac{1}{4\pi}\int\{F_{\mu\rho}^{\text{in.}}F^{\text{ret.}\,\rho}{}_\nu+F_{\mu\rho}^{\text{ret.}}F^{\text{in.}\,\rho}{}_\nu+\tfrac{1}{2}g_{\mu\nu}F_{\rho\sigma}^{\text{in.}}F^{\text{in.}\,\rho\sigma}\}\{s^\nu(1-\kappa')-\epsilon v^\nu\}\,\epsilon\,d\Omega. \quad (118)$$

Now the ingoing field has no singularity on the world line. Hence its value at any point x_ρ on the surface of the sphere can be expressed by the help of Taylor's theorem in terms of its value at the retarded point $z_\rho(\tau_0)$; thus

$$(F_{\mu\nu}^{\text{in.}})_{x_\rho} = (F_{\mu\nu}^{\text{in.}})_{z_\rho(\tau_0)}+s^\rho\left(\frac{\partial}{\partial x^\rho}F_{\mu\nu}^{\text{in.}}\right)_{z_\rho(\tau_0)}.$$

Now dS^ν is at least of order ϵ^2, while the highest singularity in $F_{\mu\nu}^{(1)}$ given by (113) is of order ϵ^{-2}. Hence the g_1 terms in $T_\mu^{\text{mix.}}$ will contain the ingoing field strengths but not their derivatives. The highest singularity in $F_{\mu\nu}^{(2)}$ is of order ϵ^{-3}, and hence the g_2 terms in $T_\mu^{\text{mix.}}$ will contain both the ingoing field strengths and their derivatives on the world line. At first sight it would seem possible for singular terms of order ϵ^{-1} to appear in $T_\mu^{\text{mix.}}$, but calculation shows that these vanish, as we should expect. Introducing (114) for $F_{\mu\nu}^{\text{ret.}}$

in (118) and using some of the relations (116), we find after some calculation that the g_2 terms in $T_\mu^{\text{mix.}}$ reduce to

$$g_2\left[\frac{d}{d\tau}\{\tfrac{2}{3}S_\mu{}^\sigma F^{\text{in.}}_{\sigma\nu}v^\nu-\tfrac{2}{3}F^{\text{in.}}_{\mu\sigma}\mathcal{S}^\sigma+\tfrac{1}{3}v_\mu S^{\rho\sigma}F^{\text{in.}}_{\rho\sigma}\}\right.$$
$$\left.-\tfrac{1}{2}S^{\rho\sigma}\frac{\partial}{\partial x^\mu}F^{\text{in.}}_{\rho\sigma}+\{\tfrac{2}{3}S_{\mu\sigma}+\tfrac{1}{3}v_\mu\mathcal{S}_\sigma-\tfrac{1}{3}v_\sigma\mathcal{S}_\mu\}\frac{\partial}{\partial x^\nu}F^{\text{in.}\,\nu\sigma}\right]. \tag{119}$$

Use has been made of the fact that the ingoing field satisfies (9). The last term vanishes since the ingoing field satisfies (8*b*) with the right-hand side equal to zero. We thus get the result quoted in (58) in the text. The g_1 term there is the usual one which was also calculated in *A*.

Inserting (12) and (115) into the first integral of (44*a*) and remembering that this is equal to (44*b*), we find

$$M_{\lambda\mu}=\frac{1}{4\pi}\int[s_\lambda\{F_{\mu\rho}F^\rho{}_\nu+\tfrac{1}{4}g_{\mu\nu}F_{\rho\sigma}F^{\rho\sigma}\}\{s^\nu(1-\kappa')-\epsilon v^\nu\}]_-\epsilon\,d\Omega. \tag{120}$$

$M^{\text{mix.}}_{\lambda\mu}$ therefore differs from (119) in containing an extra s_λ in the integrand, the same terms with λ and μ interchanged being then subtracted. The result of this extra s_λ is that there will be no g_1 terms in $M^{\text{mix.}}_{\lambda\mu}$, while the g_2 terms will contain the ingoing field but not its derivatives. After some easy calculation we get the result given in the text by (59).

We now come to the radiation reaction terms. In the notation of (80),

$$T^{(\epsilon)}_\mu=g_1^2T^{(\epsilon)}_\mu(0)+g_1g_2T^{(\epsilon)}_\mu(1)+g_2^2T^{(\epsilon)}_\mu(2) \tag{121}$$

and

$$T^{(0)}_\mu=g_1^2T^{(0)}_\mu(0)+g_1g_2T^{(0)}_\mu(1)+g_2^2T^{(0)}_\mu(2). \tag{122}$$

The terms in g_1^2 are the well-known reaction terms for a pure point charge and have been calculated in A. It was shown there that

$$T^{(\epsilon)}_\mu(0)=-\frac{1}{2}\frac{\dot v_\mu}{\epsilon}, \tag{123}$$

$$T^{(0)}_\mu(0)=\tfrac{2}{3}v_\mu\dot v^2. \tag{124}$$

The terms in g_1g_2 can be calculated in a similar manner. Introducing (113) and (114) into (117) and using the relations (116), we find after some calculation that

$$T^{(\epsilon)}_\mu(1)=\frac{1}{\epsilon}\frac{d}{d\tau}[\tfrac{1}{3}v_\mu(\mathcal{S}\dot v)+\tfrac{2}{3}S'_\mu+\tfrac{1}{3}S_{\mu\sigma}\dot v^\sigma], \tag{125}$$

and

$$T^{(0)}_\mu(1)=\frac{d}{d\tau}[\tfrac{1}{15}\mathcal{S}_\mu\dot v^2-\tfrac{2}{3}v_\mu(S'\dot v)-\tfrac{8}{15}\dot v_\mu(\mathcal{S}\dot v)]$$
$$+\tfrac{1}{3}(S'_\mu-S_{\mu\sigma}\dot v^\sigma)\dot v^2-\tfrac{2}{3}\ddot S_{\mu\sigma}\dot v^\sigma+\tfrac{2}{3}\dot v_\mu(\mathcal{S}\ddot v)$$
$$+v_\mu\{\tfrac{2}{3}(S'\ddot v)+\tfrac{2}{3}(\ddot vS\dot v)-\tfrac{4}{3}(S''\dot v)-2(\mathcal{S}\dot v)\dot v^2\}. \tag{126}$$

We finally come to the g_2^2 terms. The calculation of $T_\mu^{\text{ret.}}(2)$ is carried out in exactly the same way. (114) is introduced into (117) and then the relations (116) are used to calculate each integral. Since $F_{\mu\nu}^{(2)}$ given by (114) contains no less than 18 terms, $T_{\mu\nu}$ which is quadratic in $F_{\mu\nu}$ contains some 324 terms. Some of these, of course, vanish at once from symmetry, or due to (18), but nevertheless the calculation is very lengthy and tedious. We have not found a way of shortening it. It is interesting to notice that with the expression (114) for $F_{\mu\nu}^{(2)}$, there are no terms of order ϵ^{-3} and ϵ^{-2} in $F_{\rho\sigma}^{(2)}F^{(2)\rho\sigma}$, so that the contribution to $T_\mu^{(0)}(2)$ comes only from the first product in (117). Moreover, $F_{\rho\sigma}^{(2)}F^{(2)\rho\sigma}$ contributes nothing to $M_{\lambda\mu}^{(0)}(2)$ since the only other terms which could do this are those of order ϵ^{-4}, and (120) shows that these are multiplied by the factor $(s_\lambda s_\mu - s_\mu s_\lambda)\kappa'$ which vanishes. We find

$$\begin{aligned}
T_\mu^{(\epsilon)}(2) = \frac{d}{d\tau}\Big[\frac{1}{\epsilon^3}\{&-\tfrac{1}{6}v_\mu S^2 + \tfrac{1}{3}v_\mu \not{S}^2 - \tfrac{1}{3}S_{\mu\sigma}\not{S}^\sigma\} \\
&+\frac{1}{\epsilon^2}\{\tfrac{2}{3}v_\mu(\not{S}S') + \tfrac{2}{5}v_\mu(\not{S}S\dot{v}) + \tfrac{8}{15}\dot{v}_\mu\not{S}^2 - \tfrac{1}{5}\dot{v}_\mu S^2 - \tfrac{1}{3}S_{\mu\sigma}S'^\sigma \\
&-\tfrac{4}{15}S_{\mu\sigma}S^{\sigma\nu}\dot{v}_\nu - \tfrac{1}{3}\dot{S}_{\mu\sigma}\not{S}^\sigma\} + \frac{1}{\epsilon}\{v_\mu[-\dot{v}^2\not{S}^2 + \tfrac{1}{5}\dot{v}^2S^2 \\
&-\tfrac{1}{3}\dot{S}^2 + \tfrac{4}{3}S'^2 + \tfrac{4}{15}(S'S\dot{v}) - \tfrac{1}{15}(\dot{v}SS\dot{v}) + \tfrac{14}{15}(\not{S}\dot{S}\dot{v})] \\
&+\dot{v}_\mu[\tfrac{14}{15}(\not{S}S') + \tfrac{4}{15}(\not{S}S\dot{v})] + \tfrac{4}{15}S_{\mu\sigma}\dot{S}^{\sigma\nu}\dot{v}_\nu - \tfrac{2}{15}S_{\mu\sigma}\not{S}^\sigma\dot{v}^2 \\
&-\tfrac{2}{5}\dot{S}_{\mu\sigma}S^{\sigma\nu}\dot{v}_\nu + \tfrac{2}{3}\not{S}_\mu(S'\dot{v}) - \tfrac{2}{3}S'_\mu(\not{S}\dot{v})\}\Big],
\end{aligned} \tag{127}$$

$$\begin{aligned}
T_\mu^{(0)}(2) = \frac{d}{d\tau}[v_\mu\{&\tfrac{12}{5}(S'\dot{S}\dot{v}) - \tfrac{32}{35}(\not{S}S\dot{v})\dot{v}^2 - \tfrac{2}{5}(\dot{v}S\dot{S}\dot{v})\} \\
&+\dot{v}_\mu\{-\tfrac{16}{35}\not{S}^2\dot{v}^2 + \tfrac{2}{5}(\not{S}\dot{S}\dot{v}) + \tfrac{2}{35}S^2\dot{v}^2 - \tfrac{4}{35}(\dot{v}SS\dot{v}) + \tfrac{2}{15}\dot{S}^2 \\
&+\tfrac{4}{5}(\not{S}S'') + \tfrac{2}{5}(S'S\dot{v})\} + \tfrac{2}{5}\dot{S}_{\mu\sigma}\dot{S}^{\sigma\nu}\dot{v}_\nu - \tfrac{4}{35}S_{\mu\sigma}S^{\sigma\nu}\dot{v}_\nu\dot{v}^2] \\
&+v_\mu\{-\tfrac{1}{3}\ddot{S}^2 + 2S''^2 + \tfrac{4}{5}(S''S\ddot{v}) - \tfrac{2}{5}(\dot{v}S\ddot{S}\dot{v}) + \tfrac{4}{5}(\not{S}\ddot{S}\ddot{v}) \\
&+\tfrac{16}{5}(\not{S}S'')\dot{v}^2 + \dot{S}^2\ddot{v}^2 - \tfrac{12}{5}(S'\dot{S}\ddot{v}) + \tfrac{8}{5}(\dot{v}\dot{S}\dot{S}\dot{v}) - \tfrac{24}{5}S'^2\dot{v}^2 - \tfrac{2}{15}(\ddot{v}SS\ddot{v}) \\
&-\tfrac{16}{5}(\not{S}S')(\dot{v}\ddot{v}) + \tfrac{1}{15}S^2\ddot{v}^2 + \tfrac{32}{15}(\not{S}S\ddot{v})\dot{v}^2 - \tfrac{1}{3}S^2\dot{v}^4 - \tfrac{8}{15}\not{S}^2\ddot{v}^2 \\
&-\tfrac{4}{5}(\dot{v}SS\dot{v})\dot{v}^2 + \tfrac{10}{3}\not{S}^2\dot{v}^4\} + \dot{v}_\mu\{-\tfrac{2}{3}(\dot{S}\ddot{S}) + \tfrac{8}{5}(S'S'') - \tfrac{2}{5}(S''S\dot{v}) \\
&-\tfrac{2}{5}(\not{S}\ddot{S}\dot{v}) - \tfrac{4}{5}(S'\dot{S}\dot{v}) + \tfrac{2}{5}(\dot{v}S\dot{S}\dot{v}) + \tfrac{8}{5}(\not{S}S\dot{v})\dot{v}^2 - \tfrac{4}{5}(\not{S}S''')\} \\
&+\ddot{v}_\mu\{-\tfrac{2}{15}S^2\dot{v}^2 + \tfrac{4}{15}(\not{S}S\ddot{v}) + \tfrac{16}{15}\not{S}^2\dot{v}^2\} + \tfrac{2}{15}S_{\mu\sigma}\ddot{S}^{\sigma\nu}\ddot{v}_\nu + \tfrac{2}{5}S_{\mu\nu}S''^\nu\dot{v}^2 \\
&-\tfrac{2}{5}S_{\mu\nu}S'^\nu(\dot{v}\ddot{v}) - \tfrac{2}{15}S_{\mu\nu}\not{S}^\nu\ddot{v}^2 + \tfrac{4}{15}S_{\mu\sigma}S^{\sigma\nu}\ddot{v}_\nu\dot{v}^2 + \tfrac{2}{3}S_{\mu\nu}\not{S}^\nu\dot{v}^4 - \tfrac{6}{5}\dot{S}_{\mu\nu}S'^\nu\dot{v}^2 \\
&-\tfrac{2}{5}\dot{S}_{\mu\nu}\not{S}^\nu(\dot{v}\ddot{v}) - \tfrac{2}{5}\dot{S}_{\mu\nu}\dot{S}^{\nu\rho}\ddot{v}_\rho + \tfrac{2}{3}\ddot{S}_{\mu\nu}S''^\nu + \tfrac{2}{15}\ddot{S}_{\mu\sigma}S^{\sigma\rho}\ddot{v}_\rho + \tfrac{2}{5}\ddot{S}_{\mu\nu}\not{S}^\nu\dot{v}^2.
\end{aligned} \tag{128}$$

The calculation of $M^{\text{ret.}}_{\lambda\mu}$ can be carried out in exactly the same way by introducing (113) and (114) into (120). We give only the result. As before (Bhabha 1939*b*), $M^{(\epsilon)}_{\lambda\mu}(0) = 0$, while

$$M^{(0)}_{\lambda\mu}(0) = -\tfrac{2}{3}(v_\lambda \dot{v}_\mu - v_\mu \dot{v}_\lambda), \tag{129}$$

$$M^{(\epsilon)}_{\lambda\mu}(1) = [\tfrac{1}{2}v_\lambda(\tfrac{2}{3}S'_\mu + \tfrac{1}{3}S_{\mu\sigma}\dot{v}^\sigma) + \tfrac{1}{3}\dot{S}_{\lambda\mu}]_-, \tag{130}$$

$$\begin{aligned} M^{(0)}_{\lambda\mu}(1) = {} & \frac{d}{d\tau}[\tfrac{1}{3}\dot{S}_{\lambda\mu} + \tfrac{1}{3}\dot{v}_\lambda \mathcal{S}_\mu - \tfrac{1}{3}v_\lambda S_{\mu\sigma}\dot{v}^\sigma]_- + [v_\lambda\{\tfrac{1}{15}\mathcal{S}_\mu \dot{v}^2 - \tfrac{8}{15}\dot{v}_\mu(\mathcal{S}\dot{v})\}]_- \\ & + [v_\lambda\{2\dot{S}_{\mu\sigma}\dot{v}^\sigma + \tfrac{4}{3}S''_\mu + \tfrac{2}{3}S_{\mu\sigma}\ddot{v}^\sigma + \tfrac{1}{3}\mathcal{S}_\mu \dot{v}^2 + \tfrac{4}{3}\dot{v}_\mu(\mathcal{S}\dot{v})\}]_-. \end{aligned} \tag{131}$$

Finally,

$$\begin{aligned} M^{(\epsilon)}_{\lambda\mu}(2) = {} & \Bigg[\frac{1}{\epsilon^3}(-\tfrac{1}{3}v_\lambda S_{\mu\sigma}\mathcal{S}^\sigma) + \frac{1}{\epsilon^2}\Big\{\tfrac{8}{15}v_\lambda \dot{v}_\mu \mathcal{S}^2 - \tfrac{1}{5}v_\lambda \dot{v}_\mu S^2 \\ & - \tfrac{1}{3}v_\lambda S_{\mu\sigma}S'^\sigma - \tfrac{4}{15}v_\lambda S_{\mu\sigma}S^{\sigma\nu}\dot{v}_\nu - \tfrac{1}{3}v_\lambda \dot{S}_{\mu\sigma}\mathcal{S}^\sigma) - \tfrac{1}{3}\frac{d}{d\tau}(v_\lambda S_{\mu\sigma}\mathcal{S}^\sigma)\Big\} \\ & + \frac{1}{\epsilon}\Big\{v_\lambda[\tfrac{14}{15}\dot{v}_\mu(\mathcal{S}S') + \tfrac{4}{15}\dot{v}_\mu(\mathcal{S}S\dot{v}) + \tfrac{4}{15}S_{\mu\sigma}\dot{S}^{\sigma\nu}\dot{v}_\nu - \tfrac{2}{15}S_{\mu\sigma}\mathcal{S}^\sigma \dot{v}^2 \\ & - \tfrac{2}{5}\dot{S}_{\mu\sigma}S^{\sigma\nu}\dot{v}_\nu + \tfrac{2}{3}\mathcal{S}_\mu(S'\dot{v}) - \tfrac{2}{3}S'_\mu(\mathcal{S}\dot{v})] + \frac{d}{d\tau}[-\tfrac{2}{15}v_\lambda \dot{v}_\mu S^2 \\ & + \tfrac{4}{5}v_\lambda \dot{v}_\mu \mathcal{S}^2 - \tfrac{4}{3}\mathcal{S}_\lambda S'_\mu - \tfrac{2}{3}S_{\lambda\sigma}\dot{S}^\sigma{}_\mu - \tfrac{4}{3}v_\lambda S_{\mu\sigma}S'^\sigma \\ & - \tfrac{2}{5}v_\lambda S_{\mu\sigma}S^{\sigma\nu}\dot{v}_\nu - \tfrac{2}{3}\dot{v}_\lambda S_{\mu\sigma}\mathcal{S}^\sigma]\Big\}\Bigg]_-, \end{aligned} \tag{132}$$

$$\begin{aligned} M^{(0)}_{\lambda\mu}(2) = {} & \frac{d}{d\tau}[v_\lambda\{\tfrac{4}{5}\dot{v}_\mu(\mathcal{S}S') - \tfrac{2}{5}\dot{v}_\mu(\mathcal{S}S\dot{v}) - \tfrac{4}{3}S_{\mu\sigma}S''^\sigma \\ & + \tfrac{2}{15}S_{\mu\nu}\dot{S}^{\nu\rho}\dot{v}_\rho - \tfrac{8}{15}\dot{S}_{\mu\nu}S^{\nu\rho}\dot{v}_\rho + \tfrac{1}{5}S_{\mu\sigma}\mathcal{S}^\sigma \dot{v}^2 + \tfrac{4}{5}\mathcal{S}_\mu(S'\dot{v}) - \tfrac{4}{5}S'_\mu(\mathcal{S}\dot{v})\} \\ & - \dot{v}_\lambda\{\tfrac{2}{15}S_{\mu\sigma}S'^\sigma + \tfrac{8}{15}\dot{S}_{\mu\sigma}\mathcal{S}^\sigma\} - \tfrac{2}{3}S_{\lambda\sigma}\ddot{S}^\sigma{}_\mu + \tfrac{2}{15}S_{\lambda\mu}(S'\dot{v}) \\ & - \tfrac{2}{15}\dot{S}_{\lambda\mu}(\mathcal{S}\dot{v}) + \tfrac{2}{15}\mathcal{S}_\lambda \dot{S}_{\mu\sigma}\dot{v}^\sigma - \tfrac{2}{15}S'_\lambda S_{\mu\sigma}\dot{v}^\sigma - \tfrac{4}{3}\mathcal{S}_\lambda S''_\mu]_- \\ & + [v_\lambda\{\dot{v}_\mu[-\tfrac{16}{35}\mathcal{S}^2\dot{v}^2 + \tfrac{2}{5}(\mathcal{S}\dot{S}\dot{v}) + \tfrac{2}{35}S^2\dot{v}^2 - \tfrac{4}{35}(\dot{v}SS\dot{v}) + \tfrac{2}{15}\dot{S}^2 \\ & + \tfrac{4}{5}(\mathcal{S}S'') + \tfrac{2}{5}(S'S\dot{v})] + \tfrac{2}{5}\dot{S}_{\mu\nu}\dot{S}^{\nu\sigma}\dot{v}_\sigma - \tfrac{4}{35}S_{\mu\nu}S^{\nu\sigma}\dot{v}_\sigma \dot{v}^2\}]_- \\ & + [v_\lambda\{\tfrac{4}{3}S_{\mu\nu}S'''^\nu + \tfrac{16}{15}S_{\mu\nu}\ddot{S}^{\nu\rho}\dot{v}_\rho + \tfrac{2}{5}\ddot{S}_{\mu\nu}S^{\nu\rho}\dot{v}_\rho - \tfrac{2}{3}\dot{v}_\mu \dot{S}^2 - \tfrac{12}{5}\dot{v}_\mu(\mathcal{S}S'') \\ & - \tfrac{6}{5}\dot{S}_{\mu\nu}\dot{S}^{\nu\rho}\dot{v}_\rho + \tfrac{8}{5}\dot{v}_\mu S'^2 - \dot{S}_{\mu\nu}\mathcal{S}^\nu \dot{v}^2 + S_{\mu\nu}S'^\nu \dot{v}^2 + \tfrac{1}{5}S_{\mu\nu}S^{\nu\sigma}\dot{v}_\sigma \dot{v}^2 \\ & + \tfrac{1}{5}\dot{v}_\mu S^2\dot{v}^2 + \tfrac{4}{5}\ddot{v}_\mu(\mathcal{S}S\dot{v}) - \tfrac{8}{5}\dot{v}_\mu \mathcal{S}^2\dot{v}^2 - \tfrac{2}{5}\dot{v}_\mu(\dot{v}SS\dot{v})\} \\ & + \dot{v}_\lambda\{\tfrac{4}{3}S_{\mu\nu}S''^\nu + \tfrac{2}{3}\ddot{S}_{\mu\nu}\mathcal{S}^\nu - \tfrac{4}{3}\dot{S}_{\mu\nu}S'^\nu + \tfrac{4}{15}\dot{S}_{\mu\nu}S^{\nu\rho}\dot{v}_\rho - \tfrac{2}{5}S_{\mu\nu}\dot{S}^{\nu\rho}\dot{v}_\rho \\ & + \tfrac{3}{5}S_{\mu\nu}\mathcal{S}^\nu \dot{v}^2 - \tfrac{1}{15}\ddot{v}_\mu S^2 + \tfrac{2}{5}\ddot{v}_\mu \mathcal{S}^2\} - \tfrac{2}{15}\dot{v}_\lambda S_{\mu\nu}S^{\nu\sigma}\dot{v}_\sigma \\ & + \tfrac{4}{3}\mathcal{S}_\lambda S'''_\mu + \tfrac{2}{3}S_{\lambda\nu}S'''^\nu{}_\mu - \tfrac{2}{3}S''_\lambda S_{\mu\sigma}\dot{v}^\sigma + \tfrac{2}{3}\mathcal{S}_\lambda \ddot{S}_{\mu\nu}\dot{v}^\nu \\ & - \tfrac{2}{3}S_{\lambda\sigma}\dot{v}^\sigma \dot{S}_{\mu\rho}\dot{v}^\rho + \tfrac{2}{3}S_{\lambda\sigma}\dot{S}^\sigma{}_\mu \dot{v}^2 + 2\mathcal{S}_\lambda S'_\mu \dot{v}^2]_-. \end{aligned} \tag{133}$$

The singular terms in all the above expressions have already been dealt with in the text. We now have to determine $A^{(0)}_{\mu}$ and $B^{(0)}_{\lambda\mu}$. We can see from (126) and (128) that certain terms of $T^{(0)}_{\mu}(1)$ and $T^{(0)}_{\mu}(2)$ are perfect differentials. It simplifies the calculation to add these terms straight away to $A^{(0)}_{\mu}(1)$ and $A^{(0)}_{\mu}(2)$, for these terms then fall out of the translational equation. They cancel one another on the right-hand side of (69*a*). Their inclusion in $A^{(0)}_{\mu}$, however, alters the left-hand side of (79) and is equivalent to subtracting certain terms from $M^{(0)}_{\lambda\mu}$. It appears that this actually effects a simplification in $M^{(0)}_{\lambda\mu}$. The terms that are so cancelled in $M^{(0)}_{\lambda\mu}(1)$ and $M^{(0)}_{\lambda\mu}(2)$ have been written separately in the second square brackets in (131) and (133) respectively. Further we see that the terms in the first square brackets in (131) and (133) are perfect differentials. These can therefore be eliminated at once by including them in $B^{(0)}_{\lambda\mu}$. These terms then also drop out of the rotational equations. We may therefore work as if the terms in the first square brackets in $T^{(0)}_{\mu}(1)$ and $T^{(0)}_{\mu}(2)$, and the terms in the first and second square brackets in $M^{(0)}_{\lambda\mu}(1)$ and $M^{(0)}_{\lambda\mu}(2)$, were absent. This effects some simplification in the subsequent calculation, and we henceforth assume that these terms have been eliminated.

Consider first $A^{(0)}_{\mu}(0)$. This must not contain $S_{\lambda\mu}$ and must have one differentiation with respect to τ. It can easily be seen that it must be $-\frac{2}{3}\dot{v}_{\mu}$. With this substitution the right-hand side of (69*a*) vanishes at once, and the left-hand side of (79) also vanishes by (129), provided that $B^{(0)}_{\lambda\mu}(0) = 0$. This is in any case inevitable since no term in $B^{(0)}_{\lambda\mu}(0)$ is possible which only contains v_{μ} but none of its derivatives. We thus find that

$$T^{\text{react.}}_{\mu}(0) = \tfrac{2}{3}(v_{\mu}\dot{v}^2 + \ddot{v}_{\mu}), \tag{134}$$

while $M^{\text{react.}}_{\lambda\mu}(0) = 0$. These are the well-known radiation reaction terms for a point charge.

Now consider $A^{(0)}_{\mu}(1)$ and $B^{(0)}_{\lambda\mu}(1)$. Expressions (126) and (131) show that the terms of these must be linear in $S_{\lambda\mu}$ and contain respectively two and one differentiations with respect to τ. The most general expressions for these quantities are then of the following form:

$$\begin{aligned} A^{(0)}_{\mu}(1) = {} & f_1 v_{\mu}(\mathcal{S}\ddot{v}) + f_2 v_{\mu}(S'\dot{v}) + f_3 \dot{v}_{\mu}(\mathcal{S}\dot{v}) \\ & + f_4 \mathcal{S}_{\mu}\dot{v}^2 + f_5 S''_{\mu} + f_6 \dot{S}_{\mu\sigma}\dot{v}^{\sigma} + f_7 S_{\mu\sigma}\ddot{v}^{\sigma}, \end{aligned} \tag{135}$$

and

$$B^{(0)}_{\lambda\mu}(1) = [h_1 \dot{S}_{\lambda\mu} + h_2 v_{\lambda} S'_{\mu} + h_3 v_{\lambda} S_{\mu\sigma}\dot{v}^{\sigma} + h_4 \dot{v}_{\lambda}\mathcal{S}_{\mu}]_{-}. \tag{136}$$

The f's and h's are arbitrary constants which have to be determined. Using (131) (without the terms in the first two brackets), (135) and (136), we build the expression on the left-hand side of (79). The coefficients of those terms in this which are not of the form of the right of (79) must be put equal to zero. Thus, the coefficient of $v_\lambda \dot{v}_\mu(\dot{S}\dot{v})$ is $-(f_3-\frac{4}{3})$, and this must be zero; whence $f_3 = \frac{4}{3}$. Similarly, the coefficient $v_\lambda \dot{S}_\mu \dot{v}^2$ is $-(f_4-\frac{1}{3})$; whence $f_4 = \frac{1}{3}$. The coefficient of $v_\lambda S_{\mu\sigma} \ddot{v}^\sigma$ is $-(f_7+h_3-\frac{2}{3})$. This need not be zero, but it must be equal to minus the coefficient of $\ddot{v}_\lambda \dot{S}_\mu$ which is $-h_4$. Hence $h_4 = -(f_7+h_3-\frac{2}{3})$. These two terms then combine to give

$$h_4[S_{\mu\sigma}(\ddot{v}^\sigma v_\lambda - v^\sigma \ddot{v}_\lambda)]_-,$$

which is of the form of the right-hand side of (79) and is permissible. Proceeding in this way we can show that the left-hand side of (79), which is equal to $M^{\text{react.}}_{\lambda\mu}(1)$ by (88), must be reduced to

$$M^{\text{react.}}_{\lambda\mu}(1) = h_2[S_{\lambda\sigma}(\ddot{v}^\sigma v_\mu - v^\sigma \ddot{v}_\mu)]_-. \tag{137a}$$

Finally, using (126) and (135), we form the right-hand side of (69a) and equate it to the left-hand side, which in this case becomes just $h_2(S'\ddot{v})$. The coefficients of each term on the two sides of (69a) must be equal, and this gives us another set of equations determining the coefficients. It is found that all the coefficients can be determined in terms of one of them, namely h_2. We call this h below. The result is given in the table:

$f_1 = \frac{2}{3}$	$f_2 = -3h+\frac{8}{3}$	$f_3 = \frac{4}{3}$	$f_4 = \frac{1}{3}$
$f_5 = -h+\frac{4}{3}$	$f_6 = -2h+2$	$f_7 = \frac{2}{3}$	
$h_1 = 0$	$h_2 = h$	$h_3 = h$	$h_4 = -h$

If we use (126) and (135) with these values of the coefficients, $T^{\text{react.}}_\mu(1)$ given by (85) can easily be worked out. Similarly, by (56) and with h for h_2, the equation (137a) leads to

$$C^{\text{react.}}_{\rho\mu}(1) = h(\ddot{v}_\rho v_\mu - \ddot{v}_\mu v_\rho). \tag{137b}$$

$T^{\text{react.}}_\mu(2)$ and $M^{\text{react.}}_{\lambda\mu}(2)$ can be found in the same way, but due to the fact that they are quadratic in $S_{\lambda\mu}$ and contain respectively four and three derivatives with respect to τ, they are very much more complicated. $A^{(0)}_\mu(2)$ contains 56 terms which may be grouped in the following way. One group has terms of the type $v(SS)v^2$ with three derivatives (dots) distributed over the different symbols. By (4), (5) and (7), there are five independent terms in this group, namely $\dddot{v}_\mu S^2$, $\dot{v}_\mu \dot{S}^2$, $\dot{v}_\mu S^2\dot{v}^2$, $v_\mu(\dot{S}\ddot{S})$, and $v_\mu(\dot{v}\ddot{v})$. Another group has terms of the type $v_\mu(vSSv)v^2$ and contains 23 terms. The other groups are characterized by terms of the type $v_\mu(vSv)(vSv)$, $(S_{\mu\sigma}S^{\sigma\nu}v_\nu)v^2$ and $(S_{\mu\sigma}v^\sigma)(vSv)v^2$, and contain 3, 13 and 12 terms respectively. There are thus in all 56 independent terms with arbitrary coefficients in $A^{(0)}_{\mu}(2)$. Similarly, the terms of $B^{(0)}_{\lambda\mu}(2)$ can be classified in the following groups:

$$[v_\lambda S_{\mu\sigma} S^{\sigma\nu} v_\nu]_- v^2, \quad [v_\lambda S_{\mu\sigma} v^\sigma]_-(vSv), \quad (v_\lambda v_\mu]_-(vSSv),$$
$$[S_{\lambda\sigma} v^\sigma S_{\mu\rho} v^\rho]_-, \quad \text{and} \quad S_{\lambda\mu}(vSv),$$

with two dots distributed over the symbols in each term, plus two other terms, $[v_\lambda \ddot{v}_\mu S^2]_-$ and $[S_{\lambda\rho} \ddot{S}^{\rho}{}_{\mu}]_-$, which do not belong to these groups. There are 11, 5, 3, 4 and 3 terms respectively in each group, making 28 terms in all. It is remarkable that the conditions (79) and (69a) are so stringent that the coefficients of all these terms can be determined in terms of six arbitrary constants which we denote by k_1 to k_6. We give only the result here. $T^{\text{react.}}_{\mu}(2)$ is an extremely cumbersome expression. However, when $\dot{v}_\mu$, $\ddot{v}_\mu$, $v^{\text{iii}}{}_{\mu}$ and $\dot{S}_{\lambda\mu}$, $\ddot{S}_{\lambda\mu}$ and $S^{\text{iii}}{}_{\lambda\mu}$ vanish, it reduces to

$$-\tfrac{1}{15} v^{\text{iv}}_{\mu} S^2 + \tfrac{2}{5} v^{\text{iv}}_{\mu} \ddot{S}^2 + \tfrac{2}{15} v_\mu (\ddot{S} S v^{\text{iv}}) + (k_1 + k_3 + \tfrac{2}{3})\, v_\mu (\ddot{S} S''')$$
$$+ (k_1 + \tfrac{2}{3})\, S^{\text{iv}}_{\mu\nu} \ddot{S}^{\nu} + k_3 S_{\mu\nu} S'''^{\,\nu}. \tag{138}$$

Finally, $M^{\text{react.}}_{\lambda\mu}(2)$ can be written

$$M^{\text{react.}}_{\lambda\mu}(2) = [S_\lambda{}^{\rho} C^{\text{react.}}_{\rho\mu}(2)]_-, \tag{139}$$

with
$$\begin{aligned} C^{\text{react.}}_{\rho\mu}(2) = {} & \tfrac{2}{3} S^{\text{iii}}_{\rho\mu} + \tfrac{2}{3} \dot{S}_{\rho\mu} \dot{v}^2 + [\tfrac{4}{3} v_\rho S'''_{\mu} + 2 v_\rho S'_{\mu} \dot{v}^2 \\ & - k_1 v^{\text{iii}}_{\rho} \ddot{S}_{\mu} - (k_1 + k_2 + \tfrac{2}{15})\, \ddot{v}_\rho S_{\mu\sigma} \dot{v}^\sigma - (k_1 - k_3 - k_4 + \tfrac{2}{3})\, \ddot{v}_\rho S'_{\mu} \\ & + (k_1 - k_3 + k_4 + \tfrac{2}{3})\, v_\rho \dot{S}_{\mu\sigma} \ddot{v}^\sigma - (k_2 + k_3 - \tfrac{8}{15})\, \dot{v}_\rho S_{\mu\sigma} \ddot{v}^\sigma \\ & - (k_3 - \tfrac{2}{3})\, v_\rho S_{\mu\sigma} v^{\text{iii}\,\sigma} + (k_4 + \tfrac{2}{3})\, \{v_\rho \ddot{S}_{\mu\sigma} \dot{v}^\sigma + \dot{v}_\rho S''_{\mu}\} \\ & + (2k_4 - \tfrac{2}{3})\, \dot{v}_\rho \dot{S}_{\mu\sigma} \ddot{v}^\sigma - 2k_5 v_\rho \ddot{S}_{\mu} (\dot{v}\ddot{v}) - (k_5 - \tfrac{3}{5})\, \{v_\rho S_{\mu\sigma} \dot{v}^\sigma \dot{v}^2 \\ & + \dot{v}_\rho \ddot{S}_{\mu} \dot{v}^2\} + k_6 \{v_\rho \ddot{v}_\mu (\ddot{S}\dot{v}) + v_\rho \dot{v}_\mu (\ddot{S}\ddot{v})\}]_-. \end{aligned} \tag{140}$$

We see from (138) that $S^{\text{iv}}_{\lambda\mu}$ appears in the translational equation, but the arguments given in the text show that this does not prevent the equations from being used to determine the motion of the particle. The only terms which contain $S^{\text{iv}}_{\lambda\mu}$ are in fact just the last three terms in (138). (No term containing $S^{\text{iv}}_{\lambda\mu}$ vanishes by putting any of the lower derivatives of v_μ or $S_{\lambda\mu}$ equal to zero since the terms in $T^{\text{react.}}_{\mu}(2)$ have in all four derivatives, and in those terms where four derivatives appear in $S_{\lambda\mu}$ no dots can appear over any other symbol.) (138) shows that by putting $k_1 + \tfrac{2}{3} = 0$, $k_3 = 0$, we could eliminate $S_{\lambda\mu}$ from the equations of motion altogether. This specialization simplifies the coefficients in (140). Out of the remaining four coefficients, $k_6 = 0$ effects an obvious simplification.

To obtain the specialized equation when either $S_{\mu\rho}v^{\rho} = 0$ or $S^{*}_{\mu\rho}v^{\rho} = 0$, we have to replace $C^{\text{react.}}_{\rho\mu}$ by

$$D_{\rho\mu} \equiv C^{\text{react.}}_{\rho\mu} - (C^{\text{react.}}_{\rho\sigma} v^{\sigma} v_{\mu} - C^{\text{react.}}_{\mu\sigma} v^{\sigma} v_{\rho}), \tag{141}$$

as shown in the text. This expression is in general no simpler than (140). However, in the particular case $\not{S}_{\mu} = 0$ we can use the relations (94). The expression for $D_{\rho\mu}$ then reduces to

$$D_{\rho\mu} = \tfrac{2}{3} S^{\text{iii}}_{\rho\mu} + \tfrac{2}{3}\dot{S}_{\rho\mu}\dot{v}^{2} - [-\tfrac{2}{3} v_{\rho} S'''_{\mu} + (d-\tfrac{2}{3}) v_{\rho} S'_{\mu}\dot{v}^{2} + (d-\tfrac{2}{3})\dot{v}_{\rho} S''_{\mu} + d\ddot{v}_{\rho} S'_{\mu} + 2(d+\tfrac{1}{3})\dot{v}_{\rho}\dot{S}_{\mu\sigma}\dot{v}^{\sigma}]_{-}, \tag{142}$$

where we have written d in place of $-(k_{2}+k_{3}+k_{4}-\tfrac{8}{15})$. It is interesting to note that in this case three of the six arbitrary constants automatically fall out, while the other three only appear in the above combination, so that in effect there is only one arbitrary constant in this case. (142) is exactly the radiation reaction term found for this case in a previous paper (B, (46)) by a direct method. $T^{\text{self.}}_{\mu}(2)$ is given explicitly in that paper (B, appendix).

Forming the expression on the right-hand side of (141) from (137*b*), we see that it vanishes, which shows that there are no $g_{1}g_{2}$ terms in $D_{\rho\mu}$. We thus get the result quoted in the text that even in the case $g_{1} \neq 0$ the charge g_{1} adds nothing to the radiation reaction terms in the rotational equation.

In the case $\not{S}_{\mu} = 0$, the radiation reaction terms in the translational equation (101) are then

$$T^{\text{self.}}_{\mu} = g_{1}^{2} T^{\text{self.}}_{\mu}(0) + g_{1}g_{2} T^{\text{self.}}_{\mu}(1) + g_{2}^{2} T^{\text{self.}}_{\mu}(2).$$

$T^{\text{self.}}_{\mu}(0)$ is just given in (134), while

$$T^{\text{self.}}_{\mu}(1) = \tfrac{4}{3} v_{\mu}(S'\ddot{v}) + \tfrac{2}{3} S'_{\mu}\dot{v}^{2} - \tfrac{2}{3} S'''_{\mu} - 2\ddot{S}_{\mu\sigma}\dot{v}^{\sigma} - \tfrac{2}{3}\dot{S}_{\mu\sigma}\ddot{v}^{\sigma}, \tag{143}$$

and thus contains no arbitrary constant. $T^{\text{self.}}_{\mu}(2)$ contains the one arbitrary constant d which occurs in (142) and is given explicitly in B (appendix). We see clearly that, whereas the reaction terms in the general equations (72) and (73) contain no less than seven arbitrary constants, in the special case $\not{S}_{\mu} = 0$ (but not in the case $S^{*}_{\mu\rho}v^{\rho} = 0$) there is only one arbitrary constant, and the radiation reaction terms both in the translational and rotational equations are vastly simpler.

REFERENCES

Bhabha 1939*a* *Proc. Roy. Soc.* A, **172**, 384–409; referred to here as A.
Bhabha 1939*b* *Proc. Indian Acad. Sci.* A, **10**, 324–332.
Bhabha 1940*a* *Proc. Indian Acad. Sci.* A, **11**, 247–267, 467; referred to here as B.
Bhabha 1940*b* *Nature, Lond.*, **145**, 819.
Dirac 1938 *Proc. Roy. Soc.* A, **167**, 148–169.
Heitler 1936 *Quantum theory of radiation*, p. 158 ff.
Pauli 1933 *Handbuch der Physik*, **24**/1, Quantentheorie.
Pryce 1938 *Proc. Roy. Soc.* A, **168**, 389–401.

General classical theory of spinning particles in a meson field

BY H. J. BHABHA, PH.D.
Department of Physics, Indian Institute of Science, Bangalore

(*Communicated by P. A. M. Dirac, F.R.S.—Received* 18 *December* 1940)

An exact classical theory of the motion of a point dipole in a meson field is given which takes into account the effects of the reaction of the emitted meson field. The meson field is characterized by a constant $\chi = \mu/\hbar$ of the dimensions of a reciprocal length, μ being the meson mass, and as $\chi \rightarrow 0$ the theory of this paper goes over continuously into the theory of the preceding paper for the motion of a spinning particle in a Maxwell field. The mass of the particle and the spin angular momentum are arbitrary mechanical constants. The field contributes a small finite addition to the mass, and a negative moment of inertia about an axis perpendicular to the spin axis.

A cross-section (formula (88*a*)) is given for the scattering of *transversely* polarized neutral mesons by the rotation of the spin of the neutron or proton which should be valid up to energies of 10^9 eV. For low energies E it agrees completely with the old quantum cross-section, having a dependence on energy proportional to p^4/E^2 (p being the meson momentum). At higher energies it deviates completely from the quantum cross-section, which it supersedes by taking into account the effects of radiation reaction on the rotation of the spin. The cross-section is a maximum at $E \sim 3{\cdot}5\mu$, its value at this point being 3×10^{-26} cm.^{2}, after which it decreases rapidly, becoming proportional to E^{-2} at high energies. Thus the quantum theory of the interaction of neutrons with mesons goes wrong for $E \gtrsim 3\mu$. The scattering of longitudinally polarized mesons is due to the translational but not the rotational motion of the dipole and is at least twenty thousand times smaller.

With the assumption previously made by the present author that the heavy partilesc may exist in states of any integral charge, and in particular that protons of charge $2e$ and $-e$ may occur in nature, the above results can be applied to *charged* mesons. Thus transversely polarised mesons should undergo a very big scattering and consequent absorption at energies near $3{\cdot}5\mu$. Hence the energy spectrum of transversely polarized mesons should fall off rapidly for energies below about 3μ. Scattering plays a relatively unimportant part in the absorption of longitudinally polarized mesons, and they are therefore much more penetrating.

The theory does *not* lead to Heisenborg explosions and multiple processes.

It has been shown in the preceding paper† with Corben that it is possible to give a complete classical theory of the motion of a point dipole in a Maxwell field. This theory is free from the infinite energies associated in the usual theory with a point charge or a point dipole, and it was shown that the appearance of these infinities in the usual theory is fictitious and due to an incorrect definition of field energy when singularities are present in the field. It appears that the effects of radiation reaction are even more important for a point dipole than for a point charge, and this makes the scattering of light decrease as ω^{-2} for high frequencies ω instead of increasing as ω^2, as would be the case if radiation reaction were neglected.

The work of this paper is an extension to the meson field of the work of the preceding paper with Corben. It will constantly be necessary to refer to the results of that paper. The underlying ideas and assumptions are exactly the same, as is also the method of procedure. It must be understood that whenever the charge g_1 and the dipole moment g_2 are referred to in this paper, these are quantities which interact with and create the meson field and not the Maxwell field. In other words, the charge is not an electric charge, nor the dipole moment an electromagnetic moment. When need arises for specifically distinguishing these quantities from the corresponding electromagnetic quantities, I shall refer to them as a mesic charge and a mesic dipole moment, and correspondingly I shall talk of an electromesic force and a magnetomesic force.

The extension of the theory to the case of spinning particles moving in a meson field is of both theoretical and practical interest, for it is known that protons and neutrons have an explicit spin interaction with the meson field involving the interaction constant g_2, whereas this term appears to be absent in the interaction of electrons or protons with the Maxwell field. The meson field has a characteristic constant χ which is connected, when the field is quantized, with the rest mass μ of the meson by the relation $\chi = \mu/\hbar$ (the velocity of light is taken to be unity). In the classical theory neither μ nor $\hbar$ appear explicitly, but only in the combination χ which has the dimensions of a reciprocal length. Maxwell's theory is the particular case of meson theory in which $\chi = 0$. Now it was shown in a previous paper (Bhabha 1939, referred to in this paper as A) that the Green's function for the meson field is just the Green's function for the Maxwell field plus a non-singular part which has a plain discontinuity on the light cone. This additional part tends to zero continuously as $\chi \rightarrow 0$. It follows from this that in any given case, the highest singularities in the meson field are the same as those in the Maxwell field, and all additional terms are singular to a lesser degree. One would expect from this that it would be possible to extend the theory of spinning dipoles of the previous paper to a meson field. This is done in the present paper. Exact equations are derived for the motion of a point dipole in a meson field which contain the constant χ explicitly, and go over continuously into the equations of the previous paper as $\chi \rightarrow 0$. Even for the simplest type of point dipole, namely one whose mechanical properties are those of a pure gyroscope, there are three constants having the dimensions of a reciprocal length which enter into the equations of motion. These are $3M/2g_1^2$, $(3I/2g_2^2)^{\frac{1}{2}}$, and χ, where M and I denote the mass and spin angular momentum of the particle, and g_1 and g_2 the mesic charge and dipole moment respectively. If these constants are given the values which they have in nuclear theory, it appears that the first and second are respectively about 450 and 3 times the third. As stated above, Maxwell's theory corresponds to the limit $\chi = 0$, so that it follows from the magnitude of the constants that all processes which involve only the first and third constants, as, for example, the scattering of transverse waves by a point charge, will differ very slightly in the Maxwell and meson theories. This is confirmed by the results of a previous paper (A). On the other hand, in processes which involve the second constant also, the differences in the magnitudes of corresponding processes in the Maxwell and meson theories may be expected to be considerable, since the second constant is only about three times the third. The results of this paper confirm this. For frequencies ω_0 large compared with χ, the difference between the two theories is small and gets continuously smaller with increasing ω_0.

---

† Bhabha and Corben (1941), referred to in this paper as C.

A cross-section is given for the scattering of meson waves due to the g_2 spin interaction by a particle which is free to rotate but not to translate. This cross-section goes over continuously as $\chi \rightarrow 0$ into the corresponding cross-section for the scattering of light. It has the same general dependence on frequency (formula (88) and the curve marked $\beta = 0$ in the figure). For low frequencies it increases as $(\omega_0^2 - \chi^2)^2/\omega_0^2$, and, if the angular momentum of the spin of the particle is put equal to $\frac{1}{2}\hbar$, it agrees completely[†] with the quantum cross-section for the scattering of neutral mesons by neutrons.

[†] See, however, second footnote on p. 341.

However, it differs from the behaviour of the quantum cross-section, which continues to increase as ω_0^2 to the highest energies, in that it reaches a maximum at $\omega_0 \sim 3{\cdot}5\chi$, and finally decreases for high frequencies as ω_0^{-2}. This decrease is entirely due to the effect of radiation reaction on the rotation of the spin, which is completely neglected in the quantum theory. Moreover, this behaviour at high frequencies is similar to the scattering by a point charge. For scattering by a point charge the cross-section decreases but slowly up to a certain frequency, after which the decrease becomes more rapid, finally becoming proportional to ω_0^{-2}. Since the scattering by the translational motion of a point charge and the rotation of a dipole are very different processes, it seems plausible to suppose that *this decrease of the scattering at high frequencies proportionally to* ω_0^{-2} *is a fundamental property of radiation fields, both Maxwellian and mesic.*

A non-relativistic attempt to avoid the increase of the quantum cross-section for the scattering of mesons due to the *spin* of the heavy particles has recently been made by Heitler (1940) in which it is assumed that the heavy particles can exist in states of spin $\frac{3}{2}\hbar$, $\frac{5}{2}\hbar$, etc. There are a number of objections to this assumption. First, it is known that the effect of the reaction of the emitted radiation is neglected in the quantum theory, so that a failure of the quantum formulae at high energies is in any case to be expected. The classical theory of this paper then shows that the effect of this radiation reaction is to make all cross-sections decrease at high frequencies like ω_0^{-2}, and hence it completely removes all necessity for assuming that the heavy particles may exist in higher spin states. Secondly, the assumption that the heavy particles can exist in higher spin states is an assumption about the *mechanical properties of the heavy particles*, and would only alter the scattering of mesons by heavy particles, whereas the difficulty is equally pronounced in the scattering of light by an electron *having an explicit spin interaction* with the Maxwell field, as is theoretically possible, although for the actual electron which occurs in nature this spin interaction happens to be zero. *There is complete parallelism between the two cases*, and the theories of this paper and the preceding paper with Corben deal with both on the same footing. To apply Heitler's idea to the scattering of light in the above hypothetical case we should have to assume that the electron could also exist in states of higher spin, and there is no evidence whatever for this. It is not unreasonable to suppose that all elementary particles with a spin $\frac{1}{2}\hbar$ in their normal state have the *same mechanical characteristics* and there is *only one relativistic* theory for a particle of spin $\frac{1}{2}\hbar$, namely, that in which the particle is described by the Dirac equation. It is not possible to say yet whether Heitler's idea allows of formulation in a way consistent with the theory of relativity. Thus, whereas the treatment of this paper is complete within the limits of classical theory, the approach of Heitler falls short of the completeness of present quantum mechanics by not being in relativistic form. Finally, the assumption of allowing the heavy particles to exist in states of higher spin merely puts the scattering by the spin on the same footing as the scattering by a point charge. In this it does not seem to me to go far enough. For it is well known that the formulation of the interaction of a point charge with a field in quantum theory neglects the effect of radiation reaction and leads to divergence difficulties in higher approximations. These have been discussed at length elsewhere (Bhabha 1940*b*). Dirac (1938) has shown how these difficulties may be removed for a point electron within the limits of classical theory, and the work of this paper is but an extension of the work of Dirac to a spinning particle moving in a meson field, and shows that in classical theory the complete treatment of the spin presents no more difficulty than the treatment of a point charge. Thus it would be reasonable to suppose that the difficulties concerning the spin in the quantum theory are to be removed in the same way as the difficulties concerning a point charge, namely, by introducing into quantum theory the effects of radiation reaction both for a point charge and for a point dipole. A quantum translation of the classical theory of Dirac and of this paper, if possible, would do this, though it may require a far-reaching extension of the basis of quantum mechanics.

An interesting feature appears in the scattering of meson waves. As shown in A, the scattering of longitudinal waves, due to the motion of a point charge is less than the scattering of transverse waves of the same frequency ω_0 by a factor χ^2/ω_0^2. This difference is very much accentuated in the scattering by a dipole. As far as concerns scattering by a magnetomesic dipole which is free to rotate but not to translate, it is only the magnetomesic force of the wave which acts on the dipole and causes it to oscillate. Now the magnetomesic force of a longitudinal wave is zero, so that no scattering of longitudinal waves by the dipole will occur at all. The scattering of longitudinal waves can therefore only be due to the translational motion of the point charge or dipole. With the actual values of the constants as they occur in nature the scattering of transverse waves due to the rotation of the dipole is more than twenty thousand times greater than the scattering of longitudinal waves due to the translational motion of the particle. Hence transverse and longitudinal waves behave quite differently. The difference only disappears for low frequencies, ω_0 very close to χ, when in any case the scattering of both is negligible. However, as shown in A, when a longitudinal wave is scattered it is more probable that the emerging wave will be transversely polarized, and hence the probability of its being scattered again will be very much greater.

The above remarks apply strictly to neutral mesons. The cause of the difference in the scattering of charged and neutral mesons was analysed in a previous paper (Bhabha 1939), and it was shown there (and also by Pauli) that it is due entirely to the fact that whereas in the usual theory a positive meson can only be emitted by a proton and a negative meson by a neutron, a neutral meson can be emitted by both a proton and a neutron. There are thus twice as many intermediate states leading to the scattering of neutral as of charged mesons, and the effects of these largely cancel each other, thus reducing the scattering of neutral mesons. To avoid this difference the present author put forward the idea that the heavy particles could exist in states of all integral charge, positive and negative, having different rest energies, of which only the two of lowest energy (rest mass), namely the proton and neutron, occur normally in nature. This idea was communicated to Dr Heitler and has been adopted by him to calculate the scattering of mesons due to the charge of the heavy particles (Heitler 1940). With this assumption, as was shown in a previous paper (1940*b*), the theory of charged mesons is put on the same footing as the theory of neutral mesons, so that the above-mentioned classical cross-sections which should be valid for energies up to 10^9 eV can at once be applied to charged mesons.†

This idea by itself is, however, not sufficient to remove the difficulties in the scattering of mesons due to the *spin* of the heavy particles. Heitler (1940) has attempted to overcome these difficulties by allowing the heavy particles to exist in states of higher spin, whereas the approach of this paper has been to show that the difficulties disappear if proper account is taken of the effects of radiation reaction. The scattering of mesons due to the *spin* of the heavy particles is therefore different in his theory from that given here. The two cross-sections have a different dependence on energy, and experiment could easily distinguish between them. Thus the cross-section given in this paper is small at low and high energies but becomes very large at energies near $3{\cdot}5\mu$. The effect of this would be that the energy spectrum of transversely polarized mesons would fall off rapidly for energies below about 3μ. Further, one would expect the mesons in cosmic radiation to fall into two groups depending on their polarization, longitudinally polarized mesons being scattered twenty thousand times less than transversely polarized mesons of the same energy and hence being far more penetrating. On the rare occasion, however, that a longitudinally polarized meson is scattered, the probability that the scattered meson is transversely polarized is of the order

---

† Cf. Bhabha and Madhava Rao, 1941, *Proc. Indian Acad. Sci.* A, **13**, 9–24.

$2\omega_0^2/(2\omega_0^2+\chi^2)$, so that the chance of a subsequent scattering is very much greater. For mesons of cosmic-ray energies, the difference in the scattering of longitudinally and transversely polarized mesons is so great that it might almost lead them to appear as different particles, whereas the difference is only in their polarization and consequently in their penetrating power. This difference vanishes for mesons of extremely small velocities, but then the scattering is in any case very small and negligible compared with a number of other processes.

It must be recognized, however, that the application of the cross-sections of this paper to *charged* mesons definitely implies an assumption that among other things protons of charge $2e$ and $-e$ may be expected to occur in nature. The circumstances under which these particles might be observed and the probability of processes leading to their creation have already been fully investigated in the paper mentioned (Bhabha 1940*b*). If the cross-section for the scattering of mesons given in this paper could be shown experimentally to be in agreement with the scattering of charged mesons, then this would be evidence, though not proof, that the assumption made about the nature of the heavy particles and the possible appearance of protons of charge $2e$ and $-e$ was correct. The theory of the motion of spinning particles in meson fields developed in this paper is, however, complete in itself, and does not depend on the correctness or otherwise of its application to *charged* mesons through the *independent assumption* about the nature of the heavy particles.

Finally, the work of this paper shows that the spin itself does *not* lead to multiple processes and Heisenberg explosions as hitherto supposed. In a previous paper (A) I showed that the mass of the meson cannot lead to explosions either. The only remaining possibility of the appearance of Heisenberg explosions then lies in the difference in the behaviour of charged and neutral mesons, and, as shown in the paper mentioned (Bhabha 1940*b*) this difference is removed by the assumption that the heavy particles can exist in states of all integral charge, so that even this possibility of the appearance of explosions disappears. It may then be concluded that large Heisenberg explosions are not possible theoretically. This does not, of course, mean that occasionally two and on rare occasions more mesons may not be simultaneously produced.

THE MESON FIELD OF A DIPOLE

I keep to the notation of the preceding paper. The velocity of light is put equal to unity, and I take the metric tensor $g_{\mu\nu}$ in the form $g_{00}=1$,

$g_{11} = g_{22} = g_{33} = -1$ with all the other components vanishing. The coordinate of the particle is denoted by z_μ which can be considered as a function of the proper time τ, measured from some arbitrary point on the classical world line of the particle. A dot over a symbol denotes differentiation with respect to τ. The velocity $\dot{z}_\mu$ is denoted by v_μ. The spin of the particle is described by an antisymmetric tensor $S_{\mu\nu}$ which may likewise be considered as a function of τ. The mesic charge and current density P_μ at any point x_ρ may then be written

$$\mathrm{P}_\mu(x_\rho) = g_1\int_{-\infty}^{\infty} d\tau\, v_\mu\, \delta(x_0-z_0)\,\delta(x_1-z_1)\,\delta(x_2-z_2)\,\delta(x_3-z_3), \tag{1}$$

and the dipole density $\Sigma_{\mu\nu}$ at the point x_ρ by

$$\Sigma_{\mu\nu}(x_\rho) = g_2\int_{-\infty}^{\infty} d\tau\, S_{\mu\nu}(\tau)\,\delta(x_0-z_0)\,\delta(x_1-z_1)\,\delta(x_2-z_2)\,\delta(x_3-z_3). \tag{2}$$

As in the preceding paper, the invariant formed from any two tensors $X_{\mu\nu}$ and $Y_{\mu\nu}$ is written

$$(XY) \equiv X_{\mu\nu}Y^{\mu\nu}, \quad X^2 \equiv (XX) = X_{\mu\nu}X^{\mu\nu}.$$

The invariant formed from any combination of tensors and two vectors is written in the usual matrix notation; thus

$$(\dot{v}\dot{S}\dot{S}v) = \dot{v}^\mu \dot{S}_{\mu\sigma}\dot{S}^{\sigma\nu}v_\nu, \quad \dot{v}^2 = \dot{v}_\rho\dot{v}^\rho.$$

The antisymmetric tensor formed from two other antisymmetric tensors $X_{\mu\nu}$ and $Y_{\mu\nu}$ will sometimes be written in the vector product notation

$$[X\,.\,Y]_{\lambda\mu} = X_{\lambda\sigma}Y^\sigma{}_\mu - X_{\mu\sigma}Y^\sigma{}_\lambda.$$

The vector v_μ by definition satisfies

$$v^2 = 1. \tag{3}$$

The equations derived from this by successive differentiation are†

$$(v\dot{v}) = 0, \tag{4a}$$

$$(v\ddot{v}) + \dot{v}^2 = 0, \tag{4b}$$

$$(vv^{\text{iii}}) + 3(\dot{v}\ddot{v}) = 0, \tag{4c}$$

$$(vv^{\text{iv}}) + 4(\dot{v}v^{\text{iii}}) + 3\ddot{v}^2 = 0. \tag{4d}$$

Further,

$$S^2 \equiv S_{\mu\nu}S^{\mu\nu} = \text{constant}, \tag{5}$$

---

† I write v^{iii} and v^{iv} for the third and fourth derivatives with respect to τ.

and the equations derived from this by successive differentiation are

$$(S\dot{S}) = 0, \tag{6a}$$

$$(S\ddot{S})+\dot{S}^2 = 0, \tag{6b}$$

$$(SS^{\text{iii}})+3(\dot{S}\ddot{S}) = 0. \tag{6c}$$

If the potentials of the meson field are denoted by U_ν and the field strengths by $G_{\mu\nu}$, the meson equations may be written in the form†

$$\left(\frac{\partial}{\partial x^\mu}U_\nu-\frac{\partial}{\partial x^\nu}U_\mu\right) = G_{\mu\nu}, \tag{7a}$$

$$\frac{\partial}{\partial x_\mu}G_{\mu\nu}+\chi^2U_\nu = 4\pi \mathrm{P}_\nu+4\pi\frac{\partial}{\partial x_\mu}\Sigma_{\mu\nu}. \tag{7b}$$

From (7*a*) it follows that

$$\frac{\partial}{\partial x^\lambda}G_{\mu\nu}+\frac{\partial}{\partial x^\mu}G_{\nu\lambda}+\frac{\partial}{\partial x^\nu}G_{\lambda\mu} = 0, \tag{8}$$

and from (7*b*)

$$\chi^2\frac{\partial}{\partial x_\nu}U_\nu = 4\pi\frac{\partial}{\partial x_\nu}\mathrm{P}_\nu = 0, \tag{9}$$

for a neutral meson field,‡ since then the divergence of the charge and current density P_μ vanishes. Inserting (7*a*) into (7*b*) and using (9) I get

$$\frac{\partial}{\partial x_\rho}\frac{\partial}{\partial x^\rho}U_\nu+\chi^2U_\nu = 4\pi\mathrm{P}_\nu+4\pi\frac{\partial}{\partial x_\mu}\Sigma_{\mu\nu}. \tag{10}$$

The usual energy-momentum tensor of the meson field $T_{\mu\nu}$ is given by

$$4\pi T_{\mu\nu} = G_{\mu\rho}G^\rho{}_\nu+\tfrac{1}{4}g_{\mu\nu}G_{\rho\sigma}G^{\rho\sigma}+\chi^2(U_\mu U_\nu-\tfrac{1}{2}g_{\mu\nu}U_\rho U^\rho). \tag{11}$$

The angular momentum density tensor $M_{\lambda\mu\nu}$ of the field is defined as in C by

$$M_{\lambda\mu\nu} = x_\lambda T_{\mu\nu}-x_\mu T_{\lambda\nu}. \tag{12}$$

Since I am interested in investigating the action of the meson field on the dipole, I shall henceforth put $g_1 = 0$ for simplicity. If $g_1 \neq 0$, I have only to add to the equations of motion the terms calculated in A for the case $g_1 \neq 0$, $g_2 = 0$, and further calculate the cross-terms in $g_1 g_2$ exactly on the lines of the preceding paper. These are much simpler than the reaction terms in g_2^2 which will be treated below.

---

† These differ from the form given in A in that the field strengths of this paper are equal to $-(G_{\mu\nu}-4\pi\Sigma_{\mu\nu})$ of A. This is only a matter of definition, and is more convenient for our purpose, although superficially it makes the equations less symmetrical.

‡ On the old theory of charged mesons and their interaction with the heavy particles, the charge current density leading to the creation of positive mesons was different from that leading to the creation of negative mesons, and neither satisfied a conservation equation, so that the right-hand side of (9) did not vanish. With the new assumption of allowing the heavy particles to exist in states of all integral charge this is altered, and the right-hand side of (9) vanishes again.

As shown in A, the solution of (10) when $P_\nu = 0$ can be written as an integral with the help of a Green's function G:

$$U_\nu(x_\rho) = \iiiint_{-\infty}^{\infty} dx'_\rho\, G(x_\rho, x'_\rho) \left\{ \frac{\partial}{\partial x'_\mu} \Sigma_{\mu\nu}(x'_\rho) \right\}, \tag{13}$$

where x'_ρ stands for the four variables x'_0, x'_1, x'_2 and x'_3. G is a function of $x_\rho - x'_\rho$ only. There are, as usual, two independent solutions corresponding to the retarded and advanced potentials. I shall only deal with the retarded potentials since the result does not depend on which are taken.

If I write, for the moment, $u_\rho \equiv x_\rho - x'_\rho$, $u \equiv (u_\rho u^\rho)^{\frac{1}{2}}$ and $u_r = \left(\sum_1^3 u_k^2\right)^{\frac{1}{2}}$, the Green's function G can be written in the form

$$G(x_\rho, x'_\rho) = \frac{\partial}{u\,\partial u} F(u), \tag{14}$$

with the function F defined, as shown in A (48*a*), for the retarded potentials by

$$F(u) = \begin{cases} J_0(\chi u) & u_0 > u_r, \\ 0 & u_0 < u_r. \end{cases} \tag{15}$$

Here J_0 is the Bessel function of order zero. The function F therefore has a plain discontinuity on the light cone $u = 0$. I shall frequently have to use the following properties of Bessel functions.

$$s^{-n} J_{n+1}(s) = -\frac{d}{ds}\{s^{-n} J_n(s)\}, \tag{16}$$

$$\operatorname*{Lt}_{s \to 0} \frac{1}{s^n} J_n(s) = \frac{1}{2^n\, n!}, \tag{17}$$

$$J_{n-1}(s) + J_{n+1}(s) = \frac{2n}{s} J_n(s). \tag{18}$$

For $\Sigma_{\mu\nu}$ given by (2), the differentiation with respect to x'_μ in (13) can be made to operate on G by partial integration, and, since G is a function of $x_\rho - x'_\rho$ only, it can be written as a differentiation with respect to x_μ, which can then be taken outside the integral. Introducing (2) into (13) I thus find

$$U_\nu^{\text{rot.}}(x_\rho) = g_2 \frac{\partial}{\partial x_\mu} \int_{-\infty}^{\infty} d\tau\, S_{\mu\nu}(\tau) \frac{\partial}{u\,\partial u} F(u), \tag{19}$$

where, in the notation that will be used henceforth,

$$u_\rho = x_\rho - z_\rho(\tau), \tag{20a}$$

$$u = (u_\rho u^\rho)^{\frac{1}{2}}, \tag{20b}$$

$$u_r = \left(\sum_1^3 u_k^2\right)^{\frac{1}{2}}. \tag{20c}$$

I introduce the following symbols as abbreviations:

$$\kappa = u_\mu v^\mu, \quad \kappa' = u_\mu \dot{v}^\mu, \quad \kappa'' = u_\mu \ddot{v}^\mu, \tag{21}$$

and

$$S_\mu = S_{\mu\nu} v^\nu, \quad S'_\mu = \dot{S}_{\mu\nu} v^\nu, \quad S''_\mu = \ddot{S}_{\mu\nu} v^\nu, \quad S'''_\mu = S^{\mathrm{iii}}_{\mu\nu} v^\nu, \quad S''''_\mu = S^{\mathrm{iv}}_{\mu\nu} v^\nu. \tag{22}$$

Now, for any function of u,

$$\frac{\partial}{\partial x_\mu} F(u) = \frac{\partial u}{\partial x_\mu} \frac{\partial F(u)}{\partial u} = \frac{u^\mu}{u} \frac{\partial F(u)}{\partial u}, \tag{23}$$

and, by (20a) for a fixed point x_ρ,

$$\frac{\partial u^2}{\partial \tau} = -2\kappa. \tag{24}$$

By (23), (19) reduces to

$$U_\nu^{\text{ret.}} = g_2 \int_{-\infty}^{\infty} d\tau \frac{u^\rho S_{\rho\nu}}{u} \frac{\partial}{\partial u}\left(\frac{1}{u}\frac{\partial F}{\partial u}\right),$$

or, by (24),

$$U_\nu^{\text{ret.}} = g_2 \int_{-\infty}^{\infty} d\tau \frac{u^\rho S_{\rho\nu}}{\kappa} \frac{\partial}{\partial \tau}\left(\frac{1}{\kappa}\frac{\partial F}{\partial \tau}\right).$$

After repeated integration by parts we get

$$U_\nu^{\text{ret.}} = g_2 \int_{-\infty}^{\infty} d\tau F(u) \frac{\partial}{\partial \tau}\left\{\frac{1}{\kappa}\frac{\partial}{\partial \tau}\left(\frac{u^\rho S_{\rho\nu}}{\kappa}\right)\right\}.$$

Hence, by (15),

$$U_\nu^{\text{ret.}} = g_2 \int_{-\infty}^{\tau_0} d\tau\, J_0(\chi u) \frac{d}{d\tau}\left\{\frac{1}{\kappa}\frac{d}{d\tau}\left(\frac{u^\rho S_{\rho\nu}}{\kappa}\right)\right\} \tag{25a}$$

$$= g_2 \int_0^{\infty} du\, J_0(\chi u) \frac{d}{du}\left\{\frac{d}{u\,du}\left(\frac{u^\rho S_{\rho\nu}}{\kappa}\right)\right\}. \tag{25b}$$

Here τ_0 is the retarded time, determined by

$$\{x_\rho - z_\rho(\tau_0)\}\{x^\rho - z^\rho(\tau_0)\} = 0. \tag{26a}$$

I shall write

$$s_\rho = x_\rho - z_\rho(\tau_0), \tag{26b}$$

so that (26a) may be written $s^2 = 0$.

Now, if $\chi = 0$, the equations (7) become the Maxwell equations, and we should expect (25) to become the expression for the Maxwell potential $\phi_\nu^{(2)}$ given in the preceding paper. This is obvious from (25), for when $\chi = 0$, $J_0(\chi u) = 1$ by (17), and (25*a*) does in fact become exactly the expression for $\phi_\nu^{(2)}$ given in (23) of C. Integrating (25*a*) by parts, I have

$$U_\nu^{\text{ret.}} = g_2\left[J_0(\chi u)\frac{1}{\kappa}\frac{d}{d\tau}\left(\frac{u^\rho S_{\rho\nu}}{\kappa}\right)\right]_{-\infty}^{\tau_0} - g_2\int_{-\infty}^{\tau_0} d\tau\,\frac{1}{\kappa}\frac{d}{d\tau}\left(\frac{u^\rho S_{\rho\nu}}{\kappa}\right)\frac{d}{d\tau}J_0(\chi u). \tag{27}$$

By (17) and (21), the first part just becomes $\phi_\nu^{(2)}$ given by†

$$\phi_\nu^{(2)} = g_2\left\{\frac{\mathcal{S}_\nu}{\kappa^2} + \frac{s^\rho S_{\rho\nu}}{\kappa^3},\quad -\frac{s^\rho S_{\rho\nu}}{\kappa^3}\kappa' + \frac{s^\rho \dot{S}_{\rho\nu}}{\kappa^2}\right\}, \tag{28}$$

which is just the Maxwell potential given by (23) of C. I make the convention that all quantities are to be taken at the retarded time τ_0 except when they enter in the integrand of an integral along the world line. Thus the first term of (28) is $\mathcal{S}_\nu(\tau_0)\{s_\mu v^\mu(\tau_0)\}^{-2}$. By (24) and (16), the second integral becomes

$$-g_2\chi\int_{-\infty}^{\tau_0}\frac{d}{d\tau}\left(\frac{u^\rho S_{\rho\nu}}{\kappa}\right)\frac{1}{u}J_1(\chi u),$$

which, on again integrating by parts, becomes

$$-g_2\chi\left[\frac{u^\rho S_{\rho\nu}}{\kappa}\frac{J_1(\chi u)}{u}\right]_{-\infty}^{\tau_0} + g_2\chi\int_{-\infty}^{\tau_0}\frac{u^\rho S_{\rho\nu}}{\kappa}\frac{d}{d\tau}\left(\frac{J_1(\chi u)}{u}\right).$$

Hence using (16) and (17) again we may write finally,‡

$$U_\nu^{\text{rot.}} = \phi_\nu^{(2)} + U_\nu^{(\chi)}, \tag{29}$$

where

$$U_\nu^{(\chi)} = -\tfrac{1}{2}g_2\chi^2\frac{s^\rho S_{\rho\nu}}{\kappa} + \breve{U}_\nu, \tag{30}$$

with

$$\breve{U}_\nu = g_2\chi^2\int_{-\infty}^{\tau_0} d\tau\,\frac{u^\rho S_{\rho\nu}}{u^2}J_2(\chi u). \tag{31}$$

The integral in (31) remains finite even when the point χ_ρ approaches the world line. The first term of (30) is finite but not one-valued on the world line, its value depending on the direction from which the point on the world line is approached. $U_\nu^{(\chi)} \to 0$ as $\chi \to 0$.

---

† Following Dirac, I separate terms which correspond (as $\kappa \to 0$) to singularities of different orders by a comma.

‡ For a consistent notation I should write the second part as $U_\nu^{(2,\chi)}$. I have, however, written it as $U_\nu^{(\chi)}$ for simplicity, since g_1 has been put equal to zero in this paper.

By using ($7a$) we can now find the retarded field $G^{\text{ret.}}_{\mu\nu}$. Corresponding to (29) we can write

$$G^{\text{ret.}}_{\mu\nu} = F^{(2)}_{\mu\nu} + G^{(\chi)}_{\mu\nu}, \tag{32}$$

where $F^{(2)}_{\mu\nu}$ is the expression for the retarded field in the Maxwell theory, and is defined by

$$F^{(2)}_{\mu\nu} = \frac{\partial}{\partial \chi^{\mu}}\phi^{(2)}_{\nu} - \frac{\partial}{\partial \chi^{\nu}}\phi^{(2)}_{\mu}. \tag{33}$$

It is given explicitly in C (114). $G^{(\chi)}_{\mu\nu}$ is derived from $U^{(\chi)}_{\nu}$. In differentiating (30) it must be remembered that a change in the point x_ρ also changes the retarded point τ_0. The method has been given in A. I find†

$$G^{(\chi)}_{\mu\nu} = -\tfrac{1}{2}g_2\chi^2\left[\frac{S_{\mu\nu}}{\kappa} + \frac{s_\mu \dot{S}_\nu}{\kappa^2} - \frac{v_\mu s^\rho S_{\rho\nu}}{\kappa^2} + \frac{s_\mu s^\rho S_{\rho\nu}}{\kappa^3}(1-\kappa') + \frac{s_\mu s^\rho \dot{S}_{\rho\nu}}{\kappa^2}\right]_- + \tfrac{1}{8}g_2\chi^4\left[\frac{s_\mu s^\rho S_{\rho\nu}}{\kappa}\right]_- + \bar{G}_{\mu\nu}, \tag{34}$$

with

$$\bar{G}_{\mu\nu} = 2g_2\chi^2\int_{-\infty}^{\tau_0} d\tau S_{\mu\nu}\frac{J_2(\chi u)}{u^2} - g_2\chi^3\int_{-\infty}^{\tau_0} d\tau \frac{u_\mu u^\rho S_{\rho\nu} - u_\nu u^\rho S_{\rho\mu}}{u^3} J_3(\chi u). \tag{35}$$

The part proportional to χ^2 in (34) has a singularity of order κ^{-1}, while the part proportional to χ^4 vanishes on the world line. The expressions (29) and (32) show quite clearly that the retarded meson potential and field is the same as the corresponding Maxwell potential and field plus a part containing χ which is singular to a lesser degree and vanishes when $\chi \to 0$. Both $\bar{U}_\nu$ given by (31) and $\bar{G}_{\mu\nu}$ given by (35) are finite and one-valued on the world line.

Now, as in the previous papers, I write the actual potentials U_ν and field strengths $G_{\mu\nu}$ at a point as the sum of the retarded and ingoing potentials and field strengths respectively at that point; thus

$$U_\nu = U^{\text{ret.}}_\nu + U^{\text{in.}}_\nu, \tag{36a}$$

$$G_{\mu\nu} = G^{\text{ret.}}_{\mu\nu} + G^{\text{in.}}_{\mu\nu}. \tag{36b}$$

The ingoing potentials and field strengths satisfy the equations (7) and (10) with P_ν and $\Sigma_{\mu\nu}$ put equal to zero. Using (29) and (32) we may write (36) as

$$U_\nu = \phi^{(2)}_\nu + U^{(\chi)}_\nu + U^{\text{in.}}_\nu, \tag{37a}$$

$$G_{\mu\nu} = F^{(2)}_{\mu\nu} + G^{(\chi)}_{\mu\nu} + G^{\text{in.}}_{\mu\nu}. \tag{37b}$$

---

† The minus sign at the end of a bracket means that the same terms with μ and ν interchanged are to be subtracted.

The ingoing field can always be written as a superposition of plane waves, a typical solution being

$$U_\nu = \gamma_\nu \cos(\omega_\nu x^\nu), \tag{38}$$

where, by (9) and (10),

$$\omega_\nu \gamma^\nu = 0, \tag{39a}$$

$$\omega^2 \equiv \omega_\nu \omega^\nu = \chi^2. \tag{39b}$$

The field strengths for this wave are

$$G_{\mu\nu} = -(\omega_\mu \gamma_\nu - \omega_\nu \gamma_\mu) \sin(\omega_\sigma x^\sigma). \tag{40}$$

A transversely polarized wave is defined as one in which the amplitude† γ_k of the vector potential is perpendicular to the direction of propagation ω_k. Then, by (39a), $\gamma_0 = 0$, and $U_0 = 0$. The field strengths $G_{\mu\nu}$ are perpendicular to the direction of propagation. A longitudinally polarized wave is defined as one in which the amplitude γ_k is parallel to the direction of propagation ω_k. Then, by (40), G_{kl} vanishes exactly, so that a longitudinally polarized wave has no magnetomesic force. The 'electromesic force' G_{0k} is now along the direction of propagation. Inserting (38) and (40) into (11), the energy-momentum tensor for this plane wave averaged over a period is

$$-\frac{1}{8\pi} \omega_\mu \omega_\nu \gamma^2. \tag{41}$$

The vector γ_μ is perpendicular to the time-like vector ω_μ, so that γ^2 is negative.

THE EQUATIONS OF MOTION

To find the equations of motion of the particle in a given meson field I use the method of the previous papers. Assume the world line of the particle to be given and the direction of the spin at every point of it. Now surround the world line between the points τ_1 and τ_2 by a thin world tube, and using the tensors (11) and (12) calculate the flow of energy, momentum and angular momentum into the tube. For the conservation laws to hold, the flow of each of these quantities into the tube should equal the increase in the amounts stored at the two ends of the tube. As before, I take the world tube to be defined by

$$\kappa \equiv s_\mu v^\mu = \epsilon, \tag{42}$$

where ultimately ϵ will be made to tend to zero.

---

† A Latin suffix only takes on the values 1, 2 and 3. A repeated Latin suffix therefore implies a summation from 1 to 3 only.

If we denote an element of the three-dimensional surface of the tube by dS^ν taken as positive when the normal is directed outwards, the flow of energy and momentum into the tube is

$$\int T_{\mu\nu} dS^\nu,$$

which, as shown in C, can always be written in the form

$$\int_{\tau_1}^{\tau_2} T_\mu d\tau.$$

For conservation of energy and momentum, this must only depend on the conditions at the two ends of the tube, so that the integrand must be a perfect differential. We must then have

$$T_\mu = \dot{A}_\mu, \tag{43}$$

and if A_μ is *known, this becomes the equation determining the translational* motion of the dipole.

Similarly, the flow of angular momentum into the tube is given by

$$\int M_{\lambda\mu\nu} dS^\nu.$$

Defining $M_{\lambda\mu}$ by $$\int_{\tau_1}^{\tau_2} M_{\lambda\mu} d\tau = \int (s_\lambda T_{\mu\nu} - s_\mu T_{\lambda\nu})\, dS^\nu, \tag{44}$$

we can show, as in C, that the conservation of angular momentum requires that $M_{\lambda\mu} - (v_\lambda A_\mu - v_\mu A_\lambda)$ shall be a perfect differential, so that I have to put

$$M_{\lambda\mu} - (v_\lambda A_\mu - v_\mu A_\lambda) = \dot{B}_{\lambda\mu}. \tag{45}$$

If $B_{\lambda\mu}$ is fixed, this becomes the equation determining the rotational motion of the dipole.

The calculation follows the work of C step by step. The only difference is that I get additional terms involving χ in T_μ and $M_{\lambda\mu}$ besides the terms already given in the previous paper. These arise from two causes. First, the retarded field strengths differ from the Maxwell field strengths $F^{(2)}_{\mu\nu}$ by having the extra terms $G^{(\chi)}_{\mu\nu}$. Secondly, the energy tensor (11) itself has additional terms proportional to χ^2 and involving the potentials U_ν explicitly. I can therefore write

$$T_\mu = T_\mu^{\text{max.}} + T_\mu^{\text{mes.}}, \tag{46}$$

where $T_\mu^{\text{max.}}$ is just the expression calculated in C for the Maxwell field, with the only difference that the ingoing meson field strengths $G^{\text{in.}}_{\mu\nu}$ appear in place of the ingoing Maxwell field strengths $F^{\text{in.}}_{\mu\nu}$. Then $T_\mu^{\text{mes.}}$ is the additional part that appears for a meson field due to the two causes mentioned above. It contains χ explicitly and vanishes as $\chi \rightarrow 0$. Corresponding to this, I write A_μ in (43) as the sum of two parts,

$$A_\mu = A_\mu^{\text{max.}} + A_\mu^{\text{mes.}}, \tag{47}$$

where $A_\mu^{\text{max.}}$ is the expression for A_μ found in C for a Maxwell field. Similarly, write

$$M_{\lambda\mu} = M_{\lambda\mu}^{\text{max.}} + M_{\lambda\mu}^{\text{mes.}}, \tag{48}$$

$$B_{\lambda\mu} = B_{\lambda\mu}^{\text{max.}} + B_{\lambda\mu}^{\text{mes.}}. \tag{49}$$

By substituting these into (43) and (45), and using the expressions for $T_\mu^{\text{max.}}$, $A_\mu^{\text{max.}}$, $M_{\lambda\mu}^{\text{max.}}$ and $B_{\lambda\mu}^{\text{max.}}$ found in C, the translational equation (43) becomes

$$\begin{aligned} M\dot{v}_\mu + \frac{d}{d\tau} v_\mu \{\tfrac{1}{4}K\dot{S}^2 + \tfrac{1}{4}K'(\dot{S}\dot{S}^*) - \tfrac{1}{2}g_2(SG^{\text{in.}})\} \\ = -\tfrac{1}{2}g_2 S^{\rho\sigma} \frac{\partial}{\partial x^\mu} G_{\rho\sigma}^{\text{in.}} + T_\mu^{\text{react.}} + (T_\mu^{\text{mes.}} - \dot{A}_\mu^{\text{mes.}}), \end{aligned} \tag{50}$$

and the rotational equation (45) becomes

$$\begin{aligned} I\dot{S}_{\lambda\mu} + I'\dot{S}^*_{\lambda\mu} + K[S \,.\, \ddot{S}]_{\lambda\mu} + K'[S \,.\, \ddot{S}^*]_{\lambda\mu} \\ = g_2[S \,.\, G^{\text{in.}}]_{\lambda\mu} + [S \,.\, C^{\text{react.}}]_{\lambda\mu} + \{M_{\lambda\mu}^{\text{mes.}} - (v_\lambda A_\mu^{\text{mes.}} - v_\mu A_\lambda^{\text{mes.}}) - \dot{B}_{\lambda\mu}^{\text{mes.}}\}. \end{aligned} \tag{51}$$

These are just equations (72) and (73) of C which give the motion of a spinning particle in a Maxwell field, with additional terms. M, I, I', K and K' are arbitrary constants, and have the dimensions of mass, angular momentum and moment of inertia respectively. $S^*_{\lambda\mu}$ is the six-vector adjunct† (dual) to $S_{\lambda\mu}$. Finally, $T_\mu^{\text{react.}}$ and $C_{\lambda\mu}^{\text{react.}}$ are the terms proportional to g_2^2 giving the reaction of radiation for a Maxwell field. Now, by the arguments given in C, we must have

$$[M_{\lambda\mu}^{\text{mes.}} - (v_\lambda A_\mu^{\text{mes.}} - v_\mu A_\lambda^{\text{mes.}}) - \dot{B}_{\lambda\mu}^{\text{mes.}}] \equiv S_\lambda{}^\rho C_{\rho\mu}^{\text{mes.}} - S_\mu{}^\rho C_{\rho\lambda}^{\text{mes.}}, \tag{52}$$

that is, $A_\mu^{\text{mes.}}$ and $B_{\lambda\mu}^{\text{mes.}}$ must be so chosen that the left-hand side of (52) has the form of the right-hand side of this equation. Further, in order that the invariant equation got by contracting (50) with v^μ should be consistent with an invariant equation which can be derived from (51) as shown in C, one must demand that

$$(\dot{S} \,.\, C^{\text{mes.}}) = 2v^\mu(T_\mu^{\text{mes.}} - \dot{A}_\mu^{\text{mes.}}). \tag{53}$$

---

† Its components are connected with those of $S_{\mu\nu}$ as in C(26) by $S^{*01} = S_{23}$, $S^*_{01} = -S^{23}$, etc., the other relations being derived by a cyclical permutation of any three suffixes.

Now consider the contribution to $T_\mu^{\text{mes.}}$ that comes from the fact that the retarded field strengths in (37*b*) contain the extra term $G_{\mu\nu}^{(\chi)}$. The highest singularities in the three terms on the right-hand side of (37*b*) are respectively of order ϵ^{-3}, ϵ^{-1}, and 1, while the surface element dS^ν is of order ϵ^2. Hence the addition to $T_\mu^{\text{mes.}}$ due to the extra term $G_{\mu\nu}^{(\chi)}$ in (37*b*) will come from product terms in $T_{\mu\nu}$ involving $F_{\mu\nu}^{(2)}$ and $G_{\mu\nu}^{(\chi)}$, and from terms quadratic in $G_{\mu\nu}^{(\chi)}$. There will be no extra terms containing $G_{\mu\nu}^{\text{in.}}$. Now $G_{\mu\nu}^{(\chi)}$ contains the term $\tilde{G}_{\mu\nu}$ given by (35), which, as has been mentioned before, has no singularities even on the world line. This term will therefore appear in the equations of motion in terms of the same form as those involving the ingoing field $G_{\mu\nu}^{\text{in.}}$. Moreover, since the highest singularity in $F_{\mu\nu}^{(2)}$ is of order ϵ^{-3}, the derivative of $\tilde{G}_{\mu\nu}$ will also appear in the translational equations, just like the derivative of $G_{\mu\nu}^{\text{in.}}$. The derivative appears as before because the value of $\tilde{G}_{\mu\nu}$ at a point x_ρ on the world tube has to be expressed in terms of its value at the retarded point $z_\rho(\tau_0)$ on the world line by a Taylor's series; thus

$$(\tilde{G}_{\mu\nu})_{x_\rho} = (\tilde{G}_{\mu\nu})_{z_\rho(\tau_0)} + s^\rho\left(\frac{\partial}{\partial x^\rho}\tilde{G}_{\mu\nu}\right)_{z_\rho(\tau_0)}. \tag{54}$$

Now, using (35), I find

$$\begin{aligned}\frac{\partial}{\partial x^\rho}\tilde{G}_{\mu\nu} = {} & \tfrac{1}{4}g_2\chi^4 S_{\mu\nu}\frac{s_\rho}{\kappa} - 2g_2\chi^3\int_{-\infty}^{\tau_0} S_{\mu\nu}u_\rho\frac{J_3(\chi u)}{u^3} \\ & -\tfrac{1}{48}g_2\chi^6(s_\mu s^\lambda S_{\lambda\nu} - s_\nu s^\lambda S_{\lambda\mu})\frac{s_\rho}{\kappa} - g_2\chi^3\int_{-\infty}^{\tau_0} d\tau[g_{\mu\rho}u^\lambda S_{\lambda\nu} + u_\mu S_{\rho\nu}]_-\frac{J_3(\chi u)}{u^3} \\ & +g_2\chi^4\int_{-\infty}^{\tau_0} d\tau(u_\mu u^\lambda S_{\lambda\nu} - u_\nu u^\lambda S_{\lambda\mu})\,u_\rho\frac{J_4(\chi u)}{u^4} \\ = {} & \tfrac{1}{4}g_2\chi^4 S_{\mu\nu}\frac{s_\rho}{\kappa} - \tfrac{1}{48}g_2\chi^6(s_\mu s^\lambda S_{\lambda\nu} - s_\nu s^\lambda S_{\lambda\mu})\frac{s_\rho}{\kappa} + \tilde{G}_{\mu\nu,\rho},\end{aligned} \tag{55}$$

where
$$\begin{aligned}\tilde{G}_{\mu\nu,\rho} = {} & -g_2\chi^3\int_{-\infty}^{\tau_0} d\tau[u_\rho S_{\mu\nu} + g_{\mu\rho}u^\lambda S_{\lambda\nu} + u_\mu S_{\rho\nu}]_-\frac{J_3(\chi u)}{u^3} \\ & +g_2\chi^4\int_{-\infty}^{\tau_0} d\tau[u_\mu u^\lambda S_{\lambda\nu}]_-\frac{J_4(\chi u)}{u^4}.\end{aligned} \tag{56}$$

The minus sign means that terms with μ and ν interchanged have to be subtracted. The first two terms on the right-hand side of (55) come from the fact that a change in the point x_ρ changes the retarded point τ_0 according to (26*a*). The second term is of order ϵ^3 and hence contributes nothing to T_μ and $M_{\lambda\mu}$, as will be seen in the appendix. It vanishes on the world line. The expression (55) is, moreover, contracted with s^ρ in (54), so that the first term on the right-hand side of (55) also vanishes by (26). Hence $\tilde{G}_{\mu\nu,\rho}$ will play the part of $\frac{\partial}{\partial x^\rho}\tilde{G}_{\mu\nu}$ in the equations of motion. Contracting (55) with v^ρ and remembering (21), I get at a point on the world line

$$\frac{d}{d\tau}\tilde{G}_{\mu\nu} \equiv v^\rho \frac{\partial}{\partial x^\rho}\tilde{G}_{\mu\nu} = \tfrac{1}{4}g_2\chi^4 S_{\mu\nu} + \tilde{G}_{\mu\nu,\rho}v^\rho. \tag{57}$$

$T_\mu^{\text{mes.}}$ and $M_{\lambda\mu}^{\text{mes.}}$ are given by (97) and (99) in the appendix, and $A_\mu^{\text{mes.}}$ and $B_{\lambda\mu}^{\text{mes.}}$ are chosen to satisfy (52) and (53). If we introduce the expressions for $T_\mu^{\text{mes.}} - \dot{A}_\mu^{\text{mes.}}$ given in (102) of the appendix, the translational equation (50) becomes

$$\begin{aligned} M\dot{v}_\mu + \frac{d}{d\tau}v_\mu\{\tfrac{1}{4}K\dot{S}^2 + \tfrac{1}{4}K'(\dot{S}\dot{S}^*) - \tfrac{1}{2}g_2(S[G^{\text{in.}} + \tilde{G}])\} \\ = -\tfrac{1}{2}g_2 S^{\rho\sigma}\left(\frac{\partial}{\partial x^\mu}G_{\rho\sigma}^{\text{in.}} + \tilde{G}_{\rho\sigma,\mu}\right) + g_2^2\chi^4(-\tfrac{1}{8}v_\mu S^2 + \tfrac{1}{4}S_{\mu\rho}\ddot{S}^\rho + \tfrac{1}{4}v_\mu\ddot{S}^2) \\ + T_\mu^{\text{react.}} + (T_\mu'^{\text{mes.}} - \dot{A}_\mu'^{\text{mes.}}), \end{aligned} \tag{58}$$

where $T_\mu'^{\text{mes.}} - \dot{A}_\mu'^{\text{mes.}}$ is an expression proportional to $g_2^2\,\chi^2$ and is given by (109) in the appendix. The terms in χ^4 are important. On contracting (58) with v^μ, the last two terms proportional to χ^4 cancel each other, while the first combines according to (57) with $\tilde{G}_{\rho\sigma,\mu}$ to give

$$\tfrac{1}{2}g_2\{S^{\rho\sigma}\tilde{G}_{\rho\sigma,\mu} + \tfrac{1}{4}g_2\chi^4 v_\mu S^2\}\,v^\mu = \tfrac{1}{2}g_2\,S^{\rho\sigma}\frac{d}{d\tau}\tilde{G}_{\rho\sigma},$$

which is analogous to

$$\tfrac{1}{2}g_2\left(S^{\rho\sigma}\frac{\partial}{\partial x^\mu}G_{\rho\sigma}^{\text{in.}}\right)v^\mu = \tfrac{1}{2}g_2\,S^{\rho\sigma}\frac{d}{d\tau}G_{\rho\sigma}^{\text{in.}}.$$

By using (104) of the appendix, the rotational equation (51) becomes

$$\begin{aligned} I\dot{S}_{\lambda\mu} + I'\dot{S}_{\lambda\mu}^* + K[S\,.\,\ddot{S}]_{\lambda\mu} + K'[S\,.\,\ddot{S}^*]_{\lambda\mu} \\ = g_2[S\,.\,(G^{\text{in.}} + \tilde{G})]_{\lambda\mu} + [S\,.\,C^{\text{react.}}]_{\lambda\mu} + [S\,.\,C'^{\text{mes.}}]_{\lambda\mu}, \end{aligned} \tag{59}$$

where $C_{\rho\mu}'^{\text{mes.}}$ is given in the appendix by (110) and is proportional to $g_2^2\,\chi^2$. The reaction terms $T_\mu'^{\text{mes.}} - \dot{A}_\mu'^{\text{mes.}}$ and $C_{\rho\mu}'^{\text{mes.}}$ contain one arbitrary dimensionless constant k. This completely determines the exact equations of motion of a spinning particle in a meson field. As $\chi \to 0$, the equations go over continuously into those derived in C for the motion of a spinning particle in a Maxwell field.

Specialized equations can be derived from (58) and (59) which are consistent with the condition that the mesic dipole moment shall always be a pure 'magnetic' moment in the system in which the particle is at rest. This condition is expressed by

$$S_{\mu\nu}v^{\nu} = 0. \tag{60}$$

To derive equations consistent with (60) I follow the procedure given in C. Take all the terms in (59) on to the left-hand side and contract this expression with v^{μ}. I then have to add the resulting expression to A_{μ} in (43). Any addition to A_{μ} naturally also alters the rotational equation (51) or (59), since A_{μ} occurs on the left-hand side of (45). The alteration in the terms not involving χ has already been given in the previous paper. I have only to consider the alteration in the additional terms involving χ. By (60), the effect of the above operation is to replace $T_{\mu}^{\text{mes.}} - \dot{A}_{\mu}^{\text{mes.}}$ in (50) by

$$T_{\mu}^{\text{mes.}} - \dot{A}_{\mu}^{\text{mes.}} + \frac{d}{d\tau}(S_{\mu}{}^{\rho}C_{\rho\nu}^{\text{mes.}}v^{\nu}). \tag{61}$$

The corresponding change in terms involving χ on the right-hand side of (59) is to replace $[S_{\lambda}{}^{\rho}\dot{C}_{\rho\mu}^{\text{mes.}}]_{-}$ by $[S_{\lambda}{}^{\rho}(\dot{C}_{\rho\mu}^{\text{mes.}} - \dot{C}_{\rho\nu}^{\text{mes.}}v^{\nu}v_{\mu})]_{-}$. Using (102) and (104) of the appendix, and the results of C for the modification of the other terms not involving χ, I find that the translational equation becomes

$$\begin{aligned} M\dot{v}_{\mu} + \frac{d}{d\tau}\{IS'_{\mu} + \tfrac{1}{4}Kv_{\mu}\dot{S}^{2} + KS_{\mu\rho}S''^{\rho} - \tfrac{1}{2}g_{2}v_{\mu}(S[G^{\text{in.}} + \tilde{G}]) - g_{2}S_{\mu}{}^{\rho}(G_{\rho\nu}^{\text{in.}} + \tilde{G}_{\rho\nu})v^{\nu}\} \\ = -\tfrac{1}{2}g_{2}S^{\rho\sigma}\left(\frac{\partial}{\partial x^{\mu}}G_{\rho\sigma}^{\text{in.}} + \tilde{G}_{\rho\sigma,\mu}\right) - \tfrac{1}{8}g_{2}^{2}\chi^{4}v_{\mu}S^{2} + T_{\mu}^{\text{self}} + T_{\mu}^{\text{self},\chi}. \end{aligned} \tag{62}$$

Here, as in C, I have put $K' = 0$ for simplicity. I' must necessarily be put equal to zero. T_{μ}^{self} is the reaction term in g_{2}^{2} given explicitly in an earlier paper (Bhabha 1940*a*, referred to here as B). $T_{\mu}^{\text{self},\chi}$ is the reaction term in g_{2}^{2} which involves χ, and is given by (111) in the appendix.

Similarly, the rotational equation (59) is now to be modified to

$$\begin{aligned} I\{\dot{S}_{\lambda\mu} + v_{\lambda}S'_{\mu} - v_{\mu}S'_{\lambda}\} + K[S_{\lambda}{}^{\rho}(\ddot{S}_{\rho\mu} - S''_{\rho}v_{\mu})]_{-} \\ = g_{2}[S_{\lambda}{}^{\rho}\{(G_{\rho\mu}^{\text{in.}} + \tilde{G}_{\rho\mu}) - (G_{\rho\nu}^{\text{in.}} + \tilde{G}_{\rho\nu})v^{\nu}v_{\mu}\}]_{-} \\ + [S_{\lambda\rho}D^{\rho}{}_{\mu}]_{-} + g_{2}^{2}\chi^{2}[S_{\lambda}{}^{\rho}(\dot{S}_{\rho\mu} - S'_{\rho}v_{\mu})]_{-}. \end{aligned} \tag{63}$$

$D_{\rho\mu}$ is the reaction term proportional to g_{2}^{2} given explicitly in B (46) and C (142). It is such that $D_{\rho\mu}v^{\mu} = 0$. We see that $\tilde{G}_{\rho\mu}$ appears in the equations (58) and (59) in the same way as the ingoing field $G_{\mu\nu}^{\text{in.}}$. It embodies the effect of the previous motion of the dipole on the motion of the particle at the instant under consideration and may be interpreted as the resultant of the fields which the particle has itself radiated in moving along the preceding part of the world line. It should be noticed that the arbitrary constant k

in $C'^{\text{mes.}}_{\rho\mu}$ has dropped out of the specialized equations (62) and (63) for the case $\ddot{S}_\mu = 0$.

Contracting (62) with v^μ and using (53) I get the invariant equation

$$K(\dot{S}\ddot{S}) - 2K(S'S'') - g_2(\dot{S}\,.\{G^{\text{in.}} + \tilde{G}\})$$
$$+ 2g_2 S'^\rho (G^{\text{in.}}_{\rho\nu} + \tilde{G}_{\rho\nu})\, v^\nu - (\dot{S}D) - g_2^2\chi^2(\dot{S}^2 - S'^2) = 0. \tag{64}$$

On contracting (63) with v^μ it vanishes identically. Thus (63) vanishes identically in the rest system when either λ or μ takes on the value zero. It therefore only consists of three equations determining $\dot{S}_{lm}$, $\dot{S}_{mk}$ and $\dot{S}_{kl}$, while $\dot{S}_{0k}$, $\dot{S}_{0l}$ and $\dot{S}_{0m}$ are determined explicitly by the equation derived by differentiating (60). Corresponding to this, (64) in the rest system takes the form

$$K(\dot{S}_{kl}\ddot{S}^{kl}) - g_2\dot{S}^{kl}(G^{\text{in.}}_{kl} + \tilde{G}_{kl}) - \dot{S}^{kl}D_{kl} - g_2^2\chi^2\dot{S}^{kl}\dot{S}_{kl} = 0. \tag{65}$$

THE SCATTERING OF MESONS BY A DIPOLE

In considering the scattering of meson radiation by a dipole, we may simplify the problem by putting the mass of the dipole $M = \infty$. All derivatives of the velocity will then vanish, and (63) can be considered in the rest system. Put the dipole at the origin of coordinates. Henceforth write t, x, y, z in place of x_0, x_1, x_2 and x_3. If we introduce a space vector $\mathbf{M}$ defined by

$$M_k = S_{lm}, \quad M_l = S_{mk}, \quad M_m = S_{kl},$$

and denoting the magnetomesic force $G^{\text{in.}}_{lm}$, $G^{\text{in.}}_{mk}$, $G^{\text{in.}}_{kl}$ of the ingoing field by $\mathbf{H}$ the equation (63) takes the form†

$$I\mathbf{M} + K[\mathbf{M}\,.\,\dot{\mathbf{M}}] = g_2[\mathbf{M}\,.\,\mathbf{H}] + \tfrac{2}{3}g_2^2[\mathbf{M}\,.\,\mathbf{M}'''] + g_2[\mathbf{M}\,.\,\tilde{\mathbf{G}}] + g_2^2\chi^2[\mathbf{M}\,.\,\dot{\mathbf{M}}], \tag{66}$$

where $\tilde{\mathbf{G}}$ stands for the vector $\tilde{G}_{lm}$, $\tilde{G}_{mk}$, $\tilde{G}_{kl}$. Its components are defined by (35). The quantities u_ρ in (35) written out explicitly are

$$u_k = z_k(\tau) - z_k(\tau') = 0, \quad u_0 = z_0(\tau) - z_0(\tau') = t - t', \quad u = u_0 = t - t', \tag{67}$$

t being the time at the proper time τ. Hence, on account of (60) and (67), the second integral in (35) vanishes, and I get

$$\tilde{\mathbf{G}}(t) = 2g_2\chi^2\int_{-\infty}^{t} dt'\,\mathbf{M}(t')\,\frac{J_2(\chi u)}{u^2}$$
$$= 2g_2\chi^2\int_0^\infty du\,\mathbf{M}(t-u)\,\frac{J_2(\chi u)}{u^2}. \tag{68}$$

---

† Henceforth the square brackets have their usual meaning in three-dimensional vector theory.

Let us suppose that a periodic force $\mathbf{H}$ with a frequency ω_0 acts on the dipole:

$$\mathbf{H} = \mathbf{H}_0 \cos \omega_0 t. \tag{69}$$

Solve (66) for small oscillations of the dipole. I write

$$\mathbf{M}(t) = \mathbf{M}_0 + \mathbf{M}_1 \sin \omega_0 t + \mathbf{M}_2 \sin(\omega_0 t + \delta). \tag{70}$$

$\mathbf{M}_0$ is the initial direction of the dipole, and I assume that $\mathbf{M}_0^2 = 1$. The vectors $\mathbf{M}_0$, $\mathbf{M}_1$ and $\mathbf{M}_2$ are perpendicular to each other and such that $[\mathbf{M}_0 . \mathbf{M}_1]$ is in the direction $\mathbf{M}_2$. I neglect quantities quadratic in $\mathbf{M}_1$, $\mathbf{M}_2$, and $\mathbf{H}_0$.

Introducing (70) into (68), I get

$$\bar{\mathbf{G}} = 2g_2 \chi^2 \mathbf{M}_0 \int_0^\infty du \frac{J_2(\chi u)}{u^2}$$
$$+ 2g_2 \chi^2 \int_0^\infty du \, [\mathbf{M}_1 \sin \omega_0 (t-u) + \mathbf{M}_2 \sin \{\omega_0 (t-u) + \delta\}] \frac{J_2(\chi u)}{u^2}.$$

The integrals which occur in this expression can be easily evaluated and are

$$\int_0^\infty du \frac{J_2(u)}{u^2} = \tfrac{1}{3},$$

$$\int_0^\infty du \frac{J_2(u)}{u^2} e^{-i\nu u} = \begin{cases} \tfrac{1}{3}[(1-\nu^2)^{3/2} + i\nu^3 - \tfrac{3}{2} i\nu] & 0 < \nu < 1, \\ \tfrac{1}{3}[-i(\nu^2-1)^{3/2} + i\nu^3 - \tfrac{3}{2} i\nu] & \nu > 1. \end{cases}$$

With the help of these I get at once

$$\bar{\mathbf{G}} = \tfrac{2}{3} g_2 \chi^3 \mathbf{M}_0 + \tfrac{2}{3} g_2 \chi^3 \mathbf{M}_1 \{P \sin \omega_0 t + Q \cos \omega_0 t\}$$
$$+ \tfrac{2}{3} g_2 \chi^3 \mathbf{M}_2 \{P \sin(\omega_0 t + \delta) + Q \cos(\omega_0 t + \delta)\}, \tag{71}$$

where

$$\left.\begin{aligned} P &= \begin{cases} \left(1 - \dfrac{\omega_0^2}{\chi^2}\right)^{3/2} & \omega_0 < \chi, \\ 0 & \omega_0 > \chi, \end{cases} \\ Q &= \begin{cases} \dfrac{\omega_0^3}{\chi^3} - \dfrac{3}{2}\dfrac{\omega_0}{\chi} & \omega_0 < \chi, \\ \dfrac{\omega_0^3}{\chi^3} - \dfrac{3}{2}\dfrac{\omega_0}{\chi} - \left(\dfrac{\omega_0^2}{\chi^2} - 1\right)^{3/2} & \omega_0 > \chi. \end{cases} \end{aligned}\right| \tag{72}$$

Now write as abbreviations

$$\alpha = \frac{3}{2}\frac{I}{g_2^2}, \quad \beta = \frac{3}{2}\frac{K}{g_2^2}. \tag{73}$$

Introducing (70) and (71) into (66), using (72) and remembering the relation between the three directions $\mathbf{M}_0$, $\mathbf{M}_1$ and $\mathbf{M}_2$, I find, neglecting terms quadratic in $\mathbf{M}_1$, $\mathbf{M}_2$ and $\mathbf{H}_0$, that (66) becomes

$$\omega_0 \mathbf{M}_1\left[\alpha\cos\omega_0 t+\left|\frac{M_2}{M_1}\right|\{\xi\sin(\omega_0 t+\delta)-\zeta\cos(\omega_0 t+\delta)\}\right]$$
$$+\omega_0 \mathbf{M}_2\left[\alpha\cos(\omega_0 t+\delta)-\left|\frac{M_1}{M_2}\right|\{\xi\sin\omega_0 t-\zeta\cos\omega_0 t\}\right]=\frac{3}{2g_2}[\mathbf{M}_0.\mathbf{H}_0]\cos\omega_0 t, \tag{74}$$

where
$$\xi\equiv\beta\omega_0-\frac{\chi^3}{\omega_0}(1-P)=\begin{cases}\beta\omega_0-\dfrac{\chi^3}{\omega_0}+\dfrac{(\chi^2-\omega_0^2)^{\frac{3}{2}}}{\omega_0} & \omega_0<\chi,\\[2ex] \beta\omega_0-\dfrac{\chi^3}{\omega_0} & \omega_0>\chi,\end{cases} \tag{75a}$$

$$\zeta\equiv-\frac{\chi^3}{\omega_0}\left\{Q-\frac{\omega_0^3}{\chi^3}+\frac{3}{2}\frac{\omega_0}{\chi}\right\}=\begin{cases}0 & \omega_0<\chi,\\[1ex] \dfrac{(\omega_0^2-\chi^2)^{\frac{3}{2}}}{\omega_0} & \omega_0>\chi.\end{cases} \tag{75b}$$

Now, each square bracket on the left-hand side of (74) can always be written as the sum of a term proportional to $\cos\omega_0 t$ and a term proportional to $\sin\omega_0 t$, and, since $\mathbf{M}_1$ and $\mathbf{M}_2$ are perpendicular, the coefficients of the terms proportional to $\sin\omega_0 t$ in each bracket must vanish. The coefficient of the term proportional to $\sin\omega_0 t$ in the first bracket vanishes if

$$\xi\cos\delta+\zeta\sin\delta=0,$$

that is, if
$$\tan\delta=-\frac{\xi}{\zeta}, \tag{76}$$

while the coefficient of the term proportional to $\sin\omega_0 t$ in the second bracket vanishes if

$$\alpha\sin\delta+\left|\frac{M_1}{M_2}\right|\xi=0.$$

Hence, with the help of (76),

$$\left|\frac{M_1}{M_2}\right|=-\frac{\alpha\sin\delta}{\xi}=\frac{\alpha}{\sqrt{(\xi^2+\zeta^2)}}. \tag{77}$$

By using (76) and (77) and dividing through by $\cos\omega_0 t$, equation (74) becomes

$$\mathbf{M}_1\left(\frac{\alpha^2-\xi^2-\zeta^2}{\alpha}\right)+\mathbf{M}_2\left|\frac{M_1}{M_2}\right|(2\zeta)=\frac{3}{2g_2\omega_0}[\mathbf{M}_0.\mathbf{H}_0].$$

Let θ be the angle between $\mathbf{M}_0$ and $\mathbf{H}_0$, and η the angle between $\mathbf{M}_1$ and $[\mathbf{M}_0 . \mathbf{H}_0]$, $\mathbf{M}_1$ lying in such a direction that the angle between the $\mathbf{M}_1 \mathbf{M}_0$ plane and the $\mathbf{M}_0 \mathbf{H}_0$ plane is $\frac{1}{2}\pi - \eta$. Then it follows from the above equation that

$$\tan \eta = \frac{2\alpha\zeta}{\alpha^2 - \xi^2 - \zeta^2}, \tag{78}$$

and

$$| M_1 | = \frac{3\alpha H_0 \sin\theta}{2g_2 \omega_0 \{(\alpha^2 - \xi^2 - \zeta^2)^2 + 4\alpha^2\zeta^2\}^{\frac{1}{2}}}. \tag{79}$$

The work done by the external force on the dipole is on the average

$$\begin{aligned} -g_2 \overline{(\mathbf{H}\dot{\mathbf{M}})} &= -\tfrac{1}{2} g_2 \omega_0 \{(\mathbf{H}_0 . \mathbf{M}_1) + (\mathbf{H}_0 \mathbf{M}_2) \cos\delta\} \\ &= -\tfrac{1}{2} g_2 \omega_0 H_0 \{| M_1 | \sin\theta \sin\eta - | M_2 | \sin\theta \cos\eta \cos\delta\}. \end{aligned}$$

By (76), (77), (78) and (79), this becomes

$$\tfrac{3}{4} H_0^2 \sin^2\theta \frac{\zeta(\alpha^2 + \xi^2 + \zeta^2)}{(\alpha^2 - \xi^2 - \zeta^2)^2 + 4\alpha^2\zeta^2}. \tag{80}$$

When $\omega_0 < \chi$, this expression vanishes since, by (75*b*), ζ is then zero. This is what one would expect, for no meson waves exist for $\omega_0 < \chi$, and hence no radiation by the dipole is possible. The amplitude of the oscillation $\mathbf{M}_1$ as given by (79) is now proportional to $(\alpha^2 - \xi^2)^{-1}$. For very low frequencies $\omega_0 \ll \chi$,

$$\xi \approx \beta\omega_0 - \tfrac{3}{2}\chi\omega_0 = \frac{3\omega_0}{2g_2^2}(K - g_2^2 \chi). \tag{81}$$

This shows quite clearly that as far as slow oscillations are concerned the constant K, which, as was shown in C, is to be interpreted as the moment of inertia of the particle perpendicular to the axis of the spin, is diminished by a quantity $g_2^2 \chi$. We must interpret $-g_2^2 \chi$ as an added moment of inertia due to the meson field. For the Maxwell field where $\chi = 0$, there is no such added moment of inertia due to the field. Now the energy density as given by (11) is a positive definite form, so that if the expression (11) were used for calculating the addition to the moment of inertia due to the field, the addition would always be positive. For a point dipole it would be infinite. The arguments of the preceding paper show that this infinity is spurious and (11) is not the correct expression for the energy density when point charges or point dipoles are present. (11) has to be modified in the presence of point dipoles as Pryce (1938) has modified the energy tensor for a point charge. The result that the addition to the moment of inertia given above is negative then shows that the modified energy tensor will no longer be a positive definite expression.

Exactly as in the case of a point charge investigated in A, the mass of the particle is changed due to the mass of the meson field. We could calculate it by working out the amplitude of the translatory motion of a dipole of finite mass M due to an external force of low frequency in a way exactly analogous to the one used above for calculating the change in the moment of inertia. Its order of magnitude can be estimated by dimensional considerations. The mass of the field must be proportional to g_2^2, and the only other constant which the expression for it can contain is χ. The only combination of these two constants which has the dimensions of a mass is $g_2^2\chi^3$. With the actual values of the constants for neutrons and mesons as they occur in nature, $g_2^2\chi^3 = \mu(g_2^2\chi^2/\hbar) \sim M/150$, M being the neutron mass, so that this is extremely small compared with the neutron mass, and of the same order as the alteration in the mass calculated in A due to the meson field of a point charge g_1. It is seen that the dipole field makes a very small negative contribution to the mass of a neutron. This result is contrary to a non-relativistic classical theory by Heisenberg (1939) in which the field was made to account for the whole mass of the neutron.

I now return to the more interesting case $\omega_0 > \chi$. To get the scattering cross-section we have to suppose that the force H is the magnetomesic force of a plane wave of the type (38). Now, as mentioned before, the magnetic force of a longitudinal wave is zero, so that a dipole free to rotate only will not scatter longitudinal meson waves at all. Any scattering of these waves must be due to the translation of the dipole, and the scattering will be of the same order as the scattering due to a point charge calculated in A. For transverse waves the rate of energy transfer per unit area of a wave with a magnetic force **H** is, by (41), $H_0^2\omega_0(\omega_0^2-\chi^2)^{-\frac{1}{2}}/8\pi$. Dividing (80) by this, it is found that the total effective cross-section for the scattering of a transverse meson wave is

$$6\pi\sin^2\theta\,\frac{(\omega_0^2-\chi^2)^2}{\omega_0^2}\,\frac{\alpha^2+\xi^2+\zeta^2}{(\alpha^2-\xi^2-\zeta^2)^2+4\alpha^2\zeta^2}. \tag{82}$$

If χ is put equal to zero, this at once reduces to the cross-section for the scattering of light by a dipole given in C. ζ may be regarded as expressing the effects of radiation reaction for a meson field, for it reduces when $\chi \rightarrow 0$ to ω_0^2, the reaction term for a Maxwell field. ξ may then be taken to express the effects of the sum of the mechanical moment of inertia K of the particle perpendicular to the axis of the spin plus that due to the field. When $\omega_0 \gg \chi$,

$$\xi = \beta\omega_0 - \frac{\chi^3}{\omega_0} = \frac{3}{2}\frac{\omega_0}{g_2^2}\left(K - \tfrac{2}{3}g_2^2\frac{\chi^3}{\omega_0^2}\right).$$

This clearly shows that the moment of inertia of the field is $-\frac{2}{3}g_2^2\chi^3/\omega_0^2$, and tends to zero as ω_0 increases. This is what one would expect, since, as the frequency increases, less and less of the static field swings with the dipole. In the absence of the radiation reaction term ζ, the cross-section (82) would become infinite when $\xi = \alpha$, i.e. at frequencies ω_0 given by

$$\omega_0 = \frac{\alpha}{\beta - \chi^3/\omega_0^2} = \frac{I}{K - \frac{2}{3}g_2^2\chi^3/\omega_0^2}. \tag{83}$$

This is a resonance phenomenon. The expression on the right of (83) is the normal gyration frequency of the spin in a meson field for small amplitudes. The effect of the radiation reaction term ζ is to make the scattering finite even for this frequency, but the cross-section still has a more or less strong maximum at this point, as shown by the curves in the figure, which are drawn for different values of β and hence of K. For $I < (K - \frac{2}{3}g_2^2\chi)\chi$, the gyration frequency is less than χ and hence no resonance occurs in the scattering of meson waves. (This is shown below by the curve marked $\beta = 15$ in the figure.)

To get the angular distribution of the scattered radiation one must calculate the potentials at a large distance $\mathbf{r}$ due to the vibration of the dipole given by (70). It is shown in the appendix that, if quantities of the order $1/r^2$ are neglected, the potentials at a large distance r are given by

$$U_0^{\text{ret.}} = 0,$$

$$U_k^{\text{ret.}} = \begin{cases} g_2\sqrt{(\chi^2-\omega_0^2)}\, e^{-r\sqrt{(\chi^2-\omega_0^2)}}\{[\mathbf{r}\,.\,\mathbf{M}_1]\sin\omega_0 t + [\mathbf{r}\,.\,\mathbf{M}_2]\sin(\omega_0 t+\delta)\}/r^2 & \omega_0 < \chi, \\ g_2\sqrt{(\omega_0^2-\chi^2)}\{[\mathbf{r}\,.\,\mathbf{M}_1]\cos(\omega_0 t - r\sqrt{(\omega_0^2-\chi^2)}) + [\mathbf{r}\,.\,\mathbf{M}_2]\cos(\omega_0 t - r\sqrt{(\omega_0^2-\chi^2)}+\delta)\}/r^2 & \\ & \omega_0 > \chi. \end{cases} \tag{84}$$

For $\omega_0 < \chi$ the field falls off exponentially, and no radiation takes place. For $\omega_0 > \chi$ the radiated wave is purely transverse. The average rate of radiation of energy per unit area in the direction $\mathbf{r}$ is, according to (11),

$$\frac{1}{8\pi}g_2^2\frac{\omega_0(\omega_0^2-\chi^2)^{\frac{3}{2}}}{r^2}\left\{\frac{[\mathbf{r}\,.\,\mathbf{M}_1]^2}{r^2} + \frac{[\mathbf{r}\,.\,\mathbf{M}_2]^2}{r^2} + 2\frac{([\mathbf{r}\,.\,\mathbf{M}_1]\,.\,[\mathbf{r}\,.\,\mathbf{M}_2])}{r^2}\cos\delta\right\}. \tag{85}$$

$\mathbf{M}_1$, $\mathbf{M}_2$ and δ are given by (79), (77) and (76) respectively. Thus the angular distribution has no very simple relation to the direction of the incident field. Moreover, as (78) and (77) show, it varies with the frequency. If we integrate (85) over all directions and use (75*b*), (77) and (79), the total rate of radiation just becomes equal to (80).

Discussion

The scattering cross-section (82) is plotted in the figure for $I = \frac{1}{2}\hbar$, and $\chi = 4{\cdot}42 \times 10^{12}$ cm.$^{-1}$ corresponding to a meson mass μ of 85×10^6 eV. I have taken $\alpha = 10\chi^2$ corresponding to $g_2^2\chi^2/\hbar = 1/13{\cdot}3$, as is required by the theory of nuclear forces. The different curves correspond to different values of K given by $\beta = 0$, χ, 5χ, 10χ and 15χ.

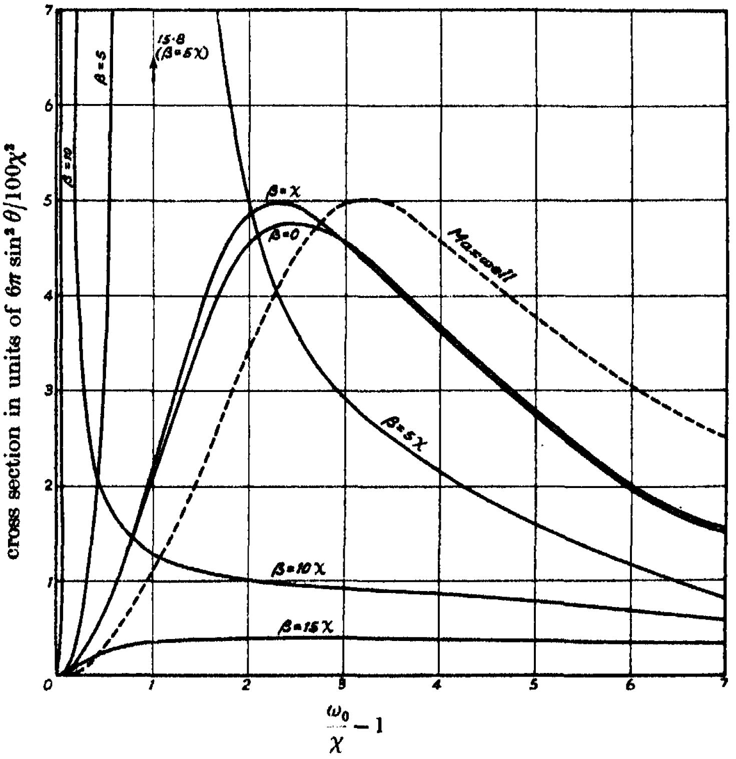

FIGURE 1

The dipole moment g_2 only appears in (82) in the denominator of α, and of β in ξ. For small g_2 and frequencies which are not too high, these are large compared with ω_0, and (82) can be expanded in a series in ascending powers of g_2. The first term of this series is

$$\frac{8\pi}{3}\sin^2\theta\,\frac{g_2^4}{I^2}\,\frac{(\omega_0^2-\chi^2)^2}{\omega_0^2}\,\frac{1+K^2\omega_0^2/I^2}{(1-K^2\omega_0^2/I^2)^2}. \tag{86}$$

This differs completely from the quantum cross-section for the scattering of mesons by neutrons (or protons) due to the appearance of the constant K, since for frequencies near I/K, (86) has a strong resonance peak and becomes infinite. There is no such constant in the quantum theory. If $K = 0$, then (86) does in fact become the quantum cross-section. To apply it to the scattering of neutral mesons by neutrons or protons I must put $I = \frac{1}{2}\hbar$, and replace $\sin^2\theta$ by 2/3, its value averaged over all initial orientations of the dipole.† If I write for greater similarity with the quantum formula $E = \hbar\omega_0$ for the energy of a meson, and

$$p = \hbar(\omega_0^2 - \chi^2)^{\frac{1}{2}}$$

for its momentum, and further, if I put $g_2 - g_2'/\chi$, I find that (86) becomes, in the case $K = 0$,

$$\frac{64}{9}\pi\left(\frac{g_2'^2}{\hbar}\right)^2 \frac{1}{\chi^2}\frac{p^4}{\mu^2 E^2}, \tag{87}$$

which is exactly the cross-section for the scattering of neutral mesons due to the spin of the neutron as given by quantum theory. Now, as is well known, quantum theory neglects the reaction of the radiated field, so that for high frequencies important deviations from formulae (86) and (87) should be expected, as indeed the exact formula (82) shows. There is, however, no reason to doubt that the Dirac equation adequately describes the mechanical properties of a particle of spin $\frac{1}{2}\hbar$. There is therefore no reason for doubting that the formula (87) is correct for low frequencies. The above argument then shows that for the elementary particles as they occur in nature, K is zero, and the elementary particles have the simplest possible mechanical properties for a spinning particle. Thus the exact classical equations of motion for a neutron or proton (with $g_1 = 0$) in a meson field are got by putting $K = 0$ in (62) and (63). A glance at these equations shows that the case $I = 0$, $K \neq 0$ is formally not as simple as the case $I \neq 0$, $K = 0$ which seems to occur in nature and is described by the quantum theory of elementary particles.

Thus a formula which goes beyond the quantum formula (87) and which may be used for describing the scattering of mesons by neutrons or protons is obtained by putting $K = 0$ in (82). The resulting formula is

$$6\pi\sin^2\theta(\omega_0^2 - \chi^2)^2 \frac{\alpha^2\omega_0^2 + (\omega_0^2 - \chi^2)^3 + \chi^6}{\{\alpha^2\omega_0^2 + (\omega_0^2 - \chi^2)^3 + \chi^6\}^2 - 4\alpha^2\omega_0^2\chi^6}. \tag{88}$$

---

† $\frac{2}{3}$ is the classical average. Detailed calculations (see second footnote on p. 341) have shown that in the quantum theory of a particle of spin $\hbar/2$, $\sin^2\theta$ is to be replaced by 2. The quantum cross-section is therefore exactly three times (87).

As mentioned at the beginning of this section, $\alpha = 10\chi^2$, so that the explicit χ^6 terms in (88) may be omitted with an error of less than 2 %. To this degree of accuracy the scattering cross-section may be written

$$6\pi \sin^2\theta \frac{\hbar^2 p^4}{\alpha^2\hbar^4 E^2 + p^6}. \tag{88a}$$

The formula (88) has a very wide range of validity. In deriving it the following approximations have been made. First, the translational motion of the particle was neglected. Due to the largeness of the neutron mass this approximation is fully justified. The scattering due to the translational motion of the dipole would be smaller by a factor of the order $(\mu/M)^2$. Secondly, the meson field has been treated classically. A comparison of the Klein-Nishina formula with the Thomson formula, as well as the corresponding quantum formula of Booth and Wilson (1940)† for the scattering of neutral mesons due to the g_1 interaction with the classical formula given in A, shows that this is a good approximation so long as the wave-length of the quanta or mesons is large compared with the Compton wave-length of the electron or neutron respectively. Thus no appreciable error is introduced by the classical treatment provided that $\omega_0 < M/\hbar$. This frequency $M/\hbar$ corresponds to mesons with an energy of the order of 10^9 eV, and thus formula (88) should correctly give the scattering of mesons up to these energies. Quantum deviations from formula (88) would only make their appearance near and above this energy. Lastly, the spin of the neutron (or proton) has been treated classically. Since the neutron spin is $\frac{1}{2}\hbar$, so that its angular momentum in any direction can only take on the two values $\pm\frac{1}{2}\hbar$, it may be doubted whether a classical treatment of the spin would give correct results. The complete agreement‡ of the classical formula (88) with the quantum formula (87) for low frequencies shows that a classical treatment also gives the right result. There is no reason to suppose that it will go wrong at high frequencies on this account alone.

---

† I am indebted to Dr A. H. Wilson for communicating this result to me before publication.

‡ Subsequent calculation has shown (Bhabha and Madhava Rao, 1941, *Proc. Indian Acad. Sci.* A, **13**, 9–24) that the quantum cross-section is greater than the classical by a constant factor 3, though *the two agree completely in their dependence on frequency, scattering angle, and polarization of the incident and scattered meson.* This difference of a constant factor 3 results from differences in the averaging over the initial orientations of the spin of the heavy particle. In the quantum theory the average value of the square of the cosine of the angle which the spin makes with some fixed direction is 1, if the spin is $\hbar/2$, whereas in the classical theory it is always $\frac{1}{3}$. As a consequence it can be shown that $\sin^2\theta$ in formulae (88) and (88a) must be replaced by 2 and not $\frac{2}{3}$.

We therefore meet with a very unusual state of affairs. The above arguments show that the quantum theory of the interaction of the heavy particles with mesons goes wrong owing to its neglect of the effects of radiation reaction on the rotation of the spin at the point where the quantum cross-section (87) diverges from the classical cross-section (88a), i.e. at momenta satisfying $p^3 \lesssim E\alpha\hbar^2$. With $\alpha = 10\chi^2$, this gives $E \sim 3\mu$. On the other hand, quantum effects would not invalidate the classical formulae (88) and (88a) until we reach energies comparable with the rest energy of the heavy particles. Thus, there is a region of energies E, defined by $3\mu < E < M$, for which the classical formulae (88) and (88a) still hold, but the quantum formula (87) is quite wrong.

The cross-section (88) is given by the curve marked $\beta = 0$ in the figure. For comparison the corresponding cross-section for the scattering of light is given in the figure by the broken curve marked 'Maxwell'. This is got from (88) by putting $\chi = 0$, in which case (88) becomes the cross-section for the scattering of light given in the previous papers (B(56) and C(111)). The abscissa for the broken curve is ω_0/χ and not $\omega_0\chi^{-1} - 1$. The difference between the two curves is considerable, contrary to what is found for the scattering by a point charge. This is what one would expect from the argument given in the introduction.

With the assumption that the heavy particles can exist in states of all integral charge positive or negative (Bhabha 1940b), the above results can at once be applied to charged mesons as they appear in cosmic radiation. To sum up, then, the scattering of *transversely* polarized mesons is given correctly by formula (88) (curve marked $\beta = 0$ in the figure) up to energies of 10^9 eV. The scattering is greatest at energies $E \sim 3{\cdot}5\mu$, the cross-section at this point being 3×10^{-26} cm.^{2}. For higher and lower energies the scattering is much less, so that it is *not* possible to exclude the above cross-section as being too large to be reconciled with experiment. That would only be the case if the cross-section at higher energies were also of the same order, whereas (88) decreases roughly as E^{-2} at high energies. The largeness of the cross-section for $E \sim 3{\cdot}5\mu$, however, will have the effect that relatively very few transversely polarized mesons will fall below these energies. Thus the energy spectrum of mesons will fall away rapidly for energies below about 3μ, if they are transversely polarized.

Longitudinally polarized mesons are not scattered by the rotation of the spin. They can only be scattered by the translational motion of the dipole; the cross-section for this is of the same order as the cross-section for the scattering of longitudinal waves by the g_1 term as calculated in A (43), namely†

$$6\pi\frac{\chi^2}{\omega_0^2}\left(1+\frac{1}{2}\frac{\chi^2}{\omega_0^2}\right)\frac{1}{\left\{\left(\frac{3M}{2g_1^2}\right)^2+\frac{1}{2}\frac{\chi^3}{\omega_0^2}\right\}^2+\left\{\omega_0^2-\frac{3}{4}\frac{\chi^4}{\omega_0^2}-\frac{1}{4}\frac{\chi^6}{\omega_0^4}\right\}},$$

The ratio of this cross-section to the cross-section given above for scattering by the spin at a frequency $\omega_0 \sim 3{\cdot}5\mu$ where the latter is a maximum, is of the order $(g_1^2/\hbar)^2(\mu/M)^2$. With $(\mu/M)^2 \sim 1/137$ and $g_1^2/\hbar \sim 1/14$, this ratio is of the order 4×10^{-5}. For higher energies the cross-section due to the spin falls away very rapidly but so also does the cross-section given above for scattering of *longitudinally polarized* mesons by a point charge, due mainly to factor χ^2/ω_0^2. The ratio is therefore not much altered at high energies. Thus the scattering of longitudinally polarized mesons is always more than twenty thousand times less than the scattering of transversely polarized mesons except for very small velocities, when in any case the scattering is negligibly small for both. Scattering will therefore play an important part in the absorption of transversely polarized mesons, but a quite unimportant part in the absorption of longitudinally polarized mesons.

In comparing the theory of this paper with experiment it should be remembered that if the observed mesons do not show the above large scattering at energies near $3{\cdot}5\mu$, as given by formulae (88) and (88*a*) with $\sin^2\theta$ replaced by 2, in the absence of other evidence this could be interpreted to mean that the observed mesons were mostly longitudinally polarized at the place of observation. On the other hand, if the observed mesons showed a large scattering for energies near $3{\cdot}5\mu$, it would mean that a large number of the actual mesons at the place of observation were transversely polarized. It would also be evidence in favour of the correctness of the theory of this paper, for no other theory predicts a behaviour of this type for mesons.

I wish to express my thanks to Professor Sir C. V. Raman and the Director, Dr J. C. Ghosh, for having afforded me every facility for doing this work at the Institute.

APPENDIX

One must calculate $T_\mu^{\text{mes.}}$ and $M_{\lambda\mu}^{\text{mes.}}$ as defined by (46) and (48). First consider the contribution to these due to the extra terms containing the potentials in (11). These are proportional to χ^2. The potential U_μ at a point on the world tube is the sum of three parts as given by (37*a*), the first being independent of χ and of order ϵ^{-2} and the second proportional to χ^2 and of order 1. Thus, remembering that, for the world tube defined by (42),

---

† Obvious misprints in A (43) have been corrected.

$$dS^\nu = \{s^\nu(1-\kappa') - \epsilon v^\nu\}\,\epsilon\, d\Omega\, d\tau, \tag{89}$$

as shown in A, where $d\Omega$ is a solid angle about the retarded point in the rest system of that point, it is seen that the potentials will contribute to $T_\mu^{\text{mes.}}$ an amount

$$\frac{\chi^2}{4\pi}\int\{\phi_\mu^{(2)}\phi_\nu^{(2)} - \tfrac{1}{2}g_{\mu\nu}\phi_\rho^{(2)}\phi^{(2)\rho}\}\{s^\nu(1-\kappa') - \epsilon v^\nu\}\,\epsilon\, d\Omega$$
$$+\frac{\chi^2}{4\pi}\int\{\phi_\mu^{(2)}(U_\nu^{(\chi)} + U_\nu^{\text{in.}}) + (U_\mu^{(\chi)} + U_\mu^{\text{in.}})\,\phi_\nu^{(2)} - g_{\mu\nu}\phi^{(2)\rho}(U_\rho^{(\chi)} + U_\rho^{\text{in.}})\}\,(s^\nu - \epsilon v^\nu)\,\epsilon\, d\Omega. \tag{90}$$

By using (28), the first integral can be evaluated as shown in C. All its terms are proportional to χ^2, and are of orders ϵ^{-1} and 1. As far as the second integral is concerned, the two parts of $U_\nu^{(\chi)}$ given in (30) can be treated separately. The first part will give a contribution proportional to χ^4 and calculation shows that it is

$$g_2^2\chi^4(\tfrac{1}{3}S_{\mu\rho}\,\mathcal{S}^\rho + \tfrac{1}{6}v_\mu\,\mathcal{S}^2). \tag{91}$$

The second part $\bar{U}_\nu$ is non-singular and can be treated along with the ingoing field. This gives

$$g_2\chi^2\{\tfrac{2}{3}S_{\mu\sigma} + \tfrac{1}{3}v_\mu\,\mathcal{S}_\sigma - \tfrac{1}{3}v_\sigma\,\mathcal{S}_\mu\}\,(\bar{U}^\sigma + U^{\text{in.}\sigma}). \tag{92}$$

The terms containing the ingoing field, $T_\mu^{\text{mix.}}$, as calculated in C (119), are

$$T_\mu^{\text{mix.}} = g_2\Big[\frac{d}{d\tau}\{\tfrac{2}{3}S_\mu{}^\sigma\, G_{\sigma\nu}^{\text{in.}}\, v^\nu - \tfrac{2}{3}G_{\mu\sigma}^{\text{in.}}\,\mathcal{S}^\sigma + \tfrac{1}{3}v_\mu\, S^{\rho\sigma}G_{\rho\sigma}^{\text{in.}}\}$$
$$-\tfrac{1}{2}S^{\rho\sigma}\frac{\partial}{\partial x^\mu}G_{\rho\sigma}^{\text{in.}} - \{\tfrac{2}{3}S_{\mu\sigma} + \tfrac{1}{3}v_\mu\,\mathcal{S}_\sigma - \tfrac{1}{3}v_\sigma\,\mathcal{S}_\mu\}\Big]\frac{\partial}{\partial x^\nu}G^{\text{in.}\sigma\nu}, \tag{93}$$

where the ingoing meson field strengths $G_{\mu\nu}^{\text{in.}}$ have been written in place of the ingoing Maxwell field strengths $F_{\mu\nu}^{\text{in.}}$. Now the terms containing $U_\nu^{\text{in.}}$ in (92) combine with the last three terms in (93) to form

$$(\tfrac{2}{3}S_{\mu\sigma} + \tfrac{1}{3}v_\mu\,\mathcal{S}_\sigma - \tfrac{1}{3}v_\sigma\,\mathcal{S}_\mu)\left(\frac{\partial}{\partial x^\nu}G^{\text{in.}\nu\sigma} + \chi^2 U^{\text{in.}\sigma}\right),$$

which vanishes on account of (7*b*). $T_\mu^{\text{mix.}}$ therefore remains the same as in the Maxwell case, except that $G_{\mu\nu}^{\text{in.}}$ now replaces $F_{\mu\nu}^{\text{in.}}$.

Now consider the contribution to $T_\mu^{\text{mes.}}$ which comes from the first two terms in (11). It is

$$\frac{1}{4\pi}\int\{F^{(2)}_{\mu\rho}G^{(\chi)\rho}{}_\nu+G^{(\chi)}_{\mu\rho}F^{(2)\rho}{}_\nu+\tfrac{1}{2}g_{\mu\nu}F^{(2)\rho\sigma}G^{(\chi)}_{\rho\sigma}\}\{s^\nu(1-\kappa')-\epsilon v^\nu\}\,\epsilon\,d\Omega$$
$$+\frac{1}{4\pi}\int\{G^{(\chi)}_{\mu\rho}G^{(\chi)\rho}{}_\nu+\tfrac{1}{4}g_{\mu\nu}G^{(\chi)}_{\rho\sigma}G^{(\chi)\rho\sigma}\}(s^\nu-\epsilon v^\nu)\,\epsilon\,d\Omega. \tag{94}$$

$G^{(\chi)}_{\mu\nu}$ consists of three parts as shown by (34). The first is of order ϵ^{-1}, the second of order ϵ and the last of order 1. Therefore, as far as the second integral of (94) is concerned, only the first will give a finite contribution and it will be proportional to χ^4. Calculation shows that it vanishes. In the first integral, the first part of $G^{(\chi)}_{\mu\nu}$ will give a contribution proportional to χ^2, the second to χ^4. The latter is

$$\tfrac{1}{8}g_2^2\chi^4\{-\tfrac{2}{3}S_{\mu\nu}\mathcal{S}^\nu-\tfrac{1}{3}v_\mu S^2+\tfrac{2}{3}v_\mu\mathcal{S}^2\}. \tag{95}$$

The third term in $G^{(\chi)}_{\mu\nu}$ is non-singular, and therefore it can be treated with $G^{\text{in.}}_{\mu\nu}$. Its value on the world tube must be expressed in terms of its value at the retarded point by a Taylor series as given by (54). $\tilde{G}_{\mu\nu,\rho}$ will play the part of the derivative $\dfrac{\partial}{\partial x^\rho}\tilde{G}_{\mu\nu}$. Hence there will be terms containing $\tilde{G}_{\mu\nu}$ and $\tilde{G}_{\mu\nu,\rho}$ exactly like the terms containing $G^{\text{in.}}_{\mu\nu}$ and $\dfrac{\partial}{\partial x^\rho}G^{\text{in.}}_{\mu\nu}$. Thus, corresponding to the last three terms of (93) the first integral of (94) gives

$$-g_2\{\tfrac{2}{3}S_{\mu\sigma}+\tfrac{1}{3}v_\mu\mathcal{S}_\sigma-\tfrac{1}{3}v_\sigma\mathcal{S}_\mu\}\tilde{G}^{\sigma\nu}{}_{,\nu}.$$

This combines with the terms containing $\tilde{U}^\sigma$ in (92) to give an expression containing $\tilde{G}_{\sigma\nu,}{}^\nu-\chi^2\tilde{U}_\sigma$ as a factor. Using (31) and (56), and remembering (20*b*) we get

$$\tilde{G}_{\sigma\nu,}{}^\nu-\chi^2\tilde{U}_\sigma=-6g_2\chi^3\int_{-\infty}^{\tau_0}d\tau\,S_{\sigma\nu}u^\nu\frac{J_3(\chi u)}{u^3}+g_2\chi^4\int_{-\infty}^{\tau_0}d\tau\,S_{\sigma\nu}u^\nu\frac{J_4(\chi u)}{u^2}$$
$$+g_2\chi^4\int_{-\infty}^{\tau_0}d\tau\,S_{\sigma\nu}u^\nu\frac{J_2(\chi u)}{u^2}$$
$$=g_2\chi^4\int_{-\infty}^{\tau_0}d\tau\,\frac{S_{\sigma\nu}u^\nu}{u^2}\left\{J_2(\chi u)+J_4(\chi u)-6\frac{J_3(\chi u)}{\chi u}\right\}=0$$

by (18).

Now consider the second term in (93). It really appears as the sum of two terms

$$-\tfrac{2}{3}g_2\left[v^\rho\left(\frac{\partial}{\partial x^\rho}G^{\text{in.}}_{\mu\sigma}\right)\mathcal{S}^\sigma+G^{\text{in.}}_{\mu\sigma}\dot{\mathcal{S}}^\sigma\right]=-\tfrac{2}{3}g_2\frac{d}{d\tau}(G^{\text{in.}}_{\mu\sigma}\mathcal{S}^\sigma).$$

Corresponding to the first two terms on the left of this equation, the first integral of (94) will give

$$-\tfrac{2}{3}g_2[v^\rho \tilde{G}_{\mu\sigma,\rho}\,\mathcal{S}^\sigma+\tilde{G}_{\mu\sigma}\dot{\mathcal{S}}^\sigma],$$

which, on account of (57), may be written

$$-\tfrac{2}{3}g_2\left[\left(\frac{d}{d\tau}\tilde{G}_{\mu\sigma}-\tfrac{1}{4}g_2\chi^4S_{\mu\sigma}\right)\mathcal{S}^\sigma+\tilde{G}_{\mu\sigma}\dot{\mathcal{S}}^\sigma\right]=\tfrac{1}{6}g_2^2\chi^4S_{\mu\sigma}\mathcal{S}^\sigma-\tfrac{2}{3}g_2\frac{d}{d\tau}(\tilde{G}_{\mu\sigma}\mathcal{S}^\sigma).$$

Thus, corresponding to the first four terms of (93), it is seen by the same reasoning that (94) will give

$$g_2\left[\frac{d}{d\tau}\{\tfrac{2}{3}S_{\mu\sigma}\tilde{G}^{\sigma\nu}v_\nu-\tfrac{2}{3}\tilde{G}_{\mu\sigma}\mathcal{S}^\sigma+\tfrac{1}{3}v_\mu S^{\rho\sigma}\tilde{G}_{\rho\sigma}\}-\tfrac{1}{12}g_2\chi^4v_\mu S^2-\tfrac{1}{2}S^{\rho\sigma}\tilde{G}_{\rho\sigma,\mu}\right]. \tag{96}$$

The calculation of the terms proportional to χ^2 is straightforward. The terms proportional to χ^4 are given by (91), (95) and (96). Adding up all the terms the final result is

$$\begin{aligned}T_\mu^{\text{mes.}}=g_2\biggl[&\frac{d}{d\tau}\{\tfrac{2}{3}S_{\mu\sigma}\tilde{G}^{\sigma\nu}v_\nu-\tfrac{2}{3}\tilde{G}_{\mu\sigma}\mathcal{S}^\sigma+\tfrac{1}{3}v_\mu S^{\rho\sigma}\tilde{G}_{\rho\sigma}\}\\&-\tfrac{1}{2}S^{\rho\sigma}\tilde{G}_{\rho\sigma,\mu}+g_2\chi^4(-\tfrac{1}{8}v_\mu S^2+\tfrac{1}{4}S_{\mu\sigma}\mathcal{S}^\sigma+\tfrac{1}{4}v_\mu\mathcal{S}^2)\biggr]\\&-g_2^2\frac{\chi^2}{\epsilon}\frac{d}{d\tau}(\tfrac{1}{6}v_\mu\mathcal{S}^2)+T'^{\text{mes.}}_\mu,\end{aligned} \tag{97}$$

where

$$\begin{aligned}T'^{\text{mes.}}_\mu=g_2^2\chi^2[&v_\mu\{\tfrac{1}{2}\dot{S}^2-\tfrac{5}{3}S'^2+\tfrac{1}{3}(\mathcal{S}S'')-\tfrac{11}{15}(\mathcal{S}\dot{S}\dot{v})-\tfrac{11}{15}(S'S\dot{v})\\&+\tfrac{4}{15}(\mathcal{S}S\ddot{v})-\tfrac{1}{6}S^2\dot{v}^2+\mathcal{S}^2\dot{v}^2+\tfrac{1}{15}(\dot{v}SS\dot{v})\}-\dot{v}_\mu\{\tfrac{7}{5}(\mathcal{S}S')+\tfrac{4}{5}(\mathcal{S}S\dot{v})\}\\&+\tfrac{1}{30}\ddot{v}_\mu S^2-\tfrac{1}{5}\ddot{v}_\mu\mathcal{S}^2+\tfrac{1}{3}\mathcal{S}_\mu(S'\dot{v})+\tfrac{1}{3}\mathcal{S}_\mu(\mathcal{S}\ddot{v})+\tfrac{1}{3}S_{\mu\rho}\dot{v}^\rho(\mathcal{S}\dot{v})\\&+\tfrac{1}{3}S'_\mu(\mathcal{S}\dot{v})+\tfrac{1}{2}S_{\mu\nu}S''^\nu+\tfrac{13}{30}S_{\mu\nu}\dot{S}^{\nu\rho}\dot{v}_\rho+\tfrac{4}{15}S_{\mu\nu}S^{\nu\rho}\ddot{v}_\rho\\&+\tfrac{1}{3}S_{\mu\nu}\mathcal{S}^\nu\dot{v}^2-\tfrac{2}{3}\dot{S}_{\mu\nu}S'^\nu-\tfrac{7}{30}\dot{S}_{\mu\nu}S^{\nu\rho}\dot{v}_\rho-\tfrac{1}{6}\ddot{S}_{\mu\nu}\mathcal{S}^\nu].\end{aligned} \tag{98}$$

The calculation of $M_{\lambda\mu}^{\text{mes.}}$ is straightforward. I have to calculate the integrals (90) and (94) with an extra s_λ in the integrand, the expressions being then made antisymmetrical in λ and μ. As before I obtain an expression like $M_{\lambda\mu}^{\text{mix.}}$ given in C (59), with $\tilde{G}_{\mu\nu}$ written in place of $F_{\mu\nu}^{\text{in.}}$. The final result is

$$M_{\lambda\mu}^{\text{mes.}}=g_2[S_\lambda{}^\sigma\tilde{G}_{\sigma\mu}+\tfrac{2}{3}v_\lambda S_\mu{}^\sigma\tilde{G}_{\sigma\nu}v^\nu-\tfrac{2}{3}v_\lambda\tilde{G}_{\mu\sigma}\mathcal{S}^\sigma]_-+M'^{\text{mes.}}_{\lambda\mu}, \tag{99}$$

where

$$M'^{\text{mes.}}_{\lambda\mu} = g_2^2\chi^2[S_{\lambda\rho}\,\dot{S}^{\rho}{}_{\mu} + \not{S}_{\lambda}\,S'_{\mu} + \tfrac{1}{2}\dot{v}_{\lambda}\,S_{\mu\sigma}\,\not{S}^{\sigma}$$

$$+v_{\lambda}\{S_{\mu\sigma}\,S'^{\sigma} - \tfrac{2}{3}\dot{S}_{\mu\sigma}\,\not{S}^{\sigma} + \tfrac{13}{30}S_{\mu\sigma}\,S^{\sigma\nu}\dot{v}_{\nu} + \tfrac{1}{5}\dot{v}_{\mu}\,S^2 - \tfrac{13}{30}\dot{v}_{\mu}\,\not{S}^2 + \tfrac{1}{3}\not{S}_{\mu}(\not{S}\dot{v})\}]_{-}. \quad (100)$$

I may straightaway write

$$A^{\text{mes.}}_{\mu} = g_2\{\tfrac{2}{3}S_{\mu\sigma}\,\tilde{G}^{\sigma\nu}v_{\nu} - \tfrac{2}{3}\tilde{G}_{\mu\sigma}\,\not{S}^{\sigma} + \tfrac{1}{6}v_{\mu}\,S^{\rho\sigma}\tilde{G}_{\rho\sigma}\} - g_2^2\frac{\chi^2}{\epsilon}(\tfrac{1}{6}v_{\mu}\not{S}^2) + A'^{\text{mes.}}_{\mu}, \quad (101)$$

where $A'^{\text{mes.}}_{\mu}$ contains only terms proportional to $g_2^2\chi^2$, so that

$$T^{\text{mes.}}_{\mu} - \dot{A}^{\text{mes.}}_{\mu} = -\tfrac{1}{2}g_2\,S^{\rho\sigma}\tilde{G}_{\rho\sigma,\mu} + g_2^2\chi^4(-\tfrac{1}{5}v_{\mu}\,S^2 + \tfrac{1}{4}S_{\mu\rho}\not{S}^{\rho}$$

$$+\tfrac{1}{4}v_{\mu}\not{S}^2) + \tfrac{1}{2}g_2\frac{d}{d\tau}(v_{\mu}S^{\rho\sigma}\tilde{G}_{\rho\sigma}) + (T'^{\text{mes.}}_{\mu} - \dot{A}'^{\text{mes.}}_{\mu}), \quad (102)$$

and $$M^{\text{mes.}}_{\lambda\mu} - (v_{\lambda}A^{\text{mes.}}_{\mu} - v_{\mu}A^{\text{mes.}}_{\lambda}) - \dot{B}^{\text{mes.}}_{\lambda\mu} = [S_{\lambda}{}^{\rho}C^{\text{mes.}}_{\rho\mu}]_{-}, \quad (103)$$

where $$C^{\text{mes.}}_{\rho\mu} = g_2\tilde{G}_{\rho\mu} + C'^{\text{mes.}}_{\rho\mu} \quad (104)$$

and $$[S_{\lambda\rho}C'^{\text{mes.}\,\rho}{}_{\mu}]_{-} = M'^{\text{mes.}}_{\lambda\mu} - (v_{\lambda}A'^{\text{mes.}}_{\mu} - v_{\mu}A'^{\text{mes.}}_{\lambda}) - \dot{B}^{\text{mes.}}_{\lambda\mu}. \quad (105)$$

The expressions (102) and (103) show that $\tilde{G}_{\rho\sigma,\mu}$ occurs in the translational equation (50) exactly like the ingoing field $\frac{\partial}{\partial x^{\mu}}G^{\text{in.}}_{\rho\sigma}$, while $\tilde{G}_{\rho\mu}$ occurs in the rotational equation (51) exactly like $G^{\text{in.}}_{\rho\mu}$. The terms of order χ^4 in (102) are most essential. Not having any differentiation with respect to τ, they cannot be altered by any addition to $A^{\text{mes.}}_{\mu}$. They are just such that, on contracting (102) with v^{μ}, and remembering (57), I get

$$v^{\mu}(T^{\text{mes.}}_{\mu} - \dot{A}^{\text{mes.}}_{\mu}) = \tfrac{1}{2}g_2(\dot{S}^{\rho\sigma}\tilde{G}_{\rho\sigma}) + v^{\mu}(T'^{\text{mes.}}_{\mu} - \dot{A}'^{\text{mes.}}_{\mu}). \quad (106)$$

This, according to (53), must be equal to $\frac{1}{2}(\dot{S}C^{\text{mes.}})$, that is, by (104),

$$\tfrac{1}{2}g_2(\dot{S}\tilde{G}) + \tfrac{1}{2}(\dot{S}\,.\,C'^{\text{mes.}}). \quad (107)$$

If any substitution other than (101) had been made for $A^{\text{mes.}}_{\mu}$, (106) and (107) would not have been equal.

Finally, then, $A'^{\text{mes.}}_{\mu}$ and $B^{\text{mes.}}_{\lambda\mu}$ have to be determined so that

$$M'^{\text{mes.}}_{\lambda\mu} - (v_{\lambda}A'^{\text{mes.}}_{\mu} - v_{\mu}A'^{\text{mes.}}_{\lambda}) - \dot{B}^{\text{mes.}}_{\lambda\mu} \equiv [S_{\lambda}{}^{\rho}\,.\,C'^{\text{mes.}}_{\rho\mu}]_{-}, \quad (108a)$$

$$(\dot{S}C'^{\text{mes.}}) = 2v^{\mu}(T'^{\text{mes.}}_{\mu} - \dot{A}'^{\text{mes.}}_{\mu}). \quad (108b)$$

Both $A'^{\text{mes.}}_{\mu}$ and $B^{\text{mes.}}_{\lambda\mu}$ must be proportional to $g_2^2\chi^2$, as is seen from (98) and (100). They must be quadratic in $S_{\lambda\mu}$ and contain terms with respectively one and no dots. They may be found by the method given in C. There are eight possible independent terms in $A'^{\text{mes.}}_\mu$ and only one in $B^{\text{mes.}}_{\chi\mu}$. The conditions (107) determine the coefficients of all these in terms of one arbitrary constant k. The result is that

$$\begin{aligned} T'^{\text{mes.}}_\mu - \dot{A}'^{\text{mes.}}_\mu = g_2^2\chi^2[&k\ddot{S}_{\mu\nu}\not{S}^\nu + (2k-1)\dot{S}_{\mu\nu}S'^\nu + k\dot{S}_{\mu\nu}S^{\nu\rho}\dot{v}_\rho \\ &+ kS_{\mu\nu}S''^\nu + kS_{\mu\nu}\dot{S}^{\nu\rho}\dot{v}_\rho + \tfrac{1}{3}S_{\mu\nu}S^{\nu\rho}\ddot{v}_\rho + \tfrac{1}{3}S_{\mu\nu}\not{S}^\nu\dot{v}^2 \\ &+ v_\mu\{2(k-1)S'^2 + (2k-1)(S'S\dot{v}) + 2k(\not{S}S'') + (2k-1)(\not{S}\dot{S}\dot{v}) \\ &+ \tfrac{1}{3}(\not{S}S\ddot{v}) + \tfrac{1}{2}\dot{S}^2 - \tfrac{1}{6}S^2\dot{v}^2 + \not{S}^2\dot{v}^2\} + 2k\dot{v}_\mu(\not{S}\dot{S}) \\ &+ \dot{v}_\mu(\not{S}S\dot{v}) - \tfrac{1}{6}\ddot{v}_\mu S^2 + \tfrac{2}{3}\ddot{v}_\mu\not{S}^2], \end{aligned} \tag{109}$$

and
$$\begin{aligned} C'^{\text{mes.}}_{\rho\mu} = g_2^2\chi^2[&(k-1)(S_{\rho\nu}\dot{v}^\nu v_\mu - S_{\mu\nu}\dot{v}^\nu v_\rho) \\ &+ (k-1)(\not{S}_\rho\dot{v}_\mu - \not{S}_\mu\dot{v}_\rho) - (S'_\rho v_\mu - S'_\mu v_\rho) + \dot{S}_{\rho\mu}]. \end{aligned} \tag{110}$$

According to (61),

$$\begin{aligned} T^{\text{self},\,\chi}_\mu &\equiv T'^{\text{mes.}}_\mu - \dot{A}'^{\text{mes.}}_\mu + \frac{d}{d\tau}(S_\mu{}^\rho C'^{\text{mes.}}_{\rho\nu}v^\nu) \\ &= g_2^2\chi^2\{v_\mu(\tfrac{1}{2}\dot{S}^2 - S'^2 - \tfrac{1}{6}S^2\dot{v}^2) - \tfrac{1}{6}\ddot{v}_\mu S^2 + \tfrac{2}{3}S_{\mu\nu}S''^\nu + \tfrac{1}{3}S_{\mu\nu}\dot{S}^{\nu\rho}\dot{v}_\rho. \end{aligned} \tag{111}$$

Further,

$$C'^{\text{mes.}}_{\rho\mu} - (C'^{\text{mes.}}_{\rho\nu}v^\nu v_\mu - C'^{\text{mes.}}_{\mu\nu}v^\nu v_\rho) = g_2^2\chi^2\{\dot{S}_{\rho\mu} - (S'_\rho v_\mu - S'_\mu v_\rho)\}. \tag{112}$$

This has already been introduced into (63) and gives the last term of that equation.

I wish to find the potentials at a distant point x_k at time t due to an oscillation of the dipole of the type

$$\dot{S}_{\mu\nu} = \omega_0 L_{\mu\nu}\cos\omega_0 t,$$

the $L_{\mu\nu}$ being constants. The dipole is taken to be fixed at the origin. Then, by (20a), $u_k = x_k$ and $u_0 = t - t'$, for a point on the world line corresponding to a time t', and, by (20b), $u_0 = \sqrt{(u^2 + r^2)}$, where $r = \sum_1^3 x_k^2$; hence

$$t' = t - \sqrt{(u^2 + r^2)}.$$

Further, by (21), $\kappa = u_0$. The potentials are given by (25b), and, for any given value of u, the position of the dipole has to be taken at a time t' as defined above. Both u_0 and t' are functions of u as the preceding expressions show, but, since I am only interested in the potentials at a very large distance r, it is sufficient to let the differentiation act only on t' and not on u_0. Differentiation of u_0 merely adds terms to the potentials which are of a higher order in $1/r$. I thus find

$$U_\nu^{\text{ret.}} \approx -g_2 \int_0^\infty u\,du\,J_0(\chi u)\left\{\frac{L_{0\nu}}{u_0^2}+\frac{x^k L_{k\nu}}{u_0^3}\right\}\omega_0^2 \sin\omega_0(t-\sqrt{(u^2+r^2)}). \qquad (113)$$

Now, by a well-known theorem of Bessel functions,

$$\int_0^\infty du\,J_0(\chi u)\frac{u}{\sqrt{(u^2+r^2)}}e^{-\omega_0\sqrt{(u^2+r^2)}} = \frac{e^{-r\sqrt{(\chi^2+\omega_0^2)}}}{\sqrt{(\chi^2+\omega_0^2)}};$$

whence

$$\int_0^\infty du\,J_0(\chi u)\frac{u}{u^2+r^2}e^{-i\omega_0\sqrt{(u^2+r^2)}} = \int_{i\omega_0}^{\infty+i\omega_0} d\omega' \int_0^\infty du\,J_0(\chi u)\frac{u}{\sqrt{(u^2+r^2)}}e^{-\omega'\sqrt{(u^2+r^2)}}$$

$$= \begin{cases} \dfrac{e^{-r\sqrt{(\chi^2-\omega_0^2)}}}{ir\omega_0} & \omega_0<\chi, \\[2ex] \dfrac{e^{-ir\sqrt{(\omega_0^2-\chi^2)}}}{ir\omega_0} & \omega_0>\chi, \end{cases}$$

where terms of order $1/r^2$ have been neglected. Similarly, by integrating twice with respect to ω_0, I find, omitting terms of order $1/r^3$, that

$$\int_0^\infty du\,J_0(\chi u)\frac{u}{(u^2+r^2)^{\frac{3}{2}}}e^{-i\omega_0\sqrt{(u^2+r^2)}} = \begin{cases} -\dfrac{\sqrt{(\chi^2-\omega_0^2)}}{r^2\omega_0^2}e^{-r\sqrt{(\chi^2-\omega_0^2)}} & \omega_0<\chi, \\[2ex] -\dfrac{i\sqrt{(\omega_0^2-\chi^2)}}{r^2\omega_0^2}e^{-ir\sqrt{(\omega_0^2-\chi^2)}} & \omega_0>\chi. \end{cases}$$

By using these integrals, (113) gives at once

$$U_0^{\text{ret.}} = \begin{cases} g_2\sqrt{(\chi^2-\omega_0^2)}\dfrac{x^k L_{k0}}{r^2}e^{-r\sqrt{(\chi^2-\omega_0^2)}}\sin\omega_0 t & \omega_0<\chi \\[2ex] g_2\sqrt{(\omega_0^2-\chi^2)}\dfrac{x^k L_{k0}}{r^2}\cos(\omega_0 t - r\sqrt{(\omega_0^2-\chi^2)}) & \omega_0>\chi \end{cases}$$

and

$$U_k^{\text{ret.}} = \begin{cases} g_2\left(\omega_0\dfrac{L_{0k}}{r}\cos\omega_0 t + \sqrt{(\chi^2-\omega_0^2)}\dfrac{x^l L_{lk}}{r^2}\sin\omega_0 t\right)e^{-r\sqrt{(\chi^2-\omega_0^2)}} & \omega_0<\chi, \\[2ex] g_2\left(\omega_0\dfrac{L_{0k}}{r}+\sqrt{(\omega_0^2-\chi^2)}\dfrac{x^l L_{lk}}{r^3}\right)\cos(\omega_0 t - r\sqrt{(\omega_0^2-\chi^2)}) & \omega_0>\chi. \end{cases}$$

Use of these results leads at once to (84) of the text.

References

Bhabha 1938 *Proc. Roy. Soc.* A, **166**, 501–528.

Bhabha 1939 *Proc. Roy. Soc.* A, **172**, 384–409; referred to here as A.

Bhabha 1940*a* *Proc. Indian Acad. Sci.* A, **11**, 247–267, 467; referred to here as B.

Bhabha 1940*b* *Proc. Indian Acad. Sci.* A, **11**, 347–368, 468.

Bhabha and Corben 1940*d* *Proc. Roy. Soc.* A, **178**, 273–314; referred to here as C.

Dirac 1938 *Proc. Roy. Soc.* A, **167**, 148–169.

Heitler 1940 *Nature, Lond.*, **145**, 29.

Heisenberg 1939 *Z. Phys.* **113**, 61–86.

Pauli 1933 *Handbuch der Physik*, **24**/1, Quantentheorie.

Pryce 1938 *Proc. Roy. Soc.* A, **168**, 389–401.

Booth and Wilson 1940 *Proc. Camb. Phil. Soc.* **36**, 446–453.

Spectroscopic observations on hydrocarbon flames in atomic oxygen

By Dr K. H. Geib, *Physikalisch Chemisches Institut der Universität, Leipzig*
and W. M. Vaidya, *University College, Rangoon*

(*Communicated by M. N. Saha, F.R.S.—Received* 15 *May* 1940—
Revised 23 *November* 1940)

[Plate 7]

Flames of hydrocarbons, burning in atomic oxygen, have been re-examined, in order to find out whether the ethylene flame bands occur in such flames. The results indicate that they are strong in benzene and acetylene, but weak and diffuse in ethylene. C_2, CH and HO are also present. Methyl alcohol gives the HO and CH bands and also 'cool flame' bands rather faintly, while formaldehyde shows only the HO band at λ 3064.

The ethylene flame bands are absent from the flame of benzene burning in atomic hydrogen, which yields only C_2 and CH bands. The Balmer lines also appear, however, due to stray light from the main discharge.

INTRODUCTORY

In view of the wide occurrence of the ethylene flame bands in the flames of carbon compounds burning in air, it was of interest to extend the investigation to similar compounds burning in atomic oxygen, in order to find out whether the ethylene flame bands also appeared in such flames. Reproductions of the spectra by previous observers (Harteck and Kopsch 1931) showed that the exposures were not long enough to warrant any definite conclusions, though in the flame of acetylene burning in atomic oxygen (see reproduction by Bonhoeffer 1936) there were suggestions that the ethylene flame bands might be present faintly. Also, in all the flames where they had appeared previously, oxygen was necessarily present; it was therefore a matter of importance, in order to ascertain their emitter, to examine a flame from which oxygen could be excluded. Such a flame was that of benzene burning in atomic hydrogen. Previous authors' (Bonhoeffer and Harteck 1928) observations on this flame were confined to the visible, while the strongest ethylene flame bands occur in the ultra-violet. In view of these facts the spectra of such flames were re-examined with longer exposures, using the quartz instruments in order to get the ultra-violet part of the spectrum.

EXPERIMENTAL DETAILS

The apparatus used was similar to that of Harteck and Kopsch. Oxygen from a compressed gas cylinder enters the apparatus at *EE* and passes into two wide pyrex glass tubes *B*, *B* in which are sealed two aluminium cylindrical electrodes. External connexions with the secondary of the transformer are made through tungsten wires sealed at *DD*. The secondary of the transformer delivers 3–5 kW at 200 mA, the primary being 300 V. After starting the discharge, a stream of atomic oxygen enters the quartz reaction vessel *S* via tube *HH*, while the hydrocarbon is let in via tube *KK*. Ethylene and acetylene were obtained from compressed gas cylinders, while in other cases the hydrocarbon was vaporized before introduction. The products of combustion are pumped away through wide tubes *M*, *N*, *R*

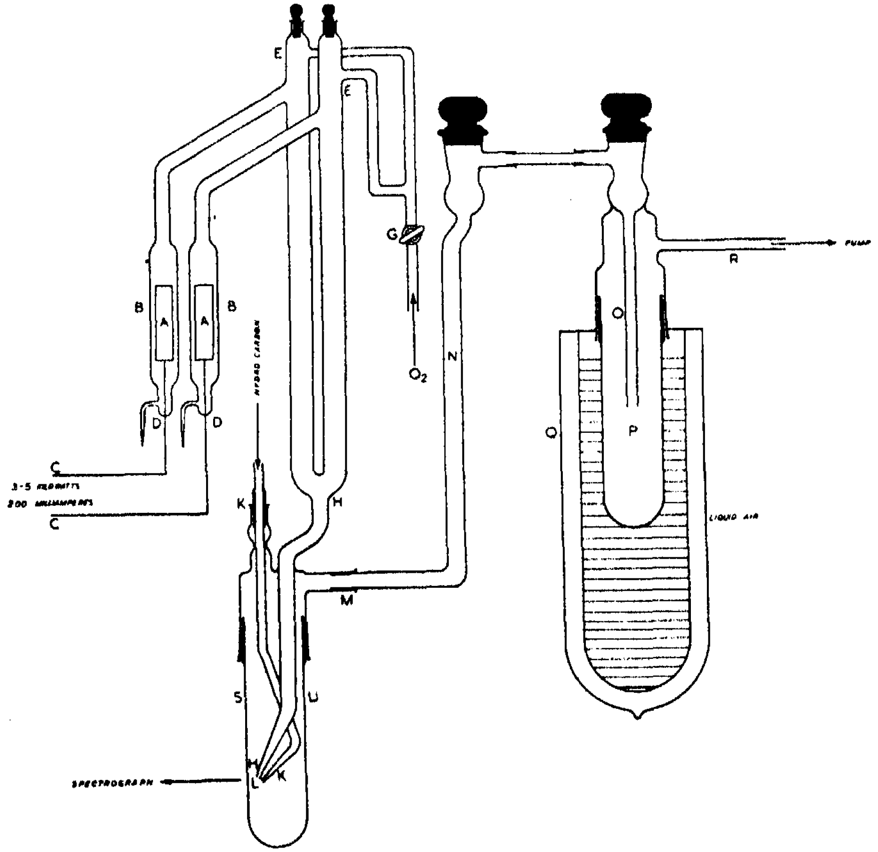

FIGURE 1. Apparatus for production of atomic flames.

by means of a mercury diffusion pump backed by an oil pump. A liquid air trap is used to freeze out harmful vapours. The pressure in the system is about 1 mm. and the temperature of the flame about 500° C. These flames appear as diffuse glows (plate 7*f*) without sharp boundaries, unlike ordinary flames. They are much brighter, for the photographs of the spectra could be easily obtained from 5 min. to an hour on a Steinheil's small quartz spectrograph similar to Hilger's E 31, with Agfa Isochrome fine-grain plates. For the acetylene flame, an instrument with dispersion of 12 A/mm. at λ3600 was used.

DESCRIPTION OF SPECTRA

Acetylene. Acetylene gave a very bright flame with central parts intensely white surrounded by a diffuse greenish outer zone. The glow is intense where the hydrocarbon meets the oxygen atoms. The disposition of the flame could be changed by regulating the flow of atomic oxygen and the hydrocarbon. If the hydrocarbon was delivered rapidly, the flame moved away from the orifice *L*; on the other hand, if the stream was slow, there was a tendency for the flame to move inside the bent tube. The adjustment of the two rates of flow was therefore critical, but with experience no difficulty was encountered in maintaining the flame for periods sufficiently long to obtain a fair intensity of the spectrum.

The spectrum is extremely bright. Unlike the acetylene flame burning in air, which gives *A* group of the HCO bands, the atomic oxygen and acetylene flame yields both *A* and *B* bands. The C_2, CH and HO bands are all strong, particularly the Swan bands.

This flame is of interest from yet another point of view, for the lesser known CH bands appear in this flame with greater intensity than in ordinary flames. The complete CH spectrum consists of the two well-known bands at λ4315 and λ3872 and three fainter bands: (1) the Raffety bands extending from λ4107 to λ4025, (2) the Fortrat bands at λ3143 and λ3157, and (3) a band at λ3628. There now remain two sets of bands of unknown origin; one has been pointed out by Grenat (1931) and the other by Raffety (1916). The former consists of three sets of bands at λ4108, λ4148 and λ4770, and Raffety's measures of the other set were λ4942, λ4937·5, λ4890·0 and λ4853 (?). It is shown elsewhere by the author (forthcoming publication) that the latter set is the (0, 1) band of the same CH system to which the CH band at λ4315 (0, 0) belongs. Another band at λ4743 noted by Raffety and also by the author can be identified with the isotope band due to C^{13}-C^{12} (Jevons 1932) (plate 7*e*).

Ethylene. Ethylene does not give such a bright flame as with acetylene. It is pale blue and is about half the size of the acetylene flame. Compared with the ordinary ethylene flame in a flame separator, the present flame is much brighter, but the ethylene flame bands are weak and diffuse in contrast with the ordinary flame where they appeared with high intensity. The ethylene flame bands are of *A* type. The C_2, CH and HO bands are also present (plate 7*c*).

Benzene. The delivery tube for the hydrocarbon was connected to a side bulb containing benzene. As soon as the bulb is joined on to the evacuating system, benzene begins to get vaporized and with careful regulation of the entry of the vapour in the reaction vessel the flame could be maintained for long periods. The flame is intense blue with strong CH emission. The C_2 and HO bands are also strong. The ethylene flame bands are of the type *A* and *B* (plate 7*b*).

Methyl alcohol. The vapour was introduced as in the case of benzene. The flame appeared like a diffuse halo, pale blue in colour. The HO band at $\lambda 3064$ is very strong, the CH band at $\lambda 4315$ is moderate. The C_2 bands seem to be absent and also the ethylene flame bands. The bands forming the cool flame spectrum of ether (Eméleus 1926; Fowler and Pearse 1935) are present very faintly.

Formaldehyde. Paraformaldehyde was heated in a side bulb and the vapour passed into the reaction vessel. The flame is extremely pale and very diffuse. Only the HO band at $\lambda 3064$ can be identified.

Since all the flames in which the ethylene flame bands appeared were obtained by burning hydrocarbons in air or oxygen, it was thought desirable to examine a flame from which oxygen, whether atomic or molecular, could be excluded. Benzene burning in atomic hydrogen gave a suitable flame from which oxygen was absent and hence this flame was studied.

For the production of atomic hydrogen the previous experimental arrangements were utilized. Hydrogen from a gas cylinder was passed slowly into the discharge tube. Benzene and atomic hydrogen reacted readily. The flame was a glow, pale blue in colour.

In this spectrum, the ethylene flame bands are absent (plate 7*a*). That there was no oxygen in the tube was shown by the absence of the HO bands at $\lambda 3064$ which usually comes out strongly if oxygen and hydrogen are together. The exposures were long enough so that if either the ethylene flame bands or the HO bands had occurred in the spectrum they would have been registered on the photographic plate.

(*f*) appearance of the flame of acetylene

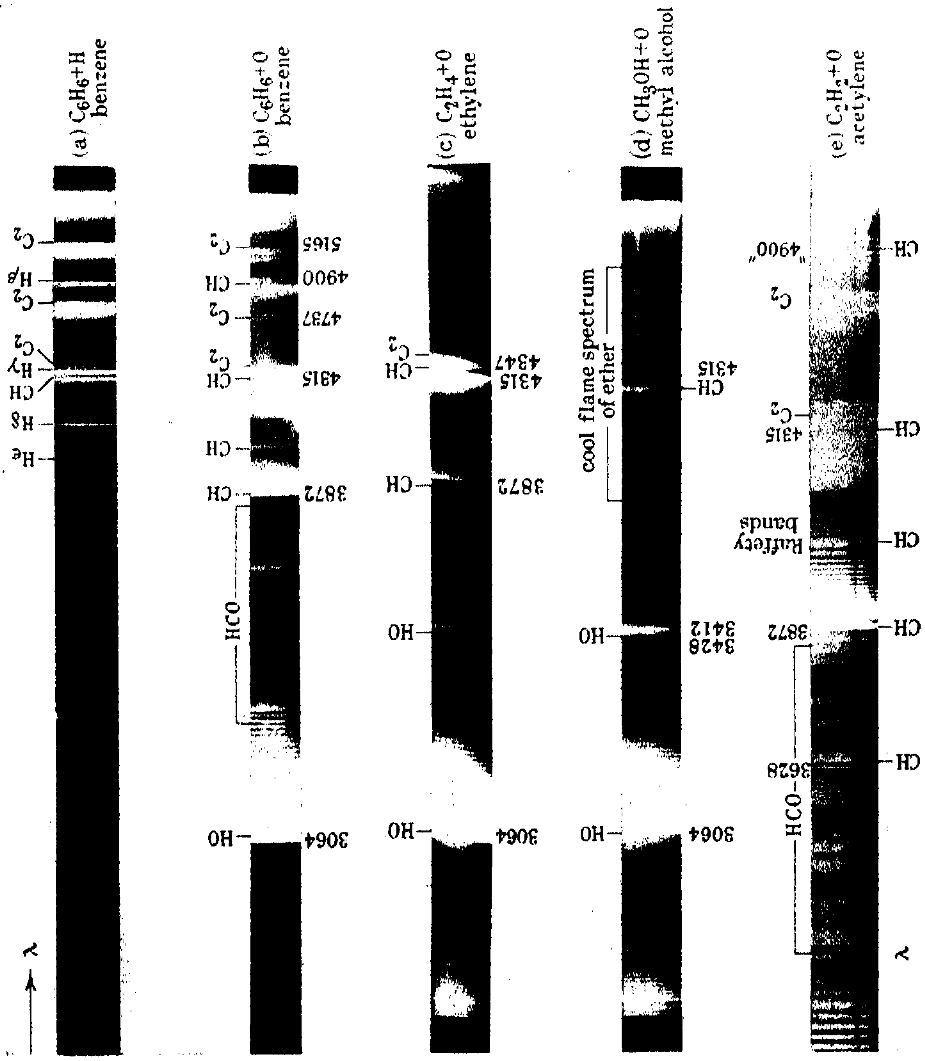

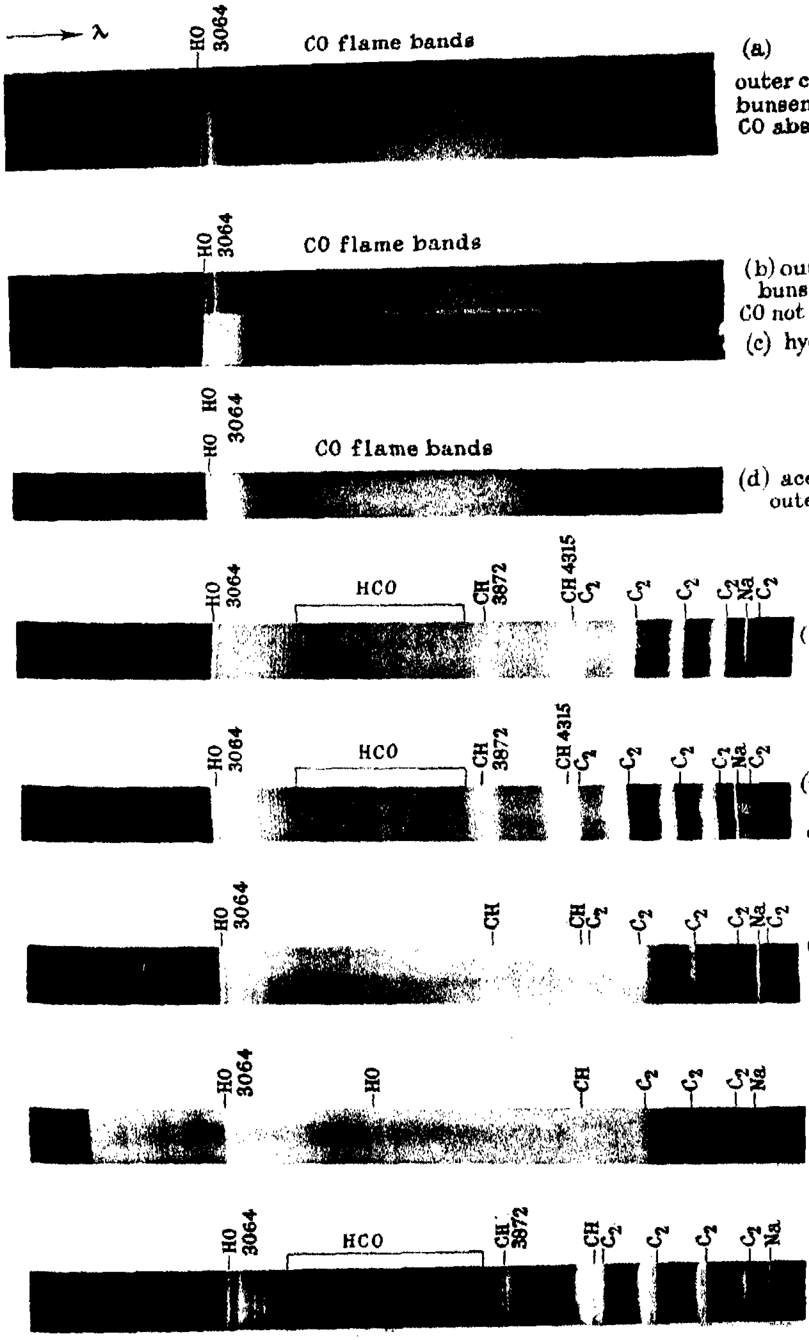

(a) outer cone bunsen flame CO absorbed

(b) outer cone bunsen flame CO not absorbed

(c) hydrogen

(d) acetylene outer cone

(e) inner cone bunsen flame

(f) Meker burner diminished air supply

(g) Meker burner increased air supply

(h) oxy-coal gas blown through

(i) oxy-coal gas mixed jet

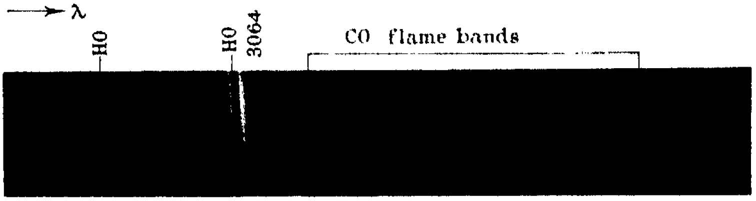

(a)
formaldehyde

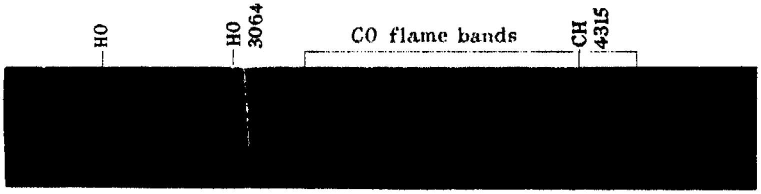

(b)
methyl alcohol

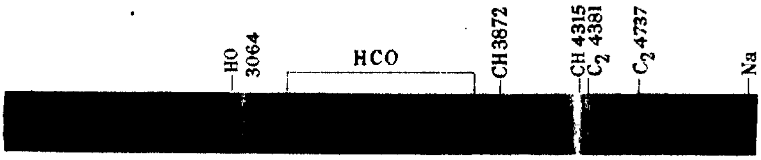

(c)
methane

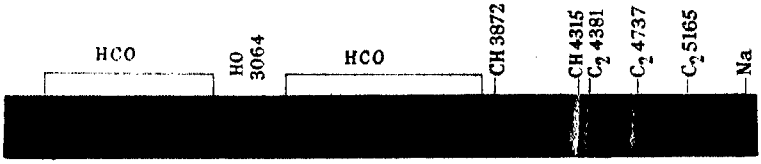

(d)
ethylene

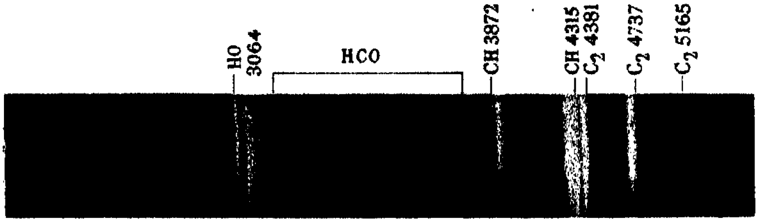

(e)
ether

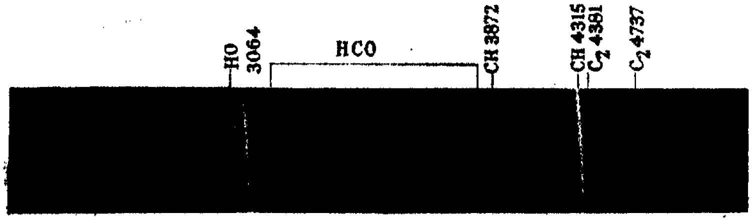

(f)
acetaldehyde

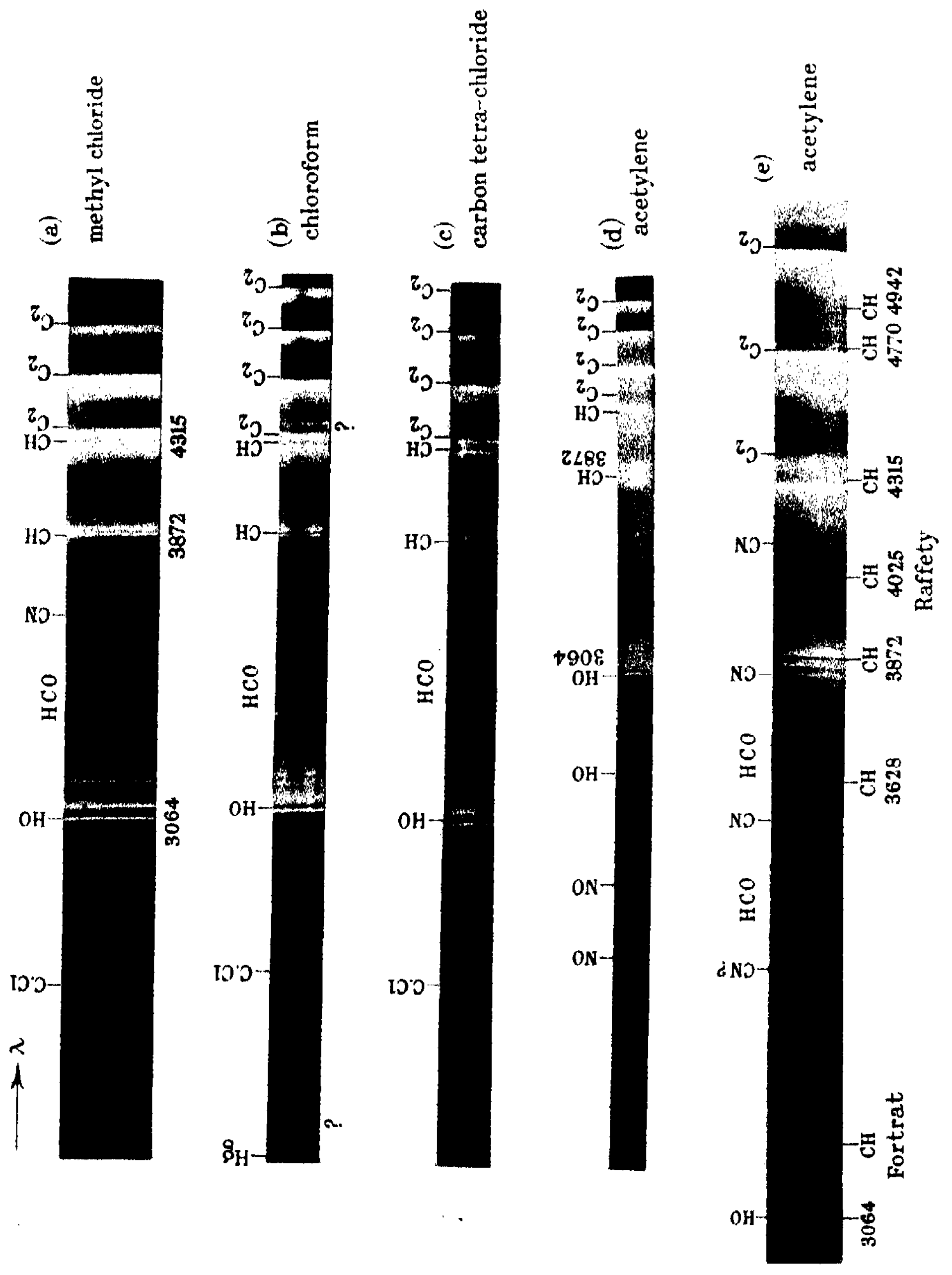
(a) methyl chloride
(b) chloroform
(c) carbon tetra-chloride
(d) acetylene
(e) acetylene
C2
CH
CN
HCO
OH
C.Cl
NO
CN?
Hg
?
4315
3872
3064
CH 4770
CH 4942
CH 4315
CH 4025
CH 3872
CH 3628
Raffety
CH Fortrat
λ

The spectrum shows the C_2 and CH bands and also the Balmer lines of hydrogen; the latter are, however, due to stray light from the brilliant red colour of the main discharge.

One of the authors is extremely thankful to Professor K. Bonhoeffer, Director of the Physikalisch Chemisches Institut, Leipzig, for his kind invitation to come and work in the Institute. Both the authors are grateful to him and Professor W. Jost for their kind interest in the investigation.

REFERENCES

Bonhoeffer 1936 *Z. Electrochem.* **42**, 455.
Bonhoeffer and Harteck 1928 *Z. phys. Chem.* A, **139**, 64.
Eméleus 1926 *J. Chem. Soc.* **128**, 2948.
Fowler and Pearse 1935 *Proc. Roy. Soc.* A, **152**, 359.
Grenat 1931 *C.R. Acad. Sci., Paris*, **192**, 1553.
Harteck and Kopsch 1931 *Z. phys. Chem.* B, **12**, 327.
Jevons 1932 *Report on band spectra*, p. 225.
Raffety 1916 *Phil. Mag.* **32**, 556.

A spectroscopic investigation of hydrocarbon flames

By W. M. Vaidya

University College, Rangoon

(*Communicated by M. N. Saha, F.R.S.—Received* 15 *May* 1940—
Revised 23 *November* 1940)

[Plates 8–10]

Spectra of flames of the three principal hydrocarbons—methane, ethylene and acetylene—and of compounds found as intermediate products in the chemical studies of their combustion, namely, methyl alcohol, formaldehyde, formic acid, and acetaldehyde, have been examined. Owing to the universal interest of the Bunsen flame and the Méker burner, their spectra are also included. Spectra of other flames, useful for comparative purposes, such as ether, ethyl alcohol, etc., are also described.

Using a flame separator, independent observations of the outer and inner cones were made in many cases. It has been found that the outer cones give a spectrum identical with the CO flame spectrum, and the inner cones give in general C_2, CH, HO and the ethylene flame bands.

It is suggested that C_2 may be produced through collisions of CH. The problem of the emitter of the ethylene flame bands is also discussed. The prevalent theories of hydrocarbon combustion are then surveyed in the light of the spectroscopic observations.

INTRODUCTORY

The present investigation was undertaken a little while ago in the laboratory of the late Professor A. Fowler, in the hope that the knowledge of molecular spectra which has been obtained in recent years might assist in tracing more fully the processes of hydrocarbon combustion. Previous chemical analyses had already yielded much valuable information, but spectroscopic studies have the advantage that they give indications of the intermediate products exactly as they arise in the flames themselves. Thus, the chemical observation $C_2H_4 + O_2 \rightarrow CO + H_2O \rightarrow CO_2 + H_2O$ does not reveal the important fact that at some stage of combustion free radicals of short duration like C_2, CH, HO, etc., are to be found.

The general results are: (1) the outer cones of many flames give a spectrum identical with the CO flame spectrum, (2) a number of other sources of the ethylene flame bands* have been found, which in some cases give the *B* bands (ethylene flame bands) without any modification of the flame such as was necessary for their appearance in the ethylene flame, and (3) the chemical composition seems to have modifying influence on the observed spectra.

---

* Since the name 'ethylene flame bands' tends to convey the wrong impression that the faint bands designated by it are something characteristic of the ethylene flame, it is proposed that they may more appropriately be called 'hydrocarbon flame

The spectra can be conveniently described under three headings: (1) spectra of coal gas, methane, ethylene and acetylene; (2) spectra of compounds found by chemists as intermediate products in the oxidation of some of the main hydrocarbons; and (3) spectra of flames useful for comparative purposes.

SPECTRA OF FLAMES OF COAL GAS, METHANE, ETHYLENE AND ACETYLENE

(1) *Coal gas.** (*a*) *The Bunsen flame.* To separate the cones a single piece of pyrex tube was mounted on a micro-burner. This tube had a short side tube which was left open to the atmosphere in the direction of the spectroscope, in order to permit observations in the ultra-violet. Under these conditions, the outer cone was pale blue, 2 cm. high, and the inner cone, about 1·5 cm. high, was bluish green.

The spectrum of the outer cone (plate 8*b*) consisted of the HO bands and a weak continuous spectrum, superposed on which was an ill-defined banded structure. The latter assumed a well-defined form when the initial content of CO, which is usually mixed with coal gas to give more heat output, was removed by passing the gas through a solution of cuprous chloride in hydrochloric acid. The bands could then be recognized as identical with the CO flame bands† (plate 8*a*). The spectrum differed from that of the hydrogen flame (plate 8*c*) in that the latter gave a very weak continuous spectrum in the same region, stronger HO bands but of course no CO flame bands.

The spectrum of the inner cone consists of the Swan bands, the two CH bands and the HO bands which extend far into the ultra-violet. The *A*

---

bands'. This will accord better with the observed fact that they occur extensively in hydrocarbon flames and are not confined to the ethylene flame only, though they appear with high intensity in that flame. In the remaining sections, the original name 'ethylene flame bands' has therefore been replaced by 'hydrocarbon flame bands'.

* The composition of the gas with which the experiments were carried out consisted mainly of H_2 40 %, CO 14 %, CH_4 23 %, with small quantities of O_2, N_2, CO_2 and C_2H_4. The analysis was kindly supplied by the Gas, Light and Coke Co., London.

† It is difficult to illustrate this point from the plate because the spectra are very feeble. The effect is, however, clear on the negatives.

group of the hydrocarbon flame bands (HCO) is also present, faint and diffuse (plate 8*e*).

(*b*) *The Méker burner*. With less air, the inner cone was greenish, the C_2 and CH bands were strong, HO moderate and HCO weak (plate 8*f*). With more air, C_2 weakened as well as CH, HO became slightly stronger and HCO practically disappeared. In addition, a continuous spectrum became visible (plate 8*g*).

(*c*) *Oxy-coal gas*. In a two-way blowpipe, with oxygen blown through, the flame was elongated and the boundary between the two cones was not very distinct. The cones, however, were very bright and the exposure time correspondingly short. The outer cone gave a spectrum with the ill-defined banded structure of the CO flame bands. In the inner cone, the HO bands were very strong, CH moderate, C_2 very weak, and the HCO diminished considerably in intensity. A continuous spectrum was also present (plate 8*h*). These intensity changes are closely similar to those observed in the Méker burner with increased air supply.

In the above-mentioned blowpipe, coal gas did not mix with oxygen until the two met at the orifice. In a mixed jet blowpipe, where the gases mix beforehand, C_2 and CH are strong, HO moderate, HCO faint and the continuous spectrum is absent (plate 8*i*). Thus, the difference in the flames from the two forms of blowpipe consists mainly in the strengthening of the HO bands, weakening of the C_2 bands and the appearance of a continuous spectrum in a two-way blowpipe.

(2) *Methane*. Methane ordinarily burns with a smoky flame, but with an adequate supply of air the flame becomes non-luminous. The cones were separated as in the ethylene flame (Vaidya 1934). The outer cone was pale blue about 4 cm. high and the inner cone was bluish green and 2 cm. high.

The spectra of both the cones were weak compared with those of the Bunsen flame. The outer cone gave a spectrum similar to that of the Bunsen flame, namely, CO flame bands and HO bands, while the spectrum of the inner cone included C_2, CH and HO bands. The hydrocarbon flame bands of group *A* were faint (plate 9*c*). Since some doubts have been expressed (Barrow, Pearson and Purcell 1939) as to whether these faint bands are the hydrocarbon flame bands, it can be definitely stated that the faint bands in the methane flame are identical with the hydrocarbon flame bands. It may be pointed out also that the same authors wrongly identify the bands in the 'cool flame' spectra with those reported by Rassweiler and Withrow as occurring in the Bunsen flame, which, as we have seen, are really the hydrocarbon flame bands.

(3) *Ethylene.* The spectrum of the inner cone has been adequately described before. In the outer cone are found the CO flame bands and the HO bands. The C_2 and CH bands also appear very faintly but they would disappear if the experimental conditions could be better controlled.

(4) *Acetylene.* With the flame separator acetylene readily separated but the cones were intensely white, giving a continuous spectrum only. The flame separator being therefore of no use, the gas was burnt in a mixed jet with compressed air. In the absence of air the gas burnt with a smoky flame giving a copious deposit of carbon, but with an increase in the air supply the flame became non-luminous giving a bright greenish inner cone.

The spectrum of the outer cone was similar to that of coal gas, methane and ethylene, namely, consisting of the CO flame bands and the HO bands (plate 8*d*).

The inner cone gave the HO, C_2 and CH bands strongly. It also gave some of the faint CH bands—the Raffety bands, the Fortrat bands and the λ 3628 band. The hydrocarbon flame bands of group *A* were faint and diffuse (plate 10*e*).

Besides the above bands, the inner cone showed the violet system of CN and the γ bands of NO. The occurrence of CN and NO is possibly associated with the high temperature of the flame (plate 10*d*).

Spectra of flames of intermediate products

(1) *Formaldehyde.* White powder of paraformaldehyde was placed in a wide pyrex tube, one end of which was drawn to a narrow neck and the other closed by a stopper. The tube was clamped in a nearly vertical position and, on heating, a copious supply of formaldehyde vapour was obtained which was ignited at the narrow end.

The flame has no luminous outer cone—it is intense blue resembling the CO flame. The spectrum consists of the CO flame bands and the HO bands only. The C_2, CH and HCO bands are absent (plate 9*a*).

(2) *Formic acid.* Formic acid was heated in the same tube as was used in formaldehyde. The temperature of the liquid had to be kept near but not at the boiling-point. Whenever boiling commenced the liquid spurted out violently and the flame was extinguished. The vapour was lighted at the narrow end and it burnt with a blue flame which could be kept steady by a careful regulation of the temperature of the pyrex tube. The flame was not so bright as the formaldehyde flame.

The spectrum was the same as that of formaldehyde, namely, the CO flame spectrum, though much weaker.

(3) *Methyl alcohol.* Methyl alcohol burning in a spirit lamp gave a blue flame without a luminous zone, the entire flame being deep blue. In the spectrum C_2 and HCO bands were absent. The CO flame bands were prominent. The HO bands were also present and the CH band at λ 4315 was rather faint (plate 9*b*).

(4) *Acetaldehyde.* Acetaldehyde is a liquid of low boiling-point which burns readily. The spectrum was examined under conditions identical with those in formaldehyde by burning the liquid in the same pyrex tube. Unlike the formaldehyde flame, the acetaldehyde has a luminous outer cone. The inner cone gives the C_2, CH and HO bands strongly and the *A* group of HCO bands faintly.

The inner cone was also examined when acetaldehyde was burnt in a micro-burner. A suitable mixture was obtained by bubbling a gentle current of air through acetaldehyde. The spectrum of the inner cone was similar to that obtained in the wide tube except that the continuous background was of greater intensity (plate 9*f*).

Spectra of flames for comparison

(1) *Methyl chloride.* This flame was studied in order to find out what change, if any, might be shown in the spectrum by the substitution of Cl for OH in methyl alcohol. To produce the flame, the vapour of methyl chloride obtained from a gas cylinder was passed over a dehydrating agent —fused lime—and ignited in a micro-burner, whose brass tube had to be heated initially in order to start the combustion. To make the flame steady a slow stream of oxygen was directed on the flame. The inner cone was deep green.

The spectrum is distinctly different from that of methyl alcohol in that the methyl chloride flame has C_2 and *A* group of HCO bands, both of which are absent from methyl alcohol. The CO flame bands found in methyl alcohol are here absent. As in methyl alcohol, the HO and CH bands are present, the latter with greater intensity. The spectrum also includes the CN bands faintly at λ 3883, λ 3580, and λ 3360, and the group of bands ascribed to CCl (Asundi and Karim 1937) are also found (plate 10*a*).

(2) *Chloroform and carbon tetrachloride.* The flames were obtained by using the multiple jet burner. Through one series of jets flowed hydrogen and through the other was blown air charged with the vapours of the liquid under examination. To provide an adequate supply of vapour the liquids were heated to 50° C.

The spectra of both the flames include the C_2, CH, HO and *A* and *B* bands of HCO. In the ultra-violet the CCl bands can be recognized (plate 10*b*, *c*).

(3) *Ethyl alcohol.* The flame was produced in two different ways: (1) a spirit lamp, and (2) a micro-burner. In the spirit lamp, the flame had a wide blue inner cone surrounding the wick and it gave the C_2, CH, HO and *A* and *B* bands of HCO with moderate intensity. The outer cone was luminous.

To obtain alcohol vapour suitable for combustion in a micro-burner the liquid was heated in a flask to 60° C. A rapid current of air was bubbled through the hot alcohol, and the air charged with the vapour was led by a connecting brass tube to the micro-burner. To prevent condensation, the brass tube and the base of the burner were kept warm. The flame was separated as in coal gas.

The CO flame bands and the HO bands constituted the spectrum of the pale blue outer cone, while the greenish blue inner cone gave the C_2, CH, HO and *A* and *B* HCO bands as in the spirit lamp.

(4) *Ether.* In an ordinary spirit lamp, ether has a luminous outer cone which gives a continuous spectrum, while the blue inner zone surrounding the wick yields the C_2, CH, and HO bands. The HCO bands of groups *A* and *B* occur with an intensity and sharpness greater than obtainable in any of the previous flames except ethylene (plate 9*e*).

For separating the cones, it was necessary to bubble air under small pressure through ether, which was surrounded by ice. Without ice, due to the volatile nature of ether, too rich a mixture was obtained, and this was unsuitable for separation of cones. The pale blue outer cone gave the CO flame bands and the HO bands. The spectrum of the inner cone was identical with that obtained in the spirit lamp.

The spectrum of the inner cone of ether thus described has nothing in common with the 'cool flame' spectrum of ether which has now been identified with the fluorescent spectrum of formaldehyde.

It is convenient to collect here (table 1) the above observations together with those given in the preceding paper, for it then becomes possible to draw certain conclusions as to the process of hydrocarbon combustion from the work viewed as a whole.

TABLE 1

Flame	C_2	CH	HO	Hydrocarbon flame bands		CO flame bands	Remarks	Exposure hr.	Plate used	Plate no.
				A	*B*					
Flames in air										
Coal gas:										
Bunsen flame	4	5	4	0·8	—	—	—	5	Special Rapid Panchromatic (Ilford)	2*e*
Méker burner (less air)	4	5	4	0·8	—	—	—	4		2*f*
Méker burner (more air)	1	3	4·5	0·1	—	—	Continuous spectrum	4		2*g*
O_2, blown through	1	4	5	0·1	—	—	Continuous spectrum	2		2*h*
O_2, mixed jet	4	5	3	1	—	—	—	2		2*i*
CH_4	2	4	2·5	0·5	—	—	—	4		3*c*
C_2H_4	3	5	3·5	2·5	—	—	—	4		3*d*
C_2H_2	5	5	4	0·7	—	—	CN, NO	1		4*d*, 4*e*
HCHO	—	—	3	—	—	3	—	2	Ordinary	3*a*
HCOOH	—	—	1·5	—	—	1	—	2	Ordinary	—
CH_3OH	—	2	3	—	—	3	—	3	Monarch	3*b*
CH_3CHO	3	5	3·5	0·5	—	—	—	3	Golden iso-zenith	3*f*
CH_3Cl	4	5	3·5	0·5	—	—	CN, CCl	3	Monarch	4*a*
$CHCl_3$, CCl_4	4	5	3·5	1	1	—	CCl	4	Special Rapid Panchromatic (Ilford)	4*c*, 4*b*
Ether	4·5	5	4	2	2	—	—	5	Golden iso-zenith	3*e*
Ethyl alcohol	4	5	4	1	1	—	—	5	Golden iso-zenith	—
Flames in atomic oxygen										
C_2H_4	2	3	4	0·5	—	—	—	1	Agfa Isochrome	1*c*
C_2H_2	4	5	3	2	2	—	—	2		1*e*
C_6H_6	4	5	4	2	2	—	—	1		1*b*
CH_3OH	?	1	4	—	—	—	Cool flame bands	1		1*d*
HCHO	—	—	4	—	—	—	—	½		—
Flame in atomic hydrogen										
C_6H_6	4	3	—	—	—	—	—	2		1*a*

Note. Different plates were used having regard to (i) the experimental difficulties in maintaining flames for a length of time, and (ii) the spectral region which was being explored.

The figures in columns 2–6 give the relative intensities.

DISCUSSION

The discussion can be conveniently divided into three sections: (1) mode of production of different radicals, (2) thermal decompositions, and (3) the nature of hydrocarbon combustion. We shall first consider the mechanism of production of the C_2 radical. For this purpose, it is relevant to consider evidence from different sources in which the C-C bands appear.

In the experiments of Peters and Wagner (1931), on the formation of acetylene in the glow discharge, it was found that as the energy input and pressure were increased the CH bands appeared stronger until at a well-defined stage the conductivity of the gas increased enormously and the Swan bands appeared so strongly that the colour of the discharge changed abruptly from blue to yellow. The reactions in the glow discharge were represented as

$$\begin{tikzcd}
CH_4 \arrow[r] & CH \arrow[r, leftrightarrow] \arrow[d, leftrightarrow] & C_2H_2 \arrow[d, leftrightarrow] \\
 & C^+ \arrow[r, dash] \arrow[d] & C\equiv C- \arrow[dl] \\
 & C\ (\mathrm{solid}) &
\end{tikzcd}$$

In the flames of hydrocarbons burning in atomic hydrogen, Bonhoeffer and Harteck (1928) observed that a pale blue cone appeared first giving the CH band, and on increasing the quantity of hydrocarbon the colour changed to green yielding the Swan bands. For the production of the Swan bands it was suggested that of the two possibilities,

$$\text{(i)}\ 2CH = C_2H_2 = C_2 + H_2, \quad \text{(ii)}\ 2CH = C_2 + H_2,$$

the former was more likely.

Examining data from hydrocarbon flames burning in air, we find that in the case of methane (Guénault 1935) the intensity of the C-C bands increases as the relative proportion of oxygen decreases. Similar conditions for the favourable production of C-C bands were found to hold good for the ethylene flame (Smith 1940).

These results suggest the possibility of C-C being produced according to either of the two equations of Bonhoeffer and Harteck.

As is well known, the Swan bands show considerable intensity changes in the Méker burner on varying the air supply. With air holes fully open, the C-C bands and the CH bands diminish in intensity, the HCO bands practically disappear, whereas the HO bands become stronger. In addition, a continuous spectrum appears. Exactly similar intensity changes are observed in a two-way blowpipe with oxygen blown through.

The chemical equations which have been suggested to account for the intensity changes in the Méker burner are those given by Bonhoeffer and Haber (1928):

$$C_2 + OH = CH + CO, \quad CH + OH = CO + H_2.$$

The continuous spectrum which appeared in both the above cases may be due to CO produced according to these equations, which receive further support if we compare the spectra of methane and methyl alcohol, where we find that the introduction of an OH group has altered the spectrum considerably. With the presence of OH, the Swan bands have disappeared or at least very considerably weakened in methyl alcohol, whereas they appear with some intensity in methane. Due to the same cause, the CO flame bands occurred prominently in the methyl alcohol flame. These changes are possibly due to chemical reactions expressed by the above equations.

The emitter of the hydrocarbon flame bands

Since the author's original suggestion of HCO as the emitter, other observers have proposed HCHO (Kondratjew 1936), CH_2 (Bell 1937) and the isomeric form of formaldehyde, HC-OH (Smith 1940). Kondratjew's proposal arose out of a misunderstanding which has since been cleared up by Withrow and Rassweiler (1938) and by the author (Vaidya 1939).

An emitter like CH_2 seems unlikely because the CH_2 frequencies—$\nu_1 = 2970$ cm.$^{-1}$, $\nu_2 = 1444$ cm.$^{-1}$, and $\nu_3 = 3000$ cm.$^{-1}$—as determined from the Raman spectra and the infra-red spectra and confirmed by the theoretical calculations of Penney and Sutherland (1936) do not appear to be related to the vibrational frequency, $\omega_e'' = 1971$ cm.$^{-1}$, of the hydrocarbon flame bands. Whether the emitter is HCO or HC-OH it is difficult to decide with the evidence at present available. If HC-OH should prove to be the emitter, the flame of methyl alcohol would be of special interest, because it has been reported (Guénault 1936, 1937) that such a flame (rich mixture) yields the 'cool flame' bands and also the hydrocarbon flame bands together, which means that the two forms of formaldehyde are existing together in this flame.

Attention may be drawn to the fact that Withrow and Rassweiler (1938) have identified the hydrocarbon flame bands in the spectrum of the internal combustion engine, when run on benzene, petrol or iso-octane.

Since it is generally believed that thermal decompositions play a prominent part in flames, the results obtained from spectroscopic observations are compared below with what is known from chemical analyses.

Thermal decompositions

Formaldehyde. The vapour of formaldehyde has been found to decompose into H_2 and CO between the temperatures of 400 and 1125° C. The same conclusions can be drawn from the experiments of Kirkbride and Norrish (1931) who showed that on ultra-violet irradiation of formaldehyde vapour H_2 and CO were obtained as if the decomposition took place according to the equation

$$H_2CO = H_2 + CO.$$

The spectrum of formaldehyde points to a similar result because it consists of the CO flame bands and the HO bands only. A rich mixture, however, yields, in addition, traces of C_2 and CH (Guénault 1937), which suggests that we should regard the major part only as decomposing according to the above equation.

Methyl alcohol. Bone and Davies (1904), from their experiments on the thermal decomposition of methyl alcohol between 650 and 1000° C, are of the opinion that it takes place in three different ways:

$$\text{(i)}\ CH_3OH = CH_2 + H_2O,$$

$$\text{(ii)}\ CH_3OH \rightarrow \begin{cases} HCHO + H_2, \\ CO + H_2 + H_2, \end{cases}$$

and (iii) the formation of CH_4 by the coalescing of CH_2 from (i) with H_2 from (ii).

The second method was found to be very prominent at temperatures about 1000° C.

With regard to (i) the decomposition does not seem to stop at CH_2 but appears to go further, giving CH which would account for the CH band in the spectrum. The spectroscopic evidence is in favour of (ii) because the spectrum of the flame has the CO flame bands and the HO bands. The existence of formaldehyde in the thermal decomposition products of methyl alcohol can also be concluded from the observations of Guénault (1936, 1937) who found that rich mixtures of methyl alcohol gave the 'cool flame' bands which are known to be due to formaldehyde. Perhaps the thermal decomposition of methyl alcohol from a spectroscopic point of view might be represented by

$$\text{(i)}\ CH_3OH = CH + H_2 + OH,$$

$$\text{(ii)}\ CH_3OH \rightarrow \begin{cases} HCHO + H_2, \\ CO + 2H_2. \end{cases}$$

As the molecule becomes heavier, it becomes difficult to deduce its thermal decomposition from spectroscopic data.

Mechanism of hydrocarbon combustion

Let us now consider the three main theories of hydrocarbon combustion in relation to these spectroscopic studies. In interpreting spectroscopic data a good deal of caution is necessary because of the possibility that although some of the radicals may actually be present they may escape detection by means of their emission spectra, either because the radicals are too few in number or because such spectra are not excited. Moreover, detailed spectroscopic observations similar to those on the chemical side are not available. There is also the uncertainty about the emitter of the hydrocarbon flame bands which occur so extensively in hydrocarbon flames. Nevertheless, certain broad facts stand out, and it seems worth while discussing them in an attempt to throw additional light on the process of hydrocarbon combustion.

The three theories are based upon material derived from extensive studies of slow and explosive combustion and may not apply directly to flames where thermal decomposition begins at very early stages. It is, however, possible that the product of an initial encounter of an oxygen molecule may be the same in all cases (Bone 1932).

The principal features of the three theories can be best presented by considering the case of a simple hydrocarbon such as methane.

(A) According to the hydroxylation theory, the course of oxidation of methane has been represented as

(*a*) *Slow combustion:*

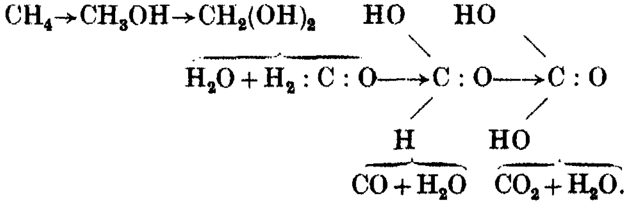

$$\begin{array}{l} CH_4 \rightarrow CH_3OH \rightarrow CH_2(OH)_2 \\ \overbrace{H_2O + H_2}:C:O \longrightarrow \overset{HO}{\underset{H}{C}}:O \longrightarrow \overset{HO}{\underset{HO}{C}}:O \\ \qquad\qquad\qquad\qquad \underbrace{}_{CO + H_2O} \qquad \underbrace{}_{CO_2 + H_2O.} \end{array}$$

(*b*) *Explosive combustion:*

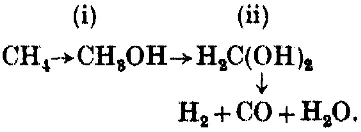

$$\begin{array}{l} \qquad\quad (i) \qquad\qquad (ii) \\ CH_4 \rightarrow CH_3OH \rightarrow H_2C(OH)_2 \\ \qquad\qquad\qquad\qquad \downarrow \\ \qquad\qquad\qquad H_2 + CO + H_2O. \end{array}$$

It is claimed that in flames the course of oxidation can be represented by the scheme (*b*) with the difference that stage (ii) is probably not reached, the thermal decomposition of CH_3OH occurring immediately after stage (i).

(B) The peroxidation theory maintains that the immediate product of oxidation is not a hydroxy compound but a peroxide formed by the direct incorporation of oxygen molecule in hydrocarbon molecule:

(i)
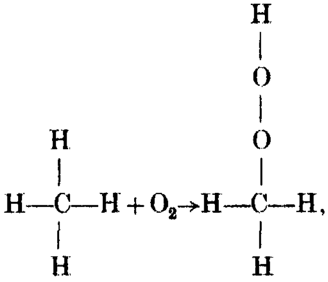

$$\text{H}-\overset{\text{H}}{\underset{\text{H}}{\overset{|}{\underset{|}{\text{C}}}}}-\text{H}+\text{O}_2\rightarrow\text{H}-\overset{\text{H}-\text{O}-\text{O}}{\underset{\text{H}}{\overset{|}{\underset{|}{\text{C}}}}}-\text{H},$$

$$\text{(ii)}\quad CH_3OOH + CH_4 = 2(CH_3OH),$$

$$\text{(iii)}\quad CH_3OOH = HCHO + H_2O.$$

(C) Norrish (1935) has recently suggested that the oxidation of methane may proceed through a chain mechanism involving a hydrocarbon radical and an oxygen atom, thus,

$$CH_4 + O = CH_2 + H_2O + 48\ \text{kcal.},$$
$$CH_2 + O_2 = HCHO + O + 15\ \text{kcal.}$$

The chain-breaking processes are

$$O + CH_4 + X = CH_3OH + X' + 88\ \text{kcal.},$$
$$O + \text{surface} = \tfrac{1}{2}O_2.$$

The oxygen atom required to initiate the chain is supposed to come from formaldehyde. Thus,

$$CH_4 + O_2 \xrightarrow{\text{surface}} HCHO + H_2O,$$
$$HCHO + O_2 \longrightarrow (H_2CO_3) \longrightarrow HCOOH + O.$$

Since, according to the hydroxylation theory, CH_3OH is the immediate product of oxidation of CH_4, it is to be expected that the spectrum of methane and that of methyl alcohol burning in a deficient supply of oxygen will be closely similar. However, we find important differences existing between their spectra. The chief dissimilarities are as follows:

(1) C_2 and CH are both strong in CH_4, but very weak in CH_3OH, particularly C_2 (table 1, Guénault 1935, 1936; Bell 1937).

(2) The hydrocarbon flame bands have fair intensity in CH_4, but are feeble in CH_3OH (Guénault 1935, 1936; Bell 1937).

(3) The CO flame bands are weak in CH_4 but more prominent in CH_3OH.

(4) 'Cool flame' bands have not yet been detected in CH_4, but they have been observed in methyl alcohol (Guénault 1937).

If methyl alcohol were an immediate product of oxidation of methane, then it would appear somewhat unlikely that so many differences between the spectra of the two would exist. It appears more probable, as suggested by Guénault (1936), that there is another compound formed between CH_4 and CH_3OH.

The possibility of formaldehyde being the immediate oxidation product as assumed by the atomic chain theory appears less likely since the spectrum of formaldehyde consists normally of the CO flame bands and HO bands only, and this type of spectrum is more likely to appear at the end of the combustion process, as the spectra of outer cones, where combustion is complete, indicate.

Further, it may be pointed out that methane and atomic oxygen do not give any flame. Objection to the assumption of an oxygen atom propagating the chain has been taken by Ubbelohde (1935) and von Elbe and Lewis (1937).

It is not to be expected that in the present stage of this research, a complete answer to all the complicated problems arising in hydrocarbon combustion can be given, but the results achieved so far sufficiently indicate the importance of the spectroscopic approach to the study of hydrocarbon combustion.

In conclusion the author wishes to express his sense of deep gratitude to the late Professor A. Fowler, F.R.S., at whose suggestion the problem was undertaken and in whose laboratory at the Imperial College, London, most of the flames were studied. The author wishes to thank also Dr J. West, D.Sc., F.Inst.P., Professor of Physics, University of Rangoon, for providing further facilities.

REFERENCES

Asundi and Karim 1937 *Proc. Indian Acad. Sci.* **6**, 328.
Barrow, Pearson and Purcell 1939 *Trans. Faraday Soc.* **35**, 882.
Bell 1937 *Proc. Roy. Soc.* A, **158**, 429.
Bone 1932 *Proc. Roy. Soc.* A, **137**, 243.
Bone and Davies 1904 *Trans. Chem. Soc.* **105**, 1691.
Bonhoeffer and Haber 1928 *Z. phys. Chem.* A, **137**, 263.
Bonhoeffer and Harteck 1928 *Z. phys. Chem.* A, **139**, 64.
von Elbe and Lewis 1937 *Chem. Rev.* **21**, 322.

Guénault 1934 *Ann. Rep. Safety in Mines Res. Bd*, **13**, 66.
Guénault 1935 *Ann. Rep. Safety in Mines Res. Bd*, **14**, 68.
Guénault 1936 *Ann. Rep. Safety in Mines Res. Bd*, **15**, 59.
Guénault 1937 *Ann. Rep. Safety in Mines Res. Bd*, **16**, 64.
Kirkbride and Norrish 1931 *Trans. Faraday Soc.* **27**, 404.
Kondratjew 1936 *Acta Phys. Chim.* **4**, 556.
Norrish 1935 *Proc. Roy. Soc.* A, **150**, 36.
Penney and Sutherland 1936 *Proc. Roy. Soc.* A, **156**, 665.
Peters and Wagner 1931 *Z. phys. Chem.* A, **153**, 183.
Smith 1940 *Proc. Roy. Soc.* A, **174**, 110.
Ubbelohde 1935 *Proc. Roy. Soc.* A, **152**, 354.
Vaidya 1934 *Proc. Roy. Soc.* A, **147**, 513.
Vaidya 1939 *J. Appl. Phys.* **10**, 26.
Withrow and Rassweiler 1938 *J. Appl. Phys.* **9**, 365.

DESCRIPTION OF PLATES 8–10

All the spectra of plates 8–10, excepting 10*e*, were taken with the Hilger's small quartz spectrograph (E 31); 10*e* was taken with an E 2 spectrograph.

Chemical equilibria of thermal associations

By Albert Wassermann

Department of Chemical Technology, Imperial College

(*Communicated by A. C. G. Egerton, Sec. R.S.—Received* 13 *January* 1941)

The equilibrium constant, K, of an association can be represented by $K = \omega\rho e^{-\Delta E_0/RT}$ or by $K = \omega\rho' e^{-\Delta E_0'/RT}$, where ΔE_0 is the energy difference between the product, at rest, and the two reactants both at rest and at infinite separation, and $\Delta E_0'$ is deduced from the heat change under the assumption that the vibrational heat capacity of the initial state agrees with that of the final state of the reaction; the factor ω as defined by the above equations is the contribution of the rigid molecules, and can be calculated by taking into account the mass and the shape of the various participants of an equilibrium and the parameters ρ and ρ' are the contributions of the internal vibrations of the reactants and of the product molecules. In this paper the non-exponential ω factors and the energy changes, $\Delta E_0'$, relating to five gaseous thermal associations are computed and by substituting these quantities and the experimental equilibrium constants in the second equation mentioned above the vibrational contributions ρ' could be deduced. In one equilibrium it was also possible to estimate the energy change, ΔE_0, and the vibrational contribution, ρ, and the relationship between the parameters ρ' and ρ is discussed. Further, an attempt is made to give a qualitative explanation for the dependence of the ρ' values on the chemical constitution of the participants of the various equilibria and it is pointed out that all the vibrational contributions are larger than unity, partly because the number of the vibrational modes increases on association, and partly because the reactants are stiffer than the associated molecules in which spectroscopically inactive vibrational modes of relatively low frequency can occur.

Introduction

In this communication the following gaseous thermal associations of the type $a + b = c$ are discussed:

hydrogen + ethylene = ethane (I)

hydrochloric acid + isobutene = *tert.*-butylchloride (II)

hydrobromic acid + isobutene = *tert.*-butylbromide (III)

acrolein + *cyclo*pentadiene = endomethylenetetrahydrobenzaldehyde (IV)

2-*cyclo*pentadiene = dicyclopentadiene (V)

The equilibrium constants can be represented by

$$K = C_c/C_aC_b = We^{-\Delta E_0/RT}, \tag{1}$$

where C_a, C_b, C_c are the concentrations in gmol./l., the subscripts relating here and below to the reactants and to the associated molecules respectively; ΔE_0, the work required to split the product at rest into the reactants both at rest and at infinite separation, can be estimated from

$$\Delta E_0 = \Delta H - \int_0^T \Delta C_p dT, \tag{2}$$

ΔH being the heat change and C_p the molecular heat capacity at constant pressure. Another representation of the equilibrium constant is

$$K = W'e^{-\Delta E_0'/RT}, \tag{3}$$

where $\Delta E_0'$ is connected with the heat change by

$$\Delta E_0' = \Delta H + 3{\cdot}5RT \quad \text{(for equilibria I–III)}, \tag{4}$$

$$\Delta E_0' = \Delta H + 4RT \quad \text{(for equilibria IV–V)}. \tag{5}$$

It will be seen that ΔE_0 and $\Delta E_0'$ would equal each other if the vibrational heat capacity of the initial state agreed with that of the final state of the chemical reaction.

The parameters W and W' in (1) and (3) are given by

$$W = \frac{N}{1000}\frac{\lambda_c}{\lambda_a\lambda_b}\frac{r_c}{r_a r_b}\frac{\sigma_a\sigma_b}{\sigma_c}\rho = \omega\rho, \tag{6}$$

$$W' = \omega\rho', \tag{7}$$

where λ is the translational partition function (without volume factor), r is the rotational partition function, σ is the external symmetry number, and ρ the ratio of the vibrational partition functions, q, is defined by

$$\rho = q_c/q_a q_b, \tag{8}$$

each partition function λ, r or q referring to an energy zero which is that of the lowest state of the relevant degree of freedom.

There is the possibility that in ethane, isobutene, *tert.*-butylchloride, *tert.*-butylbromide, acrolein and endomethylenetetrahydrobenzaldehyde a polyatomic part of the molecule rotates freely with respect to another polyatomic part of the molecule. It is known, however, that under the conditions of the equilibrium and heat measurements the internal rotation of ethane is far from being free; this result strongly suggests that a situation similar to that of ethane exists in the other molecules and, therefore, it is assumed for the following discussion that the participants of all the equilibria are so stiff that internal rotations about single bonds can be treated as torsional harmonic oscillations of low frequency. It is possible that further experiments will prove that some modes can best be represented by free or restricted internal rotations; in this case the method now to be described, involving equations (4)–(7), could nevertheless be applied, provided the 'vibrational' heat capacity and the factors ρ and ρ' are defined in such a way as to include the contributions of both harmonic vibrations and internal rotations. Thus the latter contributions would have to be lumped together with the vibrational partition functions and not with the partition functions and symmetry numbers relating to the external rotations.

It would be of interest to determine both factors ρ and ρ', as defined by (6) and (7), for all five above equilibria, but this is not possible at present. The only case for which ρ and ρ' can be deduced is the reaction between hydrogen, ethylene and ethane, which has already been the subject of various discussions.* The ρ values of the other four equilibria are unknown, but it is shown in this paper that the ρ' factors of all the reactions can be calculated. These latter quantities can also be computed for a number of other associations which are not in the above list. It is intended, however, to deal with a few typical examples only, and it is not within the scope of this paper to discuss all the known thermal associations.

The following discussion relates, inter alia, to torsional vibrations of simple open-chain compounds and of complex cyclic molecules. The first problem can admittedly be treated in a more satisfactory way by using the results of specific heat and spectroscopic measurements. In dealing with complex cyclic molecules, however, the present method can be useful, since in these cases an assignment of vibrational modes is very difficult or impossible and the application of the usual methods for the determination of specific heats is sometimes prevented, because under the conditions of the experimental measurements decomposition accompanied by consecutive reactions can take place.

RESULTS OF HEAT AND EQUILIBRIUM MEASUREMENTS

Numerical values of the heat and energy changes, of the equilibrium constants and of the non-exponential W and W' factors are listed below. The measurements from which these data were deduced have been carried out by a number of workers whose names are given (in alphabetical order) in the first set of references. The constants of equilibrium I have been determined at eleven temperatures in the range 673–973° abs.; the equilibrium constant in the second column of table 1 is believed to be especially reliable, since at 863° abs. more measurements than at any other temperatures were carried out (cf. Teller and Topley 1935). The energy changes of reaction I are independent of the equilibrium measurements and were calculated by using the most reliable calorimetrically determined heat change and the specific heats of hydrogen, ethylene and ethane. The less accurate ΔE_0 value has been obtained by evaluating the integral in (2) by a graphical method, whereas the more accurate figure which was used for the calculation of the W factor has been computed by Guggenheim (1941).

---

* Fowler and Guggenheim (1939), Guggenheim (1941) and earlier papers referred to there.

TABLE 1. HEAT AND ENERGY CHANGES, EQUILIBRIUM CONSTANTS AND W AND W' VALUES RELATING TO FIVE GASEOUS THERMAL ASSOCIATIONS

Association ...	I	II	III	IV	V	
$-\Delta H$ (kcal.)	$32{\cdot}83 \pm 0{\cdot}05$ ($T = 355°$)	$17{\cdot}1 \pm 0{\cdot}5$ ($T = 436°$)	$18{\cdot}9 \pm 0{\cdot}5$ ($T = 453°$)	$19{\cdot}3 \pm 2{\cdot}5$ ($T = 448°$)	$18{\cdot}8 \pm 1{\cdot}3$ ($T = 353°$)	—
$-\Delta E_0$ (kcal.)	$31{\cdot}1 \pm 0{\cdot}3$ $30{\cdot}8 \pm 0{\cdot}1$	—	—	—	—	—
$-\Delta E_0'$ (kcal.)	$30{\cdot}36 \pm 0{\cdot}05$	$14{\cdot}1 \pm 0{\cdot}5$	$15{\cdot}8 \pm 0{\cdot}5$	$15{\cdot}7 \pm 2{\cdot}5$	$16{\cdot}0 \pm 1{\cdot}3$	—
$\log_{10} K$ ($K =$ l./gmol.)	$3{\cdot}462 \pm 0{\cdot}020$ ($T = 863°$)	$2{\cdot}255 \pm 0{\cdot}040$ ($T = 436°$)	$2{\cdot}591 \pm 0{\cdot}050$ ($T = 453°$)	$2{\cdot}72 \pm 0{\cdot}08$ ($T = 448°$)	$3{\cdot}97 \pm 0{\cdot}04$ ($T = 353°$)	$2{\cdot}77 \pm 0{\cdot}04$ ($T = 425°$)
$-\log_{10} W$ ($W =$ l./gmol.)	$4{\cdot}32 \pm 0{\cdot}05$ ($T = 863°$)	—	—	—	—	—
$-\log_{10} W'$ ($W =$ l./gmol.)	$4{\cdot}23 \pm 0{\cdot}03$ ($T = 863°$)	$4{\cdot}8 \pm 0{\cdot}3$ ($T = 436°$)	$5{\cdot}0 \pm 0{\cdot}3$ ($T = 453°$)	$4{\cdot}9 \pm 1{\cdot}2$ ($T = 448°$)	$6{\cdot}0 \pm 0{\cdot}8$ ($T = 353°$)	$5{\cdot}5 \pm 0{\cdot}7$ ($T = 425°$)

The data relating to the associations II–V were deduced either from equilibrium or from velocity measurements. In each case runs were made at least at six different temperatures within a range of 150°, the temperatures which are given in the columns 3–7 being the means of the lowest and highest temperatures. The least reliable heat changes and equilibrium constants relate to reaction IV; these were deduced from the velocity coefficients of the formation and decomposition of endomethylenetetrahydrobenzaldehyde, which, according to Kistiakowsky and Lacher (1936), can be represented in the following form:

$$k_{\text{formation}} = 1{\cdot}5 \times 10^{6} \exp\,(-15{,}200/RT)\,\text{l./gmol.-sec.,} \tag{9}$$

$$k_{\text{decomposition}} = 2 \times 10^{12} \exp\,(-33{,}600/RT)\,\text{sec.}^{-1}. \tag{10}$$

Harkness, Kistiakowsky and Mears (1937) and Kistiakowsky and Ransom (1939) pointed out that Lacher's kinetic measurements of the decomposition reaction were possibly inaccurate, and the latter authors suggested the following expression:

$$k_{\text{decomposition}} = 10^{15} \exp\left(-39{,}700/RT\right) \text{sec.}^{-1}. \tag{11}$$

The decomposition of endomethylenetetrahydrobenzaldehyde has been reinvestigated (Wassermann, unpublished experiments) and it has been found that the velocity coefficient is given by

$$k_{\text{decomposition}} = 10^{12\pm1} \exp\{(-34{,}500 \pm 15{,}000)/RT\} \text{sec.}^{-1}, \tag{12}$$

which is in agreement with (10) and shows that (11) is incorrect. The values in the fifth column of table 1 have, therefore, been deduced from (9) and (10), and it is believed that the inaccuracies listed above account for the experimental errors. The non-exponential factors W and W' in the lines 9 and 11 of table 1 were obtained by substituting in (1) and (3) the relevant data of lines 5, 6 and 7.

PARTITION FUNCTIONS AND SYMMETRY NUMBERS

The translational partition function (without volume factor) and the rotational partition function are given by*

$$\lambda = (2\pi\Sigma mkT)^{\frac{3}{2}}/h^3, \tag{13}$$

$$r = (8\pi^2 i'kT)/h^2 \quad \text{(diatomic molecules)}, \tag{14}$$

$$r = \{8\pi^2(8\pi^3 i'i''i''')^{\frac{1}{2}}(kT)^{\frac{3}{2}}\}/h^3 \quad \text{(non-linear polyatomic molecules)}, \tag{15}$$

where Σm is the mass of the molecules and i', i'', i''' are the principal moments of inertia. Numerical values of these latter quantities, of the symmetry numbers σ, and of the partition functions (at temperature T) are given in table 2.

The principal moments of inertia of the polyatomic molecules are the roots of the following secular equation:

$$\begin{vmatrix} \Sigma m(y^2+z^2)-i & \Sigma mxy & \Sigma mxz \\ \Sigma myx & \Sigma m(z^2+x^2)-i & \Sigma myz \\ \Sigma mxz & \Sigma myz & \Sigma m(x^2+y^2)-i \end{vmatrix} = 0, \tag{16}$$

---

* Cf. Fowler and Guggenheim (1939), where the more accurate and complete expressions of all the partition functions are given. The nuclear spin factors have been omitted in (14) and (15) because they cancel in (6) and (7). The notation of the partition functions in this paper is that suggested by Fowler and Guggenheim; it is different from the notation of Khambata and Wassermann (1939).

where m is the mass of the various atoms and x, y and z are their rectangular co-ordinates referred to the centre of gravity of the molecule as origin and with arbitrary directions. The molecules, their centre of gravity and the co-ordinates were represented by models of steel wire which were so large that x, y and z could be deduced with sufficient accuracy from measurements which were carried out by using a ruler. In constructing these models the most probable values for the bond length and angles were chosen from the available data in the literature (cf. second set of references). The models of endomethylenetetrahydrobenzaldehyde and dicyclopentadiene are shown in figure 1. Geometrical isomeres of these molecules also exist, but the equilibrium measurements relate to the molecules represented above.

TABLE 2. PRINCIPAL MOMENTS OF INERTIA, SYMMETRY NUMBERS, TRANSLATIONAL PARTITION FUNCTIONS AND ROTATIONAL PARTITION FUNCTIONS

	i'	i''	i'''			$10^{-26}\lambda$	
	(10^{39} g.cm.^{2})			σ	T (° K)	(cm.$^{-3}$)	$10^{-4}r$
Ethylene	0·57	2·8	3·3	4	863	6·76	0·40
Hydrogen	0·047	—	—	2	863	0·129	0·00102
Ethane	1·07	4·0	4·0	6	863	7·50	0·741
Hydrochloric acid	0·26	—	—	1	436	3·61	0·0028
Isobutene	11	9	19	2	436	6·87	4·4
					453	7·28	4·7
tert.-Butylchloride	14 (14)	20 (27)	37 (43)	3	436	14·6	22 (28)
Hydrobromic acid	0·33	—	—	1	453	12·6	0·0038
tert.-Butylbromide	14 (14)	44 (71)	58 (88)	3	453	27·8	40 (62)
Acrolein	32	19	12	1	448	7·18	19
*cyclo*Pentadiene	11	17	17	2	448	9·14	12
					425	8·45	11
					353	6·40	9·4
Endomethylenetetra-hydrobenzaldehyde	22	45	50	1	448	23·0	47
Dicyclopentadiene	30	43	51	1	425	23·9	52 (60)
	(42)	(43)	(51)		353	18·0	43 (45)

The moments of inertia of the participants of equilibrium I are considerably more accurate than those of the polyatomic participants of the equilibria II–V. Some of the moments of inertia and also some symmetry numbers of these latter molecules relate to particular configurations. In the case of acrolein, for instance, it is assumed that the $CH_2{=}CH$ and the 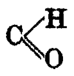 $\mathrm{C}{<}^{\mathrm{H}}_{\mathrm{O}}$ groups are situated in the same plane, while for certain other mutual orientations of these groups the moments of inertia are up to 10 % smaller than the values in table 2 and the symmetry number is 2. The moments of inertia of the *tert.*-butylhalides, of endomethylenetetrahydrobenzaldehyde and of dicyclopentadiene are least reliable; these values were calculated by using respectively the same carbon-halogen distance as in simple organic chlorine and bromine compounds, viz. 1·7 and 2·2 A and the same ring strain as in camphor.* The use of these values is admittedly only a first approximation but it is believed that the inaccuracies will not exceed 30 %. If values for the carbon-halogen distances and for the ring strain in dicyclopentadiene are used which are 30 % larger, then the moments of inertia and the rotational partition functions in brackets are obtained; the difference between the decadic logarithms of the two sets of the relevant rotational partition functions amounts only to 0·03–0·2 units, and it will be seen that such inaccuracies are smaller than those of the W' factors in the columns 3–7 of table 1.

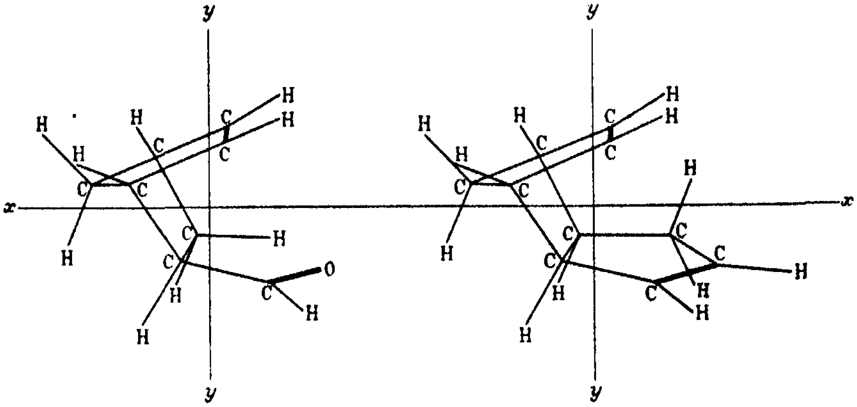

Endomethylenetetra-hydrobenzaldehyde

Dicyclopentadiene

FIGURE 1

The product of the vibrational partition functions of the reactants, $q_a \times q_b$, and the vibrational partition function of the associated molecules, q_c, can be represented by

$$q_a \times q_b = \prod_{n_a+n_b} (1-e^{-h\nu/kT})^{-1}, \tag{17}$$

$$q_c = \prod_{n_a+n_b} (1-e^{-h\nu/kT})^{-1} \times \prod_{5 \text{ or } 6} (1-e^{-h\nu/kT})^{-1}. \tag{18}$$

Here n_a+n_b and n_a+n_b+5 or n_a+n_b+6 are the numbers of the fundamental vibrational modes of the reactants and of the associated molecules respectively, and the ν's are the relevant frequencies. It will be seen that the vibrational partition functions become large if one or more of the vibrational frequencies ν become sufficiently small.

---

* For references relating to the problem of ring strain in such compounds as camphor and dicyclopentadiene see Freudenberg (1933) and Wassermann (1935).

DISCUSSION

The logarithms of the vibrational contributions ρ and ρ' in table 3 were calculated by substituting the relevant data of the tables 1 and 2 in (6) and (7), the inaccuracies including both the experimental errors of the non-exponential factors of the equilibrium constants and the effects discussed on p. 378.

TABLE 3. VIBRATIONAL CONTRIBUTIONS

Association ...	I	II	III	IV	V	
$\log_{10}\rho$	0.57 ± 0.05	—	—	—	—	
$\log_{10}\rho'$	0.68 ± 0.03	1.6 ± 0.4	1.6 ± 0.5	5.2 ± 1.7	3.3 ± 0.9	4.0 ± 0.7
temp. (° K)	863	436	453	448	353	425

In order to establish a relationship between the vibrational contributions ρ and ρ', defined by (6) and (7), it has to be taken into account that the difference between the parameters ΔE_0 and $\Delta E_0'$ is due to the fact that, in general, the vibrational energy of the associated molecules will be larger than the sum of the vibrational energies of the reactants. It follows from the Planck-Einstein formula for the energy of the harmonic oscillator and from the equations (1) and (3) that

$$\log_{10}\rho' - \log_{10}\rho = \log_{10} e \left\{\Delta\Sigma\left(\frac{h\nu/kT}{e^{h\nu/kT}-1}\right)\right\}, \tag{19}$$

where T is the temperature at which the heat change has been determined and the other symbols, on the right-hand side, have the same significance as in (17) and (18). The figures in the second column of table 3 show that the vibrational contribution, ρ', and the numerical value of (19) amount respectively to about 5 and 0.11 ± 0.08; similar small values will probably obtain, not only in the ethane equilibrium, but also in other associations involving relatively simple reactants. If the participants of an association are more complex than the difference between $\log\rho'$ and $\log\rho$ may become larger but in such cases the vibrational contribution ρ will also be relatively large. The ρ' values listed in the columns 3–7 of table 3 indicate, therefore, that the numerical values of the vibrational partition functions of the various associated molecules will exceed those of the products of the vibrational partition functions of the relevant reactants.

The vibrational contributions relating to the reactions II and III involving the addition of a diatomic molecule to the same olefine are identical and those of the chemically similar Diels-Alder reactions IV and V, in which 1 : 2–1 : 4 addition of two diene molecules takes place, are probably of the same order of magnitude. Apart from such particular cases, however, the vibrational contributions of different association reactions are not constant and eventually very large variations can occur; this is shown by the fact that the ρ' value of the ethane equilibrium is at least 400 times smaller than the vibrational contributions of the Diels-Alder reactions.

The partition function (18) relating to the product molecules of the various reactions has been split into two factors in order to make it clear that the number of the fundamental vibrational modes increases on association by 5 or 6 as the case may be. It is obvious, therefore, that quite generally the vibrational contributions ρ and ρ' will be larger than unity, but in order to understand the numerical values in table 3 it is necessary to make special assumptions relating to the 'additional' modes in the partition functions of the associated molecules. In ethylene and ethane one fundamental vibrational mode, consisting in a twisting of one half of the molecule relative to the other half, is inactive both in the Raman and in the infra red spectrum. If it is tentatively assumed that these twisting modes have the same frequencies as the lowest spectroscopically observed modes, then the vibrational contribution would amount to 2, at 863°, which is smaller than the ρ value in the second column of table 3. The discrepancy can be explained and the spectroscopically observed modes can be brought into concordance with the specific heats if it is assumed that the frequency of the twisting mode of ethane is considerably lower than that of the twisting mode of ethylene and that the frequencies of both twisting modes are lower than the lowest spectroscopically observed frequencies. These considerations are not new* and they are merely pointed out because it is very probable that in the other reactions, which are here considered, similar effects as in the ethane equilibrium, but giving rise to much larger vibrational contributions, are operative. In isobutene and acrolein there will be a twisting of CH_3 or $\mathrm{C}\begin{smallmatrix}\diagup\!\!\diagup\mathrm{O}\\ \diagdown\mathrm{H}\end{smallmatrix}$ relative to the rest of the molecule but the influence of these modes is possibly not predominant, since similar modes occur respectively in the *tert.*-butylhalides and in endomethylenetetrahydrobenzaldehyde. There are, however, other modes viz. in the *tert.*-butylhalides a twisting of the third methyl group relative to the rest of the molecule and in endomethylenetetrahydrobenzaldehyde and dicyclopentadiene, represented in figure 1, a vibration of the parts above the x-axis relative to the parts below the x-axis. The frequencies of such modes, which might be spectroscopically inactive, will be low and it is qualitatively understandable, therefore, that the vibrational contributions in the columns 3–7 of table 3 are so large. Further, the marked increase of the values in passing from reaction I to reactions II–V can be explained by the plausible assumption that some of the modes of the *tert.*-butylhalides and especially some vibrations of endomethylenetetrahydrobenzaldehyde and dicyclopentadiene are lower than the lowest mode of ethane.

---

* They can easily be deduced from the data which are given by Guggenheim (1941).

I am indebted to Professor A. C. G. Egerton, Dr E. A. Guggenheim and Professor D. M. Newitt for stimulating criticism and to the trustees of the van't Hoff Fund for a research grant.

REFERENCES

Benford, Khambata and Wassermann 1937 *Nature, Lond.*, **139**, 669.
Benford and Wassermann 1939 *J. Chem. Soc.* p. 363.
Eucken and Parts 1933 *Z. phys. Chem.* B, **120**, 184.
Frey and Huppke 1933 *Industr. Engng Chem.* **23**, 54.
Heuse 1919 *Ann. Phys., Lpz.*, **59**, 86.
Hunsmann 1938 *Z. phys. Chem.* B, **39**, 23.
Khambata and Wassermann 1939 *J. Chem. Soc.* p. 363.
Kistiakowsky and Lacher 1936 *J. Amer. Chem. Soc.* **58**, 123.
Kistiakowsky, Lacher and Stitt 1939 *J. Chem. Phys.* **7**, 289.
Kistiakowsky and Nazmi 1938 *J. Chem. Phys.* **6**, 18.
Kistiakowsky, Romeyn, Ruhoff, Smith and Vaughan 1935 *J. Amer. Chem. Soc.* **57**, 68.
Kistiakowsky and Stauffer 1937 *J. Amer. Chem. Soc.* **59**, 165.
Koenig 1938 Inaugural Dissertation, Berlin.
Pease and Durgan 1928 *J. Amer. Chem. Soc.* **50**, 2715.
Scheel and Heuse 1913 *Ann. Phys., Lpz.*, **40**, 473.
Schulze 1938 *Oel und Kohle*, No. 6, p. 113.
Travers and Hockin 1932 *Proc. Roy. Soc.* A, **136**, 1.
Travers and Pearce 1934 *J. Chem. Ind.* **53**, 322.
Vidensky and Vinikowa 1934 *J. Gen. Chem., Moscow*, **4** (46), 120.

Fowler and Guggenheim 1939 *Statistical thermodynamics*. Cambridge.

Freudenberg 1933 *Stereochemie*. Vienna.
Pauling 1939 *The nature of the chemical bond and the structure of molecules and crystals*. London.
Shomaker and Pauling 1939 *J. Amer. Chem. Soc.* **61**, 1769.
Smith 1940 *J. Chem. Phys.* **8**, 798.
Thompson 1939 *Trans. Faraday Soc.* **35**, 697.

Guggenheim 1941 *Trans. Faraday Soc.* **37**, 97 and another article in Press.

Harkness, Kistiakowsky and Mears 1937 *J. Chem. Phys.* **5**, 682.

Kistiakowsky and Ransom 1939 *J. Chem. Phys.* **7**, 734.

Teller and Topley 1935 *J. Chem. Soc.* p. 873.

Wassermann 1935 *J. Chem. Soc.* p. 828.

The diffusion and thermal diffusion of hydrogen-deuterium, with a note on the thermal diffusion of hydrogen-helium

By H. R. Heath, T. L. Ibbs and N. E. Wild
Physics Department, University of Birmingham

(*Communicated by M. L. Oliphant, F.R.S.—Received* 18 *February* 1941)

The diffusion coefficient D_{12} has been determined for hydrogen-deuterium and is found to be in close agreement with the value predicted by the classical theory. The case is one of particular interest because the diffusing molecules have the same size and the same molecular field.

The thermal separation in mixtures of this pair of gases has also been measured. As the molecules are of the same size, the thermal separation is due entirely to difference in mass. By using Chapman's theory, the value of the repulsive force index (ν_{12}) is deduced.

By combining the values of ν_{12} and D_{12}, the repulsive force constant κ_{12} can be determined, and so the complete law of force operating in collisions between unlike molecules can be obtained. On classical considerations this law of force would apply to either gas separately.

Measurements of thermal separation in mixtures of hydrogen-helium have also been made and the value of ν_{12} determined. It is shown that this pair of molecules is 'harder' than hydrogen-deuterium. Comparison is made with earlier results of Elliott and Masson.

Introduction

The diffusion of pairs of gases in which there are similarities between the molecules provides problems of particular interest in the kinetic theory. In the special case where the molecules are identical we have self-diffusion, for which Chapman's exact classical theory (1916, 1918) gives

$$D_{11} = \frac{k\eta}{\rho},$$

where η is the coefficient of viscosity, ρ the density, and k a constant, the value of which varies from 1·504 for Maxwellian molecules to 1·200 for rigid elastic spheres. Massey and Mohr (1933), applying the quantum mechanics to this collision process, have deduced that the coefficient D_{11} should be about half the value given by the classical theory. They point out that it is impossible to test their conclusion experimentally, as it is based on the assumption that the molecules in the diffusion experiment are indistinguishable. It is of interest, however, to consider the diffusion of pairs of gases which are alike in many of their physical properties. Boardman and Wild (1937) working in this laboratory have measured the diffusion of carbon monoxide-nitrogen, and carbon dioxide-nitrous oxide, pairs of gases of approximately the same molecular weight, molecular diameter, and having the same molecular and intermolecular fields. The results they obtain are, as would be expected, in good agreement with the classical theory.

The diffusion of hydrogen-deuterium provides a further case where the diffusing molecules, although unequal in mass, have the same diameter and molecular field (Cleave and Maass 1935) and also the same intermolecular field (Grew and Atkins 1936). The fact that these gases are isotopes gives special interest to their investigation. It appears on classical ideas of collision processes that the intermolecular fields of the unlike molecules in hydrogen-deuterium mixtures would probably be the same as the ordinary molecular field of either gas. Experiments on thermal diffusion will provide evidence on the intermolecular fields of the unlike molecules. For most pairs of isotopes the ratio of the molecular masses m_1/m_2 (where m_1 refers to the heavier molecules and m_2 to the lighter molecules) is not sufficiently great to enable a measurable thermal separation to be obtained without difficulty by simply applying a temperature gradient, but in this case the relatively large difference in mass enables the experiment to be made. Viscosity measurements on deuterium and hydrogen show that the diameters σ_1 and σ_2 are the same, so that thermal separation will be entirely due to the difference in mass of the molecules.

THE DIFFUSION MEASUREMENTS

The principle of the method is that of Loschmidt (1870). It consists in allowing the pure gases in vessels of equal lengths and equal uniform cross-sections to diffuse into one another for a given time, after which the composition of the gas mixture in each vessel is determined.

Full details of the apparatus and experimental procedure have already been given in a previous paper (Boardman and Wild 1937).

Experimental results

The diffusion coefficient was measured with the gas at atmospheric pressure, beginning with hydrogen in the upper half of the apparatus. The results were corrected to 76 cm. of mercury pressure and 15° C. Four separate experiments were performed, the results of which are given in table 1.

TABLE 1

barometric pressure cm. Hg	mean temp. ° C	upper half % D_2	lower half % D_2	diffusion time min.	D_{12} 76 cm. 15° C
75·0	15·21	33·1	65·8	10	1·188
75·1	15·04	31·5	67·4	9	1·180
75·1	15·97	35·8	62·9	11	1·296
75·1	16·30	35·4	66·0	10	1·296

Mean $D_{12} = 1{\cdot}24$ cm.^{2} sec.$^{-1}$.

Discussion of results

The classical value for the diffusion coefficient is given by Maxwell's formula (Kelvin 1904, p. 293):

$$D_{12} = \frac{k^2}{\sigma_{12}^2}\sqrt{\left(\frac{1}{w_1}+\frac{1}{w_2}\right)},$$

where $k^2 = \dfrac{1}{2\sqrt{6\pi}}\dfrac{V}{N}$ for rigid elastic spherical molecules. In this formula,

$N =$ the number of molecules per c.c.,

$V =$ the mean velocity of the molecules of hydrogen,

$w_1, w_2 =$ the masses of the molecules with respect to the mass of the hydrogen molecule as unity,

$\sigma_{12} = \frac{1}{2}(\sigma_1 + \sigma_2)$, i.e. the mean molecular diameter.

The value given by the formula in this case is $1{\cdot}25$ cm.^{2} sec.$^{-1}$, which is extremely close to the measured value, the difference being less than the probable error of the experiments. A good agreement may be expected for hydrogen-deuterium, as these molecules are 'hard', i.e. they approximate closely to the rigid elastic sphere model. This agreement in no way conflicts with the deductions from quantum mechanics, as the wave-function symmetry does not occur in this case or in any other case capable of being investigated experimentally.

THE THERMAL DIFFUSION MEASUREMENTS

The thermal separation was measured with apparatus essentially similar to that described in earlier papers (Ibbs 1937). A steam-jacketed bulb with capacity about 2 or 3 cm.^{3} was attached to the Shakespear katharometer (Daynes 1920), one cell of which thus formed the cold side of the thermal diffusion apparatus, at room temperature. The change in concentration on the cold side when the temperature gradient was applied was thus directly observed and the change in concentration on the hot side had to be added. This could not be found accurately from the volumes of the two sides because of the uncertainty introduced by the relatively large volume of the connecting tube. The factor for obtaining the total separation from the observed separation was therefore determined by separate experiments with mixtures of hydrogen-nitrogen which were made under identical conditions. The cold-side separation for these gases was thus measured, and comparison with the known total separation for these gases gave the required factor. The total separation for these gases had previously been measured using a very large hot side so that practically all the change in concentration occurred on the cold side and was observed directly. The small correction for the hot-side separation could be safely applied in this case from an approximate knowledge of the relative volumes of the hot and cold sides.

Experiments were confined to the determination of k_t between two fixed temperatures, the temperature of condensing steam on the hot side and room temperature on the cold side, and the whole range of concentration of mixtures of the pair of gases was investigated.

Preparation and purity of the gases

The deuterium used in these experiments was prepared by distilling heavy water over clean sodium in vacuo, the method employed by Grew and Atkins (1936). The heavy water contained 99·2 % deuterium oxide, and the deuterium produced was compared by means of the katharometer, with a specimen of deuterium analysed by Dr Farkas. Assuming the impurity in both specimens of gas to be hydrogen (from the ordinary water present in the heavy water), it was concluded that the prepared specimen contained 99 % of deuterium. The katharometer calibration was made regarding the deuterium as 100 % pure, the remaining 1 % (being hydrogen) then produces a negligible effect on either the diffusion or the thermal diffusion measurements. Thermal diffusion itself provides the most suitable test of purity of the gases for these experiments, no effect being observed for a sufficiently pure gas. The presence of a very minute amount of heavy impurity in light gases results in thermal separation and produces a large effect with this method of gas analysis. 1 % of hydrogen in deuterium produces a very small thermal separation to which the katharometer is comparatively insensitive, and hence it is not surprising that the specimen of deuterium gave no measurable effect in this test. The hydrogen used was 99·9 % pure and was found to be satisfactory in the thermal diffusion test.

Experimental results

The standard katharometer used for most purposes has air in the closed cell, but such an instrument is unsuitable for analysing mixtures of light gases such as hydrogen and deuterium. A katharometer with one of these gases in the open cell and air in the closed cell would be in a very unbalanced condition, because the spiral in the open cell would be much cooler than that in the closed cell owing to the greater thermal conductivity of the light gas. This is undesirable for two reasons. First, a small change in the composition of the mixture of hydrogen and deuterium can only produce a very slight change in the temperature of the already cold spiral and consequently the katharometer is very insensitive. But also, the resistances of the spirals are so different that they are not affected equally by the small variations in room temperature, and so the katharometer zero reading is unsteady.

The katharometer used in these experiments therefore had hydrogen sealed in the closed cell, so that for all mixtures of hydrogen and deuterium, the katharometer was in a sensibly balanced condition. By using the standard bridge current of 0·10 amp. both spirals would now be fairly cool owing to the high thermal conductivity of hydrogen, but the temperature can easily be raised to the normal working temperature by increasing the current. The current actually used in these experiments was 0·18 amp.

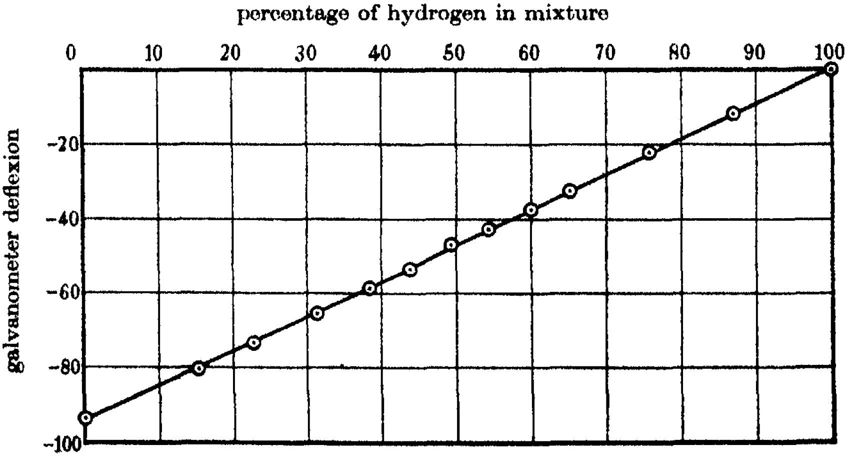

FIGURE 1. Katharometer calibration curves for mixtures of hydrogen and deuterium.

Figure 1 shows the katharometer calibration curve for mixtures of these two gases, which was obtained in order to interpolate the change in concentration from the galvanometer deflexion resulting from the application of the temperature gradient. This graph is very nearly linear over the whole range of concentration. The calibration curve gives a very close approximation in shape to the curve of thermal conductivity against concentration, when the difference in the thermal conductivity of the pure component gases is small. It is interesting therefore to compare this curve with results recently obtained by Archer (1938) on absolute thermal conductivities of mixtures of this pair of gases. Archer also obtains a relation which is very nearly linear but rising rather more sharply near the hydrogen end.

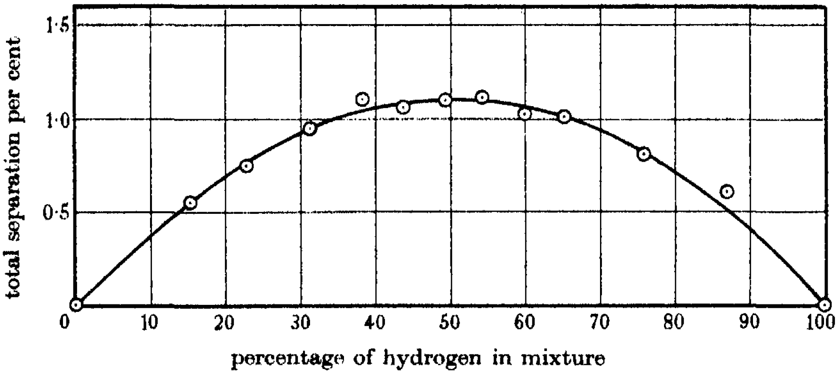

FIGURE 2. Thermal separation in mixtures of hydrogen and deuterium. $T_1 = 100°$ C, $T_2 = 15°$ C.

Figure 2 shows how the total separation varies with the concentration of hydrogen in the mixture of hydrogen and deuterium, individual points having been corrected to $\log_{10} T_1/T_2 = 0{\cdot}112$ (hot-side temperature 100° C and cold-side temperature 15° C). Eleven mixtures were made, and each experimental point represents the mean of four separate observations. The difference in the thermal conductivity of hydrogen and deuterium is so small that measurements of a change in concentration of 0·6% (the maximum actually observed on the cold side) is a matter of some experimental difficulty. Minute secondary effects, normally quite negligible, became relatively important. Thus it was necessary to introduce very effective screening of the katharometer from the hot side, and it was also found necessary to pass hydrogen through the apparatus repeatedly before consistent results were obtainable. The katharometer block was protected from draughts and other refinements were introduced which have hitherto been quite unnecessary in thermal diffusion measurements.

The values of k_t were obtained at intervals of 10% from this curve (figure 2), and were compared with the values of k_t for the same mixtures. calculated as if the molecules behaved like rigid elastic spheres, using Chapman's first approximation formula

$$k_t\,(\text{r.e.s.}) = \frac{5}{2}\left\{\frac{0{\cdot}1752\lambda_1 + 0{\cdot}2198\lambda_2}{3{\cdot}668 + 1{\cdot}724\lambda_1/\lambda_2 + 1{\cdot}764\lambda_2/\lambda_1}\right\},$$

where λ_1 and λ_2 are the concentrations by volume of the heavier and lighter gases respectively, and $\lambda_1 + \lambda_2 = 1$. This formula was obtained by substituting the values of m_1, m_2, σ_1, σ_2, in the general expression given by Chapman (1924). The corresponding values of $R_t = \dfrac{k_t(\text{exp.})}{k_t(\text{r.e.s.})}$ were thus found and are shown in table 2.

TABLE 2

. % H_2	total separation %	k_t (exp.)	k_t (r.e.s.)	R_t
10	0·374	0·0145	0·0232	0·63
20	0·685	0·0265	0·0418	0·63
30	0·920	0·0356	0·0558	0·64
40	1·071	0·0416	0·0649	0·64
50	1·112	0·0432	0·0690	0·63
60	1·071	0·0416	0·0676	0·61
70	0·938	0·0362	0·0605	0·60
80	0·726	0·0281	0·0473	0·60
90	0·420	0·0166	0·0273	0·61

The curve (figure 2) is very nearly symmetrical, and this agrees with the predictions of the theory when the mass ratio and the diameter ratio are small. The general tendency in the separation-concentration curve is for the maximum to move over in the direction of 100 % of the lighter gas as m_1/m_2 and σ_1/σ_2 become large. The good agreement (in shape) with the theoretical curve is shown by the values of R_t which remain constant and equal to 0·62 within about the limit of experimental error over the whole range of concentration.

DISCUSSION OF RESULTS

The results show that an appreciable thermal separation is produced in mixtures of this pair of gases solely as a consequence of the difference in mass of the two constituents, the diameters being the same.

The value of the constant R_t depends on the nature of the collisions between unlike molecules in the gas mixture. If the molecules obey an inverse power law of repulsion during collisions, the force F between them can be expressed as

$$F = \kappa_{12} r^{-\nu_{12}},$$

where r = the distance between the point centres,

κ_{12} = a constant (the force constant),

ν_{12} = the repulsive force index.

Such a law of force is known to hold for many gas molecules over a considerable range of ordinary temperature. Chapman has shown that the repulsive force index ν_{12} can be obtained from R_t by the following relation:

$$R_t = \frac{13}{10}\left\{\frac{\nu_{12}-5}{\nu_{12}-1}\right\},$$

a formula which applies exactly to the case of a Lorentzian gas, but there is reason to believe that application to the present case would not affect it very greatly.

The value of ν_{12} in the case of hydrogen-deuterium is thus found to be 8·6. It is interesting to compare the values of ν_{12} obtained from thermal diffusion for other pairs of gases. Thus the case of hydrogen-helium recorded later in this paper gives the value 9·8, which means that helium is 'harder' than hydrogen or deuterium. Numerous previous observations which we have made support this conclusion. On the other hand, nitrogen is known to be 'softer' than the hydrogen isotopes and the value of ν_{12} for hydrogen-nitrogen and for deuterium-nitrogen is 8·3 (from the measurements of Grew and Atkins 1936). The chief interest in the present case, however, is that the value $\nu_{12} = 8·6$ can probably be applied independently to hydrogen and deuterium. The value of the repulsive force index ν_{11} given by viscosity for both hydrogen and deuterium separately is 11·3. This higher value may be expected as viscosity appears to yield values of the repulsive force index higher than those given by thermal diffusion. [In the following paper Dr K. E. Grew extends the interpretation of the results by Chapman's theory, and is able to show that the value of ν obtained from thermal diffusion can be brought into good agreement with the value obtained from viscosity.]

By combining the measurements of thermal diffusion and ordinary diffusion for hydrogen-deuterium the force constant κ_{12} can be obtained, thus giving the complete description of the law of force in molecular encounters for this pair of gases. Using the equations (32″), (26″) and (27″) (Chapman 1929) a value of $\kappa_{12} = 1·0 \times 10^{-70}$ was obtained. The complete law of force between molecules of hydrogen in collision, molecules of deuterium in collision, or a molecule of hydrogen in collision with a molecule of deuterium, may therefore be given as

$$F = 1{\cdot}0 \times 10^{-70}\, r^{-8\cdot6}.$$

[From his experiments Grew obtains $R_t = 0{\cdot}61$ which is in close agreement with the value we have obtained. From this, using his revised method of calculation, he gets $\nu_{12} = 12{\cdot}6$ and shows that it is in good agreement with the values obtained from the most recent viscosity measurements for hydrogen. Combining Grew's value of ν_{12} with our experimental value of the diffusion coefficient we obtain

$$F = 3{\cdot}8 \times 10^{-101}\, r^{-12\cdot6}.$$

This should be regarded as a much closer approximation to the complete description of the law of force operating between these pairs of molecules.]

NOTE ON THE THERMAL DIFFUSION OF HYDROGEN-HELIUM

Measurements have also been made on mixtures of hydrogen and helium with the same apparatus. This again is a case of peculiar interest because the heavier molecule has the smaller diameter. Hence the effect of the mass ratio is to produce a tendency for helium to move to the cold side, but the diameter ratio produces a tendency for helium to move to the hot side. The formula for k_t (r.e.s.) is found in the usual way and is expressed with the usual notation as follows:

$$k_t\,(\text{r.e.s.}) = \frac{5}{2}\left\{\frac{0{\cdot}1390\lambda_1 + 0{\cdot}2056\lambda_2}{3{\cdot}646 + 2{\cdot}156\lambda_1/\lambda_2 + 1{\cdot}379\lambda_2/\lambda_1}\right\}.$$

This predicts that helium will always move to the cold side, the mass effect overcoming the opposite tendency due to the diameter ratio. This has already been observed by Elliott and Masson (1925) and is confirmed by our results. Seven measurements of thermal separation have been made for gas mixtures of different concentration ranging from 50 to 100% of hydrogen. Values of k_t exp. were found from a graph similar to that shown in figure 2, the results being given in table 3.

The case does not appear to be of the normal type in which R_t is reasonably constant. The results now obtained appear to be in agreement with the observations of Elliott and Masson, which suggested that the maximum separation occurred in mixtures containing less than 50% of the lighter gas. The considerable decrease of R_t as the proportion of hydrogen is increased now appears to be of special interest in view of Chapman's (1940) recent extension of the theory in which he discusses how k_t will depend upon the different variables involved.

TABLE 3

% H_2	total separation %	k_t (exp.)	k_t (r.e.s.)	R_t
50	1·24	0·0481	0·0600	0·80
60	1·14	0·0442	0·0575	0·77
70	0·90	0·0350	0·0500	0·70
80	0·64	0·0284	0·0380	0·66
90	0·34	0·0132	0·0313	0·63

The experimental values of k_t obtained by Elliott and Masson give a mean value of $R_t = 0{\cdot}61$, which corresponds to a repulsive force index $\nu_{12} = 8{\cdot}5$. The mean value from our results is 0·71, which gives a value of $\nu_{12} = 9{\cdot}8$. As has already been observed, this value of 9·8 agrees well with the general scheme of molecular fields deduced from measurements of thermal diffusion. Elliott and Masson's value of $\nu_{12} = 8{\cdot}5$ is therefore probably rather low. The apparent variation in the value of R_t suggests that further examination of this pair of gases could profitably be made.

REFERENCES

Archer, C. T. 1938 *Proc. Roy. Soc.* A, **165**, 474–485.

Boardman, L. E. and Wild, N. E. 1937 *Proc. Roy. Soc.* A, **162**, 511–520.

Chapman, S. 1916 *Phil. Trans.* A, **216**, 279–348.

Chapman, S. 1918 *Phil. Trans.* A, **217**, 115–198.

Chapman, S. 1929 *Phil. Mag.* **7**, 1–16.

Chapman, S. 1924 *Phil. Mag.* **48**, 593–607.

Chapman, S. 1940 *Proc. Roy. Soc.* A, **177**, 38–62.

van Cleave, A. B. and Maass, O. 1935 *Canad. J. Res.* **12**, 1.

Daynes, H. A. with a note by Shakespear, G. A. 1920 *Proc. Roy. Soc.* A, **97**, 273–280.

Elliott, G. A. and Masson, I. 1925 *Proc. Roy. Soc.* A, **108**, 378–385.

Grew, K. E. and Atkins, B. E. 1936 *Proc. Phys. Soc.* **48**, 415–420.

Ibbs, T. L. 1937 *Physica*, IV, **10**, 1133–1140, where full references to previous experiments are given.

Kelvin 1904 *Baltimore Lectures*. London: C. J. Clay and Sons.

Loschmidt 1870 *S.B. Akad. Wiss. Wien*, **61**, 367; **62**, 468.

Massey, H. S. W. and Mohr, C. B. O. 1933 *Proc. Roy. Soc.* A, **141**, 434–453.

Thermal diffusion in hydrogen-deuterium mixtures

By K. E. Grew

Heriot-Watt College, Edinburgh

(*Communicated by M. L. Oliphant, F.R.S.—Received* 18 *February* 1941)

The separation produced by thermal diffusion in hydrogen-deuterium mixtures has been measured at temperatures between -183 and 425° C, and the thermal diffusion ratio R_T found.

Theoretical values of R_T for the same mixture have been calculated for various values of the force index ν from Chapman's general expression appropriate to molecules behaving as point centres of repulsive force $F = \kappa r^{-\nu}$. The evaluation of R_T in this way is possible only for isotopic mixtures, in which the interactions between like and between unlike molecules are the same.

Comparison of the experimental value of R_T with these theoretical values indicates that the fields of the hydrogen and deuterium molecules have an index $\nu = 12{\cdot}6$. This agrees with the value $\nu = 12{\cdot}5$ deduced from viscosity results. It is higher than the value $\nu = 8{\cdot}6$, which is found if the theoretical values of R_T for a Lorentz gas are assumed to apply—an assumption necessarily made in the case of the non-isotopic mixtures examined so far. This result suggests that the discrepancies between values of ν hitherto deduced from thermal diffusion measurements and those expected from viscosity values are attributable to this assumption.

The calculation shows that R_T depends slightly on the concentration of the mixture, a point on which the experimental evidence is inconclusive.

Introduction

Measurements of thermal diffusion in hydrogen-deuterium mixtures have been made which, extending over a range of temperature from -183 to 425° C, supplement those described by Heath, Ibbs and Wild in the preceding paper. Moreover, in estimating the index of the molecular repulsive field from the results, advantage has been taken of the simplification effected in the theoretical expressions by the fact that the mixture is isotopic and consequently the interactions between like and unlike molecules are the same. It has thus been possible to avoid an assumption necessarily made in other cases in finding the force index ν from thermal diffusion measurements. This has led to a value of ν in good agreement with that deduced from viscosity measurements. Hitherto, the value of ν from thermal diffusion measurements has been generally smaller than would be expected from the viscosity results.

EXPERIMENTAL METHOD

A diagram of the diffusion vessel and analysing apparatus is shown in figure 1.

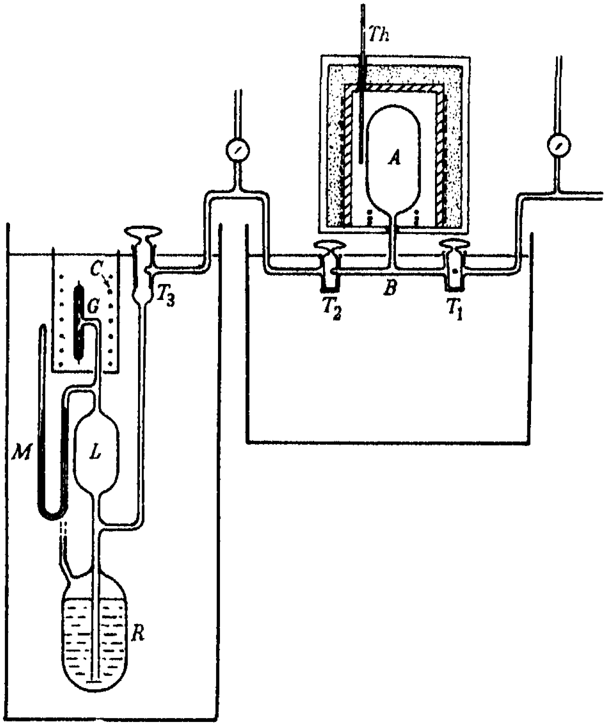

FIGURE 1. The diffusion vessel and analysing apparatus.

The hydrogen-deuterium mixture was prepared in a system of burettes not shown in the figure, and was admitted through the stopcock T_1 to the diffusion vessel *AB*, previously evacuated. The upper part, *A*, of this vessel was situated inside a small electric furnace; the lower, *B*, consisting of the tube between the stopcocks T_1 and T_2, was immersed in a water thermostat maintained at 20° C. The volumes of *A* and *B* were respectively 18·1 and 2·4 cm.^{3}, including the appropriate parts of the connecting tube. *A* could be heated to temperatures up to 450° C. Uniformity of temperature over the bulb to within 2° C was attained by winding the heating element on a thick-walled, nickel-plated copper tube, and by the provision of a supplementary heating coil near the mouth of the furnace. The temperature was measured by a chromel-alumel thermocopule *Th* placed close to the bulb.

Some measurements were made at low temperatures also, as earlier work with other gas mixtures (Ibbs and Grew 1931) had shown this temperature range to yield interesting results. For these measurements the diffusion vessel was inverted, the bulb *A* lying below the tube *B*, and the bath surrounding *B* suitably modified. *A* was immersed in a bath of liquid oxygen or cooled pentane, the temperature of which was measured by a copper-constantan couple.

The gas mixture in *B* was analysed before and after diffusion by a thermal conductivity method. The analyser, originally intended for measurements on vapours, was based on the microgauge described by Bolland and Melville (1937). A spiral tungsten filament, 2·5 cm. long, taken from an Osram 'Striplite' lamp, was welded to short platinum wires which were then sealed in 2 mm. capillary tubing, as shown at *G*. A capillary side tube led to the bulb *L*, of about 14 cm.^{3} capacity, and the mercury reservoir *R*. The space above the mercury in *R* could be connected either with the pump or with an air reservoir, so that the mercury could be raised or lowered, and the pressure of a sample of gas, admitted to the evacuated bulb through T_3, adjusted to the desired value. The pressure was measured by the mercury manometer *M*, made from 2 mm. capillary tubing; a little Apiezon oil introduced into the capillary prevented the mercury from sticking. The whole was immersed in a paraffin thermostat maintained by a toluene regulator within 0·01 of 21·20° C.

The tungsten filament formed one arm of a Wheatstone bridge; its temperature, and therefore also its resistance, depended on the conductivity of the gas surrounding it and on the current flowing through it. At 21° C its resistance was 23·0 ohms. The second arm of the bridge was adjusted so that when the bridge was balanced the filament was about 20° C above the thermostat temperature. This was done by varying the thermostat temperature and determining the temperature coefficient of resistance of the filament, using bridge currents sufficiently small to produce no appreciable heating of the filament. The second resistance was then made equal to the calculated filament resistance at a temperature of 41° C, that is, 20° above the normal thermostat temperature. Moreover, by combining suitable lengths of nickel and manganin wires, this second resistance was given a temperature variation the same as that of the tungsten filament, measured under the operating conditions described later. Thus any fluctuations in thermostat temperature affected equally both arms of the bridge. It was necessary that this resistance, unlike the filament resistance, should be independent of the bridge current; s.w.g. 39 nickel was used in its construction so that the heating effect was negligible. It was wound as a coil *C* on an open bakelite frame, 6 cm. long and 3 cm. diameter, which surrounded the microgauge. The other two arms of the bridge were both manganin resistances of 10 ohms, supported in the thermostat, and connected to the gauge and second arm by short lengths of stout copper wire. In operation, the potential difference across the bridge was adjusted until the filament resistance reached its equilibrium value and the bridge was balanced. A constant fraction, obtained by a potential divider, of the potential difference was measured by a Tinsley potentiometer reading to 0·0001 V.

Satisfactory results were obtainable with a gas pressure in the gauge of 50 mm., which required the introduction into the analyser of only 0·15 cm.^{3} of gas at 76 cm. pressure. This amount of gas was conveniently withdrawn from the diffusion vessel *B* by rotating the partially drilled stopcock T_2 and spilling the small amount of gas in the barrel into the evacuated analyser through T_3. The gas in *L* was then compressed to 50 mm., the manometer reading being taken by a travelling microscope. The pressure adjustment was important as at 50 mm. the conductivity varied appreciably with the pressure. With hydrogen a change in pressure of 1 mm. caused a change in potentiometer reading of 0·0025 V, when the normal reading was 1·5114 V; an accuracy of 0·1 mm. was therefore aimed at in setting the pressure.

Considerable difficulty in obtaining steady and reproducible readings was at first experienced. The trouble was due to the response of the coil *C* to the small temperature fluctuations (which necessarily occurred with the intermittent operation of the heating coil) being more rapid than that of the gauge. Several modifications in the design of the thermostat, relay and stirrer were made in an attempt to reduce these temperature fluctuations, but without success. Eventually a solution was found in placing the gauge and coil *C* in a celluloid enclosure filled with paraffin. The contents of the enclosure were therefore partly insulated thermally from the paraffin circulating around it; the temperature fluctuations were consequently inappreciable. Consistent readings were now readily obtained, even over long periods. For example, the following readings were taken approximately monthly with hydrogen in the gauge: 1·5112, 1·5110, 1·5114, 1·5114 V. This constancy was rather unexpected, as Trenner (1937) had found, using a somewhat similar apparatus, though with a platinum filament, a small continuous change of resistance.

The procedure was as follows. Deuterium was prepared from heavy water, containing 99·65 % deuterium oxide, by reaction with sodium. Hydrogen from a cylinder was purified by passage through sodium hydrosulphite to remove oxygen, and subsequently dried. A mixture of hydrogen and deuterium was made in measured proportions, and after allowing some hours for the composition to become uniform, it was admitted to the evacuated diffusion vessel, with the bulb *A* at room temperature. The gas pressure was made roughly 1 atm. The gauge was then evacuated by a Hyvac pump, the pressure being indicated by the potential difference necessary to balance the bridge in this condition. The stopcock T_2 was turned twice and the gas so introduced into the analyser compressed to 50 mm. The current was then adjusted approximately to balance the bridge and 10 or 15 min. allowed for the temperature of the gauge and surrounding paraffin to become steady. The current was then exactly adjusted, and the potential difference across the bridge measured.

Sufficient gas was next withdrawn from the diffusion vessel into the burette so that the pressure should be still about 1 atm. when the bulb *A* was heated to a given temperature. After allowing time for the diffusion to occur and the composition of the gas in *B* to become uniform, a sample was introduced into the gauge. The change in composition due to thermal diffusion was determined from the change in potential difference balancing the bridge and the slope of the potential difference-concentration curve. The total thermal separation was calculated from the observed change in composition in *B* in the usual way: the multiplying factor determined from the ratio of the volumes of *A* and *B* was checked by making separation measurements on a hydrogen-nitrogen mixture and comparing the values with the accepted ones for that mixture. This procedure was then repeated with the bulb *A* at a different temperature.

For measurements at low temperatures it was not convenient to work at constant pressure. The bulb containing the gas mixture at atmospheric pressure when at room temperature was immersed in the cooling bath and the diffusion took place at reduced pressure. Earlier measurements had shown that this pressure change was without effect on the separation.

In this way a series of thermal separation measurements was made with five mixtures, each taken over a temperature range extending to 425° C, and with three mixtures at temperatures down to $-183°$ C. The precision of the measurements was not high. The conductivities of hydrogen and deuterium are not widely different—the potentiometer readings for the two gases differed by only 0·17 V—and the thermal separation is small because of the small molecular mass ratio. The separation at any temperature was consequently liable to an error of 5–10 %, attributable mainly to disturbance of the balance point of the bridge by small fluctuations in the thermostat temperature and to errors in adjusting the pressure within the gauge.

EXPERIMENTAL RESULTS

Five hydrogen-deuterium mixtures ranging from 38 to 70 % hydrogen content were examined at temperatures up to 425° C. A curve showing the separation as a function of log T/T' (where T and T' are the temperatures of the hot and cold sides respectively) for one of these mixtures is given in figure 2. In all cases the relation was a linear one: that is, the thermal diffusion coefficient k_T in the Chapman expression for the separation

$$n'_{10} - n_{10} = k_T \ln T/T'$$

is constant over the range from 0 to 400° C.

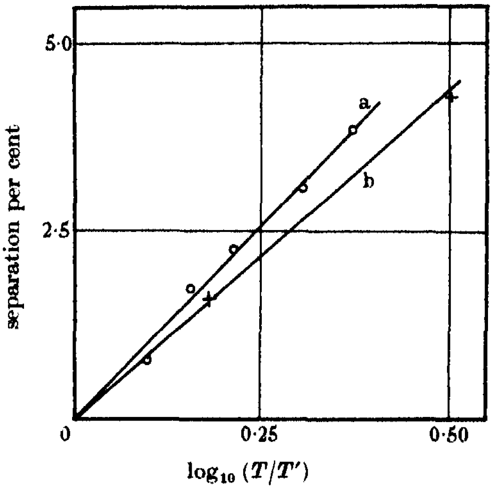

FIGURE 2. Thermal separation in hydrogen-deuterium mixtures as a function of log T/T'. (*a*) 56·9 % H_2. $T' = 293°$ K; $273 < T < 700°$ K. (*b*) 65·5 % H_2. $T = 293°$ K; $273 > T' > 90°$ K.

In the low-temperature range three mixtures were examined at two or three temperatures only. The measurements are thus of a preliminary nature, a more complete investigation being unavoidably prevented. They suffice, however, to show that k_T is constant also over temperatures down to −183° C. Thus in hydrogen-deuterium mixtures there is no indication of a change in the force index, implied by a change in k_T, which has been observed over this range in other gases (Ibbs and Grew 1931). The curve for one mixture is given in figure 2.

The values of k_T deduced from the slopes of the curves are given in table 1. As in earlier work, the thermal diffusion ratio R_T, which is the ratio of the experimental value of k_T to the theoretical, first approximation, value $[k_T]_{1\atop\infty}$, for rigid elastic spheres, has been calculated. R_T, as shown later, depends slightly on the concentration, but the variation is small and of the order of the experimental error. A mean value of $R_T = 0{\cdot}61$ has therefore been taken and is considered appropriate to a 50 % mixture. This mean value agrees within experimental error with the value 0·62 obtained by Heath, Ibbs and Wild reported in the preceding paper.

TABLE 1. VALUES OF k_T AND R_T

% hydrogen	k_T (exp.)	$[k_T]_{1\atop\infty}$	R_T
38·5	0·040	0·064	0·63
47·1	0·041	0·068	0·60
56·9	0·045	0·069	0·65
62·6	0·037	0·066	0·56
69·2	0·040	0·061	0·66
48·5	0·038	0·068	0·55
54·5	0·044	0·069	0·65
65·5	0·038	0·064	0·59

Mean $R_T = 0{\cdot}61 \pm 0{\cdot}01$.

DISCUSSION OF RESULTS

The significance of R_T is its marked dependence on the law of molecular interaction, which is assumed to be of the form $F = \kappa r^{-\nu}$. A comparison therefore of the experimental value of R_T with theoretical values for different types of interaction should lead to an estimate of the force field actually operative. Theoretical expressions for R_T in the general case, however, cannot be evaluated since they involve the three force constants κ_1, κ_2, κ_{12} and the three indices ν_1, ν_2, ν_{12} applicable to the three types of collision occurring in a mixture of molecules 1 and 2. In the special case of the Lorentzian gas (a gas mixture in which the mass ratio and the number ratio both tend to infinity) an exact expression for R_T in terms of ν_{12} is available, viz.

$$R_T = \frac{13}{10}\,\frac{\nu_{12}-5}{\nu_{12}-1}$$

It has hitherto been assumed that this same relation holds for the non-Lorentzian mixtures studied experimentally, and values of ν_{12} have been deduced from the experimental value of R_T using it. A summary of these values, which are mainly due to Ibbs and his collaborators, has been given by Chapman and Cowling (1939). A comparison with values of ν_1, ν_2 deduced from viscosity measurements on the simple gases shows that the value of ν_{12} from diffusion is generally lower than would be expected from the viscosity results. In isotopic mixtures the assumption of the applicability of the Lorentz expression is unnecessary. Here the same force constant κ and force index ν apply to collisions between both like and unlike molecules, and R_T can consequently be evaluated for various values of ν. This has been done for hydrogen-deuterium mixtures.

The value of $[k_T]_1$ for a series of values of ν was calculated from the expression 9·83. i given by Chapman and Cowling (1939), which is a first approximation to k_T. The values which apply to a 50 % mixture are given in table 2. The error of this first approximation is not known exactly, and it is necessary to make an assumption in estimating it. To take the error as being the same as in the Lorentzian case, for which it is known exactly, is not justifiable, as Professor Chapman kindly pointed out privately. This is because the error of the first approximation to quantities which can also be evaluated exactly is much greater in the Lorentzian than in the general case. For example, the error in the coefficients of conductivity, viscosity, and self-diffusion for a simple gas whose molecules are rigid elastic spheres is about 2 %; for a Lorentz gas the errors are 8, 12, 15 % respectively (Clark Jones 1940). The same is likely to be true of k_T. Failing more definite knowledge, it seems best to assume that the error of $[k_T]_1$ for hydrogen-deuterium bears the same ratio to that for the Lorentz case as does the error of the coefficient of self-diffusion for a simple gas to that for the Lorentz gas. These errors have been tabulated for various values of ν by Chapman and Cowling (1939, pp. 196, 198).

TABLE 2. THEORETICAL VALUES OF k_T AND R_T FOR A 50 % HYDROGEN-DEUTERIUM MIXTURE

ν	$[k_T]_1$	k_T	R_T	R_T (Lorentz)
5	0	0	0	0
7	0·0203	0·0205	0·297	0·43
9	0·0307	0·0313	0·452	0·65
11	0·0374	0·0382	0·553	0·78
15	0·0456	0·0468	0·678	0·93
∞	0·0690	0·072	1·043	1·30

On this basis the values of $[k_T]_1$ given in table 2 have been corrected to those under k_T. The correction amounts to 4 % for $\nu = \infty$, and decreases as ν decreases. The ratio of k_T for a particular value of ν to the first approximation for $\nu = \infty$, $\underset{\infty}{[k_T]_1}$, is then the theoretical value of R_T corresponding to the experimental value k_T (exp.)/$[k_T]_{\substack{1\\ \infty}}$. The value of R_T for a Lorentz gas is given for comparison in the last column.

The value of R_T determined experimentally is 0·61. The corresponding value of ν found from the $R_T \sim \nu$ curve is 12·6. This is markedly higher than the value $\nu = 8{\cdot}6$ which would be obtained if, as hitherto, the Lorentz values were used. Recent measurements of the viscosity of hydrogen, extending over a temperature range from a few degrees above zero to 1000° K (Trautz and Zink 1930; Itterbeek and Paemel 1940) show that from 90° K upwards the molecule conforms closely to a centre of repulsive force with index $\nu = 12{\cdot}5$. For deuterium there do not appear to be sufficient measurements for a reliable estimate of the force index to be made, though there is no reason for thinking that it differs from that for hydrogen. There is thus good agreement between the values of the force index deduced from thermal diffusion and that from viscosity measurements.

This result suggests that the reason for the values of ν_{12} hitherto deduced from thermal diffusion measurements being generally smaller than those to be expected from viscosity values is in the use of the Lorentz expression for R_T; and that, if R_T could be calculated in the general case as in the special case of isotopic and Lorentz mixtures, thermal diffusion and viscosity values would be in full agreement.

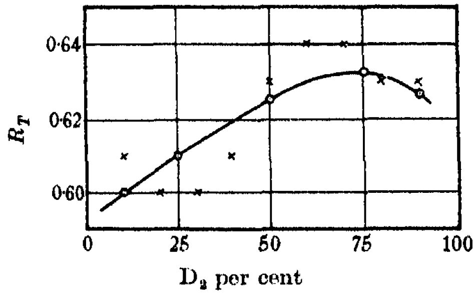

FIGURE 3. R_T as a function of concentration. ⊙ calculated, × experimental (Heath, Ibbs and Wild).

The calculation of R_T also throws light on the dependence of R_T on the concentration of a gas mixture, a point on which the experimental evidence is inconclusive. In some mixtures R_T appears to be independent of the concentration; in others it varies, though only by amounts comparable with experimental error. Such a case is that of hydrogen-deuterium mixtures, for which Heath, Ibbs and Wild have made measurements over a wide range of concentration, described in the preceding paper. The theoretical values of R_T for this mixture have been calculated for different concentrations, assuming a force index $\nu = 13$, sufficiently close, for this purpose to the experimentally determined value of 12·6. They are shown in figure 3. It appears that R_T does vary slightly with the concentration, a maximum value occurring at about 70% deuterium. The experimental points obtained by Heath, Ibbs and Wild are also marked; they are rather scattered but their trend is undoubtedly that of the theoretical curve. Thus the slight dependence of R_T on concentration observed in other cases as in this, is probably both real and in accordance with theory.

I am indebted to Drs Heath, Ibbs and Wild for their kindness in allowing me to see, prior to publication, the results of their measurements on hydrogen-deuterium mixtures, and particularly to Dr Ibbs for encouragement and criticism. My thanks are also due to Principal Cameron Smail of Heriot-Watt College for the facilities he has granted.

REFERENCES

Bolland and Melville 1937 *Trans. Faraday Soc.* **33**, 1316.
Chapman and Cowling 1939 *The Mathematical Theory of Non-uniform. Gases* Camb. Univ. Press.
Clark Jones 1940 *Phys. Rev.* **58**, 111.
Ibbs and Grew 1931 *Proc. Phys. Soc.* **43**, 142.
Itterbeek and Paemel 1940 *Physica*, **7**, 427.
Trautz and Zink 1930 *Ann. Phys., Lpz.*, **7**, 427.
Trenner 1937 *J. Chem. Phys.* **5**, 382.

Critical and co-operative phenomena. VI

The neighbour distribution function in monatomic liquids and dense gases

By J. Corner and J. E. Lennard-Jones, F.R.S.

The University Chemical Laboratory, Cambridge

(*Received* 9 *January* 1941)

A formula is given for the neighbour distribution function in liquids and dense gases, assuming that each atom is vibrating in the field of its neighbours when in their equilibrium positions. It is shown that a parabolic potential leads to a simple result. Applying this to potassium, we find a structure which bears some resemblance to a body-centred cubic. Finally we show how interatomic fields may be derived from the distribution function of a single shell of neighbours, when this has been determined from experiment.

1. Introduction

One of the main theoretical problems of liquid structure is the determination of the average distribution of atoms about any selected atom, and the most successful method of obtaining this information at present is by means of the X-ray diffraction patterns given by liquids. It was Debye (1930) who first showed how probability distribution functions could be inferred from observed intensity patterns of diffracted X-rays. A function $\rho(r)$ is used to define the probability that two atoms are at specified distances apart. This helps to define what has been called the quasi-crystalline structure of a liquid. It assumes that a liquid is homogeneous and that the average environment of each atom is the same.

The form of this distribution function has recently been found for a number of simple liquids. Mercury, gallium, potassium and sodium have recently been investigated and their distribution functions derived (Menke 1932, Gingrich 1939). These may be regarded as made up of a series of co-ordination shells somewhat similar to those in a solid but differing from them in that the shells are not at precise distances but are distributed with some degree of randomness about certain mean positions. Prins and Petersen (1936) assumed the individual peaks in the distribution function to be like Gaussian probability curves and this type has been used widely. The number of atoms (N_i) in the various co-ordination shells and the positions of their maxima were assumed by Prins to be the same as in the solid. A further development of this method is due to Bernal (1937) who assumed each shell to be distributed according to a Gaussian probability function so that it is determined by N_i, the position of its maximum r_i, and a quantity λ_i, which is a measure of the spread. He attempted to determine the geometrical conditions which must be satisfied by successive shells and tried to find the constants of all outer shells in terms of those of the first layer. The distribution function was thus expressed in terms only of three parameters.

Attempts have recently been made to calculate the shapes of these component curves for assumed models of liquids and given intermolecular forces. Thus Wall (1938) has considered a model in which each atom of a liquid is free to move in a spherical cell. Within this cell the potential energy is constant and outside it is infinite. This implies a uniform probability of finding the atom within equal elements of volume in the cell. It is then possible to calculate the probability that an atom in one cell is at a specified distance from one in another, and this is found to be a function of the size of the cells and the distance between their centres. By a comparison of theoretical and experimental distributions it is possible to fix the constants of the field. The method used by Wall can easily be generalized to apply to any model of a liquid in which the atoms are assumed to vibrate similarly and independently. Coulson and Rushbrooke (1939) have shown that for all such models the theoretical distribution has the property that $r\rho(r)$ due to each shell is symmetrical about a certain value of r, whereas it had previously been assumed, following Prins, that $\rho(r)$ itself was symmetrical.

In this paper the distribution function is calculated by similar methods for intermolecular forces of a more general type, so that once these forces have been derived, as they have now been derived for several atoms and molecules, the molecular distribution of the liquid can be calculated for various models. The theory is applied in some detail to potassium. We also indicate in this paper how to find intermolecular forces from a knowledge of the X-ray diffraction data.

This paper is restricted to monatomic substances. Polyatomic molecules with a high degree of symmetry form liquids with properties very similar to those of monatomic substances. In such cases the distribution of the molecules may be roughly the same as the distribution of atoms discussed here; it might be possible to obtain the average distribution of scattering matter by a further averaging. This would involve the types and positions of the atoms in the molecule, and so a general result would be complicated. However, special cases might be discussed on these lines.

2. GENERAL FORMULAE

Let the macroscopic density be ρ_0 atoms per c.c. The neighbour distribution function $\rho(R)$ is defined thus: the probability of finding an atom at a distance between R and $R+dR$ from any central atom is $4\pi R^2\rho_0\rho(R)\,dR$.

We will assume that the excursions of an atom from its mean position are determined by the field of its neighbours in their mean positions. Thus we neglect correlation between the motion of neighbouring atoms. This assumption must break down when a neighbouring atom can be easily displaced from its mean position, as, for example, in the critical region. At liquid and solid densities there is probably little error due to this simplifying assumption.

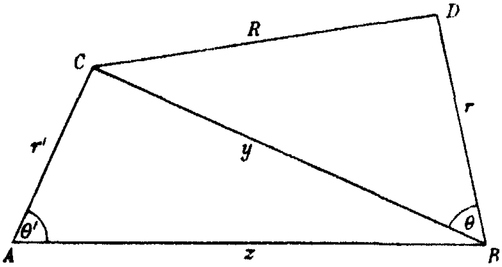

FIGURE 1. The notation used. (In general A, B, C, D are not coplanar.)

Let $p(r)\,dr$ be the probability that an atom is at a distance between r and $r+dr$ from its lattice site, when all its neighbours are at their equilibrium positions. The probability can be assumed to be a function of r only, as we have written it, if the number of neighbours of each atom is sufficiently large, say 8 or 12.

Consider two atoms, whose lattice sites are A, B, at positions C and D. With the notation shown in figure 1, we have

$$R^2 = r^2+y^2-2ry\cos\theta$$

and so the area on the sphere of radius r, which lies in a range dR of R, is

$$2\pi r^2\sin\theta\,d\theta = 2\pi r^2\frac{R\,dR}{ry}.$$

Thus the probability of such configurations, taking all positions on a sphere as equally probable, is $R\,dR/2ry$. The probability of having R in a range dR, when r', θ' are fixed, is

$$\int_{|y-R|}^{y+R}\frac{R\,dR}{2ry}p(r)\,dr = \frac{R\,dR}{2y}\int_{|y-R|}^{y+R}p(r)\frac{dr}{r}.$$

We must now average over all r' and θ'. As before, the probability of y lying in a range dy is $y\,dy/2r'z$, for fixed r', so that the probability of R lying in a range dR, averaged over all positions of C, D in their cells, is

$$\int_{y=0}^{\infty}\int_{r'=|y-z|}^{y+z}\frac{y\,dy}{2r'z}p(r')\,dr'\,\frac{R\,dR}{2y}\int_{|y-R|}^{y+R}p(r)\frac{dr}{r}$$
$$=\frac{R\,dR}{4z}\int_{0}^{\infty}dy\int_{|y-z|}^{y+z}p(r')\frac{dr'}{r'}\int_{|y-R|}^{y+R}p(r)\frac{dr}{r}.$$

Let the mean positions of the atoms form a lattice such that around any site there are successive shells of N_i sites, at distances $z_i\,(i=1,2,\ldots)$. It is convenient to denote z_1 by a. The probability of finding an atom at a distance between R and $R+dR$ from any atom is

$$R\,dR\sum_{i=1}^{\infty}\frac{N_i}{4z_i}\int_{0}^{\infty}dy\int_{|y-z_i|}^{y+z_i}p(r')\frac{dr'}{r'}\int_{|y-R|}^{y+R}p(r)\frac{dr}{r}=4\pi\rho_0R^2\rho(R)\,dR. \tag{1}$$

by definition of $\rho(R)$. Since $p(r)$ has the dimensions of the inverse of a length, this equation makes $\rho(R)$ of zero dimensions, as, of course, it should.

If the potential of an atom in its cell, relative to the centre, is $W(r)$, then

$$p(r)=\frac{r^2e^{-W(r)/kT}}{\int_{0}^{\frac{1}{2}a}r^2e^{-W(r)/kT}\,dr},$$

and so

$$\rho(R)=\frac{1}{16\pi\rho_0aR}\sum_i\frac{N_i}{z_i}\int_0^{\infty}\frac{dy}{a}\int_{|y-z_i|/a}^{(y+z_i)/a}\frac{r'}{a}\exp\left\{-\frac{W(r')}{kT}\right\}d\left(\frac{r'}{a}\right)$$
$$\times\int_{|y-R|/a}^{(y+R)/a}\frac{r}{a}\exp\left\{-\frac{W(r)}{kT}\right\}d\left(\frac{r}{a}\right)\left[\int_0^{\frac{1}{2}}\left(\frac{r}{a}\right)^2\exp\left\{-\frac{W(r)}{kT}\right\}d\left(\frac{r}{a}\right)\right]^{-2}.$$

A notation, which has been used in previous papers of this series, is

$$g=2\int_0^{\frac{1}{2}}\left(\frac{r}{a}\right)^2\exp\left\{-\frac{W(r)}{kT}\right\}d\left(\frac{r}{a}\right).$$

Then putting $\qquad \dfrac{y}{a}=\phi;\quad \dfrac{r'}{a}=\xi;\quad \dfrac{r}{a}=\eta,$

we have

$$\rho(R)=\frac{1}{4\pi\rho_0g^2aR}\sum_i\frac{N_i}{z_i}\int_0^{\infty}d\phi\int_{|\phi-z_i/a|}^{\phi+z_i/a}\xi\exp\left\{-\frac{W(\xi)}{kT}\right\}d\xi\int_{|\phi-R/a|}^{\phi+R/a}\eta\exp\left\{-\frac{W(\eta)}{kT}\right\}d\eta.$$

A considerable simplification follows from the fact that the exponential terms are negligible when ξ and η are greater than $\frac{1}{2}$, for otherwise it would not be possible to say that the atom was in the neighbourhood of a lattice site. But $z_i/a \geqslant 1$, so that the integral involving ξ is non-zero only if $|\phi - z_i/a|$ is less than $\frac{1}{2}$, in which case ϕ is greater than $\frac{1}{2}$. In this case the upper limits $\phi + z_i/a$ and $\phi + R/a$ are certainly greater than $\frac{1}{2}$, and they can be replaced by $\frac{1}{2}$, giving

$$\rho(R) = \frac{1}{4\pi\rho_0 g^2 aR}\sum_i \frac{N_i}{z_i}\int_0^\infty d\phi \int_{|\phi - z_i/a|}^{\frac{1}{2}} \xi \exp\left\{-\frac{W(\xi)}{kT}\right\} d\xi \int_{|\phi - R/a|}^{\frac{1}{2}} \eta \exp\left\{-\frac{W(\eta)}{kT}\right\} d\eta. \tag{1a}$$

It is convenient to write

$$I(\alpha) = \int_{|\alpha|}^{\frac{1}{2}} \xi \exp\left\{-\frac{W(\xi)}{kT}\right\} d\xi$$

so that
$$\rho(R) = \frac{1}{4\pi\rho_0 g^2 aR}\sum_i \frac{N_i}{z_i}\int_0^\infty I\left(\phi - \frac{z_i}{a}\right) I\left(\phi - \frac{R}{a}\right) d\phi. \tag{2}$$

$I(\alpha)$ is zero unless $|\alpha| < \frac{1}{2}$; also $z_i/a \geqslant 1$, by their definition. Hence the integral in (2) is a function of $(z_i - R)/a$ only, and we can denote it by $G\{(z_i - R)/a\}$. We then have

$$\rho(R) = \sum_i \rho_i(R), \tag{3}$$

where
$$\rho_i(R) = \frac{1}{4\pi\rho_0 g^2 aR}\frac{N_i}{z_i} G\left(\frac{z_i - R}{a}\right). \tag{4}$$

An equivalent formula has been proved by Coulson and Rushbrooke (1939).

Some special cases may be noted. In the first place, a cell potential in the form of a trough with vertical sides is the example considered by Wall (1938). He assumed free motion in a cell of radius σ, that is,

$$\begin{aligned} W(r) &= 0 \quad \text{for } r \leqslant \sigma, \\ &= \infty \text{ for } r > \sigma. \end{aligned}$$

It can be verified that in this case (4) reduces to

$$4\pi R\rho_0\rho_i(R) = \frac{N_i}{\sigma z_i}\frac{3}{5}\left\{1 - \frac{5(z_i - R)^2}{4\sigma^2}\left[1 - \frac{|z_i - R|}{2\sigma} + \frac{|z_i - R|^3}{40\sigma^3}\right]\right\} \tag{4a}$$

(for $|z_i - R| \leqslant 2\sigma$), which was obtained by Wall.

Another simple potential is a parabola, probably a fair approximation at liquid volumes. This potential can be written as

$$W\left(\frac{r}{a}\right) = A\left(\frac{r}{a}\right)^2 kT. \tag{5}$$

If we neglect quantities involving $e^{-A/4}$, that is, if we assume that the potential rises so steeply that the atom is effectively confined to a cell, then

$$I(\alpha) = \int_{|\alpha|}^{\frac{1}{2}} \xi \exp(-A\xi^2)\, d\xi = \frac{1}{2A} e^{-A\alpha^2},$$

and

$$g = \int_0^{\frac{1}{2}} 2\xi^2 e^{-A\xi^2}\, d\xi = \frac{\sqrt{\pi}}{2A^{\frac{3}{2}}}.$$

Also

$$\begin{aligned} G\left(\frac{z_i - R}{a}\right) &= \int_0^\infty \exp\left[-A\left(\phi - \frac{z_i}{a}\right)^2 - A\left(\phi - \frac{R}{a}\right)^2\right] \frac{d\phi}{4A^2} \\ &= \frac{1}{4A^2} \exp\left[-\frac{A}{2}\left(\frac{z_i - R}{a}\right)^2\right] \int_0^\infty \exp\left\{-2A\left(\phi - \frac{z_i + R}{a}\right)^2\right\} d\phi \\ &= \frac{\sqrt{\pi}}{4\sqrt{2}\, A^{\frac{5}{2}}} \exp\left\{-\frac{A}{2}\left(\frac{z_i - R}{a}\right)^2\right\}. \end{aligned}$$

Thus the distribution function from the shell i is

$$\rho_i(R) = \frac{A^{\frac{3}{2}}}{4\sqrt{2}\, \pi^{\frac{3}{2}} \rho_0 a} \frac{N_i}{z_i} \frac{1}{R} \exp\left\{-\frac{A}{2}\left(\frac{z_i - R}{a}\right)^2\right\}. \tag{6}$$

This is effectively a Gaussian distribution, such as was used by Prins and Petersen (1936) and Bernal (1937).

3. APPLICATIONS

Lennard-Jones and Devonshire (1937) have found $W(r)$ by a suitable averaging. They considered a lattice in which each atom has c nearest neighbours, and took the potential of a pair of atoms, at distance a, to be

$$\phi_0\left\{\left(\frac{r_0}{a}\right)^{12} - 2\left(\frac{r_0}{a}\right)^6\right\}. \tag{7}$$

They showed that

$$W(r) = c\phi_0\left[\left(\frac{r_0}{a}\right)^{12} l\left(\frac{r^2}{a^2}\right) - 2\left(\frac{r_0}{a}\right)^6 m\left(\frac{r^2}{a^2}\right)\right], \tag{8}$$

where

$$l(y) = \frac{1 + 12y + 25{\cdot}2y^2 + 12y^3 + y^4}{(1-y)^{10}} - 1,$$

and

$$m(y) = \frac{1+y}{(1-y)^4} - 1.$$

Therefore

$$W(r) = \frac{r^2}{a^2} c\phi_0\left[22\left(\frac{r_0}{a}\right)^{12} - 10\left(\frac{r_0}{a}\right)^6\right] + 0\left(\frac{r^4}{a^4}\right).$$

For small amplitudes, the potential is parabolic, with A of equation (5) equal to

$$\frac{c\phi_0}{kT}\left[22\left(\frac{r_0}{a}\right)^{12}-10\left(\frac{r_0}{a}\right)^{6}\right].$$

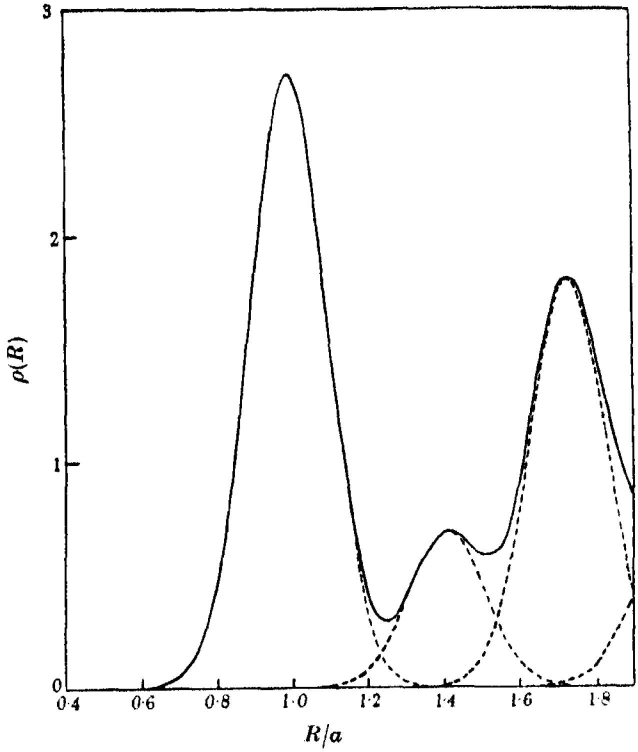

FIGURE 2. A typical distribution function of a face-centred cubic lattice, whose volume, temperature and force-constants are approximately those of argon at its boiling point. The dotted curves are the contributions of separate shells.

As an example, we may take a face-centred cubic lattice, whose volume and temperature are roughly those of argon at its boiling point. In this case $c = 12$, $V = Na^3 2^{-\frac{1}{2}}$, where N is Avogadro's number, $c\phi_0/kT \simeq 17$, $(r_0/a)^6 \simeq 0{\cdot}8$, and in round figures $A = 100$. Substituting in (6) and using the tables of N_t and z_t for this lattice, given in a paper of Prins and Petersen (1936), one finds the distribution function which has been plotted in figure 2. As there is little overlapping of the shells of neighbours, the variations of $\rho(R)$ are very pronounced.

It is unlikely that the theory will apply at the critical temperature, but tentative calculations have been made to see what kind of results would be obtained. The force-field (8) is then very far from parabolic, and the function $I(\alpha)$ must be found by numerical integration. This has been done for $\phi_0/kT = 0{\cdot}25$ and $0{\cdot}75$, the latter being the critical temperature approximately. The interatomic distance 'a' was such that $(r_0/a)^6 = 0{\cdot}228$. This corresponds, very nearly, to the critical volume on the theory of Lennard-Jones and Devonshire (1937) and is somewhat smaller than the experimental critical volume. This interatomic distance was chosen to permit comparison with the results of de Boer and Michels (1939), who have calculated an approximate distribution function from the Mayer-Born theory, and have used these volumes and temperatures. The results, based on a face-centred cubic lattice, are shown in figures 3 and 4.

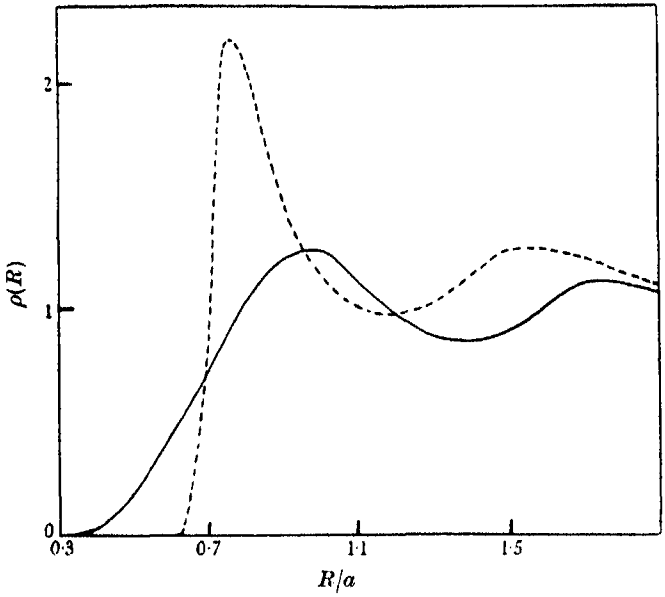

FIGURE 3. Distribution functions of a dense gas for $\phi_0/kT = 0{\cdot}75$ and $a = 1{\cdot}28r_0$, plotted as functions of r/a. The dotted curve is that from the theory of de Boer and Michels; the full curve is the result of the theory of Lennard-Jones and Devonshire. Volume and temperature in the critical region.

The results of the two theories are very different. The peaks of the present theory are much less pronounced and are also less affected by temperature changes than are those of de Boer and Michel's theory. The former also extend much more towards $R = 0$. The reason is clearly the breakdown of our approximation that each atom is restrained by the average field of its neighbours; presumably the experimental curves would have sharper peaks than ours. There do not appear to be any experimental $\rho(R)$ curves for the critical region of a monatomic gas. This is a gap in the experimental data which we hope will be filled in the near future. However, our curves show a property which was noticed by Spangler (1934) and Benz and Stewart (1934), in experiments with ethyl ether and isopentane. Their diffraction patterns varied very little with temperature at a constant volume near the critical volume.

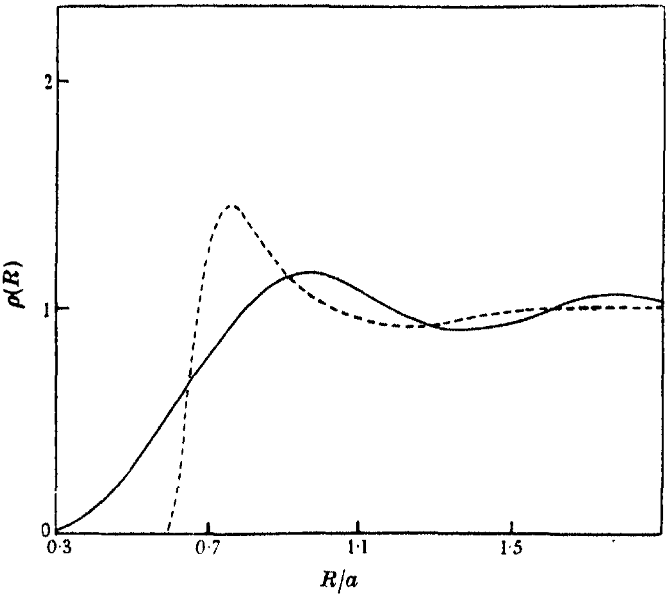

FIGURE 4. Curves similar to figure 3, except that $\phi_0/kT = 0{\cdot}25$. Temperature three times the critical temperature.

Rushbrooke (1939) has calculated the shape of the peak in liquid argon at 90° K by numerical integration. He used a potential energy of slightly different form from that which we have used.

The formulae we have given can be used for the analysis of the $\rho(R)$ curves derived from X-ray scattering data. It is first necessary to choose some simple form of potential which is at least approximately correct, and has not too many arbitrary parameters. Wall (1938) assumed free motion inside a sphere, the 'free volume' accessible to the atom; he obtained his three variables, the number of atoms in the first shell, its position, and the size of the free volume (for sodium) by fitting to the left side of the first peak, assuming that this part was entirely due to the first shell of neighbours. Using Bernal's suggestions for N_2/N_1 and z_2/a, Wall then found fair agreement with the experimental curves over the rest of the range. Coulson and Rushbrooke (1939) have repeated Wall's work, and have derived N_2/N_1 and z_2/a by adjusting these for best fit.

As an example of the use of a parabolic potential, we have examined the distribution function of liquid potassium at 70° C, given by Thomas and Gingrich (1938). This has been discussed by Gingrich and Wall (1939), following Wall's treatment for sodium.

Summing our result (6) over all the shells i, we have

$$4\pi^{\frac{3}{2}}\,2^{\frac{1}{2}}\rho_0 R\rho(R) = \sum_i \frac{N_i A^{\frac{1}{2}}}{az_i}\exp\left\{-\frac{A}{2}\left(\frac{z_i-R}{a}\right)^2\right\},$$

in which the left side is known from experiment. To represent any particular range of R, we can adjust a, A, and the N_i and z_i. These are sufficient to reproduce any reasonable experimental data; in fact, it is possible to approximate to any particular curve in an embarrassing variety of ways, because it is not known how many shells ought to be used in any range of R. The assumption that $\rho(R)$, up to the first peak, comes entirely from the first shell of neighbours, may be a good approximation in a liquid inert gas, where we expect a roughly face-centred cubic distribution. But solid sodium and potassium have a body-centred cubic structure, in which z_2/a, that is, the ratio of the radii of the second and first shells of neighbours, is only 1·155, while the number of second neighbours, 6, is not much less than the number of nearest neighbours, 8. This leads us to expect a considerable overlap of the distributions of these shells, for liquid sodium and potassium, and makes the problem more indefinite.

We have used the following process for separating the different shells. It can be used so long as the overlap is only moderate and gives the results for a small number of shells (certainly not beyond the third shell). We determine A, a, and N_1 by fitting a Gaussian distribution to the top and left side of the first peak, that is, the side with smaller R. This is best done by using the height, centre, and half-breadth. Subtracting from the whole distribution, we fit another error function to the left-hand side of the remaining distribution. A and a must be the same as before, so only N_2 and z_2 can be adjusted. Accurate values are not needed at this stage. We subtract this approximate second shell from the whole distribution, leaving a somewhat altered first peak. We now revise our values of A, a, and N_1 so that an error function fits the left and top of this new peak. Then we subtract this from the whole distribution, fit an error function to the left of the remainder, and so on. In a similar manner we can find a third shell, but after this the shells overlap so much that the method is useless. The convergence is rapid when there is only a little overlap. In the unfavourable case of potassium, we found that the process had to be carried through several cycles before the limiting result was obtained.

The results are given in table 1 assuming $A = 150{\cdot}3$. The fit obtained, and the relative contributions of these shells, are shown in figure 5. There is appreciable deviation near 3·6 A, where, however, the experimental results are not very reliable, owing to the importance of large-angle scattering.

TABLE 1. THE DISTRIBUTION FOR LIQUID POTASSIUM

Shell number, i	1	2	3
Radius, z_i, in A	4·42$_5$	5·10	5·90
Number of atoms in shell	5·5	3·8	3·6

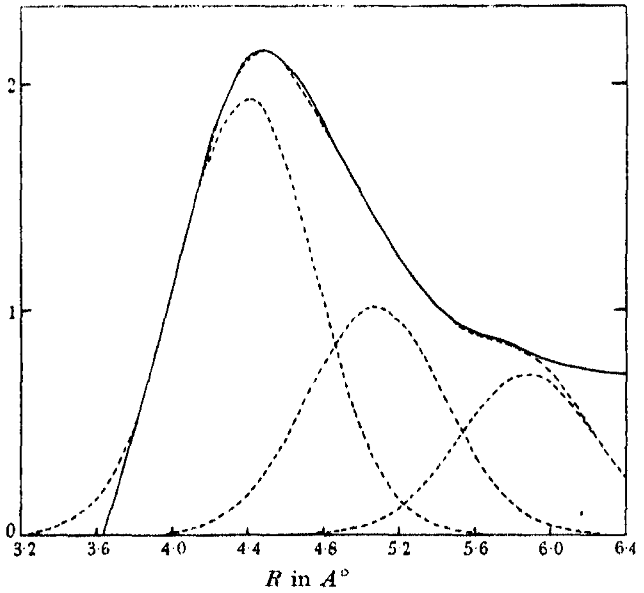

FIGURE 5. The experimental distribution function (full line) for liquid potassium at 70° C (Thomas and Gingrich), plotted as a function of distance in Ångströms, together with the separate contributions from the first three shells and their total distribution function (dotted lines).

The results differ considerably from those obtained by Wall (1938), Gingrich and Wall (1939), and Coulson and Rushbrooke (1939) in that we attribute the first peak to two overlapping shells, not to a single shell. In this respect our result shows a good deal of resemblance to the structure of solid potassium. The ratio z_2/a is 1·15, very close to the corresponding result for a body-centred cubic. However, the latter structure would not have a third shell in the position we have found, while the numbers in the first two shells would be bigger.

An unsatisfactory feature of the present method is the importance of the form of the theoretical distribution function where it tails off to zero. This depends on the repulsive potential near the wall of an atom's 'cell', so that to get a good result for the tailing-off it would be advisable to retain powers above r^2 in the general potential (8). It would then be necessary to do all the integrations numerically, just as for the critical region, already mentioned. The labour is not justified in the present case, because of the uncertainty as to the forces on an atomic ion in an alkali metal.

The numbers N_i in the shells can be altered by changes in the 'tailing-off' of the theoretical distribution, and it might be possible to make them integers by such changes. This is obviously desirable for easy visualization of the results.

We can obtain a rough check of our results in the following way. At a distance r from the centre of its cell, the potential of an atom is

$$(AkT/a^2)\,r^2 = 2\pi^2 m\nu^2 r^2,$$

where ν is the vibration frequency of the atom, of mass m. We assume that this ν, derived from an Einstein model, is the same as $\bar{\nu}$, the average frequency of a Debye spectrum. The Debye characteristic temperature is then

$$\Theta = \frac{4h\bar{\nu}}{3k} = \frac{4h(AkT)^{\frac{1}{2}}}{3\pi ka(2m)^{\frac{1}{2}}}. \tag{9}$$

Our results give Θ for potassium to be 107, which is in satisfactory agreement with the value of 100 for solid potassium, derived from specific heats (Simon and Zeidler 1926).

4. Determination of intermolecular forces from the distribution curve

The theoretical formula for the distribution function, given in equation (1), can be written in the form

$$\rho(R) = \left(\frac{1}{16\pi\rho_0 R}\right)\sum_i\left(\frac{aN_i}{z_i}\right)\int_0^\infty P\left(\frac{y-z_i}{a}\right)P\left(\frac{y-R}{a}\right)d\left(\frac{y}{a}\right), \tag{10}$$

where the P function is defined in terms of the probability function $p(r)$ by the relation

$$P(\theta) = \int_{|\theta a|}^{\frac{1}{2}a} p(r)\,dr/r. \tag{11}$$

Thus we have
$$\rho(R) = \sum_i \rho_i(R), \tag{12}$$

where
$$\rho_i(R) = \frac{aN_i}{z_i}\frac{Q\{(R-z_i)/a\}}{16\pi\rho_0 R}, \tag{13}$$

and
$$Q\left\{\frac{R-z_i}{a}\right\} = \int_{-\infty}^{\infty} P(\xi)\, P\left\{\frac{R-z_i}{a}-\xi\right\} d\xi. \tag{14}$$

According to this theory it should be possible to divide up the distribution function $\rho(R)$ into a number of component distributions $\rho_i(R)$ due to the different shells of neighbours. In principle, therefore, it should be possible, in so far as the theory is adequate, to determine the function $Q\{(R-z_i)/a\}$ from the observations. We wish to show that once the form of the function Q is found, the forces between the atoms (or molecules) of the liquid can be deduced.

If F is the Fourier transform of P, that is

$$F(t) = (2\pi)^{-\frac{1}{2}}\int_{-\infty}^{\infty} P(\theta)\exp(i\theta t)\, d\theta,$$

and so
$$P(\theta) = (2\pi)^{-\frac{1}{2}}\int_{-\infty}^{\infty} F(t)\exp(-i\theta t)\, dt, \tag{15}$$

then, by the definition of Q,

$$(2\pi)^{-\frac{1}{2}}\int_{-\infty}^{\infty} Q(\phi)\exp(i\phi t)\, d\phi = (2\pi)^{-\frac{1}{2}}\int_{-\infty}^{\infty}\exp(i\phi t)\, d\phi\int_{-\infty}^{\infty} P(\xi)\, P(\phi-\xi)\, d\xi.$$

By a known property of Fourier integrals (cf. Titchmarsh 1937), the right-hand side of this equation is equal to

$$(2\pi)^{\frac{1}{2}}\{F(t)\}^2. \tag{16}$$

It follows that

$$\begin{aligned} P(\theta) &= (2\pi)^{-\frac{1}{2}}\int_{-\infty}^{\infty} F(t)\exp(-i\theta t)\, dt \\ &= \left(\frac{1}{2\pi}\right)\int_{-\infty}^{\infty}\exp(-i\theta t)\left[\int_{-\infty}^{\infty} Q(\phi)\exp(i\phi t)\, d\phi\right]^{\frac{1}{2}} dt. \end{aligned} \tag{17}$$

These formal processes do not lead to convergence difficulties, since $Q(\phi)$ is exponentially small outside a small range of ϕ. Hence when the function Q is known, the function P can be inferred, and since P is simply related to $p(r)$, equation (11), the probability function can be deduced. From the definition of $p(r)$ it is then possible to determine the interaction energy $W(r)$.

Thus formally we have $p(r/a) = -r\dfrac{\partial}{\partial r}P(r/a),$

and so
$$r^2\exp\left\{-\frac{W(r)}{kT}\right\}\bigg/\int_0^{\frac{1}{2}a} r^2\exp\left\{-\frac{W(r)}{kT}\right\}dr$$
$$= \frac{ir}{2\pi a}\int_{-\infty}^{\infty} t\exp\left(-\frac{itr}{a}\right)\left[\int_{-\infty}^{\infty} Q(\phi)\exp\left(i\phi t\right)d\phi\right]^{\frac{1}{2}}dt. \qquad (18)$$

It is not at present possible to use this formula because the observed $\rho(R)$ cannot be divided into contributions from the different shells in a unique manner. This would require accuracy of a high order in the experimental results. Moreover, the theoretical curves for $\rho_i(R)$ do not seem to be sensitive to changes in $W(r)$, so in the converse process $W(r)$ may be expected to be sensitive to inaccuracies in the curves for $\rho_i(R)$. At present the accuracy of the experimental data is only sufficient to justify the use of simple forms of interaction energy.

One of the authors is indebted to the Goldsmiths' Company for the award of a Senior Studentship. We also wish to thank Dr A. F. Devonshire and Dr M. V. Wilkes for their assistance in the computation of the distribution functions in the critical region, and Dr Coulson and Mr G. S. Rushbrooke for a helpful discussion of this subject.

(*Added in proof.* In case recent work on this subject has been overlooked, it should be stated that this investigation was completed before the war began, since when both authors have been engaged on other work.)

REFERENCES

Benz, C. A. and Stewart, G. W. 1934 *Phys. Rev.* **46**, 703.
Bernal, J. D. 1937 *Trans. Faraday Soc.* **33**, 27.
de Boer, J. and Michels, A. 1939 *Physica*, **6**, 97.
Coulson, C. A. and Rushbrooke, G. S. 1939 *Phys. Rev.* **56**, 1216.
Debye, P. and Menke, H. 1930 *Phys. Z.* **31**, 797.
Gingrich, N. S. and Wall, C. N. 1939 *Phys. Rev.* **56**, 336.
Lennard-Jones, J. E. and Devonshire, A. F. 1937 *Proc. Roy. Soc.* **A, 163**, 53.
Menke, H. 1932 *Phys. Z.* **33**, 593.
Prins, J. A. and Petersen, H. 1936 *Physica*, **3**, 147.
Rushbrooke, G. S. 1939 *Proc. Roy. Soc., Edinburgh*, **60**, 182.
Simon, F. and Zeidler, W. 1926 *Z. phys. Chem.* **A, 123**, 383.
Spangler, R. D. 1934 *Phys. Rev.* **46**, 698.
Thomas, C. D. and Gingrich, N. S. 1938 *J. Chem. Phys.* **6**, 411.
Titchmarsh, E. C. 1937 'Fourier Integrals', p. 51. Oxford.
Trimble and Gingrich 1938 *Phys. Rev.* **53**, 278.
Wall, C. N. 1938 *Phys. Rev.* **54**, 1062.

On the electron diffraction of multilayers of esters of fatty acids. I

By A. Cameron and G. D. Coumoulos

(*Communicated by E. K. Rideal, F.R.S.—Received* 9 *December* 1940.—
Revised 25 *April* 1941)

The arrangement of the long axis of the long-chain organic molecules is revealed by electron diffraction patterns of inclined specimens.

The side spacings are estimated from a composite pattern of kaolin which has a known 'standard' structure and lattice constants.

A 3 cm. vacuum valve was designed to isolate the apparatus from the oil-diffusion pumps.

Films of long-chain organic molecules spread from petrol-ether solution in the Langmuir trough reveal molecular orientation and consist of a monolayer of molecules. Dervichian (1939) concluded that for solid films the lattice structure and the tilt of the molecules are the same both in two and three dimensions for the different crystal forms. A microscopical examination of a multilayer of long-chain esters, after a period had lapsed since deposition, indicated the presence of microscopic crystals (Stenhagen 1938), and that the molecules were arranged in some regular way (Knott, Schulman and Wells 1940) from the base of the multilayer to the surface. Bernstein (1940) suggested from X-ray measurements of an ethyl stearate multilayer that all these crystallites have the same orientation, whilst Knott, Schulman and Wells (1940) reached the conclusion that the multilayers of the long-chain esters do not consist of crystallites arranged entirely at random.

By electron diffraction it is possible to investigate the crystal structure of thin multilayers and even a monolayer (Havinga and Wael 1937) of the esters of the fatty acids. In addition, the photographs can be obtained shortly after deposition, before any alteration due to 'aging' might occur. As the multilayer is polycrystalline with a pronounced preferred orientation, the transmission pattern produced by a specimen inclined towards the incident beam will consist of features other than those appearing when the specimen is orientated normal to the beam. If the common axis of orientation of the crystallites, i.e. the 'fibre' axis, is not normal to the membrane supporting the multilayer, then patterns of the same specimen, inclined in different directions, will develop other h, k, o diffraction families.

By examining the electron-diffraction patterns of the same multilayer of a long-chain ester in different inclined positions, we can draw certain conclusions concerning the tilt of the orientation axis of the crystallites, i.e. the tilt of the long chain of the molecules.

APPARATUS AND TECHNIQUE

The camera. The electron-diffraction camera used is of the hot-cathode type, previously used in this laboratory by Lees (1935) to investigate the structure of polished metal surfaces. It was modified by insertion of a wide-bore stopcock between the apparatus and the battery of oil-diffusion pumps. The valve, of inner diameter 3 cm., is similar to that described by Du Mond (1935) and Rose (1937), and is equipped with a syphon bellows as substitute for a packing gland. It is thus possible to open the camera and change the specimen or the photographic plate while the system of oil-diffusion pumps and Hyvac pump continues running. Before the camera is reconnected to the high vacuum line it is partly evacuated by means of the Hyvac.

The voltage applied to the electron gun was determined by measuring the current in a resistance of 120 MΩ, connected across the electron gun. The resistance was made according to Bowdler's (1933) design.

Supporting membrane. The film holder consists of a ring over which a nitrocellulose supporting membrane is stretched. The ring is chromium-plated and polished, with a central aperture of 1 mm. diameter. If the edge of this opening is not quite plane and flat the supporting membrane is curved, and then the pattern of the supported specimen layer is distorted. Three screw holes are made in the ring radially and mutually at right angles to each other, and serve to hold the ring while dipping it in the Langmuir trough. The ring can be screwed into the camera's specimen-holder by either of these holes, and by inclining the ring towards the incident electron beam all possible positions required can be obtained.

The nitrocellulose membranes are deposited on the ring by means of a modified Ruska (1939) apparatus. On a clean surface of water saturated with amyl acetate a thin membrane (150 A thick) of nitrocellulose is formed from one drop of a 1 % amyl acetate solution. The surface level of the water is lowered and the nitrocellulose membrane is lowered on to the ring which is held horizontally under the water surface by means of a holder. It has been found essential to ensure that the supporting nitrocellulose membrane has preserved its amorphous state and is free from grease or impurities which give rise to the phenomenon of 'extra' rings.

. When the patterns of a specimen of a nitrocellulose membrane do not give at selected intervals up to 20 hr. any crystalline diffraction features, then the sample of the nitrocellulose solution is suitable for use. This test for intervals up to 20 hr. must always be repeated before depositing on the cellulose membrane the thin layers of the chemical compounds under examination. The electron diffraction pattern of the amorphous state of nitrocellulose consists of three characteristic halos (Kakinoki 1939).

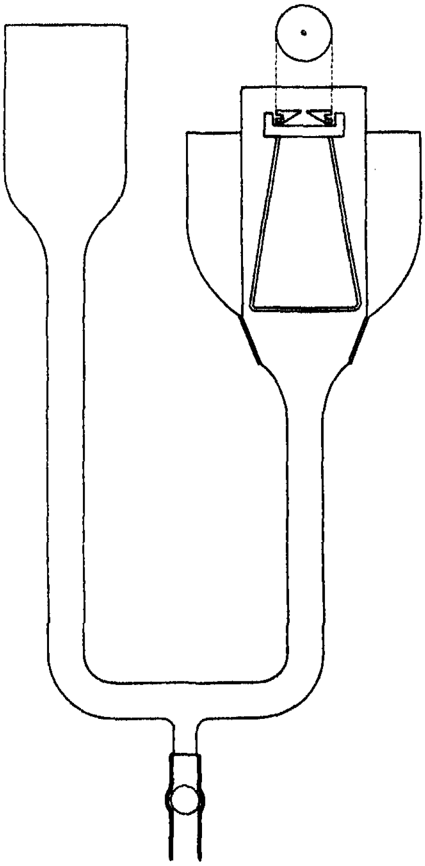

FIGURE 1

Multilayers. The multilayers were deposited from distilled water by the method described by Blodgett (1935).

Calculation of λ. The wave-length λ was either calculated from direct measurements of the voltage applied to the electron gun, or by superimposing on the photographed pattern of the compound under consideration the pattern of a calibrating substance of known structure and lattice constant. As the spacings of the ($hk0$) planes are known for kaolin (Shishacow 1937), those corresponding to the rings given by the unknown substance can be deduced. This method has been developed further by depositing the crystals of kaolin on the rear surface of the supporting cellulose membrane, before or after the deposition on the front surface of the multilayer. In this way the patterns are superimposed simultaneously and thus we can record a composite pattern. Composite patterns of kaolin and multilayers of organic long-chain molecules give distinct features of both patterns (part II, figures 2–5, plate 11).

EXPERIMENTAL

The multilayer specimen being polycrystalline with a common axis of orientation will give rise to a diffraction pattern which, while the incident beam is parallel to the orientation axis, will consist of either Debye-Scherrer rings or pairs of arcs at the opposite ends of diameters (of the same circles), in groups exhibiting a symmetry characteristic of the crystal. In the inclined positions only the planes that will remain or become parallel to the beam will give rise to two spots or arcs at the opposite ends of a diameter, this diameter being perpendicular to the reflexion plane. When dealing with built-up multilayers it may be presumed that the tilt of the long chain is in a plane perpendicular to the supporting base (i.e. parallel to the beam) and in the direction of dipping. This is a simple and special case, as in general the tilt may be in a selected perpendicular plane in an 'upward' or 'downward' sense to the dipping direction. We will examine this case.

The only planes which will reflect are those whose normals coincide closely with the axis of the specimen rotated; more than one axis must be tried to determine the angle of tilt of the long chain of the molecules. One such axis of inclination should be the direction of dipping and another at right angles to it. Furthermore, when the axis at right angles to the dipping direction is examined, both positive and negative directions of tilt must be tested. In all cases the axis of tilt lies on a plane normal to the beam. In figure 2 the tilt of the long-chain molecule is either upward or downward with respect to the dipping direction, for the position perpendicular to the beam (p) there is no difference, but two (or four) distinct positions are possible for the tilted specimen; d (I and II) and the l (I and II) (figure 2).

In the electron-diffraction pattern of long-chain molecules (paraffins, fatty acids, greases, etc.), it was suggested by Murison (1934) and shown by Motz and Trillat (1935) that the pattern is caused by interference between the successive (CH_2) groups of the carbon chain. The distance of the reciprocal points in the direction parallel to the long axis of the molecule is much larger than the distance in the perpendicular direction. So, even in the inclined position of the specimen, the only features appearing in the pattern are due to the planes which remain or become parallel to the beam and which appear as pairs of spots or arcs at opposite ends of a diameter, this latter being the projection of the axis. The sphere of reflexion does not pass through those reciprocal points corresponding to a pyramidal plane.

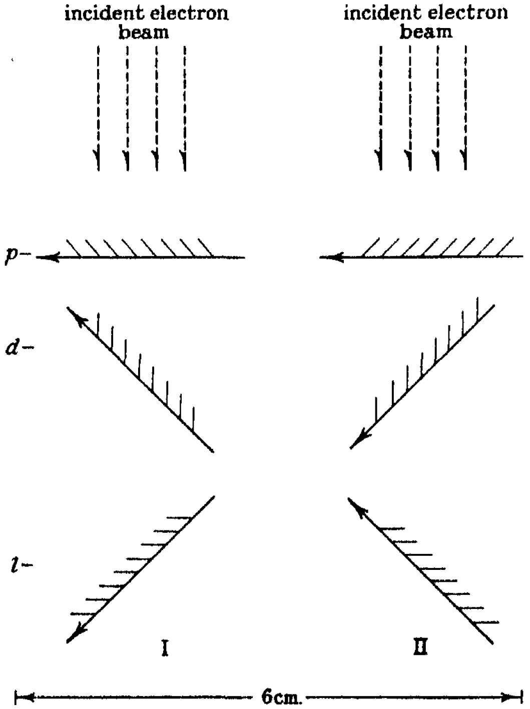

FIGURE 2

If the patterns of all the inclined positions show the same pairs of arcs at opposite ends of a diameter, then the reflecting planes in all azimuthal directions are parallel to the beam or, more accurately, there are in all directions some planes parallel to the incident electron beam. For the case of organic long-chain molecules this means many crystalline aggregate units are normal, and for a multimolecular layer, where a pronounced preferred orientation is expected, all the long axes of the organic long-chain molecules are normal. When the long-chain molecules of a multilayer are tilted in a common direction, then only one of the inclined positions gives a good pattern of pairs of arcs on opposite ends of a diameter.

These patterns resemble those which Burgers and Van Amstel (1936) succeeded in photographing with their reciprocal lattice model for paraffins, where the long chains are vertical.

RESULTS

The patterns of inclined specimens for methyl and ethyl stearate and octadecyl-acetate are all similar and have as characteristic features pairs of arcs at opposite ends of diameters for all the possible positions. The patterns of the inclined specimen of cholesterol acetate (part II, figure 1, plate 11) present entirely different features. The features of inclined specimens of the two-dimensional crystals of silica, formed by evaporating a suspension of kaolin (part II, figures 2–5, plate 11) in water on a cellulose film, give arcs of symmetrical pyramidal planes and show that the c-axis of the hexagonal symmetry is normal to the supporting film.

Our thanks are due to Professor E.K. Rideal for his stimulating criticism, also to the British Council for the grant of a scholarship (G.D.C.) and to the Salter's Institute of Industrial Chemistry for the grant of a Fellowship (A.C.).

REFERENCES

Bernstein 1940 *J. Amer. Chem. Soc.* **62**, 324.
Blodgett 1935 *J. Amer. Chem. Soc.* **57**, 1007.
Bowdler 1933 *J. Instn Elect. Engrs*, **73**, 65.
Burgers and Van Amstel 1936 *Z. Kristallogr.* **95**, 54.
Dervichian 1939 *J. Chem. Phys.* **7**, 939.
Du Mond 1935 *Rev. Sci. Instrum.* **6**, 285.
Havinga and Wael 1937 *Rec. Trav. Chim. Pays-Bas*, **56**, 375.
Kakinoki 1939 *Proc. Phys. Math. Soc. Japan*, **21**, 66.
Knott, Schulman and Wells 1940 *Proc. Roy. Soc.* A, **176**, 534.
Lees 1935 *Trans. Faraday Soc.* **31**, 1102.
Motz and Trillat 1935 *Z. Kristallogr.* **91**, 248.
Murison 1934 *Phil. Mag.* (7), **17**, 201.
Rose 1937 *Rev. Sci. Instrum.* **8**, 130.
Ruska 1939 *Naturwissenschaften*, **27**, 290.
Shishacow 1937 *Phil. Mag.* (7), **24**, 687.
Stenhagen 1938 *Trans. Faraday Soc.* **34**, 1328.

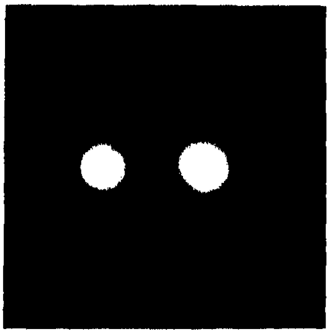

FIGURE 1. Pattern of cholesterol acetate. The (*b*) is of the tilted specimen.

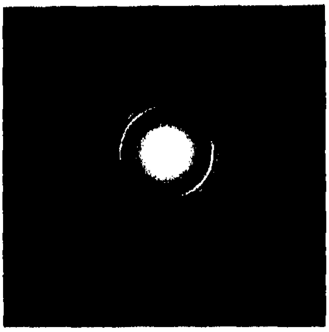

FIGURE 2

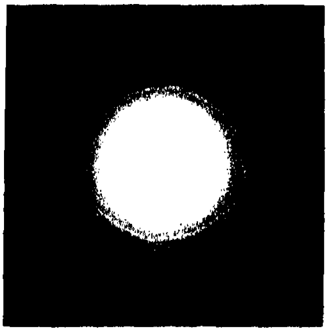

FIGURE 3

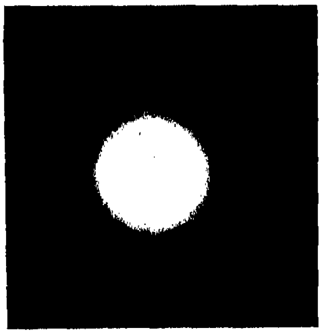

FIGURE 4

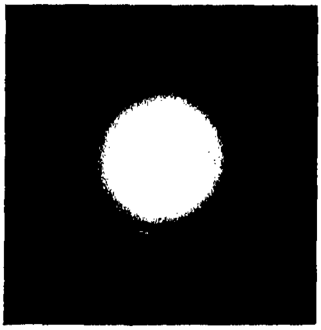

FIGURE 5

FIGURES 2–5. Composite patterns of the same specimen of methyl stearate with the 'standard' kaolin. No. 2 is perpendicular to the beam. No. 3 is tilted 30° with the 'dipping direction' as axis. No. 4 is tilted 30° in the *d*-position. No. 5 is tilted 30 in the *l*-position. The pairs of arcs on the diameter which coincide with the axis of tilt are characteristic of the multilayer.

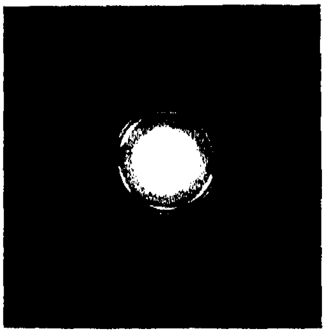

Figure 6. The 'hexagonal' arrangement of the pairs of arcs in a pattern of a methyl stearate multilayer.

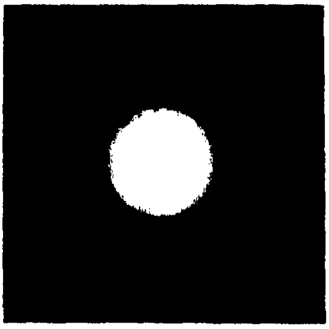

Figure 7

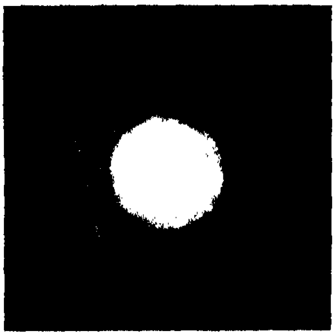

Figure 8

Figures 7, 8. 'Aged' multilayers. A 14-molecule-layers multilayer of ethyl stearate. No. 7 50 hours after deposition and No. 8 after 125 hours; the number of the irregular sited spots became smaller.

On the electron diffraction of multilayers of esters of fatty acids

II. The structure of multilayers of the esters

By G. D. Coumoulos and E. K. Rideal, F.R.S.

(*Received* 9 *December* 1940.—*Revised* 25 *April* 1941)

[Plates 11, 12]

Electron-diffraction data for the arrangement and the orientation of the molecules and the side spacings of the two-dimensional crystals of thin multilayers of methyl and ethyl stearate, and octadecyl acetate are given.

A state similar to the α-modification in crystals is a stable form for thin multilayers of long-chain esters.

The 'multilayer' state is transient and is replaced by an aggregation of micro-crystals with 'fibre' orientation.

1. Introduction

The long-chain paraffins and their simpler derivatives are known to exist in three main polymorphic crystalline modifications, the α, β and γ forms. The transparent α form exists in equilibrium with the melt, has a low melting-point, shows many of the properties of liquid crystals, and was shown by Malkin (1931, 1933), who examined melts of the esters, to give only one side (*hko*) spacing of 4·2 A when examined by X-rays. The long chains are vertical to the basal plane formed of the groups terminating the molecules. The molecules are capable of rotating round their long axis, a view confirmed by the dielectric constant measurements of Smyth and Baker (1937, 1938) for ethyl stearate and palmitate.

The β form in which the chains are tilted, reveals two side spacings of 3·7 and 4·2 A respectively and has a higher melting-point than the α form, whilst the γ has the highest melting-point of the three.

Müller (1932), in an exhaustive X-ray examination of the *n*-paraffins, showed that in the orthorhombic crystals from C_{21} to C_{27} a hexagonal symmetry is acquired near the melting-point, the *c*-axis parallel to the vertical chain remains unaltered on heating, but the *a*-axis increases at a greater rate than the *b*, thus approaching a hexagonal symmetry not quite attained in C_{18} and C_{20}. Müller thus suggests that rod-like molecules behave as if they had a cylindrical symmetry as the substance approaches the melting-point.

That the different modifications of polymorphic states are preserved in very thin layers can be noted by the identification by electron diffraction and X-rays of the three forms of the monoclinic stearic acid in a frozen lens formed on water from a benzene solution by Trillat and Hirsch (1933). Miss Denard (1939) also obtained evidence for the three forms of crystals of the acid in a built-up multilayer.

We note that Havinga and de Wael (1937) successfully obtained good electron diffraction patterns of monolayers of barium stearate, whilst Germer and Storks (1938) studied the arrangement of molecules in monolayers and multilayers of similar compounds by electron transmission, the films being deposited on a 'resoglaz' support. They found that even the monolayers had a regular arrangement.

2. THE STRUCTURE OF THE MULTILAYERS OF LONG-CHAIN ESTERS

Except for the long spacings there are no data from complete crystallographic investigation either for single crystals or for multilayers of the long-chain esters. Germer and Storks (1937) studied a thin layer of methyl stearate by the reflexion method of electron diffraction and concluded that the long chains must be tilted. A more detailed study by electron diffraction of the side spacings of long-chain esters was made by Natta and Rigamonti (1935). They examined a number of long-chain derivatives of cerotic and other acids in the form of frozen lenses formed from benzene on a water surface. All their side spacings correspond to the (*hko*) of an orthorhombic structure $a = 7{\cdot}46$ A, $b = 4{\cdot}98$ A similar to the *n*-paraffin.

Earlier, Murison (1934) and Motz and Trillat (1935) had examined similar compounds, but not in a pure state and did not give all the side spacings. These were calculated by Finch and Quarrel (1935) from observations of thin layers of grease and were found to coincide with those of the pure paraffins. Schoon (1938) found by electron diffraction that cetyl palmitate in the form of thin layers was present in the oblique β form.

Malkin (1933), from X-ray investigation, concluded that in crystals, the α form was metastable, in the case of ethyl stearate being just realizable below the melting-point. Long spacing measurements showed that it crystallized in layers of single molecules, but in the case of methyl stearate the β form in double molecular layers was formed. A similar metastability for the α form was noted in octadecyl acetate by Philip and Mumford (1934) from the thermal data, a result confirmed by other workers (Van Bellington 1938; Francis and Piper 1939).

X-ray measurements of long-chain esters in the form of thick multilayers were made by Stenhagen (1938), who found stable β forms for methyl and ethyl stearates, the former in double molecule layers. For octadecyl acetate he obtained both the single molecule α form and the double molecule β form dependent on the mode of deposition of the multilayer. The measurements for these compounds have recently been confirmed and extended by Wells, Knott and Schulman (1940).

3. EXPERIMENTAL

The apparatus and the technique for taking transmission photographs have been described in part I. The multilayers were built up in the usual way by X, Y or Z deposition (see Bikerman 1939) at intervals, during which photographs of the electron diffraction patterns were taken. Some multilayers were variable in deposition, being occasionally X- and also as Y-. Multilayers of 2 to 6 layers in thickness did not always produce good patterns. The multilayer specimens were usually built up from 2 to 20 layers. From every specimen of a multilayer, photographs were taken from all the possible positions of inclination as described in part I. The crystals of Si_2O_5 in the kaolin (which serves as a 'standard' substance) on the rear surface of the nitrocellulose support were deposited either before or after the deposition of the multilayer on the front surface.

Diffraction patterns of these multilayer specimens were taken at intervals from 1 up to 200 hr. after their preparation. When the calibrating substance was not used, the wave-length was estimated from direct voltage measurements across the electron-gun as described in part I. The long-chain esters, methyl and ethyl stearate and octadecyl acetate, were prepared as described by Alexander and Schulman (1937). Their solutions were prepared from grease-free petrol ether or benzene. Every precaution was taken to avoid contact of the specimens with grease.

4. RESULTS

The same type of pattern was obtained from the multilayers of all three compounds. The features of these patterns reveal the same orientation and arrangement of the molecules in the multilayer and the same side spacings of the reflecting planes.

All the diffractions are derived from a typical pseudo cross-grating pattern (hko), the basal plane (001) being always parallel to the supporting nitrocellulose membrane, which in its turn is normal to the beam.

Most of the fresh multilayer specimens revealed, as typical diffraction features, arcs arranged with a hexagonal symmetry (plate 12, fig. 6). This is one indication that the crystallites in the polycrystalline multilayer are relatively large and that the characteristic symmetry is due to a zone axis parallel to the incident beam. From the side spacings it can be deduced that this hexagonal symmetry is not characteristic of the crystal lattice, but is a pseudo-regularity due to twinned orthorhombic crystals.

'Aged' specimens. The hexagonal arrangement is destroyed as the multilayer-specimen becomes 'aged'. Figures 7 and 8 of plate 12 show patterns of the same specimen after 50 and 125 hr. respectively. The features of an aged specimen are those of a microcrystalline pattern with one of the axes parallel in all crystallites. The Debye-Scherrer rings corresponding to the side spacings are formed from irregularly arranged spots showing that the crystallites covered by the electron beam are not numerous. The more aged multilayers show these features more markedly.

The long chains are orientated in a vertical position to the supporting membrane, i.e. to the basal plane (001). The photographs (figures 3–5, plate 11) of the diffraction patterns of all possible inclined positions show the same pairs of arcs at opposite ends of diameters. These arcs correspond to side spacings of all the possible reflecting planes perpendicular to the basal plane (001).

The side spacings are summarized in table 1. In the majority of cases they were deduced from the known side spacings of the 'standard' kaolin. The mean values of the side spacings of all three compounds are identical, also the intensities of the rings with the same (*hko*) indices.

The rings of the fresh specimens were sharp and the radii were measured to 0·1 mm.; thus the error in estimating the side spacings is *ca* 1·0 %. These spacings correspond to an orthorhombic crystal with lattice constants $a = 7{\cdot}48$ A, $b = 5{\cdot}02$ A, with an area of the basal plane (001) of the unit cell 37·55 A^2 and $\phi = 67^\circ\ 44'$.

Garrido and Hengstenberg (1932) found the same pattern of hexagonal symmetry for the $C_{21}H_{44}$ paraffin. They also suggested that it was a pseudo-regularity due to the twinning habit of the orthorhombic paraffins. Similar side spacings and lattice constants ($a = 7{\cdot}46$ A, $b = 4{\cdot}98$ A) of the orthorhombic crystal structure were found by Natta and Rigamonti (1935) for long-chain esters. These results agree with the crystallographic data that Müller (1928) obtained by X-ray investigation for the orthorhombic paraffins. They suggest that all the compounds (esters, acids, ethers, etc.) they studied have the same configuration and possess a two-dimensional isomorphism when in very thin layers.

TABLE 1

kaolin		long-chain esters			
indices (hko)	side spacing A d_{hko}	indices (hko)	side spacing A d_{hko}	intensity of ring	azimuth of hexagonal symmetry of arcs
100	4·45	—	—	—	—
		110	4·17	v.s.	0°
		200	3·74	v.s.	0°
		210	3·00	f.	—
110	2·561	—	—	—	—
		020	2·51	s.	30°
		120	2·38	w.	—
		310	2·24	f.	30°
200	2·205	—	—	—	—
		220	2·08	s.	0°
		400	1·87	w.	0°
		320 410	1·76	w.	30°
210	1·688	—	—	—	—
		130	1·63	w.	30°
300	1·491	—	—	—	—
220	1·291	—	—	—	—
310	1·24	—	—	—	—

Intensity scale v.s. > s. > f. > w.

The different results which Germer and Storks (1937) obtained for methyl stearate may be due to their method of deposition, for their thin layer specimen was deposited on a metal surface.

Schoon (1938), in studying the polymorphic forms of organic long chains, defines three main structures for the different modifications he found by electron diffraction in thin layers. Further, he finds that the best value for the basal area is $ab \sin \beta = 37{\cdot}0\ \text{A}^2$, which is constant for all the polymorphic forms of the long-chain compounds. The multilayer specimens of the esters examined here belong to the first of these structures.

	a	b	β
(1)	5·0 A	7·5 A	90°
(2)	5·6	7·5	60
(3)	9·5	5·0	54

5. DISCUSSION OF RESULTS

The electron diffraction data obtained show that methyl and ethyl stearate and octadecyl acetate in very thin multilayers possess the orthorhombic structure of the polymorphic crystalline forms. This is deduced from the side-spacings and not from the long spacings as in X-ray investigations. The only study of polymorphic modifications of very thin multilayers by electron diffraction is that of stearic acid by Germer and Storks (1938). Stenhagen (1938) investigated by X-rays the modifications of long-chain esters in very thick multilayers by measuring the long spacings.

The more detailed X-ray investigation in 1000 layer multilayers of these compounds carried out by Wells, Knott and Schulman (1940) showed that these multilayers have good three-dimensional crystal lattices; their structure is of the oblique type.

It would thus appear that the configuration which is stable in these thin multilayers is different from that in very thick multilayers. Furthermore, it may be possible that this is generally true of very thin layers of long-chain molecules as observed in the investigations of Natta and Rigamonti.

Other indications that in very thin multilayers modifications other than in a three-dimensional state are stable are to be noted in Dervichian's (1939) study on the relations between the melting-points in two dimensions and three dimensions. The melting-point, as he defines it, of the two-dimensional state is in many cases lower than the normal three-dimensional melting-point. He measured such differences in monolayers of glycerides and acids and found that the two-dimensional melting-point of the monolayers could be correlated with the melting-point of the metastable vitreous form, which the glycerides possess in three dimensions; thus the vitreous form is more stable under monolayer than under ordinary conditions. Further, he suggests that for the acids only the vitreous form exists in two dimensions, although there is evidence for a vitreous form for bulk palmitic acid.

The vitreous state described by Dervichian coincides with the characteristic transparent solid of the α-modification. This modification is metastable for all three esters in bulk, but Stenhagen found the α-modification stable in a multilayer of octadecyl-acetate. Methyl stearate is not realizable in the metastable α-modification, while the two other esters are just below the melting-point. Thus the esters in the form of very thin multilayers may possess a stable modification only existent in two dimensions or be metastable in the three-dimensional state.

This modification resembles the α-modification of the three-dimensional crystals of the esters, but has not hexagonal symmetry which Malkin had suggested for them near their melting-point. Müller found that the n-paraffins similar in chain length to C_{18} and C_{20} did not attain hexagonal symmetry, while approaching the melting-point, as their higher homologues do.

That a fresh multilayer may possess a 'vitreous' or transparent state, the other characteristic of the α-modification, is confirmed by Bikerman's (1939) microscopical examination of fresh multilayers deposited on wire gauze. Multilayers at the moment of deposition can be compared to soap films stretched between irregularities of the surface. The multilayer undergoes changes as it becomes aged, but remains transparent at the different stages of the change. His observations were made on a multilayer of octadecyl-acetate.

The higher values of the crystal lattice constants $a = 7{\cdot}48$ A and $b = 5{\cdot}02$ A of the orthorhombic unit cell are due to thermal expansion, as the melting-points of the compounds under examination are low and near room temperature.

The experimental conditions in the electron diffraction camera are different from those of the X-ray investigation. The multilayer specimen is placed immediately after its deposition in a high vacuum, so the patterns recorded are of highly dried specimens, and during the exposure the electron beam heats up the multilayer. The energy provided by the fast electrons is even sufficient to effect melting (Trillat and Okehani 1936; Tanaka 1938). Whilst the temperature of the specimen during exposure cannot be estimated at least by the transmission method, the high values of the lattice constants present evidence for such a temperature rise.

Another feature noted in this investigation is the short life of the special 'multilayer state'. Stenhagen (1938) showed by microscopical observations that the ethyl stearate multilayer, shortly after deposition, undergoes a transformation and forms micro-crystals. These observations were extended for the three esters here studied by Wells, Knott and Schulman (1940), who found, in the 1000 layer multilayers they used, that these micro-crystals are single crystals from the base to the surface of the multilayers.

Of more interest is Bikerman's (1939) description of the stages of change of thin multilayer stretched on a wire gauze. A soap-like film develops to a dry gel which breaks up to an aggregation of gel particles or micro-crystals. These observations are in agreement with the features of the diffraction patterns of the aged multilayer specimens. The regular hexagonal arrangement of the pairs of arcs is gradually replaced by irregularly sited spots on the Debye-Scherrer rings, the number of these spots decreasing as the multilayer becomes more aged. These diffraction features may be interpreted on the view that the fresh film is in the polycrystalline state with crystallites large enough to give rise to pairs of spots or arcs revealing a symmetry characteristic of the crystal. The irregularly sited spots appear when micro-crystals are formed with a 'fibre' orientation and these are not numerous enough to give a continuous Debye-Scherrer or 'powder pattern' ring. These multilayers remain 'fresh', i.e. retain their special state at room temperature for 20–30 hr. after their deposition on the nitrocellulose base; for this period the diffraction patterns do not reveal features indicating the existence of the fibro-crystalline state. We can thus detect the stages by which the multilayer loses its special character.

Our thanks are due to the British Council for a Scholarship granted to one of us (G.D.C.).

References

Alexander and Schulman 1937 *Proc. Roy. Soc.* A, **161**, 115.
Bikerman 1939 *Proc. Roy. Soc.* A, **170**, 130.
Denard 1939 *J. Chim. Phys.* **36**, 210.
Dervichian 1939 *J. Chem. Phys.* **7**, 931.
Finch and Quarrel 1935 *Nature, Lond.*, **136**, 720.
Francis and Piper 1939 *J. Amer. Chem. Soc.* **61**, 577.
Garrido and Hengstenberg 1932 *Z. Kristallogr.* **82**, 477.
Germer and Storks 1937 *J. Chem. Phys.* **5**, 131.
Germer and Storks 1938 *J. Chem. Phys.* **6**, 281.
Havinga and de Wael 1937 *Rec. Trav. Chim. Pays-Bas*, **56**, 375.
Malkin 1931 *J. Chem. Soc.* p. 2776.
Malkin 1933 *Trans. Faraday Soc.* **29**, 977.
Motz and Trillat 1935 *Z. Kristallogr.* **91**, 248.
Müller 1928 *Proc. Roy. Soc.* A, **120**, 437.
Müller 1932*a* *Nature, Lond.*, **129**, 436.
Müller 1932*b* *Proc. Roy. Soc.* A, **138**, 514.
Murison 1934 *Phil. Mag.* (7), **17**, 201.
Natta and Rigamonti 1935 *R.C. Accad. Lincei*, (6), **22**, 342.
Philip and Mumford 1934 *J. Chem. Soc.* p. 1657.
Schoon 1938 *Z. phys. Chem.* B, **39**, 385.
Smyth and Baker 1937 *J. Chem. Phys.* **5**, 666.
Smyth and Baker 1938 *J. Amer. Chem. Soc.* **60**, 1229.
Stenhagen 1938 *Trans. Faraday Soc.* **34**, 1328.
Tanaka 1938 *Mem. Coll. Sci. Engng Kyoto*, A, **21**, 85.
Trillat and Hirsch 1933 *J. Phys. Radium*, **4**, 38.
Trillat and Okehani 1936 *C.R. Acad. Sci., Paris*, **202**, 1332.
Van Bellington 1938 *Bull. Soc. Chim. Belge*, **147**, 640.
Wells, Knott and Schulman 1940 *Proc. Roy. Soc.* A, **176**, 534.

The catalysis of the parahydrogen conversion by tungsten

By D. D. Eley and E. K. Rideal, F.R.S.

(*Received* 19 *March* 1941)

The parahydrogen conversion has been measured on a tungsten surface, as a function of the surface concentration of adsorbed oxygen, acting as a poison. This surface concentration was measured by a contact potential method. The oxygen would appear not only to cut down the fraction of surface available for reaction, but also to influence the reactivity of the neighbouring chemisorbed hydrogen. An important factor in this influence may be dipole-dipole interaction between the adsorbed atoms. A part at least of the oxygen adsorbed on tungsten can be removed at room temperature by reaction with hydrogen. Films of carbon monoxide, nitrogen and ethylene also poison the catalytic activity of tungsten and there is some evidence that the small conversion that does occur in their presence proceeds through the formation of a hydride surface on top of the film, rather than on gaps in it. Experiments with a number of different wires has led to evaluation of the constant A^0 in $k = A^0 e^{-E/RT}$. While A^0 in two cases differs considerably from the average value, in all other six cases it approximates closely to an average. In the derived equation for the absolute rate the temperature independent factor is $2{\cdot}6 \times 10^{20}$ mol./sec./cm.^{2} of catalyst surface, at 1 mm. pressure of hydrogen. From this we estimate a value of this factor $B^0_m = 10^{22}$ for the zero order reaction, which is more susceptible to simple theoretical treatment. This is considered in terms of the activated complex theory, and is shown to be more in accordance with a conversion mechanism based on an interchange between loosely adsorbed hydrogen molecules and chemisorbed hydrogen, rather than with the original idea of the recombination of chemisorbed hydrogen atoms. The $H_2 + D_2$ reaction has the same rate as the parahydrogen conversion, and so 'tunnelling' is an unimportant factor in this hydrogen reaction, even at $-150°$ C.

1. Introduction

It was found by A. Farkas (1931) that a tungsten filament, after flashing in vacuo to remove adsorbed oxygen, was an active catalyst for the conversion of parahydrogen. The observed kinetics could be explained by the mechanism advanced by Bonhoeffer and Farkas (1931),

$$p\mathrm{H}_2 + 2\mathrm{W} \rightarrow 2\mathrm{WH} \rightarrow 2\mathrm{W} + o\mathrm{H}_2$$

where W denotes a surface atom of tungsten. J. K. Roberts (1935) found that an oxygen-free tungsten surface on exposure to gaseous hydrogen takes up a stable film of the gas, which does not evaporate at an appreciable rate at room temperature and so the *para-ortho* conversion cannot proceed by this mechanism (Roberts 1939*a*). It therefore appeared desirable to re-examine this reaction, and in the first instance to establish whether or not the active filament was free from adsorbed oxygen by a physical method. The method chosen was to measure the contact potential of the catalyst filament. The importance of this point lies in the fact that many bulk oxides are good catalysts for this reaction (Taylor and Sherman 1931, 1932). Secondly, since the system is relatively simple it should be suitable for a theoretical investigation of the rate of reaction. In this connexion the reaction rates and kinetics on the oxygen-free filaments have been determined. Thirdly, the poisoning effect of adsorbed films of gases other than oxygen has been considered. The second paper is concerned with experiments more directly planned to establish the mechanism of the reaction.

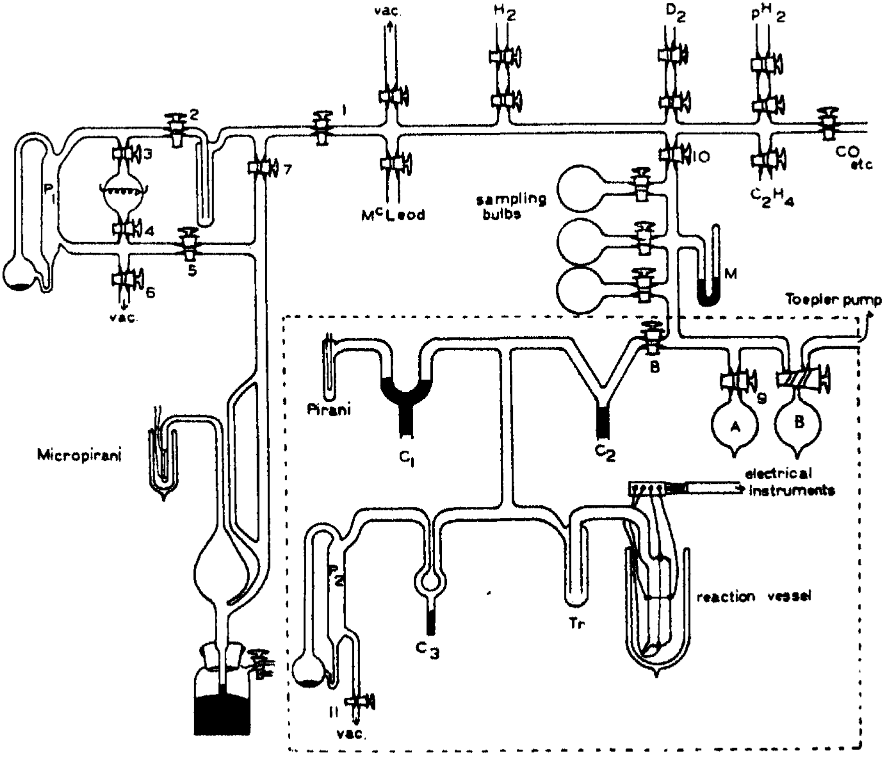

FIGURE 1. The apparatus. The dotted line encloses the high vacuum section made in pyrex glass.

2. EXPERIMENTAL DETAILS

The experiments were concerned with the measurement of (*a*) the rate of conversion of parahydrogen as a function of gas pressure and wire temperature, both on the clean wire and on wires poisoned with adsorbed films of various gases, (*b*) the contact potential of the tungsten catalyst.

The apparatus is shown in figure 1; this system was exhausted by a mercury pump backed by an oil pump, not shown in the diagram. The pump *P*2 served to evacuate the reaction system to an estimated pressure of 10^{-7} mm. This part contained no taps or greased joints and was connected to the main system by the cut-offs *C*1, *C*2, *C*3. Hydrogen gas taken from the main storage bulb could be kept over a sodium film in bulb *A* or *B* before use in an experiment. A trap *Tr* cooled in liquid air protected the reaction vessel from mercury vapour. In an experiment a suitable amount of hydrogen could be admitted to the reaction vessel via *C*2, and its pressure read on the cut-off *C*3 or on the McLeod gauge. Similarly, samples of hydrogen could be extracted from the reaction space through *C*2 and taken through the mercury pump *P*1 into the micropirani gauge for analysis. The design ensured that no appreciable leaks of air could occur into the reaction vessel during the course of an experiment. A quantity of oxygen corresponding to a pressure of 10^{-4} mm. in the reaction space would suffice to give a complete film on the wire. The tap system could be exhausted prior to the introduction or removal of gas from the reaction vessel, and would maintain 10^{-6} mm. over the time required for such manipulations. Samples of gas could be removed from the vessel and stored in the small bulbs shown, when it was desired to proceed immediately to a measurement of the contact potential of the catalyst wire.

The reaction vessel, shown in figure 2, was of pyrex glass, and contained two filaments at right angles, separated at their nearest point by about 1 mm. The vessel was designed in accordance with the requirements set forth by Bosworth and Rideal (1937), Bosworth (1937). It was necessary that the main catalyst filament should be of a sufficient length to ensure a reasonably uniform temperature when it was heated electrically. The filaments were held taut by springs of 0·3 mm. diameter molybdenum wire, which were found to be non-catalytic. The volume was about 200 c.c., and the filaments were of 0·1 mm. diameter tungsten wire.

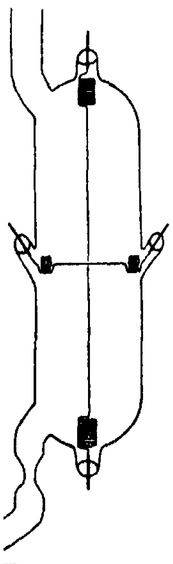

FIGURE 2. The reaction vessel.

The vertical catalyst filament was about 11 cm. long and the horizontal emitter about 3 cm. long.

After sealing the tube on to the apparatus it was baked out for 10 hr. at 450° C, in the latter stages the trap *Tr* being cooled with liquid air. The filaments were next aged at 2500° K for 5 hr., in vacuo. Sodium could then be distilled in from an appendix so as to form an even film on the walls of the vessel. Such sodium films were found to be non-catalytic, and assisted the clean-up of the filament. The temperature/resistance relationship of the catalyst filament was then determined over the range 77–473° K, using baths. The vessel was then ready for use. To obtain a clean filament the wire was first flashed in vacuo at 2500° K for 2 min. with the walls at room temperature. The reaction vessel was then immersed in liquid air, and the wire again flashed. All $p\mathrm{H}_2$ conversions and other experiments on the wire were conducted with the walls of the tube at liquid air temperature, so as to keep the wire free from oxygen and sodium. It is to be noted that a number of experiments on the conversion were also made with tubes containing only a single wire down their axis, and in these cases sodium films were not used.

The electrical apparatus was similar to that used by Bosworth and Rideal (1937).* It enabled (*a*) the catalyst wire to be heated electrically to any given temperature as measured by its resistance, (*b*) the emitter to be heated to a constant temperature in the region of 2500° K, as measured by the current (Jones and Langmuir 1927), (*c*) a variable potential to be applied between the two filaments, and the thermionic current between them measured on a microammeter. Further, a mains circuit allowed either one or both of the filaments to be flashed at 2500° K. Results were expressed as a plot of thermionic current against the applied potential (i/V curve), for constant emitter temperature. The presence of adsorbed films on the collector (catalyst) filament served to change its contact potential, and shift the i/V curve parallel to the potential co-ordinate.

The micropirani gauge was similar to that used by Bolland and Melville (1937). Mixtures of $p\mathrm{H}_2$ and $o\mathrm{H}_2$, and H_2, D_2, HD could be analysed with it. The latter of course required two measurements, before and after circulation over a red-hot nickel wire (3, 4 in figure 1). A pressure of 50 mm. of hydrogen was usually used in the gauge, which was of the tungsten spiral type and was worked with its walls at liquid air temperature. The wire was run with a constant potential drop of 2·8 V across it, and its resistance measured on a Wheatstone bridge. For $n\mathrm{H}_2$ the wire temperature was 173° K. The calibration curve is given in figure 3.

---

* We have to thank Mr H. Campbell for many valuable suggestions in arranging the electrical circuit.

Hydrogen and deuterium were purified by passage through a heated palladium tube. Parahydrogen was obtained by contacting hydrogen with a well out-gassed charcoal at 65° K. Deuterium gas was prepared by interacting liquid D_2O with previously distilled sodium metal. The ethylene used was a sample purified by distillation in vacuo and was supplied by Dr G. H. Twigg. Carbon monoxide was prepared by decomposing $Ni(CO)_4$ at 100° C, any unchanged carbonyl being frozen out with liquid air. Oxygen was obtained by heating $KMnO_4$ containing a little BaO_2. Nitrogen was freed from oxygen by a white-hot tungsten filament. Parahydrogen, nitrogen and ethylene were stored over sodium films to keep them free from traces of oxygen.

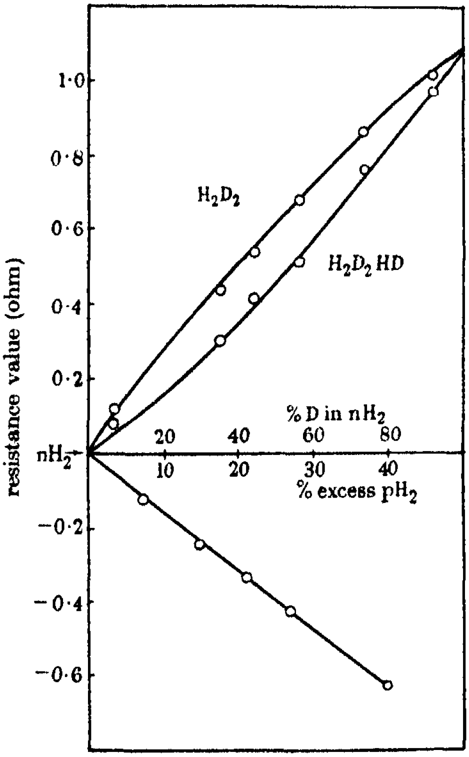

FIGURE 3. The calibration curve of the micropirani gauge.

3. Results

All known cases of the heterogeneous parahydrogen conversion obey the first order law, and we may express the constant as

$$k = \frac{1}{t}\ln\frac{C_0}{C_t},$$

where C_0 is the original concentration of parahydrogen in excess of the equilibrium concentration at the temperature of the experiment, and C_t is this 'excess' concentration at time t min. This equation may be written

$$k = \frac{1}{t}\ln\frac{\Omega_0-\Omega_\infty}{\Omega_t-\Omega_\infty},$$

where Ω denotes the 'resistance value' of the hydrogen in ohms, Ω_∞ being the resistance value of the parahydrogen sample after a sufficient time to reach equilibrium, at the temperature of the wire, has been allowed. This equation was found to hold in all cases, e.g. experiment 65. Accordingly, all rates are expressed in terms of k, in min.$^{-1}$.

Table 1

Experiment 65. 1·5 mm. $p\text{H}_2$. Wire temp. = 114° K

t, min.	$\Omega_0-\Omega_\infty$	$\Omega_t-\Omega_\infty$	k, min.$^{-1}$
3	0·39	0·26	0·14
6	0·39	0·18	0·13
9	0·39	0·11	0·14

(a) *The effect of oxygen films*

Experiments were made with tube 1*b*, with a catalyst wire of length 11 cm., and total reaction space of 300 c.c. Preliminary experiments showed that while the clean tungsten wire was active in the conversion. admission of a trace of oxygen poisoned the wire, in agreement with the results of Farkas. Subsequent flashing of the wire in vacuo restored the activity and also gave a shift in contact potential of 1·60 V. Since this is in reasonable agreement with the value found by Bosworth and Rideal (1937), namely, W/WO = − 1·74 V, we can conclude that the active wire was largely free from oxygen and that the surface metal atoms were responsible for the conversion. It seemed desirable to make a more accurate investigation of this effect, and in particular to investigate the parahydrogen conversion on tungsten surfaces partially covered with adsorbed oxygen. By using the relationship $V = 2\pi\mu c_s$, where V = measured contact potential of the film, and c_s = surface concentration of dipoles of moment μ, we have the possibility of correlating the rate constant with the surface concentration of the poison.

The contact potential measurements were made with an emitter current of 1·8 amp. and over the course of three weeks the i/V curve for W/W was found to be very reproducible. The following effect, which though fortuitous was very convenient, was found. With this emitter current sufficient heat was radiated to the adjacent collector to raise its temperature at its mid-point to the region of 800° K, as checked by a resistance measurement. This temperature was sufficiently high to evaporate all but a residual 10 % of an initially complete hydrogen film, and it was found impossible under these conditions to obtain a W/WH contact potential greater than $-0{\cdot}1$ V, in grave disagreement with that of Bosworth of $-1{\cdot}04$ V. The difference in the two tubes explains this result; our long collector wire is more easily heated than the short wire of Bosworth, which had heavy leads only 1 cm. distance from its mid-point. That this explanation is the correct one is shown by the fact that passing 1·1 amp. through our long wire, now used as emitter, and employing the short wire as collector, a W/WH value of $-0{\cdot}96$ V was obtained in reasonable agreement with Bosworth's value. So the result is not due to a spurious effect following on contamination of the tube. In these experiments therefore, our measurements refer directly to partial oxygen films and not to mixed films of hydrogen and oxygen. It is to be noted that oxygen films were quite stable to the heat rediation from the emitter.

In an experiment a pressure of 10^{-2} mm. oxygen was admitted to the vessel so as to form a full oxygen film, the tube evacuated and the emitter flashed, and the i/V curve taken. This may be denoted by curve A in figure 4. By passing a current through the collector it could be carefully heated up, and a certain amount of oxygen evaporated. A second i/V curve was then taken, curve B. The emitter was now switched off, a pressure of 1·2 mm. parahydrogen introduced into the vessel, and at zero time a current was switched on to the catalyst (collector) wire to bring it to $-131°$ C. This temperature was held by manual resistance control for the course of the experiment, during which one or more samples were extracted and stored in the sampling bulbs for subsequent analysis. At the end the vessel was pumped out, the emitter switched on and the i/V curve repeated. In all cases this was within 0·1 V of curve B, and the passage of a small current sufficient to evaporate traces of adsorbed hydrogen but not sufficient to evaporate any oxygen served to make the i/V curve exactly reproducible with B. Finally the collector was flashed and the i/V curve taken for the

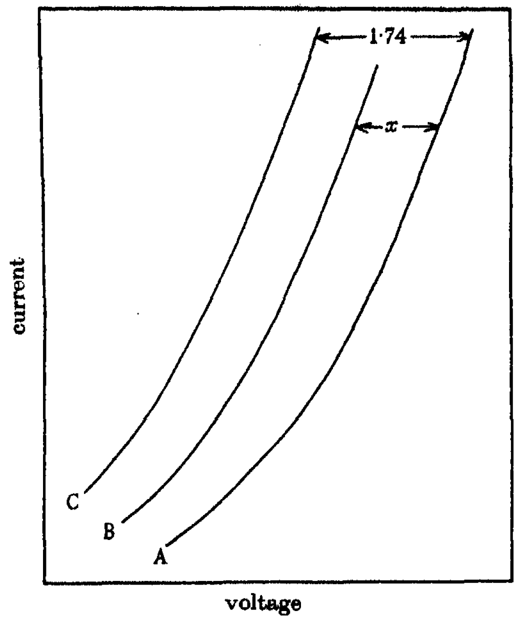

FIGURE 4. Current-voltage curves to illustrate the measurement of contact potentials.

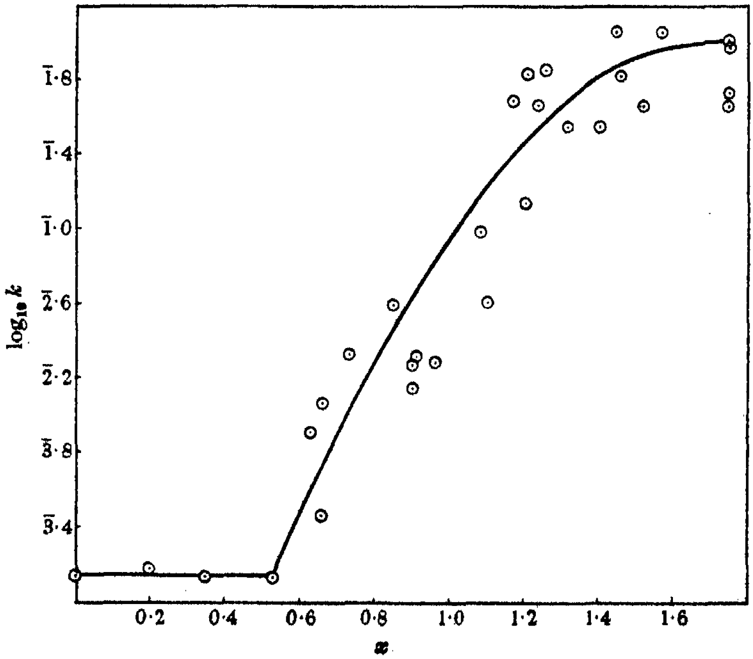

FIGURE 5. The parahydrogen conversion constant k as a function of the contact potential of a WO surface, at constant wire temperature and hydrogen pressure.

clean filament, curve C. In all cases the difference C to A agreed satisfactorily with the value of $-1{\cdot}74$ V for the oxygen film. The shift A to B we refer to as x volts.

In figure 5 we plot values of $\log_{10} k$ for the conversion against x. We note that $x = 0$ corresponds to a complete oxygen film, $x = 1{\cdot}74$ to an oxygen-free filament. During the series of experiments a small increase in the activity of the clean wire was noted, from $k = 0{\cdot}48$ to $k = 1{\cdot}1$, which is perhaps partly responsible for the spread of points, apart from experimental inaccuracy. It is significant that even a clean aged tungsten wire can alter a little in its activity. The curve shown can be given a natural explanation in terms of Roberts's picture of the oxygen film (1935, 1939*b*; Morrison and Roberts 1939). Roberts has given theoretical and experimental reasons for considering the oxygen film on tungsten as composite. It consists of a primary immobile film containing about 8 % of holes, over which are held molecules of oxygen, less strongly than in the primary film. This latter less stable part evaporates at about 1100° K, while the primary film evaporates only at temperatures above 1700° K.* The two films may be characterized by a measurement of the accommodation coefficient of the wire against neon, the primary film having $a = 0{\cdot}177$ and the primary plus secondary film having $a = 0{\cdot}226$. It is interesting for our later considerations that a relatively large change in a of 22 % results from evaporating off the oxygen from the gaps (secondary film): Starting with a full oxygen film ($x = 0$) at the lower wire temperature oxygen will be evaporated off the gaps, which can then adsorb hydrogen molecules, but not hydrogen atoms for energetic reasons since the gaps are only single sites. Such adsorbed hydrogen we should not expect to be catalytically active on any picture of the conversion process and in fact we find no alteration in the activity of the wire until about $x = 0{\cdot}52$ V. At this point we consider that the gaps have been set free and that evaporation of the primary oxygen film has commenced. While the value 0·52 V, 30 % of the total contact potential, might at first sight appear a rather large value to associate with the oxygen in the secondary film, it nevertheless is similar in magnitude to the shift in accommodation coefficient observed. There is also the possibility that it contains a part of the contribution due to the evaporation of the primary film, since in the first instance this would probably only yield single sites unable to chemisorb hydrogen. We shall, however, attribute a value of $1{\cdot}74 - 0{\cdot}52 = 1{\cdot}22$ V to the primary film, and it is then possible to plot, from the curve in figure 5, the curve shown in figure 6. Here σ is the fraction of sites free from oxygen in the primary film, taken as $(x-0{\cdot}52)/1{\cdot}22$. This assumes the validity of the equation $V = 2\pi\mu c_s$; that is, it assumes that μ for adsorbed oxygen remains constant as the surface is filled. This means that μ is the same for all sites on the tungsten surface and further that the mutual depolarization of the dipoles at high concentration can be neglected. This assumption is supported by some unpublished measurements made in this laboratory by R. C. L. Bosworth. Now if the only effect of adsorbed oxygen were to cut down the amount of chemisorbed hydrogen on a uniform set of sites we should expect k/σ to be constant, at least over the larger part of the range of σ. However, figure 6 shows a strong increase in $\log k/\sigma$ with σ up to $\sigma = 0{\cdot}75$. The linear character of the $\log k/\sigma$ against σ plot suggests that this increase is not due to a variation in the nature of the catalytically active sites but must be ascribed to the influence of a neighbouring adsorbed oxygen on the rate of reaction, this effect becoming vanishingly small when only one site in four is occupied by oxygen. This influence of a neighbouring WO on the rate of reaction may be exerted on the entropy or energy of

---

* Roberts (1940*b*) has recently modified his views as to the possible nature of the stable primary film, but this does not affect our considerations.

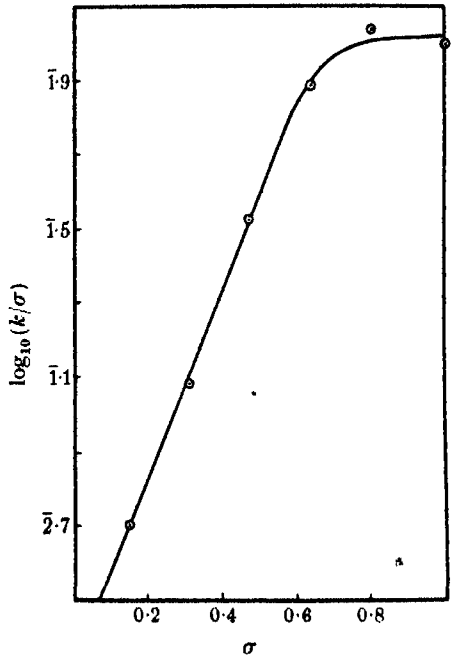

FIGURE 6. The relationship between reaction constant per unit surface bare of oxygen, and the fraction of surface bare of oxygen. This curve was derived from figure 5.

activation of the reaction. If all the change in $\log k/\sigma$ is to be ascribed to the latter, then from $\sigma = 0{\cdot}1$ to $\sigma = 1$ the activation energy need only decrease by 0·84 cal. We note there is a not inconsiderable difference in the energy of the WH dipole in the states $\sigma = 0$ and $\sigma = 1$, arising from dipole-dipole interaction alone. The summation of these interactions, derived from the computations of Roberts (1935), leads to the following expression ΔU_ϵ for this difference:

$$\Delta U_\epsilon = \frac{8{\cdot}2\mu_{\mathrm{H}}(\mu_0 - \mu_{\mathrm{H}})}{a^3} \times 14{\cdot}6 \times 10^{12}\,\text{kcal./g. atom.}$$

The lattice spacing a is taken as $3{\cdot}1 \times 10^{-8}$ cm. The contact potential measurements of Bosworth give $\mu_0 = 0{\cdot}66 \times 10^{-18}$ e.s.u., and a more uncertain value of $\mu_{\mathrm{H}} = 0{\cdot}4 \times 10^{-18}$ e.s.u. From these values we obtain $\Delta U_\epsilon = 0{\cdot}4$ kcal., the hydrogen being less strongly adsorbed in the presence of oxygen. This value is almost half the difference in the energies of activation given above. We might expect a further difference to arise from the quantum forces of cohesion and repulsion. Therefore, in the preliminary treatment of the absolute rate of reaction on the oxygen-free surface given later, it is within the error of our experiments and theoretical methods to consider all the sites as possessing a uniform activity.

(*b*) *Interaction of oxygen films with hydrogen*

An interesting point arose in an attempt to determine the temperature coefficient of k on oxygen films. With an initially complete oxygen film up to − 20° C no catalysis was observable over the time of experiment, but about 0° C a strong catalysis set in. If now the vessel were pumped out and further experiments made, appreciable values of k were found below − 20° C. It could only be concluded that at 0° C hydrogen can remove part of the oxygen film, and a simple calculation using Roberts's values for the adsorption energies (1935, 1939) shows that this occurs through a reaction a and not a displacement mechanism b.

$$\begin{array}{lll}
(a) & 2\mathrm{WO} \rightarrow 2\mathrm{W} + \mathrm{O_2} & -139\,\text{kcal.} \\
 & 2\mathrm{H_2} + \mathrm{O_2} \rightarrow 2\mathrm{H_2O} & +133\,\text{kcal.} \\
\therefore & 2\mathrm{WO} + 2\mathrm{H_2} \rightarrow 2\mathrm{W} + 2\mathrm{H_2O} & -\ \ 6\,\text{kcal.} \\
(b) & 2\mathrm{W\text{-}H} \rightarrow 2\mathrm{W} + \mathrm{H_2} & -\ 20\,\text{kcal.} \\
\therefore & 2\mathrm{W\text{-}O} + \mathrm{H_2} \rightarrow 2\mathrm{W\text{-}H} + \mathrm{O_2} & -119\,\text{kcal.}
\end{array}$$

(*b*) is therefore ruled out energetically, and (*a*) is further supported by the observation of Roberts (1935), who found a decrease of pressure when hydrogen was contacted with an oxygen film on tungsten. If 0·01 mm. of oxygen be mixed with the parahydrogen at 0° C, no onset of catalytic activity is found. In this case any gaps formed by reaction (*a*) are immediately closed by fresh oxygen from the gas phase. It is noteworthy that the constants found in this case are similar to those found with a simple reaction tube with the walls at room temperature, where the oxygen arises from the walls. It is clear that such a WO surface will show a small catalysis, a thousandfold less than that given by the oxygen free metal. A slow reaction at the gaps in the layer in this case seems to be ruled out, since such gaps would be filled with oxygen when this is present at 10^{-2} mm. It is more probable that it proceeds through the formation of a hydroxide surface, as we shall discuss later.

TABLE 2

Oxygen film. 1·0 mm. pH_2

exp.	T° C	t, min.	Ω_0 ohms	Ω_t ohms	k, min.$^{-1}$
C22	− 56	36	0·56	0·56	0·00
C25	− 10	2	0·56	0·00	—
C27	− 100	18	0·55	0·04	0·15
84	− 21	2	0·44	0·44	0·00
85	6	2	0·44	0·05	1·09
86	10	1·5	0·44	0·11	0·93
87	− 21	2	0·44	0·02	1·54
88	− 136	4	0·44	0·38	0·04
		1·0 mm. $pH_2 + 0{\cdot}01$ mm. O_2			
89	6	5	0·44	0·30	0·08
90	− 21	6	0·30	0·30	0·00
Simple reaction vessel, walls at room temp., k corrected to the same catalyst area.					
A10	18	—	—	—	0·07
A14	20	—	—	—	0·06

(*c*) *Nitrogen and ethylene films*

In figure 7 we present results at 1·5 mm. pressure of parahydrogen, as a plot of $\log_{10} k$ against $1/T$. It is apparent that nitrogen films poison the conversion, raising the activation energy from about 1000 to 5920 cal. If the difference in rates were simply due to the factor $e^{-(E_1-E_2)/RT}$, we should expect at 200° K a ratio of $2{\cdot}2 \times 10^5$ for the constants k of the poisoned and unpoisoned reactions. We actually find a ratio of $3{\cdot}4 \times 10^2$ which indicates that the increase in activation energy is offset by an alteration in the entropy of activation. This points to the view that we cannot consider these reactions simply in terms of collisions with the surface. It is to be noted that, over the temperature range examined, nitrogen films are stable in H_2, giving similar values of k at $-78°$ C, both before and after an experiment at $-21°$ C.

In figure 7 are plotted experiments on a wire poisoned by ethylene, which has a more marked effect than nitrogen. The ethylene film was quite stable at 0° C, in contradistinction to the oxygen film. A tungsten wire was heated to 450° C for 6 min. in a mixture of 0·03 mm. ethylene and 0·025 mm. hydrogen. No decrease of pressure occurred, and the amount of conversion was small, the resistance value of the parahydrogen changing from 0·44 to 0·13 ohm. It seems probable that the very strength with which ethylene is adsorbed on tungsten prevents its hydrogenation. The view of Twigg and Rideal (1940) is that tungsten will not hydrogenate ethylene since its lattice spacing will not accommodate the —CH_2—CH_2— species. This would mean that the ethylene film observed was formed by the CH_2=CH— or CH_3CH= species. At the present time we have no evidence to decide between these possibilities.

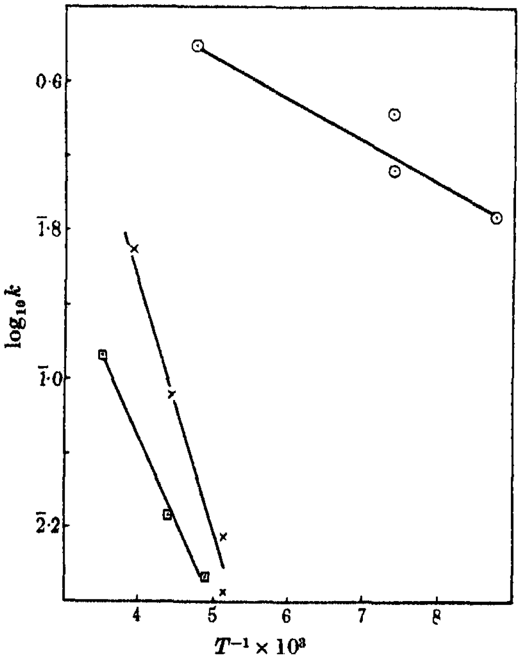

FIGURE 7. Temperature coefficients of the parahydrogen conversion at a hydrogen pressure of about 1 mm. ⊙ 'Clean' surface, i.e. free from all gases except hydrogen. × Nitrogen film on surface. ☐ Ethylene film on surface.

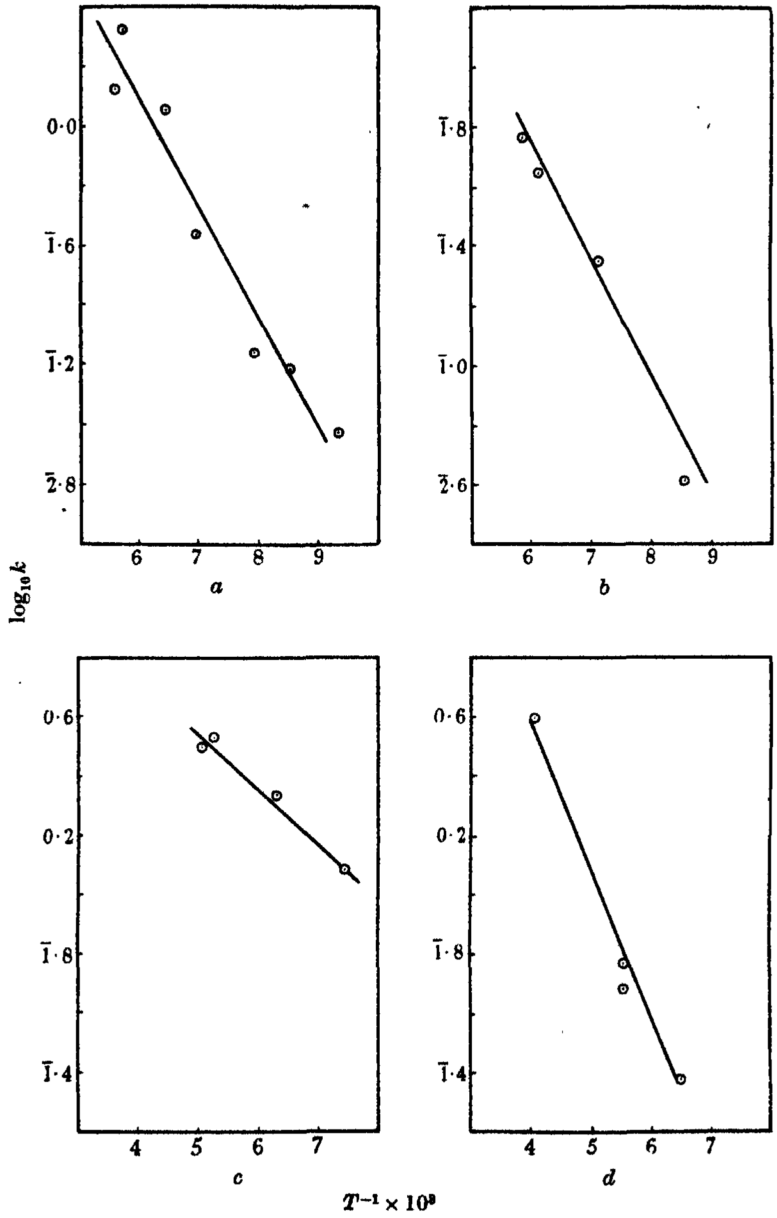

FIGURE 8. Temperature coefficients of the parahydrogen conversion on 'clean' tungsten surfaces, at constant pressures of about 1 mm. (*a*) tube 1*a*, (*b*) tube 1*a*, a second run made after (*a*), (*c*) tube 1*b*, (*d*) tube 3.

(*d*) *Carbon monoxide films*

The experiments shown and table 3 indicate that a film of carbon monoxide poisons the conversion at − 127° C but that at − 58° C a fairly rapid conversion occurs. However, the conversion is still poisoned on returning to − 127° C and we conclude that no molecules of carbon monoxide have been removed by reaction with hydrogen at the higher temperature.

TABLE 3

CO film. 0·5 mm. pH_2

exp.	temp. °C	t, min.	Ω_0 ohms	Ω_t ohms	k, min.$^{-1}$
C29	− 127	7	0·56	0·55	0
C30	− 58	28	0·55	0·00	v. rapid
C31	− 127	20	0·56	0·57	0
C32	− 54	1	0·56	0·06	2·25

(*e*) *Conversion on films*

We first note that in all cases a poisoning film could be removed by flashing the wire at 2500° K, when the original activity of the clean wire was restored. All the films examined poisoned the catalysis of the conversion around − 100° C, but at higher temperatures a conversion set in. The stability of the different films in hydrogen may perhaps be compared by the temperatures at which comparable rates of the parahydrogen conversion were reached. Roughly, these were for carbon monoxide films, − 50° C, nitrogen and oxygen films 0° C, and ethylene films 200° C. The case of oxygen is a special one, since the onset of activity is to be associated with a reduction of the oxide layer and the production of bare sites that can chemisorb hydrogen. It is interesting to speculate as to whether the activation of hydrogen, that occurs on these films, proceeds on top of the film itself or at gaps which may exist in it. We can only say that the balance of evidence is perhaps in favour of the former, more novel, hypothesis. Firstly, because the carbon monoxide film which is most active is the one we might expect to be relatively inactive on the gap theory. Here we should expect single site adsorption through formation of W-CO. This might be inferred from the experiments of Langmuir (1915), and also from the existence of metal carbonyls.

Gaps may arise in two ways, as Roberts had indicated (1935, p. 473). The first is when an immobile film is formed by the adsorbed molecule occupying two or more sites, as he has suggested is the case for oxygen.* Such gaps therefore probably do not arise in the case of carbon monoxide. The second is for single site adsorption when the gas molecule is sufficiently large to exclude molecules from neighbouring sites. We should on this view expect carbon monoxide and ethylene films to contain similar numbers of gaps, and therefore show a similar catalytic activity, as in fact they do not. Further, it is clear that such gaps could not in the first instance take up hydrogen atoms from the molecules in the gas phase, at these low temperatures. The fact that hydrogen at higher temperatures will remove oxygen from tungsten, suggests the intermediate formation of a hydroxide surface W-OH which below 0° C might be stable, i.e. it would only interchange with hydrogen and not be further reduced by it.* The bond electrons in such film bonds might be expected to resonate with the metallic electrons and therefore to behave in many respects like the surface bonds of a clean metal. In the case of ethylene films the conversion may occur through an exchange reaction with the hydrogen already present in the adsorbed ethylene. However, these points are a matter for future experimental work.

---

* Roberts (1940*b*) has recently shown that this view may require modification.

(*f*) *Conversion on the 'clean' wire*

By 'clean' we here mean free from all adsorbed films other than hydrogen. A number of different reaction vessels were used. In tubes 1*a* and 1*b* a sodium film was deposited on the walls but the other tubes contained no such film. The concordance of results indicates that a wire with care can be kept free from oxygen with no sodium present.

The activation energy and absolute rate

The constant k was determined at constant pressure of hydrogen for a number of different temperatures, and the activation energy E determined from a plot of $\log_{10} k$ against $1/T$. In table 4 we give values of A and E in the equation $k = Ae^{-E/RT}$, which we have taken as expressing our results within the experimental error. While the maximum uncertainty, from the spread of points, on the determination of E in the less exact experiments is ± 500 cal. the general agreement of A values, commented on later, suggests that the uncertainty is in reality much less than this. A will certainly be a function of pressure, but since all the measurements were made in the small range 0·4–1·5 mm. we can compare them in the first instance directly, since it will be apparent that other factors outside our control cause larger variations in A. Since k and therefore A vary with the ratio wire surface (S) : reaction volume (V) we derive $A^0 = Av/s$ in c.c. cm.$^{-2}$ min.$^{-1}$, for a temperature of 173° K.

---

* An analogous hypothesis would be that conversion on nitrogen films should occur through a surface complex of the type WNH. Such complexes have already been postulated by Messner and Frankenburger (1931) in connexion with a different kind of observation.

TABLE 4

tube	figure	p, mm.	E, cal.	A, min.$^{-1}$	S, cm.^{2}	V, c.c.	A^0 c.c. cm.$^{-2}$ min.$^{-1}$
1*a*	8*b*	0·6	1900	$1{\cdot}95 \times 10^2$	0·33	300	$1{\cdot}78 \times 10^5$
1*a*	8*a*	0·4	1860	$3{\cdot}39 \times 10^2$	0·33	300	$3{\cdot}09 \times 10^5$
1*b*	7	1·5	1000	$6{\cdot}92 \times 10^1$	0·33	300	$6{\cdot}3 \times 10^4$
1*b*	8*c*	1·5	1200	$1{\cdot}1 \times 10^2$	0·33	300	$1{\cdot}0 \times 10^5$
1*b*	10	1·5	1840	$7{\cdot}25 \times 10^1$	0·33	300	$6{\cdot}6 \times 10^4$
3	8*d*	1·5	2100	$2{\cdot}04 \times 10^2$	0·39	350	$1{\cdot}83 \times 10^5$
4	11	1·3	3070	$8{\cdot}32 \times 10^3$	0·33	350	$8{\cdot}82 \times 10^6$
F	—	*c.* 0·5	3800	$1{\cdot}18 \times 10^5$	0·6	1000	$1{\cdot}97 \times 10^8$

We include in the table Farkas's data, indicated by F, correcting his value of k to 0·5 mm. using his measured pressure dependency of k, and the value of E determined by him. In figure 9 we have plotted values of $\log_{10} A^0$ against E. We find that most of the values of A^0 lie within a factor five of each other, but that two, those for tube 4 and that from Farkas's data, lie considerably higher. There is an indication of a relationship between $\log_{10} A^0$ and E of the type that Evans and Polanyi (1936) have discussed for a number of cases. The known cases up to date in heterogeneous catalysis have arisen for relatively complex catalysts, but here we see that it holds for a clean tungsten surface. Our results would indicate that while on the average a well-aged tungsten surface is very reproducible in its catalytic properties, nevertheless it is possible to obtain clean surfaces of somewhat different catalytic behaviour. Since differences in activation energy tend

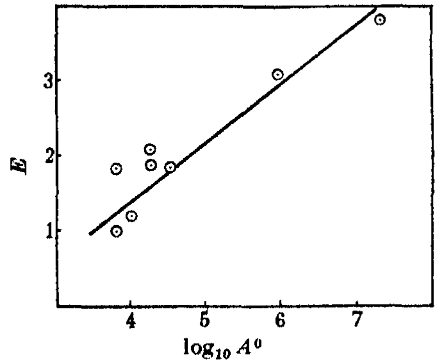

FIGURE 9. To show the calculated values of the temperature independent factor A^0, and their trend with increasing activation energy E, for 'clean' wires.

to be compensated by alterations in the entropy factor the observed effect on k, at any rate at 173° K, is small. It may be that slightly different ageing treatments, by altering the distribution of the various sites and crystal facets, can give rise to the experimental differences in A^0 and E observed. For the purposes of theory we can take a mean of the first six values as representing the well-aged clean tungsten wire, $A^0 = 1 \cdot 5 \times 10^5$, at 1 mm. pressure and 173° K.

Dependence of k on pressure

Figure 10 shows a series of runs made with tube 1*b* at pressures of 1·5 and 20·5 mm., at a variety of temperatures. This 13·7 fold increase of pressure decreases k 12·3 times at − 78° C and 8·9 times at − 159° C. We neglect the different behaviour at the two temperatures and concern ourselves only with the average behaviour of the absolute rate, which we may measure by kp. For this pressure change a 10-fold alteration in k corresponds to $kp = \text{const.}\, p^{0 \cdot 12}$. That is, the reaction is between zero and first order, being

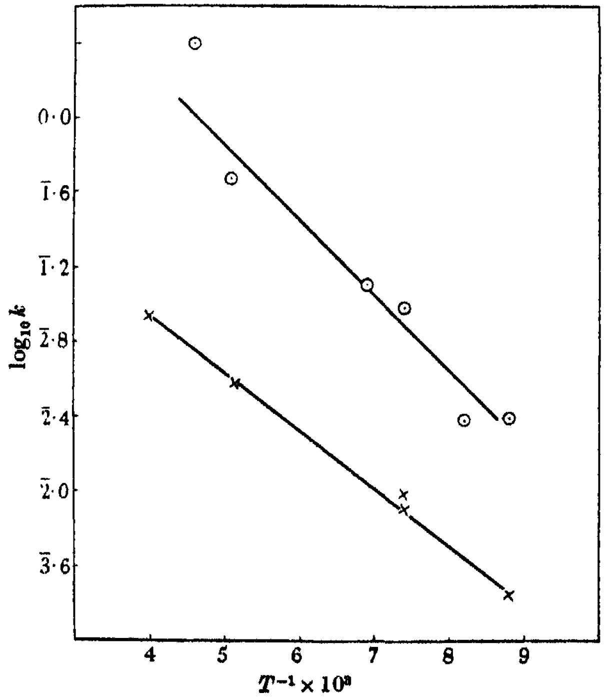

FIGURE 10. Effect of pressure on the conversion rate k, measured with tube 1*b*. ⊙, 1·5 mm. hydrogen pressure. ×, 20·5 mm. hydrogen pressure.

more nearly the first case. Such behaviour was found by Farkas, and his experiments give kp = const. $p^{0\cdot 28}$ at − 100° C. The difference in activation energies at 1·5 and 20·5 mm. is perhaps within the experimental error, when we consider the uncertainty of k at the higher temperatures. If real it is in the opposite direction to what we should expect on the view that the pressure dependency is mainly determined by the concentration of hydrogen in a Van der Waals layer. Diffusion of gas through the reaction volume may tend to limit reaction velocities at the higher temperatures. With tube 3 some experiments were made when the wire was showing a uniform increase in activity. By bracketing the experiments significant average values of k at two pressures were obtained. These were $k = 0\cdot 28$ (12 mm.) and $k = 0\cdot 9$ (1·3 mm.), all at − 93° C, and correspond to kp = const. $p^{0\cdot 5}$.

TABLE 5

p_1	p_2	$(p_1/p_2)^{0\cdot 5}$	k_2/k_1
16	1·3	3·51	3·47
1·3	0·093	3·73	3·55

In figure 11 we have plotted values of $\log_{10} k$ against $1/T$ for pressures of 16, 1·3 and 0·093 mm., using tube 4. In this case the results fairly accurately obey the relation kp = const. $p^{0\cdot 5}$. Accordingly we can say that the absolute rate kp is proportional to a power of the pressure between $p^{0\cdot 5}$ and $p^{0\cdot 1}$. Since the pressure dependency is bound up with the energy of adsorption of the hydrogen we might expect such variations from one wire to another, just as we get differences in activation energy.

For later qualitative considerations it is interesting to estimate the value of k for the zero order reaction, i.e. at a pressure where the adsorption layer of reactants is saturated. Since the observed pressure dependency is nearing zero order, we can estimate that the maximum possible increase in kp, to be occasioned by increasing the pressure, is within a factor 10^2. In all probability the factor is less than this.

Theory of the temperature independent factor A^0

We now consider the average value of $A^0 = 1\cdot 5 \times 10^5$ cm. min.$^{-1}$ for a conversion at $1\cdot 0 \pm 0\cdot 6$ mm. pressure and − 100° C, neglecting the demonstrated increases of A^0 that may be brought about either by the presence of adsorbed films or by variations in aging techniques. The former effect, however, clearly shows that such increases in A^0 are to be sought in bond strength factors modifying the entropy of activation, rather than in alterations in the active area of the wire surface. We might mention that the development of different crystal faces in the wire may be important in the second effect (see Beeck, Smith and Wheeler 1940). We have

$$k = 1{\cdot}5 \times 10^5 e^{-E/RT}\,\text{c.c. min.}^{-1}/\text{cm.}^2\ \text{catalyst.}$$

This equation can be transformed into

$$kn = Be^{-E/RT}\,\text{gmol. min.}^{-1}/\text{cm.}^2\ \text{catalyst.}^*$$

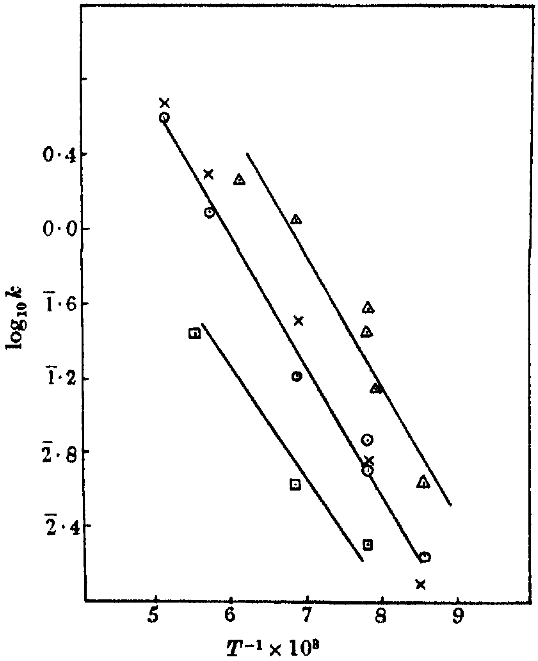

FIGURE 11. Effect of pressure on the conversion rate k, and a comparison of k with the constant k for the H_2+D_2 reaction. □, parahydrogen conversion, 16 mm. pressure. ×, parahydrogen conversion, 1·3 mm. pressure. ○, H_2+D_2 reaction, 1·3 mm. pressure. △, parahydrogen conversion, 0·093 mm. pressure, including one point for H_2+D_2 (experiment 181 at $1/T \times 10^3 \sim 8$).

n is the number of moles present in the gas phase, of volume 300 c.c. mainly at 77° K, then at 1·0 mm. pressure $n = 5{\cdot}1 \times 10^{-5}$, i.e.

$$n/v = 1{\cdot}7 \times 10^{-7}\,\text{gmol./c.c.}$$

Then $B = A^0 n/v = 2{\cdot}6 \times 10^{-2}\,\text{gmol. min.}^{-1}/\text{cm.}^2$ catalyst.

---

[*] In previous considerations it sufficed to take kp as a measurement of the absolute rate kn.

So in the equation

$$\text{No. of molecules reacting per second per cm.}^2 \text{ of catalyst} = B_m e^{-E/RT},$$

$$B_m = 2{\cdot}6 \times 10^{20}.$$

If now we use our previous estimate for the factor arising from increasing the pressure till the reaction becomes zero order, we have $B_m^0 = 2{\cdot}6 \times 10^{22}$. Within the uncertainty of estimation this may be smoothed to $B_m^0 = 10^{22}$ mol./sec./cm.^{2} tungsten surface.

In a theoretical consideration of B_m^0 we adapt the activated complex formulation of Laidler, Glasstone and Eyring (1940). We may write $B_m^0 = \alpha c_s (kT/h) e^{\Delta S*/R}$, where c_s indicates the number of tungsten sites per cm.^{2}, α the fraction of these which are active, and ΔS^* the entropy of activation for the process. At $-100°$ C the frequency factor $kT/h = 3{\cdot}6 \times 10^{12}$, and c_s may be taken as $1{\cdot}2 \times 10^{15}$.

$$\therefore \quad B_m^0 = 4{\cdot}3 \times 10^{27} \alpha e^{\Delta S*/R}.$$

There are two main possibilities for the mechanism.

(i) The mechanism of Bonhoeffer and Farkas. Since this involves the recombination of hydrogen atoms in a primary layer we should expect ΔS^* to be small and $e^{\Delta S*/R}$ to approximate to unity. For agreement with $B_m^0 = 10^{22}$ we should then require that only 2×10^{-6} sites are active. The general evidence against such an assumption has been outlined; effects in oxygen and other films and the general reproducibility of the constants k in all cases are against it.

(ii) The interchange mechanism:

$$p\text{H}_2 + \text{WH} \rightarrow \text{HW} + o\text{H}_2.$$

Experimental support for this theory is given in the second paper. Since such a mechanism involves that in the activation process a hydrogen molecule in a relatively loosely bound layer becomes localized next to a strongly bound chemisorbed H atom, it is here easy to understand a large negative entropy of activation. If we regard reaction as occurring with hydrogen molecules held over gaps in the immobile film, then $\alpha = 0{\cdot}08$, since there are 8 % of such sites. For agreement with $B_m^0 = 10^{22}$ we then require $\Delta S^* = -21$ cal. deg.$^{-1}$ mol.$^{-1}$. If the hydrogen film is mobile, however, and there is still doubt on this point (Roberts 1940*a*), it will contain no gaps and $\alpha = 1{\cdot}0$ and $\Delta S^* = -26$ cal. deg.$^{-1}$ mol.$^{-1}$. To make our present point it suffices to consider either case, and we take the first. If the molecules on these gaps be treated as particles possessing two dimensions of vibration (treated simply as a translation in a free area A_f) and rotation, we estimate (Fowler 1936)

$$S(V) = R\left[\ln\left(\frac{2\pi mkT}{h^2}\right)A_f + 1\right].$$

m is the mass of the hydrogen molecule. The area per tungsten site is $8\cdot35 \times 10^{-16}$ cm.^{2}, and the cross-sectional area of hydrogen is $1\cdot1 \times 10^{-16}$ cm.^{2}. The difference of 7×10^{-16} cm.^{2} may be considered as a reasonable approximation to A_f, when at $-100°$ C we have $S(V) = 6$ cal. deg.$^{-1}$ mol.$^{-1}$,

$$S(R) = R\left[\ln\left(\frac{8\pi^2 IkT}{h^2}\right) + 1\right].$$

With $I = 0\cdot466 \times 10^{-40}$ g.cm.^{2}, $S(R) = 3\cdot4$ cal. deg.$^{-1}$ mol.$^{-1}$. In this rough calculation, the hydrogen molecule is treated as a classical rotator.

The hydrogen on the gaps would possess an entropy of $S(V) + S(R)$, that is, about 10 cal. deg.$^{-1}$ mol.$^{-1}$, all of which might be lost on forming the transition state. However, there is still a large discrepancy between this value of $\Delta S^* = -10$ and the experimental value of $\Delta S^* = -21$, which must await a fuller treatment. At this time we merely point out that the rather large negative entropy factor required by experiment is more in accord with the interchange mechanism than the theory of Farkas.

The $H_2 + D_2$ *reaction*

In figure 11 we plot points for the $H_2 + D_2$ reaction at a pressure of 1·0 mm., at various temperatures. Here $k = \frac{1}{t}\ln\frac{a}{a-x}$, where a equals the concentration of HD in the equilibrium mixture at the temperature of the wire concerned, and x equals the concentration at time t minutes. The effect of shifts in the *para-ortho* equilibrium on the resistance value was in most cases negligible, since the wire temperatures were reasonably high in most cases (above 146° K). It is clear that the $H_2 + D_2$ reaction goes at the same rate as the parahydrogen conversion measured at 1·3 mm., and that it has about the same activation energy of 3070 cal. Further, lowering the pressure had a similar effect in increasing k, viz. at 128° K, and 0·09 ± 0·01 mm. the constants are closely similar.

TABLE 6

exp.	p, mm.	t, min.	Ω_0	Ω_t	k
180	0·085 pH_2	1·5	0·43	0·28	0·29
181	0·098 H_2D_2	1·0	0·15	0·13	0·14

The two reactions therefore are kinetically identical and may be considered to go through the same mechanism. The results indicating equality of rates at even − 150° C would appear to rule out the possibility of 'tunnelling' through potential barriers occurring in the reactions of hydrogen. This effect, if it exists, should be particularly marked at low temperatures such as these, and should lead to a big discrepancy between the rates of the two reactions. These results are further supported by experiments in the second paper, which show that on evaporated films of tungsten the $H_2 + D_2$ interchange proceeds rapidly at 77° K.

We are indebted to the Department of Scientific and Industrial Research for a senior award, and to the Chemical Society for a research grant.

REFERENCES

Beeck, O., Smith, A. E. and Wheeler, A. 1940 *Proc. Roy. Soc.* A, **177**, 62.
Bolland, J. L. and Melville, H. W. 1937 *Trans. Faraday Soc.* **33**, 1316.
Bonhoeffer, K. F. and Farkas, A. 1931 *Z. phys. Chem.* B, **12**, 231.
Bosworth, R. C. L. 1937 *Proc. Camb. Phil. Soc.* **33**, 394.
Bosworth, R. C. L. and Rideal, E. K. 1937 *Proc. Roy. Soc.* A, **162**, 1.
Evans, M. G. and Polanyi, M. 1936 *Trans. Faraday Soc.* **32**, 1333.
Farkas, A. 1931 *Z. phys. Chem.* B, **14**, 371.
Fowler, R. H. 1936 *Statistical mechanics*, 2nd ed. Camb. Univ. Press.
Jones, H. A. and Langmuir, I. 1927 *Gen. Elect. Rev.* **30**, 310.
Laidler, K. J., Glasstone, S. and Eyring, H. 1940 *J. Chem. Phys.* **8**, 667.
Langmuir, I. 1915 *J. Amer. Chem. Soc.* **37**, 1139.
Messner, G. and Frankenburger, W. 1931 *Z. phys. Chem.* Bodenstein-Festband, p. 593.
Morrison, J. L. and Roberts, J. K. 1939 *Proc. Roy. Soc.* A, **173**, 1.
Roberts, J. K. 1935 *Proc. Roy. Soc.* A, **152**, 452.
Roberts, J. K. 1939*a* *Trans. Faraday Soc.* **35**, 941.
Roberts, J. K. 1939*b* *Some problems in adsorption.* Camb. Univ. Press.
Roberts, J. K. 1940*a* *Nature, Lond.*, **146**, 372.
Roberts, J. K. 1940*b* *Proc. Camb. Phil. Soc.* **36**, 53.
Taylor, H. S. and Sherman, A. 1931 *J. Amer. Chem. Soc.* **53**, 1614.
Taylor, H. S. and Sherman, A. 1932 *Trans. Faraday Soc.* **28**, 1247.
Twigg, G. H. and Rideal, E. K. 1940 *Trans. Faraday Soc.* **36**, 533.

The interchange of hydrogen in the adsorbed film on tungsten

By D. D. Eley

(*Communicated by E. K. Rideal, F.R.S.—Received* 19 *March* 1941)

Films of tungsten have been prepared, by evaporation from a filament, which bring the reactions $pH_2 \rightleftharpoons oH_2$ and $H_2 + D_2 \rightleftharpoons 2HD$ to equilibrium in a few minutes at 77° K. Their real surface area could be estimated as about 450 cm.^{2}, from a measurement of the quantity of hydrogen which was rapidly and irreversibly adsorbed at 293° K. A WH film prepared by contacting the evaporated film with gaseous hydrogen showed a rapid interchange with deuterium gas at 193 and 293° K. From the interchange data a calculation of the surface area of the film was made, giving a value in good agreement with that cited above. An approximate treatment suggests that hydrogen and deuterium are equally strongly adsorbed on tungsten at 293° K. At 77° K the exchange equilibrium is displaced in favour of deuterium in the gas phase, so that no interchange could be detected between a WH film and gaseous deuterium. The interchange that was found to occur between gaseous hydrogen and a WD film was less than one would expect from results at 193° K. It was concluded that at 77° K only 20–40 % of the chemisorbed deuterium is sufficiently reactive to interchange with hydrogen gas, in the time of the experiment. A likely explanation for this is a slight variation over the tungsten surface of the WD adsorption energy.

1. Introduction

There are three possible mechanisms for the conversion of parahydrogen on tungsten which will be in accordance with the observed kinetics. The first is a paramagnetic conversion (Bonhoeffer, Farkas and Rummel 1933), but the equality of rates of the conversion and the $H_2 + D_2$ reaction rule this out (see the preceding paper, which I shall refer to as paper I). The second is that suggested by Bonhoeffer and Farkas (1931; Farkas 1931)

$$2W + H_2 \rightleftharpoons 2WH, \tag{1}$$

where the recombination of hydrogen atoms within a loosely bound chemisorbed layer is the rate-determining step. In paper I the reasons against this mechanism, which led to this research, have been given. A third possibility is an interchange reaction between parahydrogen molecules in a Van der Waals' layer and hydrogen atoms held in the strongly bound chemisorbed layer (Rideal 1939)

$$pH_2 + WH \rightarrow HW + oH_2. \tag{2}$$

The existence of this strongly bound layer has been experimentally demonstrated by Roberts (1935). A further possibility is that the conversion goes by mechanism (1) on a relatively small number of active spots, which would not be detected by Roberts's experiments (Farkas 1939).

To distinguish between these possibilities the following experiment may be made. A WH surface is prepared by contacting a clean tungsten surface with hydrogen gas for a minute, followed by careful evacuation at room temperature for from 5 to 10 min., until the pressure in the tube cannot be greater than 10^{-7} mm. This evacuation ensures that all the hydrogen will be removed from the active spots (if they exist) postulated by Farkas, since it is the essence of mechanism (1) that this evaporation should proceed as rapidly as does the parahydrogen conversion at room temperature. This must be complete within a fraction of a minute, since at 1 mm. pressure with a wire surface of 1 cm.^{2} in a reaction volume of 300 c.c. the half-life of the conversion is about 0·01 min., as calculated from our previous results. Deuterium gas is then admitted to the tube at a definite pressure and catalyst temperature, and the rate of interchange measured. Subsequently the parahydrogen conversion is measured under the same conditions. If now the rate of interchange of deuterium for hydrogen atoms between the gas and the adsorbed layer is the same or closely similar to the rate of conversion, we can infer that the conversion proceeds by an interchange mechanism, that is by mechanism (2).

In practice it was not possible to make a comparison of rates in quite such a clear-cut way as the above. It was only possible to detect a certain minimum amount of exchange because of the limitations imposed by the volume and sensitivity of our micropirani gauge. A calculation based on these factors showed that a tungsten surface of at least 100 cm.^{2} was necessary, and this ruled out the use of a wire. The most suitable catalyst appeared to be an evaporated film, which Farkas (1931) had already shown to possess considerable activity. On such a large surface the conversion proceeded too rapidly for a measurement of its rate to be made. Even at 77° K equilibrium was established within the few minutes required for an experiment. However, by combining data from wires with the area of the evaporated film calculated from adsorption experiments it could be shown that at this temperature the half-life of conversion on the film was of the order of half a minute, that is, only just outside the range of accurate measurement. Accordingly, to establish mechanism (2) I had merely to show that the interchange equilibrium was reached in the minimum time of experiment of 4 or 5 min. This would mean that the two rates were within a factor 5. That the actual rates of the two mechanisms (1) and (2) should be within such a factor at 77° K is extremely unlikely, and such a result would therefore rule out (1) as a possible mechanism for the conversion. A preliminary communication of these results has already been published (Eley and Rideal 1940).

2. EXPERIMENTAL DETAILS

The reaction tubes were of pyrex glass, 16 by 3·6 cm. diameter, and contained down their axis about 13 cm. of 0·1 mm. diameter tungsten wire, spot-welded at each end to heavy tungsten leads. They were sealed on to the vacuum apparatus already described in paper I, in place of the two-wire tube. The clean evaporated films were prepared as follows. The reaction vessel and trap were outgassed at 380° C for 2 days, the connecting tubing being thoroughly flamed from time to time. After this treatment the reaction system within the cut-offs held to 10^{-4} mm. overnight, with the furnaces on. Liquid air was placed on the trap adjacent to the wire, and the wire aged at 2500° K. The reaction vessel was then immersed in liquid air, the wire flashed, and the parahydrogen conversion on the wire examined. An active wire established the purity of the system and the gases used before the main experiments were made. In all cases recorded here the wire was as active as the clean wires previously examined (tubes 1*a*, 1*b*), and the results have been already recorded (paper I, tubes 2, 3, 4, 5). The only technical difference between experiments with these wires and the earlier ones was the absence of a sodium film on the walls of the vessel. Finally, the reaction tube was carefully outgassed with the walls at room temperature and a current passed through the wire, starting at 1·8 amp. and rising to 2·7 amp., which was held until the wires burnt out, usually after 10 min. In this way a visible film of tungsten was formed on the walls of the tube. It was essential from then on to exclude all traces of oxygen from the film, or it would be irreversibly poisoned and another tube would have to be prepared. Experiments were made with four such films, which were found to be very reproducible in general behaviour.

3. RESULTS

(a) *Adsorption of hydrogen by the clean film*

The freshly formed film on contacting with hydrogen gas at room temperature showed a rapid irreversible uptake of gas. Such behaviour was first observed by Roberts (1935), using the accommodation coefficient method with a tungsten wire.

(1) In the first instance a pressure of hydrogen was let into the external tubing and McLeod gauge, which we refer to as volume V_1. This gas was then expanded into the reaction vessel system, so as to occupy a total volume V_1+V_2, before the wire was evaporated. Two pressure readings, made before and after admitting the gas to V_2, served as a calibration for the subsequent measurement of adsorption.

(2) Secondly, the tube was evacuated and the evaporated film formed, and the above procedure repeated.

(3) Finally, the tube was pumped and the process repeated. To a first approximation the ratios of initial and final pressures should be the same in experiments 1 and 3. One might, however, expect a somewhat bigger pressure drop in 3 than in 1 because of Van der Waals' adsorption on the evaporated film. For the first tube experiments 1 and 3 agree well, but the second tube showed a discrepancy, the ratios being 3·3 (1) and 3·99 (3). Since the volumes in each case were identical and the value 3·99 agrees well with the ratios obtained for the first tube, I conclude that the value 3·3 is to some extent in error. Experiment 3 I take as the basis of calibration. Then for identical initial quantities of gas in experiments 2 and 3 (i.e. identical pressures in V_1), if the final pressures in (V_1+V_2) be p_2 and p_3^*, the amount of gas adsorbed corresponds to a pressure of $p_3^*-p_2$ in a volume (V_1+V_2).

TABLE 1

no.	pressure mm. in V_1	pressure mm. in V_1+V_2	pressure ratio	$p_3^*-p_2$ mm.
Experiment 183. Tube 4. H_2 gas. 296° K.				
1	0·1096	0·0288	3·81	—
2	0·1059	0·0102	—	0·0167
3	0·1059	0·0269	3·94	—
Experiment 199. Tube 5. D_2 gas. 296° K.				
1	0·1303	0·0395	3·3	—
2	0·126	0·0159	—	—
3	0·1202	0·0301	3·99	0·0157
	∴ 0·126	0·0316	—	—

In each case the volume V_1+V_2 was 500 c.c., and I neglect the effect that a small part of this system (50 c.c.) was a trap cooled in liquid air. Then in experiment 183, tube 4, $2{\cdot}74\times10^{17}$ mol. were adsorbed. Assuming $1{\cdot}2\times10^{15}$ as the number of H atoms per cm.^{2} of a chemisorbed layer on tungsten (Roberts 1939, p. 17), then the real area of the evaporated film was about 455 cm.^{2}.† From experiment 199, tube 5, I calculate an area of 428 cm.^{2}.

---

† In this and later calculations I neglect the existence of the 8 % of holes, which will be present if the film is immobile.

These calculations are based on the assumption that the film is formed by dissociation into atoms. While there is no direct evidence for this, the above reference gives the general considerations in its favour. Further, I have taken an average of the number of sites in the 100 and 110 planes as giving the actual number of sites per cm.^{2}. These assumptions do not influence a comparison of the areas with those derived from exchange experiments. A measurement of the dark zone on the walls of the reaction tube gave the apparent area of the film as 140 cm.^{2}, of similar order of magnitude as that calculated from adsorption. The film was therefore probably not microcrystalline to any great extent.

(*b*) *The parahydrogen conversion on films*

The evaporated films in their unpoisoned state were found to bring about $p\text{H}_2 \rightleftharpoons o\text{H}_2$ and $\text{H}_2 + \text{D}_2 \rightleftharpoons 2\text{HD}$ equilibria within the shortest period of experiment at both 77 and 293° K.

At 77° K† normal hydrogen $n\text{H}_2$, or hydrogen from a preceding experiment which was nearly $n\text{H}_2$ (as in no. 144), was used. Normal hydrogen means light hydrogen with the para-ortho ratio of 1:3 characteristic of room temperature, and therefore had a resistance value Ω of 0·00 ohm. At 77° K the equilibrium para-ortho mixture had Ω equal to 0·36 ohm. With H_2-D_2-HD at 77° K the equilibrium mixture contained a certain percentage of parahydrogen, so when this was passed over a hot nickel wire a rise in resistance value resulted. In table 2 the lower value in black type gives the resistance value of the sample after passage over the hot wire, while the upper value in the same column gives the resistance value before. Since each mixture of H_2-D_2 was made up in not necessarily the same proportions, we get differences in Ω_0 such as that shown between experiments 156 and 157. Qualitatively it is clear that the resistance shift $\Omega_0 - \Omega_t$ is only to be explained by considerable HD formation, and a rough calculation shows that equilibrium has been reached. That this is so is supported by the second part of experiment 156, where the continuation of the experiment over 26 min. showed no further shift in Ω_t. The calibration curve (paper I) gives for H_2-D_2 of $\Omega_0 = 0{\cdot}68$ ohm a deuterium content of 56 %. Taking the equilibrium constant as 2·2 at 77° K (Farkas 1935, p. 178), then the equilibrium concentrations will be 26 % H_2, 32 % D_2, and 42 % HD. The formation of 50 % HD from 50 % H_2, 50 % D_2 on the hot wire gives $\Delta\Omega = 0{\cdot}17$ ohm, and therefore 42 % HD corresponds to 0·14 ohm. Establishment of para-ortho equilibrium in the hydrogen will result in a shift of 0·26 × 0·36 = 0·09 ohm. One might therefore expect on these simple considerations a final resistance value of 0·45 ohm to be compared with that found of 0·42 ohm. A similar result holds for experiment 156. The discrepancy between observed and calculated values is probably outside the experimental error, and may be due to a neglect of a number of factors, e.g., ortho-deuterium formation.

---

† In these experiments the liquid air has been considered as mainly nitrogen, with a temperature of 77° K, although in many cases it was probably higher.

TABLE 2

tube	exp.	p mm.	T° K	t min.	Ω_0 ohms	Ω_t ohms
2	122	2·5 $p\mathrm{H}_2$	293	5	0·44	0·00
	125	2 $n\mathrm{H}_2$	77	2	0·00	0·36
	125	2 $n\mathrm{H}_2$	77	20	0·36	0·36
3	143	1 $p\mathrm{H}_2$	293	2	0·43	0·03
	144	1 $n\mathrm{H}_2$	77	2	0·03	0·34
	155	1 $n\mathrm{H}_2$	77	3	0·00	0·36
	156	1 $\mathrm{H}_2\mathrm{D}_2$	77	8·5	0·64	0·35
					0·46	**0·46**
	156	1 $\mathrm{H}_2\mathrm{D}_2$	77	26	0·35	0·36
					0·46	**0·46**
	157	1 $\mathrm{H}_2\mathrm{D}_2$	77	10	0·68	0·42
					0·51	**0·52**
5	202	1 $n\mathrm{H}_2$	77	3	0·00	0·37

Note. Ω is positive for H_2-D_2 mixtures, negative for $p\mathrm{H}_2$-$n\mathrm{H}_2$ mixtures.

These rapid conversions at 77° K are to be expected if the whole surface of the film is clean and therefore catalytically active. This may be shown by comparison with our experiments on wires (paper I). For tube 4, with a wire area of 0·34 cm.^{2} and a pressure of 1·3 mm., one may extrapolate to obtain at 77° K, $k = 2 \times 10^{-4}$ min.$^{-1}$ for both $\mathrm{H}_2 + \mathrm{D}_2$ and parahydrogen reactions. The evaporated film in tube 4 has an area of 455 cm.^{2} (see § 3*a*), and therefore we should expect $k = 0{\cdot}27$ min.$^{-1}$, which corresponds to a half-life of 2·5 min. Extrapolation of results with tube 1*a* gives for a wire area of 0·33 cm.^{2} $k = 2{\cdot}5 \times 10^{-3}$ min.$^{-1}$, and therefore for the film a half-life of 0·2 min. The observations show that the half-life is less than 2 min. So while one is debarred from an accurate measurement of the half-life these considerations support the view that if an appreciable interchange occurs between hydrogen in the gas phase and a well-pumped WH film at 77° K within a few minutes, then the suggested mechanism (2) is the correct one for the conversion.

(c) *Interchange experiments with adsorbed films*

(i) *Film temperature equals* 293° K. For an experiment with deuterium the tungsten film was first contacted with hydrogen at 1 mm., carefully pumped, and then a pressure p of deuterium was admitted for t min., after which it was removed to the micropirani gauge for analysis. Where experiments were made with hydrogen the film was first contacted with deuterium. This technique was modified in the experiments marked with an asterisk, where the charge of gas indicated was admitted to the reaction vessel as soon as it had been pumped out after the preceding experiment.

The results shown in table 3 indicate that for all films with the same pressure of D_2 a similar percentage exchange was observed. Experiments 128 and 129 show that equilibrium was, within experimental error, reached in 3 min. Experiments 148 and 149 show that the effect was reversible, deuterium in the film exchanging with gaseous hydrogen. It is apparent that when the amounts of hydrogen in the gas phase and the adsorbed film are comparable, as they are here, then the observed amount of exchange will be a function of the pressure. For example, if the free energies of adsorption of deuterium and hydrogen are equal, then for the cases where adsorbed gas equals in quantity that in the gas phase, we should expect only a 50 % replacement of deuterium by hydrogen in the gas phase. At lower gas pressures we should, however, obtain a greater percentage replacement, and at higher pressures a lower percentage. The absolute amount of exchange, that is, the pressure times the percentage hydrogen in the deuterium, should increase with pressure to a limit, analogously to the Langmuir isotherm. Such behaviour was in fact found, as shown in figure 1. Here I plot yp (denoted by D), where y is the fraction of hydrogen in the

TABLE 3

tube	exp.	surface	p mm.	t min.	Ω_0 ohms	Ω_t ohms
2	123	WH	$0{\cdot}21D_2$	8	1·10	0·98
	127	WH	$0{\cdot}36D_2$	5	1·10	0·93
	128	WH	$0{\cdot}33D_2$	3	1·10	0·92
	129*	—	$0{\cdot}20D_2$	6·5	1·10	1·08
3	145	WH	$0{\cdot}15D_2$	4	1·08	0·91
	148	WH	$0{\cdot}15D_2$	4	1·09	0·90
	149*	—	$0{\cdot}18H_2$	3	0·00	0·09
4	185	WH	$0{\cdot}17D_2$	4	1·09	0·98
5	204	WH	$0{\cdot}145D_2$	3	1·09	0·95
	208	WH	$0{\cdot}195D_2$	6	1·09	0·96
	209	WH	$0{\cdot}045D_2$	6	1·31	0·96
	210	WH	$0{\cdot}447D_2$	6	1·09	1·03
	213	WH	$0{\cdot}97D_2$	6	1·09	1·06

deuterium gas at the end of the experiment, read off from the calibration curve (paper I, figure 3), the resistance shifts $\Omega_0 - \Omega_t$ being taken from table 3, experiments 204–213. Treating the exchange as a reaction only involving the production of HD molecules, i.e.

$$\mathrm{WH} + \mathrm{D_2} = \mathrm{WD} + \mathrm{HD},$$

one can define an equilibrium constant,

$$K = \frac{[\mathrm{HD}][\mathrm{WD}]}{[\mathrm{D_2}][\mathrm{WH}]}.$$

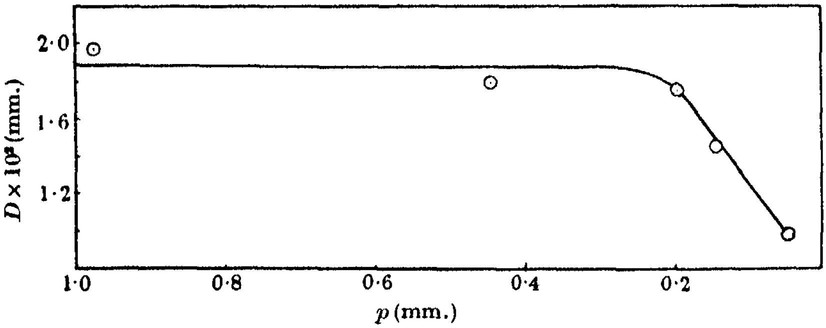

FIGURE 1. To show how the amount of interchange between gaseous $\mathrm{D_2}$ and a WH surface (D) is effected by the pressure of the $\mathrm{D_2}$ gas.

Here W indicates a surface atom of tungsten and [WD], [WH] denote surface concentrations of the adsorbed isotope, in the chemisorbed layer. Since our gas volume and surface area are constant, one can consider total quantities in the equation and not concentrations. The total number of moles of hydrogen initially present in the film we write as ψA, where A is the area of the tungsten surface, taken as 428 cm.^{2} from our adsorption measurements. Since 1 cm.^{2} of surface, containing $1{\cdot}2 \times 10^{15}$ sites, holds $0{\cdot}6 \times 10^{15}$ mol. hydrogen, ψ is 10^{-9} gmol./cm.^{2}. For a pressure p mm. let there be initially present in the gas phase N moles of deuterium, and at equilibrium let this gas contain a fraction y of hydrogen. Then at equilibrium there will be a fraction $2y$ of HD molecules present. One can write, for equilibrium

$N(1-2y)$ gmol. gaseous deuterium, $\mathrm{D_2}$,
$2Ny$ gmol. gaseous deuteride, HD,
$A - Ny$ gmol. adsorbed deuterium,
Ny gmol. adsorbed deuterium,

$$\therefore \quad \frac{2N^2y^2}{(\psi A - Ny)(1-2y)N} = K.$$

For the reaction volume of 350 c.c., $N = \alpha p$, where

$$\alpha = 1{\cdot}92 \times 10^{-5} \text{ gmol./mm.},$$

$$\therefore \quad \frac{2\alpha p^2 y^2}{(\psi A - \alpha p y)(1-2y)p} = K.$$

From figure 1 it is seen that for $p = 5 \times 10^{-2}$ mm. the total exchange $yp = 1{\cdot}0 \times 10^{-2}$ mm. ($y = 0{\cdot}2$). Therefore $(\psi A - \alpha p y) = 2{\cdot}36 \times 10^{-7}$ and $K = 0{\cdot}81$. This value is in good agreement with what one would expect on classical grounds, namely, $K = 1$. The equilibrium has not been investigated in such detail below 293° K, but later results suggest that at 77° K hydrogen is preferentially adsorbed to deuterium on tungsten.

From the limiting value of the deuterium exchange at higher pressures we can calculate the area of the film. This value is $1{\cdot}9 \times 10^{-2}$ mm. D_2 in 350 c.c., i.e. $2{\cdot}18 \times 10^{17}$ mol., each of which will occupy two sites. Since there are $1{\cdot}2 \times 10^{15}$ sites per cm.^{2} the area of the film is 364 cm.^{2}, which is only 15 % less than the value of 428 cm.^{2} determined in § 3 (*a*), and in view of the fact that the volumes concerned were not calibrated accurately but calculated from dimensions the agreement is very satisfactory. One can conclude that most of the hydrogen within the stable chemisorbed layer will interchange rapidly with deuterium at 293° K.

The reality of these experiments is confirmed in two ways. In one an interchange experiment was attempted when only a small amount of tungsten had been evaporated, with a negative result. In another a film, previously active, was poisoned by a trace of oxygen and afterwards no interchange could be observed. By partially poisoning the film in tube 4 it was possible to observe a direct correlation between the amount of interchangeable hydrogen in the film measured at 293° K, and the activity of the film in terms of the half-life ($\tau_{\frac{1}{2}}$) of the ortho-para conversion at 77° K.

Active film:

Parahydrogen conversion, pressure 1 mm., $\tau_{\frac{1}{2}} < 1$ min.
Deuterium exchange, 0·17 mm., 8 % hydrogen.

Partially poisoned film:

Parahydrogen conversion, pressure 1 mm., $\tau_{\frac{1}{2}} = 3$ min.
Deuterium exchange, 0·16 mm., 1·5 % hydrogen.

This gives strong support to the theory that a conversion goes through an interchange mechanism, between parahydrogen molecules and the strongly bound chemisorbed hydrogen.

(ii) *Film temperature equals* 193° K. The experiments given in table 4 show that a rapid reversible interchange occurs at this temperature similar in amount to that found at 293° K. All the experiments were made with tube 3.

TABLE 4

exp.	surface	p mm.	t min.	Ω_0 ohms	Ω_t ohms
150	WH	0·15D_2	3·5	1·09	0·92
151	WD	0·14H_2	2·5	0·00	0·08
152	WH	0·12D_2	4	1·09	0·92

In these experiments and those following at 77° K it is important to remember that the surfaces cited were made by contacting with the gas required, either D_2 or H_2, at a pressure of 1 mm. and a temperature of 293° K. Only after subsequent evacuation was the tube cooled to the temperature of the experiment.

(iii) *Film temperature equals* 77° K. Initially, all the experiments were made with a WH surface, the deuterium from the experiment being taken straight into the micropirani gauge. It was assumed that shifts in the para-ortho deuterium equilibrium could be neglected, but it will be shown that this is incorrect.

The average shift observed of 0·02 ohm is much less than that observed at 193 and 293° K (the experimental error is about ± 0·01 ohm). This shift

TABLE 5

tube	surface	exp.	p mm. D_2	t min.	Ω_0 ohms	Ω_t ohms
2	WH	126	0·24	5	1·10	1·06
	WD	131	0·45	4	1·10	1·09
3	WH	142	0·098	5	1·08	1·05
	WH	146	0·10	6	1·08	1·05
	WH	153	0·093	60	1·09	1·07
	—	153b*	0·10	11	1·09	1·07
4	WH	184	0·078	37	1·09	1·07
	WH	185	0·08	6	1·09	1·07
	WH	187	0·09	4·5	1·09	1·07
	—	187b*	0·09	5	1·09	1·08
	—	187c*	0·09	10	1·09	1·08
	WH	188	0·023	5	1·31	1·29
	WH	189	0·021	11	1·31	1·29
5	WH	205	0·098	6	1·09	1·07
	WH	212	0·031	6	1·31	1·29
	WD	214	1·0	15	1·09	1·07
						1·09
	WD	215	0·10	7	1·09	1·07

was independent of pressure (205, 212, 214), and also independent of whether the surface was WH or WD (cf. experiments 205, 212, with 214, 215). That equilibrium had been reached in the usual time of experiment is shown by experiment 153, made over 60 min., which also showed a shift of 0·02 ohm. If successive doses of deuterium were admitted, in each case a shift of 0·02 ohm was observed (experiments 153, 153*b*). These facts suggest that the change in resistance value was due solely to a shift in the para-ortho deuterium equilibrium from the value of 293° K to that at 77° K, under the influence of the film. At 300° K the equilibrium percentage of o-D_2 is 66·6 %, at 80° K, 69·8 % (Farkas 1935, p. 159), which would give a small change in resistance value as observed. This was confirmed by experiment 214, in which the gas sample of $\Omega_t = 1{\cdot}07$ ohm on passage over a hot nickel wire (value in black type), had $\Omega_t = 1{\cdot}09$ ohm identical with Ω_0. It is therefore concluded that under our conditions of pressure and surface area no interchange was detectable between WH and D_2 gas at 77° K. There are two possible reasons for this:

(1) While $pH_2 + WH$ interchanges rapidly, $D_2 + WH$ does not do so because of the generally remarked lower reactivity of deuterium, which will be particularly evident at temperatures as low as 77° K. This is ruled out since the reaction $H_2 + D_2 \rightarrow 2HD$ went rapidly at this temperature.

(2) The equilibrium $WH + D_2 \rightleftharpoons WD + H_2$ lies well over to the left at 77° K. The previous results at 293° K suggest that at this temperature the equilibrium is in fact equally in favour of either isotope in the gas phase. Cooling the film to 77° K may well shift the equilibrium so far to the left that no exchange is detectable using deuterium gas. However, one would be able to detect interchange between a WD surface and H_2. Table 6 shows that this has in fact been found. Before analysis the hydrogen from the experiment was passed over the hot nickel wire, since of course a negative resistance shift of 0·36 ohm was brought about by parahydrogen formation alone. The nickel wire was checked for cleanliness and reproducibility by passage of normal light hydrogen over it from time to time. The experiments were with tube 5.

From the calibration curve (paper I) it is seen that the average value of $\Omega_t = 0{\cdot}04$ ohm at 0·1 mm. corresponds to 2 % deuterium in the gas phase. At 0·1 mm. and 293° K for the reverse exchange we observed 9 % hydrogen in the gas phase. The discrepancy strongly suggests that the WD surface shows variations in activity and that in the time of experiment (6 min.) only 20–30 % of the adsorbed deuterium will exchange with hydrogen gas. This is supported by experiments 207 *a* to *e*, all at about 0·1 mm. pressure. In two experiments over a total of 13 min. (207 *a*, *b*), 4 % of deuterium appeared in the gas. A further experiment over 17 min., 207*c*, failed to remove any more deuterium. The tube was pumped and the film raised to 293° K and then contacted with deuterium, when an interchange was observed of value 4 % at 0·166 mm. At 0·1 mm. we should expect about 5 % exchange, to be compared with the 9 % observed for a WH surface prepared in the usual way. It is apparent therefore that the surface must contain a quantity of deuterium equivalent to 4 % in the gas at 0·1 mm. pressure, taken up in the previous experiment at 77° K. This value should be equal to the amount taken up in the first experiment at 77° K as, in fact, it is. These qualitative considerations suffice to show that at liquid air temperature 20–40 % of the adsorbed hydrogen only is active. This does not of course imply a wide variation in the adsorption energy of deuterium between the active and inactive sites, since at 77° K the permitted range for an appreciable reactivity will be small. An increase in activation energy of 350 cal. will slow the reaction down tenfold, at this temperature. Such a small term might arise from the difference in the repulsion energy between adjacent hydrogen atoms in the adsorbed films on the 110 and 100 planes respectively. In a later paper a fuller more quantitative theory of these experiments will be attempted. The main point here brought out is that at 77° K an appreciable amount of the strongly bound chemisorbed hydrogen will interchange with gaseous hydrogen over a few minutes. It can therefore be concluded that the para-ortho conversion goes by an interchange mechanism, referred to in the introduction as mechanism (2).

TABLE 6

surface	exp.	p mm.	T° K	t min.	Ω_0 ohms	Ω_t ohms
WD	200	0·098H_2	77	7	0·00	0·07
WD	202	0·10H_2	77	5	0·00	0·03
WD	206	0·091H_2	77	6	0·00	0·04
WD	207*a*	0·07H_2	77	6	0·00	0·04
—	207*b**	0·098H_2	77	7	0·00	0·03
—	207*c**	0·098H_2	77	17	0·00	0·00
—	207*e**	0·166D_2	293	9	1·09	1·03
WD	211	0·078H_2	77	6	0·00	0·05
WD	216	0·043H_2	77	6	0·00	0·06

My best thanks are due to Professor E. K. Rideal, F.R.S., for his encouragement and advice during the course of this work.

REFERENCES

Bonhoeffer, K. F. and Farkas, A. 1931 *Z. phys. Chem.* B, **12**, 231.
Bonhoeffer, K. F., Farkas, A. and Rummel, K. W. 1933 *Z. phys. Chem.* B, **21**, 225.
Eley, D. D. and Rideal, E. K. 1940 *Nature, Lond.*, **146**, 401.
Farkas, A. 1931 *Z. phys. Chem.* B, **14**, 371.
Farkas, A. 1935 *Light and heavy hydrogen.* Camb. Univ. Press.
Farkas, A. 1939 *Trans. Faraday Soc.* **35**, 943.
Rideal, E. K. 1939 *Proc. Camb. Phil. Soc.* **35**, 130.
Roberts, J. K. 1935 *Proc. Roy. Soc.* A, **152**, 452.
Roberts, J. K. 1939 *Some problems in adsorption.* Camb. Univ. Press.

On the α/β brass type of equilibrium

BY K. W. ANDREWS AND W. HUME-ROTHERY, F.R.S.

(*Received* 1 *April* 1941)

I

In alloys of copper and silver with many of the elements of the B subgroups, the first additions of the solute element result in the formation of a primary or α-solid solution in copper or silver, and, when the solubility limit of this is exceeded, a second phase is formed with a body-centred cubic structure, which may have a disordered (β), or an ordered (β') structure. The two-phase areas of these equilibrium diagrams are characterized by the fact that the $\alpha/\alpha+\beta$ and $\alpha+\beta/\beta$ phase boundaries are approximately parallel, and slope so that the solubility limit of the α phase increases with falling temperature; this kind of equilibrium will be called the α/β brass type of equilibrium, and is in contrast to the equilibrium between the α and β' phases, in which the phase boundaries follow quite different principles. It is well known that the α/β brass type of equilibrium is controlled largely by the electron concentration, i.e. the number of valency electrons per atom; a theory based on this assumption was advanced by H. Jones (1937*b*). In this theory the electron concentration only was considered, but it was shown by Hume-Rothery (1936) that the equilibrium was influenced by the atomic size factors and lattice distortions in the different systems. At this time lattice spacings at high temperatures could only be estimated qualitatively from measurements at room temperature, and since any complete theory must involve the lattice distortions, and atomic volumes of the alloys, it appeared very desirable to establish a really accurate set of data. The development of high temperature X-ray technique makes this possible, and in the present paper we are submitting a complete set of lattice spacings of the α, β, and β' phases in the two-phase alloys of the system copper-zinc at temperatures between 300 and 870° C, and similar lattice spacings for the α and β phases in a number of other systems at a standard temperature of 672° C. We have also measured the lattice spacings of copper at temperatures up to 871° C, since a knowledge of these is required in order to estimate the lattice distortion of the primary solid solution at the different temperatures. The positions of the phase boundaries in most of the systems are known to an accuracy which is much less than that of the present measurements of the lattice spacings, and it should be emphasized that later and more accurate determinations of the phase boundaries will not affect the present lattice spacings, which were determined from two-phase alloys.

II

The alloys used in the present work were either those from previous experiments on the determination of phase boundaries, or were prepared specially from the purest metals; the copper-zinc alloys being prepared from spectroscopically pure zinc, and from copper of 99·998 % purity kindly presented by the British Non-Ferrous Metals Research Association. The alloys were first annealed in lump form to equilibrium at the temperature at which the lattice spacing was to be measured,§ and were then quenched in cold water or iced brine according to the nature of the alloy. Filings were then prepared, and after sieving through 100-mesh gauze, were sealed in silica capillaries, and mounted in the high temperature camera. In experiments at 672° C and below, the filings were annealed in the camera for at least 4 hr. before the actual exposure was made. At the higher temperatures this preliminary annealing of the filings was gradually reduced to 2 hr. at 871° C. For the preliminary annealing treatment the temperature was controlled by hand during the early part of the work, and later by means of a Foster Potentiometric Controller. The temperature fluctuations were of the order ± 2 or ± 3° C, and very seldom exceeded these limits. For the actual exposure, control was always by hand, and the accuracy was of the order ± 1° C with only very occasional and brief fluctuations outside this limit.

---

§ This preliminary annealing in lump form at the temperature of the final experiment is essential, since filings prepared from castings may require very long periods to reach equilibrium.

The high temperature X-ray technique of Hume-Rothery and Reynolds (1938) was adopted, and nickel, cobalt, and copper radiations were used in order to obtain suitable high angle lines, the exact value of the lattice spacings being obtained by the $\cos^2\theta$ extrapolation method. The camera was originally standardized against quartz as recommended by Bradley and Jay (1933). In the course of the work, Dr H. Lipson kindly told the authors that extensive work at the Crystallographical Laboratory of the University of Cambridge had shown that the constants assumed by Bradley and Jay gave the standard angle of the type of camera approximately 0·04° too high, and the present results were recalculated using a standard angle of 84·310 instead of the value 84·350 originally assumed. The lattice spacings of the pure copper at high temperatures were measured by the methods used by Hume-Rothery and Reynolds for silver; cobalt radiation was used, and very satisfactory films were obtained over the whole range of temperature.

III

The lattice spacings obtained are summarized in tables 1 and 2 which also include other data required for the discussion of these phase boundaries. The compositions of the face-centred cubic phases at the temperatures concerned are, in general, taken from the collected tables of Hume-Rothery, Mabbott and Channel-Evans, but in some cases later and more accurate determinations have been used. Details of the exact sources of these and of the β-phase data used are given in the Appendix. The accuracy of the present lattice-spacing determinations varies in the different systems, since the presence of overlapping lines and other factors sometimes prevented really satisfactory high-angle lines from being obtained. Where a value is marked * it implies that the result appeared highly accurate. In one or two cases duplicate determinations were made with different specimens, and the results agreed to within 0·0001 A.§ The values so marked are probably accurate to within ± 0·0002 A, whilst in the results marked † the error is not likely to be more than twice as great. For the remaining values the probable accuracy is indicated in table 1. Many of the determinations were made in duplicate and every care has been taken to present an accurate set of lattice spacings.

The only data available for comparison with the present results are those obtained for the Cu-Zn β phase at the lower temperatures by Owen

---

§ The lattice spacings are in crystal Ångströms and are uncorrected for deviations from the Bragg Law.

TABLE 1

system	temp. °C	lattice spacings of α and β phases	electron concentration of α and β phases at $\alpha/\alpha+\beta$ and $\alpha+\beta/\beta$ boundaries	mean volume per atom for α and β phases	mean volume per electron for α and β phases
Cu-Zn	297	αa = 3·7105*	1·388	12·771 (4)	9·199
		$\beta' a$ = 2·9626*	1·457	13·001 (4)	8·923
	400	αa = 3·7246*	1·385	12·917 (5)	9·327
		$\beta' a$ = 2·9709†	1·45	13·115 (4)	9·045
	497·5	αa = 3·7333*	1·380	13·008 (2)	9·426
		$\beta' a$ = 2·9775*	1·438	13·198 (5)	9·178
	673	αa = 3·7433*	1·358	13·116 (5)	9·659
		$\beta' a$ = 2·9851†	1·411	13·299 (8)	9·426
	771	αa = 3·7480*	1·343	13·162 (5)	9·801
		$\beta' a$ = 2·9889†	1·393	13·350 (7)	9·584
	871	$\alpha.\ a$ = 3·7517*	1·325	13·201 (5)	9·963
		$\beta.\ a$ = 2·9907 (5)†	1·371	13·375 (5)	9·756
Cu-In	672	$\alpha.\ a$ = 3·7533*	1·205	13·221 (9)	10·973
		$\beta.\ a$ = 3·0400‡	1·372	14·047 (2)	10·238
Cu-Sn	672	$\alpha.\ a$ = 3·7425*	1·2535	13·104 (6)	10·454
		$\beta.\ a$ = 3·01385‡	1·426	13·687 (8)	9·599
Cu-Ga	672	$\alpha.\ a$ = 3·7160‡	1·394	12·828 (2)	9·202
		$\beta.\ a$ = 2·9611*	1·458	12·981 (6)	8·904
Cu-Al	672	$\alpha.\ a$ = 3·7036‡	1·380	12·700 (2)	9·205
		$\beta.\ a$ = 2·9504*	1·452	12·841 (4)	8·844

* Implies a really satisfactory film on which the error is not greater than ± 0·0001 A from the point of view of measurement, and an accuracy of ± 0·0002 A may be claimed.

† Implies a film on which the error is not more than twice that for results marked *.

‡ The accuracy here is of the order ± 0·0005 A.

TABLE 2. LATTICE SPACING OF PURE COPPER

temp. °C	lattice spacing, A
18	3·6074
300	3·6259 (5)
500	3·6398
671	3·6526
771	3·6603
871	3·6683

and Pickup (1934). These investigators used a method in which the temperature was estimated from the position of the diffraction lines of a standard substance covering one-half of the hot foil of a focusing camera, the other half being covered by the filings of the brass under examination. Copper and silver were used as standard substances, and gave slightly different results, presumably owing to volatilization of zinc from the brass to the standard. Using linear interpolation between the values given by Owen and Pickup, the following comparison may be made for the lattice spacing of the β phase in $\alpha+\beta$ alloys.

temp. °C	present result	Owen and Pickup
297	2·9626	$2{\cdot}962_4$
400	2·9709	$2{\cdot}970_8$ $2{\cdot}971_3$
497·5	2·9775	$2{\cdot}977_4$ $2{\cdot}977_9$

The agreement is very satisfactory.

The lattice spacings of pure copper at different temperatures are shown in table 2. These values all appear highly accurate, although at the higher temperatures they differ appreciably from some equations given in collected tables for the expansion of massive bars of copper; this discrepancy is being discussed in a separate paper. The value $a = 3{\cdot}6074$ A at 18° C is in exact agreement with that given by Owen and Roberts (1939).

IV

In figure 1 the results for the copper alloys are shown in such a way that the volumes per atom of the α and β phases in equilibrium in the different systems at the standard temperature of 672° C are plotted against the electron concentration of the phases as determined from the equilibrium diagram;§ the point for the solvent metal copper for which the electron concentration is 1·0 is also included. The volumes per atom are calculated on the assumption that the α and β phases are simple solid solutions with 4 and 2 atoms per unit cell respectively, whilst the electron concentrations are given by the formula $C = 1 + x(v-1)/100$, where x is the atomic percentage of solute element of valency v. When plotted in this way, several points of interest are established.

§ The phase boundaries at 672° C are known to an accuracy of the order ±0·2 atomic %, except for the β phase of the system Cu-Al where the error may be slightly greater.

(1) In the system Cu-In, the straight line joining the points for the α and β phases passes through the point for the solvent metal copper to a degree of accuracy well within that with which the positions of the phase boundaries are known, so that on passing from the α to the β phase the atomic volume increases in direct proportion to the changes in composition. In the system Cu-Sn this is almost but not quite as accurately the case. This relation does not hold in the systems Cu-Zn, Cu-Ga, or Cu-Al. It is perhaps significant that the lines joining the Cu-Zn α and β points, and the Cu-Ga α and β points intersect at the ordinate of electron concentration 1·0; this was first noted by Dr Raynor.

(2) The general relations between volume per atom and electron concentration are clearly quite different for the α and β points. For the pairs of adjacent elements In-Sn, and Zn-Ga, the lines joining the β-phase points in figure 1 are accurately parallel. For the α-phase points, no such relation holds, but the points for Cu-In, Cu-Sn, and Cu-Ga lie on one straight line, with the Cu-Zn point distinctly higher. These differences are undoubtedly connected with the way in which the lattice distortion of the α phase is produced by the different elements. In all the alloys the formation of the α solid solution in copper is accompanied by an expansion, and the mean expansion per atom of solute is in the order Sn > In > Ga > Al > Zn. At 672° C the lattice spacings of the Cu-Zn and Cu-Sn α phases in equilibrium with the corresponding β phases are almost the same, but this lattice expansion is produced by 35·8 atomic % of zinc in the system Cu-Zn, and by only 8·4 atomic % of tin in the system Cu-Sn. The distortion is thus spread out much more evenly in the system Cu-Zn than in the system Cu-Sn, and it is this fact which presumably accounts for the relatively high position of the Cu-Zn point in figure 1. The fact that the Cu-Al α point in figure 1 lies lower than would be expected from the straight line through the Cu-In, Cu-Sn, and Cu-Ga points is probably the result of the much stronger electro-chemical factor in the system Cu-Al, since this increases the forces of attraction. Figure 1 also shows that the previous suggestion (Hume-Rothery 1936) that the lattice spacings of the α phase rise to a constant limiting value is qualitatively, but not quantitatively, correct. At 672° C the α solid solubility, expressed in terms of electron concentration, decreases enormously when the mean volume per atom exceeds 13·1 A^3, but the Cu-Zn, Cu-Sn, and Cu-In points do not lie on a horizontal line.

(3) In contrast with the α phases, the β phases are not formed by the distortion of the lattice of a parent metal, and the electron concentration of the β-phase boundaries in the different systems differ much less. The

parallelism of the lines joining the CuIn-CuSn, and CuZn-CuGa points suggests that the solutes of each period follow the same principle, but unfortunately only two elements in each period form a β phase, and this point cannot be tested further.

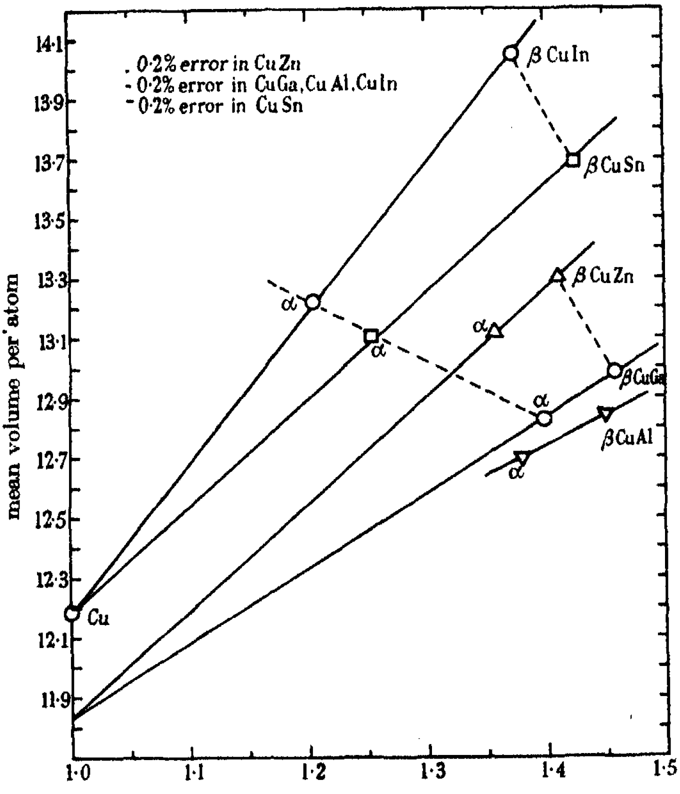

FIGURE 1

(4) Figure 1 thus establishes some points of interest, but much more general relations are shown in figure 2. In this the abscissae are again the electron concentrations of the phases in equilibrium at the standard temperature of 672° C, whilst the ordinates are the mean volumes per electron V_e, defined as the mean volume per atom divided by the number of valency electrons per atom. When plotted in this way, the lines joining the points for the β phases of the adjacent systems Cu-In, Cu-Sn, and Cu-Zn, Cu-Ga are accurately parallel, and are very nearly parallel to the lines joining the

α-phase points of the same pairs of systems.§ The lines joining the α- and β-phase points in each one of the systems Cu-Al, Cu-Zn, Cu-Ga, Cu-In, and Cu-Sn form a series of five almost parallel straight lines, and the points *a*, *b*, *c*, *d* representing the mid-points of these lines in the systems Cu-In, Cu-Sn, Cu-Zn, and Cu-Ga lie accurately on the oblique straight line *AB*. These last are the four systems in which the electro-chemical factors are small, but in the system Cu-Al where the electro-chemical factor is larger, the points for both α and β phases are clearly much lower than would be expected from the relation shown by the other systems. The oblique line *AB* in figure 2 thus shows that, when the electro-chemical factor is small,

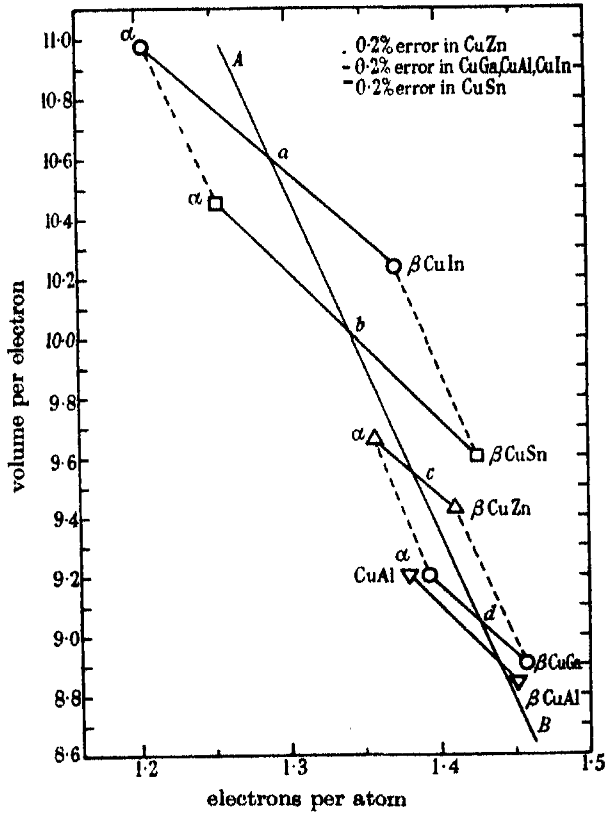

FIGURE 2

---

§ The divergence from exact parallelism is of the same order as the uncertainty in the exact position of the phase boundaries (about ± 0·2 atomic %).

the effect of lattice distortion on the $\alpha\beta$ brass equilibrium is such that at 672° C there is a linear relation between the electron concentration and the mean volume per electron of the points lying mid-way between the $\alpha/\alpha+\beta$ and $\alpha+\beta/\beta$ boundaries in the equilibrium diagrams. Increase in the volume per electron displaces these mid-points in the direction of lower electron concentration according to the oblique slope of the line *AB* in figure 2. This relation between the points mid-way between the α- and β-phase boundaries is particularly interesting in view of the fact that Jones (1937*a*) has shown that some of the relations between phases in equilibrium can be expressed in terms of the lines lying mid-way between the composition of the two phases. If the line *AB* in figure 2 were vertical, it would imply that the electron concentrations of the α and β phases were shifted by equal amounts in opposite directions. Actually this is not so, and it is particularly interesting to see how the changes are still symmetrical about the oblique line *AB*. The results for the system Cu-Al suggest that increasing electro-chemical factor interferes with this simple principle, although still leaving the line joining the Cu-Al α and β points parallel to the corresponding lines for the other systems in figure 2.

The experimental work described in this paper has been carried out at The Inorganic Chemistry Laboratory, The University Museum, Oxford, and the authors must express their gratitude to Professor C. N. Hinshelwood, F.R.S., for laboratory accommodation, and many other facilities which have greatly assisted the research. Thanks are also due to Dr G. V. Raynor for help with the X-ray work. Grateful acknowledgement of financial assistance is made to the Council of the Royal Society, the Department of Scientific and Industrial Research, the British Non-Ferrous Metals Research Association, and the Curators of the Leigh Fund of the University of Oxford, and to the Imperial Chemical Industries Ltd. for the loan of apparatus.

REFERENCES

Bradley, A. J. and Jay, A. H. 1933 *Proc. Phys. Soc.* **45**, 507.
Hume-Rothery, W. 1936 *Phil. Mag.* (vii), **22**, 1013.
Hume-Rothery, W. and Reynolds, P. W. 1938 *Proc. Roy. Soc.* A, **167**, 25.
Jones, H. 1937*a* *Proc. Phys. Soc.* **49**, 243.
Jones, H. 1937*b* *Proc. Phys. Soc.* **49**, 250.
Owen, E. A. and Pickup, L. 1934 *Proc. Roy. Soc.* A, **145**, 258.
Owen, E. A. and Roberts, E. W. 1939 *Phil. Mag.* (vii), **27**, 294.

APPENDIX

The composition of the phases in equilibrium with the β phases have been taken from the collected tables of Hume-Rothery, Mabbott and Channel-Evans (1934) except in the cases detailed below, where the sources of the data for the β phases are also indicated.

Copper-zinc. β-phase points from the diagram given by Hansen (1936).

Copper-gallium. β-phase points from the diagram of Hume-Rothery and Raynor (1937).

Copper-aluminium. β-phase points from the revised diagram given in the 1939 *Metals Handbook* (American Institute of Mining and Metallurgical Engineers), and unpublished work by the authors.

Copper-indium. α- and β-phase points from Hume-Rothery, Raynor, Reynolds and Packer (1940).

Copper-tin. β-phase points from Raper (1927).

REFERENCES

Hansen, M. 1936 *Aufbau der Zweistofflegierungen.* Berlin.

Hume-Rothery, W., Mabbott, G. W. and Channel-Evans, K. M. 1934 *Phil. Trans.* A, **233**, 1.

Hume-Rothery, W. and Raynor, G. V. 1937 *J. Inst. Metals*, **61**, 205.

Hume-Rothery, W., Raynor, G. V., Reynolds, P. W. and Packer, H. K. 1940 *J. Inst. Metals*, **66**, part 7, 209.

Raper, A. R. 1927 *J. Inst. Metals*, **38**, 217.

Deuteron-induced fission in uranium and thorium

By D. H. T. Gant and R. S. Krishnan

Cavendish Laboratory, Cambridge

(*Communicated by J. D. Cockcroft, F.R.S.—Received* 3 *February* 1941)

Nuclear fission of uranium and thorium under bombardment by deuterons of about 9 MeV has been investigated both qualitatively and quantitatively by the use of the 'active-deposit' technique.

The following results have been obtained: (i) The range of the fission fragments from both uranium and thorium is about 2·3 cm. in air. (ii) The decay curve agrees in scale and shape with that which would be expected from a complex mixture of radioactive bodies. (iii) The active deposit has been examined for emission of β-rays, positrons, γ- and X-rays, α-particles and neutrons; the radiations are found to bear a general similarity to those resulting from neutron-induced fission. (iv) Some of the radioactive bodies have been isolated by chemical methods; some correspondence with the products of neutron-induced fission is shown. (v) The ratio of the fission cross-sections for 9 MeV deuterons and (Li + D) neutrons has been measured. (vi) The excitation function has been studied.

The experimental data from (v) and (vi) are compared with calculations based on Bohr and Wheeler's treatment of the mechanism of the process.

1. Introduction

Although neutron-induced fission has been the subject of intensive study by many investigators, little work has been reported on fission induced by other methods of excitation. The techniques generally used in these studies of neutron-induced fission have been:

(i) chemical separation of the irradiated specimen,

(ii) detection of large bursts of ionization in an ionization chamber,

(iii) detection of heavily ionized tracks in a cloud chamber,

(iv) study of the active deposit formed by collection of recoiling fragment nuclei (Joliot 1939).

In considering the relative merits of these methods it may be remarked, first, that method (i) must involve considerable complexity in technique if it is to be unambiguous, and that it is not readily adapted to quantitative operation; and secondly, that methods (ii) and (iii) have the advantage of registering individual fission processes directly. In comparison, method (iv) is less direct and also less sensitive. For the present experiments, however, the technical work needed for the use of (ii) and (iii) in association with the cyclotron had not been completed at Cambridge, and method (iv) was employed. This method has enabled us to outline the outstanding features of deuteron-induced fission and to obtain some rough quantitative results. Having regard to all the circumstances our object has so far been a general survey of the phenomenon rather than a detailed study of any particular aspect of it.

This paper is intended to amplify the information contained in two earlier and shorter publications (Gant 1939; Krishnan and Banks 1940), to present some new experimental results, and briefly to review the subject from the standpoint of theory. The experimental work described was completed in August 1940, and the delay in submission of this paper has been due to circumstances attendant on the war.*

2. EXPERIMENTAL METHOD

The method consists in bombarding a target of uranium† with a beam of deuterons and placing a thin metallic foil near the target to collect any recoiling nuclei. The target was prepared by a method of crude simplicity; a 2 mm. copper plate (4 × 2 cm.) was coated on one side with a thin layer of celluloid cement, uranium metal powder was sprinkled thereon to form a thick layer, and the plate was pressed in a hydraulic press. The layer of uranium so formed was satisfactorily coherent, and such a target has withstood many bombardments over the period of a year. In order to conserve the target we have restricted the beam current to values not much greater than $1\,\mu$A, but this could probably have been exceeded without any deleterious effect. Weighing the uranium from a measured area of the target gave the surface density as 20 mg./cm.^{2}, corresponding to a stopping power of 5 cm. of air.

Details of the experimental arrangement are shown in figure 1. The target plate A was fixed on a water-cooled copper block B inside the cyclotron target chamber, and there formed the rear side of a copper box. The collecting foil F, usually of 3–4 mg./cm.^{2} aluminium, was placed on the top inside surface of the box, and was held in a pocket P having an aperture (1·5 cm. square) in the front. The collector presented a comparatively small angle to the target, but the mechanical convenience of the construction adopted was considered to outweigh this disadvantage.

---

* [*Note added in proof.* Since the submission of this paper there have come to hand reports of other work covering some of the same ground (Jacobsen and Lassen, 1940, *Phys. Rev.* 58, 867; Bohr, 1940, *Phys. Rev.* 58, 864). The conclusions appearing there are in substantial agreement with our own.]

† The technique used for thorium was similar to that described for uranium.

A piece of 2 mm. S.P. aluminium was fixed over the aperture to stop any low energy debris thrown off from the target. A lid *L* to the box protected the collector against direct bombardment by the deuteron beam, which was admitted into the box through an aperture in the lid.

In order to centre the beam in the aperture the following simple but effective method was used. A piece of white paper was fixed over the front of the box, and an irradiation of 1 μA for about 2 min. was found to demarcate the position of the deuteron beam by a definite scorch mark, roughly oval in shape and about 4 × ½ cm. By altering the voltage on the cyclotron deflector plate the beam was shifted by about ½ cm./kV, and the voltage could be adjusted so that the beam was placed symmetrically with respect to the aperture. In every subsequent run the deflector voltage was set at this value. A displacing effect due to the radio-frequency voltage on the anti-deflector plate was also evident, so a standard value of radio-frequency voltage also was used. In some of the experiments the lid of the target box was insulated from the body of the box and earthed, so that the beam galvanometer measured only the target current, but as about one-half of the beam passed through the aperture in any case, when the

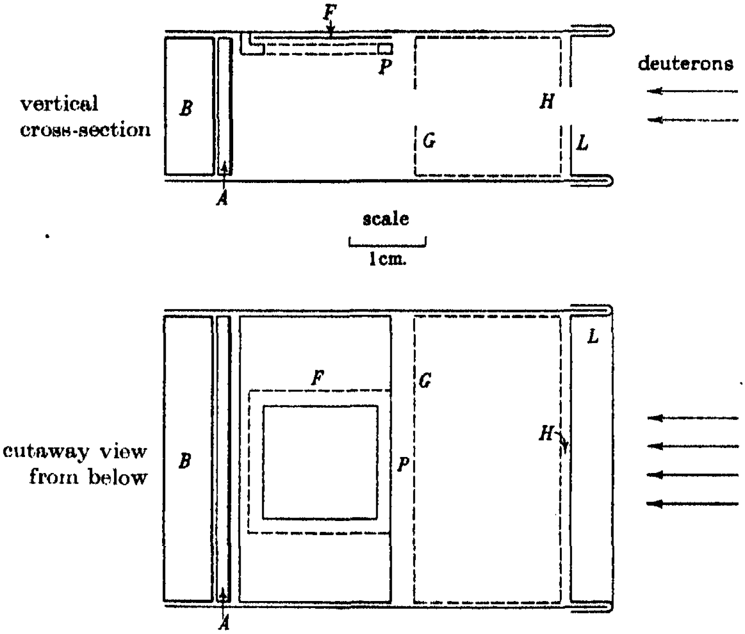

Figure 1. Target box.

absolute value of the beam was of no consequence the lid was mechanically fixed to the box for greater convenience. In order to ensure that the current registered by the beam galvanometer was due entirely to deuterons impinging on the target and not to the emission of secondary electrons, the lid of the target box was shaped so as to trap secondary electrons.

Bombardments were usually of ½–1 μA for 10 min., and in quantitative experiments the beam current was kept at a steady value throughout the irradiation. At the end of the bombardment the activity on the collecting foil was measured by means of a Geiger counter and a high-speed recording apparatus.

It was expected that a considerable activity would be induced in the collector by deuterons scattered back from the target and by neutrons produced by impact of the beam on the uranium-on-copper target with its adherent film of deuterium. To measure these effects auxiliary control foils D and N of the same size and thickness as the collector F were used. D was placed immediately behind F, and as the thickness of the latter was equivalent to about 2–3 cm. of air only (i.e. ½ MeV for 9 MeV deuterons), it was expected that any activity induced by deuterons scattered from the target would be practically equal in F and D. This was subsequently confirmed by bombarding copper, lead and bismuth in place of the uranium-on-copper target. The foil N was separated from D by a piece of copper sheet thick enough (½ mm.) to stop all the scattered deuterons, and N then registered the activity induced in the foil by neutrons only.

3. Experimental facts

In a typical case, a uranium target* was given a bombardment of 2 μA min. Five minutes after the end of the bombardment N gave a count of about 40 per min., its decay being dominated by a 10 min. half-life. The magnitude of this effect was subtracted from the activities of D and F. D then had an activity of about 100 counts per min. decaying with the well-known 2¼ min. period of Al^{28}. When both the deuteron-induced and neutron-induced activities had been subtracted, F had a strong residual count of 1500 per min. Plates of copper, lead and bismuth were substituted in turn for the uranium-on-copper target, and F then showed no activity greater than that of D. The F effect of the uranium-on-copper target was clearly due to some kind of radiation elicited from the uranium by the deuteron bombardment, any appreciable effect from the lighter nuclei present being very unlikely.

* The results with thorium were of the same kind as for uranium.

The decay of the *F* activity was characterized by no outstanding individual period; indeed the decay curve (discussed in § 6) was reminiscent of the 'composite' decay curve of the complex mixture of products resulting from neutron-induced fission. The decay curve was substantially the same whether the collector was of aluminium, silver or cine film; this suggested that radioactive nuclei were being implanted in the collector rather than that the activity was induced by bombardment of the collector.

The range of the particles was measured by a method to be described later, and was found to be equivalent to about 2 cm. of air. The particles could not have been projected merely by mechanical impact of fast particles, for then the range would have been much shorter; no explanation remained other than that the radioactive particles were fragment nuclei resulting from nuclear fission in uranium.

4. CONTROL EXPERIMENTS ON NEUTRON-INDUCED FISSION

It was of crucial importance to establish that the fission occurring under these experimental conditions was caused directly by the action of deuterons on uranium and was not merely neutron-induced fission originating in the effect of stray neutron radiation on the uranium. The tests described below proved that the major part of the fission was due to deuteron rather than to neutron action.

(i) A piece of 1 mm. copper sheet (of size 4 × 2 cm.) was coated on both sides as equally as possible with a layer of uranium. The sheet was first fixed in the target position and the fission activity measured in the usual way. It was then fixed over the aperture at the front of the box, where it occupied relative to the collector a position equivalent to that in the positive experiment, and a similar bombardment given. In the latter case the *F* activity could only be due to neutron-induced fission; it amounted to less than one-hundredth of the activity present after the positive experiment.

It could not be immediately concluded that this fraction represented the ratio of the neutron-induced and deuteron-induced fissions in the positive experiment, owing to the greater average distance of the neutron source from the layer of uranium facing the collector in the control experiment compared with the corresponding separation in the positive experiment. In the control experiment the neutron paths through the effective layer of the uranium target (equivalent in depth to 2 cm. of air), were on the whole less oblique; consequently they had a smaller part of their length in the target and could produce less effect in the layer. Even when this correction had been made, however, the result remained that the ratio of the neutron- to deuteron-induced fissions in the positive experiment was less than 1/50.

(ii) In another type of control experiment a thin plate was coated with thorium in the same manner as for the target, and this plate was enclosed within the pocket itself, just in front of the *F* foil and separated from it by a piece of 2 mm. S.P. aluminium foil. In the positive experiment neutrons from the target would cause fission in the thorium of the target, and some of the fission particles would be projected through the aperture in the pocket on to the collector; in the control experiment neutrons from the target would generate fission particles in the thorium layer inside the pocket, and some of these would be embedded in the adjacent collector. The geometrical configuration was such that neutron-induced fission effects were almost the same in the positive and control experiments, subject to a correction for the obliquity factor mentioned above. This method showed the amount of neutron-induced fission for thorium to be imperceptible under the prevailing experimental conditions.

5. RANGE OF THE FISSION PARTICLES

A rough measurement of the range of the projected particles (by a method adapted from McMillan 1939) was originally undertaken and reported by us as confirmatory evidence for the supposition that fission was occurring. The arrangement then used has been subsequently slightly refined in order to obtain a more reliable estimate than was available from the earlier measurements. For this purpose the target was inclined within the box at an angle of 45° to the direction of the beam, and a slight improvement in geometry was obtained by restricting the aperture in the pocket to a square of 0·5 cm. side. Inside the pocket were placed seven aluminium foils of 0·66 mg./cm.^{2} each. After an irradiation the activities in the foils were measured and the decay curves were drawn. These displayed a noticeable family resemblance,* and the magnitude of the activities showed a regular variation throughout the series. Activities at a time about 30 min. after the bombardment are plotted in figure 2. No appreciable deuteron-activation of the collector should remain after the lapse of this time, and the small 'background' observed (shown as a broken line in the figure) is attributed to neutron-activation. Neutron-induced fission will account for only a small fraction of each of the ordinates, and therefore does not affect the considerations of this section. The value indicated for the range is about 2·3 cm. for both uranium and thorium. A feature of interest in the curves is the increase in activity over the few uppermost foils, illustrating the greater fission intensity at the surface of the target compared with that at depths where deuterons of smaller energy are effective.

---

* Even if the fragments having different ranges are of different nuclear constitution, it is to be expected that the multiplicity of periods would tend to make the decay curves closely similar.

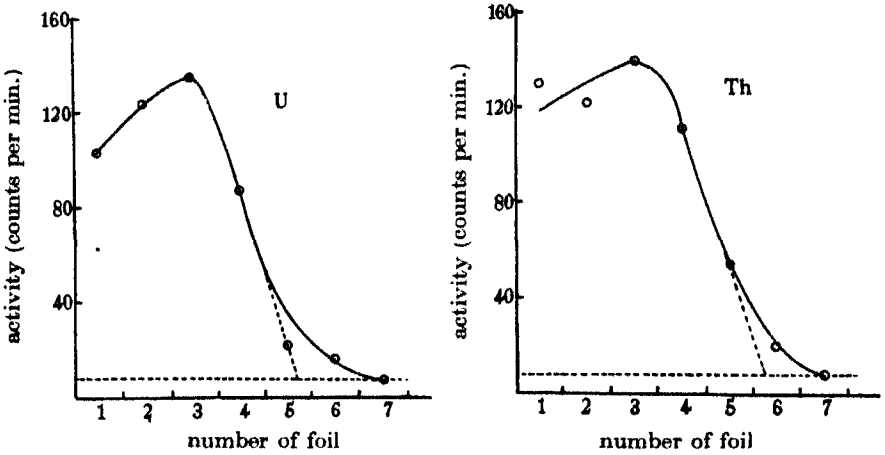

FIGURE 2. Range of the fission particles.

6. THE COMPOSITE DECAY CURVE

Individual periods are not distinguishable in the 'composite' decay curve of such a complex mixture of radioactive bodies as that which results from fission. It has been shown by Frisch (1939) that the shape of the decay curve can be calculated from the integrated effect of a continuous distribution of radioactive periods. The disintegration constants λ are connected with the corresponding disintegration energies E by the Sargent law,

$$\lambda = kE^n. \tag{1}$$

It is assumed (*ad hoc*) that the distribution function for E, $f(E)$, is independent of E over the relevant range of energies. It can then be shown that at time t measured from the end of an irradiation of duration T the number of radioactive disintegrations per unit time (I_t) is given by

$$I_t = \frac{f(E)\,\Gamma(1/n)}{nk^{1/n}}\,[t^{-1/n} - (t+T)^{-1/n}], \tag{2}$$

where Γ denotes the gamma function. The analysis is strictly true only if $f(E)$ is constant for all energies, but for values of t greater than a few minutes the approximation is sufficiently close for the present purpose if the constancy is preserved (at a value of $f(0)$) over only a small range of low energies. It is readily shown that

$$\text{counts/sec. per deuteron/sec.} = \frac{\rho\sigma s f_1 \nu f_2}{E'}\,\frac{\Gamma(1/n)}{n k^{1/n}}\,[t^{-1/n} - (t+T)^{-1/n}], \quad (3)$$

where the symbols have the following connotation:

ρ = number of nuclei per cm.^{2} in the effective layer of target,
σ = fission cross-section,
s = number of fragments per fission,
f_1 = fraction of fission fragments collected,
ν = number of β's per fission,
f_2 = fraction of the β's from the collecting foil counted,
$E' = \frac{1}{f(0)}\int_E f(E)\,dE.$

Figure 3 gives the experimental activities together with curves of the form of equation (3); the equation clearly gives an adequate representation of the experimental results. To test the validity of (3) as regards the absolute magnitude of the activity, the experimental results have been used to obtain a value for the cross-section. The following numerical values were assumed: $s = 2$; $\nu = 5$; $E' = 11$ MeV (from an analysis of data contained in figure 8 of Bohr and Wheeler 1939); $k = 3{\cdot}8 \times 10^{-5}$ in units of sec. and MeV (from an analysis of tabulated data, Nordheim and Yost 1937); other values corresponding to experimental conditions were substituted. The result obtained was: $\sigma \sim 10^{-27}$ cm.^{2} for 9 MeV deuterons on uranium. The most likely theoretical value is $0{\cdot}8 \times 10^{-27}$ cm.^{2} (§ 9, $R_0 = 1{\cdot}39 \times 10^{-13}$ cm.). The closeness of agreement can only be fortuitous owing to uncertainties involved in the derivation of both values, but the result is none the less satisfactory for that.

7. CHEMICAL SEPARATION OF THE FRAGMENT NUCLEI

In order to isolate some of the radioactive bodies, a partial chemical separation of the mixture was performed. The collecting foil from the pocket could have been used, but it was found beneficial to place the collector on top of the target itself with a piece of 2 mm. S.P. aluminium leaf between; then the activity was greatly enhanced without the deuteron-induced activity in the aluminium causing any difficulty. The collector was dissolved in aqua regia and small quantities of chloroplatinic acid, barium chloride, and lanthanum nitrate were added. The acidity of the resulting solution was adjusted to $2N$ by adding hydrochloric acid and the platinum fraction was separated by passing hydrogen sulphide gas through the boiling solution. Barium was precipitated as sulphate by the addition of concentrated sulphuric acid, and lanthanum was precipitated by adding excess of potassium hydroxide. Aluminium remained in the filtrate. The principal half-lives found in these fractions are listed in table 1. Some of the periods correspond with those obtained from neutron-induced fission in uranium and thorium (Livingood and Seaborg 1940). Control experiments with lead and bismuth targets failed to show any appreciable activity in the carriers.

TABLE 1. PRINCIPAL RADIOACTIVE PERIODS OBTAINED FROM CHEMICAL SEPARATION

	Pt fraction	Ba fraction	La fraction
Uranium	15 min., 1 hr., 30–40 hr.	11 min., 80 min.	4 hr.
Thorium	18 min., 2½ hr.	15 min.	2½ hr.

8. RADIATIONS FROM THE FRAGMENT NUCLEI

The experiments described above have been concerned more with the magnitude of the effect than with the nature of the radiations from the fission fragments. Some of the properties of the radiations have been experimentally investigated for the sake of comparison with neutron-induced fission.

(*a*) *Electron radiation.* A magnetic deflecting field was used in conjunction with a Geiger counter in order to distinguish negative and positive electron radiation. It appeared that at energies above ¼ MeV no positrons more numerous than 1/100th of the negative electrons were present. No positrons have been reported in the case of neutron-induced fission; positron-emitters could indeed result only from modes of division of the compound nucleus that are energetically unfavourable.

(*b*) *γ- and X-radiations.* In a preliminary investigation of the harder electromagnetic radiation aluminium absorbers (up to 300 mg./cm.^{2}) together with a magnetic deflecting field were used to eliminate the effect of the softer electron radiation. Under these conditions a strong activity was observed, giving a decay curve of shape similar to that illustrated in figure 3. A detailed analysis of the γ-ray activity has not yet been completed.

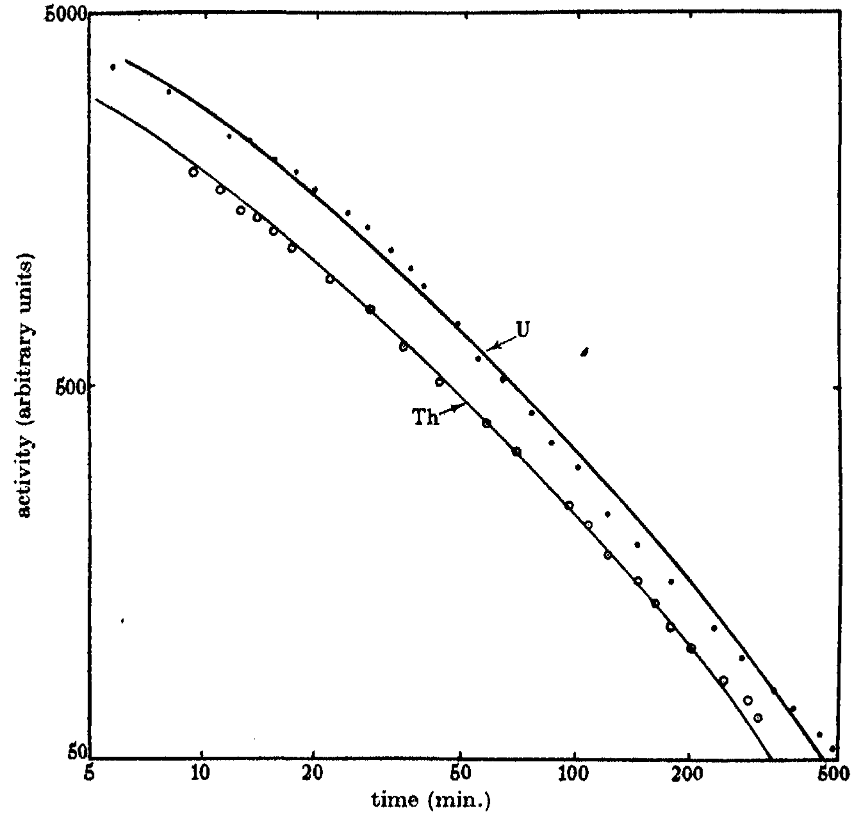

FIGURE 3. Experimental results compared with Frisch's formula for the decay curve. $T = 20$ min.

(*c*) *α-Particles.* A collector has been examined for α-particle emission by placing it in front of a 2 mm. deep pulse-recording ionization chamber of conventional type. No effect was registered in an interval of several minutes beginning about a minute from the end of bombardment, leading to the conclusion that no α-particles of energy above 1 MeV are emitted in numbers greater than 1/10,000 of the β's given in the same time. Likewise no detection of α-particles has been reported in the case of neutron-induced fission. Owing to their neutron excess the fragment nuclei would be expected to have α-particle binding energies greater even than those of neighbouring isotopes that are known to be α-stable.

(*d*) *Neutrons.* The emission of 'delayed' neutrons has been sought with the help of a neutron counter consisting of a 2 mm. deep pulse-recording ionization chamber with a surface bearing a film of paraffin wax close in front. A small block of uranium metal was used for bombardment. This could not be conveyed from the target chamber to the counter in an interval less than half a minute from the end of bombardment; at that time a rapidly decaying neutron activity giving an initial count of ten per min. was found. It was not possible to measure the periods with any accuracy.

9. THE MECHANISM OF DEUTERON-INDUCED FISSION

For the purpose of the present work use will be made of the theoretical account of the mechanism of nuclear fission given by Bohr and Wheeler (1939). An outline of relevant aspects will be given here, and application to the particular case of deuteron-induced fission will be developed slightly further than in the original presentation.

When absorption of energy into a nucleus results in an excited state, de-excitation can take place by one of a number of competitive processes, the partial probability of each depending on the excitation energy. For the particular case of de-excitation by fission, Bohr and Wheeler show that for each nucleus there is a threshold value for the excitation energy below which fission cannot occur, and this energy can be evaluated from a knowledge of Z and A.

Nuclear excitation under deuteron bombardment can be stimulated by two distinct processes, the Oppenheimer-Phillips process and the Gamow-Condon-Gurney process (deuteron capture); the cross-sections are of the same order in the two cases. The excitation energy resulting from the Oppenheimer-Phillips process is $(E_n - I)$, where E_n and I are the neutron binding energies in the heavy nucleus and in the deuteron respectively. This excitation is, in general, below the fission threshold, and consequently de-excitation will proceed not by fission but by γ-emission (neutron emission also being energetically impossible). Deuteron capture will result in an excitation of the order of $(E_d + 2E_n - I)$, where E_d is the deuteron kinetic energy, and at these levels (~ 16 MeV) fission and neutron emission will be the most eligible competitors. The cross-section for deuteron capture involves the Gamow penetration factor; following equation (71) of Bohr and Wheeler (1939) we may write

$$\sigma_c \sim \pi R^2 e^{-P}, \tag{4}$$

where R is the nuclear radius, and the penetration exponent P is given by

$$P = \frac{4Ze^2}{\hbar v}\{\arccos x^{\frac{1}{2}} - x^{\frac{1}{2}}(1-x)^{\frac{1}{2}}\}, \tag{5}$$

where $x = E_d R/Ze^2$, and the other symbols have the obvious connotation. The value of R is customarily assumed to vary according to the formula

$$R = R_0 A^{\frac{1}{3}}. \tag{6}$$

Of the several values for R_0 that have been proposed two values will be considered here:

(i) Bethe (1937): $R_0 = 2{\cdot}05 \times 10^{-13}$ cm.

(ii) Feenberg (1939): $R_0 = 1{\cdot}39 \times 10^{-13}$ cm.

Bohr and Wheeler use a value $R_0 = 1{\cdot}47 \times 10^{-13}$ cm. For later reference the factor $\pi R^2 e^{-P}$ is plotted in figure 4 for U^{238}* and Th^{232}, using each of the two values for R_0. It will be observed how profound an effect on both the shape and scale of the curve comparatively small differences in R_0 entail.

Equation (4) is more exactly written

$$\sigma_c = \pi R^2 e^{-P} \xi l_c^2/l_0^2. \tag{7}$$

ξ, the 'sticking probability', is of the order unity at the high excitation energies prevailing, and in any case will vary only slowly with deuteron energy. The factor l_c^2/l_0^2 (Bethe 1937) takes into account the angular momenta of the deuterons; an estimation based on figure 19 (Bethe 1937) indicates that for 8–9 MeV deuterons on uranium l_c^2/l_0^2 may be taken to have a value 0·1 practically independent of deuteron energy.

The compound nucleus formed by deuteron capture in U^{238} is an excited state of 93^{240}; in the case of thorium, ${}_{91}Pa^{234}$ (UX_2). Table 2 gives calculated values of the threshold energy for fission (E_f) and the neutron binding energy (E_n) for these two nuclei together with some of their isotopes mentioned below, and for the nuclei U^{239} and Th^{233}. For the calculation of E_n Dempster's estimated values for packing fractions (Dempster 1938) have been used in the form

$$f_A = 0{\cdot}52 + 0{\cdot}0080(A - 238) \tag{8}$$

(f_A in MeV per mass unit), and corrections have been applied in accordance with equation (6) of Bohr and Wheeler (1939) for deficiency in nuclear charge and for odd-even mass and charge alternations.

---

* U^{235} and U^{234} will probably not behave very differently from U^{238} in respect of deuteron-induced fission.

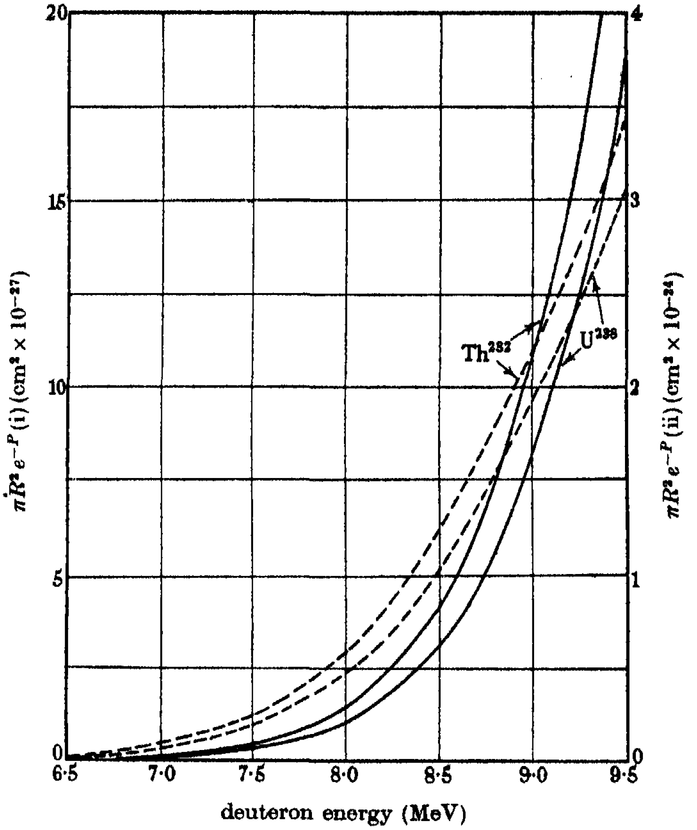

FIGURE 4. Calculated values of $\pi R^2 e^{-P}$.

(i) —— $R_0 = 1{\cdot}39 \times 10^{-13}$ cm. (ii) ···· $R_0 = 2{\cdot}05 \times 10^{-13}$ cm.

TABLE 2. THRESHOLD ENERGIES FOR FISSION (E_f) AND NEUTRON-BINDING ENERGIES (E_n) FOR SOME COMPOUND NUCLEI

	E_f (MeV)	E_n (MeV)	$E_f - E_n$ (MeV)
U^{239}	5·9	5·0	+0·9
93^{240}	5·0	5·1	−0·1
93^{239}	4·8	6·2	−1·4
93^{238}	4·6	5·4	−1·2
Th^{233}	6·9	5·1	+1·8
Pa^{234}	5·9	4·0	+1·9
Pa^{233}	5·7	6·3	−0·9
Pa^{232}	5·5	5·4	+0·1

The comparative probability of fission and neutron emission depends on the difference between E_f and E_n, and for both 93^{240} and Pa^{234} the partial probability of fission amounts to a substantial fraction. In any case, if 93^{239} is formed by the emission of a neutron the residual excitation energy will still permit of fission occurring. The partial probability of fission (Γ_f/Γ) may be expected to vary with excitation energy in the manner indicated in figure 5; this diagram is for the most part conjectural, but an attempt has been made at a quantitative representation of the various threshold energies and of the partial probabilities in the regions marked in full lines.

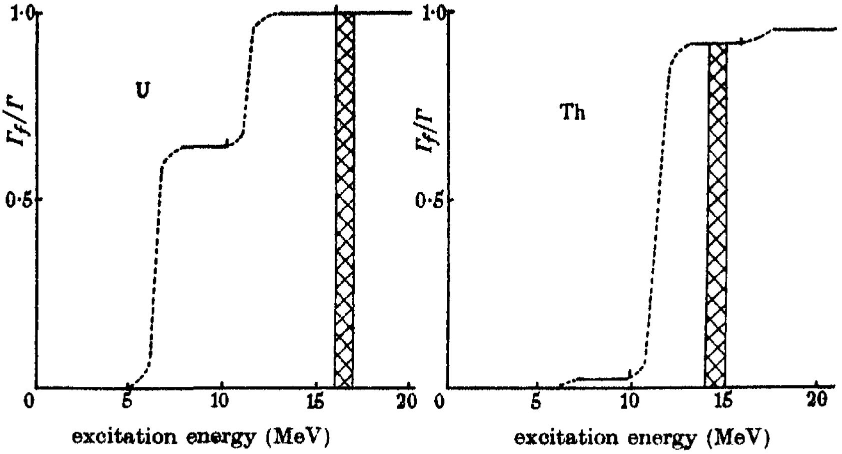

FIGURE 5. Partial probability of fission as a function of excitation energy of the compound nucleus. The cross-hatched area represents the region of importance in the experimental study of the excitation function.

It appears reasonable to assume that the partial probability of fission is of the order of unity for deuterons of 8–9 MeV, and that in any case it is a slowly varying factor within this range. The cross-section for deuteron-induced fission is given by

$$\sigma = \pi R^2 e^{-P} \xi (l_c^2/l_0^2) \Gamma_f/\Gamma. \tag{9}$$

The excitation function should therefore conform with the curves of figure 4, where the ordinates must be multiplied by 0·1 to allow for the factor l_c^2/l_0^2. In a later section these curves are to be compared with the experimental results in respect of both scale and shape.

As regards the fragment nuclei resulting from the fission process, it may be tentatively assumed that the products from deuteron-induced fission in uranium and thorium will display at least a general similarity to those from fission induced by neutrons (both fast and thermal); some points of resemblance have been remarked in §§ 7 and 8.

10. THE CROSS-SECTION FOR DEUTERON-INDUCED FISSION

It is desirable to obtain a measure of the cross-section at some particular deuteron energy for comparison with the value expected from theoretical computation. Such a determination should properly be the province of the method (ii) mentioned in the Introduction; method (iv) can only lead to the desired result by some such tortuous path as that outlined in § 6. A value for the ratio of the cross-sections for deuteron-induced and neutron-induced fission can, however, be obtained by the latter method.

Suppose that in two separate experiments the target is subjected to irradiations of the same duration by deuterons and neutrons respectively, and that the counts are taken in each case at the same time after bombardment. Referring to equation (3), if the reasonable assumption is made that s, ρ (which depends on the range of the product nuclei), ν and E' are approximately the same in the two cases

$$\frac{\sigma_d}{\sigma_n} = \frac{\text{counts/sec. per deuteron/sec.}}{\text{counts/sec. per neutron/sec.}}. \tag{10}$$

For the purpose of comparison, there is required a neutron source the strength of which is known and is sufficient to give a measurable fission activity, and for which the fission cross-section has already been measured. The first two requirements are met by using neutrons produced by bombarding with deuterons of up to 1 MeV the various targets for which neutron-yield data have been published (Amaldi, Hafstad and Tuve 1937). To fulfil the third requirement a (D + D) source would be desirable, as a reliable value for the cross-section for these neutrons is now available. Preliminary measurements with a powerful source of (Li + D) neutrons (100 μA of 900 KeV deuterons) gave counts of the order of only 10 per min., indicating that the strongest (D + D) source available to us was so unlikely to produce an activity of strength sufficient to give a reliable result that the extra difficulties involved in the preparation of a D-target were not justified, and the stronger (Li + D) source was used in spite of the fact that it is less reliable as a standard source, being prone to variation in neutron emission. No experimental value for the cross-section for fission induced by (Li + D) neutrons has been reported, so we have expressed our result in the form of a ratio, using the equation above, and have compared it with the value estimated theoretically.

The arrangement described in § 2 was used for the deuteron bombardment, except that the lid of the box was kept insulated from the body and earthed so that the current recorded by the beam galvanometer measured only the beam effective in producing fission. For the neutron irradiation the target box was placed as near as possible to a lithium target under bombardment by 900 KeV deuterons. Cine film was used as collector in preference to aluminium, as it was found to give less trouble due to neutron-induced activity. The flux of neutrons through the uranium target was derived from a knowledge of the geometrical conditions. Comparative values of the activities in the deuteron and neutron experiments were read off from the decay curves, and hence σ_d/σ_n could be calculated.

The theoretical value for the ratio σ_d/σ_n is

$$\frac{\sigma_d}{\sigma_n} = \frac{e^{-P}\,\xi_d\, l_c^2/l_0^2 (\Gamma_f/\Gamma)_d}{\xi_n (\Gamma_f/\Gamma)_n^{\text{Av.}}}. \tag{11}$$

We assume $\xi_d = \xi_n = 1$; $l_c^2/l_0^2 = 0{\cdot}1$; $(\Gamma_f/\Gamma)_d = 1$. $(\Gamma_f/\Gamma)_n^{\text{Av.}}$ can be estimated roughly by extrapolating in a somewhat speculative manner the figure 6 of Bohr and Wheeler (1939) and using published data on the spectrum of (Li + D) neutrons (Bonner and Brubaker 1935). The experimental and theoretical values for σ_d/σ_n are given in table 3; the range of variation indicated in the 'theoretical' columns reflects the uncertainty of the extrapolation of $(\Gamma_f/\Gamma)_n$. The general trend of the results is clearly in favour of the smaller value for R_0.

TABLE 3. σ_d/σ_n, THE RATIO OF THE CROSS-SECTIONS FOR DEUTERON-INDUCED AND NEUTRON-INDUCED FISSION

	experimental	theoretical	
		$R_0 = 1{\cdot}39 \times 10^{-13}$ cm.	$R_0 = 2{\cdot}05 \times 10^{-13}$ cm.
Uranium	$0{\cdot}01_5$	0·002–0·005	0·2–0·5
Thorium	$0{\cdot}07_5$	0·01–0·1	1–10

It may be mentioned here that the calculated fission-activity values for the proton and α-particle beams available from the Cambridge cyclotron would be as follows:

4½ MeV protons: 1/10,000 of the deuteron effect for the same current,
18 MeV α-particles: 1/500 of the deuteron effect for the same current.

Neither effect would be detected by the present experimental method.

11. THE EXCITATION FUNCTION FOR DEUTERON-INDUCED FISSION

If the assumption is made that the factors ρ, s, ν and E' of equation (3) are not seriously affected by variation of deuteron energy over a range about 8–9 MeV, the activity formed on the collector as a result of any bombardment can be taken as a measure of the number of fissions produced during that bombardment; this assumption has been made the basis of a determination of the excitation function for the process.

The complication introduced by the necessity for collectors, makes difficult the technique that is usually employed in excitation function measurements, namely that of measuring the activation at various energies along the path of a beam passing through an absorber, and it has been necessary to resort to the expedient of giving a separate bombardment for each energy, keeping the beam steady for the duration of each run but not necessarily at the same value for all runs. This method involved a large number of runs and the expenditure of time was minimized as far as possible by the adoption of a standard schedule in which the period 0–10 min. was occupied by the bombardment, and the period 24–47 min. by 5 min. counts on the D and F foils taken twice and alternately. D retained a small 10 min. half-life activity and this was subtracted from the F activity. As measurements were made from time to time over a period of several months, standardization of the counter was essential.

The initial energy of the deuterons was estimated from a determination of the range of the beam in air. Deceleration of the deuterons to a known energy was accomplished by inserting absorbers of aluminium foil across the aperture at the front of the box (H in figure 1). Preliminary experiments showed that this produced an intolerable scattering of the beam on to the collector, but a diaphragm placed in the position shown at G in figure 1 completely remedied this defect.

The activity at the convenient time of 35 min. from the middle of the bombardment, obtained by interpolating between experimental counts, is taken as a measure of the cross-section for the particular energy concerned. Experimental results are plotted in figures 6*a* and 6*b*; neutron effects have been subtracted, and the deuteron energies are those at the middle of the effective layer of the target. Several selected energies were dealt with twice or three times in order to get an estimate of the reliability of the method. The root-mean-square divergence of an individual result from the mean of a pair was 10 %, and the maximum divergence recorded was 20 %. The error limits marked on the experimental points in figures 6*a* and 6*b* correspond to the probable error (taken as two-thirds of the root-mean-square

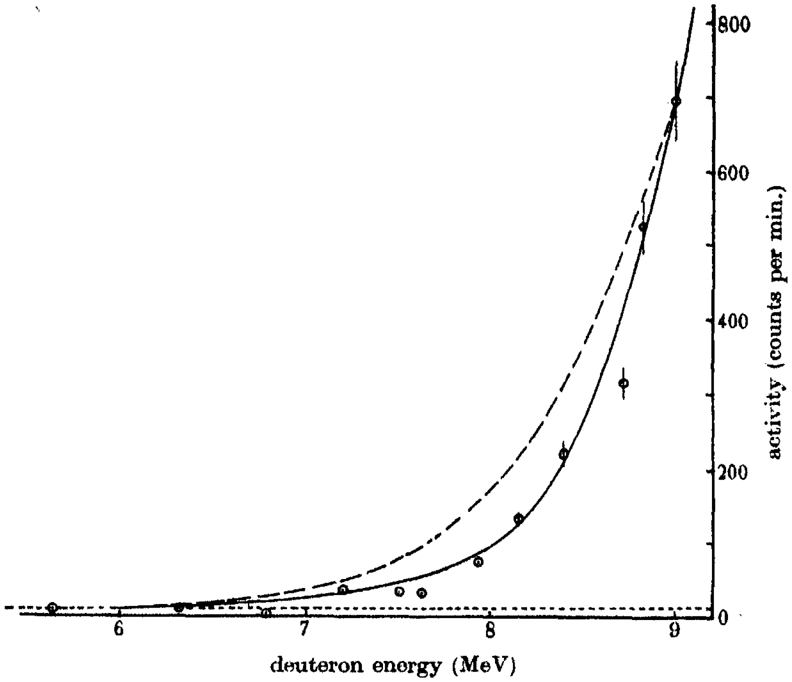

FIGURE 6*a*. Excitation function for uranium.
—— $R_0 = 1\cdot39 \times 10^{-13}$ cm. ···· $R_0 = 2\cdot05 \times 10^{-13}$ cm.

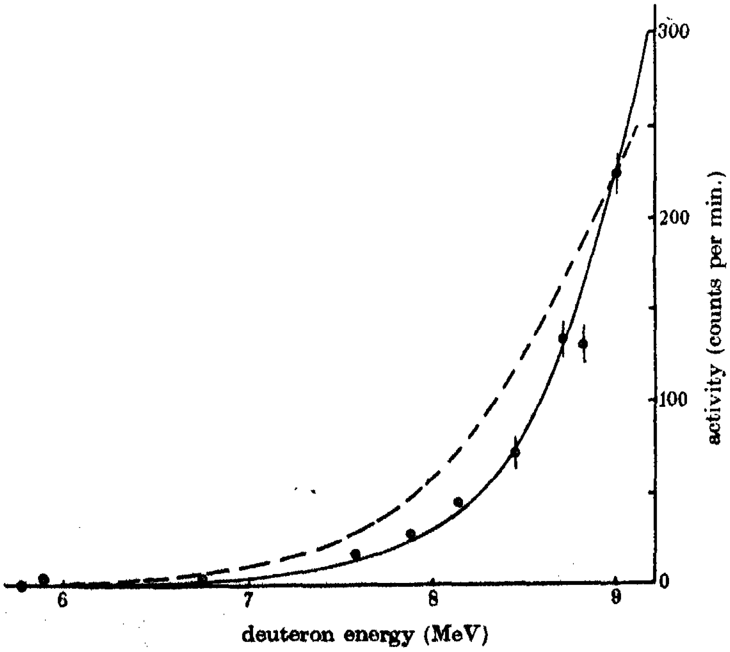

FIGURE 6*b*. Excitation function for thorium.
—— $R_0 = 1\cdot39 \times 10^{-13}$ cm. ···· $R_0 = 2\cdot05 \times 10^{-13}$ cm.

error). The residual activity observed at low energies in the case of uranium is ascribed to neutron-induced fission, and is treated as independent of deuteron energy.

Curves of the form of figure 4 have been fitted to the experimental results at 9 MeV. These results combined with those of § 10 may be interpreted as supporting theoretical predictions and favouring the lower value of R_0.

12. CONCLUSIONS

(i) The experimental method employed, though somewhat clumsy, offers a satisfactory means of studying the mechanism of nuclear fission induced by deuterons; the effects observed are practically free from any associated neutron-induced fission (§§ 2–4).

(ii) Those aspects of behaviour that depend on the course of events subsequent to nuclear excitation are similar in the case of deuteron- and neutron-induced fission (§§ 5–8).

(iii) Certain theoretical factors are not yet sufficiently well established to allow a decisive comparison of our experimental results with theoretical predictions (§§ 9–11).

We wish to express our indebtedness to various colleagues for assistance in operating the cyclotron; to Dr T. E. Banks for collaborating in some of the preliminary experiments; to those in charge of the Cavendish High Tension Laboratory for making possible the neutron irradiation; to Professor J. D. Cockcroft for suggestions, advice and encouragement. One of us (R. S. K.) acknowledges with thanks financial assistance by the Royal Commission for the Exhibition of 1851.

REFERENCES

Amaldi, Hafstad and Tuve 1937 *Phys. Rev.* **51**, 896.
Bethe 1937 *Rev. Mod. Phys.* **9**, 69.
Bohr and Wheeler 1939 *Phys. Rev.* **56**, 426.
Bonner and Brubaker 1935 *Phys. Rev.* **48**, 742.
Dempster 1938 *Phys. Rev.* **53**, 869.
Feenberg 1939 *Phys. Rev.* **55**, 504.
Frisch 1939 *Nature, Lond.*, **143**, 852.
Gant 1939 *Nature, Lond.*, **144**, 707.
Joliot 1939 *C.R. Acad. Sci., Paris*, **208**, 341.
Krishnan and Banks 1940 *Nature, Lond.*, **145**, 860.
Livingood and Seaborg 1940 *Rev. Mod. Phys.* **12**, 30.
McMillan 1939 *Phys. Rev.* **55**, 510.
Nordheim and Yost 1937 *Phys. Rev.* **51**, 942.

On the dielectric strength of mixed crystals*

By H. Fröhlich

H. H. Wills Physical Laboratory, University of Bristol

(*Communicated by N. F. Mott, F.R.S.—Received* 28 *February* 1941)

On the basis of the author's theory of dielectric breakdown, a quantitative calculation of the increase of the breakdown strength of ionic crystals due to the admixture of foreign atoms is carried out. Satisfactory agreement with von Hippel's experimental values is obtained. Furthermore, it is shown that $F^2(T) - F_p^2(T)$ should not depend on temperature. Here $F_p(T)$ is the dielectric strength of a pure crystal at temperature T, and $F(T)$ is the corresponding dielectric strength if foreign atoms are admixed in small concentration.

1. Introduction

In his fundamental experiments on the dielectric strength of alkali halides, von Hippel (1935) found that the breakdown strength of a dilute solid solution is always larger than that of the pure substance. From the point of view of the author's theory of dielectric breakdown (Fröhlich 1937, 1939) this behaviour can be explained in a way similar to the analogous increase of the electrical resistance in the theory of metals (cf. Nordheim 1931). In both cases the mean free path of electrons is decreased through additional scattering by the foreign atoms.

The assumption that the electrons causing the dielectric breakdown can be treated in a way similar to electrons in metals is essential for the author's theory. This theory is based on the idea that electrical breakdown is a phenomenon due to the acceleration of electrons, as has been suggested by von Hippel and others. The breakdown field is calculated from the condition that the electrons gain more energy from the electrical field than they can transfer to the lattice vibrations, so that no stationary state can exist. The breakdown field F, calculated in this way, was found to be inversely proportional to the mean free path of the electrons. A correct order of magnitude has been obtained for F, and it was predicted that F should increase with temperature for crystals with small residual frequencies. This increase was subsequently found experimentally (Austen and Hackett 1939; Buehl and Hippel 1939; Austen and Whitehead 1940) for KBr, which has a very low residual frequency, whereas substances with high residual frequencies, such as mica or quartz, do not show any appreciable increase of F, in accordance with the theoretical expectation. The detailed temperature dependence of F in KBr is, however, only in qualitative agreement with the theoretical formula. This may be due to too great a simplification of the theoretical treatment of the lattice vibration.

---

* Based on Report L/T 113 of the British Electrical and Allied Industries Research Association (E.R.A.).

It thus seemed desirable to treat quantitatively an effect, such as the influence of foreign atoms on the breakdown strength, in which the scattering of electrons is not entirely due to lattice vibrations. Such a calculation is carried out below, leading to satisfactory agreement with experiment. From the temperature dependence of this effect a relation is derived (equ. (14)) which depends only on the fundamental assumptions of the theory but is independent of the special way in which the mean free path of the electrons is calculated. An experimental check on this relation could, therefore, be regarded as a fundamental test of the author's theory.

2. THE EFFECT OF FOREIGN ATOMS ON THE MEAN FREE PATH

Before calculating the breakdown field, we must calculate the mean free path l of an electron. For electrons with a velocity v, the mean free path is connected with the time of relaxation τ by

$$l = \tau v. \tag{1}$$

τ is defined as

$$\frac{1}{\tau} = \sum \frac{\Delta v_x}{v_x} \Phi = \sum (1 - \cos\theta)\, \Phi. \tag{2}$$

Here Φ is the probability per second that an electron with a velocity v_x in the x-direction makes a collision which changes the x-component of the velocity to

$$v_x - \Delta v_x.$$

Since the collisions are nearly elastic,

$$\frac{\Delta v_x}{v_x} = 1 - \cos\theta,$$

where θ is the angle of scattering. The sum has to be extended over all kinds of collisions. Now suppose that we have a large crystal with a few foreign atoms present. Then, as in the pure crystal, the scattering of an electron will mainly be due to a scattering by the thermal motion of the ions. There will, however, be an additional scattering, due to the deviations from the periodic potential near the foreign atoms. Obviously we can split up the expression for $1/\tau$ (2) into two parts

$$\frac{1}{\tau} = \frac{1}{\tau_p} + \frac{1}{\tau_f}. \tag{3}$$

Here $1/\tau_p$ refers to the scattering in the pure crystal, and $1/\tau_f$ to the additional scattering by the foreign ions. Consequently, if $\Phi_f(\cos\theta)$ is the probability that the electron is scattered by a foreign atom through an angle θ

$$\frac{1}{\tau_f} = \sum_{\theta}(1-\cos\theta)\,\Phi_f(\cos\theta) = 2\pi\int_0^\pi \Phi_f(\cos\theta)\,(1-\cos\theta)\sin\theta\,d\theta.$$

A method of calculating $\Phi_f(\cos\theta)$ and τ_f was developed by Mott (1936) for the case of metals. The result of those calculations may be applied to ionic crystals of the NaCl type if the foreign ions are restricted to metal ions replacing metal ions of the original crystal. This is possible, since it was shown by Tibbs (1939) that the electronic wave functions for the normally empty bands of a NaCl lattice have a great resemblance with those in a metallic Na lattice. Mott calculates τ_f in terms of a scattering cross-section A, which is connected with τ_f by

$$\frac{1}{\tau_f} = Avnc \quad (c \ll 1),$$

or introducing the mean free path (1)

$$\frac{1}{l_f} = Anc. \tag{4}$$

Here n is the number of atoms per unit volume and c is the proportion of foreign atoms.

According to Mott, A is given by

$$A = 8\pi a^2 \left\{\frac{ma^2(E_0 - E_0')}{\hbar^2}\right\}^2 D,$$

where

$$D = \int_0^\pi f\left(\frac{2mva}{\hbar}\sin\tfrac{1}{2}\theta\right)(1-\cos\theta)\sin\theta\,d\theta = 8\left(\frac{\hbar}{2mva}\right)^4 \int_0^{2mva/\hbar} f(x)\,x^3\,dx,$$

$$x = \frac{2mva}{\hbar}\sin\tfrac{1}{2}\theta.$$

Here $4\pi a^3/3$ is the atomic volume of the metal ion of the pure lattice neglecting the presence of anions, i.e.

$$\frac{4\pi}{3}a^3 = 2a_0^3 = \frac{1}{n}, \tag{5}$$

where a_0 is the distance between neighbouring ions. E_0 and E_0' are the lowest energy states of electrons in the pure crystal, and in a crystal in which all metal ions have been replaced by the foreign metal ions, keeping the lattice distance constant. Furthermore,

$$f(x) = x^{-6}(\sin x - x\cos x)^2.$$

For most alkali halides $\quad \dfrac{2mva}{\hbar} \doteqdot 7{\cdot}6,$

if I introduce for v the electronic velocity for which, according to the theory of breakdown, the mean free path is to be calculated. Thus, by numerical calculation,

$$\int_0^{7\cdot 6} f(x)\,x^3\,dx \doteqdot 1{\cdot}2.$$

Consequently $\quad A = 1{\cdot}2\pi a^2\left(\dfrac{E_0 - E_0'}{E}\right)^2,$

where $E = \frac{1}{2}mv^2$.

Using equations (5) and (4), I obtain for the mean free path

$$\frac{1}{l_f} = \frac{0{\cdot}6\pi}{2^{\frac{2}{3}}}\left(\frac{3}{\pi}\right)^{\frac{2}{3}}\frac{1}{a_0}\left(\frac{E_0 - E_0'}{E}\right)^2 c \quad (c \ll 1). \tag{6}$$

It should be mentioned that Mott's calculation involves the assumption

$$|E_0 - E_0'| \ll E.$$

3. THE CHANGE OF THE BREAKDOWN FIELD

According to Fröhlich (1937, 1939) the breakdown field F has to be calculated from the condition

$$\frac{e^2F^2\tau(E)}{m} = B(E) \quad (E = J). \tag{7}$$

Here J is the internal ionization energy. B is the energy transferred per second to the lattice. This energy is the same as in the pure crystal, since the scattering due to the different potential field of the foreign atoms is an elastic scattering. Denoting by F_p the breakdown field of the pure crystal, I consequently find

$$B = \frac{e^2F_p^2\tau_p}{m}, \tag{8}$$

or, using expression (3) for τ,

$$F = F_p\left(\frac{\tau_p}{\tau}\right)^{\frac{1}{2}} = F_p\left(1+\frac{\tau_p}{\tau_f}\right)^{\frac{1}{2}} = F_p\left(1+\frac{l_p}{l_f}\right)^{\frac{1}{2}}. \tag{9}$$

Since I deal with small concentrations of foreign atoms only,

$$l_f \gg l_p,$$

or

$$F = F_p\left(1+\frac{1}{2}\frac{l_p}{l_f}\right). \tag{10}$$

According to Fröhlich (1939, equ. (17), 1937, equ. (5)) l_p is given by

$$l_p = \tau_p v = \frac{16E^2a_0^2}{2^{\frac{1}{2}}\pi^2(\epsilon-\epsilon_0)\,e^2h\nu}\,\psi(T), \tag{11}$$

where ν is the residual frequency, ϵ the dielectric constant, $\sqrt{\epsilon_0}$ the refractive index in the visible range and

$$\psi(T) = 1+\frac{2}{e^{h\nu/kT}-1}.$$

Thus I finally obtain, using equations (10), (11) and (6),

$$\frac{F-F_p}{F_p} = \frac{1}{2}\frac{l_p}{l_f} = 0{\cdot}63c\psi^{-1}(T)\,\frac{(E_0-E_0')^2a_0}{(\epsilon-\epsilon_0)\,h\nu e^2}. \tag{12}$$

4. DISCUSSION

In expression (12), all quantities are known except E_0-E_0'. Using von Hippel's experimental values for $F-F_p$ we find for E_0-E_0' about 0·4 eV for RbCl in KCl and 1·7 eV for AgCl in NaCl. Since KCl and RbCl have nearly the same lattice constant (3·14 and 3·27 A), E_0-E_0' is in this case equivalent to the difference of the lowest energy levels in the (normally unoccupied) conduction levels in pure KCl and pure RbCl. Professor Mott kindly informed me of calculations of these energies. According to these calculations (cf. Mott 1938, table 1) the energies are 0·07 and 0·40 eV for KCl and RbCl respectively (in Mott (1938) they are denoted by X; the polarization energy $\frac{1}{2}$eV of RbCl was estimated to 1·38). Thus, the theoretical value of $E_0 - E'_0$ is 0·33, in good agreement with the experimental value. For Ag no theoretical value is available, but $E_0 - E'_0$ should certainly be larger than for Rb, owing to the much greater differences in the energy states of the free atoms.

These considerations show that the theory, without the use of any arbitrary constant, yields the right order of magnitude for the increase of the dielectric strength by foreign atoms. The calculation of the absolute value of the breakdown strength is based on (i) a calculation of the mean free path of an electron, and (ii) on equation (7) which connects the mean free path (or the time of relaxation) with the dielectric strength. It is interesting to note that from the temperature dependence of the breakdown strength a relation can be derived which is independent of the absolute value of the mean free path, but makes use only of (ii) and of the fact that both the scattering of electrons by foreign atoms and the transfer B of energy from the electrons to the lattice are independent of temperature. To derive this relation we note that (according to (8)) with B also $F_p^2 \tau_p$ is independent of temperature, i.e.

$$F_p^2(T)\,\tau_p(T) = F_p^2(0)\,\tau_p(0). \tag{13}$$

Now from (9) it follows that at any temperature

$$F^2(T) - F_p^2(T) = F_p^2(T)\frac{\tau_p(T)}{\tau_f}.$$

Since τ_f does not depend on T it follows with (13) that the right-hand side of the above expression does not depend on T, i.e.

$$F^2(T) - F_p^2(T) = F^2(0) - F_p^2(0). \tag{14}$$

It would be interesting to test equation (14) experimentally because it allows an experimental check of the main ideas of the author's theory of dielectric breakdown.

References

Austen and Hackett 1939 *Nature, Lond.*, **143**, 637.
Austen and Whitehead 1940 *Proc. Roy. Soc.* A, **176**, 33.
Buehl and von Hippel 1939 *Phys. Rev.* **56**, 941.
Fröhlich 1937 *Proc. Roy. Soc.* A, **160**, 230.
Fröhlich 1939 *Proc. Roy. Soc.* A, **172**, 94.
von Hippel 1935 *Ergebn. exakt. Naturw.* **14**, 79.
Mott 1936 *Proc. Camb. Phil. Soc.* **32**, 281.
Mott 1938 *Trans. Faraday Soc.* **34**, 500.
Nordheim 1931 *Ann. Phys., Lpz.*, **9**, 607.
Tibbs 1939 *Trans. Faraday Soc.* **35**, 1471.

Perturbation theory for the self-consistent field

By H. W. Peng

University of Edinburgh

(*Communicated by M. Born, F.R.S.—Received* 31 *March* 1941)

The perturbation theory has been applied to the Fock-Dirac system of equations. To obtain the perturbed Fock functions, it is necessary to solve a system of linear algebraic equations. To obtain the perturbation energy of the ith order, the perturbed Fock functions up to the $(i-1)$th order are needed.

In treating n-electron problems by quantum mechanics, it is necessary to adopt approximate methods; the most accurate of these involving the use of one-electron functions is, at present, the method of the self-consistent field. When the Hamiltonian contains some terms small compared with the rest—a state of affairs that often occurs—it is convenient to regard these small terms as 'perturbations'. In what follows we shall investigate the effect of these perturbations on the wave functions and the energy of an n-electron problem to the approximation of the self-consistent field.

The wave equations for the self-consistent field are the following due to Fock (1930) and Dirac (1930):

$$(K+G-W_\gamma)\phi_\gamma = 0, \quad (\gamma = 1, 2, \ldots, n). \tag{1}$$

They form a system of n simultaneous equations. The operator K denotes the one-electron Hamiltonian in the ideal case of vanishing interaction among the electrons, while G, defined by

$$G\phi_\gamma = \sum_{\lambda=1}^{n} \{(\phi_\lambda \cdot \mathscr{G}\phi_\lambda)\,\phi_\gamma - (\phi_\lambda \cdot \mathscr{G}\phi_\gamma)\,\phi_\lambda\}, \tag{2}$$

represents the ordinary and the exchange potentials due to the interactions of the electrons. The expression $(\phi_\lambda \cdot \mathscr{G}\phi_\gamma)$ stands for

$$\sum_{s'}\int d\mathbf{r}'\,\phi_\lambda^*(\mathbf{r}'s')\,\mathscr{G}(\mathbf{r}s, \mathbf{r}'s')\,\phi_\gamma(\mathbf{r}'s'), \tag{3}$$

with $\mathscr{G}(\mathbf{r}s, \mathbf{r}'s')$ denoting the interaction between the electron at $\mathbf{r}$ with spin co-ordinate s and that at $\mathbf{r}'$ with spin co-ordinate s'. The interaction

$\mathscr{G}$ must be a self-adjoint operator and must be symmetric in the two electrons, i.e.

$$\mathscr{G}^\dagger = \mathscr{G}, \quad \mathscr{G}(\mathbf{r}s, \mathbf{r}'s') = \mathscr{G}(\mathbf{r}'s', \mathbf{r}s). \tag{4}$$

In most applications $\mathscr{G}$ is simply the Coulomb interaction $e^2/|\mathbf{r}-\mathbf{r}'|$.

The energy parameters W_γ which occur in (1) do not give the total energy E of the electrons directly. Since the interaction energy of electron pairs must be counted only once, E is given by

$$E = \sum_{\gamma=1}^{n} (\phi_\gamma \,.\, (K + \tfrac{1}{2}G)\,\phi_\gamma) = \sum_{\gamma=1}^{n} \{W_\gamma - \tfrac{1}{2}(\phi_\gamma \,.\, G\phi_\gamma)\}. \tag{5}$$

The main difficulty in solving (1) is due to the non-linear character of these equations, as may be seen from (2). We consider only the case when K and $\mathscr{G}$ can be expanded into series of descending terms

$$K = K^{(0)} + K^{(1)} + K^{(2)} + \ldots, \quad \mathscr{G} = \mathscr{G}^{(0)} + \mathscr{G}^{(1)} + \mathscr{G}^{(2)} + \ldots. \tag{6}$$

The system (1) can then be split into systems of various orders according to the usual practice of the perturbation method. As the perturbation equations are always linear, the solution of (1) is thereby greatly simplified.

1. PERTURBATION EQUATIONS

Let us suppose that the Fock-Dirac system of equations for $K^{(0)}$ and $\mathscr{G}^{(0)}$ has been solved. In order to have a complete set of orthogonal, normalized functions at our disposal so that all other functions may be expressed as linear combinations of these, we introduce the following eigenvalue problem:

$$(K^{(0)} + G^{(0)} - W_\beta^{(0)})\,\phi_\beta^{(0)} = 0, \tag{7}$$

where the linear operator $G^{(0)}$ is defined, with the help of the known functions $\phi_1^{(0)}, \phi_2^{(0)}, \ldots, \phi_n^{(0)}$, by

$$G^{(0)}\phi = \sum_{\lambda=1}^{n} \{(\phi_\lambda^{(0)} \,.\, \mathscr{G}^{(0)}\phi_\lambda^{(0)})\,\phi - (\phi_\lambda^{(0)} \,.\, \mathscr{G}^{(0)}\phi)\,\phi_\lambda^{(0)}\}, \tag{8}$$

and is, by (4), self-adjoint. It follows from the definition that the complete set $\{\phi_\beta^{(0)}\}$ of orthonormal functions includes the functions $\phi_\beta^{(0)}, \phi_2^{(0)}, \ldots, \phi_n^{(0)}$.

I can now expand the ϕ_γ's of (1) in the set $\{\phi_\beta^{(0)}\}$ and write

$$\phi_\gamma = \sum_\beta \phi_\beta^{(0)} \mathscr{U}_{\beta\gamma}. \tag{9}$$

Denoting, for brevity, the constants $(\phi_\alpha^{(0)} . K\phi_\beta^{(0)})$, $(\phi_\alpha^{(0)} . (\phi_\mu^{(0)} . \mathscr{G}\phi_\nu^{(0)})\,\phi_\beta^{(0)})$ by $K_{\alpha\beta}$, $\mathscr{G}_{\alpha\mu\nu\beta}$, we obtain, from (1), (2) and (9), the system of algebraic equations

$$\sum_\beta \left\{K_{\alpha\beta} + \sum_{\lambda=1}^n \sum_{\mu\nu} \mathscr{U}^*_{\mu\lambda}(\mathscr{G}_{\alpha\mu\nu\beta} - \mathscr{G}_{\alpha\mu\beta\nu})\,\mathscr{U}_{\nu\lambda} - W_\gamma \delta_{\alpha\beta}\right\} \mathscr{U}_{\beta\gamma} = 0. \tag{10}$$

By expanding $\mathscr{U}_{\beta\gamma}$ and W_γ in accordance with the perturbation,

$$\left.\begin{aligned} \mathscr{U}_{\beta\gamma} &= \delta_{\beta\gamma} + \mathscr{U}^{(1)}_{\beta\gamma} + \mathscr{U}^{(2)}_{\beta\gamma} + \ldots, \\ W_\gamma &= W_\gamma^{(0)} + W_\gamma^{(1)} + W_\gamma^{(2)} + \ldots, \end{aligned}\right\} \tag{11}$$

(10) splits into systems of various orders,† viz.

$$-W_\gamma^{(0)}\delta_{\alpha\gamma} + K^{(0)}_{\alpha\gamma} + \sum_{\lambda=1}^n (\mathscr{G}^{(0)}_{\alpha\lambda\lambda\gamma} - \mathscr{G}^{(0)}_{\alpha\lambda\gamma\lambda}) = 0, \tag{10·0}$$

$$\begin{aligned} -W_\gamma^{(1)}\delta_{\alpha\gamma} &+ K^{(1)}_{\alpha\gamma} + \sum_{\lambda=1}^n (\mathscr{G}^{(0)}_{\alpha\lambda\lambda\gamma} - \mathscr{G}^{(0)}_{\alpha\lambda\gamma\lambda}) \\ &+ \sum_{\lambda=1}^n \sum_{\mu\nu} (\mathscr{G}^{(0)}_{\alpha\mu\nu\gamma} - \mathscr{G}^{(0)}_{\alpha\mu\gamma\nu})(\mathscr{U}^{(1)*}_{\mu\lambda}\delta_{\nu\lambda} + \delta_{\mu\lambda}\mathscr{U}^{(1)}_{\nu\lambda}) \\ &+ \sum_\beta \left\{K^{(0)}_{\alpha\beta} + \sum_{\lambda=1}^n (\mathscr{G}^{(0)}_{\alpha\lambda\lambda\beta} - \mathscr{G}^{(0)}_{\alpha\lambda\beta\lambda}) - W_\gamma^{(0)}\delta_{\alpha\beta}\right\}\mathscr{U}^{(1)}_{\beta\gamma} = 0, \end{aligned} \tag{10·1}$$

$$\begin{aligned} -W_\gamma^{(2)}\delta_{\alpha\gamma} &+ K^{(2)}_{\alpha\gamma} + \sum_{\lambda=1}^n (\mathscr{G}^{(0)}_{\alpha\lambda\lambda\gamma} - \mathscr{G}^{(0)}_{\alpha\lambda\gamma\lambda}) \\ &+ \sum_{\lambda=1}^n \sum_{\mu\nu} (\mathscr{G}^{(1)}_{\alpha\mu\nu\gamma} - \mathscr{G}^{(1)}_{\alpha\mu\gamma\nu})(\mathscr{U}^{(1)*}_{\mu\lambda}\delta_{\nu\lambda} + \delta_{\mu\lambda}\mathscr{U}^{(1)}_{\nu\lambda}) \\ &+ \sum_{\lambda=1}^n \sum_{\mu\nu} (\mathscr{G}^{(0)}_{\alpha\mu\nu\gamma} - \mathscr{G}^{(0)}_{\alpha\mu\gamma\nu})(\mathscr{U}^{(2)*}_{\mu\lambda}\delta_{\nu\lambda} + \delta_{\mu\lambda}\mathscr{U}^{(2)}_{\nu\lambda} + \mathscr{U}^{(1)*}_{\mu\lambda}\mathscr{U}^{(1)}_{\nu\lambda}) \\ &+ \sum_\beta \left\{-W_\lambda^{(1)}\delta_{\alpha\beta} + K^{(1)}_{\alpha\beta} + \sum_{\lambda=1}^n (\mathscr{G}^{(1)}_{\alpha\lambda\lambda\beta} - \mathscr{G}^{(1)}_{\alpha\lambda\beta\lambda})\right. \\ &+ \left.\sum_{\lambda=1}^n \sum_{\mu\nu} (\mathscr{G}^{(0)}_{\alpha\mu\nu\beta} - \mathscr{G}^{(0)}_{\alpha\mu\beta\nu})(\mathscr{U}^{(1)*}_{\mu\lambda}\delta_{\nu\lambda} + \delta_{\mu\lambda}\mathscr{U}^{(1)}_{\nu\lambda})\right\}\mathscr{U}^{(1)}_{\beta\gamma} \\ &+ \sum_\beta \left\{K^{(0)}_{\alpha\beta} + \sum_{\lambda=1}^n (\mathscr{G}^{(0)}_{\alpha\lambda\lambda\beta} - \mathscr{G}^{(0)}_{\alpha\lambda\beta\lambda}) - W_\gamma^{(0)}\delta_{\alpha\beta}\right\}\mathscr{U}^{(2)}_{\beta\lambda} = 0, \end{aligned} \tag{10·2}$$

etc.

The zero-order system (10·0) is but a repetition, in algebraic form, of either the unperturbed Fock-Dirac system or the unperturbed eigenvalue problem (7) according to whether the index γ is restricted to vary from 1 to n or not. With the help of the equation obtained by putting the index γ of (10·0) equal to β, the last bracket of (10·1) and (10·2) becomes simply

---

† The restriction $(\gamma = 1, 2, \ldots, n)$ has been purposely omitted in (9)–(14) as (1) can be extended into an eigenvalue problem similar to (7) as soon as $\phi_1, \phi_2, \ldots, \phi_n$ are determined.

$$\{(W_\beta^{(0)} - W_\gamma^{(0)})\,\delta_{\alpha\beta}\} = \{(W_\alpha^{(0)} - W_\gamma^{(0)})\,\delta_{\alpha\beta}\}, \tag{12}$$

and vanishes identically when we take $\alpha = \gamma$. Because of the appearance of $\mathscr{U}_{\nu\lambda}^{(1)}$ and $\mathscr{U}_{\nu\lambda}^{(2)}$ elsewhere in (10·1) and (10·2), the perturbation energy parameters $W_\gamma^{(1)}$ and $W_\gamma^{(2)}$ cannot be calculated before $\mathscr{U}_{\nu\lambda}^{(1)}$ and $\mathscr{U}_{\nu\lambda}^{(2)}$ are obtained. To obtain $\mathscr{U}_{\nu\lambda}^{(1)}$, for example, I take the index α of (10·1) different from γ. Remembering (12), I have, for the equations for $\mathscr{U}_{\alpha\gamma}^{(1)}$ $(\alpha \neq \gamma)$,

$$\begin{aligned}(W_\alpha^{(0)} - W_\gamma^{(0)})\,\mathscr{U}_{\alpha\gamma}^{(1)} + \sum_{\lambda=1}^{n} \sum_{\mu\nu} (\mathscr{G}_{\alpha\mu\nu\gamma}^{(0)} - \mathscr{G}_{\alpha\mu\gamma\nu}^{(0)})\,(\mathscr{U}_{\mu\lambda}^{(1)*}\,\delta_{\nu\lambda} + \delta_{\mu\lambda}\,\mathscr{U}_{\nu\lambda}^{(1)}) \\ = -\left\{K_{\alpha\gamma}^{(1)} + \sum_{\lambda=1}^{n} (\mathscr{G}_{\alpha\lambda\lambda\gamma}^{(1)} - \mathscr{G}_{\alpha\lambda\gamma\lambda}^{(1)})\right\}.\end{aligned} \tag{13·1}$$

Successively the equations for $\mathscr{U}_{\alpha\lambda}^{(i)}$ $(i = 1, 2, \ldots; \alpha \neq \gamma)$ are all of the form

$$\begin{aligned}(W_\alpha^{(0)} - W_\gamma^{(0)})\,\mathscr{U}_{\alpha\gamma}^{(i)} + \sum_{\lambda=1}^{n} \sum_{\mu\nu} (\mathscr{G}_{\alpha\mu\nu\gamma}^{(0)} - \mathscr{G}_{\alpha\mu\gamma\nu}^{(0)})\,(\mathscr{U}_{\mu\lambda}^{(i)*}\,\delta_{\nu\lambda} + \delta_{\mu\lambda}\,\mathscr{U}_{\nu\lambda}^{(i)}) \\ = \text{known quantities}.\end{aligned} \tag{13·i}$$

These equations, being algebraic and linear, are in principle solvable. The elements $\mathscr{U}_{\gamma\gamma}^{(1)}$, $\mathscr{U}_{\gamma\gamma}^{(2)}$, etc. are, as usual, not determined by these equations but, owing to the normalization of the ϕ_γ's of (1) and the $\phi_\beta^{(0)}$'s of (7), they are given by

$$\mathscr{U}_{\gamma\gamma}^{(1)*} + \mathscr{U}_{\gamma\gamma}^{(1)} = 0, \quad \mathscr{U}_{\gamma\gamma}^{(2)*} + \mathscr{U}_{\gamma\gamma}^{(2)} = -\sum_{\beta} \mathscr{U}_{\beta\gamma}^{(1)*}\,\mathscr{U}_{\beta\gamma}^{(1)}, \text{ etc.} \tag{14}$$

2. PERTURBATION ENERGY

The algebraic expression for the total energy of the electrons, obtained by substituting (9) into (5), is

$$E = \sum_{\gamma=1}^{n} W_\gamma - \frac{1}{2} \sum_{\gamma,\lambda=1}^{n} \sum_{\alpha\beta\mu\nu} \mathscr{U}_{\alpha\gamma}^{*}\,\mathscr{U}_{\mu\lambda}^{*}\,(\mathscr{G}_{\alpha\mu\nu\beta} - \mathscr{G}_{\alpha\mu\beta\nu})\,\mathscr{U}_{\nu\lambda}\,\mathscr{U}_{\beta\gamma}. \tag{15}$$

This, being expanded according to the perturbation into series of the form (11), yields

$$E^{(0)} = \sum_{\gamma=1}^{n} W_\gamma^{(0)} - \frac{1}{2} \sum_{\gamma,\lambda=1}^{n} (\mathscr{G}_{\gamma\lambda\lambda\gamma}^{(0)} - \mathscr{G}_{\gamma\lambda\gamma\lambda}^{(0)}), \tag{15·0}$$

$$
\begin{aligned}
E^{(1)} = \sum_{\gamma=1}^{n} W_\gamma^{(1)} - \frac{1}{2} \sum_{\gamma,\lambda=1}^{n} (\mathscr{G}^{(1)}_{\gamma\lambda\lambda\gamma} - \mathscr{G}^{(1)}_{\gamma\lambda\gamma\lambda}) \\
- \frac{1}{2} \sum_{\gamma,\lambda=1}^{n} \sum_{\alpha\beta\mu\nu} (\mathscr{G}^{(0)}_{\alpha\mu\nu\beta} - \mathscr{G}^{(0)}_{\alpha\mu\beta\nu}) \\
\times \{(\mathscr{U}^{(1)*}_{\alpha\gamma} \delta_{\beta\gamma} + \delta_{\alpha\gamma} \mathscr{U}^{(1)}_{\beta\gamma}) \delta_{\mu\lambda} \delta_{\nu\lambda} + \delta_{\alpha\gamma} \delta_{\beta\gamma} (\mathscr{U}^{(1)*}_{\mu\lambda} \delta_{\nu\lambda} + \delta_{\mu\lambda} \mathscr{U}^{(1)}_{\nu\lambda})\},
\end{aligned}
\tag{15·1}
$$

$$
\begin{aligned}
E^{(2)} = \sum_{\gamma=1}^{n} W_\gamma^{(2)} - \frac{1}{2} \sum_{\gamma,\lambda=1}^{n} (\mathscr{G}^{(2)}_{\gamma\lambda\lambda\gamma} - \mathscr{G}^{(2)}_{\gamma\lambda\gamma\lambda}) \\
- \frac{1}{2} \sum_{\gamma,\lambda=1}^{n} \sum_{\alpha\beta\mu\nu} (\mathscr{G}^{(1)}_{\alpha\mu\nu\beta} - \mathscr{G}^{(1)}_{\alpha\mu\beta\nu}) \\
\times \{(\mathscr{U}^{(1)*}_{\alpha\gamma} \delta_{\beta\gamma} + \delta_{\alpha\gamma} \mathscr{U}^{(1)}_{\beta\gamma}) \delta_{\mu\lambda} \delta_{\nu\lambda} + \delta_{\alpha\gamma} \delta_{\beta\gamma} (\mathscr{U}^{(1)*}_{\mu\lambda} \delta_{\nu\lambda} + \delta_{\mu\lambda} \mathscr{U}^{(1)}_{\nu\lambda})\} \\
- \frac{1}{2} \sum_{\gamma,\lambda=1}^{n} \sum_{\alpha\beta\mu\nu} (\mathscr{G}^{(0)}_{\alpha\mu\nu\beta} - \mathscr{G}^{(0)}_{\alpha\mu\beta\nu}) \\
\times \{(\mathscr{U}^{(2)*}_{\alpha\gamma} \delta_{\beta\gamma} + \delta_{\alpha\gamma} \mathscr{U}^{(2)}_{\beta\gamma} + \mathscr{U}^{(1)*}_{\alpha\gamma} \mathscr{U}^{(1)}_{\beta\gamma}) \delta_{\mu\lambda} \delta_{\nu\lambda} \\
+ \delta_{\alpha\gamma} \delta_{\beta\gamma} (\mathscr{U}^{(2)*}_{\mu\lambda} \delta_{\nu\lambda} + \delta_{\mu\lambda} \mathscr{U}^{(2)}_{\nu\lambda} + \mathscr{U}^{(1)*}_{\mu\lambda} \mathscr{U}^{(1)}_{\nu\lambda}) \\
+ (\mathscr{U}^{(1)*}_{\alpha\gamma} \delta_{\beta\gamma} + \delta_{\alpha\gamma} \mathscr{U}^{(1)}_{\beta\gamma}) (\mathscr{U}^{(1)*}_{\mu\lambda} \delta_{\nu\lambda} + \delta_{\mu\lambda} \mathscr{U}^{(1)}_{\nu\lambda})\},
\end{aligned}
\tag{15·2}
$$

etc. If I had applied the ordinary perturbation method to the original Schrödinger equation for the assembly of electrons and then introduced the one-electron approximation, I should have obtained some expressions for calculating the perturbation energy of the first and the second order from the Fock functions of zero-order and the first order. Hence the explicit appearance of $\mathscr{U}^{(1)}_{\beta\gamma}$ in (15·1) and $\mathscr{U}^{(2)}_{\beta\gamma}$ in (15·2) must be only apparent. I can get rid of them by substituting (10·1) and (10·2) for $W_\gamma^{(1)}$ and $W_\gamma^{(2)}$ and then cancelling terms, as will be shown immediately.

From (4), I derive

$$
\mathscr{G}^{(i)*}_{\beta\nu\mu\alpha} = \mathscr{G}^{(i)}_{\alpha\mu\nu\beta} = \mathscr{G}^{(i)}_{\mu\alpha\beta\nu}, \quad (i = 0, 1, 2, \ldots).
\tag{16}
$$

This may be used to simplify the last term of (15·1). I then have for $E^{(1)}$,

$$
\begin{aligned}
E^{(1)} = \sum_{\gamma=1}^{n} W_\gamma^{(1)} - \frac{1}{2} \sum_{\lambda,\gamma=1}^{n} (\mathscr{G}^{(1)}_{\gamma\lambda\lambda\gamma} - \mathscr{G}^{(1)}_{\gamma\lambda\gamma\lambda}) \\
- \sum_{\gamma,\lambda=1}^{n} \sum_{\mu\nu} (\mathscr{G}^{(0)}_{\gamma\mu\nu\gamma} - \mathscr{G}^{(0)}_{\gamma\mu\gamma\nu}) (\mathscr{U}^{(1)*}_{\mu\lambda} \delta_{\nu\lambda} + \delta_{\mu\lambda} \mathscr{U}^{(1)}_{\nu\lambda}).
\end{aligned}
\tag{15·1a}
$$

To obtain $W_\gamma^{(1)}$ from (10·1), take $\alpha = \gamma$. The last line of (10·1) then drops out by (12). Hence for $W_\gamma^{(1)}$,

$$
\begin{aligned}
W_\gamma^{(1)} = K^{(1)}_{\gamma\gamma} + \sum_{\lambda=1}^{n} (\mathscr{G}^{(1)}_{\gamma\lambda\lambda\gamma} - \mathscr{G}^{(1)}_{\gamma\lambda\gamma\lambda}) \\
+ \sum_{\lambda=1}^{n} \sum_{\mu\nu} (\mathscr{G}^{(0)}_{\gamma\mu\nu\gamma} - \mathscr{G}^{(0)}_{\gamma\mu\gamma\nu}) (\mathscr{U}^{(1)*}_{\mu\lambda} \delta_{\nu\lambda} + \delta_{\mu\lambda} \mathscr{U}^{(1)}_{\nu\mu}).
\end{aligned}
\tag{17}
$$

Substituting (17) into (15·1a) and cancelling terms, I obtain for the perturbation energy of the first order,

$$E^{(1)} = \sum_{\gamma=1}^{n} K^{(1)}_{\gamma\gamma} + \frac{1}{2} \sum_{\gamma,\lambda=1}^{n} (\mathscr{G}^{(1)}_{\gamma\lambda\lambda\gamma} - \mathscr{G}^{(1)}_{\gamma\lambda\gamma\lambda}), \tag{18·1}$$

which is indeed free from $\mathscr{U}^{(1)}_{\beta\gamma}$. A similar combination of (10·2) and (15·2) yields for the perturbation energy of the second order,

$$\begin{aligned} E^{(2)} = {} & \sum_{\gamma=1}^{n} K^{(2)}_{\gamma\gamma} + \frac{1}{2} \sum_{\gamma,\lambda=1}^{n} (\mathscr{G}^{(2)}_{\gamma\lambda\lambda\gamma} - \mathscr{G}^{(2)}_{\gamma\lambda\gamma\lambda}) \\ & + \sum_{\gamma=1}^{n} \sum_{\beta} \Big\{ K^{(1)}_{\gamma\beta} + \sum_{\lambda=1}^{n} \sum_{\mu\nu} (\mathscr{G}^{(0)}_{\gamma\mu\nu\beta} - \mathscr{G}^{(0)}_{\gamma\mu\beta\nu}) (\mathscr{U}^{(1)*}_{\mu\lambda} \delta_{\nu\lambda} + \delta_{\mu\lambda} \mathscr{U}^{(1)}_{\nu\lambda}) \\ & \qquad + \sum_{\lambda=1}^{n} (\mathscr{G}^{(1)}_{\gamma\lambda\lambda\beta} - \mathscr{G}^{(1)}_{\gamma\lambda\beta\lambda}) - W^{(1)}_{\gamma} \delta_{\gamma\beta} \Big\} \mathscr{U}^{(1)}_{\beta\gamma} \\ & - \frac{1}{2} \sum_{\gamma,\lambda=1}^{n} \sum_{\alpha\beta\mu\nu} (\mathscr{G}^{(0)}_{\alpha\mu\nu\beta} - \mathscr{G}^{(0)}_{\alpha\mu\beta\nu}) (\mathscr{U}^{(1)*}_{\alpha\gamma} \delta_{\beta\gamma} + \delta_{\alpha\gamma} \mathscr{U}^{(1)}_{\beta\gamma}) (\mathscr{U}^{(1)*}_{\mu\lambda} \delta_{\nu\lambda} + \delta_{\mu\lambda} \mathscr{U}^{(1)}_{\nu\lambda}). \end{aligned} \tag{18·2}$$

Since the above expression is necessarily real, I can replace the right-hand side by its real part. The real part of the coefficient of $W^{(1)}_{\gamma}$ vanishes by (14) and the real part of the terms containing $\mathscr{G}^{(0)}$ cancel by (18). Hence I get finally for $E^{(2)}$,

$$\begin{aligned} E^{(2)} = {} & \sum_{\gamma=1}^{n} K^{(2)}_{\gamma\gamma} + \frac{1}{2} \sum_{\gamma,\lambda=1}^{n} (\mathscr{G}^{(2)}_{\gamma\lambda\lambda\gamma} - \mathscr{G}^{(2)}_{\gamma\lambda\gamma\lambda}) \\ & + \text{ real part of } \sum_{\gamma=1}^{n} \sum_{\beta} \Big\{ K^{(1)}_{\gamma\beta} + \sum_{\lambda=1}^{n} (\mathscr{G}^{(1)}_{\gamma\lambda\lambda\beta} - \mathscr{G}^{(1)}_{\gamma\lambda\beta\lambda}) \Big\} \mathscr{U}^{(1)}_{\beta\gamma}. \end{aligned} \tag{18·3}$$

The above derivation of (18·3) is quite general. Similar expressions for the perturbation energy of higher orders can all be obtained in the same way. In evaluating the energy to the third order, for example, it is necessary to solve the equations (10·2) for $\mathscr{U}^{(2)}_{\beta\gamma}$, which, however, does not present any new feature as the perturbation equations of higher orders are all of the same form as that of the equations of the first order.

3. SEPARATION OF THE SPIN

In treating $2n$-electron problems with zero resultant spin by the method of the self-consistent field, the $2n$ one-electron functions may be taken as the products of n functions $\psi_1, \psi_2, \ldots, \psi_n$ of the spatial co-ordinates r with the two spin eigenfunctions $\delta_{-1}(s)$, $\delta_{+1}(s)$. The spin eigenfunctions $\delta_{\sigma}(s)$ assume the value zero when s differs from σ and the value unity when s

equals σ. In all the scalar products (cf. (3)) of the preceding sections, the summation over the spin co-ordinates can then be performed independently according to the normalization

$$\sum_s \delta_\sigma(s)\,\delta_{\sigma'}(s) = \delta_{\sigma\sigma'}. \tag{19}$$

The important consequence of this is that all electrons contribute to the ordinary potential but only electrons with parallel spins contribute to the exchange potential. The spin eigenfunctions may be factorized and hence removed from (1). For the details of this reduction, we refer to Brillouin's book (1934).

The reduced Fock-Dirac system of equations in the case of zero resultant spin consists of n simultaneous equations in the n ψ-functions of $\mathbf{r}$. These may be obtained formally from (1) by changing ϕ into ψ provided that a factor 2 is added to the first (the ordinary potential) term on the right of (2). This means that the perturbation equations for the ψ-functions of the $2n$-electron problem may be obtained from the corresponding equations of § 1 by adding a factor 2 to the first term of every bracket containing the difference of two $\mathscr{G}$'s. The constants $K_{\alpha\beta}$, $\mathscr{G}_{\alpha\mu\nu\beta}$ now stand for $(\psi_\alpha^{(0)}\,.\,K\psi_\beta^{(0)})$, $(\psi_\alpha^{(0)}\,.\,(\psi_\mu^{(0)}\,.\,\mathscr{G}\psi_\nu^{(0)})\,\psi_\beta^{(0)})$, involving volume integrations of the spatial co-ordinates only.

To obtain the expressions for the perturbation energy for the $2n$-electron problem from those of § 2, we need to add the factor 2 in the above way and then double the whole expressions on the right-hand sides.

The above perturbation theory has been applied to the calculation of the elastic constants and the thermal frequencies of metallic crystals which will be treated in separate papers.

I wish to acknowledge my indebtedness to Professor M. Born and Dr K. Fuchs for much valuable advice.

REFERENCES

Brillouin 1934 *Actualités sci. industr.*, no. 159. Paris: Hermann Cie.
Dirac 1930 *Proc. Camb. Phil. Soc.* **26**, 376.
Fock 1930 *Z. Phys.* **61**, 126.

Two-phase equilibrium in binary and ternary systems
IV. The system ethane-propylene

By H. Lu, D. M. Newitt and M. Ruhemann
Imperial College of Science and Technology, South Kensington

(*Communicated by A. C. Egerton, Sec.R.S.—Received* 9 *April* 1941)

The liquid-vapour equilibrium of the binary system ethane-propylene has been determined at a number of temperatures between −30 and 70° C and over a wide pressure range. From dew-point, boiling-point and pressure-volume-temperature measurements the $(P, T)_x$, $(T, x)_P$ and $(P, V)_{x, T}$ relationships for the pure hydrocarbons and for nine mixtures have been determined.

In previous papers of this series (Ruhemann 1939; Guter, Newitt and Ruhemann 1940), the phase behaviour of various binary and ternary hydrocarbon systems have been examined by a method which involves the analysis of representative samples of the co-existing liquids and vapours in equilibrium. This procedure, although laborious, is particularly well adapted to the study of systems having high critical pressures, and is capable of giving the requisite degree of accuracy; it does not, however, lend itself easily to volumetric measurements. In the present instance the critical pressures of binary mixtures of ethane and propylene seldom exceed 50 atm., and it has in consequence been possible to employ an alternative and simpler method by which the dew-points, boiling-points and specific volumes of the pure hydrocarbons and of a series of their mixtures can be determined by visual observation. From the data so obtained the various P, V, T, x relationships for the system in the region of co-existing liquid and vapour can be derived.

Experimental

Purification of the hydrocarbons. As even traces of impurities have a marked effect on critical temperatures, a high degree of purity of the hydrocarbons is essential. Ethane was prepared in the laboratory by the hydrogenation of ethylene in the presence of a nickel catalyst; the impure product was scrubbed, successively, with an aqueous solution of potassium bromide saturated with bromine, and with a strong solution of caustic potash; it was subsequently cooled and condensed and the liquid allowed to boil vigorously until the thermal conductivity of the escaping vapour (as determined with a catharometer) reached a constant value. About two-thirds of the remaining liquid was then boiled off and the vapour collected in a gasholder. This procedure was repeated a second time, and the product so obtained was transferred to a fractionating apparatus for the final purification.

Propylene, purchased from the Ohio Chemical Co., was found by analysis to contain 99·5 % of the pure hydrocarbon; it was fractionated without any preliminary treatment.

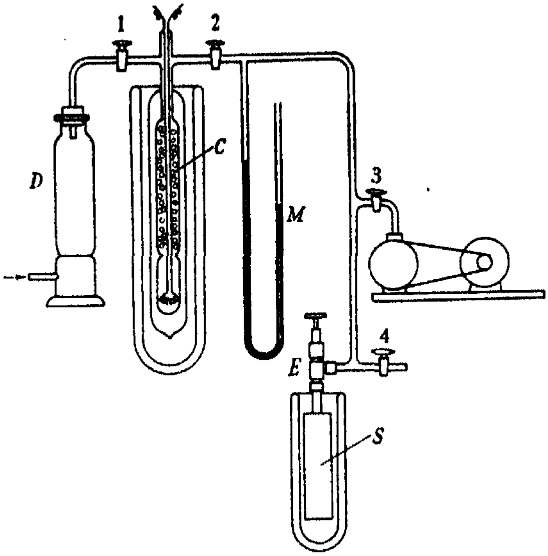

FIGURE 1. Fractionating apparatus.

The fractionating apparatus is shown in figure 1. The column *C* (packed with glass beads) is about 14 in. in length and 1 in. in diameter, and is contained in a glass jacket of 2 in. diameter; the lower end terminates in a receiver of 30 c.c. capacity fitted with a small heating coil. The column communicates with one or more copper storage vessels, *S*, by way of the valve *E*. The glass taps 1, 2, 3 and 4 enable the whole or individual parts of the system to be evacuated. Before starting a fractionation the storage vessel is heated and the whole system thoroughly pumped out. The valve *E* is then closed and a small amount of gas is introduced into the column through the drying tube *D*. The system is again evacuated and the procedure repeated several times to ensure the removal of the last traces of air from the apparatus. The column is then immersed in liquid air and condensation is allowed to proceed until the receiver is nearly full of liquid. To carry out the fractionation tap 1 is closed and the condensed gas is allowed to assume the temperature of liquid air; the column is then pumped out for 1 hr. to remove any dissolved permanent gases from the liquid. The liquid air is replaced by liquid ethylene (temperature − 104° at 1 atm.) or, in the case of propylene, by a mixture of solid carbon dioxide and alcohol. The heater is started and the liquid is allowed to boil gently. As fractionation begins the temperature of the column soon approaches that of the bath; the vapour pressure of the liquid is measured by the manometer *M*.

At the beginning of the fractionation tap 3 is opened every few minutes to allow part of the gas to escape through the pump; when about one-fourth has evaporated in this way the remainder is assumed to be substantially pure. The valve *E* is opened and the cylinder *S* is flushed with pure gas and evacuated several times. Finally, the cylinder is cooled in liquid air and two-thirds of the remaining liquid is distilled into it, the residue being rejected.

The purity of the gas is tested in the equilibrium tube by measuring the pressure change between the dew- and boiling-points, at constant temperature. The pure gas is stored in the cylinder *S*.

Determination of the dew- and boiling-points. The general arrangement of the equilibrium apparatus is shown in figure 2. The individual pure gases from their respective storage cylinders are passed successively through the drying column *D* into a calibrated gas burette *G* (300 c.c. capacity), and their volumes are measured. A known amount of the mixture is then admitted to the glass equilibrium tube *H* which is enclosed in a vacuum-jacketed bath. The upper end of the tube may be sealed by freezing a pellet of mercury in the capillary U-tube *T*; the lower end contains mercury supplied from the reservoir *R*. The pressure of gas inside the tube is indicated by the Bourdon gauge *K* and is measured accurately (to ± 0·01 atm.) on the pressure balance *B*.

The equilibrium tube is maintained at the desired temperature (± 0·02°) by circulating water or cooled alcohol through the vacuum jacket *J* from a constant temperature bath *E*. The bath (capacity 3 gal.) is fitted with a heater, regulator and stirrer and is well insulated. Two mercury thermometers reading to 0·01° are placed in the upper part of *J* in close proximity to the walls of the equilibrium tube. When the experimental temperatures are below room temperature the alcohol in the bath is pumped through a 5 ft. long copper coil immersed in a mixture of solid carbon dioxide and acetone, the rate of pumping being controlled by a thermo-regulator in series with the motor.

The equilibrium tubes (figure 2). These are of two types, the narrower tube (3 mm. bore, 6 mm. outside diameter, capacity *ca.* 4 c.c.) being used to determine boiling-points and the wider (5 mm. bore, 10 mm. outside diameter, capacity *ca.* 15 c.c.) to determine dew-points; each is provided with a magnetically controlled steel stirrer and is mounted in a steel block. A pressure-tight joint is made by two packing glands as shown in the figure (inset).

To charge a tube, it is first filled with mercury up to the tap 2 (figure 2). A part of the mixture in the burette *G* is introduced by lowering the pressure in the reservoir *R*, and the remainder is then condensed into the tube by cooling with liquid nitrogen. In order to avoid setting up big stresses in the glass during cooling the lower part of the vacuum jacket *J* is filled with ethylene glycol and *n*-pentane from the two reservoirs *S* and *P*, and the liquid nitrogen is then added slowly through a long funnel. When all the gas has condensed mercury is drawn over into the U-tube *T* up to the graduation mark and is frozen. Finally, the contents of the tube are allowed to warm up, sufficient pressure being applied to *R* to prevent any gas escaping.

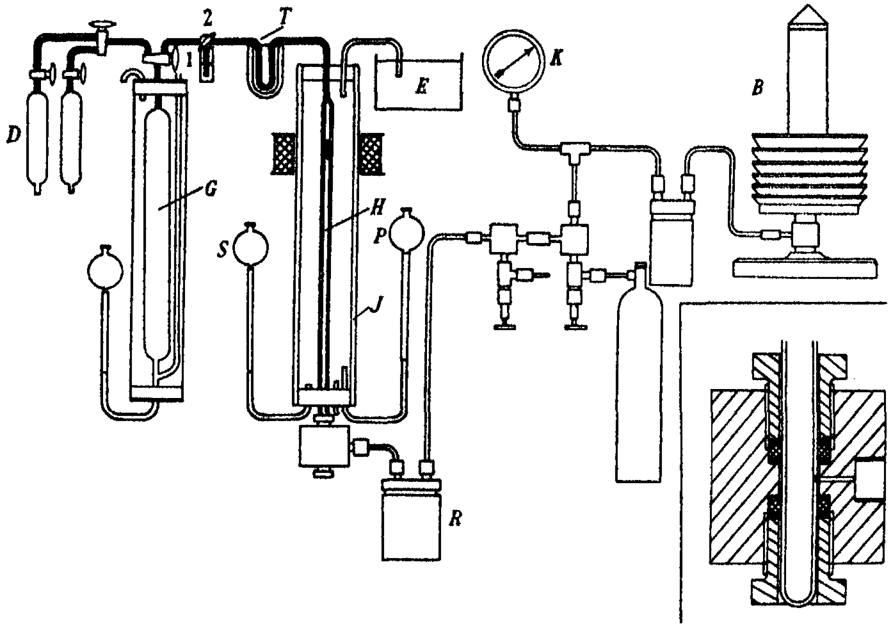

FIGURE 2. General arrangement of dew-point and boiling-point apparatus. Inset, a section through packing gland of equilibrium tube.

Observations of the boiling-points, dew-points and critical-points. To determine the boiling-point the contents of the tube are first completely liquefied by increasing the pressure, and the liquid is thoroughly stirred.

The pressure is then reduced gradually until a minute bubble of vapour appears; a slight increase of pressure will cause the bubble to disappear, whilst a slight reduction of pressure will give rise to vigorous boiling. The pressure so obtained is reproducible to within 0·05 atm.

In making an observation of the dew-point the inner wall of the tube is illuminated by reflected light and is observed through a lens. On gradually increasing the pressure on the gas the appearance of minute dark specks marks the formation of dew; on further increasing the pressure a film of liquid giving interference colours is formed. This phenomenon, described by Kay (1938), is extremely sensitive, and the pressure so obtained is reproducible to within the error of the pressure measurement.

No difficulty is experienced in determining boiling-points up to within a few degrees of the critical temperature. Beyond this limit the difference in densities between the co-existing liquid and vapour is so small that a slight increase of pressure causes the flattened meniscus to disappear at the top of the tube. A corresponding drop in pressure produces immediately a thick mist in the upper part of the tube, followed by phase separation. The exact position of the critical-point can best be located by plotting both these points and the plait-point curve on a large scale.

Volume measurements. The equilibrium tubes are calibrated from a graduation mark on the capillary U-tube T, and volume measurements are made with a cathetometer. Corrections are applied for the volume occupied by the stirrer and for the meniscus.

EXPERIMENTAL RESULTS

The complete results for the system ethane-propylene are given in table 1. Observations at the boiling-point (B.P.), the dew-point (D.P.), in the neighbourhood of the critical-point (C.P.), in the region of retrograde condensation (R.) and at certain arbitrary pressures and volumes (P.V.) are included and are distinguished by the letters in parentheses in the column 'Remarks'. The data for the vapour pressures of the pure hydrocarbons are supplemented by published data (Plank and Kambeitz 1937; Burrell, Seibert and Robertson 1915).

It should be noted that the weights of the gases introduced into the system are calculated from their volumes measured in the gas burette at constant temperature and pressure, with a correction for compressibility.

The vapour-pressure curves for the pure components, together with the border curves $(P, T)_x$ for nine mixtures and the plait-point curve for the system, are reproduced in figure 3. The general shape of the curves is normal, as is also the progressive change in the critical constants with composition; all the border curves exhibit regions of retrograde condensation, the extent of the effect depending upon mixture composition and reaching a maximum for the equimolecular mixture.

From the $(P, T)_x$ curves the $(P, x)_T$ isotherms and the $(T, x)_P$ isobars can be constructed. The latter form a series of lenticular-shaped curves enclosing

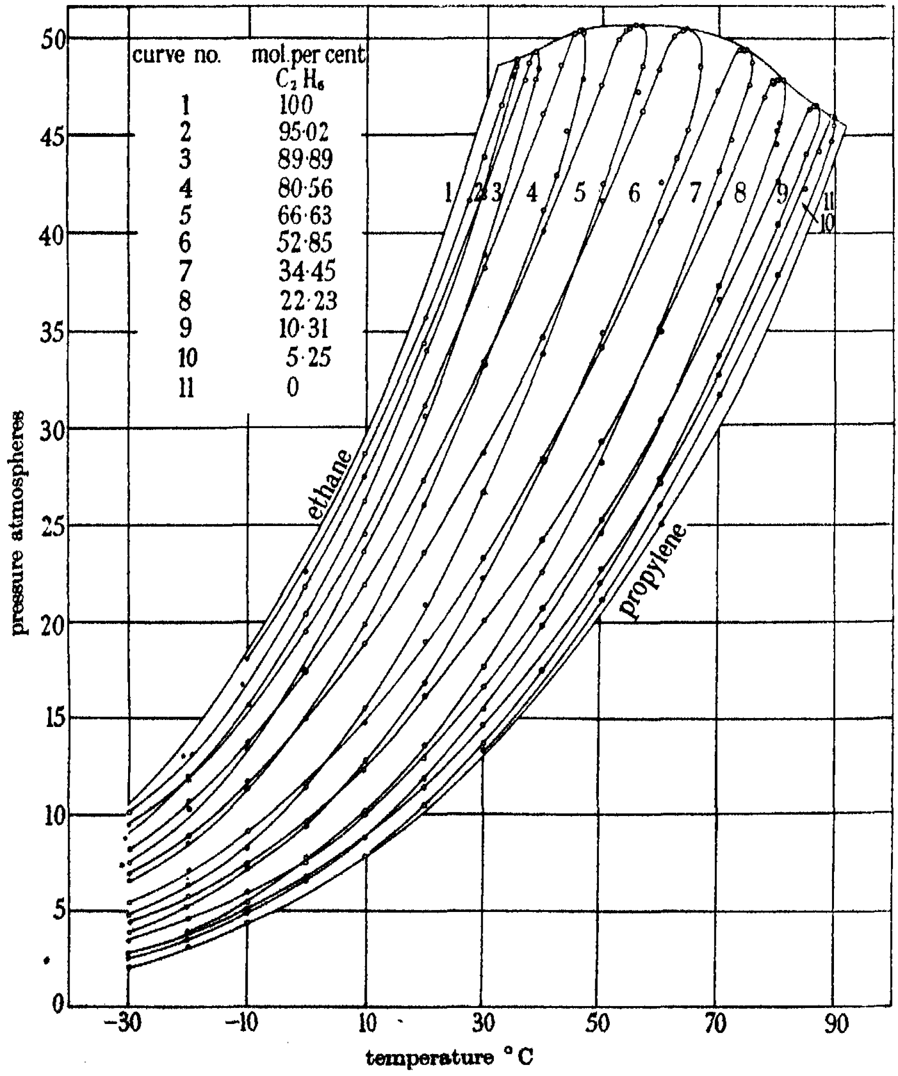

FIGURE 3. Border curves for the system ethane-propylene.

the region of co-existing liquid and vapour in equilibrium over a definite range of temperatures (see figure 4). The compositions of the two phases at any particular temperature are given by the points of contact of a horizontal line drawn through the temperature axis, with the two branches of the $(T, x)_P$ isobar.

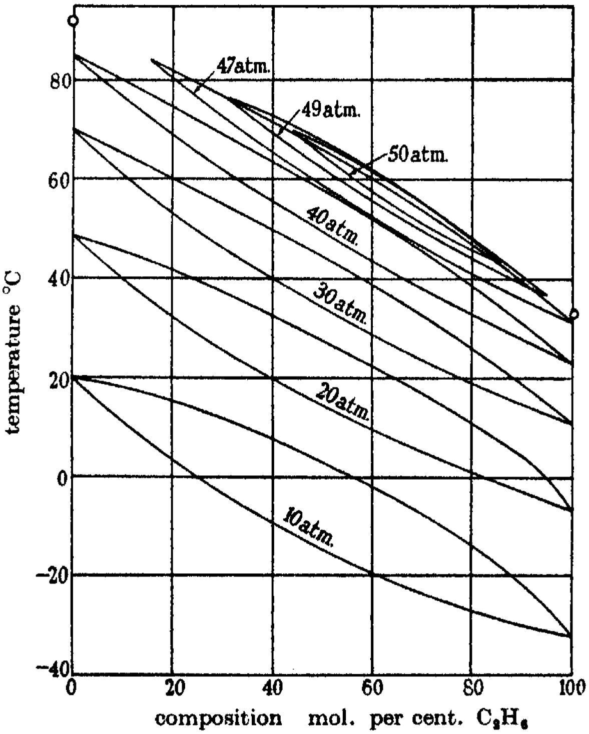

FIGURE 4. $(T, x)_P$ diagram for the system ethane-propylene.

The critical constants of the two pure hydrocarbons are:

	T_c	P_c
ethane	32·1	48·6
propylene	92·1	45·4

For temperatures and pressures above the critical values the $(T, x)_P$ curves leave the temperature axis, and the two phases can co-exist only between certain limits of composition defined by the extremities of the $(T, x)_P$ area. In the limit (defined by the maximum of the plait-point curve) there will be unique values of P, T and x for which two phases can co-exist in equilibrium, namely, $P = 51$ atm.; $T = 57°$ and $x = 66·6$ mol. % of ethane, approximately.

TABLE 1. PRESSURE-VOLUME-TEMPERATURE RESULTS FOR THE SYSTEM ETHANE-PROPYLENE IN THE REGION OF CO-EXISTING LIQUID AND VAPOUR

C_2H_6

		Liquid		Vapour	
temp. °C	pressure atm. (abs.)	volume l./mol.	density kg./l.	volume l./mol.	density kg./l.
−30·0	10·51	0·0639	0·470	1·549	0·0194
−20·0	14·04	0·0663	0·453	1·151	0·0261
−10·0	18·35	0·0693	0·434	0·866	0·0347
0·0	23·53	0·0730	0·412	0·653	0·0460
10·0	29·76	0·0779	0·387	0·485	0·0620
20·0	37·25	0·0859	0·350	0·343	0·0875
30·0	46·46	0·1051	0·286	0·212	0·142
31·0	47·52	0·1109	0·271	0·193	0·156
32·1	48·68	0·141	0·213	0·141	0·213

TABLE 1 (*continued*)

5·25 mol. % C_2H_6

Liquid					Vapour				
temp. °C	pressure atm. (abs.)	volume l./mol.	density kg./l.	remarks	temp. °C	pressure atm. (abs.)	volume l./mol.	density kg./l.	remarks
−30·5	2·77	0·0701	0·591	B.P.	−10·0	4·20	4·456	0·00930	D.P.
−30·5	4·20	0·0699	0·592	P.V.	0·0	5·68	3·186	0·01300	D.P.
−20·0	3·74	0·0717	0·578	B.P.	10·0	7·73	2·499	0·01658	D.P.
−10·0	5·06	0·0737	0·562	B.P.	20·0	10·24	1·877	0·02207	D.P.
0·0	6·74	0·0757	0·547	B.P.	30·0	13·19	1·437	0·02883	D.P.
10·1	8·77	0·0780	0·531	B.P.	50·0	21·17	0·853	0·0486	D.P.
20·0	11·36	0·0805	0·513	B.P.	70·0	31·72	0·500	0·0829	D.P.
30·0	14·55	0·0836	0·496	B.P.	85·0	42·22	—	—	D.P.
30·0	22·40	0·0831	0·499	P.V.	89·5	44·63	0·266	0·156	D.P.
30·0	40·23	0·0784	0·528	P.V.	89·5	42·03	0·350	0·118	P.V.
50·0	22·86	0·0924	0·448	B.P.	89·5	38·36	0·438	0·0946	P.V.
70·0	33·01	0·1049	0·395	B.P.	89·5	30·28	0·679	0·0610	P.V.
70·0	48·92	0·0959	0·432	P.V.	89·5	20·22	1·193	0·0347	P.V.
89·7	45·60	—	—	R.	89·5	15·67	1·624	0·0255	P.V.
89·5	46·01	0·1721	0·241	C.P.					
10·31 mol. % C_2H_6									
−30·5	3·30	0·0723	0·564	B.P.	−20·0	3·04	5·657	0·00722	D.P.
−20·0	4·50	0·0736	0·555	B.P.	−10·0	4·23	4·193	0·00974	D.P.
−10·0	5·98	0·0757	0·539	B.P.	0·0	5·72	3·241	0·01259	D.P.
0·0	7·83	0·0782	0·522	B.P.	10·0	7·88	2·452	0·01665	D.P.
10·0	9·97	0·0804	0·508	B.P.	20·0	10·45	1·837	0·02222	D.P.
20·0	12·95	0·0825	0·495	B.P.	30·0	13·40	1·457	0·02802	D.P.
20·0	19·07	0·0807	0·506	P.V.	30·0	13·31	1·471	0·03493	P.V.
30·0	16·56	0·0854	0·478	B.P.	30·0	12·34	1·627	0·02509	P.V.

30·0	37·70	0·0803	0·508	P.V.
30·0	44·44	0·0797	0·512	P.V.
40·0	20·70	0·0888	0·459	B.P.
40·0	44·41	0·0834	0·489	P.V.
40·0	47·04	0·0832	0·491	P.V.
50·0	25·27	0·0941	0·434	B.P.
50·0	47·05	0·0880	0·464	P.V.
50·0	49·35	0·0864	0·473	P.V.
60·0	30·37	0·0996	0·410	B.P.
60·0	49·24	0·0921	0·443	P.V.
60·0	52·46	0·0909	0·448	P.V.
70·0	36·82	0·1060	0·385	B.P.
70·0	52·41	0·0988	0·413	P.V.
70·0	42·19	0·1029	0·397	P.V.
80·0	42·81	0·1204	0·339	B.P.
80·0	44·99	0·1155	0·353	P.V.
80·0	51·02	0·1087	0·376	P.V.
86·8	46·45	0·1919	0·213	C.P.
86·9	46·40	—	—	R.
86·8	48·69	0·1313	0·311	P.V.
86·8	52·96	0·1198	0·341	P.V.
86·8	58·91	0·1135	0·360	P.V.

30·0	10·65	1·959	0·02084	P.V.
40·0	17·46	1·071	0·03811	D.P.
40·0	17·11	1·104	0·03698	P.V.
40·0	16·33	1·199	0·03404	P.V.
40·0	14·72	1·378	0·02962	P.V.
40·0	11·22	1·936	0·02108	P.V.
50·0	21·97	0·830	0·0492	D.P.
50·0	21·32	0·874	0·0467	P.V.
50·0	20·87	0·952	0·0429	P.V.
50·0	17·21	1·199	0·03404	P.V.
50·0	12·47	1·799	0·02269	P.V.
60·0	27·03	0·644	0·0634	D.P.
60·0	26·19	0·686	0·0595	P.V.
60·0	24·84	0·755	0·0541	P.V.
60·0	21·60	0·933	0·0438	P.V.
60·0	16·92	1·306	0·03126	P.V.
70·0	33·47	0·475	0·0859	D.P.
80·0	40·36	0·344	0·119	D.P.
80·0	39·13	0·388	0·105	P.V.
80·0	35·29	0·503	0·0812	P.V.
80·0	29·70	0·680	0·0600	P.V.
80·0	23·74	0·944	0·0432	P.V.
80·0	19·01	1·260	0·0324	P.V.
85·0	44·01	0·318	0·128	D.P.
87·5	44·16	0·324	0·126	P.V.
87·5	42·37	0·372	0·110	P.V.
87·5	36·11	0·526	0·0776	P.V.
87·5	28·86	0·752	0·0543	P.V.
87·5	22·61	1·033	0·0395	P.V.
87·5	19·50	1·265	0·0323	P.V.

TABLE 1 (*continued*

22·23 mol. % C_2H_6

Liquid					Vapour				
temp. °C	pressure atm. (abs.)	volume l./mol.	density kg./l.	remarks	temp. °C	pressure atm. (abs.)	volume l./mol.	density kg./l.	remarks
−30·0	4·27	0·0705	0·559	B.P.	−30·0	2·50	6·321	0·00623	D.P.
−20·0	5·66	0·0723	0·545	B.P.	−20·0	3·29	4·601	0·00856	D.P.
−10·0	7·41	0·0751	0·525	B.P.	−10·0	4·83	3·688	0·01068	D.P.
0·0	9·60	0·0769	0·512	B.P.	0·0	6·51	2·785	0·01414	D.P.
10·0	12·23	0·0792	0·497	B.P.	10·0	8·77	2·118	0·01860	D.P.
20·0	16·21	0·0811	0·486	B.P.	20·0	11·80	1·576	0·02500	D.P.
20·0	20·35	0·0793	0·497	P.V.	30·0	15·45	1·232	0·03197	D.P.
20·0	47·43	0·0782	0·504	P.V.	40·0	19·80	0·932	0·0423	D.P.
30·0	20·00	0·0836	0·471	B.P.	40·0	18·86	1·007	0·0391	P.V.
30·0	47·55	0·0800	0·490	P.V.	40·0	16·62	1·208	0·0326	P.V.
40·0	24·17	0·0885	0·445	B.P.	40·0	15·56	1·313	0·0300	P.V.
40·0	47·79	0·0848	0·465	P.V.	50·0	24·58	0·721	0·0546	D.P.
50·0	29·22	0·0937	0·420	B.P.	50·0	23·84	0·760	0·0518	P.V.
50·0	47·56	0·0893	0·441	P.V.	50·0	22·41	0·840	0·0469	P.V.
60·0	34·94	0·1001	0·394	B.P.	50·0	19·77	1·075	0·0366	P.V.
60·0	48·12	0·0953	0·413	P.V.	50·0	16·49	1·288	0·0306	P.V.
70·0	41·39	0·1112	0·354	B.P.	60·0	30·37	0·547	0·0720	D.P.
78·0	46·92	0·1290	0·305	B.P.	60·0	28·02	0·644	0·0612	P.V.
79·2	47·80	0·1387	0·284	B.P.	60·0	23·46	0·855	0·461	P.V.
81·2	47·82	0·1705	0·231	B.P.	60·0	17·19	1·294	0·304	P.V.
81·5	47·78	0·2171	0·181	R.	70·0	37·39	0·396	0·0995	D.P.
					80·0	44·55	0·261	0·151	D.P.
					81·5	46·03	0·275	0·143	P.V.
					81·5	42·98	0·351	0·112	P.V.
					81·5	35·28	0·540	0·0729	P.V.
					81·5	25·00	0·906	0·0435	P.V.
					81·5	19·45	1·247	0·0316	P.V.

34·45 mol. % C_2H_6

−30·0	5·39	0·0693	0·547	B.P.
−30·0	5·56	0·0690	0·550	P.V.
−30·0	10·10	0·0690	0·550	P.V.
−30·0	45·68	0·0683	0·555	P.V.
−20·0	7·12	0·0715	0·530	B.P.
−10·0	9·13	0·0729	0·520	B.P.
0·0	11·60	0·0757	0·501	B.P.
0·0	11·88	0·0753	0·504	P.V.
0·0	20·26	0·0747	0·508	P.V.
0·0	53·22	0·0741	0·512	P.V.
10·0	14·78	0·0785	0·483	B.P.
10·0	17·52	0·0774	0·490	P.V.
10·0	22·45	0·0772	0·491	P.V.
10·0	50·15	0·0760	0·499	P.V.
20·0	19·01	0·0810	0·468	B.P.
20·0	47·66	0·0790	0·480	P.V.
30·0	23·28	0·0839	0·452	B.P.
30·0	47·63	0·0799	0·475	P.V.
40·0	28·25	0·0884	0·429	B.P.
40·0	47·83	0·0842	0·450	P.V.
50·0	34·11	0·0944	0·402	B.P.
50·0	47·84	0·0898	0·422	P.V.
50·0	48·09	0·0896	0·423	P.V.
60·0	40·55	0·1034	0·367	B.P.
60·0	48·11	0·0979	0·387	P.V.
60·0	50·74	0·0969	0·391	P.V.
70·0	47·20	0·1233	0·308	B.P.
70·0	50·80	0·1128	0·336	P.V.
74·2	49·31	0·1636	0·232	B.P.
75·0	49·41	0·1807	0·210	C.P.
75·2	49·41	—	—	R.
75·0	49·82	0·1638	0·232	P.V.
75·0	51·81	0·1347	0·282	P.V.
−20·0	3·89	4·729	0·00802	D.P.
−10·0	5·43	3·381	0·01122	D.P.
0·0	7·42	2·565	0·01478	D.P.
10·0	10·15	1·878	0·02019	D.P.
20·0	13·55	1·384	0·02740	D.P.
20·0	12·63	1·527	0·02483	P.V.
20·0	10·47	1·936	0·01959	P.V.
20·0	8·04	2·621	0·01447	P.V.
20·0	5·18	4·055	0·00935	P.V.
30·0	17·63	1·040	0·03646	D.P.
40·0	22·57	0·794	0·0478	D.P.
40·0	22·07	0·827	0·0459	P.V.
40·0	20·56	0·921	0·0412	P.V.
40·0	16·18	1·280	0·02963	P.V.
50·0	28·30	0·599	0·0633	D.P.
50·0	28·27	0·602	0·0630	P.V.
50·0	27·40	0·640	0·0593	P.V.
50·0	25·25	0·736	0·0515	P.V.
50·0	22·88	0·857	0·0442	P.V.
50·0	17·26	1·256	0·03019	P.V.
60·0	35·15	0·439	0·0864	D.P.
70·0	43·20	0·296	0·128	D.P.
72·2	44·84	0·256	0·148	D.P.
75·0	47·53	—	—	D.P.
75·0	47·52	0·245	0·155	P.V.
75·0	39·89	0·437	0·0868	P.V.
75·0	30·26	0·689	0·0550	P.V.
75·0	23·62	0·968	0·0392	P.V.
75·0	19·04	1·267	0·0299	P.V.
75·3	47·60	0·221	0·172	D.P.

TABLE 1 (*continued*)

52·85 mol. % C_2H_6

Liquid					Vapour				
temp. °C	pressure atm. (abs.)	volume l./mol.	density kg./l.	remarks	temp. °C	pressure atm. (abs.)	volume l./mol.	density kg./l.	remarks
−30·0	6·95	0·0683	0·523	B.P.	−20·5	5·10	3·630	0·00984	D.P.
−20·0	8·90	0·0704	0·507	B.P.	−10·0	7·23	2·640	0·01353	D.P.
−10·0	11·73	0·0724	0·493	B.P.	0·0	9·28	2·028	0·01761	D.P.
−10·0	18·42	0·0719	0·496	P.V.	10·0	12·88	1·451	0·02461	D.P.
0·0	14·95	0·0749	0·477	B.P.	20·0	16·78	1·092	0·03270	D.P.
0·0	23·18	0·0743	0·481	P.V.	30·0	22·20	0·806	0·0443	D.P.
0·0	52·83	0·0723	0·494	P.V.	30·0	21·12	0·852	0·0419	P.V.
10·0	18·77	0·0788	0·453	B.P.	30·0	19·38	0·963	0·0371	P.V.
10·0	20·05	0·0781	0·457	P.V.	30·0	16·52	1·200	0·0298	P.V.
10·0	30·92	0·0767	0·466	P.V.	30·0	13·68	1·516	0·0236	P.V.
10·0	53·69	0·0753	0·474	P.V.	40·0	28·28	0·591	0·0604	D.P.
20·0	23·51	0·0818	0·437	B.P.	40·0	26·33	0·669	0·0534	P.V.
20·0	47·84	0·0753	0·474	P.V.	40·0	23·14	0·816	0·0438	P.V.
20·0	48·14	0·0750	0·476	P.V.	40·0	17·42	1·200	0·0298	P.V.
30·0	28·70	0·0859	0·416	B.P.	50·0	34·91	0·420	0·0850	D.P.
30·0	47·81	0·0815	0·448	P.V.	50·0	34·30	0·467	0·0765	P.V.
40·0	34·63	0·0917	0·389	B.P.	50·0	29·02	0·629	0·0568	P.V.
40·0	48·56	0·0846	0·422	P.V.	50·0	25·85	0·753	0·0474	P.V.
50·0	41·65	0·1004	0·356	B.P.	50·0	17·49	1·255	0·0285	P.V.
50·0	47·36	0·0944	0·378	P.V.	60·0	42·59	0·330	0·108	D.P.
50·0	50·43	0·0925	0·386	P.V.	63·0	43·81	0·321	0·111	D.P.
56·8	46·39	0·1107	0·323	B.P.	65·0	45·26	0·300	0·119	D.P.
60·0	48·33	0·1219	0·293	B.P.	67·0	48·50	—	—	D.P.
64·4	50·51	0·1912	0·187	C.P.					
65·1	50·32	0·2000	0·179	R.					
65·2	50·26	—	—	R.					

66·63 mol. % C_2H_6

−30·0	8·16	0·0672	0·507	B.P.	−20·0	6·29	2·852	0·01194	D.P.
−30·0	41·83	0·0648	0·526	P.V.	−10·0	8·29	2·111	0·01613	D.P.
−30·0	53·91	0·0645	0·528	P.V.	0·0	11·40	1·611	0·02114	D.P.
−20·0	10·63	0·0689	0·494	B.P.	10·0	15·45	1·172	0·02906	D.P.
−10·0	13·69	0·0710	0·480	B.P.	20·0	20·88	0·833	0·0409	D.P.
−10·0	14·73	0·0701	0·486	P.V.	30·0	26·63	0·628	0·0542	D.P.
−10·0	51·80	0·0683	0·499	P.V.	30·0	25·54	0·671	0·0508	P.V.
0·0	17·32	0·0745	0·457	B.P.	30·0	23·52	0·767	0·0444	P.V.
0·0	22·73	0·0723	0·471	P.V.	30·0	16·23	1·264	0·02695	P.V.
0·0	27·81	0·0720	0·473	P.V.	40·0	33·78	0·455	0·0749	D.P.
0·0	52·21	0·0707	0·482	P.V.	40·0	33·14	0·476	0·0716	P.V.
10·0	21·91	0·0775	0·439	B.P.	40·0	31·74	0·548	0·0622	P.V.
10·0	26·89	0·0754	0·451	P.V.	40·0	27·00	0·679	0·0502	P.V.
10·0	34·87	0·0743	0·458	P.V.	40·0	20·07	1·026	0·03319	P.V.
10·0	52·47	0·0730	0·467	P.V.	40·0	16·44	1·315	0·02590	P.V.
10·0	55·55	0·0729	0·467	P.V.	50·0	42·52	0·311	0·109	D.P.
20·0	27·20	0·0823	0·414	B.P.	56·3	47·25	0·289	0·118	D.P.
30·0	33·25	0·0875	0·389	B.P.	56·3	45·01	0·319	0·107	P.V.
30·0	48·80	0·0839	0·406	P.V.	56·3	35·05	0·525	0·0649	P.V.
40·0	40·07	0·0962	0·354	B.P.	56·3	25·01	0·854	0·0399	P.V.
40·0	48·30	0·0914	0·373	P.V.	56·3	17·71	1·303	0·02613	P.V.
40·0	52·00	0·0902	0·378	P.V.					
50·0	47·60	0·1127	0·302	B.P.					
50·0	52·00	0·1040	0·328	P.V.					
50·0	58·27	0·0983	0·346	P.V.					
53·0	49·94	0·1209	0·282	B.P.					
54·9	50·55	0·1601	0·213	B.P.					
56·0	50·65	—	—	C.P.					
56·2	50·72	0·1825	0·187	C.P.					
56·2	50·90	0·1702	0·200	C.P.					
56·2	51·46	0·1570	0·217	P.V.					
56·2	52·46	0·1385	0·246	P.V.					
56·2	54·32	0·1242	0·274	P.V.					
56·2	57·15	0·1156	0·295	P.V.					
57·0	50·70	—	—	R.					
57·0	50·30	—	—	R.					

TABLE 1 (*continued*)

80·56 mol. % C_2H_6

Liquid					Vapour				
temp. °C	pressure atm. (abs.)	volume l./mol.	density kg./l.	remarks	temp. °C	pressure atm. (abs.)	volume l./mol.	density kg./l.	remarks
−18·0	12·67	0·0703	0·461	B.P.	−25·0	7·52	2·452	0·01321	D.P.
−10·0	15·72	0·0723	0·448	B.P.	−20·0	8·44	2·152	0·01505	D.P.
0·0	19·47	0·0750	0·432	B.P.	−10·0	11·33	1·540	0·02103	D.P.
0·0	55·55	0·0732	0·443	P.V.	0·0	14·94	1·173	0·02761	D.P.
10·0	24·54	0·0791	0·409	B.P.	10·0	19·86	0·863	0·0375	D.P.
10·0	33·23	0·0781	0·415	P.V.	20·0	26·00	0·603	0·0537	D.P.
10·0	50·04	0·0761	0·426	P.V.	20·0	22·97	0·760	0·0426	P.V.
20·0	31·23	0·0840	0·386	B.P.	20·0	14·72	1·377	0·0235	P.V.
20·0	34·90	0·0811	0·399	P.V.	30·0	33·23	0·452	0·0717	D.P.
20·0	47·75	0·0796	0·407	P.V.	40·0	41·15	0·323	0·100	D.P.
20·0	53·31	0·0789	0·411	P.V.	40·0	35·00	0·466	0·0695	P.V.
20·0	56·23	0·0786	0·412	P.V.	40·0	12·79	1·766	0·0183	P.V.
30·0	38·18	0·0909	0·356	B.P.	40·0	12·79	1·766	0·0183	P.V.
30·0	42·21	0·0886	0·366	P.V.	42·4	42·93	0·308	0·105	D.P.
30·0	48·06	0·0863	0·375	P.V.	44·0	45·26	—	—	D.P.
30·0	56·24	0·0842	0·385	P.V.	46·7	47·95	0·279	0·116	D.P.
40·0	46·10	0·1061	0·305	B.P.					
40·0	48·63	0·1007	0·322	P.V.					
40·0	50·97	0·0980	0·331	P.V.					
40·0	55·22	0·0944	0·343	P.V.					
45·5	50·23	0·1367	0·237	B.P.					
46·1	50·39	0·1509	0·215	C.P.					
46·1	52·52	0·1161	0·279	P.V.					
46·1	54·88	0·1096	0·296	P.V.					
46·4	50·43	0·1782	0·182	R.					
47·1	49·91	0·2211	0·146	R.					

89·89 mol. % C_2H_6

−21·0	13·03	0·0680	0·460	B.P.	−31·0	7·32	2·328	0·01343	D.P.
−19·5	13·10	0·0682	0·459	B.P.	−30·0	7·45	2·217	0·01410	D.P.
−10·7	16·72	0·0712	0·439	D.P.	−20·0	10·30	1·647	0·01899	D.P.
0·0	21·74	0·0735	0·425	B.P.	−10·0	13·40	1·280	0·02442	D.P.
10·0	27·42	0·0784	0·399	B.P.	0·0	17·39	0·977	0·0320	D.P.
10·0	38·84	0·0738	0·424	P.V.	10·0	23·64	0·681	0·0459	D.P.
10·0	53·70	0·0719	0·435	P.V.	21·0	31·39	0·469	0·0667	D.P.
20·0	34·31	0·0848	0·369	B.P.	30·0	38·90	0·343	0·0912	D.P.
20·0	53·74	0·0772	0·405	P.V.	37·0	45·91	—	—	D.P
20·0	35·92	0·0828	0·378	P.V.					
20·0	47·82	0·0780	0·401	P.V.					
20·0	54·93	0·0767	0·408	P.V.					
30·0	42·18	0·0956	0·327	B.P.					
30·0	44·69	0·0910	0·343	P.V.					
30·0	46·37	0·0897	0·349	P.V.					
30·0	47·80	0·0883	0·354	P.V.					
36·0	47·15	0·1077	0·290	B.P.					
37·0	47·84	0·1102	0·284	B.P.					
38·4	49·16	0·1177	0·266	B.P.					
38·7	49·20	0·1223	0·256	C.P.					
38·7	49·24	0·1218	0·257	C.P.					
38·9	49·30	0·1404	0·223	R.					

TABLE 1 (*continued*)

95·02 mol. % C_2H_6

Liquid					Vapour				
temp. °C	pressure atm. (abs.)	volume l./mol.	density kg./l.	remarks	temp. °C	pressure atm. (abs.)	volume l./mol.	density kg./l.	remarks
−25·0	12·18	0·0679	0·450	B.P.	−31·0	8·45	1·978	0·0155	D.P.
−20·5	13·88	0·0674	0·455	B.P.	−20·0	11·85	1·418	0·0216	D.P.
−20·5	25·25	0·0659	0·465	P.V.	−10·0	15·87	1·020	0·0300	D.P.
−10·0	18·02	0·0714	0·429	B.P.	0·0	20·37	0·787	0·0389	D.P.
−10·0	53·26	0·0679	0·451	P.V.	10·0	26·16	0·588	0·0524	D.P.
0·0	22·45	0·0750	0·409	B.P.	20·0	33·94	0·409	0·0749	D.P.
0·0	41·15	0·0713	0·430	P.V.	30·0	42·11	0·298	0·103	D.P.
0·0	52·85	0·0705	0·435	P.V.					
10·0	28·58	0·0791	0·387	B.P.					
10·0	48·31	0·0751	0·408	P.V.					
20·0	35·67	0·0870	0·352	B.P.					
20·0	38·07	0·0841	0·364	P.V.					
20·0	54·64	0·0797	0·385	P.V.					
27·4	41·65	0·0850	0·361	B.P.					
30·0	43·88	0·1010	0·303	B.P.					
30·0	47·18	0·0944	0·325	P.V.					
30·0	49·45	0·0920	0·333	P.V.					
30·0	55·34	0·0885	0·346	P.V.					
33·0	46·54	0·1094	0·280	B.P.					
34·9	48·07	0·1178	0·260	B.P.					
35·4	48·57	0·1245	0·246	B.P.					
35·5	48·80	0·1469	0·209	C.P.					
35·8	48·75	—	—	R.					

C_3H_6

temp. °C	pressure atm. (abs.)	Liquid volume l./mol.	Liquid density kg./l.	Vapour volume l./mol.	Vapour density kg./l.
−30·0	2·07	0·0715	0·587	—	—
−20·0	3·00	0·0733	0·574	6·15	0·00684
−10·0	4·25	0·0749	0·562	4·61	0·00912
0·0	5·79	0·0770	0·546	3·42	0·0123
10·0	7·63	0·0791	0·531	2·62	0·0161
20·0	10·13	0·0815	0·516	1·98	0·0212
30·0	13·02	0·0850	0·495	1·52	0·0277
40·0	16·32	0·0884	0·476	1·19	0·0353
50·0	20·39	0·0918	0·458	0·921	0·0457
60·0	24·87	0·0962	0·437	0·708	0·0594
70·0	30·00	0·1031	0·408	0·552	0·0762
80·0	36·25	0·1137	0·370	0·419	0·100
90·0	44·02	—	—	0·308	0·137
92·1	45·40	0·175	0·240	0·175	0·240

Volumetric data. The P, V, T, x relationships for the system are shown graphically on a three-dimensional diagram in figure 5. The $(V, x)_T$ isotherms for the saturated vapours have been drawn and indicate that the orthobaric volume of the vapour phase is a linear function of composition throughout the whole temperature range. It may be pointed out that the pressure is not constant but, for each mixture, is that at which the vapour is saturated. To reduce the observations to constant pressure we may make use of the experimentally determined compressibility factors; the corrected isotherms are then found to be linear and nearly parallel to the composition axis. In the case of the liquid phase the orthobaric volume is a linear function of composition only at low temperatures; above 20° the volume increases rapidly with increase in the ethane content of the mixture.

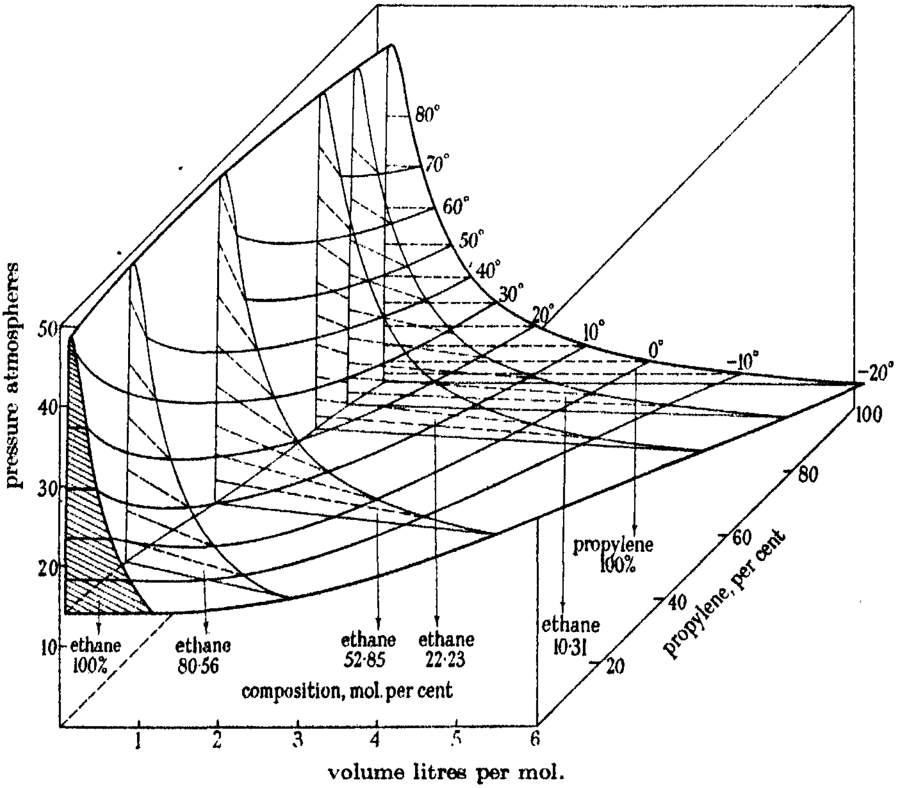

Figure 5. P, V, T, x diagram for the system ethane-propylene.

The densities of co-existing liquid and vapour in equilibrium are given in table 1. When plotted as a function of temperature the $(T, \rho)_x$ curves show a characteristic point of inflexion in the neighbourhood of the critical-point.

REFERENCES

Burrell and Robertson 1915 *J. Amer. Chem. Soc.* **37**, 2188.
Guter, Newitt and Ruhemann 1940 *Proc. Roy. Soc.* A, **176**, 140.
Kay, W. B. 1938 *J. Industr. Engng Chem.* **30**, 459.
Plank and Kamboitz 1937 *VII Congress Int. du Froid*, **3**.
Ruhemann, M. 1939 *Proc. Roy. Soc.* A, **171**, 121.
Seibert and Burrell 1915 *J. Amer. Chem. Soc.* **37**, 2683.

Systematic constructional tables for thin cemented aplanatic lenses

BY EDNA D. BROWN AND T. SMITH, F.R.S.

(*Received* 3 *July* 1941—*Deposited in Archives* 17 *July* 1941)

The tables give all the information needed for the construction of cemented aplanatic lenses made of only two refracting media, when the object is at infinity and when the image is equal in size to the object. In the former case two series of unsymmetrical doublets are specified and in the latter two series of symmetrical triplets. The refractive indices range from 1·33333 to 2·00000 and the intervals are small enough for interpolation.

CORRIGENDUM

In the paper by F. S. SHAW and R. V. SOUTHWELL, this volume, p. 2, the implication of the parenthetical reference to Richardson's paper (1908) is incorrect. Of the five diagrams there reproduced, four relate to free surfaces not initially given.

INDEX TO VOLUME 178 (A)

α/β brass type of equilibrium (Andrews and Hume-Rothery), 464.
Andrews, K. W. and Hume-Rothery, W. On the α/β brass type of equilibrium, 464.
Atomic lattice of iron, stress-strain curve (Smith and Wood), 93.

β-rays from radium (B + C), measurements of energies (Harper and Roberts), 170.
Bhabha, H. J. General classical theory of spinning particles in a meson field, 314.
Bhabha, H. J. and Corben, H. C. General classical theory of spinning particles in a Maxwell field, 273.
Bleaney, B. and Hull, R. A. The determination of the vapour-pressure curve of liquid helium below 1·6° K using a magnetic thermometer, 74.
Bleaney, B. and Hull, R. A. The effective susceptibility of a paramagnetic powder, 86.
Bolland, J. The kinetics of the polymerization of isoprene on sodium surfaces, 24.
Bose-Einstein statistics and degeneracy (Kothari and Singh), 135.
Brown, E. D. and Smith, T. Systematic constructional tables for thin cemented aplanatic lenses (abstract), 525.
Buckingham, R. A., Massey, H. S. W. and Tibbs, S. R. A self-consistent field for methane and its applications, 119.
Butene-1, catalytic isomerization (Twigg), 106.

Cameron, A. and Coumoulos, G. D. On the electron diffraction of multilayers of fatty acids, I, 415.
Carbon monoxide, flame spectrum (Gaydon), 61.
Chemical equilibria of thermal associations (Wassermann), 370.
Corben, H. C. *See* Bhabha and Corben.
Corner, J. and Lennard-Jones, J. E. Critical and cooperative phenomena, VI, 401.
Cosmic ray variations (Jánossy and Lockett), 52.
Coumoulos, G. D. and Rideal, E. K. On the electron diffraction of multilayers of fatty acids, II, 421.
Coumoulos, G. D. *See* Cameron and Coumoulos.
Critical and cooperative phenomena, VI (Corner and Lennard-Jones), 401.

Deuteron-induced fission in uranium and thorium (Gant and Krishnan), 474.
Dielectric strength of mixed crystals (Fröhlich), 493.

Electron diffraction of multilayers of fatty acids, I, II (Cameron, Coumoulos and Rideal), 415, 421.
Electronic charge (Hopper and Laby), 243.
Eley, D. D. The interchange of hydrogen in the adsorbed film on tungsten, 452.
Eley, D. D. and Rideal, E. K. The catalysis of the parahydrogen conversion by tungsten, 429.

Fage, A. and Preston, J. H. On transition from laminar to turbulent flow in the boundary layer, 201.
Fröhlich, H. On the dielectric strength of mixed crystals, 493.

γ-ray transition of radio-bromine (Siday), 189.
Gant, D. H. T. and Krishnan, R. S. Deuteron-induced fission in uranium and thorium, 474.
Gaydon, A. G. The flame spectrum of carbon monoxide, II, 61.
Geib, K. H. and Vaidya, W. M. Spectroscopic observations on hydrocarbon flames in atomic oxygen, 351.
Grew, K. E. Thermal diffusion in hydrogen-deuterium mixtures, 390.

Harper, A. F. A. and Roberts, N. F. Precise measurements of the energies of β-rays from radium (B + C), 170.
Heath, H. R., Ibbs, T. L. and Wild, N. E. The diffusion and thermal diffusion of hydrogen-deuterium, with a note on the thermal diffusion of hydrogen-helium, 380.
Hopper, V. D. and Laby, T. H. The electronic charge, 243.
Hull, R. A. *See* Bleaney and Hull.
Hume-Rothery, W. *See* Andrews and Hume-Rothery.
Hydrocarbon flames, spectroscopic investigation (Vaidya), 356.
Hydrocarbon flames, spectroscopic observations (Geib and Vaidya), 351.
Hydrogen-deuterium, diffusion and thermal diffusion (Heath, Ibbs and Wild), 380.
Hydrogen-deuterium, thermal diffusion (Grew), 390.

Ibbs, T. L. *See* Heath, Ibbs and Wild.
Isoprene, kinetics of polymerization (Bolland), 24.

Jánossy, L. and Lockett, P. The sun's magnetic field and the diurnal and seasonal variations in cosmic ray intensity, 52.

Kellermann, E. W. On the specific heat of the sodium chloride crystal, 17.
Kothari, D. S. and Singh, B. N. Bose-Einstein statistics and degeneracy, 135.
Krishnan, R. S. *See* Gant and Krishnan.

Laby, T. H. *See* Hopper and Laby.
Lennard-Jones, J. E. *See* Corner and Lennard-Jones.
Lockett, P. *See* Jánossy and Lockett.
Lonsdale, K., Robinson, J. M. and Woodward, I. Structure and molecular anisotropy of sorbic acid, 43.
Lu, H., Newitt, D. M. and Ruhemann, M. Two phase equilibrium in binary and ternary systems, IV, 506.

Massey, H. S. W. *See* Buckingham, Massey and Tibbs.
Maxwell field, classical theory of spinning particles (Bhabha and Corben), 273.
Meson field, classical theory of spinning particles (Bhabha), 314.
Methane, self-consistent field (Buckingham, Massey and Tibbs), 119.
Müller, A. Further investigations of solid n-paraffins, 227.

Newitt, D. M. *See* Lu, Newitt and Ruhemann.

Paramagnetic powder, effective susceptibility (Bleaney and Hull), 86.
Peng, H. W. Perturbation theory for the self-consistent field, 499.
Perturbation theory for the self-consistent field (Peng), 499.
Preston, J. H. *See* Fage and Preston.

Relaxation methods applied to engineering problems (Shaw and Southwell), 1, 525.
Rideal, E. K. *See* Coumoulos and Rideal *and* Eley and Rideal.
Roberts, N. F. *See* Harper and Roberts.
Robinson, J. M. *See* Lonsdale, Robinson and Woodward.
Ruhemann, M. *See* Lu, Newitt and Ruhemann.

Self-consistent field for methane and its applications (Buckingham, Massey and Tibbs), 119.
Shaw, F. S. and Southwell, R. V. Relaxation methods applied to engineering problems, VII, 1, 525.
Siday, R. E. The γ-ray transition of radio-bromine, 189.
Singh, B. N. *See* Kothari and Singh.
Smith, S. L. and Wood, W. A. A stress-strain curve for the atomic lattice of iron, 93.
Smith, T. *See* Brown and Smith.
Solid *n*-paraffins (Müller), 227.
Sorbic acid, structure and molecular anisotropy (Lonsdale, Robinson and Woodward), 43.
Southwell, R. V. *See* Shaw and Southwell.
Specific heat of the sodium chloride crystal (Kellermann), 17.
Structure and molecular anisotropy of sorbic acid (Lonsdale, Robinson and Woodward), 43.

Tibbs, S. R. *See* Buckingham, Massey and Tibbs.
Transition from laminar to turbulent flow in the boundary layer (Fage and Preston), 201.
Tungsten, catalysis of parahydrogen conversion (Eley and Rideal), 429.
Tungsten, interchange of hydrogen in adsorbed film (Eley), 452.
Twigg, G. H. The catalytic isomerization of butene-1, 106.
Two-phase equilibrium in binary and ternary systems, IV (Lu, Newitt and Ruhemann), 506.

Unwin, J. J. The production of waves by the sudden release of a spherical distribution of compressed air in the atmosphere, 153.

Vaidya, W. M. A spectroscopic investigation of hydrocarbon flames, 356.
Vaidya, W. M. *See also* Geib and Vaidya.
Vapour-pressure curve of liquid helium below 1·6° K (Bleaney and Hull), 74.

Wassermann, A. Chemical equilibria of thermal associations, 370.
Waves, production by sudden release of compressed air (Unwin), 153.
Wild, N. E. *See* Heath, Ibbs and Wild.
Wood, W. A. *See* Smith and Wood.
Woodward, I. *See* Lonsdale, Robinson and Woodward.

END OF THE ONE HUNDRED AND SEVENTY-EIGHTH VOLUME (SERIES A)

I. A. R. I. 75.

INDIAN AGRICULTURAL RESEARCH
INSTITUTE LIBRARY
NEW DELHI.

Date of issue.	Date of issue.	Date of issue
6 JAN 1971		

S. C. P.—1/8/47 P. J.-3-5-48-2000